Diseases of the Brain, Head and Neck, Spine 2016–2019

Jürg Hodler • Rahel A. Kubik-Huch
Gustav K. von Schulthess
Editors

Diseases of the Brain, Head and Neck, Spine 2016–2019

Diagnostic Imaging

48th International Diagnostic Course in Davos (IDKD)
Davos, April 3–8, 2016

including the
Nuclear Medicine Satellite Course "Diamond"
Davos, April 2–3, 2016

Pediatric Radiology Satellite Course "Kangaroo"
Davos, April 2, 2016

Breast Imaging Satellite Course "Pearl"
Davos, April 2, 2016

and additional IDKD Courses 2016–2019

presented by the Foundation for the
Advancement of Education in Medical Radiology, Zurich

Springer

Editors
Jürg Hodler
Orthopadische Universitatsklinik Ba
UniversitätsSpital Zürich
Zürich
Switzerland

Rahel A. Kubik-Huch
Zürich
Switzerland

Gustav K. von Schulthess
Klinik/Poliklinik Nuklearmedizin
Zürich
Switzerland

ISBN 978-3-319-30080-1 ISBN 978-3-319-30081-8 (eBook)
DOI 10.1007/978-3-319-30081-8

Library of Congress Control Number: 2016935622

Printed on acid-free paper

This Springer imprint is published by Springer Nature
The registered company is Springer International Publishing AG Switzerland

Preface

The International Diagnostic Course in Davos (IDKD) is a unique learning experience for both imaging specialists and clinicians. The course is useful for experienced radiologists, imaging specialists in training, and clinicians wishing to be updated on the current state of the art in all relevant fields of neuroimaging.

This course is organ based and disease oriented. It includes imaging of the brain, head, neck, and spine. In addition, there will be satellite courses covering pediatric radiology and nuclear medicine related to neuroimaging in more depth. These courses are also represented in the current Syllabus, as well as our traditional breast imaging satellite course.

During the last few years, there have been considerable advances in the field of neuroimaging driven by clinical as well as technological developments. These will be highlighted in the workshops given by internationally known experts in their field. The presentations encompass all the relevant imaging modalities including CT, MRI, hybrid imaging, and others.

This Syllabus contains condensed versions of the topics discussed in the IDKD workshops. As a result, this book offers a comprehensive review of the state-of-the-art neuroimaging.

This Syllabus was initially designed to provide the relevant information for the course participants in order to allow them to fully concentrate on the lectures and participate in the workshop discussions without the need of taking notes. However, the Syllabus has developed into a complete update for radiologists, radiology residents, nuclear physicians, and clinicians interested in neuroimaging.

Additional information on IDKD courses can be found on the IDKD website:
www.idkd.org

J. Hodler
R.A. Kubik-Huch
G.K. von Schulthess

Contents

Part I

Workshops

Cerebral Neoplasms

Edmond A. Knopp and Girish M. Fatterpekar

A mass-like lesion in the brain always makes us consider the possibility of an underlying tumor. We then assess the imaging pattern in order to establish an appropriate tumoral differential diagnosis. While this approach often works, a mass lesion can sometimes simulate a tumor. Identification of such a tumor mimic is essential since it can significantly influence further management. This review article will focus on imaging features of brain tumors and tumor mimics. Considering the exhaustive list of tumors (intra-axial, calvarial/dural based, sellar based, pineal region based, and intraventricular), we will limit our discussion to intra-axial tumors.

Intra-axial Brain Tumors

Astrocytic Tumors

Pilocytic Astrocytoma

Pilocytic astrocytoma is a WHO grade I well-circumscribed, slow-growing tumor seen more commonly in children and young adults. Common locations in children include the optic pathway, hypothalamus, cerebellum, and brain stem. Common locations in adult include thalamus and basal ganglia.

Characteristic imaging findings: A cystic-appearing lesion with an intensely enhancing mural nodule with minimal to no surrounding edema is often seen [1]. The intense enhancement reflects the prominent vascularity known to be associated with these lesions. Hemorrhage and calcification are uncommon. It should be noted that visual pathway and hypothalamic lesions are more solid in appearance and can show patchy enhancement. Involvement of subarachnoid space can be seen in pilocytic astrocytoma and should not make one think of a malignant transformation.

Best sequence(s) to evaluate pilocytic astrocytoma: Post-contrast T1WI/MPRAGE.

Pilomyxoid Astrocytoma

Pilomyxoid astrocytoma is a WHO grade I tumor which can be considered to be a histologic variant of pilocytic astrocytoma. As the name suggests, it has a markedly myxoid matrix which is not seen in the classic pilocytic astrocytoma. The tumor demonstrates a more aggressive behavior pattern than a typical pilocytic astrocytoma and recurs more often. It is more commonly seen in the pediatric population. Favored location is in the hypothalamic region.

Characteristic imaging findings: Pilomyxoid astrocytoma consistent with its myxoid matrix is seen as a hypointense lesion on T1WI, which appears hyperintense on long TR sequences and demonstrates moderate enhancement [2]. Hemorrhage, calcification, necrosis, and edema are uncommon.

Best sequence(s) to evaluate pilomyxoid astrocytoma: FLAIR/T2WI and post-contrast T1WI/MPRAGE.

Pleomorphic Xanthoastrocytoma

Pleomorphic xanthoastrocytoma is a WHO grade II tumor, seen in children and young adults. Often seen in the supratentorial compartment, the temporal lobe is a favored location.

Characteristic imaging findings: A cystic-appearing lesion with a mural enhancing nodule is seen. Oftentimes, the mural enhancing nodule is cortical based extending superficially up to the leptomeningeal surface (Fig. 1) [3, 4]. Hemorrhage, calcification, and surrounding edema are uncommon.

Best sequence(s) to evaluate pleomorphic xanthoastrocytoma: Post-contrast T1WI/MPRAGE.

Diffuse Astrocytoma

Diffuse astrocytomas are WHO grade II tumors, often seen in adults in the third to fifth decade of life. Characterized by

E.A. Knopp
Radiology, Zwanger-Pesiri Radiology, 150 East Sunrise Highway, Suite 208, Lindenhurst, NY 11757, USA
e-mail: eknopp@zwangerpesiri.com

G.M. Fatterpekar (✉)
Radiology, NYU School of Medicine, 660 First Avenue, New York, NY 10016, USA
e-mail: Girish.Fatterpekar@nyumc.org

J. Hodler et al. (eds.), *Diseases of the Brain, Head and Neck, Spine 2016–2019: Diagnostic Imaging*, DOI 10.1007/978-3-319-30081-8_1

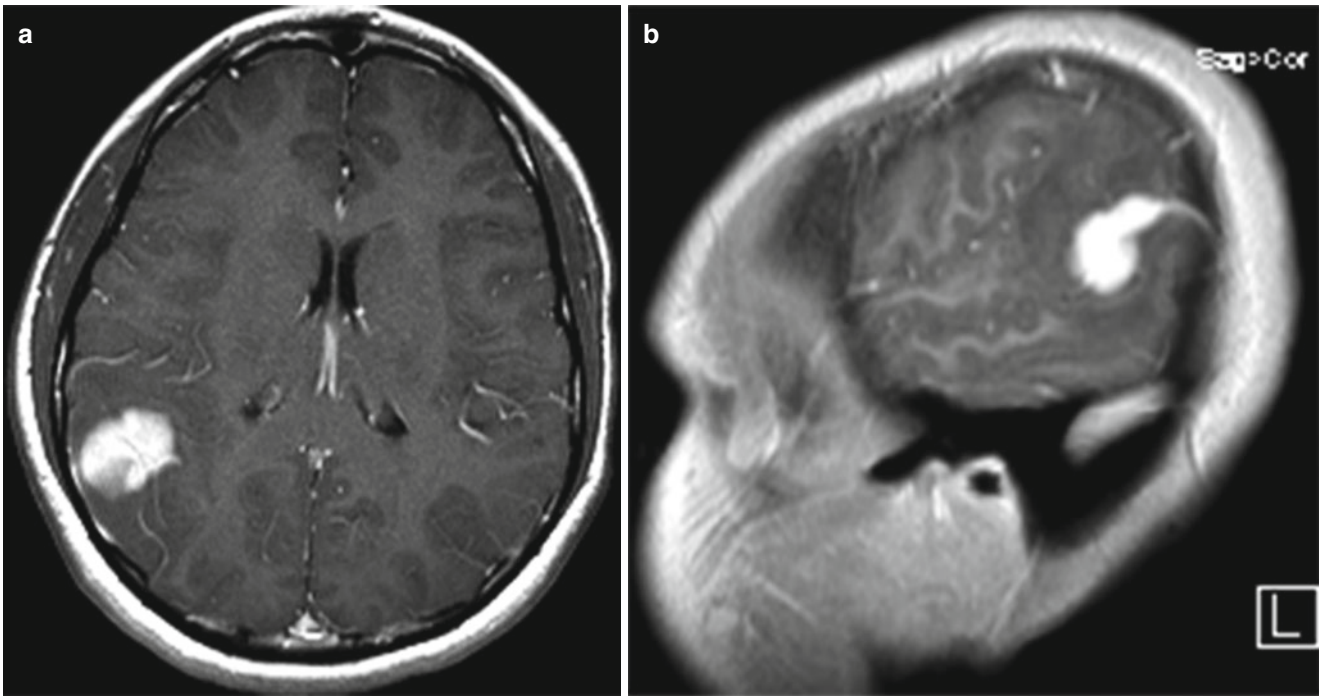

Fig. 1 Contrast-enhanced (**a**) axial and (**b**) sagittal MPRAGE images demonstrating an intensely enhancing nodule with surrounding edema in the left posterior temporal region. The nodule is seen to abut the leptomeningeal surface. Diagnosis: pleomorphic xanthoastrocytoma

slow growth, there is variable infiltration of adjacent brain structures. Malignant degeneration or degeneration into anaplastic astrocytoma can sometimes occur.

Characteristic imaging findings: An ill-defined mass hypointense on T1WI and hyperintense on T2WI, extending to and expanding the cortex, is seen. Absent to minimal contrast enhancement is seen [5]. The lack of high cellularity correlates with lack of diffusion restriction. There is no increased perfusion seen helping distinguish it from an anaplastic astrocytoma (WHO grade III) or glioblastoma (WHO grade IV). Hemorrhage, calcification, and tumoral necrosis are not seen.

Note: Brain stem gliomas, often seen as diffuse pontine lesions, are WHO grade II tumors. These tumors are most often seen in the pediatric population.

Best sequence(s) to evaluate diffuse astrocytoma: FLAIR for extent and perfusion to help distinguish from high-grade tumors.

Anaplastic Astrocytoma

Anaplastic astrocytoma is a WHO grade III tumor, often seen in adults in the third to fifth decade of life. It is defined as a diffuse astrocytoma with focal or dispersed anaplasia.

Characteristic imaging findings: Conventional imaging features are highly similar to those of diffuse astrocytoma. The presence of increased perfusion (likely reflecting neoangiogenesis) helps distinguish anaplastic astrocytoma from diffuse astrocytoma [6].

Best sequence(s) to evaluate anaplastic astrocytoma: FLAIR for extent and perfusion to help establish increased rCBV.

Gliomatosis Cerebri

Gliomatosis cerebri is a WHO grade III tumor, most commonly seen in adults in the third to fifth decade of life. It is defined as a diffusely infiltrating astrocytic tumor, involving three or more lobes. Extension across the corpus callosum and into the infratentorial compartment is common.

Characteristic imaging findings: Ill-defined infiltrative mass lesion involving the cortex and the white matter with associated mass effect and contiguously involving more than three lobes is seen [7, 8]. Extension across the splenium of corpus callosum and into the infratentorial compartment is often seen. Typically, minimal to no enhancement is noted. Hemorrhage, necrosis, and calcification are not seen.

Best sequence(s) to evaluate gliomatosis cerebri: FLAIR.

Glioblastoma

Glioblastoma is a WHO grade IV tumor, the most malignant neoplasm of the group of diffuse astrocytic tumors. It is the most common primary intra-axial brain tumor and contributes to approximately 50–60 % of all astrocytic tumors. In adults, most such tumors are seen in the supratentorial compartment; in the pediatric population, though considered an uncommon tumor, the brain stem is a favored site. Primary

glioblastomas typically develop in older individuals (sixth decade of life), whereas secondary glioblastomas derived from low-grade or anaplastic astrocytomas are seen in younger patients (fourth decade of life).

Characteristic imaging findings: An irregularly marginated, peripherally enhancing, centrally necrotic lesion with variable surrounding edema is seen. Diffusion restriction can be seen from the solid enhancing component of the lesion. Facilitated diffusion is seen from the necrotic component of the lesion. Foci of susceptibility suggestive of hemorrhage and neoangiogenesis are often seen. Increased rCBV from the solid enhancing component of the tumor is seen on perfusion-weighted imaging (Fig. 2) [9].

Best sequence(s) to evaluate glioblastoma: Contrast-enhanced T1WI/MPRAGE, diffusion-weighted imaging, and perfusion imaging.

Oligodendroglial and Oligoastrocytic Tumors

Oligodendroglioma

Oligodendroglioma is a WHO grade II tumor derived from oligodendroglia or from glial precursor cells. It is most commonly seen to involve adults in the third to fourth decade of life. Most such tumors are seen in the cerebral hemispheres, frontal lobes being the most common location.

Characteristic imaging findings: Infiltrative tumors with poorly defined margins. Closer inspection often demonstrates expansion of the involved cortex. Calcification (appreciated on gradient-echo or susceptibility-weighted imaging and still better on CT) is common. Variable degree of enhancement is seen [10–13]. Minimal edema can be seen. Small cysts and hemorrhage can be seen. Increased rCBV is noted on perfusion imaging and unlike diffuse astrocytomas does not suggest a high-grade (WHO grade III or IV) tumor.

Best sequence(s) to evaluate oligodendroglioma: FLAIR/T2WI, gradient-echo or susceptibility-weighted imaging, and non-contrast CT.

Note: Interval hemorrhage, necrosis, or ring enhancement on follow-up studies should be worrisome for anaplastic transformation of oligodendroglioma.

Oligoastrocytoma

Oligoastrocytoma is a WHO grade II tumor resembling tumor cells in both oligodendroglioma and diffuse astrocytoma. Most tumors are seen to occur in adults, in their third to fourth decade of life [14].

Characteristic imaging findings: Imaging findings demonstrating an overlap between both oligodendroglioma and astrocytoma are seen.

Best sequence(s) to evaluate oligoastrocytoma: FLAIR/T2WI and contrast-enhanced T1WI/MPRAGE.

Neuronal and Mixed Neuronal-Glial Tumors

Desmoplastic Infantile Ganglioglioma

Desmoplastic infantile ganglioglioma is a WHO grade I tumor, often seen in the first 2 years of life. This tumor is typically classified together with the desmoplastic infantile astrocytoma, which differs histologically by its lack of mature neuronal components.

Characteristic imaging findings: A complex tumor, relatively large in size and demonstrating both cystic and solid components, is seen. The solid enhancing component is superficially placed in contrast to the typically deep-seated uni- or multilocular large cyst [4, 15]. For the size of the lesion, only minimal edema is seen. Calcification and hemorrhagic foci are uncommon.

Best sequence(s) to evaluate desmoplastic infantile ganglioglioma: T2WI and contrast-enhanced T1WI/MPRAGE.

Gangliglioma

Ganglioglioma is an uncommon WHO grade I or II tumor. Most tumors are seen in the first 3 decades of life with a peak age of incidence between 10 and 20 years of age. Often seen in the supratentorial compartment, the temporal lobe is a favored site.

Characteristic imaging findings: A cortical-based cystic-appearing lesion with calcification within the temporal lobe is highly suggestive of ganglioglioma. Oftentimes, enhancement is seen [4, 16, 17].

Best sequence(s) to evaluate ganglioglioma: Contrast-enhanced T1WI/MPRAGE, gradient-echo or susceptibility-weighted imaging to look for calcification, and non-contrast CT.

Dysembryoplastic Neuroepithelial Tumor

Dysembryoplastic neuroepithelial tumor is an uncommon WHO grade I tumor, seen most commonly in the pediatric population.

Characteristic imaging findings: Superficially (cortically) located mass lesion demonstrating multiple pseudocysts causing a soap bubble appearance on T2WI is seen. No diffusion restriction, hemorrhage, or calcification is seen. FLAIR typically demonstrates a hyperintense margin along the margin of the cysts. No enhancement is seen [18, 19].

Best sequence(s) to evaluate dysembryoplastic neuroepithelial tumor: T2WI/FLAIR and contrast-enhanced T1WI/MPRAGE.

Embryonal Tumors

Medulloblastoma

Medulloblastoma is a WHO grade IV tumor, most often seen in the pediatric population in the posterior fossa. A second smaller peak occurs in the late second-early third decade of life.

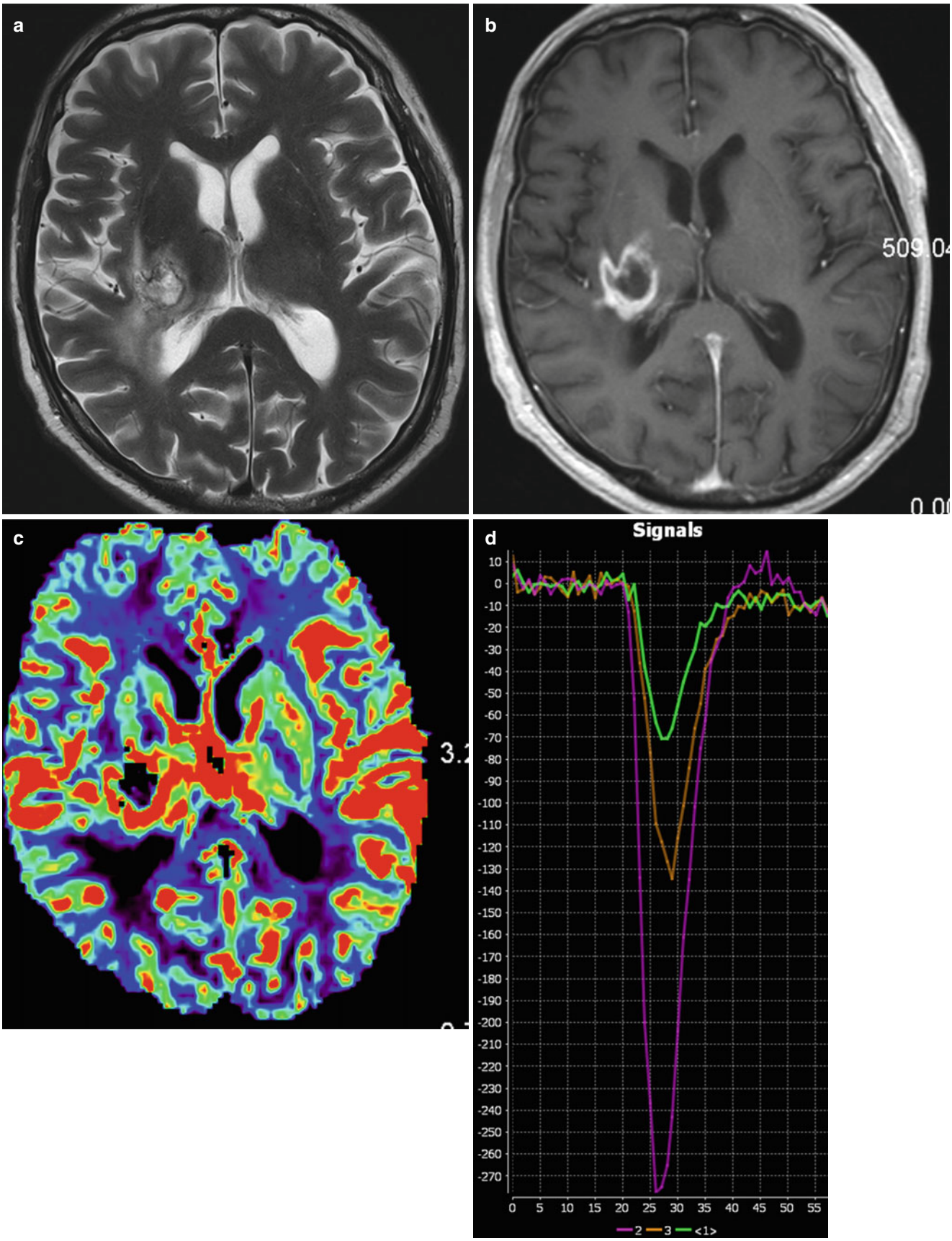

Fig. 2 (**a**) Axial T2WI and (**b**) contrast-enhanced axial T1WI demonstrate a peripherally enhancing centrally necrotic lesion in the right corona radiata. (**c**) DSC perfusion imaging demonstrates increased perfusion from the peripheral rim of the lesion. Also, there is a suggestion of increased perfusion even in the adjacent non-enhancing white matter. (**d**) Perfusion maps demonstrate markedly increased rCBV (compared to the green curve correlating to contralateral normal-appearing white matter), with values corresponding to 7.81. Diagnosis: glioblastoma

Characteristic imaging findings: Midline, posterior fossa masses arising from the roof of the fourth ventricle, displacing the fourth ventricle ventrally, and demonstrating homogenous diffusion restriction and enhancement are radiologic features of a classic medulloblastoma. Metastatic foci seeding the subarachnoid space within the intracranial compartment and in the spine can be seen [20, 21].

Best sequence(s) to evaluate medulloblastoma: Diffusion-weighted imaging and contrast-enhanced T1WI/MPRAGE.

Note: The reader is also encouraged to read about the desmoplastic medulloblastoma seen in young adults which presents more laterally, sometimes close to the cerebellopontine angle cistern, and exhibiting cysts. Part of this tumor can demonstrate diffusion restriction. Enhancement is only minimal. Imaging features of desmoplastic medulloblastoma are therefore distinct from those of classic medulloblastoma.

Primitive Neuroectodermal Tumor and Atypical Teratoid-Rhabdoid Tumors

These tumors are typically seen in infancy. In fact, atypical teratoid-rhabdoid tumor is the # 1 diagnosis to consider in a new born with an intracranial mass [22]. Also, in the first 2 years of life, a mass lesion in the brain demonstrating diffusion restriction and enhancement should strongly suggest the diagnosis of primitive neuroectodermal tumor [23].

Best sequence(s) to evaluate primitive neuroectodermal tumor: Diffusion-weighted imaging, FLAIR, and contrast-enhanced T1WI/MPRAGE.

Other Intra-axial Brain Tumors

Primary CNS Lymphoma

Primary CNS lymphoma is of the non-Hodgkin's type. It is more commonly seen in the fifth to sixth decades of life. Predisposing factors include immunodeficient states such as the AIDS population and other immunocompromised settings such as in transplant patients. It can sometimes also be seen in immunocompetent patients. The imaging appearance for both these substrata of patients is different.

Characteristic imaging findings: Immunocompromised patients: Periventricular region is a favored site. A peripherally enhancing centrally necrotic lesion with surrounding edema is seen. No diffusion restriction is seen from the centrally necrotic component of the lesion. Contiguous subependymal spread is commonly seen. Multiple lesions can be seen. Cortical-subcortical lesions can be seen. Hemorrhage and calcification are uncommon.

Immunocompetent patients: Basal ganglia, thalami, and periventricular white matter are favored locations. Solitary, solid-appearing lesion, demonstrating diffusion restriction and homogenous contrast enhancement, is seen (Fig. 3). Necrosis is occasionally seen [24]. Increased rCBV on perfusion imaging is seen. However, the rCBV values are typically < 4.0, unlike in glioblastoma where they can be higher.

Best sequence(s) to evaluate primary CNS lymphoma: DWI, FLAIR, and contrast-enhanced T1WI/MPRAGE.

Ependymoma

Ependymoma typically is seen in the pediatric population as a posterior fossa (4th ventricular) tumor. However, when it occurs in the adult population, it is seen more often as an intraparenchymal tumor. Heterogenously enhancing lesion is seen. Calcification is common. It is a difficult diagnosis to make considering the nonspecific imaging features and the rarity of its occurrence.

Metastases

Approximately 60 % of new intracranial tumors reported every year are metastatic tumors. Common primary sites include the lung and breast. Other common metastatic tumors to the brain include melanoma and gastrointestinal tumors. Imaging findings are nonspecific and include nodular deposits, large solid enhancing tumors, and peripherally enhancing centrally necrotic lesions. Hemorrhage can be seen. Surrounding edema is often seen. Calcification is uncommon. Some imaging pearls: New enhancing infratentorial tumor in an elderly patient is most likely a metastatic tumor. Also, multiple enhancing lesions at the gray-white matter interface in an appropriate clinical setting are most likely metastatic foci.

Best sequence(s) to evaluate metastases: Contrast-enhanced T1WI/MPRAGE. Perfusion imaging can help distinguish metastatic tumors from primary brain tumors [9].

Tumor Mimics

This category includes multiple etiologies including inflammatory, infectious, and vascular conditions. Also included are normal variants such as Virchow-Robin spaces. Treatment-related changes such as pseudoprogression and pseudoresponse have also been included to complete the discussion. Again, similar to brain tumors, tumor mimics includes an extensive list of underlying etiologies. We will limit our discussion to commonly occurring tumor mimics.

Inflammatory Conditions

While there are multiple etiologies in this subset, we will limit our discussion to demyelinating disease and amyloid angiopathy-related inflammation.

Tumefactive Demyelinating Lesion (TDL)

TDL is one of the most common tumor mimics. In its most classic form, TDL is defined as a single, large (>2.0 cm) lesion in the brain, most often in the periventricular location. There are no other imaging lesions to suggest an underlying demyelinating condition.

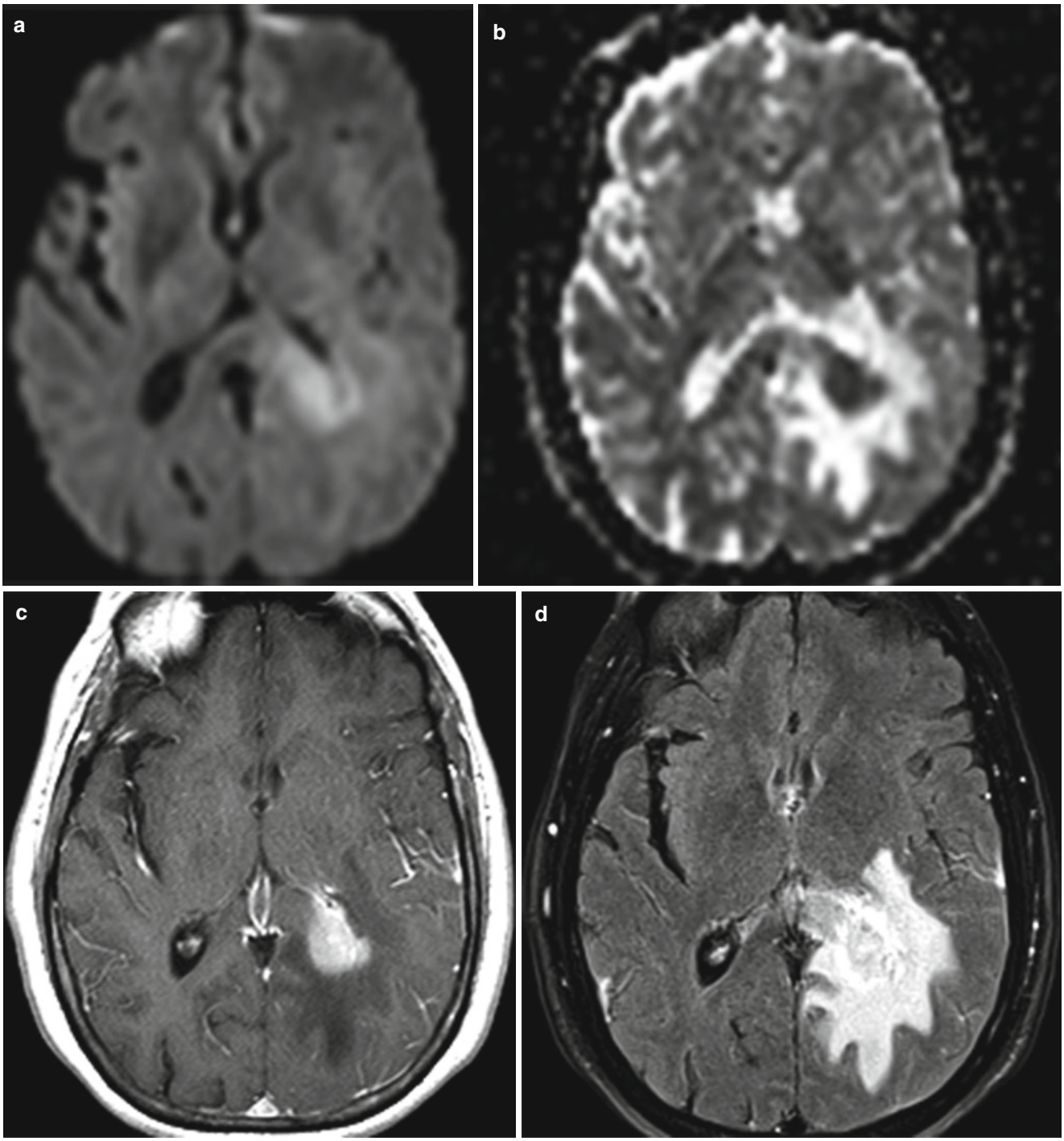

Fig. 3 (**a**) Axial DWI and corresponding (**b**) ADC map confirm diffusion restriction in the left periatrial region and extending into the splenium of corpus callosum. (**c**) Axial FLAIR demonstrates significant surrounding vasogenic edema and mass effect. (**d**) Contrast-enhanced axial T1WI demonstrates homogenous enhancement of the solid-appearing lesion. There is a suggestion of subependymal enhancement. Diagnosis: primary CNS lymphoma

Characteristic imaging findings: Large hypodense lesion on CT which appears hypointense on T1WI and hyperintense on T2WI/FLAIR is seen. Minimal surrounding edema and minimal mass effect, disproportionate to the size of the lesion, is seen. No hemorrhage or calcification is seen. An incomplete ring of enhancement is a hallmark feature of this lesion (Fig 4). This incomplete ring oftentimes corresponds to a band of diffusion restriction. Typically no increased perfusion is seen [25, 26]. In addition on either the perfusion source dataset or a SWI image, venular structures may be seen coursing through the mass lesion.

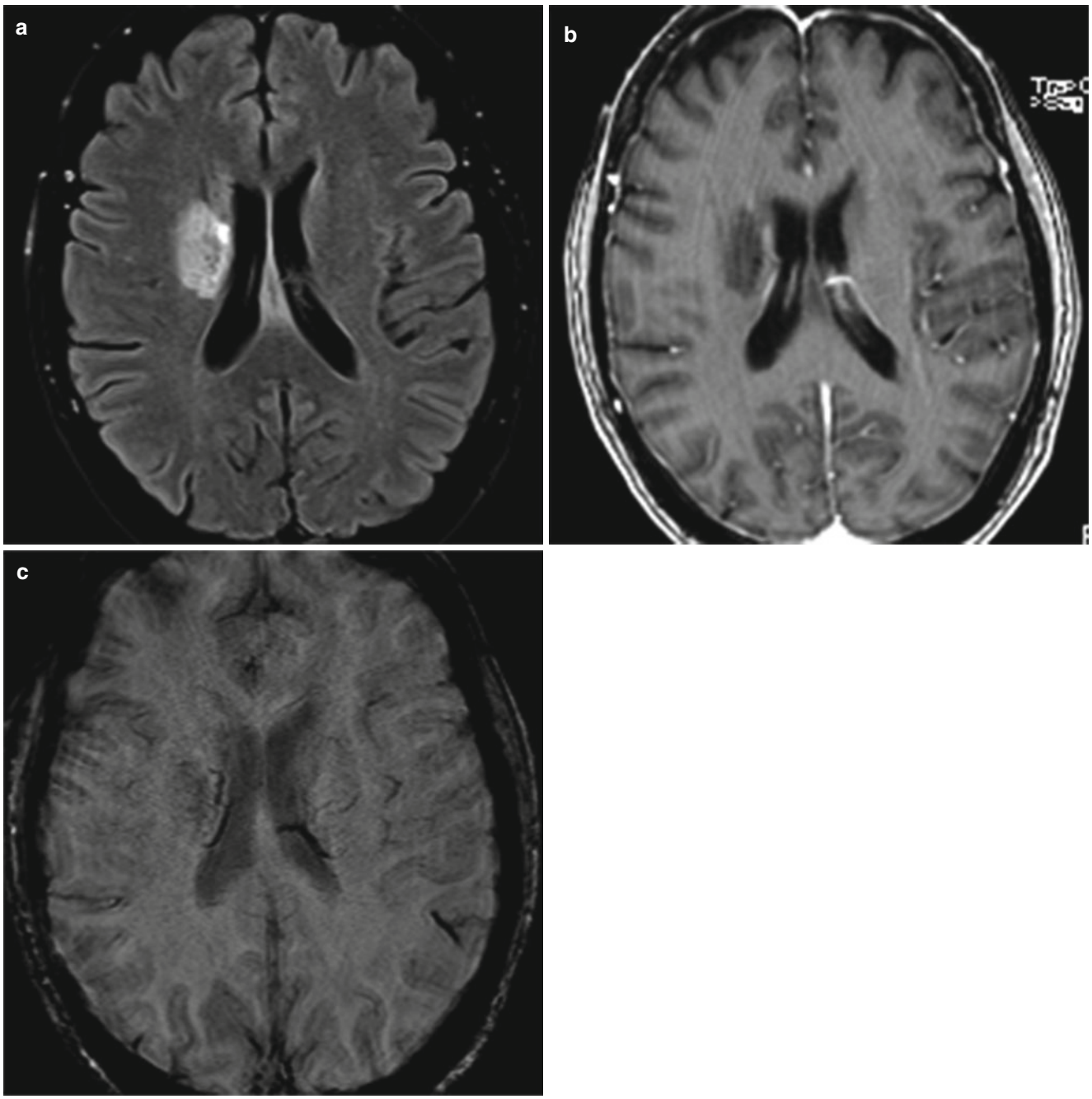

Fig. 4 (**a**) Axial FLAIR demonstrates an area of abnormal signal in the right corona radiata. No surrounding edema is seen. Minimal mass effect is noted. (**b**) Contrast-enhanced axial T1WI demonstrates a peripheral incomplete ring of enhancement. (**c**) Susceptibility-weighted image demonstrates wispy linear susceptibility foci coursing through the lesion. Diagnosis: tumefactive demyelinating lesion

Best sequence(s) to evaluate TDL: T2WI/FLAIR and contrast-enhanced T1WI/MPRAGE.

Amyloid Angiopathy-Related Inflammation

Cerebral amyloid angiopathy is seen in the elderly population. It results from extracellular deposition of amyloid, an amorphous eosinophilic fibrillary protein, in the walls of small- and medium-sized arteries. Occasionally, such deposition causes an inflammatory response in the brain. Patients present with headache, cognitive decline, encephalopathy, seizures, and occasionally focal deficits.

Characteristic imaging findings: Peripherally located foci of susceptibility in an elderly person should raise the possibility of amyloid angiopathy. Focal area of the brain demonstrating FLAIR hyperintense signal in an appropriate clinical setting should suggest amyloid angiopathy-related inflammation. Associated mass effect and subtle enhancement in the overlying leptomeningeal space can be seen [27].

Best sequence(s) to evaluate amyloid angiopathy-related inflammation: Susceptibility-weighted imaging or gradient-echo image, FLAIR/T2WI, and contrast-enhanced T1WI/MPRAGE.

Infectious Etiologies

This primarily includes bacterial, including mycobacterial, and fungal etiologies. Occasionally, parasitic infections can mimic brain tumors.

Abscess

Characteristic imaging findings: A centrally necrotic peripherally enhancing lesion is seen. The central necrotic component demonstrates diffusion restriction due to the inherent viscosity of pus. This diffusion restriction seen from the central necrotic component helps distinguish infection from tumor. There are certain exceptions to the rule which are mentioned below.

Note: Diffusion restriction from mucinous adenocarcinoma metastases can mimic an infection. On the other hand, lack of diffusion restriction from tuberculous abscess can mimic a tumor.

Best sequence(s) to evaluate an abscess: Diffusion-weighted imaging and contrast-enhanced T1WI/MPRAGE.

Encephalitis

Rhombencephalitis or brain stem encephalitis is often associated with infectious or autoimmune disease conditions. Occasionally, it is also associated with paraneoplastic syndromes. In the infectious category, listeria is the most common offending agent.

Characteristic imaging findings: Diffuse abnormal signal involving the brain stem and cerebellum is best appreciated on FLAIR sequences. The abnormal signal when involving the brain stem can mimic the appearance caused by diffuse intrinsic pontine glioma. However, the involvement of the cerebellum (in the presence or absence of involvement of the cerebral periventricular white matter) when seen should suggest the diagnosis of rhombencephalitis. Associated scattered foci of susceptibility reflecting hemorrhage should suggest the diagnosis of listeria encephalitis.

Best sequence(s) to evaluate listeria rhombencephalitis: FLAIR/T2WI, susceptibility-weighted imaging, or gradient-echo imaging.

Vascular Causes

In this basket of vascular causes, we will discuss ischemic and vasculitic processes.

Ischemic processes especially subacute infarction.

Subacute Infarction

Subacute infarction is the classic tumor mimic. The enhancement associated sometimes with subacute infarction is primarily responsible for considering it as a mass-like lesion.

Characteristic imaging findings: The sharply demarcated boundaries of the enhancement area, typically seen to involve a region of arterial branch distribution, should suggest the diagnosis of subacute infarction. The presence of luxury perfusion should also help establish this diagnosis. Also, most such lesions will have a characteristic acute onset of neurologic deficit versus a tumor which has a progressive worsening of focal neurologic deficit.

Best sequence(s) to evaluate subacute infarction: Contrast-enhanced T1WI/MPRAGE and perfusion imaging.

Vasculitic Processes

This will include etiologies such a primary angiitis of central nervous system and Behcet's disease among other vasculitides.

Behcet's Disease

Characteristic imaging findings: Most often the dorsal aspect of the brain stem is involved. Ill-defined hyperintense signal on long TR sequences will be seen. Patchy enhancement is occasionally seen. No diffusion restriction, hemorrhage, or calcification is seen. Imaging features are nonspecific. However, it is the association with characteristic clinical features including aphthous ulcers that helps diagnose this disease condition [28].

Best sequence(s) to evaluate Behcet's disease: FLAIR/T2WI.

Treatment-Related Changes

Pseudoprogression

The Stupp-combined protocol is the standard treatment of care for glioblastoma [29]. Both radiation therapy and temozolomide are toxic to tumor cells. However, at the same time, they incite an inflammatory response in the brain. As a result, the surgical bed on follow-up imaging can demonstrate interval progression in enhancement (due to increased breakdown of blood-brain barrier) and increased FLAIR signal abnormality (inflammatory response). These imaging findings look similar to those seen in tumor recurrence. However, this appearance in fact represents a favorable response to treatment. Hence, though the imaging appearance looks bad, it ideally is not and therefore the term pseudoprogression.

Best sequence(s) to evaluate pseudoprogression: Conventional imaging has no role to play in distinguishing pseudoprogression from tumor recurrence. Advanced imaging can help. Interval decreased rCBV on perfusion imaging

suggests pseudoprogression. In contrast, interval increased rCBV favors tumor progression [30].

Pseudoresponse

Bevacizumab is the standard treatment of care for recurrent glioblastoma. Bevacizumab is an antiangiogenic agent. It stabilizes the blood-brain barrier. Therefore, upon administration of bevacizumab, follow-up imaging often demonstrates reduced enhancement and interval decrease in FLAIR signal abnormality. On conventional imaging, therefore, the imaging findings suggest a good response. However, bevacizumab has no toxic effect on tumor cells. Hence, though imaging suggests a good response, the lack of antitumoral effect in fact allows the tumor to grow along white matter tracts (not visible on conventional imaging) and therefore the term pseudoresponse.

Best sequence(s) to evaluate pseudoresponse: New FLAIR signal abnormality remote from surgical bed should suggest tumor recurrence in a patient with pseudoresponse. Increasing enhancement, increasing FLAIR signal abnormality, and increasing rCBV from the surgical treatment bed also suggest tumor recurrence [30].

References

1. Koeller KK, Rushing EJ (2004) From the archives of AFIP: pilocytic astrocytoma: radiologic pathologic correlation. Radiographics 24:1693–1708
2. Linscott LL, Osborn AG, Blaser S et al (2008) Pilomyxoid astrocytoma: expanding the imaging spectrum. AJNR Am J Neuroradiol 29:1861–1866
3. Crespo-Rodriguez AM, Smirniotopoulos JG, Rushing EJ (2007) MR and CT imaging of 24 pleomorphic xanthoastrocytomas (PXA) and a review of the literature. Neuroradiology 49:307–315
4. Koeller KK, Henry JM (2001) From the archives of AFIP: superficial gliomas: radiologic-pathologic correlation. Radiographics 21:1533–1536
5. Al-Okaili RN, Krejza J, Woo JH et al (2007) Intra-axial brain masses: MR imaging-based diagnostic strategy – Initial experience. Radiology 243:539–550
6. Law M, Yang S, Wang H et al (2003) Glioma grading: sensitivity, specificity, and predictive values of perfusion MR imaging and proton MR spectroscopic imaging compared with conventional MR imaging. AJNR Am J Neuroradiol 24:1989–1998
7. Felsberg GJ, Silver SA, Brown MT et al (1994) Radiologic-pathologic correlation: gliomatosis cerebri. AJNR Am J Neuroradiol 15:1745–1753
8. Spagnoli MV, Grossman RI, Packer RJ et al (1987) Magnetic resonance imaging determination of gliomatosis cerebri. Neuroradiology 29:15–18
9. Cha S, Lupo JM, Chen MH et al (2007) Differentiation of glioblastoma multiforme and single brain metastasis by peak height and percentage of signal intensity recovery derived from dynamic susceptibility-weighted contrast-enhanced perfusion MR imaging. AJNR Am J Neuroradiol 28:1078–1084
10. Jenkinson MD, du Plessis DG, Smith TS et al (2006) Histological growth patterns and genotype in oligodendroglial tumours: correlation with MRI features. Brain 129:1884–1891
11. Koeller KK, Rushing EJ (2005) From the archives of the AFIP. Oligodendroglioma and its variants: radiologic-pathologic correlation. Radiographics 25:1669–1688
12. Engelhard HH, Stelea A, Mundt A (2003) Oligodendroglioma and anaplastic oligodendroglioma: clinical features, treatment, and prognosis. Surg Neurol 60:443–456
13. Giannini C, Burger PC, Berkey BA et al (2008) Anaplastic oligodendroglial tumors: refining the correlation among histopathology, 1p 19q deletion and clinical outcome in Intergroup Radiation Therapy Oncology Group Trial 9402. Brain Pathol 18:360–369
14. van den Bent MJ (2007) Anaplastic oligodendroglioma and oligoastrocytoma. Neurol Clin 25:1089–1093
15. Shin JH, Lee HK, Khang SK et al (2002) Neuronal tumors of the central nervous system: radiologic findings and pathologic correlation. Radiographics 22:1177–1189
16. Castillo M, Davis PC, Takei Y et al (1990) Intracranial gangliogliomа: MR, CT, and clinical findings in 18 patients. AJR Am J Roentgenol 154:607–612
17. Zenter J, Wolf HK, Ostertun B et al (1994) Gangliogliomas: clinical, radiological, and histopathological findings in 52 patients. J Neurol Neurosurg Psychiatry 57:1497–1502
18. Campos AR, Clusmann H, von Lehe M et al (2009) Simple and complex dysembryoplastic neuroepithelial tumors (DNT) variants: clinical profile, MRI, and histopathology. Neuroradiology 51:433–443
19. Stanescu Cosson R, Varlet P, Beuvon F et al (2001) Dysembryoplastic neuroepithelial tumors: CT, MR findings and imaging follow-up: a study of 53 cases. J Neuroradiol 28:230–240
20. Koeller KK, Rushing EJ (2003) Medulloblastoma: a comprehensive review with radiologic-pathologic correlation. Radiographics 23:1613–1637
21. Rumboldt Z, Camacho DL, Lake D et al (2006) Apparent diffusion coefficients for differentiation of cerebellar tumors in children. AJNR Am J Neuroradiol 27:1362–1369
22. Han L, Qiuu Y, Xie C et al (2010) Atypical teratoid/rhabdoid tumors in adult patients: CT and MR imaging features. AJNR Am J Neuroradiol 32:103–108
23. MacDonald TJ, Rood BR, Santi MR et al (2003) Advances in diagnosis, molecular genetics, and treatment of pediatric embryonal CNS tumors. Oncologist 8:174–186
24. Erdag N, Bhorade RM, Alberico RA et al (2001) Primary lymphoma of the central nervous system: typical and atypical CT and MR imaging appearances. AJR Am J Roentgenol 176:1319–1326
25. Cha S, Pierce S, Knopp EA et al (2001) Dynamic contrast-enhanced T2*-weighted MR imaging of tumefactive demyelinating lesions. AJNR Am J Neuroradiol 22:1109–1116
26. Dagher AP, Smirniotopoulos J (1996) Tumefactive demyelinating lesions. Neuroradiology 38:560–565
27. Savoiardo M, Erbetta A, Storchi G et al (2010) Case 159: cerebral amyloid angiopathy-related inflammation. Radiology 256: 323–327
28. Kocer N, Islak C, Siva A et al (1999) CNS involvement in neuro-Behcet syndrome. AJNR Am J Neuroradiol 20:1015–1024
29. Stupp R, Mason WP, van den Bent MJ et al (2005) Radiotherapy plus concomitant and adjuvant temozolomide for glioblastoma. N Engl J Med 352:987–996
30. Fatterpekar GM, Galheigo D, Narayana A et al (2012) Treatment-related change versus tumor recurrence in high-grade gliomas: a diagnostic conundrum – use of dynamic susceptibility contrast-enhanced (DSC) perfusion MRI. AJR Am J Roentgenol 198: 19–26

Mass Lesions of the Brain: A Differential Diagnostic Approach

Michael N. Brant-Zawadzki
and James G. Smirniotopoulos

Though not as common as lung cancer, breast cancer, or others, 70,000 new cases of primary brain tumors are diagnosed annually in the USA. There are nearly 700,000 people in the USA living with a brain tumor. Meningiomas represent 34 % of all primary brain tumors, and their prevalence at autopsy is approximately 1 % making them the most common primary brain tumor. Gliomas represent 30 % of all primary brain tumors and 80 % of all primary malignant tumors. There are more than 120 types of brain tumors. Approximately 50 % of solitary tumors discovered in the brain relate to metastatic disease; when multiple tumors are found, metastatic disease is easier to suspect. Finally, there are many disease entities in the brain that simulate the morphology of a neoplasm yet are caused by infection, stroke, demyelination, etc.

Needless to say, the choice of an imaging modality, and particularly the specific algorithms within an imaging modality that are used, greatly influences not just detection of masses in the brain but their characterization which helps to lead the radiologist toward a concise differential diagnosis. Patient history, objective clinical findings, and the demographics are always useful in that effort.

The clinical presentation of brain tumors varies widely. Headache is a frequent symptom; however the widespread prevalence of headaches in the general population makes it an extremely nonspecific one. Many tumors discovered on imaging for headaches are really incidentally found, the headache only occasionally being associated with the tumor. More worrisome patient complaints suggesting the presence of an underlying tumor are the onset of a seizure beyond the age of 15, progressive sensory or motor disturbance of a subacute or subtle nature, progressive alteration of cognition or mental status in a young or middle-aged adult, or slow onset of visual change. Imbalance, nausea and vomiting, and hearing loss can herald the presence of a posterior fossa mass or increased intracranial pressure from tumor-induced obstructive hydrocephalus.

The development of CT scanning greatly improved the ability to detect intracranial neoplasms. Iodinated contrast agents help characterize them in terms of vascularity and loss of the integrity of the blood-brain barrier, a marker of greater degrees of malignancy. However, CT suffers from beam-hardening artifacts in the region of the middle and posterior fossa, and its ability to delineate subtle alteration of tissue in the form of differential x-ray attenuation detracts from its sensitivity. Physics that rely on changes in electron density for differentiation of normal and abnormal tissue are not as robust as the physics of the hydrogen relaxation parameters, magnetic susceptibility of intrinsic tissue constituents, restriction in the diffusion of water molecules, etc., that are the hallmarks of the greater tissue differentiation capability of magnetic resonance imaging, improving its sensitivity. Only the presence of calcification is arguably more sensitive with CT as compared to MRI on routine imaging studies.

Once detected, the location of tumors to a specific compartment aids the differential diagnosis from a purely anatomic perspective. Allocating the origin or location of a tumor into either the intra-axial or the extra-axial space is the first basic step. Localizing to the intraventricular, subarachnoid, and extra leptomeningeal spaces likewise helps further differentiation. Although special allocation sounds simple, especially when the tumor is well within the brain substance, the distinction may be difficult when the mass is in the periphery of the brain or in such regions as the cerebellopontine angle, the skull base, and even the anterior fossa. The angle between the mass and the adjacent cranium, presence of displaced vessels, and menisci in the spinal fluid space help this distinction.

Certain general locations narrow the differential diagnosis. For instance, lesions in the cerebellopontine angle have a

M.N. Brant-Zawadzki, MD (✉)
Neurosciences Institute, Hoag Memorial Hospital Presbyterian,
1 Hoag Drive, Newport Beach, CA 90745, USA
e-mail: mbrant@hoag.org; monica.figueroa@hoag.org

J.G. Smirniotopoulos
Radiology and Radiological Sciences,
Uniformed Services University of the Health Sciences,
4301 Jones Bridge Road, Bethesda, MD 20814, USA

J. Hodler et al. (eds.), *Diseases of the Brain, Head and Neck, Spine 2016–2019: Diagnostic Imaging*, DOI 10.1007/978-3-319-30081-8_2

relatively limited differential which includes acoustic neuroma, meningioma, aneurysm of the vertebral artery branches, and neuromas of the various cranial nerves at the level of the foramen magnum but also less common lesions such as lipomas and arachnoid cysts. A lesion in the region of the pineal gland creates another category of differential diagnoses, which includes benign pinealomas and the more malignant pineoblastomas, germ cell layer tumors such as germinomas and teratomas, and also glial tumors given the proximity of glial cells to the pineal region. In fact, ependymomas, even meningiomas, can occasionally stimulate the pineal gland as the originating cell types are found in the vicinity. Intraventricular tumors again have a more specific differential, including ependymoma and meningioma, in children tumors related to congenital syndromes such as giant cell astrocytoma. In older adults, intraventricular neurocytomas can be found, as can paraventricular neurocytomas. Masses around the pituitary fossa can be better analyzed by first determining if the normal pituitary gland can be identified, as large tumors of the pituitary (craniopharyngiomas, nonfunctioning giant adenomas) can simulate intra-axial brain tumors.

As magnetic resonance has become the staple for characterizing brain tumors, the basic parameters of T1 and T2 relaxation, magnetic susceptibility characteristics of inherent constituents [1], and the diffusion of water molecules in the microarchitecture help tumor characterization. Additional parameters that can be used with MR include perfusion imaging with its components of blood volume and contrast transit time, as well as spectroscopy. Though as a general rule, T2 high signal connotes malignancy, certain tumors such as lymphoma and mucinous carcinoma exhibit relatively low T2-weighted signal features due to the presence of specific components such as free radicals and mucin, respectively, although hemorrhagic components of tumors can likewise lower T2 relaxation and demonstrate low signal on T2-weighted images. Melanoma is a tumor which can lower T2 weighting due to both blood by-products (it is frequently hemorrhagic) or intrinsic components such as free radicals and even melanin itself. High T1 signal is also associated with blood by-products, particularly methemoglobin due to a component of subacute hemorrhage within the tumor, but occasionally follicular calcification can produce T1 shortening of hydrogen nuclei at the surface of such microcalcific foci, mimicking hemorrhagic components.

A hallmark of several subtypes of low-grade astrocytomas (e.g., protoplasmic astrocytoma) is the low T1-weighted signal intensity of a well-circumscribed lesion without surrounding edema, while the bubbly appearance of a localized lesion in the gray matter convolutions in a youngster with seizures should raise the consideration of a dysembryoplastic neuroepithelial tumor to a low-grade lesion with a very good prognosis. Cystic components can be seen with relatively benign tumors such as craniopharyngiomas (the cysts highly variable in signal depending on protein concentration within) and pilocytic astrocytomas which have highly enhancing solid components, but are well circumscribed with little or no edema. Also demonstrating necrotic cysts, but showing ill-defined borders and varying degrees of surrounding edema, are the malignant gliomas and the medulloblastomas of childhood which tend to be midline in the posterior fossa.

Two other features that help in the differential diagnosis are the presence of multiple foci, most often associated with metastatic disease, but sometimes due to nonneoplastic conditions such as infection, vasculitis, demyelinating disease, and others. One must remember, however, that there is multifocality seen in glial primary brain tumors, with gliomatosis cerebri and multicentric glioblastomas being the most notable examples. When a single lesion presents on both sides of the brain midline, particularly by spread through the corpus callosum, the differential diagnosis becomes significantly limited to such infiltrating lesions as malignant gliomas, lymphomas, and epidermoids (which cross the midline through the subarachnoid space) and dural tumors such as meningiomas and metastatic lesions to the dura of the interhemispheric falcine structure. Epidermoids can simulate expanded spinal fluid spaces, but FLAIR and diffusion sequences clearly separate the two.

Paramagnetic contrast agents provide considerable support for the diagnostic capability of MRI, making the diagnosis of blood-brain barrier disruption demonstrable, as well as physiologic evaluation of perfusion and blood volume parameters. It is notable that certain chemotherapeutic agents may actually mistake reduction in vascularity and blood volume for tumor remission (e.g., Avastin). However, overall, cerebral blood volume and contrast permeability analysis can help distinguish degrees of malignancy and thus help monitor disease treatment. Recent advances with MRI include the development of PET MRI capability [2], which has been found helpful in distinguishing radiation necrosis from recurrent tumor. Spectroscopy helps in this type of differential as well, as it allows for specific analysis of various metabolites within brain tissue. Tumors, especially primary brain tumors, show elevation of choline (a marker of cell membrane turnover) and loss of an N-acetylaspartate (a neuronal marker). However, it should be noted that MR spectroscopy, like perfusion analysis, is not totally specific. Any rapidly evolving process which produces membrane breakdown or turnover, including demyelinating disease, can show elevation of choline (although the decrease in an acetylaspartate is not as prominent in demyelinating disease).

Diffusion imaging can be specifically used for tractography, allowing surgical planning in certain cases where involvement of important white matter tracts is questioned,

but the most common use of diffusion imaging is to demonstrate restricted diffusion and resulting high signal on appropriately reconstructed images in highly cellular tumors such as lymphoma and in differentiating abscesses from brain tumors (the former almost always demonstrate diffusion restriction). This is particularly pertinent in separating necrotic tumor cavities from infected ones. Any significant increases of membranes in the micro environment can also restrict diffusion, so hypercellular tumors in addition to demyelination can show high signal on diffusion images, but the finding is not tumor specific. Even hematomas will demonstrate diffusion restriction, despite no underlying neoplasms.

Despite our advanced technology, it is still challenging to specifically differentiate certain lesions in terms of a non-neoplastic versus neoplastic histology. Masses such as tumefactive multiple sclerosis, certain fungal infections (e.g., toxoplasmosis), encephalitides, congenital dysplasias such as migrational disorders, and even hematomas can simulate neoplasms. Careful attention to the numerous MR parameters as expressed on specific pulse sequences of a given lesion can usually solve the quandary, but occasionally full specificity in this distinction will evade us. Any unexplained hematoma should be followed until resolution to exclude a possible underlying pathology, including malignancy.

Once detection of localization and characterization of neoplasms is determined, MRI can help considerably in treatment planning. Its three-dimensional capability, and other characterization capabilities, allows much better delineation of tumor extent and relationships to eloquent brain structures. For instance, we have been using the combination of FLAIR imaging and MR spectroscopy to better delineate stereotactic radiation of infiltrating gliomas, treating the "leading edge" of the tumor as determined on multivoxel spectroscopy applied to FLAIR images. Further, surface contours which can easily be created with 3D techniques, inherent in modern MRI instruments, help couple the data to intraoperative navigation techniques creating a "virtual reality" for the neurosurgeon, aiding more accurate resection. We have found such techniques useful in helping prolong the median survival time of infiltrating gliomas, suggesting a survival advantage using such gamma knife radiosurgery for patients with glioblastomas and other malignant gliomas [3].

Given this very broad overview and in summary, the radiologist now has available extremely advanced imaging capabilities that aids in the detection of brain tumors at much earlier stages and to a greater degree of accuracy. The availability of multiple instruments, some melded into one (as in the case of PET/MR and MR/CT) [2], the ability to fuse images from one modality with another, and the various algorithms greatly help characterization of lesions as well as monitoring of therapy. A concise differential in a newly referred patient starts with lesion localization, then its characterization. The patient's age, gender, clinical history and objective signs are always important.

References

1. Haacke EM, Mittal S, Wu Z et al (2009) Susceptibility-weighted imaging: technical aspects and clinical applications, part 1. AJNR 30(1):19–30
2. Torigian DA, Zaidi H, Kwee TC et al (2013) PET/MR imaging: technical aspects and potential clinical applications. Radiology 267(1):26–44
3. Duma CM, Kim B, Chen P et al (2015) Up-front "leading edge" gamma knife radiosurgery to tumor migration pathways in 161 patients with glioblastoma multiforme: a novel adjunctive therapy. Congress of neurologic surgeons 2015 annual meeting. New Orleans, 26–30 Sept 2015

Evaluation of the Cerebral Vessels

Robert A. Willinsky

Introduction

Evaluation of the cerebral vessels traditionally demonstrates the lumen of the vessel (the so-called luminogram). The methods include computed tomography angiography (CTA), magnetic resonance angiography (MRA), and digital subtraction angiography (DSA). All three methods can evaluate the veins, but CT venography (CTV) and MR venography (MRV) are traditionally done separately from CTA and MRA. In the last decade, dynamic 3D CTA and MRA techniques can be done that provide a hemodynamic evaluation of both the arteries and the veins. These dynamic 3D techniques give a great overview of the cerebral circulation but lack spatial resolution. DSA remains the "gold standard" in the evaluation of the arteries and the hemodynamics. We believe the gadolinium-enhanced MRV is now the "gold standard" in the evaluation of the venous system.

Aneurysmal Subarachnoid Hemorrhage

The initial imaging of the cerebral vessels for aneurysmal subarachnoid hemorrhage (SAH) is CTA. We prefer to include the great vessels in the neck to help in the management decision once an aneurysm is discovered. If the CTA is negative, we proceed to a catheter angiogram (DSA) unless the clinical findings and the pattern of the SAH are typical of the so-called non-aneurysmal perimesencephalic subarachnoid hemorrhage (PMH). In a PMH the blood is typically anterior to the brain stem and may extend into the basal parts of the sylvian fissures and the ambient cisterns but not into the lateral sylvian or anterior interhemispheric fissures. There is no intraventricular hemorrhage (IVH) in the PMH syndrome. Clinically these patients are well and alert (Hunt and Hess grade 1). In a PMH we repeat the CTA before discharge. In patients with an aneurysmal SAH that is not a PMH, we repeat the DSA in 7 days if the initial DSA is negative. If multiple aneurysms are found and we are uncertain which bled, high-resolution MR vessel wall imaging (VWI) with gadolinium may be helpful in determining which aneurysm bled.

Non-aneurysmal, Non-perimesencephalic Subarachnoid Hemorrhage

These bleeds are typically peripheral and trauma is the commonest etiology. Without trauma the list of causes includes reversible cerebral vasoconstriction syndrome (RCVS), vasculitis, amyloid vasculopathy, posterior reversible encephalopathy syndrome (PRES), and arteriovenous shunts. If amyloid and PRES are suspected, MR is our initial investigation. If RCVS, vasculitis, or a shunt is considered, then a CTA is our first investigation. CTA will frequently be diagnostic in these conditions. If CTA is negative, then DSA is indicated. On the DSA, both RCVS and vasculitis may show vessel irregularity and narrowing. If the clinical findings are not helpful in differentiating these two entities, then VWI is used since vasculitis will often show diffuse, smooth, circumferential wall enhancement and RCVS may show wall thickening but will show minimal or no enhancement. Occasionally the wall enhancement in vasculitis will be eccentric.

Intracerebral and Intraventricular Hemorrhage (ICH/IVH)

In the acute clinical setting, CTA is our initial investigation of ICH or IVH. The same holds true for a spontaneous subdural hemorrhage. In the older age group, many of the ICHs are secondary to hypertension, amyloid, or small vessel

R.A. Willinsky
Joint Department of Medical Imaging, Toronto Western Hospital, University Health Network and Mount Sinai Hospital, University of Toronto, Toronto, ON, Canada
e-mail: robert.willinsky@uhn.ca

J. Hodler et al. (eds.), *Diseases of the Brain, Head and Neck, Spine 2016–2019: Diagnostic Imaging*, DOI 10.1007/978-3-319-30081-8_3

disease. In these cases, the detection of the "spot sign" is helpful in terms of natural history and possibly management. In patients suspected to have venous thrombosis, either clinically or on the non-contrast CT, we prefer to go directly to an MR brain and MRV. In young patients with ICH/IVH, the CTA may show a vascular cause including an arteriovenous shunt, an infective aneurysm, RCVS, or vasculitis. If the CTA is negative, we do a DSA. If the DSA is negative, we do an MR brain to look for a neoplasm or underlying vascular malformation, typically a cavernous malformation (CM). If no cause for the bleed is evident, we do a delayed MR, once the blood has been resorbed, to look for an underlying tumor or CM obscured by the initial bleed. If the delayed MR shows only a hemosiderin cleft, then a delayed DSA is done to look for a micro-arteriovenous malformation (AVM) that was not initially seen due to the mass effect from the bleed.

Acute Stroke

Vascular imaging is a crucial component of our acute stroke protocol. Rapid assessment and endovascular stent thrombectomy have now been proven to be effective. Stent thrombectomy is only done when the CTA shows that the site of occlusion is suitable for this treatment. We use multiphasic CTA (two phases in our institution) to show the site of occlusion, the vascular access in the neck, and the collateral flow. The second phase is crucial to show the collateral flow. Poor collateral flow to the ischemic hemisphere is a harbinger for a poor outcome despite opening the vessel with stent thrombectomy. In our institution, CT perfusion is used in patients with acute strokes that are not eligible for stent thrombectomy. In these cases, the CT perfusion clarifies the extent of the damage and the territory at risk.

CTA in acute stroke must include the neck since many embolic strokes originate in the neck. The assessment of the carotid bifurcation should include not only the vessel lumen. Assessment of the wall may show calcification and lipids with an irregular plaque. In a dissection, careful assessment may show blood products in the wall of a vessel that is narrowed. Pseudoaneurysms and narrowing of the major arteries in the neck are telltale signs of an old dissection.

Delayed Investigation of Stroke and TIA

MR and MRA are used to investigate patients with stroke and TIA not eligible for stent thrombectomy. In many patients, this is a gadolinium-enhanced MRA of the carotids to look for eligible patients for carotid endarterectomy. This is correlated with Doppler ultrasound. This MRA of the carotids includes the circle of Willis. High-resolution MR vessel wall imaging (VWI) techniques to look at carotid plaque morphology are presently a research tool in our institution. VWI may be helpful to assess intracranial arterial narrowing. Typical intracranial atherosclerotic disease is characterized by eccentric plaques that narrow the vessel wall. Active intracranial plaques may show enhancement, whereas inactive plaques typically do not. The non-contrast component of the vessel wall study may show the lipid core within the plaque and the presence of intra-plaque hemorrhage. If there is a clinical concern for a dissection, we add axial T1 and T2 images with fat saturation through the neck to look for blood products in the wall of the carotid or vertebral arteries.

In patients with a proven stroke and normal vessels on the MRA carotids, we may do CTA due to its higher resolution. CT may show a lipid plaque at the carotid bifurcation. CTA may show intracranial arterial narrowing that was not evident on the MRA of the carotids. To further characterize the intracranial narrowing, we may do high-resolution MR VWI. VWI may show circumferential enhancement of the vessel wall in a vasculitis in distinction to the eccentric enhancement in intracranial atherosclerosis. The lack of enhancement on VWI may confirm the probable diagnosis of RCVS or Moyamoya disease.

Pulsatile Tinnitus and an Objective Bruit

The majority of patients with pulsatile tinnitus and an objective bruit over the cranium have a dural arteriovenous fistula (DAVF). Excluded from this group are those with a retrotympanic mass. In patients with a retro-tympanic mass, high-resolution CT (HRCT) is the initial investigation of choice. HRCT is ideal to diagnose an aberrant course of the internal carotid artery or a persistent stapedial artery. In patients with a DAVF, all angiographic techniques, including CTA, MRA, dynamic CTA, and dynamic MRA, are likely to detect the abnormality. I prefer a time-of-flight (TOF) MRA of the circle of Willis at 3 T due to its superior spatial resolution. The enlarged feeding arteries are easy to detect. Oxygenated blood is typically seen in the involved dural sinus. The presence of oxygenated blood is readily detected on susceptibility-weighted imaging (SWI) (Fig. 1). Time-resolved gadolinium-enhanced MRA is a good way to follow up DAVFs that are being managed conservatively. DSA is needed to fully understand the complex anatomy and the hemodynamics. DSA is critical in the evaluation of possible cortical venous reflux (CVR) that is not evident on the non-invasive imaging. The presence of CVR is important in the management since patients with CVR have a higher risk of future hemorrhage or neurological events compared to patients with only sinosal drainage.

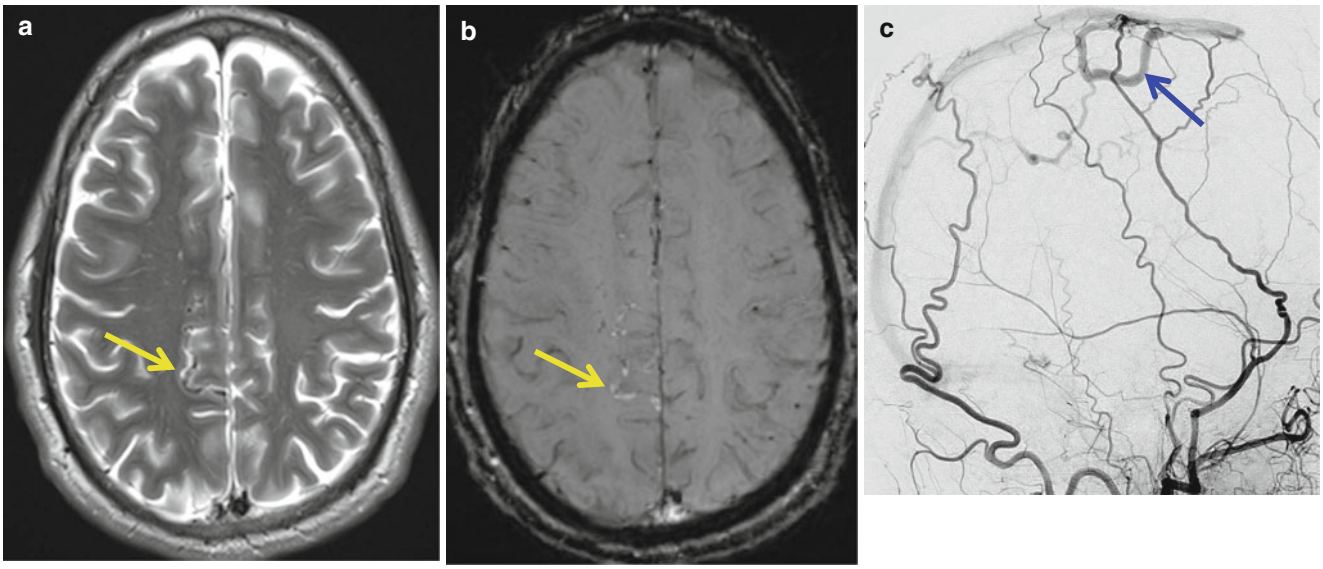

Fig. 1 (**a**–**c**) Borden 3 dural arteriovenous fistula (DAVF) in an asymptomatic 53-year-old male. (**a**) Axial T2 shows a prominent vascular structure in the right rolandic region (*arrow*). (**b**) Susceptibility-weighted image (SWI) shows hyper-intensity in the prominent rolandic vessel (*arrow*) indicating oxygenated blood. (**c**) Lateral external carotid digital subtraction arteriogram shows a direct fistula into the rolandic vein (*arrow*) that then drains into the superior sagittal sinus

Amyloid-Related Imaging Abnormalities (ARIA): Cerebral Amyloid Angiopathy (CAA), Inflammatory Cerebral Amyloid Angiopathy (I-CAA), and Amyloid-β-Related Angiitis (ABRA)

Cerebral amyloid angiopathy (CAA) results from deposition of amyloid-β in the wall of small- and medium-sized cortical vessels. Three overlapping clinical syndromes can be identified: cerebral amyloid angiopathy (CAA), inflammatory cerebral amyloid angiopathy (I-CAA), and amyloid-β-related angiitis (ABRA). In CAA, amyloid-β within the vessel wall may lead to the development of fibrinoid necrosis within the wall leading to perivascular leakage. Vascular rupture results in lobar hematomas, micro-bleeds, and high convexity SAH. The high convexity SAH leads to cortical superficial siderosis. Superficial siderosis is found in 60 % of pathologically proven cases of CAA. A subset of patients with amyloid-β deposition present with subacute cognitive decline, neuropsychiatric manifestations, seizures, headache, and T2 hyper-intense lesions. This subset includes the inflammatory CAA (I-CAA) and the amyloid-β-related angiitis (ABRA). In I-CAA there is vessel lumen obliteration and a perivascular inflammation leading to an ischemic leukoencephalopathy. There is no inflammation in the blood vessel wall. In ABRA there is an inflammatory response in the vessel wall leading to a vasculitis similar to primary angiitis of the central nervous system (PACNS). Cerebral microbleeds are the hallmark of I-CAA but may be present in all three forms of amyloid angiopathy. Micro-hemorrhages are found in approximately 50 % of pathologically proven CAA cases. The majority of patients with amyloid-related imaging abnormalities (ARIA) have underlying microangiopathic changes. The symptomatic leukoencephalopathies related to I-CAA and ABRA are subacute and progressive unlike the chronic evolution of the microangiopathic changes unrelated to amyloid deposition.

CAA increases with age. The mean age is in the seventh decade. CAA is commonly found in patients with Alzheimer's disease (AD). Aging and AD are established risk factors for CAA. Pathologically, CAA is observed mainly in the cortical vessels of the cerebral and cerebellar hemispheres. There is a predilection for the occipital lobes. CAA-related cerebral hypoperfusion may cause white matter lesions and cortical microinfarcts.

The diagnosis of I-CAA should be suspected in patients older than 50 years, who present with a progressive cognitive decline, subcortical white matter edema, and cortical micro-hemorrhages (Fig. 2). The white matter edema is often asymmetrical. There is cortical involvement that is less striking than the involvement of the white matter. There is mass effect. There may be mild leptomeningeal enhancement. I-CAA is associated with an increase in anti-B protein antibodies in the CSF. After treatment, the white matter edema may regress in some patients.

ABRA has multifocal patchy or confluent white matter T2/FLAIR hyper-intensities in the majority of cases. These white matter changes may improve with treatment. Some of

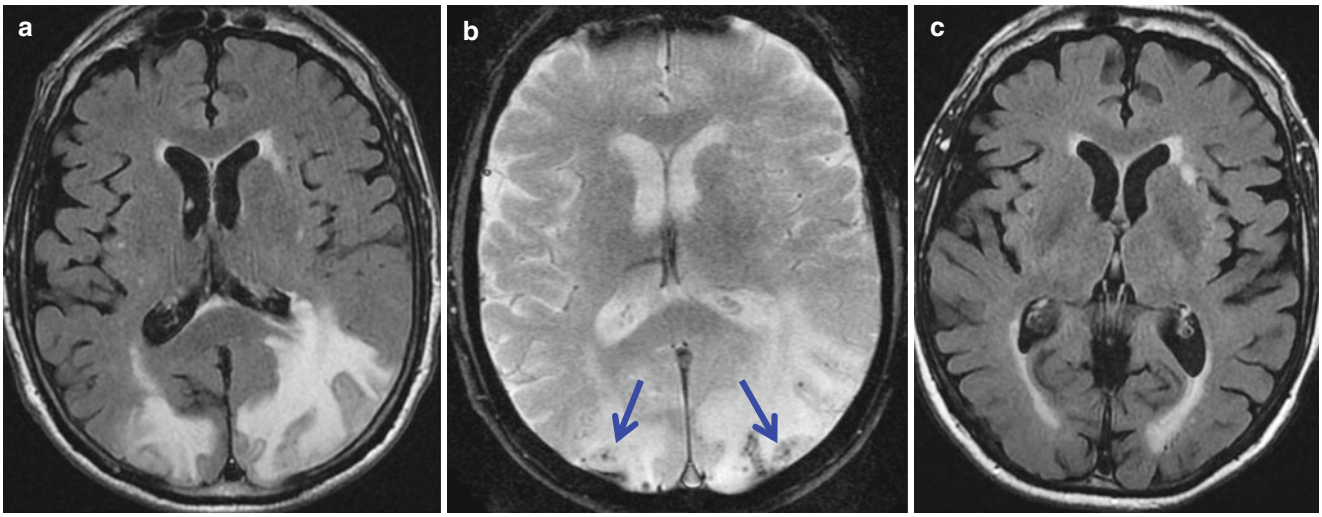

Fig. 2 (**a**–**c**) Inflammatory cerebral amyloid angiopathy (I-CAA) in a 76-year-old male who presents with a subacute progressive speech difficulty and cognitive dysfunction. (**a**) Axial flair shows bilateral posterior hyper-intensity predominantly in the white matter with slight cortical involvement and mild swelling. (**b**) Axial gradient-echo technique shows multiple cortical foci of hypo-intensity consistent with hemosiderin deposits (*arrows*). (**c**) A three-month follow-up flair image shows almost complete resolution of the leukoencephalopathy

the lesions will have mass effect. Intracerebral hemorrhages and infarcts occur in approximately 20 % of cases. Leptomeningeal enhancement is common. In ABRA, vascular imaging shows nonspecific vasculitis in medium-sized arteries similar to PACNS. The diagnosis of ABRA should be favored over PACNS in patients over the age of 50 years who have multiple cortical micro-bleeds evident on an iron-sensitive sequence and white matter T2 hyper-intensities. The presence of vasculitis distinguishes ABRA from I-CAA since in I-CAA the vascular imaging is normal.

Both I-CAA and ABRA are potentially treated encephalopathies. The commonest clinical presentations, in order of most frequent, are cognitive dysfunction, headaches, seizures, and pyramidal signs. I-CAA generally responds to short courses of immunotherapy; however, long-term recurrences can occur. Prolonged immunosuppression is recommended in ABRA. More than 50 % of patients will improve with immunosuppression; however, the long-term outcome is unfavorable, with death and dependency in almost 60 % of patients.

Reversible Cerebral Vasoconstriction Syndrome

Reversible cerebral vasoconstriction syndrome (RCVS) is a clinical and imaging syndrome characterized by a thunderclap headache and cerebral vasoconstriction that returns to normal within a few months. It may be spontaneous or be triggered by exogenous factors. The symptoms and radiology may overlap with aneurysmal subarachnoid hemorrhage and primary angiitis of the central nervous system (PACNS). RCVS has been previously reported by many different names including Call-Fleming syndrome, drug-induced angiopathy, migrainous vasospasm, benign angiopathy of the CNS, and postpartum angiopathy.

RCVS commonly affects middle-aged adults with a female predominance. The exogenous triggers are commonly vasoactive drugs and the postpartum state. The list of the vasoactive medications is long including the sympathomimetic drugs and ergotamine. Vasoactive recreational drugs including amphetamine, cocaine, ecstasy, and others have been implicated as triggers. The pathophysiology of RCVS is not known. Loss of autoregulation of the vascular tone leading to hyper-perfusion is felt to be part of the mechanism in RCVS. An overlap between RCVS and PRES suggests that endothelial dysfunction may play a role. RCVS and PRES may be part of a spectrum of findings related to a pathophysiology that alters cerebral vascular tone.

The thunderclap headache is the clinical hallmark of the syndrome and is defined as a severe headache that reaches its peak in intensity within 60 s. This thunderclap headache often may resolve within hours or waxes and wanes over the next 1–3 weeks. The cerebral vasoconstriction may not become evident for a week or more following the onset of the headache. The diagnosis is based on the presence of multifocal segmental cerebral artery vasoconstriction on CTA, MRA, or DSA. This is a uniphasic illness with no new symptoms after 1 month. The CSF analysis is normal or near normal. The diagnostic criteria include the reversibility of the angiographic abnormalities by 12 weeks.

RCVS may have a number of neurological problems including seizures, altered level of consciousness, and stroke. These may be initially present or develop in a delayed

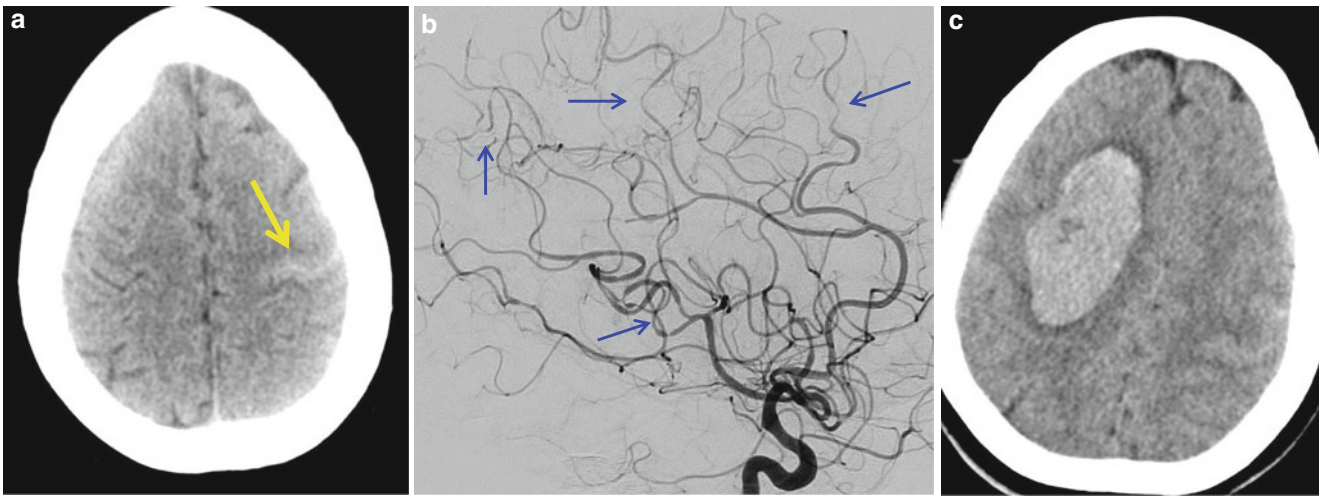

Fig. 3 (**a**–**c**) Reversible cerebral vasoconstriction syndrome (RCVS) in a 44-year-old female who presents with a thunderclap headache and a small cortical SAH. (**a**) Axial non-contrast CT shows subarachnoid hemorrhage high up over the cerebral cortex (*arrow*). (**b**) Lateral right internal carotid digital subtraction arteriogram shows multifocal areas of narrowing and irregularity in medium-sized arteries (*arrows*). (**c**) Axial non-contrast CT on the third day after presentation shows a large lobar intracerebral hemorrhage

fashion. Cortical SAH is a common at presentation (Fig. 3). Lobar intracerebral hemorrhage can occur at presentation or in follow-up. The differential diagnosis is extensive and includes aneurysmal subarachnoid hemorrhage, PRES, venous thrombosis, arteriovenous malformation, amyloid angiopathy, and PACNS. These conditions must be ruled out to make the diagnosis of RCVS.

Radiological investigation of possible RCVS begins with a non-contrast CT head and a CTA of the carotids and intracranial arteries. MR brain imaging is useful to look for complications of RCVS including stroke and edema similar to PRES. Strokes are often watershed infarcts reflecting hypoperfusion due to the cerebral vasoconstriction. FLAIR and iron-sensitive sequences are helpful to search for SAH and micro-hemorrhages. MR is also useful to rule out other diagnosis including venous thrombosis, arterial dissection, and pituitary apoplexy. Vessel wall imaging (VWI) can be helpful in differentiating RCVS from intracranial vasculitis. Both may have wall thickening, but vasculitis has wall enhancement, and RCVS typically has no or very mild wall enhancement. Catheter angiography is useful when the clinical picture supports the diagnosis of RCVS, and the noninvasive vascular imaging is normal. We often proceed to a DSA because the CTA may be suggestive of RCVS but not conclusive. It is important to confirm the diagnosis in order to initiate treatment.

Vasoconstriction in RCVS differs from vasospasm in aneurysmal SAH. The segmental vasoconstriction in RCVS usually involves second- and third-order branches, whereas the proximal arteries are involved in aneurysmal SAH. The vasoconstriction in RCVS occurs diffusely, while the SAH is typically localized over the cortex. In an aneurysmal bleed, the vasoconstriction is most pronounced in the vicinity of the blood, and its severity is dependent on the blood volume with the subarachnoid space. In RCVS the narrowing is typically irregular and over short segments compared to long, smooth segments of narrowing in aneurysmal SAH.

Treatment of RCVS includes control of hypertension and calcium channel blockers. Most patients do well with resolution of symptoms within a few weeks. Overall, a poor course leading to death or disability can occur in 5–10 % of patients. A poor outcome is more likely in postpartum RCVS. The poor outcomes are due to multifocal infarcts and intracranial hemorrhage.

Suggested Reading

Agid R, Andersson T, Almqvist H, Willinsky RA, Lee SK, terBrugge KG, Farb RI, Söderman M (2010) Negative CT angiography findings in patients with spontaneous subarachnoid hemorrhage: when is digital subtraction angiography still needed? AJNR Am J Neuroradiol 31(4):696–705

Castro Caldas A, Silva C, Albuquerque L, Pimentel J, Silva V, Ferro JM (2015) Cerebral amyloid angiopathy associated with inflammation: report of 3 cases and systematic review. J Stroke Cerebrovasc Dis 24(9):2039–2048

Ducros A (2012) Reversible cerebral vasoconstriction syndrome. Lancet Neurol 11:906–917

Farb RI, Agid R, Willinsky RA, Johnstone DM, Terbrugge KG (2009) Cranial dural arteriovenous fistula: diagnosis and classification with time-resolved MR angiography at 3T. AJNR Am J Neuroradiol 30(8):1546–1551

Mandell DM, Matouk CC, Farb RI, Krings T, Agid R, terBrugge K, Willinsky RA, Swartz RH, Silver FL, Mikulis DJ (2012) Vessel wall MRI to differentiate between reversible cerebral vasoconstriction syndrome and central nervous system vasculitis: preliminary results. Stroke 43(3):860–862

Martucci M, Sarria S, Toledo M, Coscojuela P, Vert C, Siurana S, Auger C, Rovira A (2014) Cerebral amyloid angiopathy-related inflammation: imaging findings and clinical outcome. Neuroradiology 56(4):283–289

Miller TR, Shivashankar R, Mossa-Basha M, Gandhi D (2015a) Reversible cerebral vasoconstriction syndrome, part 1: epidemiology, pathogenesis, and clinical course. AJNR Am J Neuroradiol 36(8):1392–1399

Miller TR, Shivashankar R, Mossa-Basha M, Gandhi D (2015b) Reversible cerebral vasoconstriction syndrome, part 2: diagnostic work-Up, imaging evaluation, and differential diagnosis. AJNR Am J Neuroradiol 36(9):1580–1588

Moussaddy A, Levy A, Strbian D, Sundararajan S, Berthelet F, Lanthier S (2015) Inflammatory cerebral amyloid angiopathy, amyloid-β-related angiitis, and primary angiitis of the central nervous system: similarities and differences. Stroke 46(9): e210–e213

Skarpathiotakis M, Mandell DM, Swartz RH, Tomlinson G, Mikulis DJ (2013) Intracranial atherosclerotic plaque enhancement in patients with ischemic stroke. AJNR Am J Neuroradiol 34(2): 299–304

Willems PW, Brouwer PA, Barfett JJ, terBrugge KG, Krings T (2011) Detection and classification of cranial dural arteriovenous fistulas using 4D-CT angiography: initial experience. AJNR Am J Neuroradiol 32:49–53

Yamada M (2015) Cerebral amyloid angiopathy: emerging concepts. J Stroke 17(1):17–30

Imaging of Traumatic Arterial Injuries to the Cervical Vessels

Mary E. Jensen

Trauma involving the cervical region can result in either blunt or penetrating injury to the cervicocerebral vessels, with attendant hemorrhagic and/or neurologic sequelae. The reported incidence of carotid or vertebral artery injury in all trauma patients is 1.2–1.6 % [1], with an associated risk of acute cerebral ischemia in 12–15 % of affected individuals. Blunt cervical vascular injury (BCVI) is increased in the setting of cervical spine, basilar skull, or severe facial fractures; spinal cord and traumatic brain injury; major thoracic injuries; and cervical hyperextension/rotation or hyperflexion [2]. The vertebral artery is more commonly injured than the carotid artery because of its close proximity to bone as it runs through the intervertebral foramina. Twenty percent of BCVI patients, however, demonstrate none of these "classic" risk factors. Damage from penetrating cervical vascular injury (PCVI) trauma is less common than blunt trauma, with carotid and vertebral artery injuries accounting for only 3 % and 0.5 %, respectively, of arterial injuries in civilians.

Anatomical Considerations

Specific anatomical features are important in the evaluation of blunt trauma. The internal carotid artery (ICA) courses ventral to the transverse processes from C1 to C3 before it enters the petrous canal at the skull base. Injury from hyperextension and contralateral rotation occurs when the vessel impinges upon the lateral articular processes and pedicles of the upper cervical spine. The ICA is also vulnerable to dissection at the skull base from deceleration injury or petrous canal fractures. The vertebral artery's course through the C2–C6 transverse foramina predisposes it to injury from subluxation or rotation or from transverse process fractures. The distal cervical (V4) segment of the vertebral artery may be crushed against the C1 vertebra or the dural edge in cases of craniocervical junction distraction or dislocation.

Historically, the approach to diagnosis and treatment of PCVI starts by determining the location of the injury within one of three anatomic zones anterior to the sternocleidomastoid muscles. The diameter of all three vascular structures (vertebral artery, carotid artery, and internal jugular vein) is greater, and their location more superficial, as the anatomical plane moves caudally. Zone I contains the origins of the brachiocephalic vessels and the subclavian and innominate veins. Here, vascular structures are most vulnerable to small fragments and shallow wounds, and penetrating injuries in this location carry the highest morbidity and mortality. Zone II (Fig. 1a) includes the distal common carotid arteries, the proximal internal and external carotid arteries, the vertebral arteries, and the internal jugular veins. The vertebral artery remains narrow and the furthest from the skin surface and is protected by 4–6 mm of bone throughout its course except in Zone I. Zone III (Fig. 1b) holds the distal cervical internal carotid arteries, the external carotid artery branches, the distal vertebral arteries, and the proximal internal jugular veins. The carotid artery and internal jugular vein are less vulnerable in Zone III due to protection from the mandible and smaller size of the vessels; the zone's posterior portion is the least common area of the neck to be injured by penetrating trauma.

Penetrating injuries in Zone II with life-threatening hemorrhage, expanding hematoma, airway compromise, or loss of the carotid pulse with a neurological deficit are often explored surgically, although patients with stable vital signs are often evaluated first by noninvasive imaging. For example, all three zones can be rapidly assessed using computed tomographic angiography (CTA), and multiplanar reconstruction in bone windows detects vertebral, skull base, and/or facial fractures associated with vascular injury [4].

M.E. Jensen, MD
Department of Radiology and Medical Imaging,
University of Virginia Health System,
P.O. Box 800170, Charlottesville, VA 22908-0170, USA
e-mail: Mej4u@virginia.edu

J. Hodler et al. (eds.), *Diseases of the Brain, Head and Neck, Spine 2016–2019: Diagnostic Imaging*, DOI 10.1007/978-3-319-30081-8_4

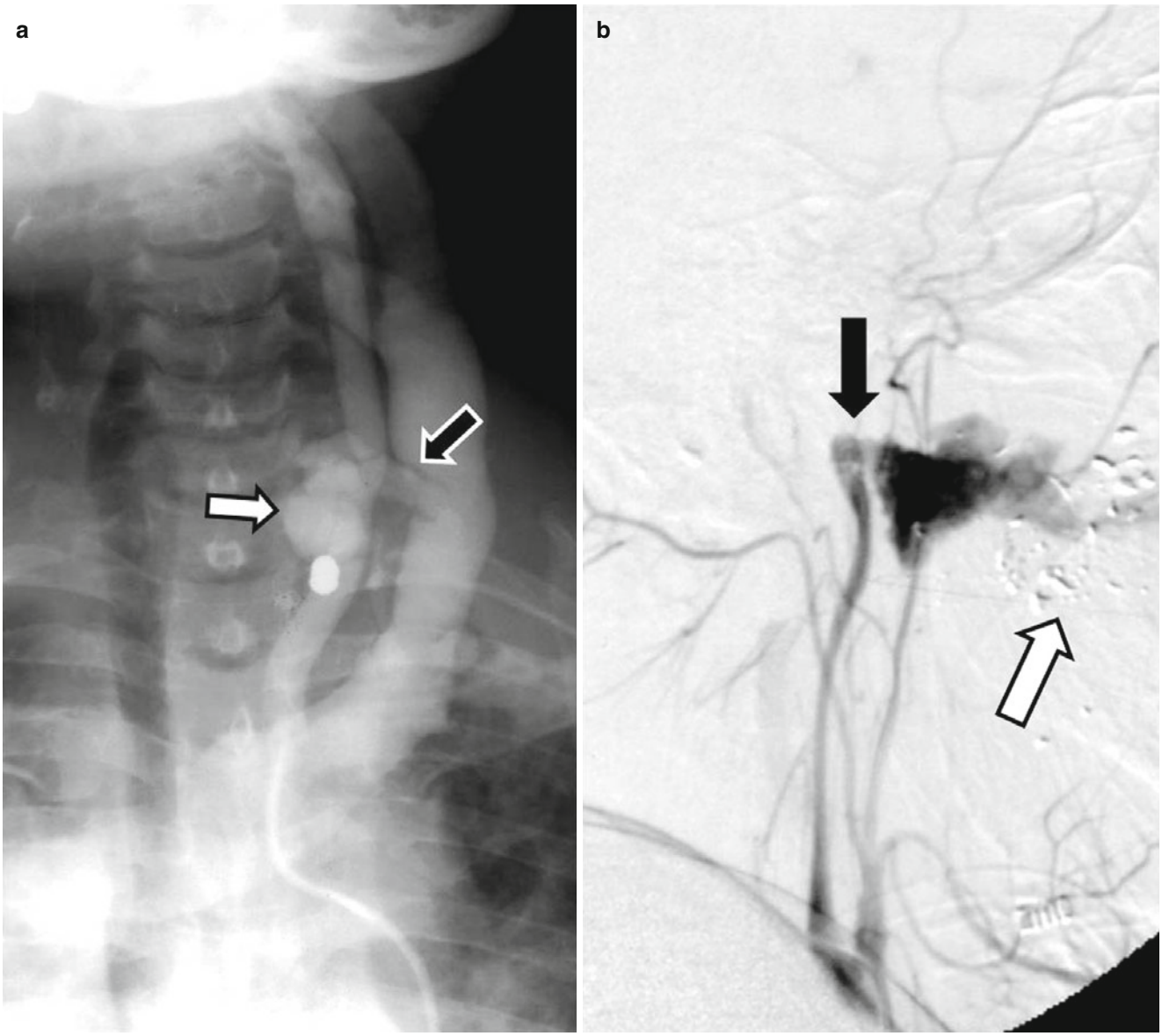

Fig. 1 (**a**, **b**) Penetrating injuries. (**a**) Zone II. AP view of a catheter angiogram (CA) done on a gunshot victim. A bullet fragment overlies the left common carotid artery (CCA) with an adjacent pseudoaneurysm (*white arrow*) and a CCA to internal jugular vein arteriovenous fistula (*black arrow*). (**b**) Zone III. Lateral digital subtraction angiogram (DSA) view of a self-inflicted gunshot to the mouth shows transection (*black arrow*) of the distal left cervical ICA with extravasation along the bullet path. Multiple bullet fragments are noted in the soft tissues (*white arrow*)

Imaging Modalities

Medical imaging is a central component of the diagnostic evaluation of vascular injuries. Each imaging modality plays a unique role in the diagnosis of these lesions.

Duplex Sonography

Duplex sonography is ideal for use in the emergency department as it is portable and requires no contrast. Doppler imaging demonstrates endoluminal flow characteristics, while gray-scale imaging provides detailed imaging of the vessel wall and extraluminal structures. Occlusion, dissection, intramural hematoma, pseudoaneurysm, laceration, transection, or arteriovenous fistula have been reliably identified in several studies [8, 9], with a reported sensitivity as high as 92–100 % in penetrating neck trauma.

Ultrasound has several limitations in the evaluation of traumatic lesions. The study is time-consuming and operator dependent; metallic foreign bodies, subcutaneous gas, and osseous structures limit visibility of the vascular structures;

and detailed evaluation is particularly difficult for vessels located above the angle of the mandible or running through bony foramina.

Magnetic Resonance Imaging

Magnetic resonance imaging (MRI) offers a high degree of tissue contrast and spatial resolution that allow for reliable disease detection. In the setting of cervical trauma, MRI is the test of choice to evaluate the spinal cord, brachial plexus, and musculotendinous and ligamentous elements. MRI also provides the most effective evaluation of the intracranial compartment for ischemic and hemorrhagic complications of cervical vascular injury.

Two- and three-dimensional time-of-flight (TOF) and contrast-enhanced MR angiography (MRA), as well as fat-saturated T1- and T2-weighted sequences, are effective at evaluating arterial wall integrity, especially when arterial dissection is suspected [10].

In the largest series of MRI use in suspected dissections, Levy et al. reported an overall sensitivity and specificity of 83 % and 99 %, respectively, using 3D-TOF angiography, although sensitivity was much lower for the vertebral arteries (20 %).

MR imaging of cervical vascular injury is limited by the presence of metallic fragments, the lack of detailed evaluation of the osseous structures, and time constraints associated with seriously injured individuals. In the United States, emergency department imaging of cervical trauma relies primarily on computed tomography (CT).

Computed Tomography

With the development of multi-detector CT (MDCT) technology, computed tomography is the predominant triage tool for trauma patients [11]. High spatial resolution and isometric voxelation allow for seamless multiplanar reconstructions and volume-rendered three-dimensional imaging of large tissue volumes. In cervical trauma, MDCT can image the entire cervicocerebral vascular system within a few seconds, along with the adjacent soft tissue and osseous structures. CT imaging carries no absolute contraindications and very few relative contraindications, e.g., contrast allergy, which allows for safe and rapid performance of the procedure.

Computed tomographic angiography (CTA) has a spatial resolution that rivals catheter angiography. A recent evaluation of CTA with 16-slice MDCT scanners demonstrated 97.7 % sensitivity and 100 % specificity compared to conventional angiography. Because of these attributes, MDCTA has usurped catheter angiography as the predominant imaging modality in the diagnosis of cervical vascular injury [7].

Digital Subtraction Angiography

For years, digital subtraction angiography [DSA] represented the "gold standard" for imaging evaluation of vascular injuries. However, continued improvements in noninvasive vascular imaging have caused a shift away from this invasive technology for the bulk of the diagnostic evaluation. Two major limitations in DSA contribute to this shifting diagnostic paradigm—DSA is limited in its assessment of the extravascular structures and mural integrity, and there is the potential for neurologic and non-neurologic complications. On the positive side, DSA allows for very high spatial resolution, as well as provides temporal information relating to the hemodynamics of the cerebrovascular tree. DSA remains the test of choice for detecting flow-related complications of cervical and cerebral vascular injury, such as arteriovenous fistulas, and for the evaluation of collateral circulation. DSA is often used when noninvasive imaging is inconclusive or necessary for preoperative planning and as an endovascular alternative to open surgical vascular repair.

Patterns of Injury

Intimal damage is the final common pathway for vascular injury, regardless of the mechanism of action. Even minimal intimal disruption may promote the cascade of platelet aggregation and clot formation, leading to distal embolization or vascular thrombosis.

Focal spasm or mild luminal irregularity (Fig. 2a) may be all that is noted. However, more substantial injury includes subintimal dissection with (Fig. 2b) or without intramural thrombus, raised intimal flap (Fig. 2c), pseudoaneurysm formation (Figs. 1a and 2c), occlusion (Fig. 2d), transection with active extravasation (Fig. 1b), and arteriovenous fistula (AVF) development (Fig. 1a). Progression of subintimal thrombus in a false lumen or a subendothelial tear with false channel (Fig. 2c) or pseudoaneurysm enlargement may lead to luminal stenosis with subsequent hemodynamic compromise and cerebral ischemia. Rapid change in the appearance of the injury can occur. Combinations of injuries may occur in the same vessel (Fig. 1a), and multivessel injury has been reported in 18–38 % of cases.

In an effort to predict the risk of stroke, Biffl et al [5]. devised a grading scale based upon the angiographic appearance of blunt carotid injuries. The scale was modified in 2002 to include arteriovenous fistulas (AVFs) and to apply also to vertebral artery injuries. Grade I lesions are vessels which show luminal irregularity with less than 25 % luminal narrowing (Fig. 2a). Grade II lesions are those with dissection or intramural hematoma with greater than 25 % luminal narrowing (Fig. 2b), intraluminal thrombus (Fig. 2b), raised intimal flap (Fig. 2c), or hemodynamically insignificant

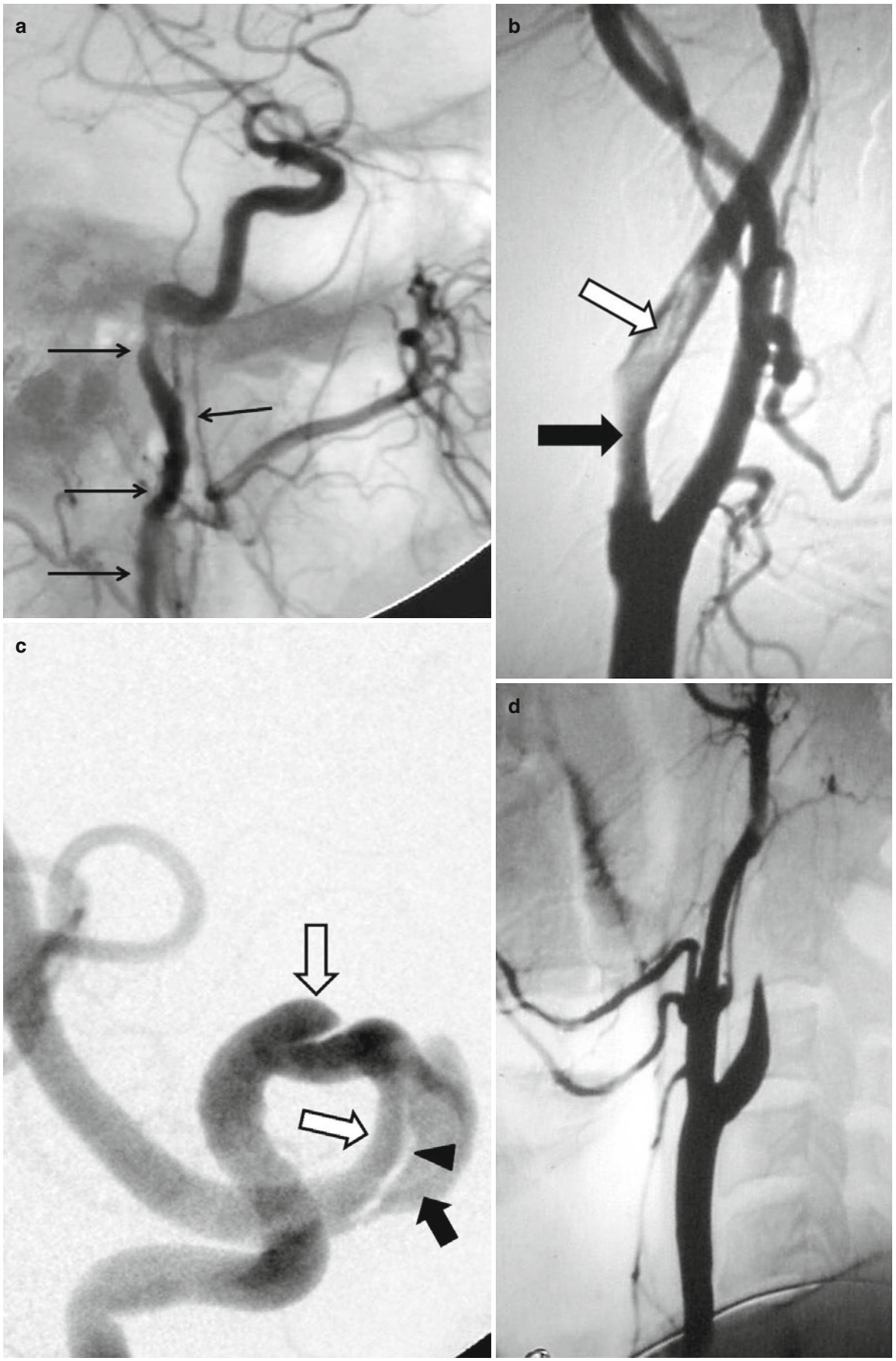
a
b
c
d

arteriovenous fistula (AVF). Grade III lesions are pseudoaneurysms (Figs. 1A and 2c); Grade IV, vessel occlusion (Fig. 2d); and Grade V, transaction (Fig. 1b) or hemodynamically significant AVF (Fig. 1a). In the carotid territory, the higher the Biffl grade, the higher the risk of stroke. In the vertebral system, Grade II lesions carry the highest risk.

It is important to recognize that vascular injury, usually in the form of a dissection, can occur after trivial trauma or in otherwise healthy individuals with no obvious risk factors. The average annual incidence of these "spontaneous" occurrences is between 2.6 and 2.9 per 100,000 people and accounts for 13–22 % of ischemic strokes in patients younger than 45 years of age. Known collagen-vascular disorders (CVDs), such as Ehlers-Danlos syndrome (Type IV), fibromuscular dysplasia, and Marfan's syndrome, are associated with the development of spontaneous dissection. Skin biopsies in patients with spontaneous dissection often demonstrate structural abnormalities of their connective tissue, making them more prone to injury from insignificant trauma such as coughing or sneezing [3].

Vasospasm

Vasospasm is a physiological response of the arterial wall to mechanical or chemical irritation resulting in contraction of the smooth muscle within the wall and appearing as segmental areas of associated vascular narrowing on imaging. Vasospasm is a uniformly reversible and self-limited event and usually responds favorably to vasodilators such as nitroglycerine, papaverine, and calcium channel blockers.

Vasospasm can mimic subtle intimal injury, which can manifest as segmental narrowing, but vasospasm should never be associated with an intimal flap or pseudoaneurysm. It can also be indistinguishable from mild forms of connective tissue disorders, particularly fibromuscular dysplasia, and can be subtle enough to be overlooked or undetectable on CTA and MRA.

Intimal Flap

An intimal flap is the separation of a short segment of the intimal layer from the medial layer of the arterial wall. It appears on imaging as a linear intraluminal filling defect that is in continuity with the arterial wall, but without an associated wall hematoma or distinct false lumen (Fig. 3a). Intimal flaps have similar imaging characteristics on CTA and MRA, but they are more reliably detected with CTA (Fig. 3b). Because they are focal and often subtle, the ability to detect them on imaging is impaired by adjacent metallic foreign bodies or other sources of beam-hardening artifact, such as venous contrast reflux into the internal jugular vein, or by quantum mottle caused by the shoulders.

Intimal flaps can be a nidus for, and a mimic of, thromboembolus formation. They may also progress to frank dissection. In practice, the vast majority of minor intimal injuries heal spontaneously without sequelae. There is considerable debate over the incidence, significance, and appropriate treatment of intimal flaps. Observation may be all that is necessary, but when appropriate, short-term use of an antiplatelet agent, e.g., aspirin, can be considered.

Dissection and Pseudoaneurysm

Cervical arterial dissections are the most common vascular injury following blunt cervical trauma, representing as many as 76 % of these injuries, but they can also occur after mild trauma, i.e., chiropractic manipulation, roller coaster riding, or spontaneously without an identifiable traumatic event. There is clearly an association between spontaneous dissections and hereditary connective tissue disorders, although the estimates of the prevalence in the spontaneous dissection population vary dramatically, ranging from 0 to 18 %. Cervical arterial dissections can also arise as an extension of aortic aneurysms involving the aortic arch.

Pathophysiologically, arterial dissection represents a separation of the intimal layer of the arterial wall away from the medial layer, with the creation of a false channel between the two layers (Fig. 2c). Radiographically, cervical arterial dissections demonstrate a variety of appearances ranging from an uncomplicated intimal flap to complete occlusion. A dissection may look like a blind-ended pouch with an adjacent stenotic lumen, often eccentric, and varying degrees of contrast opacification (Fig. 4). If blood in the false channel creates a "reentrance" intimal tear or fenestration, the vessel takes on the "double-barrel" appearance of two parallel vascular channels (Fig. 2c), which, upon healing, may become permanent (Fig. 5). If the hemorrhage does not create a fen-

Fig. 2 (**a**) Left CCA lateral DSA view of a patient in a motor vehicle accident (MVA) with neck pain. The study shows mild luminal irregularity along the course of the distal ICA (*black arrows*) to the carotid canal indicative of intimal injury (Biffl Grade I). (**b**) Right CCA lateral DSA view of another MVA patient with stroke shows luminal narrowing of the carotid bulb of greater than 25 % (*black arrow*) consistent with an intraluminal hematoma and adherent intraluminal thrombus (*white arrow*) (Biffl Grade II). (**c**) Left vertebral artery (VA) oblique submentovertex DSA view of a patient in a snowboarding accident. A large intimal flap (*arrowhead*) is identified with compression of the true lumen (*white arrow*) by the false lumen (*black arrow*) (Biffl Grade II). In addition, a pseudoaneurysm is identified proximal to the flap (*open arrow*) (Biffl Grade III). (**d**) Right CCA lateral DSA view of an MVA patient with stroke shows complete occlusion of the internal carotid artery (Biffl Grade IV)

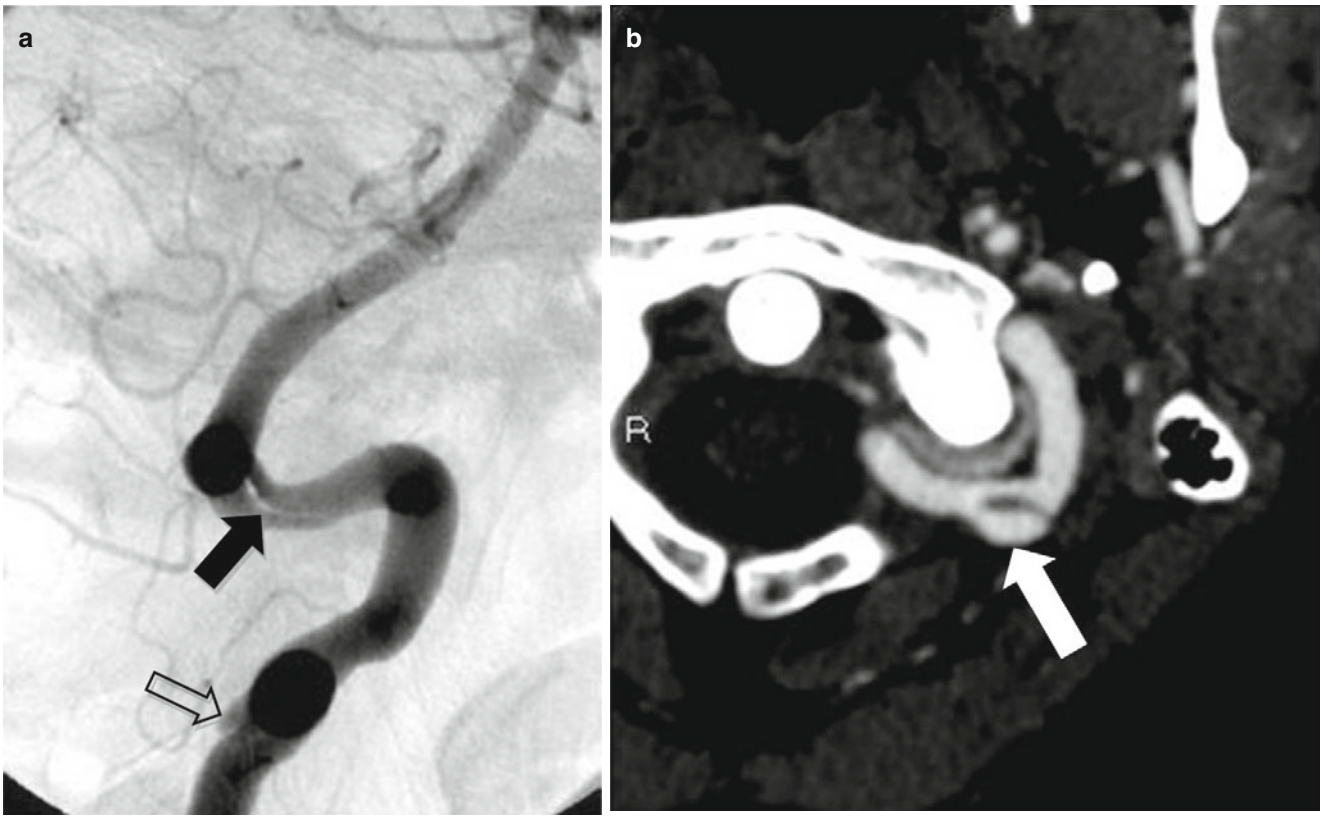

Fig. 3 (**a**) Left VA lateral DSA view in a patient with an athletic injury. A small intimal flap is identified (*black arrow*) in addition to a small intimal irregularity seen more proximally (*open arrow*). (**b**) A subsequently CTA shows the flap well on the axial view, with some early pseudoaneurysm formation (*white arrow*)

estration, the false lumen may lead to stenosis or occlusion of the true lumen or pseudoaneurysm formation. When the dissection involves the *subintimal* media, it will evolve into stenosis (Fig. 4) or occlusion (Fig. 2d). Stenosis usually appears as a smooth, tapered narrowing that varies in severity and length depending on the extent of the dissection. DSA imaging can elucidate the luminal narrowing associated with dissection, but cross-sectional imaging optimizes visibility of the offending intramural hematoma. On CTA, this manifests as luminal narrowing with paradoxical enlargement of the total diameter of the vessel (Fig. 6a). Intramural hematoma may appear iso- or mildly hyperdense to adjacent muscle. On MRI, the intramural hematoma becomes even more conspicuous on fat-saturated T1-weighted images, appearing as an intramural hyperintensity paralleling the vascular flow artifact (Figs. 6b and 7b) or as a hyperintense "crescent" sign on images perpendicular to the long axis of the vessel (Fig. 7a). The intramural thrombus can also be seen on susceptibility-weighted imaging (SWI) as a hypointense area (Fig. 6c) and will restrict diffusion on diffusion-weighted imaging (DWI). These findings are more reliably conspicuous in the carotid artery (Fig. 7) than the vertebral artery, as normal sluggish flow in the closely approximated vertebral venous system can mimic the "crescent" sign of vertebral dissection.

Occlusive dissection possesses a characteristic flame-shaped, tapered luminal narrowing (Figs. 2d and 8). The wall hematoma will possess the same imaging characteristics as described above, but differentiating intramural hematoma from intraluminal thrombus can be difficult, if not impossible, in the setting of occlusion.

Pseudoaneurysms (Figs. 1a, 2c, and 4) result from *subadventitial* dissection and appear as a saccular outpouching projecting beyond the expected confines of the vessel wall. The term "pseudoaneurysm" is used due to the fact that the aneurysmal outpouching does not consist of all three vascular wall layers. On DSA and cross-sectional vascular imaging, pseudoaneurysms appear as contrast-filled outpouchings adjacent to and in continuity with the vessel lumen (Fig. 4). On cross-sectional imaging, adjacent hematoma may be evident. Color-flow Doppler shows the "yin-yang" appearance of swirling flow within the pseudoaneurysm sac.

Pseudoaneurysms may form from a dissection caused by blunt injury or by penetrating trauma. Unlike dissecting pseudoaneurysms, pseudoaneurysms caused by laceration contain no vessel wall (Fig. 9), with the sac instead being

Fig. 4 (**a**) Left CCA DSA, AP view shows a subacute dissection from an MVA. There is abrupt tapering of the internal carotid artery from the C3 level to the carotid canal, where the lumen returns to normal diameter (*black arrow*). A blind-ended pouch representing contrast in the proximal portion of the dissection with pseudoaneurysm formation is noted. (**b**) The corresponding CTA shows the luminal narrowing and the false lumen pouch (*black arrow*), which extends outside of the vessel lumen as a pseudoaneurysm (*open arrow*). The ascending pharyngeal artery (APA) (**a,b** *white arrows*) parallels the ICA lumen and may be mistaken for a "string sign" in patients who actually have ICA occlusion. The APA, however, does not enter the carotid canal

comprised of perivascular connective tissue and/or surrounding hematoma. This results in an instability that invariably leads to pseudoaneurysm growth and could lead to a vascular "blowout." For these reasons, pseudoaneurysms related to vessel laceration are usually treated surgically or endovascularly.

Follow-up imaging in cervical arterial dissections is important, as dissections show a variable evolution. Many dissections heal without obvious abnormality, and follow-up imaging will appear normal or with minimal luminal irregularity. However, some dissections heal with chronic stenosis or pseudoaneurysm. Occlusive dissections may recanalize and become a source for distal embolization; dissecting pseudoaneurysms may enlarge and compress the adjacent vessel (Fig. 10). Understanding these changes aids in treatment decisions both in the acute and chronic stages of the disease.

Fig. 5 Right CCA DSA, AP view in a trauma patient shows evidence of a healed dissected ICA with three separate channels (*arrows*)

Occlusion

Vascular occlusion is the most common imaging appearance of cervical carotid arterial injury in both blunt and penetrating cervical trauma, with a prevalence as high as 33 % and 36 %, respectively. The imaging appearance of occlusion varies relative to the acuity and etiology of the event. In situ thrombosis often demonstrates an abrupt, blunt occlusion that ends at or near a branch point (Fig. 11). Contrast tracking around intraluminal thrombus may appear as a "meniscus" or "tram-track" sign, and vessels tend to thrombose retrograde to a branch point. Conversely, occlusive dissection may be seen as a tapered, flame-shaped occlusion (Fig. 1d).

In CTA, arterial occlusion is usually readily apparent as an abrupt termination of the contrast column. Occlusion of a vessel in the early arterial phase may show no contrast enhancement within its lumen, misidentifying the level of the lesion. However, contrast opacification to the level of the occlusion occurs eventually as contrast material slowly percolates into the stagnant column and will be identified on delayed images if obtained.

In the acute phase of cervical arterial occlusion, collateral channels distal to obstruction may reconstitute the vessel downstream of the obstruction. Patterns of collateralization vary depending on the vessel and the site of the occlusion. In common carotid artery occlusion, retrograde filling of the external carotid artery to the internal carotid artery is often seen. In cervical ICA occlusion, antegrade filling of the intracranial ICA can occur through ECA collaterals with the petrous and cavernous segments of the ICA and via retrograde flow from the ophthalmic arteries. In cervical vertebral artery occlusion, potential collateral pathways at each vertebral level exist for vertebral artery reconstitution. Robust collaterals from the thyrocervical and costocervical trunks, as well as muscular vertebral and occipital artery branches, often revascularize an injured vertebral artery just distal to the occlusion.

When satisfactory collateral circulation is not present to maintain distal flow, the artery will thrombose retrograde to the last point of inflow or may consist of several discontinuous segments of filling. Differentiating between occlusion and severe stenosis is important because of the potential for future thromboembolic events in vessels with slow flow. As a noninvasive study, CTA shows a high degree of accuracy for differentiating these two entities, but when the results are inconclusive, catheter angiography can be performed to delineate between the two with a high degree of certainty.

Contrast-enhanced MRA (CE-MRA) results in similar imaging characteristics to those described above for CTA although its lower spatial resolution makes it more difficult to differentiate between occlusion and severe stenosis. Time-of-flight (2D and 3D) MR angiographic techniques have even less sensitivity and specificity than contrast-enhanced MRA.

Arteriovenous Fistulas

Arteriovenous fistulas (AVFs) are abnormal communication between arteries and veins that result in arterialization of the venous systems. Traumatic cervical AVFs almost always arise from penetrating trauma (Fig. 1b), although blunt trauma is implicated in some cavernous-carotid and vertebrovenous fistulas. Although not always the case, AVFs may be unsuspected initially, but enlarge and mature over time with symptoms presenting in a delayed fashion. Audible bruit or neck pain may indicate the presence of a fistula, but the initial signs may be more ominous, such as those related to cerebral ischemia, venous hypertension, or high-output failure.

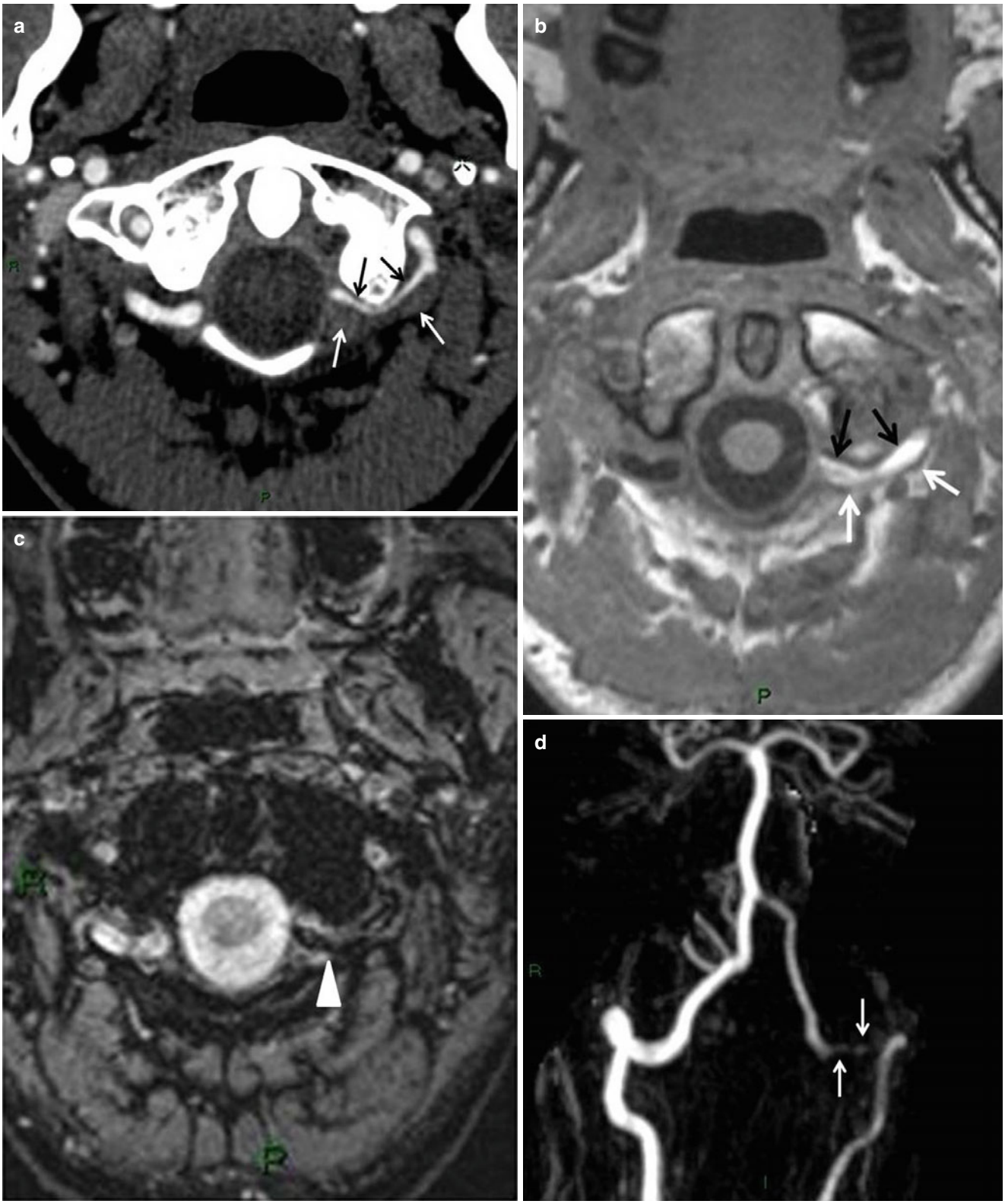

Fig. 6 (**a**) Axial CTA image through the distal vertebral arteries in a patient in a minor car accident with neck pain. The study shows compression of the contrast-filled lumen (*black arrows*) by intramural thrombus in the dissected segment (*white arrows*). Notice how the overall diameter of the vessel (distance from the *black arrows* to the *white arrows*) is larger than the diameter of the normal right vertebral artery. (**b**) Corresponding axial T1-weighted MRI shows the flow void within the compressed lumen (*black arrows*) and the hyperintense mural thrombus (*white arrows*). (**c**) The intramural thrombus on susceptibility-weighted imaging (*arrowhead*) is hypointense, and the contrast-enhanced MRA (**d**) shows the irregular and narrowed residual lumen through the affected area

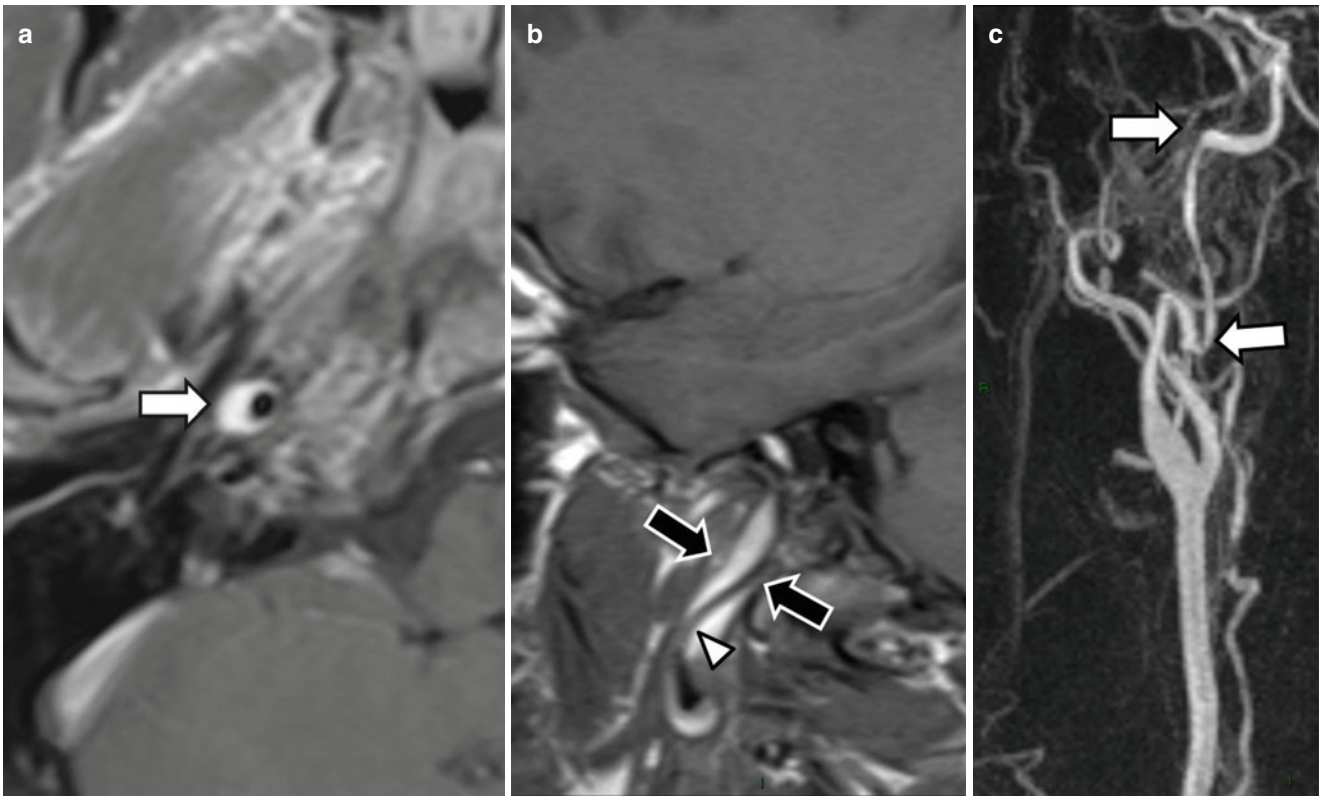

Fig. 7 MRI and MRA in a patient who sustained a fall show the "crescent sign" (*white arrow*) involving the right ICA at the skull base on axial T1-weighted imaging (**a**). The sagittal view nicely demonstrates the enlarged vascular structure with intramural thrombus (*black arrows*), and the residual lumen flow void coursing through the center (*arrowhead*). The corresponding gadolinium-enhanced MRA (**c**) shows the rapid tapering of the distal ICA with variable lumen size from the cervical loop to the vertical portion of the petrous carotid segment (*white arrows*)

Noninvasive vascular imaging may be able to detect obvious AVFs, but catheter angiography remains the gold standard or evaluating these lesions. Cross-sectional imaging may show a caliber change of the affected artery and enlargement of the affected vein. In some cases the fistulous connection is identified, particularly with time-resolved CT and MR sequences; detection and characterization of these lesions noninvasively remain suboptimal. If the lesion is in a location that can be studied with color-flow and spectral Doppler, ultrasound may show low-resistance arterial and arterialized venous waveforms or the actual fistulous connection. But these lesions are obvious on DSA, demonstrating the enlarged feeding artery, rapid arteriovenous transit time, and early filling of the affected veins. The size and location of the fistulous connection are identified, and the presence of collateral circulation can be identified in cases of arterial steal. In some cases, the fistula can be closed by endovascular means at the same time as the diagnosis (Fig. 12).

Transection

Transection represents the most severe form of cervical arterial injury and is often lethal. Penetrating trauma is the most likely cause of vascular transection, but excessive blunt force can be the inciting factor, particularly in severe spinal and skull base fractures. Radiographically, arterial transections can present with any of three imaging appearances: vessel occlusion (Fig. 9), active extravasation (Fig. 1b), or arteriovenous fistula (all described above). High-flow and/or retrograde steal may give the appearance of a transection in the presence of an arteriovenous fistula; however, antegrade flow is restored after fistula closure, demonstrating vessel patency.

Fig. 8 Sagittal CTA in a patient with spontaneous carotid dissection shows the flame-shaped, rapid tapering of the ICA, which is occluded (*black arrow*). The enlarged, thrombus-filled distal carotid artery is seen (*white arrows*) and consistent with a thrombosed dissection. Intramural thrombus cannot be distinguished from intraluminal thrombus

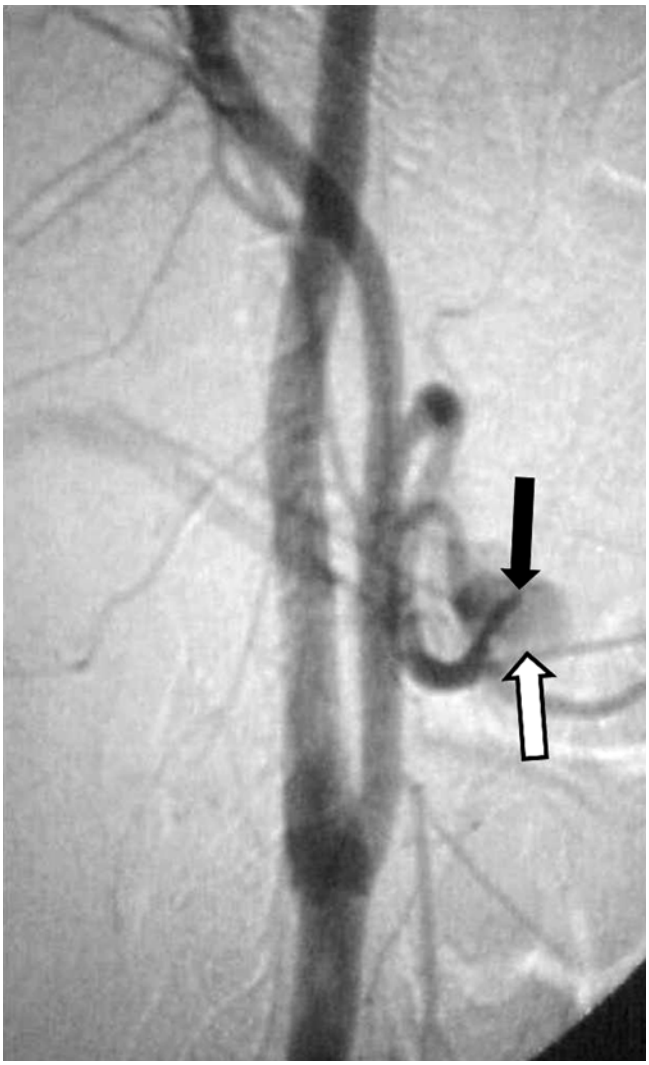

Fig. 9 Left CCA DSA, lateral view, in a farmworker who fell onto his shears, with a resulting injury to the facial artery. The vessel is transected (*white arrow*), and a traumatic pseudoaneurysm is identified at the site of the injury (*black arrow*). The vessel was completely occluded endovascularly using platinum microcoils (not shown)

Treatment

Image-guided therapy has evolved into the first line of treatment for many traumatic cerebrovascular injuries [6]. When DSA is employed in the diagnosis of these lesions, endovascular techniques and appropriate devices allow treatment to take place at the same time. Flow-limiting or symptomatic dissections can be treated with balloon angioplasty or endovascular stenting; pseudoaneurysms are now being closed with coil embolization or the placement of a flow diverter. Life-threatening transections and active extravasation can be treated with vessel sacrifice; and arteriovenous fistulas can be closed via transarterial (Fig. 12) or transvenous embolization. Unfortunately, a detailed discussion of these exciting techniques is beyond the scope of this syllabus.

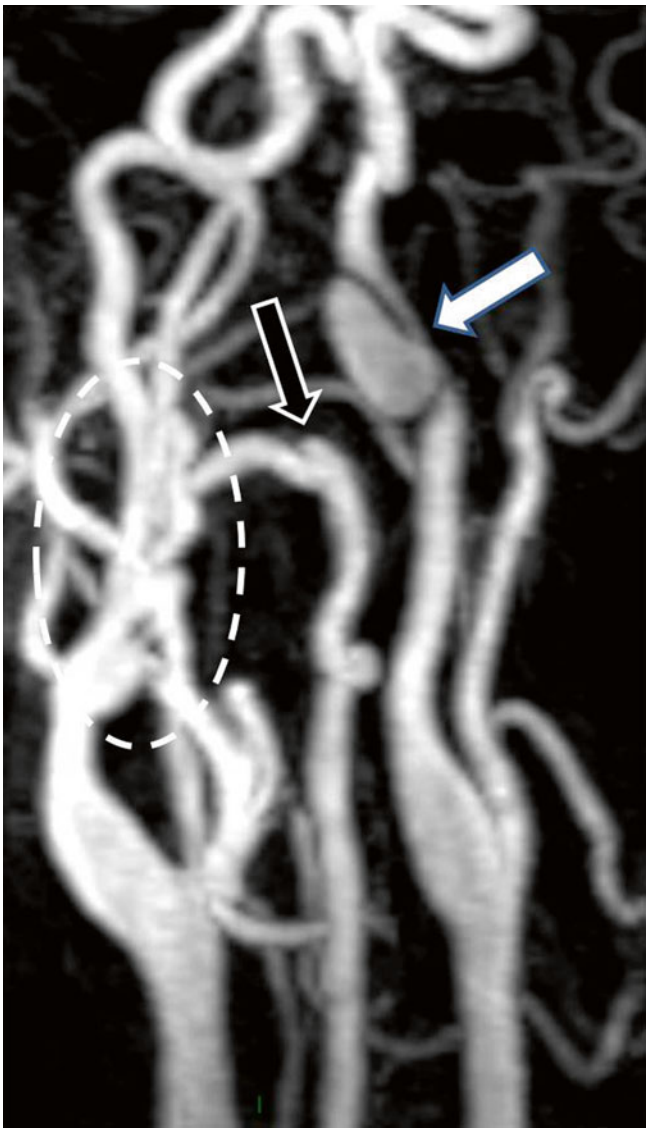

Fig. 10 Follow-up contrast-enhanced MRA of patient with multiple vascular injuries and of the same patient as in Fig. 5. This study shows a stable multichannel right ICA dissection (*dashed circle*); a small, stable left vertebral artery pseudoaneurysm (*black arrow*); and a progressively enlarging left ICA pseudoaneurysm causing significant stenosis of the left ICA (*white arrow*). The pseudoaneurysm was treated with carotid stenting (not shown)

Fig. 11 Right VA DSA, AP view shows a blunt, rounded termination of flow with thinning of the contrast column (*arrow*), consistent with an acute occlusion. The posterior meningeal artery arises just proximal to the stump

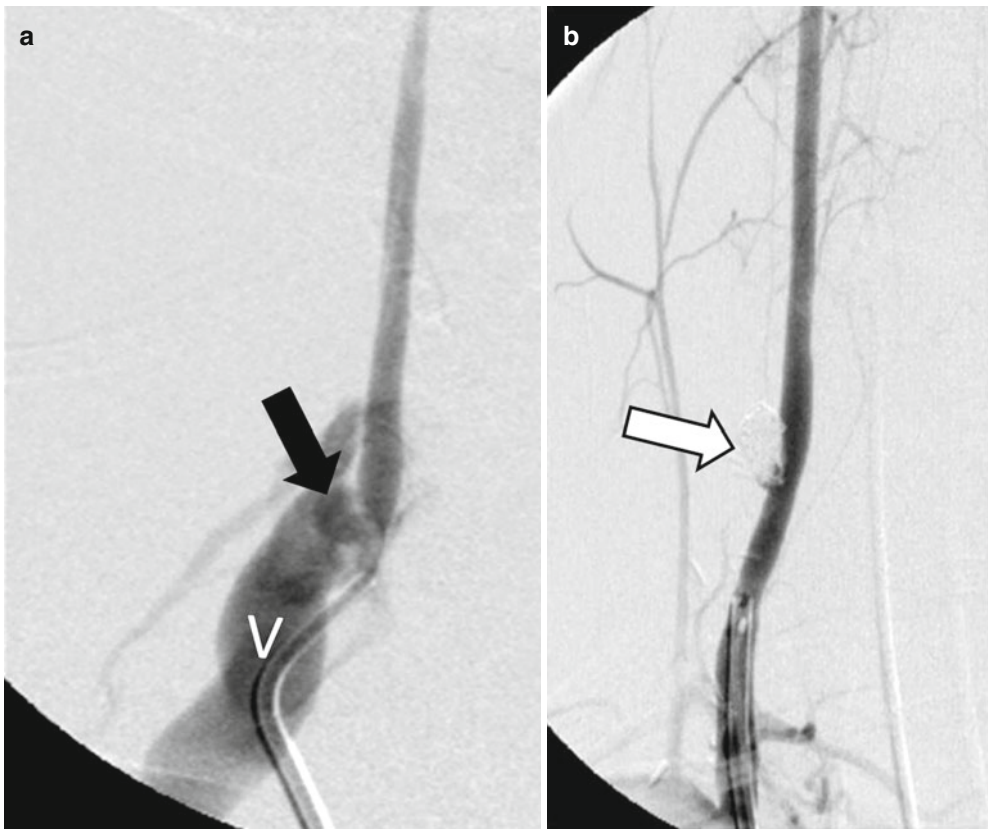

Fig. 12 Iatrogenic injury to the right vertebral artery during attempted central line placement resulted in a vertebral artery to vertebral venous fistula, seen on a right VA DSA (**a**, *arrow*). The fistulous connection is identified (*black arrow*), as well as rapid shunting into markedly enlarged vein (V). After closure of the fistula using platinum coils (**b**, *white arrow*), the vertebral artery fills normally, and the draining vein is no longer seen in the arterial phase. The white arrow on b is pointing to the coil ball, which is difficult to see because it is masked out

References

1. Berne JD, Reuland KS, Villarreal DH et al (2006) Sixteen slice multi-detector computed tomographic angiography improves the accuracy of screening for blunt cerebrovascular injury. J Trauma 60:1204–1209
2. Biffl WL, Moore EE, Offner PJ et al (2001) Blunt carotid and vertebral arterial injuries. World J Surg 25:1036–1043
3. Gdynia HJ, Kuhnlein P, Ludoph AC et al (2008) Connective tissue disorders in dissections of the carotid or vertebral arteries. J Clin Neurosci 15:489–494
4. Munera F, Danton G, Rivas LA et al (2009) Multidetector row computed tomography in the management of penetrating neck injuries. Semin Ultrasound CT MRI 30:195–204
5. Biffl WL, Ray CE, Moore EE, Franciose RJ et al (2002) Treatment-related outcomes from blunt cerebrovascular injuries: importance of routine follow-up arteriography. Ann Surg 235:699–706
6. Seth R, Obuchowski AM, Zoarski GH (2013) Endovascular repair of traumatic cervical internal carotid artery injuries: a safe and effective treatment option. AJNR Am J Neuroradiol 34(6):1219–1226
7. Anaya C, Munera F, Bloomer CW et al (2009) Screening multidetector computed tomographic angiography in the evaluation of blunt neck injuries: an evidence based approach. Semin Ultrasound CT MRI 30:205–214
8. Gardner DJ, Gosink BB, Kallman CE (1991) Internal carotid artery dissections: duplex ultrasound imaging. J Ultrasound Med 10:607–614
9. Montalvo BM, LeBlanq SD, Nunez DB Jr et al (1996) Color flow Doppler sonography in penetrating injuries of the neck. AJNR Am J Neuroradiol 17:943–951
10. Provenzale JM, Sarikaya B (2009) Comparison of test performance characteristics of MRI, MR angiography, and CT angiography in the diagnosis of carotid and vertebral artery dissection: a review of the medical literature. AJR Am J Roentgenol 193(4):1167–1174
11. Chokshi FH, Munera F, Rivas LA et al (2011) 64-MDCT angiography of blunt vascular injuries of the neck. AJR Am J Roentgenol 196(3):W309–W315

Brain Ischemia: CT and MRI Techniques in Acute Stroke

Howard A. Rowley and Pedro Vilela

Introduction

The past year has seen rapid advances in acute stroke therapy based on advanced imaging selection [1–5]. The main aim of imaging in acute ischemic stroke (AIS) is to rule out hemorrhage and stroke mimics, to define the extension of established infarct (core), and to identify the occlusion site, which are the main factors involved in the acute treatment decision: conservative, IV thrombolysis, and mechanical thrombectomy [1–5]. Additional relevant information includes the extension of the core (or penumbra), the type and length of the clot, and the individual collateral circulation that may allow the individual AIS treatment strategies.

From an initial PPP (parenchyma, pipe, penumbra) evaluation, we have been witnessing the introduction of the CCC concept (core, clot, and collaterals). The different imaging techniques that address these factors and the rationality beneath its use will be overviewed.

Computed tomography (CT) and magnetic resonance imaging (MRI) protocols both provide excellent tools in the evaluation of acute ischemic stroke [6]. The choice of modality is driven by many factors, which must balance practical availability, clinical urgency, critical information required, and range of possible interventions under consideration. Although there is controversy about which method is "best," we are fortunate that both methods can be effectively used and refined to optimize diagnosis and patient management [7, 8]. Whether based on CT or MR, comprehensive stroke imaging protocols can be used to triage patients to rationale therapy based on individual vascular anatomy and physiology. Parenchymal imaging establishes the diagnosis and extent of ischemia, CTA or MRA determines site of occlusion and interventional access options, and perfusion studies provide a view of collateral flow and autoregulation. Refinements and guidelines for advanced imaging techniques are still being worked out in clinical trials, but these tools already play a central role in clinical practice. Here we review new developments and concepts in acute stroke imaging and acute intervention, highlight practical aspects of the diagnosis of stroke using basic and advanced CT and MRI protocols, and look at future directions in the field.

H.A. Rowley (✉)
Department of Radiology, University of Wisconsin,
600 Highland Avenue, Box 3252, Madison, WI 53792, USA
e-mail: hrowley@uwhealth.org

P. Vilela
Neuroradiology, Hospital Beatriz Ângelo,
Avenida Carlos Teixeira, 3, Loures, Lisbon 2674-514, Portugal
e-mail: ferrovilela@sapo.pt

The "Golden Hour" of Stroke Triage

The timing of comprehensive neurovascular studies may be critical not only for acute TPA decisions but also for additional practical management reasons. The concept of "the Golden Hour" in trauma evaluation grew from French military data from World War I suggesting that delay to treatment beyond an hour reduced likelihood of survival. Since we lose about 1.9 million neurons per minute in an acute MCA occlusion, "time is brain," and we need to think of stroke as urgently as trauma triage and treatment [9]. If we are to meet a "door to needle" target of less than 60 min for TPA delivery, current guidelines suggest acute imaging be completed within 25 min and interpreted within 20 min [10]. However this first hour is also a golden opportunity to get beyond the TPA decision and use comprehensive imaging to help with definitive clinical management, including stent retrievers for proven proximal clot [11]. Getting beyond the basic CT or MRI, our vascular and perfusion imaging can help establish diagnosis, prognosis, and underlying cause of stroke and identify treatable causes of stroke in a timely fashion. For example, timely detection and treatment of cervical carotid disease in a stroke or TIA patient can reduce the risk of second stroke. In our well-intended rush to make the TPA decision, we also need to consider the larger role of imaging and try to efficiently and quickly provide more complete data to help with global management. Advanced centers have

J. Hodler et al. (eds.), *Diseases of the Brain, Head and Neck, Spine 2016–2019: Diagnostic Imaging*, DOI 10.1007/978-3-319-30081-8_5

found that multimodal imaging need not delay time to treatment for TPA [12]. Deployment of fast, streamlined workflow for comprehensive CT and MR protocols also provides an imaging foundation to facilitate triage and management of patients with either ischemic or hemorrhagic stroke.

CT Protocols in Acute Stroke

CT is the most commonly used imaging technique employed for acute neurologic problems worldwide. Although CT is not as sensitive for detection of ischemia as MRI with diffusion-weighted imaging (DWI), it is an efficient, readily available diagnostic tool in emergency situations. In addition to identifying candidates for intravenous tissue plasminogen activator (TPA) therapy, newly published trials [1–5] support immediate endovascular intervention for those with proven proximal occlusions. Therefore the practicality and evidence base for CT have kept it frontline for acute treatment decisions in most hospitals [13]. A directed review of the native non-contrast CT in acute stroke gleans key diagnostic information in less than a minute. For TPA and endovascular decisions, patients with any hemorrhage or signs of extended cortical ischemia (e.g., > 1/3 MCA) must be excluded. The ASPECT (Alberta Stroke Program Early CT) score provides an easy structured method to facilitate acute stroke CT reading and treatment triage (Fig. 1). This divides the middle cerebral territory into 10 areas (6 cortical and 4 deep), encompassing slices from the basal nuclei to the top of the ventricles. The reader takes a point off for each region showing ischemic changes and tallies the result. A normal score is therefore 10 and complete territorial infarction is an ASPECTs of 0. When scans from several large trial databases were scored using ASPECTs, scores of 7 and below were found to correlate with poor outcome, either with or without subsequent therapy [14]. A similar target ASPECTs was used in the recent successful endovascular trials. This serves to remind us that patients with large infarcts at baseline are unlikely to do well with therapy, whether we read images qualitatively or with a scoring system. ASPECTs also provides an excellent shorthand for communication among the stroke team members during urgent triage. The state of the parenchyma needs to be carefully evaluated as acute treatment decisions are weighed, since thrombolytic treatment of large ischemic lesions is not only fruitless but potentially dangerous. A similar scale (pcASPECTS) has been proposed for the posterior circulation AIS with similar advantages for predicting the patient outcome [15, 16].

The hyperdense artery sign on CT (and corresponding T2*/SWI clot sign on MRI) can be very helpful in not only diagnosis but may also prompt consideration of intra-arterial revascularization in the acute setting. Patients with proximal clot (ICA or M1 segment MCA), and especially extensive clot burden (e.g., clot length >5–8 mm), are unlikely to recanalize with intravenous TPA [17, 18]. The non-contrast CT done at 5 mm increments is only about 1/3 sensitive for detection of the hyperdense MCA sign, but thin sections will double the HDMCA detection rate and also help distinguish clot from mural atherosclerosis.

Complementary CTA can directly show not only the location of vascular occlusion but also more proximal (and treatable) clot sources such as atherosclerosis of the carotid

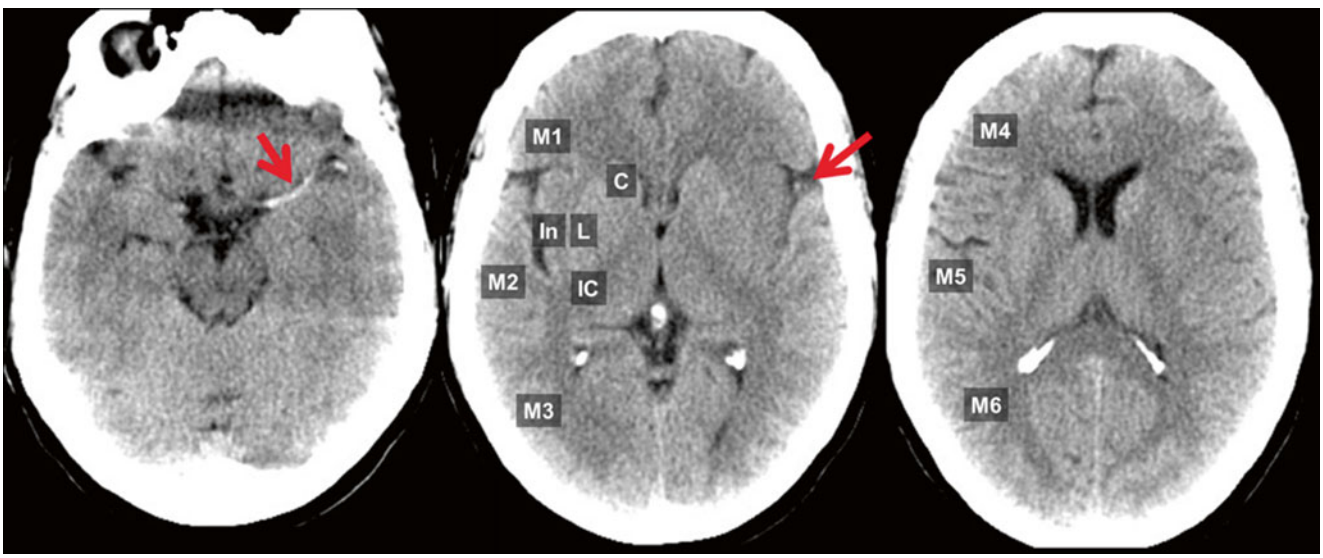

Fig. 1 Acute left MCA occlusion and early ischemic changes on CT. There is a hyperdense MCA sign (*arrows*) and subtle edema in the left insula, lentiform nucleus, and frontal operculum. ASPECT score template is shown over the right hemisphere for the 6 MCA cortical regions (M1–M6) and 4 deep regions (insula, caudate, lentiform nucleus, and internal capsule). This patient would receive an ASPECTs of 6 with points off for left insula, lentiform, M2, and M5

bifurcation or cervicocephalic dissection. Recent endovascular stroke trials indicate that good TPA candidates with proximal clot or occlusion should still receive IV TPA acutely, but they should simultaneously be considered for immediate endovascular therapy (using clot suction/retrieval devices, thrombolytics, or combinations), and that such combined IV-IA therapy improves clinical outcomes over IV TPA alone.

MRI Protocols in Acute Stroke

Magnetic resonance imaging (MRI) protocols for studying acute ischemic stroke patients are widely used in high-volume stroke centers worldwide. Multiparametric stroke imaging combining diffusion- and perfusion-weighted MRI (DWI and PWI), MR angiography (MRA), and conventional MR sequences such as fluid-attenuated inversion recovery (FLAIR) is utilized as the primary imaging modality in several major stroke centers. Short acquisition times reduce motion artifacts and enable the study of acute stroke patients with moderate cooperation. Fast image reconstruction makes the results of MRA or PWI available within a few minutes, optimally including maps to operationally estimate the size of the ischemic core and putative penumbra [19]. Detectability and detection rate of acute hemispherical stroke are significantly higher with DWI than with computed tomography (CT). The advantage of a multiparametric MRI approach lies in the characterization of the lesion extension and of the stroke mechanism, thus providing a pathophysiological basis for rational decision-making. The major advantage of MRI in stroke is the availability of DWI. Thus, we will discuss the pathophysiological basis of DWI in particular depth and just deal briefly with perfusion imaging and the detection of cerebral microbleeds.

Overview of Perfusion Techniques in Stroke

It is increasingly important to understand the physiology of brain perfusion and its complementary role alongside anatomy and vasculature in acute stroke protocols (Fig. 2). The "neurovascular unit" of the brain (a working assemblage of neurons, astrocytes, and vascular capillary endothelium) actively adjusts local cerebral blood flow (CBF) according to neural activity and overall metabolic needs. Below the normal CBF threshold of approximately 55 ml/100 gram tissue/minute, compensatory mechanisms such as recruitment of collaterals and elevation of blood volumes can help maintain overall brain function, even in the face of falling systemic perfusion pressures. Below a critical ischemic CBF threshold of approximately 15–20 ml/100 gm/min, the brain becomes ischemic, clinical deficits appear, and there is rapid progression to infarction unless flow is restored quickly. These perfusion changes can be seen immediately in acute stroke, while traditional parenchymal imaging signs of cytotoxic edema will take at least minutes (DWI) to hours (CT, T2, FLAIR) to appear.

The dynamic nature of blood delivery can be captured using CT and MR bolus perfusion studies. Using a small intravenous contrast injection, the first pass of either iodine (for CT) or gadolinium (for MR) is measured every 1–2 s for about a minute, covering as much of the brain as possible for the particular scanner. Modern CT protocols typically at least half the brain and MRI using echo-planar T2* sequences usually encompass the whole brain. Resulting data sets are analyzed using tracer kinetic modeling to produce various parameter maps related to: the time of arrival or transit in seconds (e.g., mean transit time (MTT), first moment transit time (FMT), or time to peak (TTP)); the estimated amount of blood on the vascular bed in ml/100 gm, cerebral blood volume (CBV); and the overall rate of blood delivery, cerebral blood flow (CBF), in ml/100 gm/min. Ideally post-processing is performed automatically using an arterial input function, and thresholded quantitative (or semiquantitative) maps are rapidly provided.

Perfusion Imaging

Up-to-date MRI criteria for patient selection are especially based on the relation of diffusion-weighted imaging (DWI) to perfusion imaging (PI), and a variety of methods have been used to evaluate the presence and degree of mismatch [20–25]. Although several investigators have predicted brain tissue outcome based on this hypothesis, there is growing evidence that this traditionally used ADC/perfusion mismatch concept only provides a weak approximation of the real penumbra. A recent systematic review found only two studies using true visual inspection of lesion volumes, while all others measured lesion volume on a workstation, even though in the acute situation the majority of stroke centers and major stroke studies rely on visual inspection of perfusion abnormalities ("eyeballing") for clinical decisions. Different perfusion parameters, e.g., cerebral blood volume (CBV), cerebral blood flow (CBF), mean transit time (MTT), and time to peak (TTP), define different perfusion lesion volumes in a single patient, but the perfusion lesions in these maps are less conspicuous. It is therefore worth considering the relationship of lesion volumes of different perfusion parameters and their individual predictive value for lesion growth.

It has already been shown that different perfusion parameters delineate different lesion areas and volumes (Fig. 3). Currently, TTP or rMTT maps are most widely used for lesion volume measurements, as lesion boundaries are

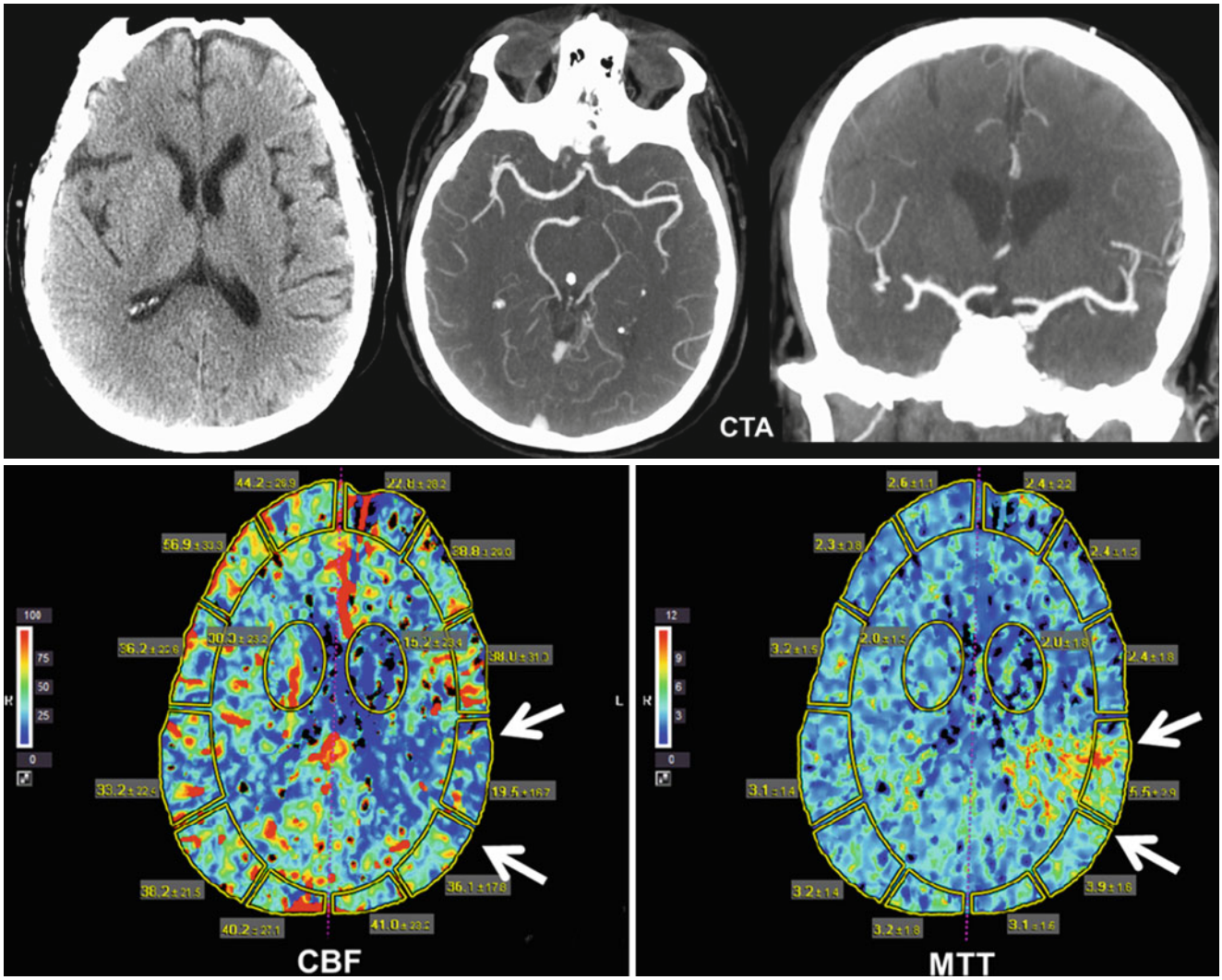

Fig. 2 Complementary information derived from traditional imaging and perfusion. This 63-year-old man was imaged less than 1 h after abrupt-onset right hemiparesis and aphasia. All sections from non-contrast CT and CT angiography were normal, even in retrospect. CT perfusion metrics (including CBF and MTT shown here) objectively confirm a wedge-shaped area of evolving ischemia in the left parietal lobe (arrows)

visually distinct. However, TTP and MTT lesions are indirect indicators of tissue perfusion including oligemic tissue not at risk of infarction and thus overestimate the penumbra. In contrast CBF and CBV maps are believed to provide a more direct estimation of tissue perfusion physiology. When comparing the ADC lesion volume with each PI parameter map (CBV, CBF, TTP, and MTT), the PI lesion exceeds the ADC lesion in most of the patients. In studies dealing with this issue in the hyperacute stage of stroke, >75 % of the patients showed perfusion exceeding corresponding diffusion lesions. In addition it has been stated that DWI and CBV maps generally show underestimation of the final infarct size, whereas the area of prolonged MTT shows an overestimation of the final infarct size.

The MTT lesion was rated to exceed all other lesion volumes in at least about 1/3 of the patients. From these results a common pattern with CBV≤CBF≤TTP≤MTT can be derived. These results indicate that different PI parameters provide complementary physiological information concerning the ischemic tissue, and therefore different PI parameter maps should be considered. Another approach for the prediction of lesion growth in stroke patients has been suggested considering the combination of the occlusion of a proximal artery and a CBF>ADC mismatch as a possible MR criterion. By using this method, lesion growth was predicted with a sensitivity of 0.79, a specificity of 0.64, a PPV of 0.56, and an NPV of 0.83 [26].

Diffusion-Weighted Imaging

Within the last two decades, a considerable number of studies were dedicated to the physiological background of DWI in experimental ischemia and human stroke. The translation of free water molecules from the extra- to the intracellular

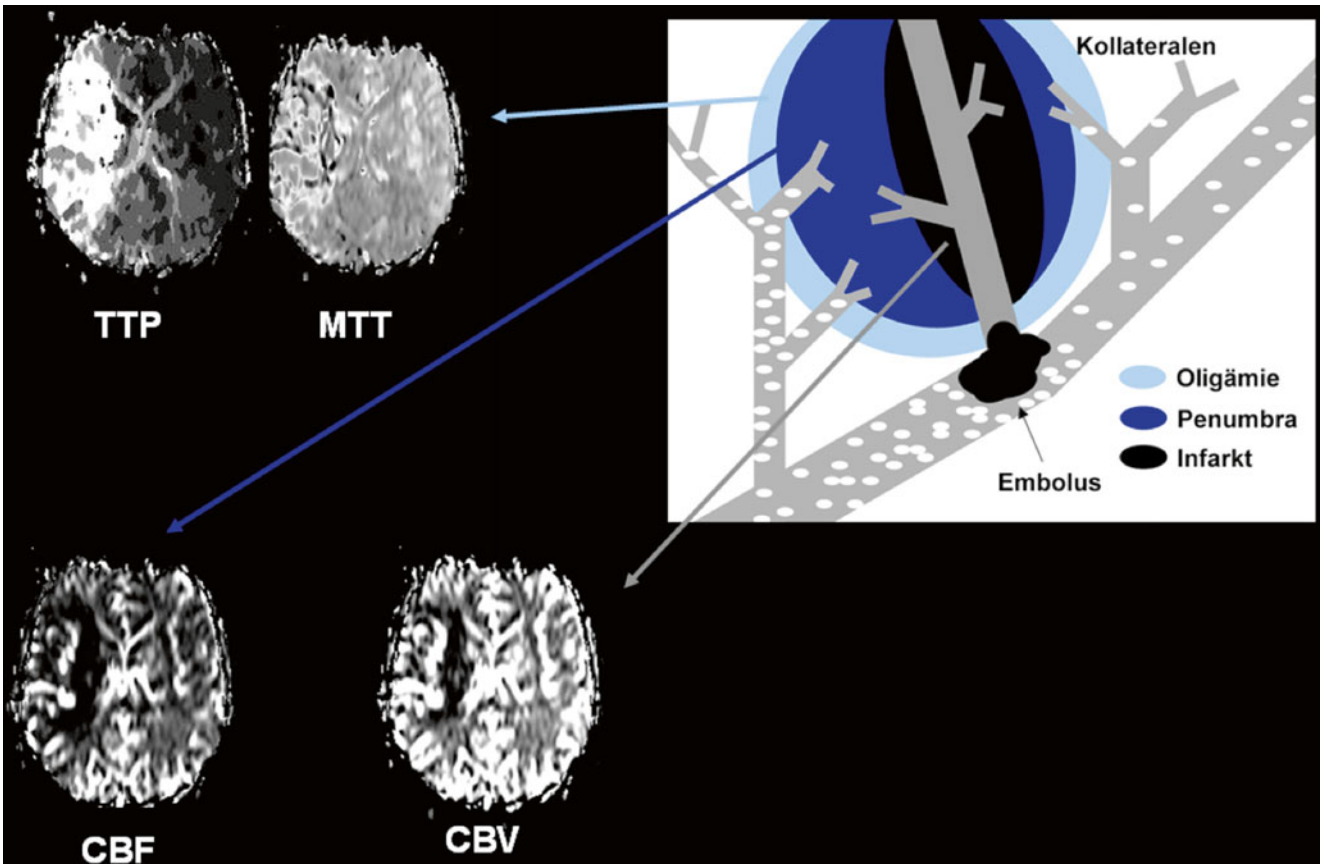

Fig. 3 Relation of the perfusion parameters to the penumbra concept

space along with ischemic cell depolarization is regarded as the hallmark for diffusion slowing. Whereas numerous animal studies were dedicated to the temporal development of acute cerebral ischemia, human DWI data on acute stroke within 6 h or less after stroke onset, the time window relevant for thrombolytic therapy is still limited.

A widely accepted hypothesis among clinicians applying DWI was that lesions with diffusion slowing represent tissue prone to infarction even though animal research indicated that this is not necessarily true. Another hypothesis was that absolute values of the apparent diffusion coefficient (ADC) might deliver a measure of tissue viability. Both hypotheses have not only been challenged by experimental work but also by several stroke studies. With increasing numbers of DWI studies in acute stroke patients, a normalization of initially decreased ADC values is reported in patients with spontaneous or therapeutic reperfusion. On the other hand, reports on the absence of early DWI abnormalities in later on infarcted tissue emerge.

What is diffusion? Diffusion is referred to as a random microscopic motion of water molecules. In principle, DWI is based on the signal intensity loss by phase dispersion accumulated by randomly moving spins between two diffusion-sensitizing magnetic field gradients. Thus, diffusion weighting in an MR image reflects random motion along the direction of the applied gradients. Typical ADC values in the human brain are age dependent and range between 0.67 and $0.83 \times 10–3$ mm^2 s-1 in gray matter (caudate nucleus and frontal cortex) and 0.64 and $0.71 \times 10–3$ mm^2 s^{-1} in white matter. Usual human stroke studies typically used a standard DWI sequence with a multislice, single-shot spin-echo echo-planar imaging (SE-EPI) sequence including 2–3 different b-values. Typically, gradients in 3 orthogonal directions are applied in order to acquire the mean diffusivity in space independent of gradient direction ("trace images"), which reduces potentially confounding directional effects in tight white matter bundles (anisotropy). As a quantitative measure of water diffusion, a map of the apparent diffusion coefficient is calculated pixel-wise as the logarithm of the signal intensity in dependence of the b-value ($ADC = \ln [S0/S1]/[b1–b0]$) (Fig. 4). The major non-diffusion effect contributing to hyperintensity in DWI is the "T2 shine-through" effect. This effect is due to the "contamination" of DW images by T2 signal hyperintensity resulting from lesions with T2 prolongation (i.e., vasogenic edema). Since T2 contamination does not influence quantitative maps of the ADC, ADC maps are informative for the estimation of the age of an ischemic lesion. To avoid pitfall and help determine the chronicity of ischemic injury, imaging should include DWI, quantitative ADC maps, and T2w (Bo) images for a complete diagnostic evaluation.

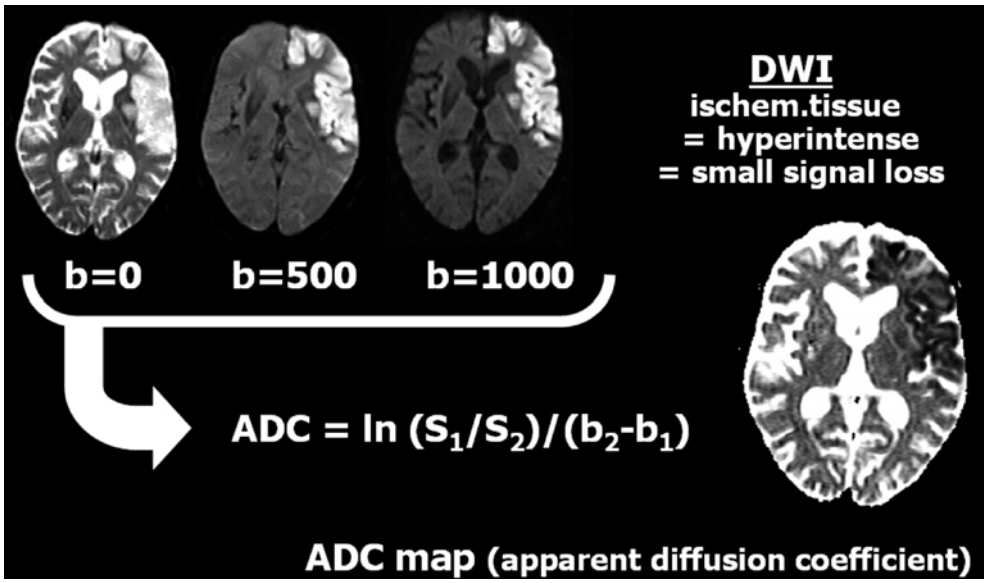

Fig. 4 Calculation of the apparent diffusion coefficient (ADC)

Why does ADC decrease and increase in cerebral ischemia? Comparably to CT, where changes of radiolucency reflect elevated total tissue water content due to tissue edema and loss of blood volume, increased signal intensities in T2w MRI appear approximately 2–4 h after cerebral ischemia and are usually thought to reflect irreversible tissue damage. For the ADC as a measure of diffusivity, the situation is more complex. ADC values in acute stroke show an early decrease (minutes to <1 h (cell depolarization and cytotoxic edema)) when T2w imaging may still be normal and "pseudonormalization" after 1–10 days (increased extracellular water content = vasogenic edema), followed by a further rise above normal ranges (cell lysis and necrosis). Several exceptions to this rule exist that will be explained in the section below. Cerebral ischemia below a critical CBF threshold results in the disruption of energy metabolism with consequent failure of ion pumps and anoxic cell membrane depolarization. As a result of increased membrane permeability and loss of ion homeostasis, water and cations simultaneously shift from the extracellular space (ECS) into the intracellular space (ICS) resulting in cell swelling (cytotoxic edema).

Diffusion and Tissue Viability

The contribution of the two paths of neuronal death, apoptosis and necrosis, and the role of reperfusion in the pathophysiology of transient ischemia is still subject to discussion. The degree of ADC decrease was related to the location and extent of neuronal injury, with pronounced changes occurring within the areas displaying the most severe histological damage. However, no association of an ADC threshold with irreversible injury was found. Thus, even with severe ADC changes, lesions may be reversible, particularly with early and effective reperfusion. This effect of treatment is welcome but also complicates the ability to predict which DWI-positive regions represent true core tissue at baseline assessment. However, normalization of MR parameters (ADC, T2w) does not necessarily indicate true tissue salvage. Within normal-appearing T2w regions in postischemic MRI scans, a partial neuronal necrosis can be observed. Surprisingly with shorter occlusion times, the average lesion size in T2w at 7 days, which is thought to represent the vasogenic edema, can be strikingly smaller than the histologically determined infarct size. Even after 10 min of vessel occlusion, a partial neuronal necrosis was observed in the absence of any T2w lesion in the chronic stage.

With thrombolytic treatment, large ischemic lesions on DWI may transiently and permanently appear normal on follow-up MRI without differences in the clinical course between both patient groups (Fig. 5). Even if areas with reversible DWI hyperintensities tend to display higher mean ADC values, an absolute ADC viability threshold in humans does not seem to exist. A complete ADC recovery without lesion in T2w imaging on day 7 has been found even within regions with initially severely decreased ADC values (<50 % of the mean contralateral value) [27, 28]. In human stroke, the degree of ADC decreases is correlated with the ischemic impairment, but does not predict the fate of the tissue after potential reperfusion. Many experts suggest that, in general, DWI-visible ischemia (confirmed by low ADC) measuring more than 70 ml, or a DWI-ASPECTs of less than 7, indicates a large core volume, a threshold beyond which intervention may be fruitless [29].

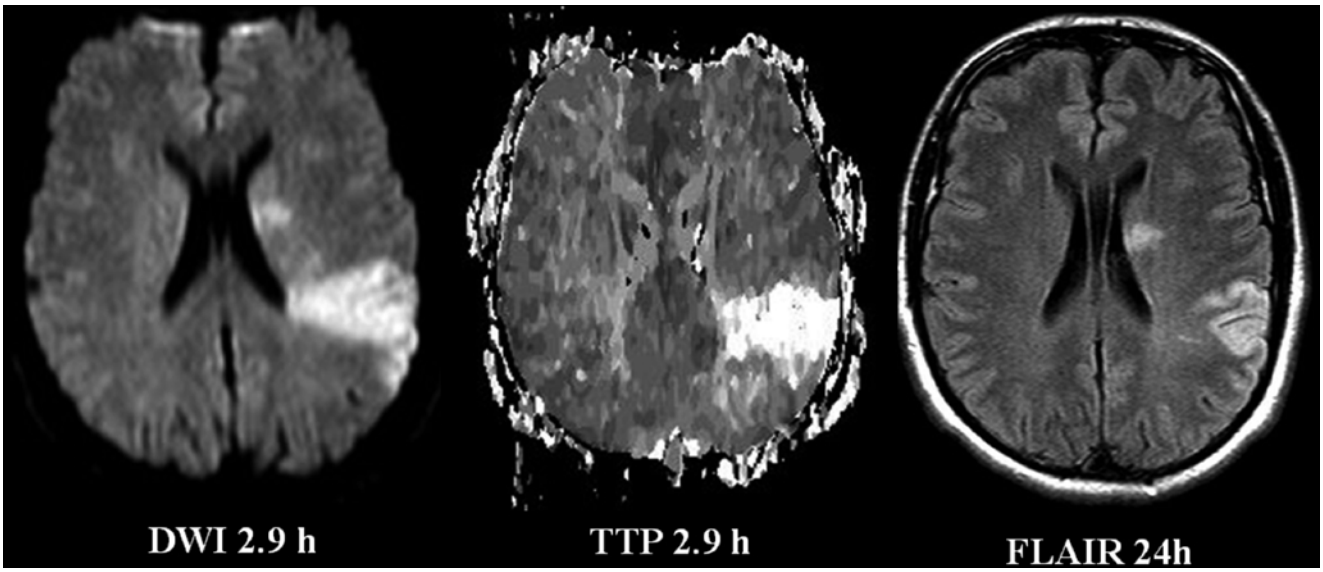

Fig. 5 Partial normalization of a DWI lesion after TPA

Imaging of the Penumbra and Core

The "penumbra" in acute ischemic stroke patients is defined as brain tissue with loss of electric activity and potential recovery after timely recanalization of the occluded artery [6]. This penumbra is the target of therapeutic approaches such as systemic thrombolysis or mechanical recanalization to save this brain tissue by early recanalization. Thus, the identification of a penumbra is important to exclude patients without salvageable tissue from a potentially harmful treatment. Tissue at risk as defined by function and metabolism can be visualized using positron emission tomography [30]. Because of its higher availability, it was our aim to establish a method to assess cerebral metabolism in stroke patients with MRI. Although patient selection in recent successful endovascular trials was mostly based on CT and CTA, those trials that also included CTA collateral scoring [4, 31] or penumbral selection showed the best clinical outcomes. Whether to include collateral assessment or perfusion routinely in clinical practice, and the exact method to use, is still controversial [32–34] and will require more trials before a definitive answer is established.

The area of mismatch between perfusion abnormality and restricted diffusion was suggested as brain tissue at risk of irreversible infarction but with the potential to recover after reperfusion. This concept to identify the penumbra with MRI has raised high hopes to prolong the narrow 3–4.5 h time window for intravenous thrombolysis [35]. Even if the "mismatch concept" (lesion growth if PI > DWI) shows positive results in clinical trials, there is growing evidence that it only represents a very rough approximation of the true salvageable tissue. This mismatch approach is primarily based on tissue perfusion and appears to be an oversimplification: perfusion imaging is inherently unable to discriminate between benign oligemia and penumbra.

It is widely accepted that acute ischemic strokes with smaller core infarct volumes have better outcomes. In opposition, baseline larger core infarcts are associated with worse clinical outcome, even with intra-arterial treatment and despite the recanalization rate, with larger infarct areas and increased risk for symptomatic intracranial hemorrhage [19, 36–41].

Moreover, it has been suggested that the major clinical outcome determinant is the size of the core and not the presence of the ischemic penumbra, as the latter can be anticipated as the remaining arterial territory fed by the occluded artery [42, 43]. Therefore, the core identification to select patients with a small core could be sufficient to depict those that will have better prognosis.

Regarding the infarct core assessment, several imaging features have been proposed, with DWI being the best parameter within the acute phase (first 6 h of stroke onset), with both high sensitivity (91–100 %) and specificity (86–100 %) [13, 44]. One should be aware that DWI lesion reversibility may occur in 8–44 % of cases [27, 28, 45–47] depending on the duration of the stroke and ADC decrease magnitude. However, this potential reversibility may not be consistently associated with improved clinical outcomes nor with changes in the treatment decision [27, 48, 49], and the real reversibility could be residual in both incidence and amount of tissue involved, as shown in the DEFUSE-EPITHET trial analysis (6.7 % with a median volume of 2.3 cm^3) [50].

For CT and MR perfusion imaging, there is neither well-validated parameter nor threshold to distinguish core,

penumbra, and benign oligemia [20, 51, 52] The thresholds differ significantly between studies reflecting a poor standardization with high variability among study protocols, regions of interest evaluated (generally combined gray/white matter which has distinct perfusions), algorithms, and post-processing techniques, with large sources of variability in parametric quantification and with associated low interobserver reproducibility [20, 51, 53]. Therefore, presently it may not be suitable for systematic patient selection for treatment [32].

MR perfusion (PWI-DSC) may be not appropriate for reliable quantitative perfusion measurements [54, 55], with qualitative assessments being preferable to use. A promising alternative would be the use of arterial spin labeling (ASL), allowing noninvasive and quantitative (CBF) perfusion assessment [56]. However, with the current commercial sequences, the arterial transit time differences introducing quantification errors, the long acquisition times, and the need for high-field scans are among the major current drawbacks for the implementation of this sequence.

Besides DWI for core assessment, CT perfusion parameters have also been used to define core, such as CBF decrease (rCBF reduction greater than 30–45 %) [51, 57, 58], CBV decrease (below 2–2.5 mL/100 g) [51, 59], and MTT increase (above 8.3 s) [60]. Although there is still some debate regarding which is the best CTP parameter to define the infarct core, namely, CBV [58, 61] or CBF [62, 63]decreases, it seems that CBF reduction (rCBF reduction greater than 31 %) may correlate better with the DWI findings [64, 65]. Concerning the penumbra, the most common parameters/thresholds suggested have been the increased T_{max} (PWI-T_{max} longer than 6.5 s and CTP-T_{max} longer than 5.5 s) [66], the MTT increase (longer than 6 to 12–13 s or 145–249 % rMTT of the contralateral) [51, 60, 67], and the decreased CBF (rCBF lower than 66 % or CBF below ~28 ml/100 g/min) [51, 57–59, 65, 68].

It should be emphasized that it is a "snapshot" in time and the arterial ischemic stroke is a continuous dynamic process with multiple parameter fluctuations over time. However, the use of these individualized physiological imaging (core/penumbra/collaterals) could allow better patient selection for treatment within and beyond the time therapeutic window. Other potential uses of core/penumbra imaging include the identification of stroke mimics avoiding unnecessary treatments.

Imaging of the Collateral Circulation

Brain arterial collateral circulation represents an important factor for the AIS clinical outcome, since patients with good collateral circulation (either through the circle of Willis or leptomeningeal anastomosis) have more favorable outcomes [69, 70], presumably by decreasing the size of the area at risk and by increasing the time window for treatment due to reduction of the infarct progression rate.

It has been proposed that collateral circulation pattern is a more stable parameter, being constant over time, meaning that the collateral circulation present (or absent) initially does not change over time, in opposition to perfusion parameters that have a decremental relationship between penumbra and time [71].

Arterial collateral circulation may be assessed by CTA or DSA. There are several classifications grading the collateral circulation between the total absence of collaterals and complete collateral filling of the arterial territory supplied by the occluded artery [72].

Imaging of the Clot

Vessel imaging is mandatory to define the site of occlusion and select patients for intra-arterial treatment. Clot/occlusion location predicts the recanalization rate for intravenous thrombosis, with low recanalization rates for proximal occlusions, namely, ICA-T (4.4 %), M1 (32.3 %), M2 (30.8 %), and basilar (4 %) segments/arteries [10, 73].

As abovementioned, both CTA (sensitivity 98.4 %; specificity 98.1 %) [74–77] and MRA (sensitivity 84–87 %; specificity 85–98 %) [74, 78] have been shown to be highly accurate for the detection of arterial occlusion. CTA has some diagnostic accuracy compared with MRA[75, 78].

Additionally, both clot length and type have shown prognostic value. Clots with lengths over 8 mm and/or that are hypodense (fibrin-rich) compared to a smaller and hyperdense (red blood cell-rich) thrombus have lower recanalization with IV thrombolysis [18, 79, 80].

Role of Microbleeds

Anecdotal case reports describe patients with cerebral microbleeds (CMBs) who developed catastrophic post-ischemic hemorrhage related or unrelated to therapy. Histopathological studies suggest that most focal areas of MRI signal loss on T2*w scans indicate focal hemosiderin deposition from previous small bleeds. Differential diagnosis of CMBs, however, also includes microcalcifications and even the release of prosthetic heart valve material which both certainly do not increase the risk for secondary brain hemorrhage after ischemic stroke. The distribution of CMBs is very similar to the usual sites of ICH and the existence of higher numbers of CMB represents an independent factor for the overall incidence of ICH. Based on these observations it has been hypothesized that CMB may represent an independent risk factor

for devastating hemorrhage after thrombolytic therapy. Based on the data of a large multicenter study (BRASIL) [81], a minor increase in hemorrhage risk cannot be ruled out. Based on data from thirteen high-volume stroke centers, BRASIL represents the highest available level of evidence on the prognostic value of CMBs for clinically relevant secondary bleeding complications in acute ischemic stroke patients after thrombolytic therapy. The data suggest that even the maximal risk estimate of hemorrhage in the presence of CMBs does not exceed the benefit of thrombolytic treatment as expected from the literature. A conclusion about the rare patients with multiple CMBs cannot be derived.

Conclusions

Imaging is essential in AIS treatment for patient selection. Nowadays, parenchymal and vascular imaging are mandatory, either by CT or MRI depending on the local availability.

Advanced stroke CT and MRI protocols provide precise information about individual stroke pathophysiology. Individual assessment can improve patient selection for the most invasive treatment techniques.

Interpretation requires careful consideration of physiology, image construction, and post-processing factors. Simple ideas such as the "mismatch concept" can be misleading in a particular patient.

Acknowledgments The authors acknowledge the contribution of Prof Dr Jens Fiehler for his generous contributions to the manuscript, figures, and concepts.

References

1. Berkhemer OA, Fransen PSS, Beumer D, van den Berg LA, Lingsma HF, Yoo AJ et al (2015) A randomized trial of intraarterial treatment for acute ischemic stroke. N Engl J Med 372(1):11–20
2. Saver JL, Goyal M, Bonafe A, Diener H-C, Levy EI, Pereira VM et al (2015) Stent-retriever thrombectomy after intravenous t-PA vs. t-PA alone in stroke. N Engl J Med 372(24):2285–2295
3. Jovin TG, Chamorro A, Cobo E, de Miquel MA, Molina CA, Rovira A et al (2015) Thrombectomy within 8 hours after symptom onset in ischemic stroke. N Engl J Med 372(24):2296–2306
4. Goyal M, Demchuk AM, Menon BK, Eesa M, Rempel JL, Thornton J et al (2015) Randomized assessment of rapid endovascular treatment of ischemic stroke. N Engl J Med 372(11):1019–1030
5. Campbell BCV, Mitchell PJ, Kleinig TJ, Dewey HM, Churilov L, Yassi N et al (2015) Endovascular therapy for ischemic stroke with perfusion-imaging selection. N Engl J Med 372(11):1009–1018
6. Muir KW, Buchan A, von Kummer R, Röther J, Baron J-C (2006) Imaging of acute stroke. Lancet Neurol 5(9):755–768
7. Wintermark M, Rowley HA, Lev MH (2009) Acute stroke triage to intravenous thrombolysis and other therapies with advanced CT or MR imaging: pro CT. Radiology 251(3):619–626
8. Köhrmann M, Schellinger PD (2009) Acute stroke triage to intravenous thrombolysis and other therapies with advanced CT or MR imaging: pro MR imaging. Radiology 251(3):627–633
9. Saver JL (2006) Time is brain--quantified. Stroke 37(1):263–266
10. Jauch EC, Saver JL, Adams HP, Bruno A, Connors JJB, Demaerschalk BM et al (2013) Guidelines for the early management of patients with acute ischemic stroke: a guideline for healthcare professionals from the American Heart Association/American Stroke Association. Stroke 44:870–947
11. Rowley HA (2013) The alphabet of imaging in acute stroke: does it spell improved selection and outcome? Stroke 44(6 Suppl 1):S53–S54
12. Salottolo KM, Fanale CV, Leonard KA, Frei DF, Bar-Or D (2011) Multimodal imaging does not delay intravenous thrombolytic therapy in acute stroke. Am J Neuroradiol 32(5):864–868
13. Latchaw RE, Alberts MJ, Lev MH, Connors JJ, Harbaugh RE, Higashida RT et al (2009) Recommendations for imaging of acute ischemic stroke: a scientific statement from the American Heart Association. Stroke 40(11):3646–3678
14. Hill MD, Rowley HA, Adler F, Eliasziw M, Furlan A, Higashida RT et al (2003) Selection of acute ischemic stroke patients for intra-arterial thrombolysis with pro-urokinase by using ASPECTS. Stroke 34(8):1925–1931
15. Puetz V, Sylaja PN, Coutts SB, Hill MD, Dzialowski I, Mueller P et al (2008) Extent of hypoattenuation on CT angiography source images predicts functional outcome in patients with basilar artery occlusion. Stroke 39(9):2485–2490
16. Puetz V, Khomenko A, Hill MD, Dzialowski I, Michel P, Weimar C et al (2011) Extent of hypoattenuation on CT angiography source images in basilar artery occlusion: prognostic value in the Basilar Artery International Cooperation Study. Stroke 42(12):3454–3459
17. Kimura K, Sakamoto Y, Aoki J, Iguchi Y, Shibazaki K, Inoue T (2011) Clinical and MRI predictors of no early recanalization within 1 hour after tissue-type plasminogen activator administration. Stroke 42(11):3150–3155
18. Riedel CH, Zimmermann P, Jensen-Kondering U, Stingele R, Deuschl G, Jansen O (2011) The importance of size: successful recanalization by intravenous thrombolysis in acute anterior stroke depends on thrombus length. Stroke 42(6):1775–1777
19. Lansberg MG, Straka M, Kemp S, Mlynash M, Wechsler LR, Jovin TG et al (2012) MRI profile and response to endovascular reperfusion after stroke (DEFUSE 2): a prospective cohort study. Lancet Neurol 11(10):860–867
20. Dani KA, Thomas RGR, Chappell FM, Shuler K, Muir KW, Wardlaw JM (2012) Systematic review of perfusion imaging with computed tomography and magnetic resonance in acute ischemic stroke: heterogeneity of acquisition and postprocessing parameters: a translational medicine research collaboration multicentre acute stroke imaging study. Stroke 43(2):563–566
21. Lansberg MG, Lee J, Christensen S, Straka M, De Silva DA, Mlynash M et al (2011) RAPID automated patient selection for reperfusion therapy: a pooled analysis of the Echoplanar Imaging Thrombolytic Evaluation Trial (EPITHET) and the Diffusion and Perfusion Imaging Evaluation for Understanding Stroke Evolution (DEFUSE) Study. Stroke 42(6):1608–1614
22. Mlynash M, Lansberg MG, De Silva DA, Lee J, Christensen S, Straka M et al (2011) Refining the definition of the malignant profile: insights from the DEFUSE-EPITHET pooled data set. Stroke 42(5):1270–1275
23. Olivot J-M, Albers GW (2011) Diffusion-perfusion MRI for triaging transient ischemic attack and acute cerebrovascular syndromes. Curr Opin Neurol 24(1):44–49
24. Rowley HA (2005) Extending the time window for thrombolysis: evidence from acute stroke trials. Neuroimaging Clin N Am 15(3):575–587, x
25. Thomalla G, Cheng B, Ebinger M, Hao Q, Tourdias T, Wu O et al (2011) DWI-FLAIR mismatch for the identification of patients with acute ischaemic stroke within 4·5 h of symptom onset (PRE-FLAIR): a multicentre observational study. Lancet Neurol 10(11):978–986

26. Kucinski T, Majumder A, Knab R, Naumann D, Fiehler J, Väterlein O et al (2004) Cerebral perfusion impairment correlates with the decrease of CT density in acute ischaemic stroke. Neuroradiology 46(9):716–722
27. Fiehler J, Knudsen K, Kucinski T, Kidwell CS, Alger JR, Thomalla G et al (2004) Predictors of apparent diffusion coefficient normalization in stroke patients. Stroke 35(2):514–519
28. Fiehler J, Foth M, Kucinski T, Knab R, von Bezold M, Weiller C et al (2002) Severe ADC decreases do not predict irreversible tissue damage in humans. Stroke 33(1):79–86
29. Yoo AJ, Pulli B, Gonzalez RG (2011) Imaging-based treatment selection for intravenous and intra-arterial stroke therapies: a comprehensive review. Expert Rev Cardiovasc Ther 9(7):857–876
30. Baron JC (2001) Mapping the ischaemic penumbra with PET: a new approach. Brain 124(Pt 1):2–4
31. Menon BK, d'Esterre CD, Qazi EM, Almekhlafi M, Hahn L, Demchuk AM et al (2015) Multiphase CT angiography: a New tool for the imaging triage of patients with acute ischemic stroke. Radiology 275(2):510–520
32. Gonzalez RG (2012) Low signal, high noise and large uncertainty make CT perfusion unsuitable for acute ischemic stroke patient selection for endovascular therapy. J NeuroIntervent Surg 4(4):242–245
33. Gonzalez RG, Copen WA, Schaefer PW, Lev MH, Pomerantz SR, Rapalino O et al (2013) The Massachusetts General Hospital acute stroke imaging algorithm: an experience and evidence based approach. J NeuroIntervent Surg 5(Supplement 1):i7–i12
34. Schaefer PW, Souza L, Kamalian S, Hirsch JA, Yoo AJ, Kamalian S et al (2015) Limited reliability of computed tomographic perfusion acute infarct volume measurements compared with diffusion-weighted imaging in anterior circulation stroke. Stroke 46(2):419–424
35. Hacke W, Kaste M, Bluhmki E, Brozman M, Dávalos A, Guidetti D et al (2008) Thrombolysis with alteplase 3 to 4.5 hours after acute ischemic stroke. N Engl J Med 359(13):1317–1329
36. Singer OC, Humpich MC, Fiehler J, Albers GW, Lansberg MG, Kastrup A et al (2008) Risk for symptomatic intracerebral hemorrhage after thrombolysis assessed by diffusion-weighted magnetic resonance imaging. Ann Neurol 63(1):52–60
37. Lansberg MG, Thijs VN, Bammer R, Kemp S, Wijman CAC, Marks MP et al (2007) Risk factors of symptomatic intracerebral hemorrhage after tPA therapy for acute stroke. Stroke 38(8):2275–2278
38. Yoo AJ, Verduzco LA, Schaefer PW, Hirsch JA, Rabinov JD, Gonzalez RG (2009) MRI-based selection for intra-arterial stroke therapy: value of pretreatment diffusion-weighted imaging lesion volume in selecting patients with acute stroke who will benefit from early recanalization. Stroke 40(6):2046–2054
39. Yoo AJ, Barak ER, Copen WA, Kamalian S, Gharai LR, Pervez MA et al (2010) Combining acute diffusion-weighted imaging and mean transmit time lesion volumes with National Institutes of Health Stroke Scale Score improves the prediction of acute stroke outcome. Stroke 41(8):1728–1735
40. Olivot J-M, Mosimann PJ, Labreuche J, Inoue M, Meseguer E, Desilles J-P et al (2013) Impact of diffusion-weighted imaging lesion volume on the success of endovascular reperfusion therapy. Stroke 44(8):2205–2211
41. Sanák D, Nosál V, Horák D, Bártková A, Zelenák K, Herzig R et al (2006) Impact of diffusion-weighted MRI-measured initial cerebral infarction volume on clinical outcome in acute stroke patients with middle cerebral artery occlusion treated by thrombolysis. Neuroradiology 48(9):632–639
42. Jovin TG, Yonas H, Gebel JM, Kanal E, Chang Y-F, Grahovac SZ et al (2003) The cortical ischemic core and not the consistently present penumbra is a determinant of clinical outcome in acute middle cerebral artery occlusion. Stroke 34(10):2426–2433
43. Hakimelahi R, Yoo AJ, He J, Schwamm LH, Lev MH, Schaefer PW et al (2012) Rapid identification of a major diffusion/perfusion mismatch in distal internal carotid artery or middle cerebral artery ischemic stroke. BMC Neurol 12:132
44. Schellinger PD, Bryan RN, Caplan LR, Detre JA, Edelman RR, Jaigobin C et al (2010) Evidence-based guideline: The role of diffusion and perfusion MRI for the diagnosis of acute ischemic stroke: report of the Therapeutics and Technology Assessment Subcommittee of the American Academy of Neurology. Neurology 75:177–185
45. Kidwell CS, Saver JL, Mattiello J, Starkman S, Vinuela F, Duckwiler G et al (2000) Thrombolytic reversal of acute human cerebral ischemic injury shown by diffusion/perfusion magnetic resonance imaging. Ann Neurol 47(4):462–469
46. Guadagno JV, Warburton EA, Jones PS, Fryer TD, Day DJ, Gillard JH et al (2005) The diffusion-weighted lesion in acute stroke: heterogeneous patterns of flow/metabolism uncoupling as assessed by quantitative positron emission tomography. Cerebrovasc Dis 19(4):239–246
47. Kranz PG, Eastwood JD (2009) Does diffusion-weighted imaging represent the ischemic core? An evidence-based systematic review. Am J Neuroradiol 30(6):1206–1212
48. Chalela JA, Kang D-W, Luby M, Ezzeddine M, Latour LL, Todd JW et al (2004) Early magnetic resonance imaging findings in patients receiving tissue plasminogen activator predict outcome: Insights into the pathophysiology of acute stroke in the thrombolysis era. Ann Neurol 55(1):105–112
49. Chemmanam T, Campbell BCV, Christensen S, Nagakane Y, Desmond PM, Bladin CF et al (2010) Ischemic diffusion lesion reversal is uncommon and rarely alters perfusion-diffusion mismatch. Neurology 75(12):1040–1047
50. Campbell BCV, Purushotham A, Christensen S, Desmond PM, Nagakane Y, Parsons MW et al (2012) The infarct core is well represented by the acute diffusion lesion: sustained reversal is infrequent. J Cereb Blood Flow amp Metab 32(1):50–56
51. Dani KA, Thomas RGR, Chappell FM, Shuler K, MacLeod MJ, Muir KW et al (2011) Computed tomography and magnetic resonance perfusion imaging in ischemic stroke: definitions and thresholds. Ann Neurol 70(3):384–401
52. Kidwell CS (2013) MRI biomarkers in acute ischemic stroke: a conceptual framework and historical analysis. Stroke 44(2):570–578
53. Fiorella D, Heiserman J, Prenger E, Partovi S (2004) Assessment of the reproducibility of postprocessing dynamic CT perfusion data. AJNR Am J Neuroradiol 25(1):97–107
54. Carroll TJ, Teneggi V, Jobin M, Squassante L, Treyer V, Hany TF et al (2002) Absolute quantification of cerebral blood flow with magnetic resonance, reproducibility of the method, and comparison with H2(15)O positron emission tomography. J Cereb Blood Flow Metab 22(9):1149–1156
55. Wintermark M, Albers GW, Alexandrov AV, Alger JR, Bammer R, Baron JC et al (2008) Acute Stroke Imaging Research Roadmap. Stroke 39(5):1621–1628
56. Bivard A, Krishnamurthy V, Stanwell P, Levi C, Spratt NJ, Davis S et al (2014) Arterial spin labeling versus bolus-tracking perfusion in hyperacute stroke. Stroke 45(1):127–133
57. Bivard A, Levi C, Spratt N, Parsons M (2013) Perfusion CT in acute stroke: a comprehensive analysis of infarct and penumbra. Radiology 267(2):543–550
58. Wintermark M, Flanders AE, Velthuis B, Meuli R, van Leeuwen M, Goldsher D et al (2006) Perfusion-CT assessment of infarct core and penumbra: receiver operating characteristic curve analysis in 130 patients suspected of acute hemispheric stroke. Stroke 37(4):979–985
59. Wintermark M, Reichhart M, Thiran J-P, Maeder P, Chalaron M, Schnyder P et al (2002) Prognostic accuracy of cerebral blood flow

measurement by perfusion computed tomography, at the time of emergency room admission, in acute stroke patients. Ann Neurol 51(4):417–432
60. Butcher K, Parsons M, Baird T, Barber A, Donnan G, Desmond P et al (2003) Perfusion thresholds in acute stroke thrombolysis. Stroke 34(9):2159–2164
61. Schaefer PW, Barak ER, Kamalian S, Gharai LR, Schwamm L, Gonzalez RG et al (2008) Quantitative assessment of core/penumbra mismatch in acute stroke: CT and MR perfusion imaging are strongly correlated when sufficient brain volume is imaged. Stroke 39(11):2986–2992
62. Bivard A, McElduff P, Spratt N, Levi C, Parsons M (2011) Defining the extent of irreversible brain ischemia using perfusion computed tomography. Cerebrovasc Dis 31(3):238–245
63. Bivard A, Levi C, Krishnamurthy V, Hislop-Jambrich J, Salazar P, Jackson B, Davis S, Parsons M (2014) Defining acute ischemic stroke tissue pathophysiology with whole brain CT perfusion. J Neuroradiol 41(5):307–315
64. Kamalian S, Kamalian S, Maas MB, Goldmacher GV, Payabvash S, Akbar A et al (2011) CT cerebral blood flow maps optimally correlate with admission diffusion-weighted imaging in acute stroke but thresholds vary by postprocessing platform. Stroke 42(7):1923–1928
65. Campbell BCV, Christensen S, Levi CR, Desmond PM, Donnan GA, Davis SM et al (2011) Cerebral blood flow is the optimal CT perfusion parameter for assessing infarct core. Stroke 42(12):3435–3440
66. Olivot J-M, Mlynash M, Thijs VN, Kemp S, Lansberg MG, Wechsler L et al (2009) Optimal Tmax threshold for predicting penumbral tissue in acute stroke. Stroke 40(2):469–475
67. Kamalian S, Kamalian S, Konstas AA, Maas MB, Payabvash S, Pomerantz SR et al (2012) CT perfusion mean transit time maps optimally distinguish benign oligemia from true "at-risk" ischemic penumbra, but thresholds vary by postprocessing technique. Am J Neuroradiol 33(3):545–549
68. Cenic A, Nabavi DG, Craen RA, Gelb AW, Lee T-Y (1999) Dynamic CT measurement of cerebral blood flow: a validation study. AJNR Am J Neuroradiol 20(1):63–73
69. Souza LCS, Yoo AJ, Chaudhry ZA, Payabvash S, Kemmling A, Schaefer PW et al (2012) Malignant CTA collateral profile is highly specific for large admission DWI infarct core and poor outcome in acute stroke. Am JNeuroradiol 33(7):1331–1336
70. Angermaier A, Langner S, Kirsch M, Kessler C, Hosten N, Khaw AV (2011) CT-angiographic collateralization predicts final infarct volume after intra-arterial thrombolysis for acute anterior circulation ischemic stroke. Cerebrovasc Dis 31(2):177–184
71. Agarwal S (2015) Is CT-based perfusion and collateral imaging sensitive to time since stroke onset? Front Neurol 6:1–7
72. Tan JC, Dillon WP, Liu S, Adler F, Smith WS, Wintermark M (2007) Systematic comparison of perfusion-CT and CT-angiography in acute stroke patients. Ann Neurol 61(6):533–543
73. Bhatia R, Hill MD, Shobha N, Menon B, Bal S, Kochar P et al (2010) Low rates of acute recanalization with intravenous recombinant tissue plasminogen activator in ischemic stroke: real-world experience and a call for action. Stroke 41(10):2254–2258
74. Vilela P, Goulão A (2005) Ischemic stroke: carotid and vertebral artery disease. Eur Radiol 15(3):427–433
75. Lev MH, Farkas J, Rodriguez VR, Schwamm LH, Hunter GJ, Putman CM et al (2001) CT angiography in the rapid triage of patients with hyperacute stroke to intraarterial thrombolysis: accuracy in the detection of large vessel thrombus. J Comput Assist Tomogr 25(4):520–528
76. Shrier DA, Tanaka H, Numaguchi Y, Konno S, Patel U, Shibata D (1997) CT angiography in the evaluation of acute stroke. AJNR Am J Neuroradiol 18(6):1011–1020
77. Knauth M, von Kummer R, Jansen O, Hähnel S, Dörfler A, Sartor K (1997) Potential of CT angiography in acute ischemic stroke. AJNR Am J Neuroradiol 18(6):1001–1010
78. Bash S, Villablanca JP, Jahan R, Duckwiler G, Tillis M, Kidwell C et al (2005) Intracranial vascular stenosis and occlusive disease: evaluation with CT angiography, MR angiography, and digital subtraction angiography. AJNR Am J Neuroradiol 26(5):1012–1021
79. Kim EY, Heo JH, Lee SK, Kim DJ, Suh S-H, Kim J et al (2006) Prediction of thrombolytic efficacy in acute ischemic stroke using thin-section noncontrast CT. Neurology 67(10):1846–1848
80. Moftakhar P, English JD, Cooke DL, Kim WT, Stout C, Smith WS et al (2013) Density of thrombus on admission CT predicts revascularization efficacy in large vessel occlusion acute ischemic stroke. Stroke 44(1):243–245
81. Fiehler J, Albers GW, Boulanger J-M, Derex L, Gass A, Hjort N et al (2007) Bleeding risk analysis in stroke imaging before thromboLysis (BRASIL): pooled analysis of T2*-weighted magnetic resonance imaging data from 570 patients. Stroke 38(10):2738–2744

Haemorrhagic Vascular Pathologies: Imaging for Haemorrhagic Stroke

James V. Byrne

Introduction

This tutorial will cover the types of intracranial haemorrhage, their appearances on CT and MRI and their causes. The term haemorrhagic stroke is used to distinguish acute bleeding from brain dysfunction due to ischaemic stroke and cerebral infarction. Stroke is a common reason for scanning patients and the most likely reason for a patient with spontaneous intracranial bleeding being referred for imaging. Teaching will focus on this indication but include other causes of spontaneous intracranial haemorrhage and the diagnosis (or exclusion) of a causative vascular pathology.

The causes of first-ever stroke have been shown to be ischaemic in 80 % and haemorrhagic in 20 %. The latter group includes intracerebral haemorrhage (ICH), subarachnoid haemorrhage (SAH) and intraventricular haemorrhage (IVH) or combinations of haematomas in these compartments. This tutorial will primarily consider the imaging involved in the management of these patients and not other issues relevant only to patients with ischaemic stroke.

Once a CT scan has shown acute intracranial haemorrhage, we need to consider its likely cause and its implications to the further clinical management. This process puts the radiologist in a central position to advise on further investigations and patient management. We will therefore be considering how to construct logical differential diagnosis of the possible pathologies causing the haemorrhage and the most appropriate investigation pathway.

J.V. Byrne
Nuffield Department of Surgical Sciences,
Oxford University, West Wing, John Radcliffe Hospital,
Headley Way, Oxford, Oxon OX7 5LJ, UK
e-mail: James.byrne@nds.ox.ac.uk

Using the Clinical History to Determine the Cause of Haemorrhage

Spontaneous intracranial haemorrhage can be broadly separated into two clinical syndromes: intracerebral and subarachnoid haemorrhages. The former is frequently indistinguishable from ischaemic stroke, and we rely on imaging to make the distinction. However, before considering the imaging and its role in diagnosing patients with haemorrhagic vascular pathologies, we should review the data available when the patient is first referred to radiology.

Obtaining an accurate clinical history and details of any abnormal physical findings on the medical examination is the crucial first step in diagnosis of the cause of bleeding. A history of trauma may simplify the analysis of the imaging, but if patients are discovered unconscious and there is no witness to confirm trauma as being the primary event, evidence of a head injury does not help because the patient may have fallen and sustained trauma as a result of the ictal event. In practice different types of spontaneous intracranial haemorrhage are associated with different patterns of clinical presentation. Being aware of the events leading to the patient's transfer to hospital and their timing helps interpretation of the subsequent imaging.

Presenting Symptoms and Signs of Intracerebral Haemorrhage Versus Subarachnoid Haemorrhage

The classic presentation of an intracerebral haemorrhage (ICH), i.e. parenchymal haemorrhage, is rapid onset of focal neurological deficit. Patients are generally quickly aware of symptoms such as hemiparesis and dysphasia but may initially ignore hemianopia and less dramatic neurological symptoms particularly those involving an element of neglect. Spontaneous ICH occurs over a variable period, and symptoms may not become apparent until the haematoma has caused a rise in intracranial pressure. It therefore may take

J. Hodler et al. (eds.), *Diseases of the Brain, Head and Neck, Spine 2016–2019: Diagnostic Imaging*, DOI 10.1007/978-3-319-30081-8_6

minutes or hours before the individual develops abnormal neurological symptoms. A distinguishing feature of the history of onset after ICH is that patients rarely present on awakening from sleep, unlike those with ischaemic stroke.

The classic presentation of subarachnoid haemorrhage (SAH) is acute sudden onset headache. This is described by patients as their worse ever headache and is frequently accompanied by nausea. The patient may lose consciousness, vomit and develop a neurological deficit. They show signs of meningism (e.g. neck stiffness) on examination and may complain of photophobia and back pain. Uncommonly, the headache is less severe and initially ignored, and patients present after a few days because it is persistent or worsens after rebleeding. The severity of presenting symptoms usually reflects the amount of haemorrhage (often termed the 'blood load') and whether it extends into the ventricles to cause acute hydrocephalus:

(a) Loss of consciousness.
The ICH patient rarely initially collapses but shows signs of confusion followed by impaired level of consciousness (LOC). This is often accompanied by headache, nausea, vomiting and elevated systemic blood pressure. In the Harvard Stroke Registry, 50–60 % of ICH patients presented with a progressive neurological deficit. This is unlike the onset of neurological deficits due to most ischaemic strokes or SAH due to rupture of an intracranial aneurysm (unless the patient develops secondary hydrocephalus). It is probably that progression of neurological deficits in ICH patients is due to continued bleeding during this hyperacute stage.
(b) Headache.
Headache is virtually universal after SAH and relatively common after ICH. In ICH it occurs in ca. 40 % of patients, compared with ca. 17 % of patients with ischemic stroke.
(c) Vomiting.
Nausea and vomiting are common features of all types of spontaneous intracranial haemorrhage. In the Harvard Stroke Registry, vomiting was recorded in 49 % of ICH patients and in 45 % of SAH patients but in only 2 % of patients after ischaemic stroke. It is particularly common if haemorrhage occurs in the posterior fossa.
(d) Seizures.
Ictal seizures are seizures occurring within 24–48 h of the onset of spontaneous intracranial haemorrhage. They may affect patients after both SAH (ca. 10–12 %) and ICH (ca. 6–10 %).

Other Important History Data

In addition to obtaining a general medical history with details of any pre-existing cardiovascular disease and enquiries concerning trauma as the possible cause of ICH, it is important to establish the patient's medication history and details of any illicit drug-taking. In particular, this should include questions about therapeutic anticoagulants or antiplatelet prescriptions as well as enquiry about possible abuse of drugs in young patients. A family history of intracranial aneurysms is important after SAH. Systemic hypertension is frequent after both SAH and ICH, since Bp levels may be raised as a response to increased intracranial pressure (ICP). It is found in up to 90 % of ICH victims but may have predated the haemorrhage.

Imaging the Patient with Spontaneous Intracranial Haemorrhage

Though the details of the patient's acute and past medical histories may point to the cause of intracranial bleeding, it is imaging that distinguishes the victims of haemorrhagic from those with ischaemic stroke. This crucial distinction triggers different diagnostic and therapeutic management paths and is made by the emergency CT brain scan. The intention of this tutorial is to describe the author's protocols for identifying aetiological vascular pathologies, but the immediate imperative is to diagnose lesions that require emergency interventions to prevent fatal rises in intracranial pressure or rebleeding. These may involve the neurosurgical haematoma evacuation, shunting for hydrocephalus and identification and embolisation of ruptured aneurysms. It is therefore important for further imaging to be appropriate and timely.

The first step is to triage patients into those likely to have an underlying structural lesion from those that do not. Identifying such lesions is important because they may complicate surgical evacuation of haematoma or make the patient more likely to suffer rebleeding. Patients with 'nonstructural' causes still require urgent diagnosis and treatment, but this process involves identifying those with little likelihood of rebleeding from an underlying vascular lesion and will not require urgent interventions. This process starts with an unenhanced CT brain scan and is summarised on the flow diagram below (Fig. 1).

The scheme outlined is based on deciding the primary site and distribution of haemorrhage, i.e. whether it is within the brain (ICH) or in an extra-cerebral compartment (subarachnoid, intraventricular or subdural). In many instances, haemorrhage may have extended into more than one compartment. The scan should be read with this possibility in mind because identifying the origin of bleeding helps to determine if a structural vascular pathology is present.

Causes of Intracranial Haemorrhage

The causes of spontaneous (i.e. non-traumatic) bleeding will be considered according to the primary site of haemorrhage:

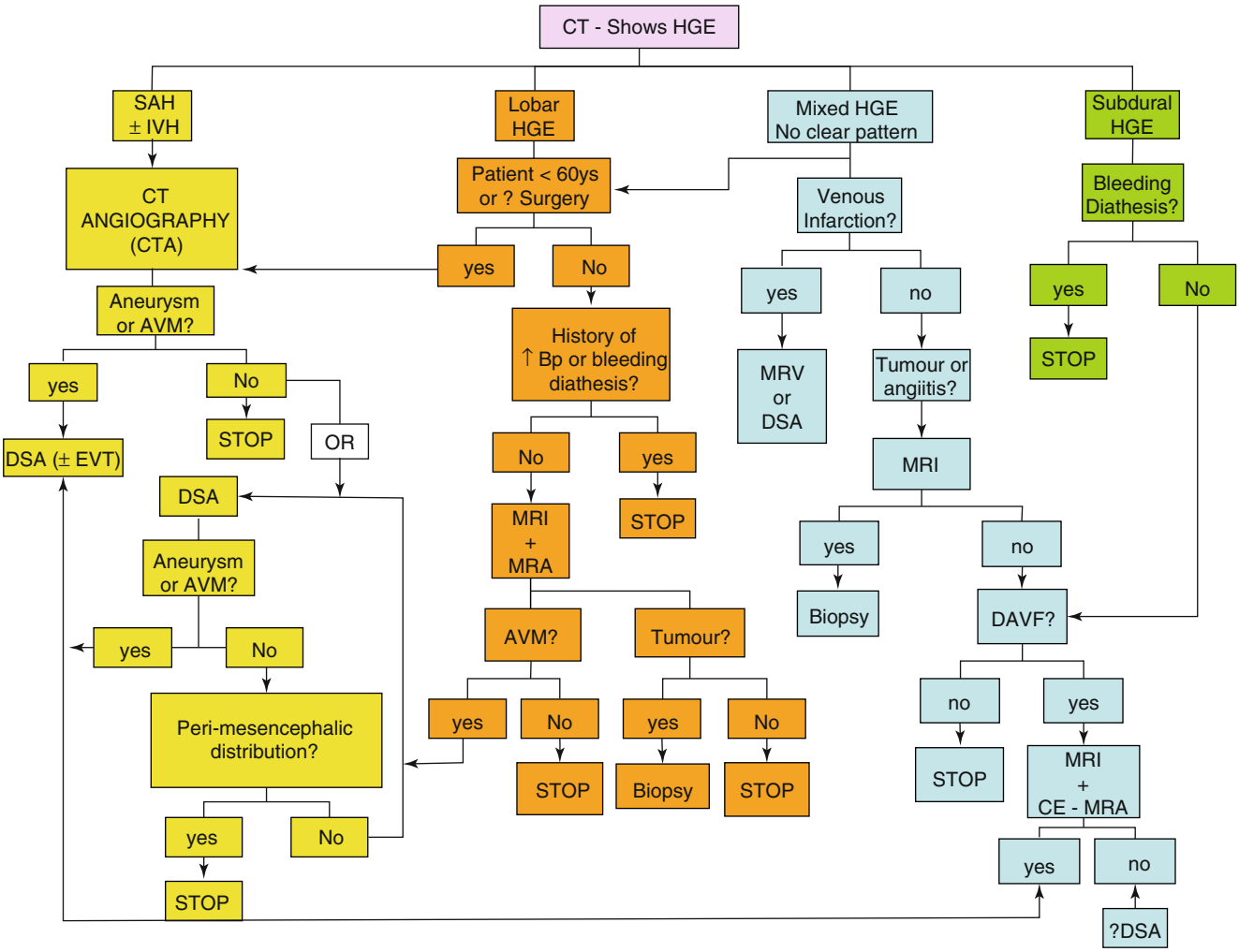

Fig. 1 Protocols for the investigation of patients after spontaneous intracranial haemorrhage

(a) ***Intracerebral haemorrhage***

Causes by location:

- **Basal ganglia/thalamus:**
  Atherosclerosis associated with systemic hypertension
  Leukoaraiosis with microbleeds
  Cerebral vasculitis
  Bleeding diathesis/haematological disorders
  Arteriovenous malformation
  Cavernous malformation
  Moyamoya syndrome
- **Lobar:**
  Haemorrhagic transformation of ischaemic stroke
  Arteriovenous malformation
  Tumour
  Saccular aneurysm (inc. infectious types)
  Venous sinus thrombosis
  Amyloid angiopathy
  Leukoaraiosis with microbleeds
  Cavernous malformation
  Substance abuse, e.g. amphetamine/cocaine abuse
  Iatrogenic (anticoagulants)
  Bleeding diathesis/haematological disorders
  Hereditary haemorrhagic telangiectasia
- **Cerebellum and brain stem:**
  Atherosclerosis associated with systemic hypertension
  Arteriovenous malformation
  Cavernous malformation
  Saccular aneurysm
  Tumour
  Dural arteriovenous malformation
  Capillary telangiectasia
  Bleeding diathesis/haematological disorders

(b) ***Subarachnoid haemorrhage***

Common causes:

Saccular aneurysm
Idiopathic, peri-mesencephalic haemorrhage
Arterial dissection

Rarer causes:

Brain or spinal arteriovenous malformation or fistula
Dural arteriovenous fistula

Pituitary apoplexy
Infectious aneurysms
Collagen disorders: Marfan's syndrome/pseudoxanthoma elasticum
Cocaine abuse
Sickle cell disease (children)
Bleeding diathesis (e.g. excessive anticoagulation)

(c) ***Subdural haemorrhage***
Idiopathic
Rupture of small trans-pial veins
Saccular aneurysm
Moyamoya syndrome
Dural arteriovenous fistula
Dural metastases
Bleeding diathesis/haematological disorders

Indications for Further Imaging

After ICH

It is salutary to remember that the prognosis of haemorrhagic stroke is very poor with 35–52 % of patients dead at 1 month. Of the estimated 67 000 Americans who experienced an ICH in the United States during 2002, only 20 % were functionally independent at 6 months [1].

Outcome has been correlated to the clinical and radiological assessments at presentation and a variety of assessment scores described. A pragmatic system was described by Hemphill et al. [2] in 2001 based on simple to adjudicate criteria. These are neurological examination (2 points for GCS score of 3–4, 1 point for GCS score of 5–12 and 0 points for GCS score of 13–15), patient age (1 point for ≥80 years and 0 point for <80 years), ICH volume (1 point for ≥30 mL and 0 points for <30 mL), the presence of intraventricular haemorrhage (1 point) and infratentorial origin (1 point). In this small study, all patients with scores equal to 5 died and scores equal to 0 survived. Subsequent variations and refinements have confirmed the approach and the prognostic value of haematoma size assessed by CT [3].

The need for catheter angiography to identify a cerebral vascular lesion responsible for the haemorrhage has reduced inversely to increasing confidence in the reliability of CT and MR angiography. In 1991, the Stroke Council of the American Heart Association made the following recommendations [4]:

(a) Angiography should be considered for all patients without a demonstrated cause of haemorrhage in whom surgical evacuation of haematoma is being considered.
(b) Further imaging should be performed in young, normotensive patients.
(c) Angiography is not required for older hypertensive patients with evidence of underlying cerebral vascular disease or with lobar haemorrhage in the basal ganglia, thalamus, cerebellum or brain stem and in whom CT findings do not suggest a structural lesion.
(d) Most older patients with deep haemorrhages die or have severe morbidity related to the haemorrhage and are therefore not candidates for DSA.

This advice has since been modified [2] and now states that

> Indications for catheter angiography include subarachnoid hemorrhage, abnormal calcifications, obvious vascular abnormalities, and blood in unusual locations, such as the sylvian fissure. Angiography may also be indicated in patients with no obvious cause of bleeding, such as those subjects with isolated IVH. The yield of angiography declines in elderly patients with hypertension and a deep hematoma. The timing of the angiogram balances the need for a diagnosis with the condition of the patient and the potential timing of any surgical intervention. A critically ill patient with hemorrhage and herniation may require urgent surgery before angiography, whereas the stable patient with imaging features of an aneurysm or arteriovenous malformation should undergo angiography before any intervention.

In practice this means that emergency DSA is decided on a case-by-case basis.

After SAH

The commonest cause for SAH is trauma. This diagnosis depends on history and CT evidence. In non-traumatic situations, the traditional approach to the investigation of patients presenting after acute SAH is to perform a catheter angiogram (DSA) after confirmation of the diagnosis by CT or CSF sampling by lumbar puncture. Because of the invasive nature of DSA, there was consensus that these steps were necessary to be sure that the patient's headache was in fact due to SAH. In practice the diagnosis may not be so simple because patients that present late (after CT can no longer be relied upon to exclude acute SAH) or local bleeding resulting from the lumbar puncture may contaminate CSF samples. The introduction of high-quality CT angiography (CTA) has changed the situation by providing a low-risk method of imaging arteries of the circle of Willis and excluding aneurysm rupture as the cause for SAH. The technique is considered reliable enough to dispense with DSA prior to neurosurgery by some and prior to EVT by most operators [5].

The author's practice is as follows:

(a) If CTA shows an aneurysm, DSA should be performed as part of an endovascular treatment (EVT) procedure (e.g. coil embolisation) under general anaesthesia and after informed consent for the planned intervention.

(b) If CTA shows an aneurysm for which EVT is not possible, then DSA under local anaesthesia may be required for planning neurosurgical clipping.
(c) If CTA is negative for aneurysm, a DSA is required only if there is a high clinical risk that another structural cause, e.g. dissection or dural arteriovenous malformation was the cause for spontaneous haemorrhage.
(d) If CTA is negative for aneurysm and no arteriovenous is suspected, MRI should be considered.

The current American Heart Association's guidelines [6] are that CT should be performed for suspected SAH (and lumbar puncture for analysis of CSF is strongly recommended when the CT scan is negative). Catheter angiography should be performed in patients with SAH to document the presence and anatomic features of aneurysms. They add that MRA and CTA may be considered when conventional angiography cannot be performed in a timely fashion, thus leaving open the question of whether positive CTA is adequate for preoperative imaging or for excluding a ruptured aneurysm.

After Subdural and Mixed Patterns of Haemorrhage

In situations when the site of primary intracranial haemorrhage is unclear on CT or when it is confined to the subdural or extradural compartments, CTA may be less useful. Atypical lobar haemorrhages, which are cortical based, raise the possibility of venous sinus thrombosis as the cause, and MR venography is generally more useful than CTV or DSA because it is easier to perform and non-invasive. MR with gadolinium enhancement may also show (or exclude) other putative lesions.

MRI After Spontaneous Intracranial Haemorrhage

The adequacy of MR to distinguish acute haemorrhage from ischaemia or infarction in stroke patients was a cause for concern. Over the last decade, its reliability has been established as we understand more about how the MR signal changes after cerebral haemorrhage. Two multicentre studies demonstrated equivalence to CT when scanning within 6 h of acute stroke onset [7, 8]. Furthermore, MRI is also more likely to show underlying causes for bleeding, so it has been adopted in centres with adequate availability.

In this tutorial, we will review the changes in magnetic susceptibility which occur with cerebral haematomas and how these influence images obtained with different examination sequence. The breakdown of the red blood cell and transition phases of red cell haemoglobin to haemosiderin takes place more slowly in the brain than in other tissues. This process changes the apparent magnetic properties of iron within haemoglobin. The timescales and signal characteristics evident on different MR sequences are summarised in Fig. 2, and readers are recommended to study a recent review of this subject by Whanga et al [9].

Summary of Learning Objectives

- Students will learn the role of CT, MRI and DSA in the diagnosis of causes of spontaneous intracranial haemorrhage.
- They will be given illustrative examples of the imaging of patients after bleeding due to a range of vascular pathologies for interpretation.
- This tutorial will emphasise the crucial role of CT as the primary imaging tool and equip students to distinguish primary lobar, subarachnoid, intraventricular and subdural locations of haemorrhage and formulate an appropriate differential diagnosis.

Age of Haemorrhage	Hyper Acute	Acute	Early Subacute	Late Subacute	Chronic
Blood Product	OxyHb	DeoxyHb	I/C MetHb	E/C MetHb	Haemosiderin
T1W	Intermediate	Intermediate	High	High	Low
T2W / FLAIR	High	Low	Low	High	Low
DWI	High	Low	Low	High	Low
ADC	Low-intermediate	Low	Low	Low-intermediate	Low
T2*	Intermediate	Low	Low	Intermediate	Low

Fig. 2 Magnetic resonance signal characteristic at different stages after intracerebral haemorrhage (Adapted from [6]). *OxyHb* oxyhaemoglobin, *DeoxyHb* deoxyhaemoglobin, *IC* intracellular *EC* extracellular, *MetHb* methaemoglobin)

- Students will be taught the evolving imaging features of cerebral haemorrhage over time on CT and MR and the situations when additional imaging is needed.

References

1. Broderick JP, Connolly S, Feldmann E et al (2007) Guidelines for the management of spontaneous intracerebral hemorrhage in adults. Stroke 38:2001–2023
2. Hemphill JC III, Bonovich DC, Besmertis L et al (2001) The ICH score: a simple, reliable grading scale for intracerebral hemorrhage. Stroke 32:891–897
3. Weimar C, Benemann J, Diener HC (2006) Development and validation of the Essen intracerebral haemorrhage score. J Neurol Neurosurg Psychiatry 77(5):601–605
4. Broderick JP et al (1999) Guidelines for the management of spontaneous intracerebral hemorrhage. A statement for healthcare professionals from a special writing group of the Stroke Council, American Heart Association. Stroke 30:905–915
5. Velthuis BK, Van Leeuwen MS, Witkamp TD et al (1999) Computerized tomography angiography in patients with subarachnoid hemorrhage: from aneurysm detection to treatment without conventional angiography. J Neurosurg 91:761–767
6. Jb B, Connolly ES, Batjar HH (2009) Guidelines for the management of aneurysmal subarachnoid hemorrhage. A statement for healthcare professionals from a special writing group of the Stroke Council, American Heart Association. Stroke 40:994–1025
7. Kidwell CS, Chalela JA, Saver JL et al (2004) Comparison of MRI and CT for detection of acute intracerebral hemorrhage. JAMA 292:1823–1830
8. Fiebach JB, Schellinger PD, Gass A et al (2004) (Stroke magnetic resonance imaging is accurate in hyperacute intracerebral hemorrhage: a multicenter study on the validity of stroke imaging. Stroke 35:502–506
9. Whanga JS, Kolbera M, Powell DK et al (2015) Diffusion-weighted signal patterns of intracranial haemorrhage. Clin Radiol 70(8):909–916

Suggestions for Further Reading

Fink JN, Caplan LR (2003) The importance of specific diagnosis in stroke patient management. Magnetic resonance imaging in Stroke. Davis S, Fisher M, Warach S (eds), Cambridge University Press. Cambridge, New York.

Moritani T, Ekholm S, Westesson PL (2009) Diffusion-weighted MR imaging of the brain. Springer, Berlin, Heidelberg

Warlow CP (1996) Stroke. A practical guide to management. Blackwell Science, Oxford

Hemorrhagic Vascular Pathology

Martin Wiesmann

Introduction

Intracranial hemorrhage is a frequent indication for neuroimaging and accounts for about 15 % of all "strokes." The term intracranial hemorrhage includes epidural, subdural, subarachnoid, intracerebral, and intraventricular bleeds. Computed tomography (CT) remains the standard method to detect intracranial hemorrhage although radiologists need also be familiar with the appearance of hematomas using magnetic resonance imaging (MRI).

The first step is to confirm or exclude the presence of a hemorrhage, identify the anatomic compartment it is located in, and approximate the age of the hemorrhage. The next step is to triage patients into those likely to have an underlying cause that requires urgent diagnosis and treatment and those who do not require urgent interventions. To do this, neuroimaging findings need to be considered in combination with the age and medical history of the patient [1–3].

In the setting of acute intracranial hemorrhage, CT angiography can be used to screen for the presence of vascular abnormalities such as intracranial aneurysms, arteriovenous malformations, or dural arteriovenous fistulae. In addition, in cases of parenchymal hemorrhage, CT angiography images may show acute contrast extravasation within the hemorrhage ("spot sign"). This sign has a high specificity to predict hematoma expansion and worsening of the patients' condition, thus allowing for improved therapeutic decision-making [4].

M. Wiesmann
Department of Diagnostic and Interventional Neuroradiology, University Hospital, Technical University of Aachen RWTH, Aachen, Germany
e-mail: mwiesmann@ukaachen.de

Imaging Intracranial Hemorrhage

To understand the appearance of blood clots on CT and MRI, some knowledge on clot formation is helpful. Initially, an intracerebral hematoma consists of intact red blood cells (RBCs) containing mainly oxygen-saturated hemoglobin (oxyhemoglobin, OxyHb). The hemoglobin is then gradually deoxygenated. At 48 h after hemorrhage, the clot consists almost entirely of deoxyhemoglobin (DeoxyHb). The hematoma is surrounded by a rim of edema. In the early subacute phase (3–7 days), DeoxyHb is gradually converted to methemoglobin (MetHb). These changes begin at the periphery of the clot and then progress toward the center. In the late subacute phase (2–4 weeks), the RBCs lyse and MetHb is released from the intracellular into the extracellular space. In this stage the edema gradually dissolves. Later on, in the chronic phase (>4 weeks), the hematoma shrinks to finally form a small cavity, which is often slit like. The cavity often contains ferritin- and hemosiderin-laden macrophages as long-standing markers of bleeding [5–9].

On CT, fresh blood clots typically appear as hyperdense lesions. Only in rare cases of extreme anemia or coagulation disorders, acute hematomas may also appear iso- or even hypodense. Density of blood clots then gradually diminishes to become slightly hypodense at 2–4 weeks after hemorrhage. Typically, clots may appear isodense to the brain at 8–14 days after hemorrhage. Late subacute or chronic hematomas are usually hypodense and may approach cerebrospinal fluid (CSF) in attenuation.

On MR, the signal intensity depends on the sequence used, the predominant degradation product of hemoglobin, and whether the RBCs are still intact (see Table 1).

Subarachnoid hemorrhage can lead to subsequent superficial cortical hemosiderosis. This is an important diagnostic sign to be recognized by radiologists. Its presence can help to suspect prior subarachnoid hemorrhage or to substantiate the differential diagnosis of amyloid angiopathy [2, 5].

J. Hodler et al. (eds.), *Diseases of the Brain, Head and Neck, Spine 2016–2019: Diagnostic Imaging*, DOI 10.1007/978-3-319-30081-8_7

Table 1 CT and MR characteristics of intracranial hemorrhage

Time	NECT	CECT	T1w	T2w	T2*w
Hyperacute (<6 h)	Hyperdense		Iso	Hyper	Hypo
Acute (6 h–3 days)	Hyper		Iso	Hypo	Hypo
Early subacute (3–7 days)	Hyper/iso		Iso (center) Hyper (rim)	Hypo	Hypo
Late subacute (1–4 weeks)	Iso/hypo	Rim enhancement	Hyper	Hyper	Hypo
Chronic (months to years)	Hypo		Hypo	Hypo	Hypo

Density/signal intensity compared to the cortex

NECT non-enhanced CT, *CECT* contrast-enhanced CT

Etiology of Nontraumatic Intracranial Hemorrhage by Age Group and Anatomic Location

Perinatal Hemorrhage

- Premature infants
  - Periventricular – intraventricular hemorrhage:
    Hypoxia may cause hypertension and subsequent rupture of vessels within the germinal matrix.
  - Periventricular leukomalacia (PVL):
    Ischemic infarct causes coagulation necrosis of deep periventricular white matter.
    Subsequent hemorrhage is found in up to 20 % of cases.
- Term infants
  - Traumatic delivery (scalp edema, subgaleal hemorrhage, cephalohematoma, subdural hematoma)
  - Hypoxic-ischemic injury (hemorrhagic transformation in deep gray nuclei, perirolandic hemorrhage)

Subarachnoid Hemorrhage

- Aneurysm
- Arterial dissection
- Angiogram-negative perimesencephalic hemorrhage
- Arteriovenous malformation
- Dural arteriovenous fistulae
- Sickle cell disease (in children)
- Bleeding diathesis (e.g., excessive anticoagulation)

Nontraumatic Subdural Hemorrhage

- Dural arteriovenous fistulae
- Aneurysm
- Moyamoya syndrome
- Dural metastases
- Bleeding diathesis/hematological disorders

Intracerebral Hemorrhage (ICH) in Elderly Adults

- Hypertensive intracerebral hemorrhage
  - Most common cause of nontraumatic ICH in adults
  - Typical locations: putamen/external capsule (60–65 %), thalamus (15–20 %), pons (5–10 %), cerebellum (2–5 %), and hemispheric white matter (1–2 %)
- Cerebral amyloid angiopathy
- Hemorrhagic infarction
- Coagulopathies
- Neoplasms

Intracerebral Hemorrhage (ICH) in Young/Middle-Aged Adults

- Arteriovenous malformations
- Cavernous angioma
- Aneurysms
- Hemorrhagic infarction
- Venous infarction (thrombosis of dural sinus or cortical veins)
- Hypertensive encephalopathies (preeclampsia, renal failure, hemolytic-uremic syndrome)
- Drug abuse (e.g., cocaine)
- Neoplasms

Summary of Learning Intentions

In this presentation students will be taught to distinguish between different anatomical locations of intracranial hemorrhage, as well as to recognize typical CT and MRI patterns of intracranial hemorrhages over time. Imaging strategies to triage patients with intracranial hemorrhage will be discussed. Illustrative examples of typical underlying pathologies will be given.

References

1. Atlas SW (2008) Magnetic resonance imaging of the brain and spine. Lippincott Williams & Wilkins, Baltimore, pp 644–771
2. Falter B, Wiesmann M, Freiherr J et al (2015) Frequency and appearance of hemosiderin depositions after aneurysmal subarachnoid hemorrhage treated by endovascular therapy. Neuroradiology 57:999–1006
3. Huber P (1982) Cerebral angiography. Thieme, Stuttgart/New York
4. Khosravani H, Mayer SA, Demchuk A et al (2013) Emergency noninvasive angiography for acute intracerebral hemorrhage. AJNR Am J Neuroradiol 34:1481–1487
5. Linn J, Herms J, Dichgans M et al (2008) Subarachnoid hemosiderosis and superficial cortical hemosiderosis in cerebral amyloid angiopathy. AJNR Am J Neuroradiol 29:184–186
6. Linn J, Michl S, Katja B et al (2010) Cortical vein thrombosis: the diagnostic value of different imaging modalities. Neuroradiology 52:899–911
7. Linn J, Wiesmann M, Brückmann H (2011) Atlas Klinische Neuroradiologie des Gehirns. Springer, Berlin/Heidelberg, pp 77–192
8. Osborn AG (2010) Osborn's brain: imaging, pathology, and anatomy. Amirsys, Salt Lake City, pp 73–292
9. Wiesmann M, Brückmann H (2004) Magnetic resonance imaging of subarachnoid hemorrhage. RoFo 176:500–505

Acquired Demyelinating Diseases

Àlex Rovira and Kelly K. Koeller

Introduction

Demyelinating disorders of the central nervous system (CNS) have a variety of etiologies and can be separated into primary (e.g., multiple sclerosis (MS) and other idiopathic inflammatory-demyelinating diseases) and secondary (e.g., infectious, ischemic, metabolic, or toxic) diseases. Brain and spinal cord magnetic resonance imaging (MRI) is the imaging modality of choice to assess demyelinating disorders and, together with the clinical and laboratory findings, can accurately classify them in most cases [1–3]. This review will highlight the important imaging manifestations of some acquired demyelinating diseases that allow more specific diagnosis.

Idiopathic Inflammatory-Demyelinating Diseases of the CNS

The term idiopathic inflammatory-demyelinating disease (IIDD) encompasses a broad spectrum of CNS disorders that can be differentiated according to their severity, clinical course, and lesion distribution, as well as their imaging, laboratory, and pathological findings. The spectrum includes monophasic, multiphasic, and progressive disorders, ranging from highly localized forms to multifocal or diffuse variants [2]. Relapsing-remitting and secondary progressive MS are the two most common forms of IIDD. MS can also have a progressive course from onset (primary progressive and progressive-relapsing MS). Fulminant forms of IIDD include a variety of disorders that have in common the severity of the clinical symptoms, an acute clinical course, and atypical findings on MRI. The classic fulminant IIDD is Marburg disease. Balo concentric sclerosis, Schilder disease, and acute disseminated encephalomyelitis (ADEM) can also present with severe, acute attacks.

Some IIDDs have a restricted topographic distribution, as is the case with neuromyelitis optica spectrum disorders (NMOSDs), which can have a monophasic or, more often, a relapsing course.

Multiple Sclerosis

MS is a progressive inflammatory, demyelinating, and neurodegenerative autoimmune disease characterized pathologically by perivascular infiltrates of mononuclear inflammatory cells, demyelination, and axonal loss and gliosis, with the formation of focal and diffuse abnormalities in the brain and spinal cord, mainly affecting the optic nerves, brainstem, spinal cord, and cerebellar and periventricular white matter, although cortical and subcortical gray matter damage is also prominent, resulting in chronic progressive disability for the majority of people with the disorder.

The high sensitivity of MRI in depicting brain and spinal cord demyelinating plaques has made this technique the most important paraclinical tool in current use, not only for the early and accurate diagnosis of MS but also for understanding the natural history of the disease and monitoring and predicting the efficacy of disease-modifying treatments.

MRI is the most sensitive imaging technique for detecting MS plaques throughout the brain and spinal cord. Proton density (PD) or T2-weighted MR images (especially those of fluid-attenuated inversion recovery (FLAIR) sequence) show areas of high signal intensity in the periventricular white matter in 98 % of MS patients. MS plaques are generally round to ovoid in shape and range from a few millimeters to more than one centimeter in diameter. They are typically discrete and focal at the early stages of the disease but become

À. Rovira
Section of Neuroradiology and MR Unit (IDI), Department of Radiology, Hospital Universitari Vall d'Hebron, Autonomous University of Barcelona, Barcelona, Spain
e-mail: Alex.rovira@idi.gencat.cat

K.K. Koeller (✉)
Section of Neuroradiology, Department of Radiology, Mayo Clinic, Rochester, MN, USA
e-mail: Koeller.Kelly@mayo.edu

J. Hodler et al. (eds.), *Diseases of the Brain, Head and Neck, Spine 2016–2019: Diagnostic Imaging*, DOI 10.1007/978-3-319-30081-8_8

confluent as the disease progresses, particularly in the posterior hemispheric periventricular white matter. MS plaques tend to affect the deep white matter rather than the subcortical white matter, whereas small vessel ischemic lesions tend to involve the subcortical white matter more than the periventricular white matter [4, 5]. The total T2 lesion volume of the brain increases by approximately 5 %–10 % each year in the relapsing forms of MS.

Both acute and chronic MS plaques appear hyperintense on T2-weighted sequences, reflecting their increased tissue water content. The signal increase indicates edema, inflammation, demyelination, reactive gliosis, and/or axonal loss in proportions that differ from lesion to lesion. The vast majority of MS patients have at least one ovoid periventricular lesion, whose major axis is oriented perpendicular to the outer surface of the lateral ventricles. The ovoid shape and perpendicular orientation are derived from the perivenular location of the demyelinating plaques noted on histopathology (Dawson's fingers).

MS lesions tend to affect specific regions of the brain, including the periventricular white matter situated superolateral to the lateral angles of the ventricles, the calloso-septal interface along the inferior surface of the corpus callosum, the cortico-juxtacortical regions, and the infratentorial regions. Focal involvement of the periventricular white matter in the anterior temporal lobes is typical for MS and rarely seen in other white matter disorders. The lesions commonly found at the calloso-septal interface are best depicted by sagittal T2-FLAIR images; so this sequence is highly recommended for diagnostic MRI studies.

Histopathological studies have shown that a substantial portion of the total brain lesion load in MS is located within the cerebral cortex. Presently available MRI techniques are not optimal for detecting cortical lesions because of poor contrast resolution between normal-appearing gray matter (NAGM) and the plaques in question and because of the partial volume effects of the subarachnoid spaces and CSF surrounding the cortex. Cortical lesions are better visualized by 2D or 3D T2-FLAIR sequences and newer MR techniques such as 3D double inversion recovery (DIR) MR sequences which selectively suppress the signal from white matter and cerebrospinal fluid (CSF). Juxtacortical lesions that involve the "U" fibers are seen in two-thirds of patients with MS. They are a rather characteristic finding in early stages of the disease and are best detected by T2-FLAIR sequences.

Posterior fossa lesions preferentially involve the floor of the fourth ventricle, the middle cerebellar peduncles, and the brainstem. Most brainstem lesions are contiguous with the cisternal or ventricular CSF spaces and range from large confluent patches to solitary, well-delineated paramedian lesions or discrete "linings" of the CSF border zones. Predilection for these areas is a key feature that helps to identify MS plaques and to differentiate them from focal areas of ischemic demyelination and infarction that preferentially involve the central pontine white matter. Because of their short acquisition time and greater sensitivity, T2-weighted sequences are preferred over T2-FLAIR sequences for detecting posterior fossa lesions [6].

Approximately 10–20 % of T2 hyperintensities are also visible on T1-weighted images as areas of low signal intensity compared with normal-appearing white matter. These so-called T1 black holes have a different pathological substrate that depends, in part, on the lesion age. The hypointensity is present in up to 80 % of recently formed lesions and probably represents marked edema, with or without myelin destruction or axonal loss. In most cases, the acute (or wet) "black holes" become isointense within a few months as inflammatory activity abates, edema resolves, and reparative mechanisms like remyelination become active. Less than 40 % evolve into persisting or chronic black holes [7], which correlate pathologically with the most severe demyelination and axonal loss, indicating areas of irreversible tissue damage. Chronic black holes are more frequent in patients with progressive disease than in those with relapsing-remitting disease and more frequent in the supratentorial white matter as compared with the infratentorial white matter. They are rarely found in the spinal cord and optic nerves.

MS lesions of the spinal cord resemble those in the brain. The lesions can be focal (single or multiple) or diffuse and mainly affect the cervical cord segment. On sagittal scans, the lesions characteristically have a cigar shape and rarely exceed two vertebral segments in length. On cross section, they typically occupy the lateral and posterior white matter columns, extend to involve the central gray matter, and rarely occupy more than one half the cross-sectional area of the spinal cord [8].

Acute spinal cord lesions can produce a mild-to-moderate mass effect with spinal cord swelling and may show contrast enhancement. Active lesions are rarer in the spinal cord than the brain and are almost always associated with new clinical symptoms. The prevalence of spinal cord abnormalities is as high as 74–92 % in established MS and depends on the clinical phenotype of MS. In a clinically isolated syndrome (CIS), the prevalence of spinal cord lesions is lower, particularly if there are no referable symptoms such as myelopathy. Nevertheless, asymptomatic spinal cord lesions are found in 30–40 % of patients with a CIS. In relapsing-remitting MS, the spinal cord lesions are typically multifocal. In secondary progressive MS, the abnormalities are more extensive and diffuse and are commonly associated with spinal cord atrophy. In primary progressive MS, spinal cord abnormalities are quite extensive as compared with brain abnormalities. This discrepancy may help to diagnose primary progressive MS in patients with few or no brain abnormalities.

Longitudinal and cross-sectional MR studies have shown that the formation of new MS plaques is often associated

with contrast enhancement, mainly in the acute and relapsing stages of the disease [9]. The gadolinium enhancement varies in size and shape but usually lasts from a few days to weeks, although steroid treatment shortens this period. Incomplete ring enhancement on T1-weighted gadolinium-enhanced images, with the open border facing the gray matter of the cortex or basal ganglia, is a common finding in active MS plaques and is a helpful feature for distinguishing between inflammatory-demyelinating lesions and other focal lesions such as tumors or abscesses [10].

Focal enhancement can be detected before abnormalities appear on unenhanced T2-weighted scans and can reappear in chronic lesions with or without a concomitant increase in size. Although enhancing lesions also occur in clinically stable MS patients, their number is much greater when there is concomitant clinical activity. Contrast enhancement is a relatively good predictor of further enhancement and of subsequent accumulation of T2 lesions but shows no (or weak) correlation with progression of disability and development of brain atrophy. In relapsing-remitting and secondary progressive MS, enhancement is more frequent during relapses and correlates well with clinical activity. For patients with primary progressive MS, serial T2-weighted studies show few new lesions and little or no enhancement with conventional doses of gadolinium, despite steady clinical deterioration. Contrast-enhanced T1-weighted images are routinely used in the study of MS to provide a measure of inflammatory activity in vivo. The technique detects disease activity 5–10 times more frequently than clinical evaluation of relapses, suggesting that most of the enhancing lesions are clinically silent. Subclinical disease activity with contrast-enhancing lesions is four to ten times less frequent in the spinal cord than the brain, a fact that may be partially explained by the large volume of brain as compared with the spinal cord. High doses of gadolinium and a long postinjection delay can increase the detection of active spinal cord lesions.

Multiple Sclerosis Variants

Marburg Disease

Marburg disease (also termed malignant MS) is a rare, acute MS variant that occurs predominantly in young adults. It is characterized by a confusional state, headache, vomiting, gait unsteadiness, and hemiparesis. This entity has a rapidly progressive course with frequent, severe relapses leading to death or severe disability within weeks to months after onset of the clinical signs, mainly due to brainstem involvement or mass effect with herniation. Most patients who survive subsequently develop a relapsing form of MS. Because Marburg disease is often preceded by a febrile illness, it can also be considered a fulminant form of ADEM when it has a monophasic course. At the time of the clinical presentation, it may be difficult to find good predictors of whether the patient will have a fulminant course, develop mild or severe MS, or even develop MS at all. Pathologically, Marburg lesions are more destructive than those of typical MS or ADEM and are characterized by massive macrophage infiltration, demyelination (not restricted to the perivascular areas), hypertrophic astrocytes, and severe axonal injury, with features compatible with the histomorphologic diagnosis of a severe, acute demyelinating disease. Despite the destructive nature of these lesions, areas of remyelination are often observed [11]. In Marburg disease, MRI typically shows multiple focal T2 lesions of varying sizes, which may coalesce to form large white matter plaques disseminated throughout the hemispheric white matter and brainstem. Perilesional edema is often present, and enhancement is commonly seen. A similar imaging pattern is seen in ADEM.

Schilder Disease

Schilder disease is a rare acute or subacute disorder that can be defined as a specific clinical-radiologic presentation of MS. It commonly affects children and young adults. The clinical spectrum of Schilder disease includes psychiatric predominance, acute intracranial hypertension, intermittent exacerbations, and progressive deterioration. Imaging studies show large ring-enhancing lesions involving both hemispheres, sometimes symmetrically, and located preferentially in the parieto-occipital regions. These large, focal demyelinating lesions can resemble a brain tumor, an abscess, or even an adrenoleukodystrophy. MRI features that suggest possible Schilder disease include large and relatively symmetric involvement of the brain hemispheres, incomplete ring enhancement, minimal mass effect, restricted diffusivity, and sparing of the brainstem [2, 12]. Histopathologically, Schilder disease consistently shows well-demarcated demyelination and reactive gliosis with relative sparing of the axons. Microcystic changes and even frank cavitation can occur. The clinical and imaging findings usually show a dramatic response to steroids.

Balo Concentric Sclerosis

Balo concentric sclerosis is a rare IIDD subtype, considered a variant of MS, with characteristic radiologic and pathologic features. The disease was formerly considered an aggressive MS variant, leading to death in weeks to months after onset, and in which the diagnosis was made on histopathologic findings at postmortem examination. However, with the widespread use of MRI, this MS variant is often

identified in patients who later have a complete or almost complete clinical recovery [13]. The pathologic hallmarks of the disease are large demyelinated lesions showing a peculiar pattern of alternating layers of preserved and destroyed myelin. One possible explanation for this pattern is that sublethal tissue injury is induced at the edge of the expanding lesion, which would then stimulate expression of neuroprotective proteins to protect the rim of periplaque tissue from damage, thereby resulting in alternating layers of preserved and nonpreserved myelinated tissue [14]. These alternating bands are best identified with T2-weighted sequences, which typically show thick concentric hyperintense bands corresponding to areas of demyelination and gliosis, alternating with thin isointense bands corresponding to normal myelinated white matter. This pattern can be also identified on T1-weighted images as alternating isointense (preserve myelin) and hypointense (demyelinated) concentric rings. These bands, which may eventually disappear over time, can appear as multiple concentric layers (onion skin lesion), as a mosaic, or as a "floral" configuration. The center of the lesion usually shows no layering because of massive demyelination ("storm center"). Contrast enhancement and decreased diffusivity are common in the outer rings (inflammatory edge) of the lesion [13].

The Balo pattern can be isolated, multiple, or combined with typical MS-like lesions, and the lesion structure can vary from one or two to several alternating bands, with a total size from one to several centimeters. Lesions occur predominantly in the cerebral white matter, although brainstem, cerebellum, and spinal cord involvement has also been reported.

Neuromyelitis Optica Spectrum Disorders

Neuromyelitis optica (NMO) is an autoimmune inflammatory disorder of the CNS with a predilection for the optic nerves and spinal cord. The discovery of NMO-IgG and an NMO-specific autoantibody directed against aquaporin-4 (AQP4-Ab), the major water channel in the CNS, clearly identified NMO as a disease separate from MS.

This uncommon and topographically restricted form of IIDD is characterized by severe unilateral or bilateral optic neuritis and complete transverse myelitis, which occur simultaneously or sequentially over a varying period of time (weeks or years). AQP4-Ab has been also demonstrated in patients with conditions other than classic NMO, including isolated longitudinally extensive transverse myelitis, defined by lesions spanning over more than three segments; monophasic or recurrent isolated optic neuritis; and certain types of brainstem encephalitis (particularly if the diencephalon or medulla oblongata is affected). As most of these patients later develop NMO, various groups have suggested classifying these symptoms as high-risk syndromes for NMO when they occur in AQP4-Ab-seropositive patients. In addition, it has been proposed that AQP4-Ab-positive classic NMO and AQP4-Ab-positive high-risk syndromes be referred to as NMO-spectrum disorder (NMOSD) or autoimmune AQP4 channelopathy [15]. The incidence and prevalence of NMO are unknown, and there are important differences in its regional distribution worldwide.

The index events of new-onset NMO are severe unilateral or bilateral optic neuritis, acute myelitis, or a combination of these symptoms. The myelitis attacks appear as complete transverse myelitis with severe bilateral motor deficits, sensory-level, bowel and bladder dysfunction, pain and significant residual neurologic injury. Optic neuritis attacks are generally more severe than those typically seen in MS. Approximately 85 % of patients have a relapsing course with severe acute exacerbations and poor recovery, which leads to increasing neurologic impairment and a high risk of respiratory failure and death due to cervical myelitis. Patients who experience acute optic neuritis and transverse myelitis simultaneously or within days of each other are much more likely to have a monophasic course. On the other hand, a relapsing course correlates with NMO-IgG seropositivity, a longer interval between attacks, older age at onset, female gender, and less severe motor impairment after the myelitic onset. Although the initial attacks are more severe in patients proven to have monophasic NMO, the long-term neurologic prognosis is somewhat better in this group because patients do not accumulate disability from recurrent attacks.

Clinical features alone are insufficient to diagnose NMO; CSF analysis and MRI are usually required to confidently exclude other disorders. CSF pleocytosis (>50 leukocytes/mm^3) is often present, while oligoclonal bands are seen less frequently (20–40 %) than in MS patients (80–90 %). AQP4-Ab detection is reported to have a sensitivity of 73 % and a specificity of 91 % for NMO. AQP4-Ab may be helpful to distinguish this form of IIDD from MS and it can predict relapse and conversion to NMO in patients presenting with a single attack of longitudinally extensive myelitis. NMO-IgG is positive in 52 % of patients with relapsing transverse myelitis and in 25 % of patients with recurrent idiopathic optic neuritis [16].

Wingerchuk et al. [17] proposed a revised set of criteria for diagnosing NMO. These criteria remove the absolute restriction on CNS involvement beyond the optic nerves and spinal cord, allow any interval between the first events of optic neuritis and transverse myelitis, and emphasize the specificity of longitudinally extensive spinal cord lesions on MRI and NMO-IgG-seropositive status. More recently the International Panel for NMO diagnosis developed new diagnostic criteria that define the unifying term NMOSD, which is stratified by serologic testing (with or without AQP4-IgG) [18]. These new criteria require, in patients with AQP4-IgG, core clinical and MRI findings related to optic nerve, spinal

cord, area postrema, other brainstem, diencephalic, or cerebral presentations. However, more stringent clinical and MRI criteria are required for diagnosis of NMO-spectrum disorders without AQP4-IgG or when serologic testing is unavailable.

MRI of the affected optic nerve demonstrates swelling and loss of blood–brain barrier integrity with gadolinium enhancement that can extend into the optic chiasm. The spinal cord lesions in NMO typically extend over three or more contiguous vertebral segments and occasionally the entire spinal cord (longitudinally extensive spinal cord lesions); they are centrally located (preferential central gray matter involvement) and affect much of the cross-section on axial images. During the acute and subacute phase, the lesions are tumefactive and show contrast uptake. In some cases, the spinal cord lesions are small at the onset of symptoms, mimicking those of MS, and then progress in extent over time. The presence of very hyperintense spotty lesions on T2-weighted images ("bright spotty sign") is a specific feature that helps differentiate NMO from MS, particularly in patients without longitudinally extensive spinal cord lesions [19], and likely reflects the highly destructive component of the inflammatory lesion. Spinal cord lesions can progress to atrophy and necrosis, and may lead to syrinx-like cavities on T1-weighted images.

NMO was long considered a disease without brain involvement, and a negative brain at disease onset was considered a major supportive criterion for the diagnosis of NMO. However, various studies have shown that brain MRI abnormalities exist in a significant proportion (50–85 %) of patients [20]. Brain MRI lesions are often asymptomatic but sometimes are associated with symptoms even at disease onset. The brain lesions are commonly nonspecific. They can be dot-like or patchy, <3 cm in diameter, and located in the deep white matter, brainstem, or cerebellum. Nonetheless, some brain MRI features appear to be quite characteristic and distinct from MS lesions. These abnormalities may have parallel sites with high AQP4 expression adjacent to the ventricular system at any level, such as the hypothalamus, periependymal areas surrounding the third and lateral ventricles, cerebral aqueduct, corpus callosum, and dorsal brainstem adjacent to the fourth ventricle. The appearance of periventricular lesions in NMO is quite characteristic. In contrast to MS, where periventricular lesions are discrete, oval-shaped, and perpendicular to the ependymal lining due to their perivenular distribution (Dawson's fingers), NMO lesions are not oval-shaped, located immediately adjacent to the lateral ventricles following the ependymal lining in a disseminated pattern, and are often edematous and heterogeneous [20]. As opposed to what occurs in MS, NMO lesions do not affect the cortical gray matter.

Involvement of the corpus callosum has been described in 18 % of AQP4-seropositive NMO patients. The lesions are multiple, large, and edematous, show heterogeneous signal intensity on T2-weighted images, and sometimes affect the entire thickness of the corpus callosum.

Lesions may also affect areas where AQP4 expression is not particularly high, such as the corticospinal tracts. These lesions, which can be unilateral or bilateral and may affect the posterior limb of the internal capsule and cerebral peduncle of the midbrain, are contiguous and often longitudinally extensive [20].

Other brain MRI findings described in NMO include extensive and confluent hemispheric white matter lesions and radial hemispheric lesions (sometimes corresponding to an extension of periventricular lesions), which are likely related to vasogenic edema involving the white matter tracts. These lesions usually do not show mass effect or contrast enhancement but there may be a "cloud-like" pattern of enhancement, defined as multiple patches of enhancing lesions with blurred margins [20].

Some of the typical brain MRI findings may be specific to clinical presentations, such as intractable vomiting and hiccup (linear dorsal medullary lesions involving the area postrema and nucleus tractus solitarius) or a syndrome of inappropriate antidiuretic hormone secretion (hypothalamic and periaqueductal lesions) [21].

Distinguishing NMO from MS is critical, particularly in the early stages, since the treatment and prognosis of these disorders differ. In fact, some evidence suggests that MS-modifying treatments such as interferon-ß, natalizumab, and laquinimod exacerbate NMO. By contrast, several immunosuppressants (e.g., azathioprine, rituximab, mitoxantrone) seem to help in preventing NMO relapses.

NMOSD can be associated with systemic autoimmune diseases such as systemic lupus erythematosus and Sjögren syndrome). Whether the neurologic manifestations are solely due to NMO-spectrum disorder or are a manifestation of these diseases is controversial, although optic neuritis and transverse myelitis are rare presentations of them, and several studies have shown that patients with systemic autoimmune diseases and NMO-IgG-positive antibodies always have optic neuritis, myelitis, or NMO.

Acute Disseminated Encephalomyelitis

ADEM is a severe, immune-mediated inflammatory disorder of the CNS that predominantly affects the white matter of the brain and spinal cord. In the absence of specific biologic markers, the diagnosis of ADEM is based on clinical and radiologic features. This disorder affects children more commonly than adults, and, in contrast to MS, shows no gender preponderance. The estimated incidence is 0.8 per 100,000 population per year. In most cases, the clinical onset of disease is preceded by viral or bacterial infections, usually

nonspecific upper respiratory tract infections. ADEM may also develop following a vaccination (postimmunization encephalomyelitis). Patients commonly present with nonspecific multifocal symptoms, which developed subacutely over a period of days, frequently associated with encephalopathy (relatively uncommon in MS), defined as an alteration in consciousness (e.g., stupor, lethargy) or a behavioral change unexplained by fever, systemic illness, or postictal symptoms. Although ataxia, encephalopathy, and brainstem symptoms are frequently present in both pediatric and adult cases, certain signs and symptoms appear to be age related. In childhood ADEM, long-lasting fever and headaches occur more frequently, while in adult cases, motor and sensory deficits predominate. In general, the disease is self-limiting and the prognostic outcome favorable.

Although ADEM usually has a monophasic course, multiphasic forms have been reported, raising diagnostic difficulties in distinguishing these cases from MS. This multiphasic form, which accounts for less than 4 % of ADEM cases, is defined as a new encephalopathic event consistent with ADEM, separated by 3 months after the initial illness but not followed by any further events. The second ADEM event can involve either new or re-emergent neurologic symptoms, signs, and MRI findings. Relapsing disease following ADEM that occurs beyond a second encephalopathic event is no longer consistent with multiphasic ADEM but rather indicates a chronic disorder, most often leading to the diagnosis of MS or NMO [22].

An ADEM event as the first manifestation of the classic relapsing form of MS occurs in 2–10 %. According to the International Pediatric Multiple Sclerosis Study Group, the diagnosis of MS is met if, after the initial ADEM, a second clinical event meets the following three requirements: [1] it is nonencephalopathic; [2] it occurs 3 months or more after the incident neurologic illness; and [3] it is associated with new MRI findings consistent with the 2010 McDonald criteria for dissemination in space [22]. The presence of hypointense lesions and two or more periventricular lesions is an MRI feature that supports an MS diagnosis in children with acute CNS demyelination [23]. Unlike the lesions in MS, ADEM lesions are often large, patchy, and poorly marginated on MRI. There is usually asymmetric involvement of the subcortical and central white matter and cortical gray–white junction of the cerebral hemispheres, cerebellum, brainstem, and spinal cord. Lesions confined to the periventricular white matter and corpus callosum are less common than in MS. The gray matter of the thalamus and basal ganglia is often affected, particularly in children, and typically in a symmetric pattern [40]. However, the frequency of thalamic involvement in adult ADEM does not differ from that of adult MS. This can be explained by the fact that involvement of this structure is less common in adult ADEM than in childhood ADEM. Four patterns of cerebral involvement have been proposed to describe the MRI findings in ADEM [24]: (1) ADEM with small lesions (less than 5 mm); (2) ADEM with large, confluent, or tumefactive lesions and frequent extensive perilesional edema and mass effect; (3) ADEM with additional symmetric deep gray matter involvement; and (4) acute hemorrhagic encephalomyelitis. Gadolinium enhancement of one or more lesions occurs in 14–30 % of cases [22]. The pattern of enhancement varies and can be complete or incomplete ring shaped, nodular, gyral, or spotty. Although ADEM is usually a monophasic disease, new lesions may be seen on follow-up MRI within the 1st month of the initial attack.

Most MRI lesions appear early in the course of the disease, supporting the clinical diagnosis of ADEM. Nonetheless, in some cases, there may be a delay of more than 1 month between the onset of symptoms and the appearance of lesions on MRI. Therefore, a normal brain MRI obtained within the first days after the onset of neurologic symptoms suggestive of ADEM does not exclude this diagnosis.

The spinal cord is affected in less than 30 % of ADEM patients [24], predominantly in the thoracic region. The spinal cord lesion is typically large, causes swelling, and shows variable enhancement. In most ADEM patients, partial or complete resolution of the MRI abnormalities occurs within a few months of treatment. This course is positively associated with a final diagnosis of ADEM.

Infectious Inflammatory-Demyelinating Disorders

Progressive Multifocal Leukoencephalopathy

Progressive multifocal leukoencephalopathy (PML) is overwhelmingly a disease of the immunocompromised patient, and most (55–85 %) cases are related to acquired immunodeficiency syndrome (AIDS). There is a wide age range of involvement, with the peak age of presentation in the sixth decade. The disease is caused by reactivation of a papovavirus (JC virus) that selectively attacks the oligodendrocyte, leading to demyelination. Treatment with monoclonal antibody therapy (natalizumab, rituximab, efalizumab) or other immunomodulatory drugs, commonly used in patients with MS and other disorders, has also been linked with PML [25]. Unlike patients with ADEM, untreated patients with PML have an extremely poor prognosis, with death common in the first 6 months following establishment of the diagnosis. Although there is no specific treatment, combination antiretroviral therapy (cART) has not only resulted in a lower incidence of PML in AIDS patients but also substantially improved survival times of afflicted patients, now at 50 % 1-year survival [25]. Unfortunately, about 20 % of PML cases are linked to a robust inflammatory response to

pathogens associated with recovery of the immune system after a period of immunosuppression. This condition, known as PML–IRIS (immune reconstitution inflammatory syndrome), has been associated with intracranial masses with generous amounts of surrounding vasogenic edema on MRI. Enhancement may also occur [41].

Like ADEM, the lesions of PML are characterized by little mass effect or enhancement. Most lesions involve the subcortical white matter and deep cortical layers of the parieto-occipital or frontal white matter, although gray matter and posterior fossa lesions are also common, occurring in up to 50 % of cases. PML lesions tend to be more confluent in their appearance than ADEM lesions, and scalloping of the lateral margin of the lesion at the gray matter–white matter junction is common. Subtle signal intensity changes in the white matter may precede clinical suspicion of the PML–IRIS. While development of mass effect and temporary enhancement in the early phase of cART has been linked to better survival, similar imaging manifestations may also be seen in monoclonal antibody-treated PML patients [25, 26].

Human Immunodeficiency Virus Encephalopathy

Human immunodeficiency virus (HIV) encephalopathy results from direct infection of the brain by the virus itself. Since the advent of cART, the prevalence of the disease has markedly decreased, and the temporal progression has been slowed. Most patients are severely immunocompromised at the time of onset and exhibit psychomotor slowing, impaired mental status, and memory difficulties. Histologically, demyelination and vacuolation with axonal loss are noted, along with occasional microglial nodules. Mild cerebral atrophy is the first and sometimes only imaging feature of the disease, which is also known as AIDS dementia complex, HIV dementia, HIV-associated dementia complex, and HIV-associated neurocognitive disorder (HAND). Involvement of the central white matter, basal ganglia, and thalamus is characteristic. Typically, bilaterally symmetric abnormal T2 hyperintensity in the basal ganglia and small focal areas in the periventricular regions are noted on T2-weighted MR images [27]. Regression of these findings has been seen following institution of cART.

White Matter Disease from Toxic Imbalance

Chronic Alcohol Ingestion and Its Consequences

Brain abnormalities in alcoholics include atrophy, Marchiafava-Bignami disease, Wernicke encephalopathy, osmotic myelinolysis, and consequences of liver cirrhosis such as hepatic encephalopathy and coagulopathy [28]. All the reported entities are not specific of alcohol and can be found in many other toxic or metabolic conditions. Ethanol direct brain toxicity is caused by under-regulation of receptors of N-methyl-D-aspartate and abnormal catabolism of homocysteine, resulting in an increased susceptibility to glutamate excitatory and toxic effects. Moreover, immune response occurs mediated by lipid peroxidation products that bind to neurons resulting in neurotoxicity. Neuroimaging studies show a characteristic distribution of loss of volume: initially there is infratentorial predominance with atrophy of the cerebellar vermis and hemispheres. Frontal and temporal atrophy is subsequently evident, followed by diffuse atrophy of the brain. The possibility of partial reversibility of these alterations is also observed. In pregnancy, ethanol determines inhibition of maturation of Bergmann's fibers of cerebellum, with consequential marked cerebellar atrophy.

Hepatic Encephalopathy

The term *hepatic encephalopathy* (HE) includes a wide spectrum of neuropsychiatric abnormalities occurring in patients with liver dysfunction. Most cases are associated with cirrhosis and portal hypertension or portal-systemic shunts, but the condition can also be seen in patients with acute liver failure and rarely those with portal-systemic bypass and no associated intrinsic hepatocellular disease. Although HE is a clinical condition, several neuroimaging techniques, particularly MRI, may eventually be useful for the diagnosis because they can identify and measure the consequences of CNS increase in substances, which, under normal circumstances, are efficiently metabolized by the liver. Classical MR abnormalities in chronic HE include high signal intensity in the globus pallidum on T1-weighted images, likely a reflection of increased tissue concentrations of manganese and an elevated glutamine/glutamate peak coupled with decreased myoinositol and choline signals on proton MR spectroscopy, representing disturbances in cell volume homeostasis secondary to brain hyperammonemia [29]. Recent data have shown that white matter abnormalities, also related to increased CNS ammonia concentration, can also be detected with several MRI techniques: magnetization transfer ratio measurements show significantly low values in otherwise normal-appearing brain white matter, T2-Flair sequences reveal diffuse and focal high-signal intensity lesions in the hemispheric white matter, and diffusion-weighted imaging (DWI) discloses increased white matter diffusivity. All these MR abnormalities, which return to normal with restoration of liver function, probably reflect the presence of mild diffuse interstitial brain edema, which seems to play an essential role in the pathogenesis of HE.

In acute HE, bilateral symmetric signal intensity abnormalities on T2-weighted images, often with associated restricted diffusion involving the cortical gray matter, are commonly identified. Involvement of the subcortical white matter and the basal ganglia, thalami, and midbrain may also be seen. These abnormalities that can lead to intracranial hypertension and severe brain injury reflect the development of cytotoxic edema secondary to the acute increase of brain hyperammonemia.

Marchiafava-Bignami Disease

Marchiafava-Bignami disease is a rare complication of chronic alcoholism, characterized by demyelination and necrosis of the corpus callosum, with rare involvement of extracallosal regions. Etiology remains unknown but is believed to be caused by toxic agents in red wine of low quality and lack of group B vitamins. Rarely, the disease has also been reported in nonalcoholic patients. Symptoms are mainly represented by cognitive deficits, psychosis, hypertonia, and interhemispheric disconnection, until coma and death. Typical MRI features in the acute phase are corpus callosum hyperintensity on T2-weighted sequences and FLAIR, without significant mass effect, with peripheral enhancement. Diffusion is restricted due to cytotoxic edema. In chronic forms, necrosis of the genu and splenium can be detected [30].

Wernicke Encephalopathy

Wernicke encephalopathy (WE) is an acute condition first described by the French ophthalmologist Gayet in 1875 and later by the German neurologist Wernicke in 1881, caused by a deficiency of vitamin B1 (thiamine). WE develops frequently but not exclusively in alcoholics. Other potential causes include extended fasting, malabsorption, digitalis poisoning, and massive infusion of glucose without vitamin B1 in weak patients. The autoptic incidence is reported to be 0.8–2 % in random autopsies and 20 % in chronic alcoholics. The classic clinical triad of ocular dysfunctions (nystagmus, conjugate gaze palsy, ophthalmoplegia), ataxia, and confusion is observed in only 30 % of cases. Treatment consists of thiamine infusion and avoids irreversible consequences including Korsakoff dementia or death. Memory impairment and dementia are related to damage of the mammillary bodies, anterior thalamic nuclei, and interruption of the diencephalic–hippocampal circuits. Depletion of thiamine leads to failure of conversion of pyruvate to acetyl CoA and α-ketoglutarate to succinate, altered pentose monophosphate shunt, and the lack of Krebs cycle, with cerebral lactic acidosis, intra- and extracellular edema, swelling of astrocytes, oligodendrocytes, myelin fibers, and neuronal dendrites. Neuropathological aspects include neuronal degeneration, demyelination, hemorrhagic petechiae, proliferation of capillaries and astrocytes in periaqueductal gray substance, mammillary bodies, thalami, pulvinar, III cranial nerves nuclei, and cerebellum. On MRI, bilateral and symmetric hyperintensities on T2-weighted sequences and FLAIR are evident at the level of the already mentioned structures, mainly mammillary bodies and thalami [31, 32]. DWI shows areas of high signal with apparent diffusion coefficient (ADC) signal reduced due to cytotoxic edema, although the ADC can sometimes be high due to the presence of vasogenic component. Rarely, T1-weighted images show bleeding ecchymotic hemorrhages in the thalami and mammillary bodies, a sign considered clinically unfavorable. In 50 % of cases, contrast enhancement is present in periaqueductal regions. Marked contrast enhancement of mammillary bodies is evident in 80 % of cases, even prior to the development of visible changes in T2-weighted sequences, and is considered highly specific for WE. In chronic forms, change of signal in T2-weighted sequences becomes less prominent due to the diffuse brain atrophy, more pronounced at the level of mesencephalon and mammillary bodies.

Osmotic Demyelination Syndrome

Osmotic demyelination syndrome (ODS) usually occurs in the setting of osmotic changes, typically with the rapid correction of hyponatremia. This causes destruction of the blood–brain barrier with hypertonic fluid accumulation in extracellular space, resulting in a noninflammatory demyelination. The most common damage is in the pontine fibers [33]. ODS is observed in alcoholics with nutritional deficiency. The most common symptoms include paralysis, dysphagia, dysarthria, and pseudobulbar palsy. Death is frequent. Rarely, ODS affects other regions, especially the basal ganglia, thalami, and deep white matter. MRI usually shows an area of high signal on T2-weighted sequences in the central part of the pons, sparing ventrolateral portions and corticospinal tracts. The lesion is moderately hypointense in T1 and may show positive contrast enhancement. If the patient survives, the acute phase can evolve into a cavitated pontine lesion.

White Matter Disease Associated with Radiation Therapy and Chemotherapy

Treatment strategies designed to target cancer cells are commonly associated with deleterious effects to multiple organ systems, including the CNS. As both radiation and

chemotherapy alone can be associated with significant toxicity, the combination of radiation and chemotherapy may be particularly harmful to the CNS. With advanced treatment regimens and prolonged survival, neurologic complications are likely to be observed with increasing frequency.

Neurotoxicity can result from direct toxic effects of the drug or radiation on the cells of the CNS or indirectly through metabolic abnormalities, inflammatory processes, or vascular adverse effects.

Recognition of treatment-related neurologic complications is critically important, because symptoms may be confused with metastatic disease, tumor progression, paraneoplastic disorders, or opportunistic infections, and discontinuation of the offending drug may prevent irreversible CNS injury.

Radiation Injury and Necrosis

It is widely accepted that the white matter of the CNS is prone to radiation-induced injury, compared with gray matter. Radiation encephalopathy has been classically divided into three stages according to its timing after radiotherapy: early, early-delayed, and late-delayed reactions [34]. Within the first several weeks of therapy, patients may experience acute declines with focal neurologic deficits. These effects are possibly related to increased edema, which has been supported by the observation that steroid treatment often results in clinical improvement. Early- delayed adverse effects usually occur within 1–6 months of treatment and are thought to be a result of demyelination. This syndrome is characterized by somnolence, fatigue, and cognitive dysfunction, consistent with dysfunction of the frontal network systems. Late-delayed side effects occur months to years after cessation of treatment and are largely irreversible and progressive. These late changes are commonly associated with progressive cognitive deficits. In more severe cases of late-delayed radiation injury, imaging and histopathological studies may demonstrate leukoencephalopathy and/or focal necrosis.

In all types of white matter radiation-induced damage, CT and mainly MRI may demonstrate variable degrees of white matter signal changes related to an increase in free tissue water in the involved areas. This may result from endothelial damage, causing increased capillary permeability and vasogenic edema, or from demyelination. However, the degree of these white matter changes correlates poorly with the functional deterioration observed in the patients. MRI findings in early reactions occurring during course of treatment are nonspecific. MRI may be normal or demonstrate poorly defined multifocal lesions in both hemispheres that usually disappear spontaneously. MRI in early-delayed reactions also may show signal changes involving not only the hemispheric white matter but also the basal ganglia and the cerebral peduncles, which resolve completely without treatment. These early-delayed changes have been reported in children with acute lymphatic leukemia who have been treated with both whole brain irradiation and chemotherapy. These changes have no correlation with clinical manifestations and have no clear prognostic significance. Late-delayed reactions can be subdivided into diffuse and focal radiation necrosis injury. Diffuse radiation injury is characterized by white matter changes that are “geographic” in nature, i.e., the areas of abnormal signal intensity or attenuation are limited to the regions of the brain that conform to the radiation portal. This can produce striking differences between the involved zones and the spared surrounding white matter. The involved territories are often symmetric and do not enhance on post-contrast studies. While originally reported in children with leukemia, diffuse necrotizing leukoencephalopathy has also been observed following treatment for many other malignancies in both children and adults. The disease may occur following chemotherapy alone, but the incidence of disease is highest when chemotherapy is combined with radiation therapy. Both the histologic findings and imaging features bear resemblance to radiation necrosis. Axonal swelling, demyelination, coagulation necrosis, and gliosis dominate the histologic picture.

Diffuse white matter changes, with hypoattenuation on CT and T1 and T2 prolongation on MRI, are common and often involve an entire hemisphere. Microbleeds can occur as a sign of vasculopathy. Radiation-induced leukoencephalopathy may be associated with progressive brain atrophy, and patients may present with cognitive decline, gait abnormalities, and urinary incontinence. However, the more common mild-to-moderate cognitive impairment is inconsistently associated with radiological findings and frequently occurs in patients with normal appearing. Recently, more sensitive tools to quantify the damage to brain tissue, such as diffusion tensor imaging (DTI), have been applied in patients treated with brain radiotherapy and have shown early and progressive diffuse changes in normal-appearing white matter indicating radiation-induced demyelination and mild structural degradation of axonal fibers, which are indetectable with conventional MRI.

Focal radiation necrosis usually manifests as a ring-like or irregular enhancing mass lesion located in the white matter, which may become hemorrhagic. The MRI features commonly seen in radiation necrosis include a soap bubble-like interior and Swiss cheese-like interior. Compared with lesions with the soap bubble pattern, Swiss cheese lesions are larger, more variable in size, and more diffuse. This pattern can be visualized as a result of diffuse necrosis affecting the white matter and cortex with diffuse enhancement at the margins with intermixed foci of necrosis. The rim of enhancement is often thinner, more uniform, and more aligned to the gray matter–white matter junction than in

malignant tumors. As radiation necrosis progresses, it can lead to severe shrinkage of the white matter and cortex and result in focal brain atrophy with hydrocephalus.

Quite frequently is impossible to distinguish radiation necrosis from recurrent malignant brain tumor, such as glioblastoma multiforme, using conventional MRI. Metabolic imaging (e.g., positron emission tomography) may facilitate differentiating between the two diseases as radiation necrosis is iso- to hypometabolic, while recurrent high-grade tumors are typically hypermetabolic. MR spectroscopy (MRS) may also be useful as radiation necrosis frequently shows a characteristic lactic acid peak and near-normal peaks for N-acetyl-aspartate (NAA) and choline, while recurrent high-grade gliomas typically show elevated choline levels compared to NAA without or with elevated lactic acid levels. Perfusion imaging can identify the areas of increased blood flow associated with tumor recurrence whereas radiation necrosis is not expected to contain any increased blood flow [35].

Chemotherapy-Associated Neurotoxicity

Neurotoxicity has been observed with virtually all categories of chemotherapeutic agents. Neurologic complications may range from acute encephalopathy, headache, seizures, visual loss, cerebellar toxicity, and stroke to chronic side effects, including chronic encephalopathy, cognitive decline, and dementia.

Among the most puzzling aspects of cancer therapy-related toxicity is the occurrence of delayed and progressive neurologic decline, even after cessation of treatment. Anticancer agents affect brain function through both direct and indirect pathways. It is also conceivable that additional variables play important roles, including the timing of treatment, combination of different treatment modalities, patient age, integrity of the blood–brain barrier, and cognitive function prior to treatment initiation.

Imaging studies have provided evidence that structural and functional CNS changes occur in a significant number of patients treated with chemotherapy. Some agents, such as methotrexate or carmustine, are well known to cause a leukoencephalopathy syndrome, especially when administered at a high dose, intrathecally, or in combination with cranial radiotherapy. Nonenhancing, confluent, periventricular white matter lesions, necrosis, ventriculomegaly, and cortical atrophy characterize this syndrome. White matter abnormalities following high-dose chemotherapy have been detected in up to 70 % of treated individuals and usually have a delayed onset of several months [36].

A delayed leukoencephalopathy syndrome with distinct DWI abnormalities on MRI indicative of cytotoxic edema within cerebral white matter has been recently described. This syndrome appeared to mimic a stroke-like syndrome and has seen mainly in patients receiving methotrexate, 5-fluorouracil (5-FU), carmofur, and capecitabine [37].

Mineralizing Microangiopathy

In children with cancer who have been treated with either chemotherapy alone or in combination with radiation therapy, deposits of calcium in and around small penetrating blood vessels of the deep brain lead to local areas of necrosis. This process is termed mineralizing microangiopathy and is the most common neuroradiologic abnormality noted in this group of patients. The disease has a predilection for the basal ganglia, especially the putamen, and, more rarely, the cerebral cortex. On CT and MRI, evidence of cortical atrophy and abnormal attenuation/signal intensity changes within the white matter are commonly noted. Of all chemotherapeutic agents, methotrexate is the one classically associated with mineralizing microangiopathy. Patients younger than 5 years of age who have meningeal leukemia and have received high-dose methotrexate therapy are at greatest risk of developing this complication of therapy [38].

Vascular Causes of White Matter Disease

Reversible Encephalopathy Syndrome

Although not a truly demyelinating condition, reversible encephalopathy syndrome is noteworthy because of its affinity for the posterior cerebral white matter territories and is important in the differential diagnosis of demyelinating disease. Under normal circumstances, cerebral perfusion pressure is maintained at a relatively constant level by autoregulation, a physiologic mechanism that compensates for wide changes in systemic blood pressure. Hypertensive encephalopathy is believed to result from loss of normal autoregulation, with competing regions of vasodilatation and vasoconstriction and endothelial dysfunction. The vessels of the posterior cerebral circulation, lacking less sympathetic innervation compared to those of the anterior circulation, are unable to vasoconstrict in a normal manner and bear the brunt of these vascular changes. Reversible vasogenic edema is the result and is associated with visual field deficits, as well as headaches, somnolence, and an overall impaired mental status. The terms posterior reversible encephalopathy syndrome (PRES) and reversible posterior leukoencephalopathy syndrome (RPLS) have been popularized in the literature to describe this scenario that is most commonly seen in hypertensive states and/or the presence of immunosuppression (particularly cyclosporine A and tacrolimus), chemotherapy, eclampsia, and renal failure. While it commonly

involves the posterior cerebral white matter, other sites may also be affected including unilateral cerebral hemispheric or isolated brainstem involvement in patients following aortic valve surgery [39, 40]. Accordingly, it has been suggested that perhaps the terminology should be changed to simply "reversible encephalopathy" [40].

On MR studies, bilaterally symmetric abnormal T2 hyperintensity, representing vasogenic edema, is most commonly seen in the distribution of the posterior circulation, although other sites including the frontal lobes and corpus callosum may be noted as well. Cortical and subcortical lesions may be better detected on FLAIR sequences [41]. Diffusion-weighted imaging (DWI) may be normal or show restricted water diffusion in regions of infarction that correlate with poorer prognosis [42]. Susceptibility-weighted imaging may show areas of hemorrhage within involved territories. With early treatment and limited involvement of the brain, many of these imaging abnormalities will completely resolve, and most patients recover within 2 weeks [43]. However, when larger areas or regions of infarction are involved, permanent neurologic deficits or even death are possible [42]. Vascular narrowing has been observed on angiographic studies. Perfusion studies reported in the literature indicate normal to increased perfusion in these zones. When biopsies of these regions have been performed, white matter edema is seen histologically.

Aging and Ischemic Demyelinating Disorders

Small focal lesions on T2-weighted images are quite common in the white matter of adult subjects [44]. They are not associated with mass effect, do not enhance, and are typically isointense compared to normal white matter on T1-weighted images. When these lesions have been biopsied, histologic examination reveals a spectrum of findings including gliosis (partial), loss of myelination, and vasculopathy. They tend to be located in the periventricular white matter, centrum semiovale, and optic radiations. In contrast to MS, they do not involve the corpus callosum or the juxtacortical U-fibers, important distinguishing features [3]. Since the lesions are so ubiquitous and appear to be a part of "normal" aging, various terms have been proposed: senescent white matter changes or disease, deep white matter ischemia, leukoaraiosis, etc. In general, the more lesions present, the more likely it is that the patient will have cognitive problems or difficulties with neuropsychologic testing. However, it is not possible to predict a particular patient's status simply based on the imaging appearance alone.

In adult patients between 30 and 50 years of age, the presence of periventricular and subcortical lesions in a patient with a family history of similarly affected relatives should raise the possibility of cerebral autosomal dominant arteriopathy with subcortical infarcts and leukoencephalopathy (CADASIL). A defect in the notch3 gene on the long arm of chromosome 19 has been identified and apparently evokes an angiopathy affecting small- and medium-sized vessels. Most lesions occur in the frontal and temporal lobes and less commonly in the thalamus, basal ganglia, internal and external capsules, and brainstem [45].

Conclusions

Several neuroradiologic imaging techniques have been extensively applied to the study of white matter disorders. These examinations play an important role in narrowing the differential diagnosis of this heterogeneous group of disorders. Due to the lack of specificity of imaging findings in many of these conditions, the imaging features should be correlated with clinical manifestations and laboratory results to improve their diagnostic value.

References

1. Smith AB, Smirniotopoulos JG (2010) Imaging evaluation of demyelinating processes of the central nervous system. Postgrad Med J 86:218–229
2. Cañellas AR, Gols AR, Izquierdo JR et al (2007) Idiopathic inflammatory-demyelinating diseases of the central nervous system. Neuroradiology 49:393–409
3. Aliaga ES, Barkhof F (2014) MRI mimics of multiple sclerosis. Handb Clin Neurol 122:291–316
4. Rovira A, León A (2008) MR in the diagnosis and monitoring of multiple sclerosis: an overview. Eur J Radiol 67:409–414
5. Filippi M, Rocca MA (2011) MR imaging of multiple sclerosis. Radiology 259:659–681
6. Rovira À, Wattjes MP, Tintoré M et al (2015) Evidence-based guidelines: MAGNIMS consensus guidelines on the use of MRI in multiple sclerosis-clinical implementation in the diagnostic process. Nat Rev Neurol 11:471–482
7. Bagnato F, Jeffries N, Richert ND et al (2003) Evolution of T1 black holes in patients with multiple sclerosis imaged monthly for 4 years. Brain 126:1782–1789
8. Lycklama G, Thompson A, Filippi M et al (2003) Spinal-cord MRI in multiple sclerosis. Lancet Neurol 2:555–562
9. Cotton F, Weiner HL, Jolesz FA et al (2003) MRI contrast uptake in new lesions in relapsing-remitting MS followed at weekly intervals. Neurology 60:640–646
10. Masdeu JC, Quinto C, Olivera C et al (2000) Open-ring imaging sign: highly specific for atypical brain demyelination. Neurology 54:1427–1433
11. Popescu BF, Lucchinetti CF (2012) Pathology of demyelinating diseases. Annu Rev Pathol 7:185–217
12. Mehler MF, Rabinowich L (1989) Inflammatory myelinoclastic diffuse sclerosis (Schilder's disease): neuroradiologic findings. AJNR Am J Neuroradiol 10:176–180
13. Hardy TA, Miller DH (2014) Baló's concentric sclerosis. Lancet Neurol 13:740–746
14. Stadelmann C, Ludwin S, Tabira T et al (2005) Tissue preconditioning may explain concentric lesions in Baló's type of multiple sclerosis. Brain 128:979–987
15. Trebst C, Jarius S, Berthele A et al (2014) Update on the diagnosis and treatment of neuromyelitis optica: recommendations of the Neuromyelitis Optica Study Group (NEMOS). J Neurol 261:1–16

16. Lennon VA, Wingerchuk DM, Kryzer TJ et al (2004) A serum autoantibody marker of neuromyelitis optica: distinction from multiple sclerosis. Lancet 364:2106–2112
17. Wingerchuk DM, Lennon VA, Pittock SJ et al (2006) Revised diagnostic criteria for neuromyelitis optica. Neurology 66:1485–1489
18. Wingerchuk DM, Banwell B, Bennett JL et al (2015) International consensus diagnostic criteria for neuromyelitis optica spectrum disorders. Neurology 85:177–189
19. Yonezu T, Ito S, Mori M et al (2014) "Bright spotty lesions" on spinal magnetic resonance imaging differentiate neuromyelitis optica from multiple sclerosis. Mult Scler 20:331–337
20. Kim HJ, Paul F, Lana-Peixoto MA et al (2015) MRI characteristics of neuromyelitis optica spectrum disorder: an international update. Neurology 84:1165–1173
21. Misu T, Fujihara K, Nakashima I et al (2005) Intractable hiccup and nausea with periaqueductal lesions in neuromyelitis optica. Neurology 65:1479–1482
22. Krupp LB, Tardieu M, Amato MP et al (2013) International Pediatric Multiple Sclerosis Study Group criteria for pediatric multiple sclerosis and immune-mediated central nervous system demyelinating disorders: revisions to the 2007 definitions. Mult Scler 19:1261–1267
23. Verhey LH, Branson HM, Shroff MM et al (2011) MRI parameters for prediction of multiple sclerosis diagnosis in children with acute CNS demyelination: a prospective national cohort study. Lancet Neurol 10:1065–1073
24. Tenembaum S, Chamoles N, Fejerman N (2002) Acute disseminated encephalomyelitis: a long-term follow-up study of 84 pediatric patients. Neurology 59:1224–1231
25. Tan CS, Koralnik IJ (2010) Progressive multifocal leukoencephalopathy and other disorders caused by JC virus: clinical features and pathogenesis. Lancet Neurol 9:425–437
26. Wattjes MP, Barkhof F (2014) Diagnosis of natalizumab-associated progressive multifocal leukoencephalopathy using MRI. Curr Opin Neurol 27:260–270
27. Gottumukkala RV, Romero JM, Riascos RF et al (2014) Imaging of the brain in patients with human immunodeficiency virus infection. Top Magn Reson Imaging 23:275–291
28. Geibprasert S, Gallucci M, Krings T (2010) Alcohol-induced changes in the brain as assessed by MRI and CT. Eur Radiol 20:1492–1501
29. Rovira A, Alonso J, Cordoba J (2008) MR imaging findings in hepatic encephalopathy. AJNR Am J Neuroradiol 29:1612–1621
30. Arbelaez A, Pajon A, Castillo M (2003) Acute Marchiafava-Bignami disease: MR findings in two patients. AJNR Am J Neuroradiol 24:1955–1957
31. Gallucci M, Bozzao A, Splendiani A et al (1990) Wernicke encephalopathy: MR findings in five patients. AJR Am J Roentgenol 155:1309–1314
32. Zuccoli G, Santa Cruz D, Bertolini M et al (2009) MR imaging findings in 56 patients with Wernicke encephalopathy: nonalcoholics may differ from alcoholics. AJNR Am J Neuroradiol 30:171–176
33. Ruzek KA, Campeau NG, Miller GM (2004) Early diagnosis of central pontine myelinolysis with diffusion-weighted imaging. AJNR Am J Neuroradiol 25:210–213
34. Soussain C, Ricard D, Fike JR et al (2009) CNS complications of radiotherapy and chemotherapy. Lancet 374:1639–1651
35. Cha S (2006) Update on brain tumor imaging: from anatomy to physiology. AJNR Am J Neuroradiol 27:475–487
36. Rimkus Cde M, Andrade CS, Leite Cda C et al (2014) Toxic leukoencephalopathies, including drug, medication, environmental, and radiation-induced encephalopathic syndromes. Semin Ultrasound CT MR 35:97–117
37. Baehring JM, Fulbright RK (2008) Delayed leukoencephalopathy with stroke-like presentation in chemotherapy recipients. J Neurol Neurosurg Psychiatry 79:535–539
38. Davis P, Hoffman JJ, Pearl G et al (1986) CT evaluation of effects of cranial radiation therapy in children. AJR Am J Roentgenol 147:587–592
39. Wijdicks EF, Campeau N, Sundt T (2008) Reversible unilateral brain edema presenting with major neurologic deficit after valve repair. Ann Thorac Surg 86:634–637
40. McKinney AM, Short J, Truwit CL et al (2007) Posterior reversible encephalopathy syndrome: incidence of atypical regions of involvement and imaging findings. AJR Am J Roentgenol 189:904–912
41. Casey SO, Sampaio RC, Michel E, Truwit CL (2000) Posterior reversible encephalopathy syndrome: utility of fluid-attenuated inversion recovery MR imaging in the detection of cortical and subcortical lesions. AJNR Am J Neuroradiol 21:1199–1206
42. Covarrubias D, Luetmer P, Campeau N (2002) Posterior reversible encephalopathy syndrome: prognostic utility of quantitative diffusion-weighted MR images. AJNR Am J Neuroradiol 23:1038–1048
43. Post JD, Beauchamp NJ (1998) Reversible intracerebral pathologic entities mediated by vascular autoregulatory dysfunction. Radiographics 18:353–367
44. Kloppenborg RP, Nederkoorn PJ, Geerlings MI, van den Berg E (2014) Presence and progression of white matter hyperintensities and cognition: a meta-analysis. Neurology 82:2127–2138
45. van dem Boom R, Lesnick Oberstein S et al (2006) Cerebral autosomal dominant arteriopathy with subcortical infarcts and leukoencephalopathy: MR imaging changes and apolipoprotein E genotype. AJNR Am J Neuroradiol 27:359–362

Movement Disorders and Metabolic Disease

Marco Essig and Hans Rolf Jäger

Movement Disorders

Introduction

Movement disorders include a large number of diseases that clinically present as neurological conditions that affect the speed, quality, fluency or ease of movements. Clinically movement disorders can present with one or a combination of the following clinical conditions:

- *Dyskinesia*, the abnormal fluency or speed of movement
- *Hyperkinesia* defined as excessive involuntary movement
- *Hypokinesia*, the absence or slowing of voluntary movement
- *Ataxia*, the lack of coordination, associated with jerky movements
- *Dystonia*, which is defined by involuntary movement and prolonged muscle contraction
- *Myoclonus* that includes rapid, brief and irregular movement
- *Tremor*

These pathologic movement patterns might be also present in other diseases of neurodegeneration or as a result from previous injuries or metabolic disorders.

Pathologic movement however is the primary findings in the following conditions and diseases that will be later described in more detail:

Parkinson's disease (PD)
Multiple system atrophies (MSA)
Wilson disease
Amyotrophic lateral sclerosis (ALS)
Huntington's disease also called chronic progressive chorea
Progressive supranuclear palsy (PSP)
Restless legs syndrome (RLS) and reflex sympathetic dystrophy/periodic limb movement disorder (RSD/PLMD)
Tourette's syndrome
Hallervorden-Spatz disease (or NBIA: neurodegeneration with brain iron accumulation)
Creutzfeldt-Jakob disease (CJD)

Parkinson's disease (PD)

PD is a degenerative disorder of the central nervous system that often impairs the sufferer's motor skills and speech. It is characterised by muscle rigidity, tremor, a slowing of physical movement (bradykinesia) and, in extreme cases, a loss of physical movement (akinesia). Secondary symptoms may include high-level *cognitive dysfunction* and subtle language problems. PD exists in a chronic and a progressive form. The idiopathic form, also named paralysis agitans, is a common progressive disorder, which appears spontaneously between age 50 and 80.

As the changes in the iron accumulation may vary and are much dependent from the field strength used, imaging studies in PD often present unspecific atrophy which is in most of the cases diffuse. The loss of the normal swallow tail appearance of the substantia nigra on GRE or SWI imaging proved to be of value (up to 90 % accuracy). On high-resolution scanning, a decreased width of the pars compacta or a decreased definition of the gap between the pars reticularis and the red nucleus can be found. The underlying mechanism is an increased iron deposition in the pars compacta.

PET and SPECT imaging allow to assess the presynaptic dopaminergic system at high sensitivity. Both methods are also able to differentiate PD from atypical parkinsonism.

M. Essig (✉)
Department of Radiology, University of Manitoba,
GA216-820 Sherbrook Street, Winnipeg, MB R3A 1R9, Canada
e-mail: messig@exchange.hsc.mb.ca

H.R. Jäger
Neuroradiological Academic Unit,
Department of Brain Repair & Rehabilitation,
UCL Institute of Neurology, Box 65, Queen Square,
London WC1N 3BG, UK
e-mail: r.jager@ucl.ac.uk

J. Hodler et al. (eds.), *Diseases of the Brain, Head and Neck, Spine 2016–2019: Diagnostic Imaging*, DOI 10.1007/978-3-319-30081-8_9

Multiple system atrophy (*MSA*) is a collection of diseases that involve several systems. The associated cell degeneration causes problems with movement, balance and automatic functions of the body such as bladder control, presence of pyramidal sign and parkinsonoid symptoms.

Based on the consensus statement from 2007, MSA has been divided into two main subtypes, MSA-C and MSA-P. The before-used MSA-A or Shy-Drager symptom has been included in the MSA-C subtype.

MSA-C presents clinically with cerebellar symptoms and shows on MR imaging typical findings in the pontocerebellar tracts known as hot cross bun sign and other T2 hyperintensities in the middle cerebellar peduncles, the cerebellum and the pons in combination with atrophic changes. More common but not binding findings are the more pronounced susceptibility in the globus pallidus, the red nucleus and the susceptibility rim surrounding the putamen, the so-called putaminal rim sign. Changes vary significantly with different field strengths.

With progression of the disease, the imaging abnormalities become more pronounced.

Wilson disease or hepatolenticular degeneration is one of the few movement disorders in which a kind of specific imaging finding exists. On T2-weighted MRI, prominent hyperintensities in the putamen, the thalami, the brain stem and the dentate nuclei have been reported. Within the putaminal hyperintensities, irregular areas of reduced signal may be present which represent focal iron depositions causing a susceptibility artefact. The deposition of copper causes the same finding. With progression of the disease, a diffuse atrophy of the above-described areas will occur.

The face of the giant panda sign in the midbrain is described as a typical finding of Wilson disease.

Amyotrophic lateral sclerosis (*ALS*) is a progressive, usually fatal, neurodegenerative disease caused by the degeneration of motor neurons, the nerve cells in the central nervous system that control voluntary muscle movement. While the diagnosis of ALS is made on the basis of clinical findings, imaging is used to exclude treatable causes of the symptoms like syringomyelia. Typical ALS findings in MRI are abnormal high signal intensities along the corticospinal motor tracts. Those changes can only be found along the intracranial portion of the tracts down to the pons. Along the spinal cord, only atrophic changes can be observed (Fig. 9.1).

Huntington's disease (*HD*) is an autosomal dominant disorder that presents with the clinical picture of choreoathetosis, rigidity, emotional disturbance and dementia. The disease is expressed mainly in the fourth and fifth decades but can also present at younger age. Histologically, HD is characterised by neuronal loss, demyelination, gliosis and iron accumulation in the striatum. On cross-sectional imaging, the most striking feature of HD is atrophy of the caudate nucleus and putamen. This is apparent as the loss of the usual bulge of the inferolateral borders of the frontal horns of the lateral ventricles. Coexisting abnormalities may be diffuse cerebral atrophy and hyper- and hypointensity of the striatum on T2-weighted images.

Progressive supranuclear palsy (*PSP*) is a movement disorder that is clinically characterised by eye movement abnormalities including vertical saccades and supranuclear gaze palsy. With an onset at the age of over 40, symptoms like postural instability and falls appear late.

On imaging, patients with PSP may present with nonspecific findings like high signal in the periaqueductal grey matter on T2-weighted images and a progressive midbrain atrophy.

The midbrain atrophy can be qualitatively described with the Mickey Mouse sign or the hummingbird or penguin sign (Fig. 1).

For quantitative assessments, authors have calculated a midbrain to pons area ratio with a reduced area ratio in patients with PSP to 0.12. The AP diameter of the midbrain at the level of the superior colliculi toe < 12 mm leads to the characteristic Mickey Mouse ears appearance.

NBIA – Neurodegeneration with brain iron accumulation (former Hallervorden-Spatz disease) is a hereditary neurodegenerative disease with excessive degeneration of the basal ganglia with gliotic changes and excessive iron deposition that lead to the classical eye-of-the-tiger appearance of the globus pallidus. Clinically, most paediatric patients present with a rapid progressive gait impairment, rigidity, dystonia and pronounced mental deterioration or decline.

Creutzfeldt-Jakob disease (*CJD*) is a very rare and incurable degenerative neurological disorder (brain disease) that is ultimately fatal. Among the types of transmissible spongiform encephalopathy found in humans, it is the most common. CJD is normally caused by prions but can also be acquired genetically through a mutation of a gene (5–10 % of cases).

The diagnosis of CJD is suspected when there are typical clinical symptoms and signs such as rapidly progressing dementia with myoclonus. Further investigation can then be performed including MRI. Imaging is unspecific in the majority of cases and may present unspecific atrophy and in some cases symmetric bilateral high signal intensity in the caudate nucleus and putamen bilaterally on the T2- or FLAIR-weighted images.

Huntington's disease is an autosomal dominant (chromosome 4) movement disorder with an onset at the age of 30–40. The disease presents clinically with progressive chorea and dementia in the later stage. Imaging characteristics are nonspecific and include a diffuse cerebral atrophy, most pronounced in the basal ganglia including the striatum and putamen. These structures present with high signal on T2, FLAIR and DWI.

The striatal atrophy leads to a specific form of the lateral ventricles, also known as boxlike configuration. This can be further quantified by measuring the width of the frontal horns or the intercaudate distance from the inner table.

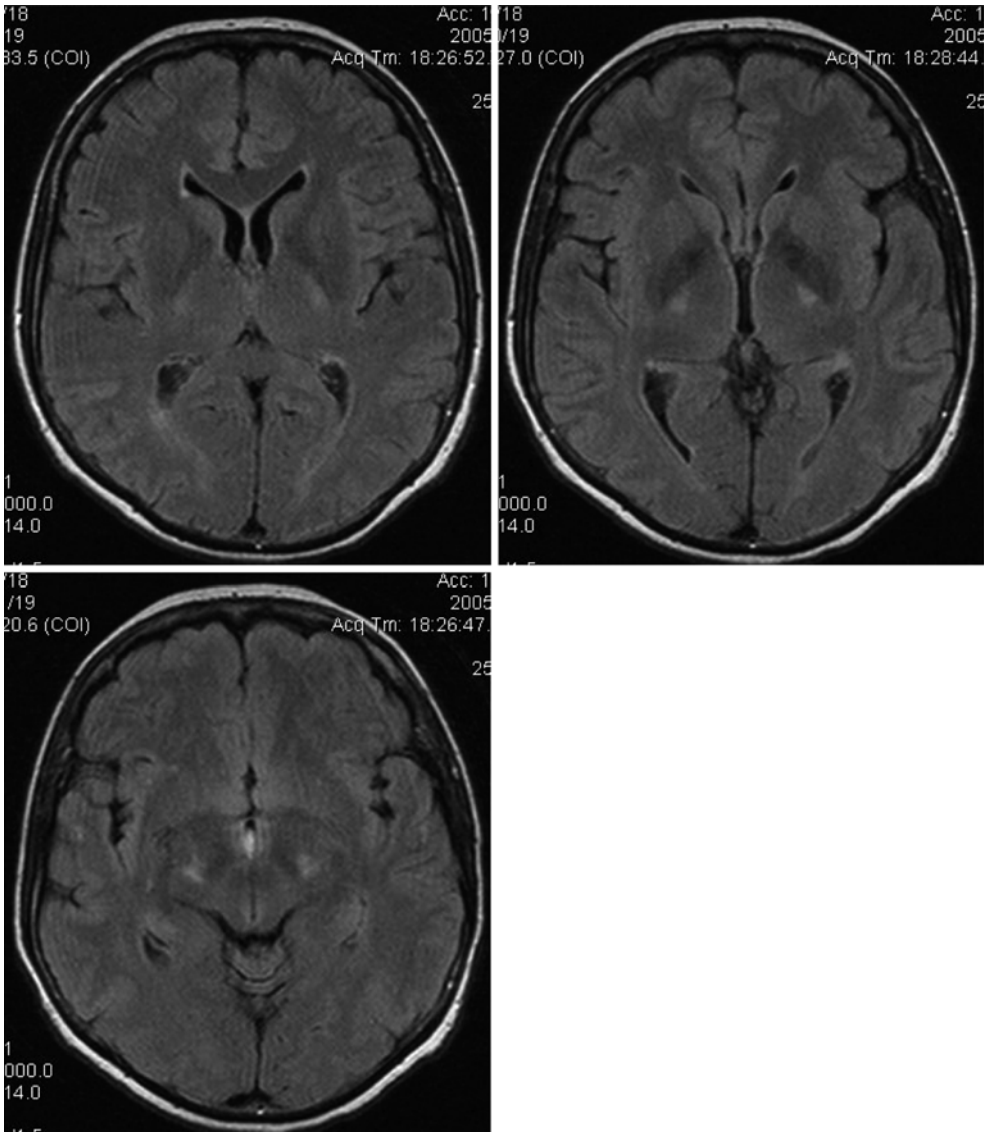

Fig. 1 Fifty-five-year-old patient with ALS. Note the signal changes along the corticospinal tract

Metabolic Disease

Metabolic diseases in children are mostly congenital inborn errors of metabolism, whereas metabolic diseases in adults are usually acquired.

Congenital metabolic disorders in children are a vast and highly specialist field, and detailed knowledge of these belongs to the remit of tertiary referral centres.

The syllabus will focus on the most common inborn errors of metabolism that can present or persist into adulthood, as well as on acquired metabolic disorders.

Although a number of metabolic disorders are closely related to alcohol abuse, a discussion of toxic effects from other substances, including therapeutic and recreational drugs, is beyond the scope of this section. Disorders of iron accumulation (Wilson disease and NBIA) have been discussed above under movement disorders.

Most Common Congenital Metabolic Disorders Presenting or Persisting into Adulthood

X-Linked Adrenoleukodystrophy

This is a disorder of peroxisomal fatty acid beta oxidation leading to accumulation of long-chain fatty acids, which can manifest itself in childhood (typically around 7 years of age) or in adult life. Adult-onset cerebral ALD accounts for about 5 % and usually presents with psychiatric features followed by dementia, ataxia and seizures. As an X-linked disorder, ALD is more frequent in males, but around 15–20 % of heterozygote female carriers become symptomatic.

The typical MRI appearance is T2 and FLAIR hyperintense white matter abnormalities starting in the parieto-occipital regions with early involvement of the splenium of the corpus callosum and corticospinal tracts. These signal abnormalities correspond to areas of demyelination. Active

demyelination at the edge of the lesions is associated with contrast enhancement and restricted diffusion on DWI.

Adrenomyelo-neuropathy (AMN) is a later-onset adult phenotype presenting with slowly progressive spastic paraparesis, bladder and bowel dysfunction, sexual dysfunction and peripheral neuropathy. Typical imaging appearances include increased T2/FLAIR signal in the posterior limbs of the internal capsules, brainstem and cerebellar white matter which may be followed by spinal cord atrophy.

Globoid Cell Leukodystrophy (Krabbe Disease)

Globoid cell leukodystrophy (GLD) has been linked to a mutation in the GALC gene on chromosome 14, leading to a deficiency of galactosylceramide β-galactosidase that causes accumulation of sphingolipids in the lysosomes.

Late adolescent and adult forms (10 %) present with slowly progressive gait abnormalities or spastic paresis. Other features include cognitive decline, seizures and cortical blindness.

MRI shows predominantly posterior T2/FLAIR hyperintense white matter changes with sparing of the U fibres and involvement of the splenium of the corpus callosum, extending along the corticospinal tracts into the posterior limbs of the internal capsules and the pyramidal tracts.

Metachromatic Leukodystrophy (MLD)

Several variants have been described, all of which have deficient activity of arylsulfatase A, which results in defective degradation of sulfatides in the lysosomes.

Approximately 20 % of MLD presents in adulthood often with psychiatric symptoms, followed by spastic paraparesis, cerebellar ataxia and cognitive decline.

MRI demonstrates symmetrical areas of T2 prolongation in the periventricular white matter with sparing of the subcortical U fibres. Early involvement of the peritrigonal white matter, corpus callosum and cerebellar white matter is common, showing typically a "tigroid" pattern of radiating stripes. As opposed to ALD, there is no contrast enhancement of the lesion edge.

Mitochondrial Encephalomyopathy with Lactic Acidosis and Stroke-Like Episodes (MELAS)

Mitochondrial encephalomyopathy with lactic acidosis and stroke-like episodes (MELAS) syndrome is a typical example of a mitochondrial disorder. About 40 % of patients present in late childhood or early adulthood.

Clinical features are led by encephalomyopathy, lactic acidosis and stroke-like episodes; other features include seizures, hearing loss and neuropsychiatric dysfunction.

MRI demonstrates T2/FLAIR hyperintense areas involving cortical and deep grey matter, not confined to any of the major vascular territories. On diffusion-weighted imaging, ADC values can be elevated or decreased, depending on the acuity of symptoms.

Fabry Disease (Galactocerebrosidase Deficiency)

Fabry disease is a lysosomal storage disease related to a deficiency of a-galactosidase. It is an X-linked inherited disorder with varied clinical presentations and an estimated prevalence of 1 in 50,000 persons.

The deposition of globotriaosylceramide-3 in the endothelium and smooth muscles leads to involvement of multiple organ systems, including the blood vessels, heart and kidneys.

Macro- and microvascular complications are the leading CNS manifestations, with the first cerebrovascular event usually occurring usually around 40 years of age.

CT and MRI features are those of macrovascular disease (acute or chronic infarcts and parenchymal haemorrhage) and signs of microvascular disease (hyperintense foci in the periventricular and subcortical white matter and cerebral microhaemorrhages).

Characteristic MRI features of Fabry's disease are T1 hyperintensity within the pulvinar nuclei of the thalamus (the "pulvinar sign") and ectasia of the basilar artery on MRA, which has been found to be one of the best indicators of the presence of the disease in adults.

Alexander Disease

Defects in the glial fibrillary acidic protein gene have been identified as the underlying cause of this disease, in which approximately 25 % of patients present in adulthood, most commonly with bulbar dysfunction, pyramidal involvement, cerebellar ataxia and sleep abnormalities.

The MRI findings of the infantile and juvenile form include extensive white matter change with frontal predominance, a periventricular rim with high signal on T1-weighted images and low signal on T2-weighted images, abnormalities of the basal ganglia and thalami, brainstem abnormalities and contrast enhancement.

In adult onset disease, MRI findings consist of atrophy and abnormal signal within the medulla and upper cord, which has been termed a "tadpole" appearance and may be accompanied by periventricular white matter change.

Primary Familial Brain Calcification

Primary familial brain calcification, idiopathic basal ganglia calcification and bilateral striopallidodentate calcinosis are terms used for what was formerly called Fahr disease. This is a group of genetic disorders with currently four known mutations that are inherited in an autosomal dominant pattern. Symptomatic patients present in their late 40s with a mostly Parkinsonian movement disorder, followed by cognitive decline, cerebellar features and speech disorders. Symmetrical calcification involving the lentiform nuclei, caudate nuclei, thalami and dentate nuclei is mostly readily detected by CT. On MRI, the structures involved may show high signal on T1-weighted spin echo sequences and signal loss on susceptibility-weighted imaging.

Acquired Metabolic Disorders

Wernicke's Encephalopathy

Wernicke's encephalopathy (WE) is caused by a deficiency of vitamin B1 (thiamine), which may be due to alcohol abuse, malabsorption, poor nutrition, increased metabolism or iatrogenic elimination (haemodialysis).

Thiamine depletion leads to failure of conversion of pyruvate to acetyl-CoA and α-ketoglutarate to succinate and the lack of Krebs cycle resulting in cerebral lactic acidosis with intra- and extracellular oedema, swelling of astrocytes, oligodendrocytes, myelin fibres and neuronal dendrites.

The classic clinical triad of ocular dysfunctions (nystagmus, conjugate gaze palsy, ophthalmoplegia), ataxia and confusion is observed only in 30 % of cases. Treatment consists of thiamine infusion, which can prevent progression to Korsakoff's dementia or death.

MRI shows T2/FLAIR hyperintensities in the periaqueductal and medial thalamic regions, mammillary bodies, hypothalamus, tectum and cerebellum.

Contrast enhancement occurs in 80 % in the mammillary bodies (often prior to T2 hyperintensities) and in 50 % in the periaqueductal regions.

Imaging abnormalities can regress with treatment, but the prognosis is usually poor once there is cortical involvement or T1 hyperintensity in the thalami and mammillary bodies indicating haemorrhagic change.

Chronic cases show atrophy of the mammillary bodies.

Subacute Combined Degeneration

This is a disorder of the spinal cord secondary to vitamin B12 deficiency, characterised by gliosis and spongiform degeneration of the posterior and lateral columns. Clinical presentations are in spastic paraparesis and spinal ataxia.

MRI demonstrates T2 hyperintensities in the posterior and lateral columns of the spinal cord, which can reverse after adequate B12 administration. Chronic non- or undertreated cases show spinal cord atrophy.

Osmotic Myelinolysis Syndrome

This entity includes central pontine myelinolysis (CPM) and extrapontine myelinolysis and occurs usually in patients with hyponatremia that has been corrected too quickly.

The traditionally proposed pathophysiological mechanism is a disruption of the blood-brain barrier resulting in vasogenic oedema, fibre tract compression and myelinolysis. Additional implicated mechanisms are cerebral dehydration, intramyelinic oedema and oligodendrocyte degeneration. The most common damage is in the central pontine fibres (CPM). Extrapontine demyelination (in sites such as basal ganglia, thalami, lateral geniculate body, cerebellum and cerebral cortex) may occur together with CPM or in isolation (in approximately 10 %).

Clinical symptoms of CPM include paralysis, dysphagia, dysarthria and pseudobulbar palsy.

Typical MRI features of central pontine myelinolysis are T2/FLAIR hyperintensity in the central pons showing a symmetric "trident" or "bat-wing" pattern, due to sparing of the peripheral fibres and the axons of the corticospinal tracts.

In the acute phase, DWI shows restricted diffusion with a decreased ADC. This may occur within 24 h of symptom onset and precede the signal abnormalities seen on T2 or FLAIR images. The ADC values usually return to baseline within 3–4 weeks.

CPM can appear moderately hypointense in T1 and may infrequently show contrast enhancement. If the patient survives the acute phase, the pontine lesions can cavitate and appear markedly hypointense on T1-weighted images.

Hepatic Encephalopathy

The term hepatic encephalopathy includes a spectrum of neuropsychiatric abnormalities in patients with liver dysfunction. Most cases are associated with cirrhosis and portal hypertension or portal-systemic shunts, but the condition can also occur in acute liver failure.

Classical MR abnormalities in chronic hepatic encephalopathy include high signal intensity in the globus pallidus on T1-weighted images and, less frequently, in the substantia nigra and the tegmentum of the midbrain, secondary to increased concentrations of manganese.

Magnetisation transfer imaging, fast FLAIR and DWI sequences may demonstrate white matter abnormalities secondary to increased CNS ammonia concentration. These return to normal with restoration of liver function and are thought to reflect mild diffuse interstitial brain oedema, which appears to play an essential role in the pathogenesis of hepatic encephalopathy.

In acute hepatic encephalopathy, bilateral symmetric T2 hyperintensities of the cortical grey matter are often associated with restricted diffusion. There may be additional involvement of the subcortical white matter, basal ganglia, thalami and midbrain. These imaging abnormalities are thought to reflect cytotoxic oedema secondary to acute hyperammonemia.

Hypoglycemic Encephalopathy

An acute decrease in serum glucose levels can arise from an excess of exogenous or endogenous insulin- and hypoglycaemia-inducing drugs. This causes a decline of the cell membrane ATPase pump activity and release of excitatory neurotransmitters such as aspartate.

CT can demonstrate enhancing hypodensities in the basal ganglia, cerebral cortex, hippocampus and substantia nigra.

MRI is more sensitive and shows T2 hyperintensities as well as restricted diffusion in the posterior limb of the internal capsules, hippocampi, the basal ganglia and cortical

areas and splenium of the corpus callosum. These changes are likely to reflect cytotoxic oedema, and extensive DWI changes in the basal ganglia and deep white matter are associated with poor clinical outcome.

Hyperglycemic Encephalopathy

Hyperglycaemia occurs in uncontrolled diabetes mellitus and can lead to osmotic derangements the basal ganglia and subthalamic region.

Imaging findings are hyperdense changes on CT and T1 hyperintensities on MRI within the putamen and caudate nuclei, which may be uni- or bilateral. SPECT has been reported to show hypoperfusion in the basal ganglia. After correction of blood glucose, the imaging abnormalities usually regress.

References

Movement Disorders General

1. Amogh NH, Mohan S, Lath N, Tchoyoson Lim CC (2001) Differential diagnosis for bilateral abnormalities of the basal ganglia and thalamus MR NR. Radiographics 31:5–30

Parkinsons Disease

2. Darcourt J, Booij J, Tatsch K et al (2010) EANM procedure guidelines for brain neurotransmission SPECT using (123)I-labelled dopamine transporter ligands, version 2. Eur J Nucl Med Mol Imaging 37(2):443–450
3. Brooks DJ (2010) Imaging approaches to Parkinson disease. J Nucl Med 51(4):596–609
4. Weingarten CP, Sundman MH, Hickey P, Chen NK (2015) Neuroimaging of Parkinson's disease: expanding views. Neurosci Biobehav Rev 59:16–52. doi:10.1016/j.neubiorev.2015.09.007, Epub ahead of print

Multi-System-Atrophy

5. Ozawa T, Paviour D, Quinn NP et al (2004) The spectrum of pathological involvement of the striatonigral and olivopontocerebellar systems in multiple system atrophy: clinicopathological correlations. Brain 127(Pt):2657–2671
6. Lee JY, Yun JY, Shin CW et al (2010) Putaminal abnormality on 3-T magnetic resonance imaging in early parkinsonism-predominant multiple system atrophy. J Neurol 257(12):2065–2070

Wilsons Disease

7. King AD, Walshe JM, Kendall BE et al (1996) Cranial MR imaging in Wilson's disease. AJR Am J Roentgenol 167(6):1579–1584

Amyotrophic Lateral Sclerosis

8. Cheung G, Gawel MJ, Cooper PW et al (1995) Amyotrophic lateral sclerosis: correlation of clinical and MR imaging findings. Radiology 194(1):263–270

Huntington Diseases

9. Chan S, Shungu DC, Douglas-Akinwande A et al (1999) Motor neuron diseases: comparison of single-voxel proton MR spectroscopy of the motor cortex with MR imaging of the brain. Radiology 212(3):763–769

PSP

10. Quattrone A, Nicoletti G, Messina D et al (2008) MR imaging index for differentiation of progressive supranuclear palsy from Parkinson disease and the Parkinson variant of multiple system atrophy. Radiology 246(1):214–221
11. Righini A, Antonini A, De Notaris R et al (2004) MR imaging of the superior profile of the midbrain: differential diagnosis between progressive supranuclear palsy and Parkinson disease. AJNR Am J Neuroradiol 25(6):927–932
12. Gröschel K, Kastrup A, Litvan I et al (2006) Penguins and hummingbirds: midbrain atrophy in progressive supranuclear palsy. Neurology 66(6):949–950

NBIA

13. Sener RN (2003) Pantothenate kinase-associated neurodegeneration: MR imaging, proton MR spectroscopy, and diffusion MR imaging findings. AJNR Am J Neuroradiol 24(8):1690–1693
14. Guillerman RP (2000) The eye-of-the-tiger sign. Radiology 217(3):895–896

CJD

15. Lee H, Hoffman C, Kingsley PB et al (2010) Enhanced detection of diffusion reductions in Creutzfeldt-Jakob disease at a higher B factor. AJNR Am J Neuroradiol 31(1):49–54
16. Kallenberg K, Schulz-schaeffer WJ, Jastrow U et al (2006) Creutzfeldt-Jakob disease: comparative analysis of MR imaging sequences. AJNR Am J Neuroradiol 27(7):1459–1462
17. Finkenstaedt M, Szudra A, Zerr I et al (1996) MR imaging of Creutzfeldt-Jakob disease. Radiology 199(3):793–798

Metabolic Disease

18. Ahmed RM, Murphy E, Davagnanam I et al (2014) A practical approach to diagnosing adult onset leukodystrophies. J Neurol Neurosurg Psychiatry 85:770–781
19. Alonso J, Córdoba J, Rovira A (2014) Brain magnetic resonance in hepatic encephalopathy. Semin Ultrasound CT MR 35(2):136–52 A

20. Alleman AM (2014) Osmotic demyelination syndrome: central pontine myelinolysis and extrapontine myelinolysis. Semin Ultrasound CT MR 35(2):153–159
21. Krishna SH, McKinney AM, Lucato LT (2014) Congenital genetic inborn errors of metabolism presenting as an adult or persisting into adulthood: neuroimaging in the more common or recognizable disorders. Semin Ultrasound CT MR 35(2):160–191
22. Rovira A, Sundgren P, Gallucci M (2014) Inflammatory and metabolic disease. Chapter 64 in Grainger & Allison's diagnostic Radiology, 6th edn. Churchill Livingstone, Kirjastus
23. Sutter R, Kaplan PW (2015) What to see when you are looking at confusion: a review of the neuroimaging of acute encephalopathy. J Neurol Neurosurg Psychiatry 86(4):446–459

Neuroimaging in Dementia

Frederik Barkhof and Mark A. van Buchem

Dementia: Clinical Background

Dementia is usually defined as an acquired condition involving multiple cognitive impairments that are sufficient to interfere with activities of daily living. It is usually but not necessarily progressive. Memory impairment is one of the most common deficits, but other domains such as language, praxis, visual-perceptive and most notably executive functions are often involved. With increasing loss of function due to these cognitive problems, there is progressive difficulty with activities of daily living. Many of the diseases that cause dementia have a relentlessly progressive course with an insidious onset; many have long durations (e.g. 5–10 years from diagnosis) and relatively prolonged end-stage period of where all self-care and independence is lost. Dementia places tremendous burdens on patients, their families and carers and on health and social care systems. The most important causes of dementia have an age-related incidence. As a result the prevalence and societal costs of dementia are predicted to rise dramatically over the coming decades.

In 2000, prevalence data of 11 European population-based studies were pooled to obtain stable estimates of prevalence of dementia in the elderly (>65 years). Age-standardized prevalence was 6.4 % for dementia (all causes), 4.4 % for Alzheimer's disease (AD) and 1.6 % for vascular dementia (VaD). Prevalence of dementia was higher in women than in men and nearly doubled with every 5 years increase of age: from 0.8 % in the group age 65–69 years to 28.5 % over the age of 90 years.

Need for a Nosological Approach

Dementia is a syndrome, not a disease, and has many and varied causes. The diagnostic workup is meant to identify the underlying cause with a particular emphasis on picking up treatable conditions. Diagnosis is critically dependent on careful history taking from patient and informant followed by clinical and cognitive examination supported by ancillary investigations, of which neuroimaging is one of the most important. The a priori chance of a particular disease being present is dependent on age. The younger the patient, the greater the chance that one of a wide range of underlying pathologies is the cause of the cognitive problems. Diseases like frontotemporal lobe degeneration (FTLD) and Huntington's disease (HD) tend to occur more often before the age of 70; genetic forms of AD almost exclusively occur at young ages and rare metabolic causes are more likely in early adulthood (see Table 1). In the older patient AD, Lewy body dementia (LBD) and vascular disease are by far the most common pathologies; mixed disease is very common: notably AD with vascular disease has been shown to be the most prevalent in post-mortem series of older individuals (>85 years).

The nosological approach is facilitated by the use of clinical criteria. In the table below, the main disease categories and their published clinical criteria are listed with the use of imaging highlighted. From the table, it may be inferred that for the majority of diseases, no specific imaging criteria have been formulated; however, it is also notable that more recent revisions of criteria are increasingly including imaging (for positive as well as negative predictive value).

F. Barkhof (✉)
Department of Radiology & Nuclear Medicine,
VU University Medical Centre, Amsterdam, The Netherlands

Institutes of Neurology and Biomedical Engineering,
University College London, London, UK
e-mail: f.barkhof@vumc.nl; f.barkhof@ucl.ac.uk

M.A. van Buchem
Department of Radiology, Leiden University Medical Centre,
Leiden, The Netherlands
e-mail: m.a.van_buchem@lumc.nl

J. Hodler et al. (eds.), *Diseases of the Brain, Head and Neck, Spine 2016–2019: Diagnostic Imaging*, DOI 10.1007/978-3-319-30081-8_10

Table 1 Differential diagnosis in young-onset dementia

Disease	MRI findings	Clinical clues	Additional tests
Alzheimer's disease	Posterior cingulate atrophy, medial temporal atrophy	Family history, visuospatial and apraxia > memory	CSF (abeta and tau); FDG-PET; amyloid PET
Frontotemporal lobe degeneration	Frontotemporal atrophy Temporal atrophy (asymmetrical or symmetrical)	Family history, language, behaviour	FDG-PET
Corticobasal degeneration	Frontoparietal atrophy; may be asymmetrical	Asymmetrical parkinsonism, dyspraxia and myoclonus; alien limb	CSF; dopamine imaging
Small vessel disease	Strategic infarcts, lacunes, WMH, microbleeds, microinfarcts, dilated VRS	TIA; stroke	Vascular risk factors
Vasculitis	WMH, patchy enhancement, multifocal diffusion restriction	TIA, multifocal	ESR and CRP elevation; CSF, DSA, serology
Multiple sclerosis	Disseminated WM lesions, black holes Gad enhancement	Relapses; other neurological findings	CSF oligoclonal bands
Creutzfeldt-Jakob disease	Abnormal DWI basal ganglia or neocortex	Myoclonus; cerebellar ataxia	EEG, CSF tau and 14-3-3 protein
Paraneoplastic or limbic encephalitis	Temporal lobe lesions; thalamic swelling	Subacute onset; other neurological findings	CSF antibodies
Infectious	WM lesions, enhancement	Fever, HIV, lues	Serology, CSF, culture
Metabolic	WM lesions, GM lesions, lactate in spectroscopy, diffusion restriction	Stroke-like episode	CSF, serology, muscle biopsy, genetics

Modified from Ridha B, Josephs KA. *Neurologist*. 2006;12:2–13

The Toolbox

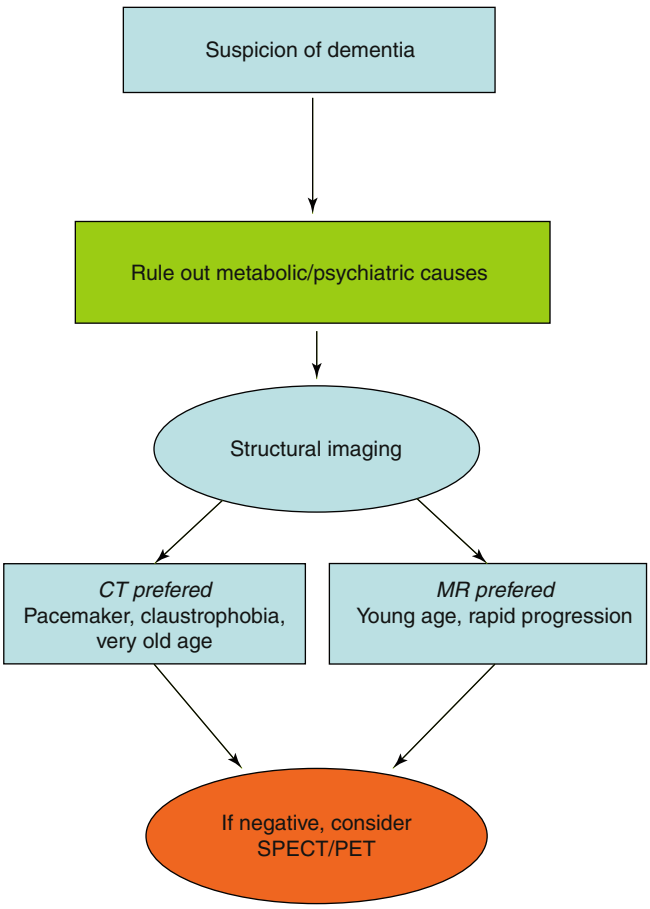

When structural imaging is equivocal or does not lead to the diagnosis, functional imaging may add diagnostic value. Second-line neuroimaging investigation includes metabolic information obtained by using SPECT or PET or physiological information obtained by using diffusion or perfusion MRI. For example, in the early stages of FTLD, there may not exist any discernible atrophy. FDG-PET or HMPAO-SPECT might demonstrate decreased metabolism or hypoperfusion preceding tissue loss on structural imaging. In the future, molecular imaging may provide even more disease-specific information. PET tracers binding to amyloid are a good example of such developments, although their role in the diagnostic algorithm still remains to be established.

Standard Structural MR Imaging Protocol

The prevalence of AD and vascular pathology means that suggested first aims in the imaging evaluation of a patient suspected of having dementia – beyond exclusion of a surgically treatable disorder – are:

(I) To assess the extent and pattern of brain atrophy, in particular medial temporal lobe atrophy (for evidence of Alzheimer's pathology)
(II) To determine the degree of vascular damage, including the occurrence of strategic vascular lesions

Standard Structural MRI Protocol: No Routine Contrast Administration

- Sagittal 3D T1-weighted gradient echo with 1 mm isotropic voxels
  - Coronal reformats (MPR) perpendicular to long axis of hippocampus
  - Detection of regional atrophy patterns (e.g. hippocampal)
- Transverse FLAIR with 3–5 mm slices (can be MPR form 3D-FLAIR)
  - Detection of ischemic white matter lesions and lacunes
- Transverse T2-weighted TSE/FSE with 3–5 mm slices
  - Detection of thalamic lesions and vessel patency
- Transverse T2* gradient echo with 3–5 mm slices
  - Detection of microbleeds
- Transverse DWI/ADC
  - Detection of recent infarcts and CJD

Table 2 Visual assessment of medial temporal lobe atrophy (MTA)

Score	Width of choroid fissure	Width of temporal horn	Height of hippocampus
0	N	N	N
1	↑	N	N
2	↑↑	↑	↓
3	↑↑↑	↑↑	↓↓
4	↑↑↑	↑↑↑	↓↓↓

According to Scheltens et al.
(↑ increase, ↓ decrease, *N* normal)

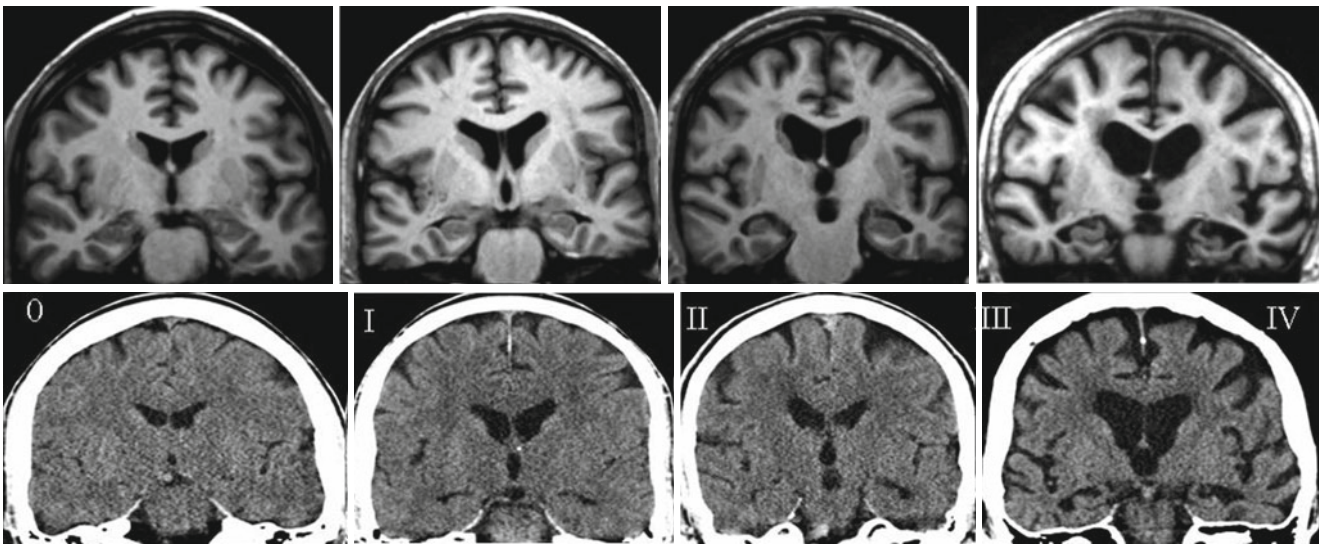

Visual rating of MTA. In these same-day scans, a perfect similarity between MRI and CT is noted for assessment of the medial temporal lobe for visual rating of MTA (Modified with permission from *Radiology*. 2009;253:174–83)

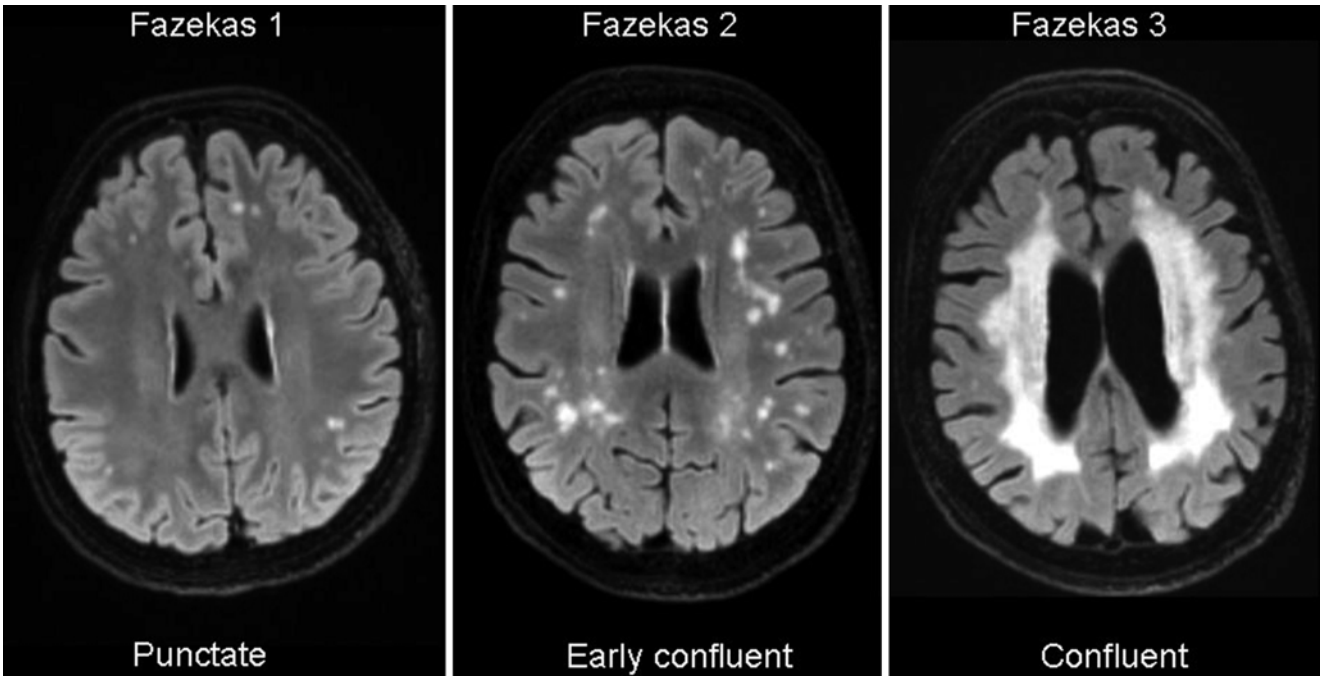

WMH scoring using Fazekas' rating scale

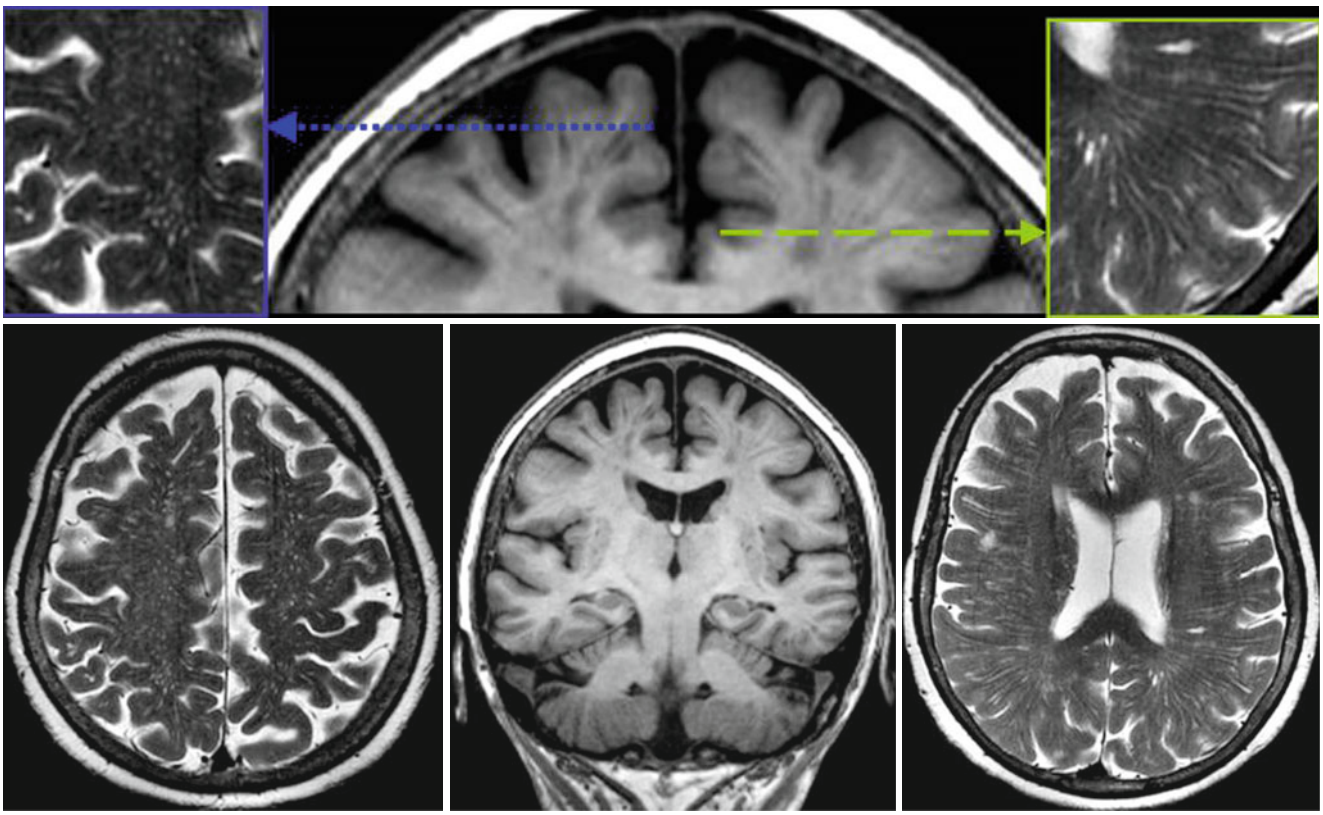

Virchow-Robin spaces (VRS). This 71-year-old woman presented with subjective memory complaints only. The coronal T1-weighted image in the middle show normal hippocampi and ventricles. There is diffuse widening of the VRS which are seen as sharply demarcated structures with signal intensity close to CSF. Note that their appearance on axial T2-weighted images depends on their orientation relative to the imaging plane, leading to a dot-like appearance when cut cross-sectionally (*left*) or stripe-like when cut tangentially (*right*)

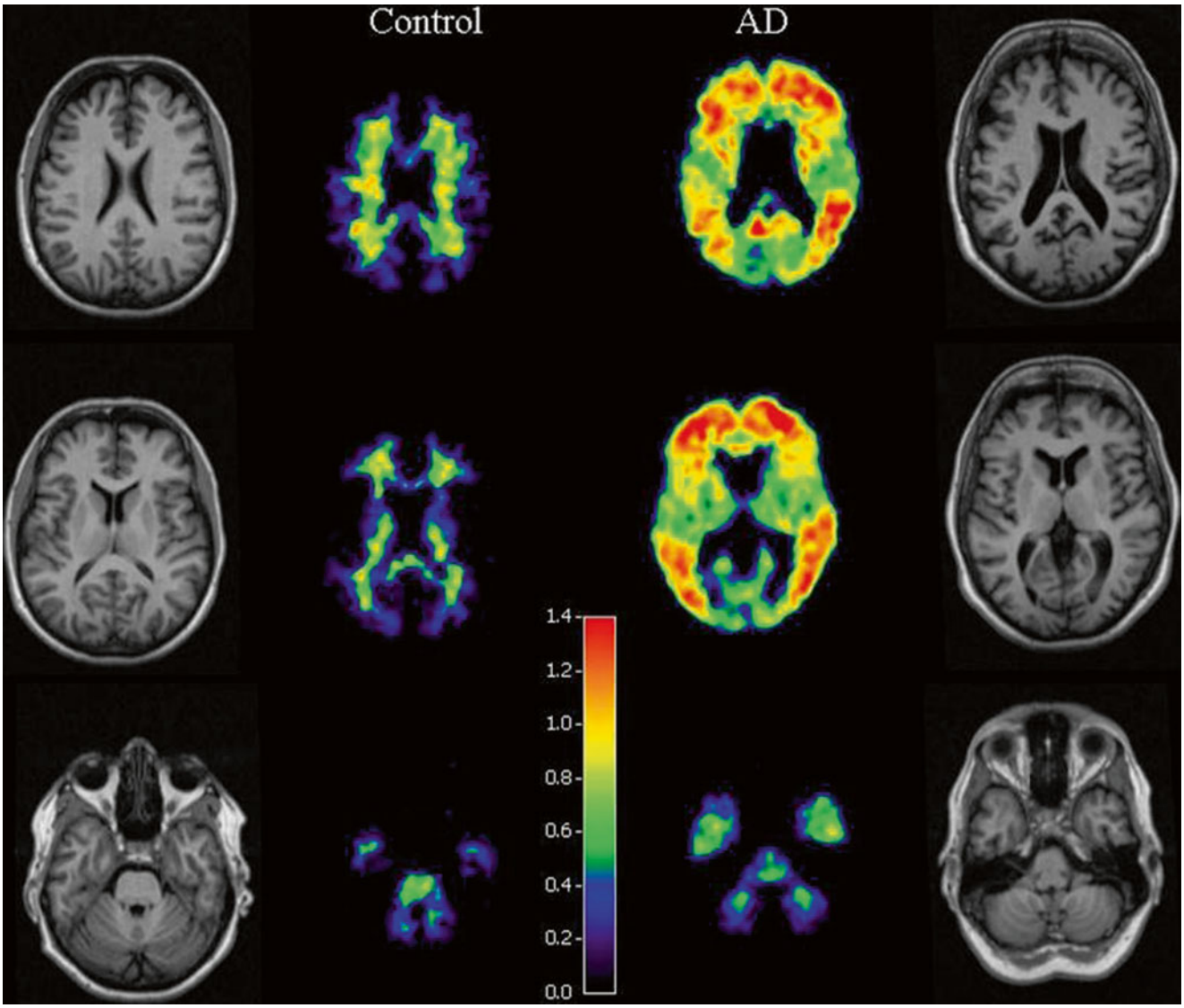

Amyloid PET in AD. The binding potential of the tracer ^{11}C-Pittsburgh compound-B (PIB) is low in healthy controls and confined to the white matter. By contrast, abnormal uptake occurs in the cortex of AD patients, probably many years before the diagnosis due to abnormal amyloid deposition.

Normal Ageing

Age-related abnormalities do not occur in all elderly persons. Some elderly individuals have a perfectly normal brain that is indistinguishable from that of a young person. This observation is in line with the concept of subdividing human ageing in *successful ageing* and *usual ageing*. Successful ageing is defined as minimal physiologic loss, even when compared with younger individuals, and usual ageing as the presence of disturbance of physiologic functions (such as systolic hypertension, abnormal glucose tolerance test) without overt neurologic symptoms. Elderly individuals with a normal appearance of the brain on imaging might be representatives of the group of successful ageing human beings. Age-related changes that are apparent on radiological examinations do not always have functional consequences. An impressive load of brain lesions may be an incidental finding in an elderly individual, who has no neurological or intellectual complaints whatsoever and who, apparently, is capable of having a normal, independent life.

Normal ageing and neurodegenerative disorders may be difficult to distinguish. One reason is the similarity of the abnormalities that are associated with these conditions. In several neurodegenerative disorders, the abnormalities only differ in pattern from those occurring in normal ageing. In other neurodegenerative disorders, the abnormalities really are similar, also in pattern, and the amount of abnormalities in relation to a patient's age is the only factor that permits

distinction from normal ageing. Another phenomenon that complicates distinguishing normal ageing from other neurodegenerative disorders is the fact that due to the high prevalence of the latter, these conditions often coexist in the elderly with changes that are due to normal ageing. In such circumstances it may be impossible to separate the abnormalities in terms of their origin.

An important task for radiologists, when confronted with a brain study in an elderly patient, is to screen for the presence of neurodegenerative disorders. In this process, changes should not be attributed too easily to normal ageing. In order to be able to separate usual ageing and other neurodegenerative disorders, a radiologist should be familiar with the changes that occur in normal ageing. In the following section, such changes will be described.

Structured Evaluation of MRI in Workup of Dementia

1. Exclude a structural lesion which may be amenable for neurosurgical intervention. Consider both lesions with significant mass effect (e.g. subdural hematoma, meningioma) and lesions with minor mass effect (e.g. AVM).
2. Exclude brain swelling, either generalized swelling (e.g. associated with dural AVF or hydrocephalus) or focal swelling (e.g. medial temporal lobe swelling in HSV encephalitis). Whenever swelling is present, consider adding DWI and Gd-enhanced images.
3. Assess signal increase on T2/FLAIR, both in white matter (e.g. white matter changes (WMC) in vascular disease) and in grey matter (e.g. thalamic infarction in vascular disease or pulvinar sign in Creutzfeldt-Jakob disease). Consider applying a white matter rating scale, such as the Fazekas scale or the ARWMC scale. When describing vascular changes, assess/report specifically lacunes, état criblé and (bilateral) thalamic lesions and whether changes involve the brain stem or basal ganglia.
4. Assess microbleeds (MBs) on T2*GE, especially in subjects with white matter changes.
5. Determine the degree and pattern of general cortical atrophy (GCA) and specifically report whether the atrophy:
   (a) Is abnormal for age or not
   (b) Is symmetric of asymmetric
   (c) Has a regional pattern
   (d) Has a posterior or anterior gradient
6. Assess focal atrophy, especially in the following regions:
   (a) Medial temporal lobe (e.g. MTA as seen in AD) (see Table 2)
   (b) Temporal pole and/or frontal lobes (e.g. consistent with FTLD)
   (c) Biparietal atrophy (posterior cortical atrophy, mostly AD)
   (d) Occipital atrophy (posterior cortical atrophy or the Balint syndrome, usually AD but there is a considerable overlap with other neurodegenerative pathologies)
   (e) Posterior cingulate and precuneus (e.g. presenile or posterior AD)
   (f) Mesencephalic atrophy (e.g. PSP)
   (g) Pontine (and cerebellar) atrophy (e.g. MSA)
   (h) Cerebellar atrophy (e.g. alcohol abuse, prion, etc.)

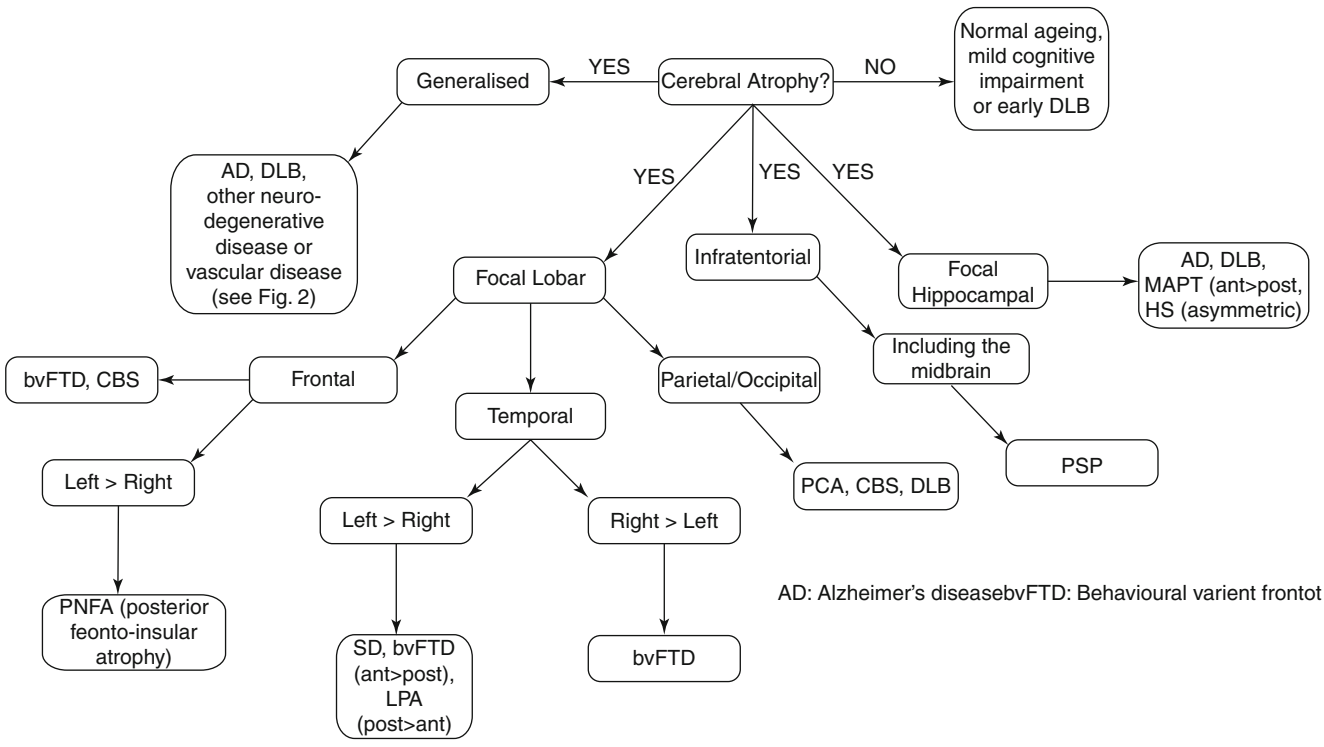

AD: Alzheimer's diseasebvFTD: Behavioural varient frontot

Suggested Reading

Harper L, Barkhof F, Scheltens P, Schott JM, Fox NC (2014) An algorithmic approach to structural imaging in dementia. J Neurol Neurosurg Psychiatry 85(6):692

Frederik Barkhof, Nick C. Fox, António J. Bastos-Leite, Philip Scheltens (2002) Neuroimaging in dementia hardcover. Lancet Neurol 1(1):13–21

http://www.radiologyassistant.nl/en/p43dbf6d16f98d/dementia-role-of-mri.html

Traumatic Neuroemergency: Imaging Patients with Traumatic Brain Injury – an Introduction

Paul M. Parizel and C. Douglas Philips

Introduction

Traumatic brain injury (TBI) is a leading cause of mortality and disability among young individuals, especially in high-income countries [1]. According to a meta-analysis, combining reports from 23 European countries between 1980 and 2003, the incidence rate is about 235 per 100,000 [2]. Increasingly, imaging techniques play a crucial role in the diagnosis and management of patients with craniocerebral trauma, often influencing life or death decisions.

Imaging Techniques

The diagnostic efficacy of plain skull films in TBI is poor. At present, for the management of patients with traumatic brain injury, plain X-ray films no longer play a role; they have been replaced by computed tomography (CT) imaging [3].

CT is the initial imaging technique for evaluation of craniocerebral trauma. In most trauma centers and emergency rooms, CT is readily available. More and more emergency departments position a CT scanner in the receiving area for rapid triage. Moreover, a CT examination can be performed in a few seconds with a modern, state-of-the art multidetector CT scanner. These machines allow acquisition of multiple thin sections in a much shorter scan time than a single-detector system [4]. Image data can be reconstructed in every plane as well as in 3D views (Fig. 1). Routine utilization of these multiplanar reconstructed (MPR) images also appears to improve diagnosis of traumatic injuries and has been supported in the literature to increase CT accuracy [5]. Modern hospitals almost invariably utilize multi-detector computed tomography (MDCT) scanners. Cranial CT is used for evaluation of all forms of intracranial hemorrhage,

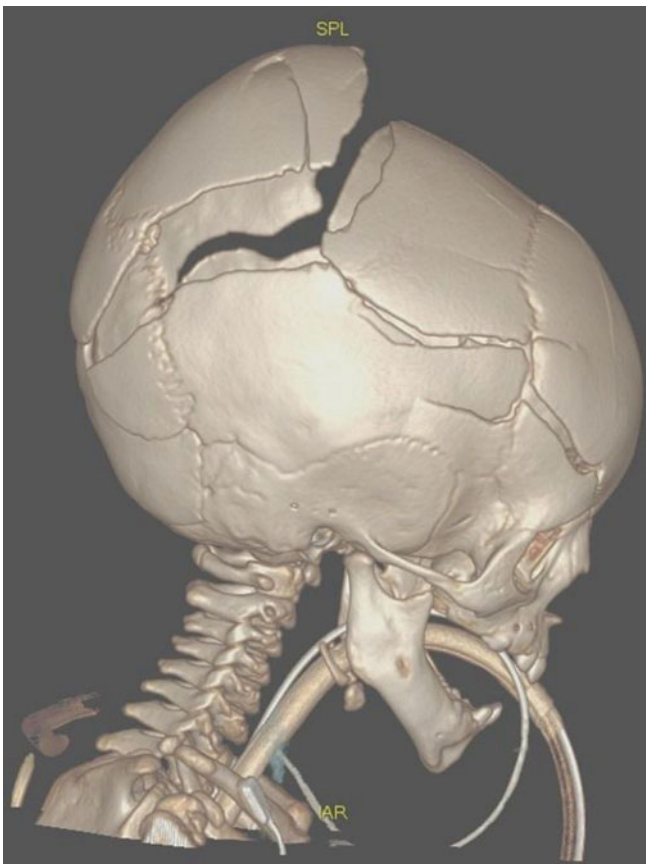

Fig. 1 Volume rendering technique (*VRT*), obtained from a 3D CT scan data set, reveals multiple skull fractures and displaced bone fragments. The sharp outline of the fracture lines is clearly distinct from the jagged and serrated edges of the cranial sutures in this young child with severe craniocerebral trauma

P.M. Parizel, MD, PhD (✉)
Department of Radiology,
Antwerp University Hospital & University of Antwerp,
Wilrijkstraat 10, Antwerp (Edegem) B-2650, Belgium
e-mail: paul.parizel@uantwerpen.be

C.D. Philips, MD, FACR
Head and Neck Imaging, Weill Cornell Medical Center,
NewYork-Presbyterian Hospital, 525 East 68th Street,
New York, NY NY 10065, USA
e-mail: dphillips@med.cornell.edu

J. Hodler et al. (eds.), *Diseases of the Brain, Head and Neck, Spine 2016–2019: Diagnostic Imaging*, DOI 10.1007/978-3-319-30081-8_11

fractures, brain edema, herniation, and other associated injuries, as well as to evaluate foreign bodies. CT angiography (dynamic contrast-enhanced CT to visualize vascular structures) may be indicated whenever vascular injury is suspected and also in patients with a high-risk mechanism trauma, such as, for example, intraoral trauma, high energy crashes, near hanging, and fractures of skull base and midface [6] or for suspicious hemorrhage patterns.

MRI is more sensitive than CT for the detection of parenchymal lesions [7, 8]. It is also indicated whenever there is a discrepancy between the clinical neurological status of the patient and the CT findings.

In this review paper, we aim to present a systematic guide toward interpretation of imaging studies in the patient with TBI.

Scalp Lesions

Scalp lesions are common in head trauma victims (Figs. 2 and 3). Although they are of little clinical importance, the identification of scalp lesions may direct the attention of the radiologist toward the point of impact [9]. CT is rarely performed for isolated scalp injury, but to detect the more critical and suspected intracranial injuries. CT not only visualizes the soft tissue swelling but through correct window (W) and level (L) settings will also illustrate intracranial abnormalities [8]. One important factor influencing the detection rate of soft tissue lesions in CT is the perception of density differences within the lesions and the surrounding tissues such as blood, subcutaneous fatty tissue, or cerebrospinal fluid [10].

Table 1 provides an overview of some of the most commonly encountered scalp lesions.

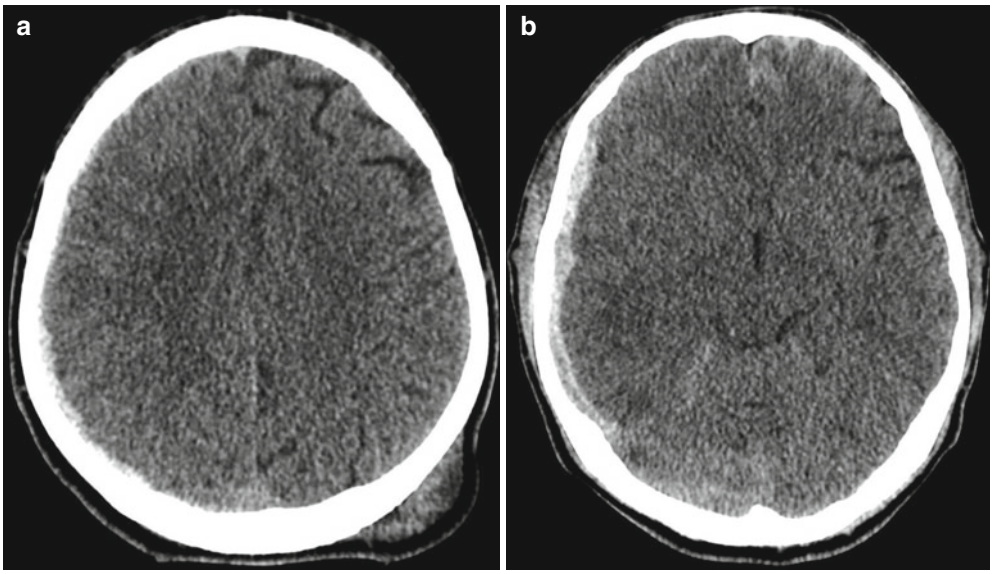

Fig. 2 (**a**, **b**) Axial noncontrast CT scan, revealing a left parietal subgaleal hematoma ("coup" side). On the "contrecoup" side, there is a hyperdense subdural hematoma overlying the right cerebral hemisphere, as well as a basifrontal hemorrhagic contusion. Notice the brain swelling with obliteration of the ambient cisterns around the brainstem

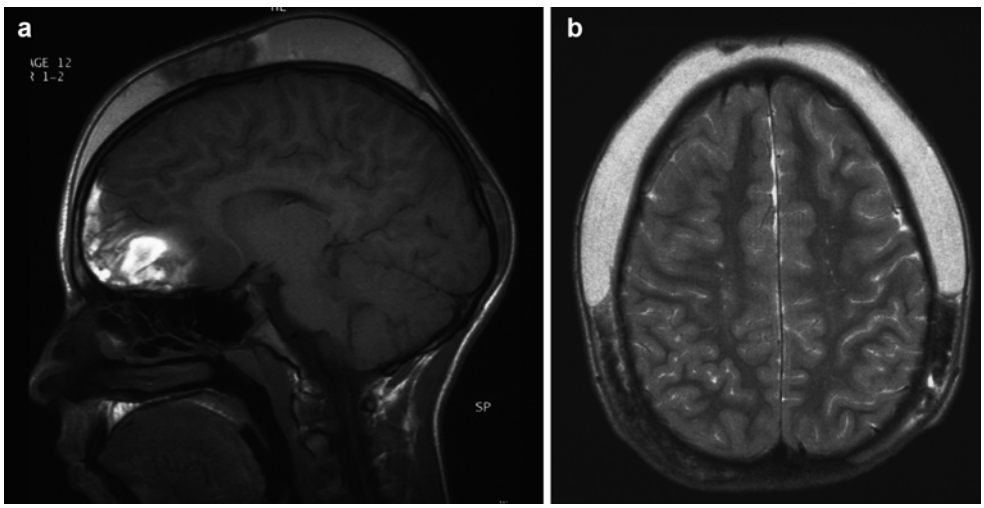

Fig. 3 (**a**, **b**) Hemorrhagic cerebral contusions and subgaleal hematoma. MRI examination performed with (**a**) sagittal SE T1-weighted images and (**b**) axial TSE T2-weighted images. Extracranially, there is marked swelling of the subcutaneous soft tissues, due to a massive subgaleal hematoma, which extends from the frontal to the posterior parietal region. Intracranially, there are hemorrhagic cerebral contusions in the right frontal and anterior temporal lobes

Table 1 Overview of scalp lesions

Lesion type	Caput succedaneum	Subgaleal hematoma (extracranial subdural hematoma)	Subgaleal hygroma	Cephalohematoma (extracranial epidural hematoma)
Occurrence	After normal vaginal delivery	After head trauma (or after birth)	Birth trauma (forceps delivery)	Birth trauma (skull fracture during birth)
Location	Superficial of the galea aponeurotica	Beneath the galea aponeurotica	Beneath the galea aponeurotica	Subperiosteal (flat skull bones)
Composition	Edema (with microscopic hemorrhages)	Venous blood	Cerebrospinal fluid	Subperiosteal hemorrhage
Clinical presentation	Pitting edema	Diffusely spreading, firm fluctuating mass	–	Well-defined, focal, firm mass
Skull fracture		Yes or no	Yes	Yes
Crosses suture lines?	Yes	Yes	Yes	No

Skull Fractures

Skull fractures constitute a diverse group of traumatic bone injuries with different mechanism of occurrence, topography, complications, and required management. They can be classified according to various parameters:

- Shape of the fracture: linear, comminuted, and stellate
- Depressed, non-depressed, and open
- Anatomic location and extent of the fracture: skull vault, skull base, and craniofacial junction

Simple linear fractures are most common type, especially in children younger than 5 years. Temporal bone fractures represent 15–48 % of all skull fractures and are considered as a separate category of skull injury. Skull base and temporal bone fractures have their own clinical significance; a detailed discussion of these injuries is beyond the scope of this text.

CSF leaks, cranial nerve injuries, orbital injuries, and craniocervical junction injuries are common accompaniments of fractures, especially near the skull base.

Depressed skull fractures (with displacement of the outer table of the skull to at least the level of the inner table) occur in 75 % of cases in the frontoparietal region and are often open (75–90 %).

Patients with skull fractures have a fivefold increased risk of having an intracranial hemorrhage (ICH), and CT is mandatory [11]. Linear skull fractures may be occult on skull radiographs because of the double-layered skull along fractures, when the cross section is oblique to the direction of the X-rays [12]. Similarly, skull fractures may be difficult to see on CT, when parallel to the display plane. The interpreting physician may need to correlate MPR images as well as occasionally rely on the scout image to depict these linear fractures.

In patients with significant TBI, skull fractures are common and are often overlooked on clinical examination. However, in some cases, there is a poor correlation between skull fractures and intracranial injury; severe brain injuries can occur, even without the presence of a skull fracture [8].

Extra-axial Lesions

There are four types of extra-axial hemorrhage to be considered: epidural, subdural, subarachnoid, and intraventricular.

Epidural Hematoma

Epidural hematoma (EDH) is an extracerebral collection of blood between the inner table of the skull and the dura, essentially underlying a bare bone surface. EDH occurs in less than 1 % of patients with head injuries [13]. EDH is typically found on the "coup" injury side and is commonly associated with a skull fracture and laceration of the underlying blood vessel(s) [14]. The recommended imaging method is CT, because it is fast, accessible, and depicts both the fracture and resulting hemorrhage. EDHs are commonly biconvex in appearance and typically do not cross suture lines but may cross the tentorium or falx; their mass effect is mostly caused by the size of extracerebral collection [14]. In the early stage, an epidural hematoma may appear heterogeneous on CT with hyperdense areas of clotted blood and hypodense whirls of non-coagulated blood that in time becomes more homogeneous [14]. This "swirl sign" is an ominous feature and should be carefully noted and communicated to the treating physicians, as it represents active hemorrhage into the collection [15].

EDH may be arterial or venous in origin (Table 2). Arterial EDH is caused by injury of a meningeal artery, commonly the middle meningeal artery. The typical location is the temporoparietal region, with 75 % of EDH occurring adjacent to the temporal bone (Fig. 4). When the blood vessel is lacerated, arterial bleeding results in a rapidly expanding hematoma that

Table 2 Epidural versus subdural hematoma

Epidural hematoma (EDH)	Subdural hematoma (SDH)
"Coup" side	"Contrecoup" side
Associated with skull fracture in ±90 % of cases	No consistent relationship with skull fractures
Does not cross suture lines	Does cross suture lines
Not limited by falx or tentorium (may extend from supra- to infratentorial or across midline)	Limited by falx and tentorium (confined to supra- or infratentorial compartment, does not cross midline)
Origin: Arterial (majority, due to tearing of one or more branches of the meningeal arteries, most commonly the middle meningeal artery) Venous (minority, due to laceration of a dural venous sinus, e.g., along the sphenoparietal sinus)	Origin: Venous, due to laceration of superficial bridging cortical veins
Medical emergency	May be chronic
Magnitude of the mass effect caused by EDH is directly related to the size of the extracerebral collection	Magnitude of the mass effect caused by SDH is more often associated with underlying parenchymal injury
CT is the preferred imaging technique because: Of rapid accessibility It shows both the hemorrhage and the skull fracture MR can be useful for: Detection of parenchymal repercussions (edema, mass effect, herniations)	MRI is the preferred imaging technique because: MRI is more sensitive than CT, especially in the detection of so-called isodense SDHs which may be difficult to see on CT Multiplanar imaging capability Better definition of multi-compartmental nature of SDH

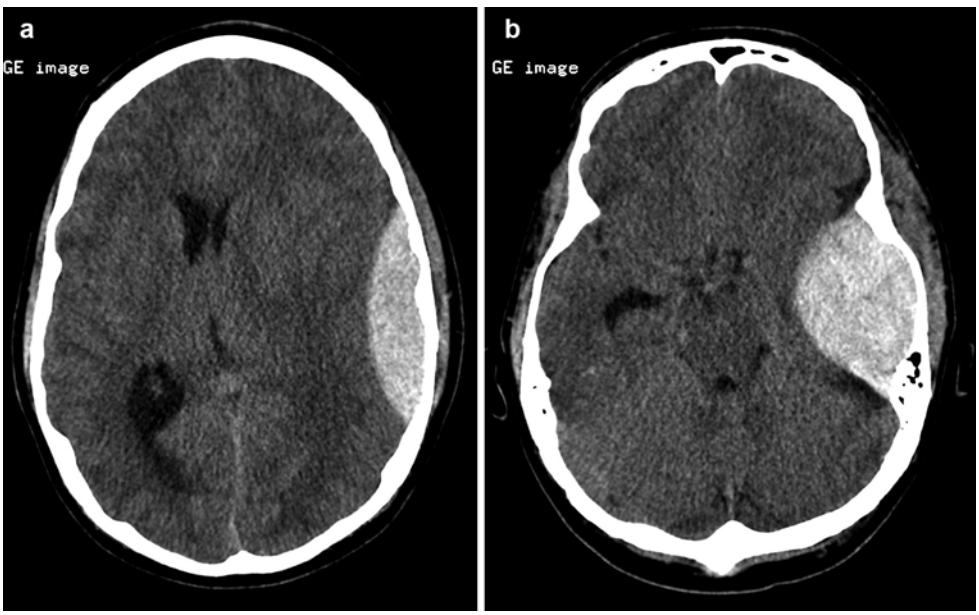

Fig. 4 (**a**, **b**) Acute left arterial epidural hematoma. Noncontrast CT scan upon admission. The left-sided hematoma is biconvex and is limited by the coronal suture anteriorly and by the lambdoid suture posteriorly. The mass effect causes a shift of the midline structures with compression of the left lateral ventricle and dilatation of the right lateral ventricle

exerts mass effect on the brain, focal deformity of the brain, and an increase in intracranial pressure (ICP). The size of the EDH may continue to increase until the arterial perfusion pressure is equilibrated with the elevated ICP. Emergency decompressive surgery is indicated to remove the EDH, stop hemorrhage, and reduce compression on the brain.

Venous EDH results from rupture/laceration of a dural venous sinus, or bleeding from diploic veins, again often associated with a skull fracture [16]. Venous EDH is usually located near the anterior wall of the middle cranial fossa (injury of sphenoparietal sinus and/or fracture of the greater wing of the sphenoid bone) and the vertex (injury of the superior sagittal sinus and/or fracture of the frontal or parietal bone) or against the occiput near the tentorium (injury of the transverse sinus and/or occipital fracture) [8] (Fig. 5). Anterior temporal EDH is often a low-pressure hemorrhage, and usually there is no requirement for surgical intervention [16]. Conversely, posterior fossa EDH may urgently require surgical evacuation because of early brainstem compression [16].

Subdural Hematoma

A subdural hematoma (SDH) represents an extracerebral collection of blood in the potential space between the dura mater and the arachnoid membrane or "epiarachnoid."

SDHs are relatively common and occur in about 30 % cases of severe head trauma [13]. They are more commonly found on the contrecoup injury side and are not as strongly associated with fractures as EDH [14]. The origin is almost invariably venous, caused by injury of superficial bridging cortical veins. They do cross sutures and may be holohemispheric and are typically limited by the falx and tentorium [14].

On CT, an acute SDH is seen as crescentic hyperdense structure between the brain and the inner border of the skull (Fig. 6). On modern CT scanners, the arachnoid space may be seen adjacent to the brain opposing the SDH. SDHs do not penetrate into sulci. Over time, the density decreases and they may become isodense to the adjacent brain. Therefore, MRI may be a preferred imaging method in later stages.

Subacute SDH occurs as hyperintense lesion on T1- and T2-weighed images due to extracellular methemoglobin [17] (Fig. 7). Chronic subdural hematoma is also well evaluated by MRI, which can clearly distinguish the size and extent of the collection as well as the development of the enhancing, capillary-rich membrane associated with resorbing SDH [17]. Chronic subdural hematomas are variable in signal but may retain T1 or FLAIR hyperintensity (Fig. 8).

The development of the vascular membranes, that are common in chronic SDH, is an important feature in the subsequent development of rehemorrhage into these collections, representing the "acute or chronic" form of SDH. These collections may appear quite complex in nature, with mixed and layered signal intensities, and are difficult to manage [18].

Traumatic Subarachnoid Hemorrhage

Traumatic subarachnoid hemorrhage (SAH) is common and often focal. It can be due to superficial cerebral abrasions, direct leptomeningeal vascular injury, or intraventricular hemorrhage with subarachnoid reflux [8]. The estimated incidence rates for SAH are 10–25 per 100,000 per year [19]. Acute SAH is easily recognizable on noncontrast CT as gyriform high attenuation in the subarachnoid space. It will penetrate sulci. The attenuation of blood on CT decreases as the hemoglobin concentration decreases [20]. The combination of SWI and FLAIR yields a distinctly higher detection rate for SAH due to their complementary detection capabilities [21]. FLAIR is sensitive for superficial/convexity SAH, while SWI adds value for the centrally located SAH, e.g., the interhemispheric fissure, interpeduncular fossa, supracerebellar cistern, and intraventricular subarachnoid blood [21]. The recognition of subtle SAH is important in the trauma setting, as this finding alone will typically result in an extended in-hospital evaluation of the patient.

Traumatic Intraventricular Hemorrhage

Traumatic intraventricular hemorrhage (IVH) occurs as a result of the tearing of subependymal or choroidal veins or reflux of SAH into the ventricular system. It may also be seen in association with diffuse axonal injury of the corpus callosum. The incidence of IVH in nonpenetrating head injury is 1.5–3 % and 10–25 % of patients with severe head injury [22].

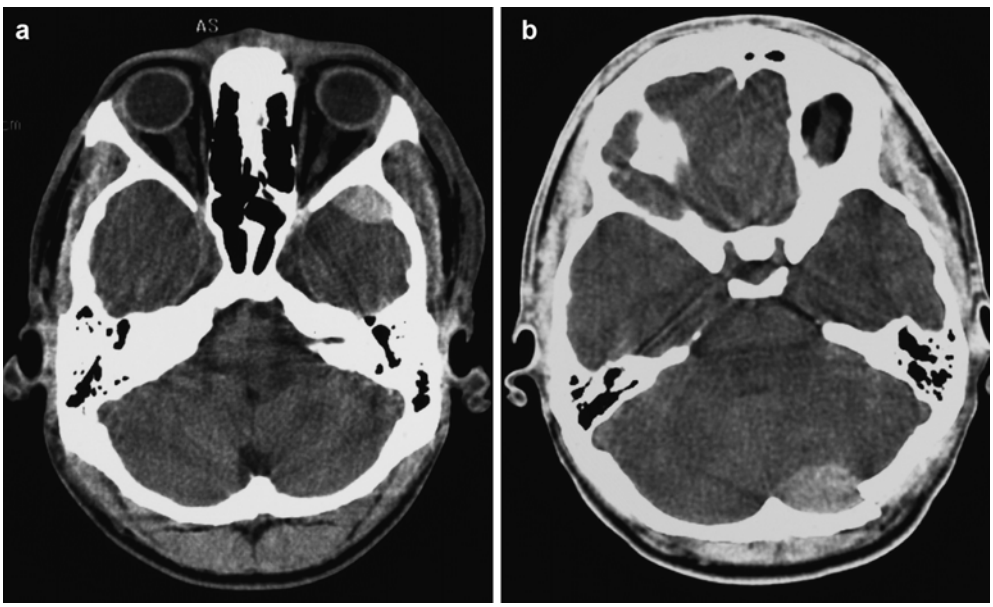

Fig. 5 (**a**, **b**) Venous epidural hematomas, shown in two different patients. Venous epidural hematomas typically are found (**a**) anteriorly in the middle cranial fossa adjacent to the sphenoparietal sinus and greater wing of the sphenoid bone or (**b**) adjacent to the transverse sinus. They present a typical, biconvex lens-shaped configuration

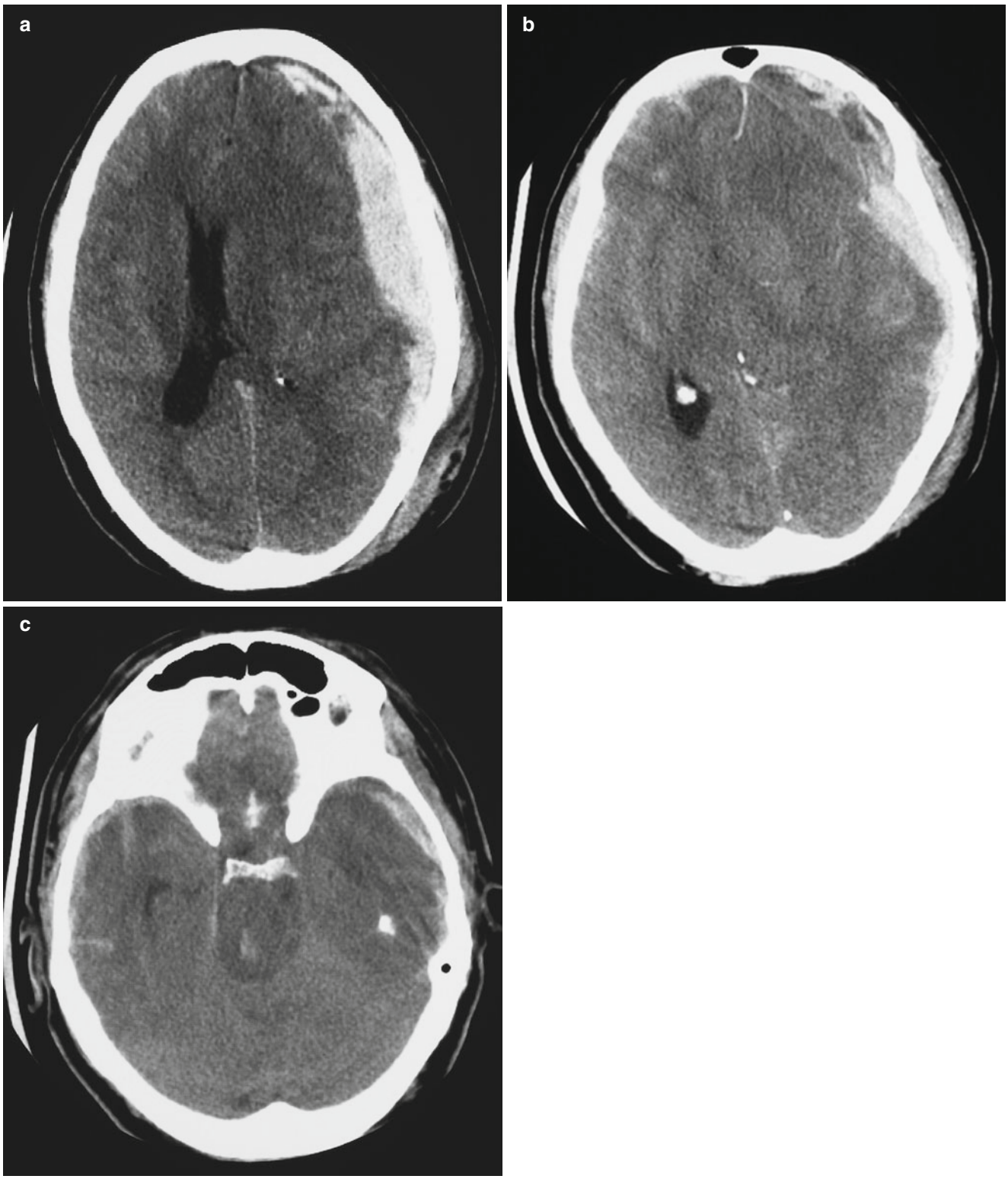

Fig. 6 (**a**–**c**). Acute left subdural hematoma. The CT scan shows hyperdense areas of clotted blood and some hypodense components indicating active bleeding. There is mass effect on the left cerebral hemisphere, with transtentorial herniation. The high-density area in the brainstem indicates a secondary brainstem hemorrhage or so-called Duret hemorrhage. There are also hemorrhagic cerebral contusions in both cerebral hemispheres

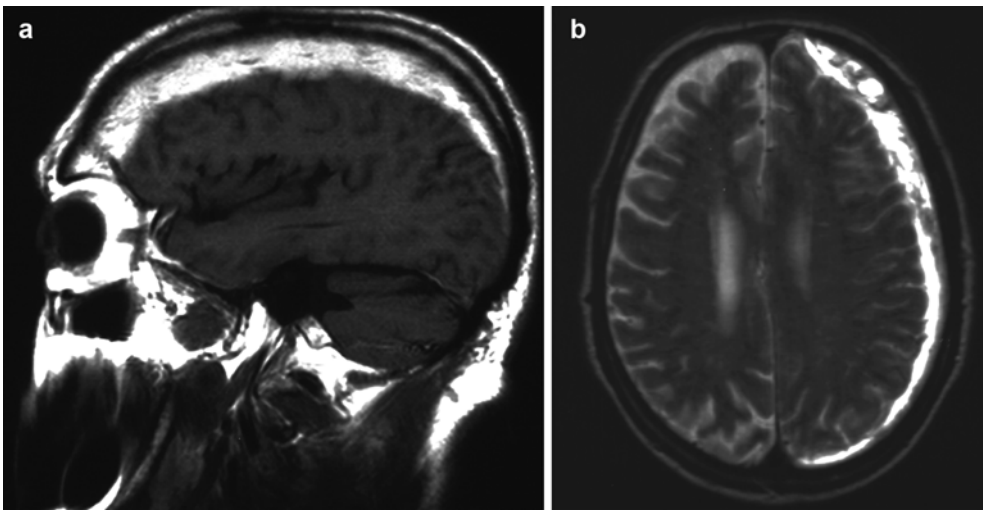

Fig. 7 (**a**, **b**) Subacute left subdural hematoma. MRI examination performed with (**a**) sagittal SE T1-weighted image and (**b**) axial TSE T2-weighted image. The MR images show the typical appearance of a crescent-shaped left subdural hematoma. There are multiple internal septations, representing strands of fibrovascular granulation tissue, derived from the inner (meningeal) layer of the dura. The hematoma extends over the surface of the left cerebral hemisphere from the frontal to the occipital region. The blood is hyperintense on T1-WI and on T2-WI, indicating the presence of extracellular methemoglobin

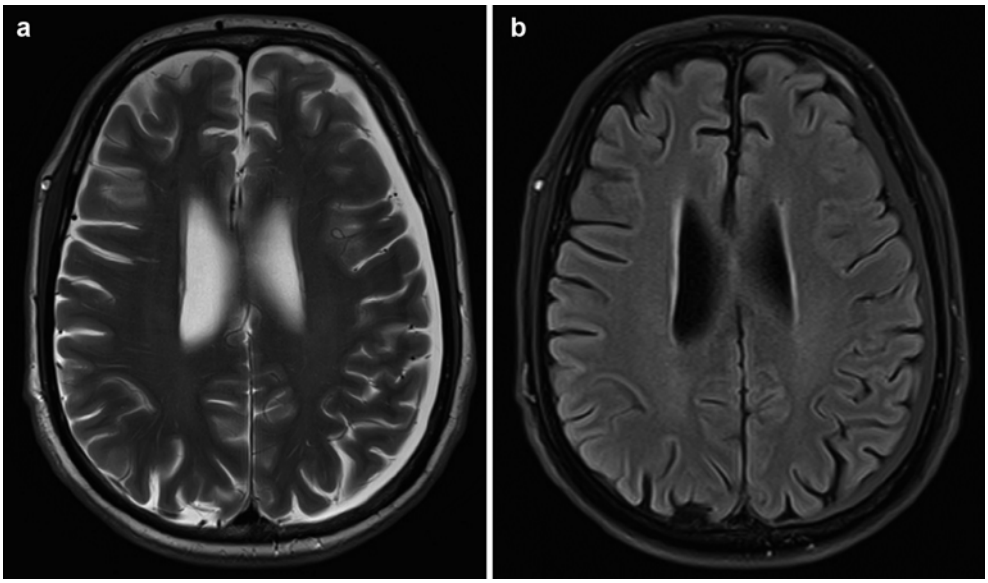

Fig. 8 (**a**, **b**) Chronic left subdural hematoma. MRI examination, including (**a**) axial TSE T2-weighted image and (**b**) axial turbo-FLAIR image with fat saturation. On the T2-weighted scan, the chronic subdural hematoma overlying the left cerebral hemisphere is hyperintense and appears isointense to cerebrospinal fluid (*CSF*); however, on the FLAIR image, the signal intensity is higher than CSF, indicating a different protein content

On CT IVH may appear as a hyperdense collection in the ventricular system. MRI is more sensitive to IVH, and DWI and FLAIR are the preferred sequences for identifying IVH (Fig. 9). During the first 48 h, IVH appears hyperintense on FLAIR, but subsequently the signal intensity may be variable [23]. Pulsatile flow artifacts in the third and fourth ventricle may compromise the usefulness of the FLAIR technique [8]. 3D-FLAIR techniques are more useful in this regard. SWI is extremely sensitive in detecting intraventricular hemorrhage. IVH appears as a typical hypointense area of susceptibility [24].

Intra-axial Lesions

Cerebral Contusion, Hemorrhagic Versus Nonhemorrhagic, and Coup Versus Contrecoup

Cerebral contusions are focal injuries of the brain surface due to direct impact with the skull and are most common at sides of bony protuberances. They are, in essence, to be considered as "a bruise of the brain." The consequent lesions are hemorrhagic or edematous and may progress to necrosis [25].

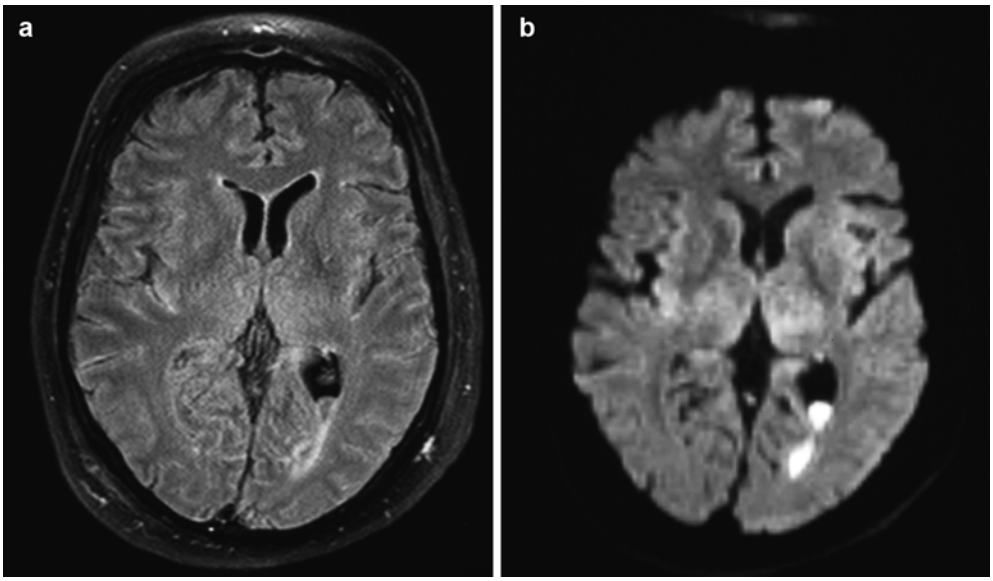

Fig. 9 (**a**, **b**) Posttraumatic intraventricular and subarachnoid hemorrhage. MRI examination, including (**a**) axial turbo-FLAIR image with fat saturation and (**b**) axial diffusion-weighted trace image (b =1000). In the left occipital horn, there is intraventricular blood, with a hemorrhagic sedimentation level, and markedly restricted diffusion. In addition, there is evidence of subarachnoid hemorrhage, best seen on the FLAIR images

Table 3 Sequential signal intensity changes of intracranial hemorrhage on MRI (1,5 T)

	Hyperacute hemorrhage	Acute hemorrhage	Early subacute hemorrhage	Late subacute hemorrhage	Chronic hemorrhage
What happens	Blood leaves the vascular system (extravasation)	Deoxygenation with formation of deoxy-Hb	Clot retraction and deoxy-Hb is oxidized to met-Hb	Cell lysis (membrane disruption)	Macrophages digest the clot
Time frame	<12 hours	Hours–days (weeks in center of hematoma)	A few days	Four to seven days –1 month	Weeks–years
Red blood cells	Intact erythrocytes	Intact, but hypoxic erythrocytes	Still intact, severely hypoxic	Lysis (solution of lysed cells)	Gone; encephalomalacia with proteinaceous fluid
State of Hb	Intracellular oxy-Hb (HbO2)	Intracellular deoxy-Hb (Hb)	Intracellular met-Hb (HbOH) (first at periphery of clot)	Extracellular met-Hb (HbOH)	Hemosiderin (insoluble) and ferritin (water soluble)
Oxidation state	Ferrous (Fe2+)	Ferrous (Fe2+)	Ferric (Fe3+)	Ferric (Fe3+)	Ferric (Fe3+)
	No unpaired e–	Four unpaired e–	Five unpaired e–	Five unpaired e–	2,000×5 unpaired e-
Magnetic properties	Diamagnetic (c<0)	Paramagnetic (c>0)	Paramagnetic (c>0)	paramagnetic (c>0)	FeOOH is superparamagnetic
SI on T1-WI	≈ or ↓	≈ (or ↓) (no PEDD interaction)	↑↑ (PEDD interaction)	↑↑ (PEDD interaction)	≈ (or ↓)(no PEDD interaction)
SI on T2-WI	↑ (high water content)	↓ T2 PRE (susceptibility effect)	↓↓ T2 PRE (susceptibility effect)	↑↑ No T2 PRE	↓↓ T2 PRE (susceptibility effect)
Notes	*Hb* hemoglobin	*e–* electrons	*FeOOH* ferric oxyhydroxide	↑ increased SI relative to normal gray matter	↓ decreased SI relative to normal gray matter

Hemorrhagic contusions are superficial and have either a "salt-and-pepper" appearance or may appear more solid [26]. When a traumatic brain injury results in a cerebral contusion and hemorrhagic contusion, they may progress during the first several hours and can be associated with SAH [27]. Predominantly affected areas are located in the supratentorial region – anterior frontal and temporal lobes and the gyri around the sylvian fissure.

On CT, hemorrhagic contusions appear as heterogeneous, hyperdense cortical lesions surrounded by an irregularly marginated hypodense (edematous) component. In the acute stage, CT may be more sensitive than MRI, as acute hemorrhage can be nearly indistinguishable from brain parenchyma on MRI. Subsequent CT performed between 24 and 48 h after traumatic brain injury often demonstrates previously undetected contusions or more extensive hemorrhage and increased edema. MRI is more sensitive than CT to depict cerebral contusions after the first 24 h because of the visualization of "nonhemorrhagic" contusion or contusions with predominant edema. This is particularly true of FLAIR

[8, 25]. The ability of MRI to detect hemorrhagic brain lesions increases proportionally to the evolution of blood products in these lesions. Hemosiderin and also deoxyhemoglobin have increased magnetic susceptibility that make SWI or T2* gradient-echo sequences very sensitive for detecting hemorrhagic lesions [28, 29]. Four to six months after injury, the lesions become cystic and lose volume and therefore become hypodense on CT [30], although MR findings of hemorrhage persist.

Table 3 provides an overview of sequential signal intensity changes of intracranial hemorrhage on MRI.

Contusions may be bihemispheric and occur along the vector of the force applied to the skull on the site of impact and the opposite region of the brain. These injuries are referred to as "coup" (side of injury) or "contrecoup" (opposite the injury). In closed head injury, for example, after an abrupt stop, the force translation can result in this pattern [30]. The coup injury is on the side of primary impact, often identified by scalp lesions or skull fracture. "Contrecoup" lesions are the mechanical consequence of an acceleration/deceleration trauma and occur on the opposite side of impact. They are often larger and more extensive than the coup lesions, perhaps because of the initial displacement of the brain toward the contrecoup location [8, 30, 31].

Diffuse Axonal Injury (DAI)

Diffuse axonal injury is a common type of primary neuronal injury in patients with severe head trauma with an incidence up to 50 % of trauma victims [30, 32]. DAI occurs when the brain is exposed to shear strain forces that lead to lesions at interfaces between two adjacent tissues with different densities or rigidities, such as gray and white matter [33], or areas where the brain is relatively anchored to an adjacent structure, such as the cerebral or cerebellar peduncles or corpus callosum. Predominantly affected areas in decreasing order of frequency are the gray-white matter junction, corpus callosum, basal ganglia, brainstem, and mesencephalon. The severity of the lesions increases toward the cerebellum, whereas axonal injury in the brainstem is considered to be an indicator for degeneration to coma in DAI [8, 33].

Its important clinical relevance and various clinical manifestations have contributed to the development of radiological imaging techniques for detection of DAI. As mentioned, DAI is a common primary injury in brain trauma, and CT examination is still the mode of choice in severe trauma patients in the acute phase because of its great value in detecting petechial hemorrhagic lesions and fractures and because of its rapid and convenient acquisition. Unfortunately, CT severely underestimates the extent and number of DAI lesions, especially of nonhemorrhagic lesions [34] (Fig. 10). Therefore, whenever there is a discrepancy between the clinical status of the patient and the CT findings, MRI should be recommended. In the early stage, diffusion-weighted images are of great importance to detect DAI. In addition, FLAIR sequences are useful for the detection of areas of gliosis. Gradient-echo sequences (GRE) are also superior to CT in subacute or chronic hemorrhagic head injuries because of paramagnetic blood degradation products [33, 34].

New advanced MRI techniques like diffusion tensor imaging (DTI) offer more sensitive detection and differentiation of DAI. In DTI, the specific water diffusion direction in the white matter is used to detect microstructural conditions that result in restriction in the diffusion of the molecules and alter the values seen on FA (fractional anisotropy) maps [35, 36]. A recent study showed that DTI is a very qualitative and useful way for clinical evaluation of DAI. The authors found decreased anisotropy in the corpus callosum even in patients with normal results on FLAIR and GRE [37]. Multiple additional studies demonstrate the utility of DTI, but application to individual patients remains challenging because of a wide number of variables [38].

Vessel Injury

Carotid Artery-Cavernous Sinus Fistula (CCF)

In the traumatic carotid artery-cavernous sinus fistula (CCF), there occurs a direct communication between the cavernous segment of the internal carotid artery (ICA) and the cavernous sinus. The underlying cause is often a laceration of the ICA due to blunt or penetrating head trauma. The fistula leads to engorgement and dilatation of the cavernous sinus with successive congestion of the superior ophthalmic vein (SOV) and inferior petrosal sinus [28].

Specific imaging signs of CCF are enlargement of the cavernous sinus or ipsilateral SOV on CT or MR and multiple flow voids on MRI. MRA may demonstrate arterialized flow in the cavernous sinus or SOV.

Traumatic Aneurysms

Traumatic intracranial aneurysms are rare and represent less than 1 % of all aneurysms. They are most common in children [39]. Predominant locations are the cavernous and infraclinoid segment of ICA, as well as along the anterior cerebral artery.

The gold standard in imaging of traumatic aneurysms is cerebral angiography, but CT angiography (CTA) is widely used because of its speed and ease of acquisition [40].

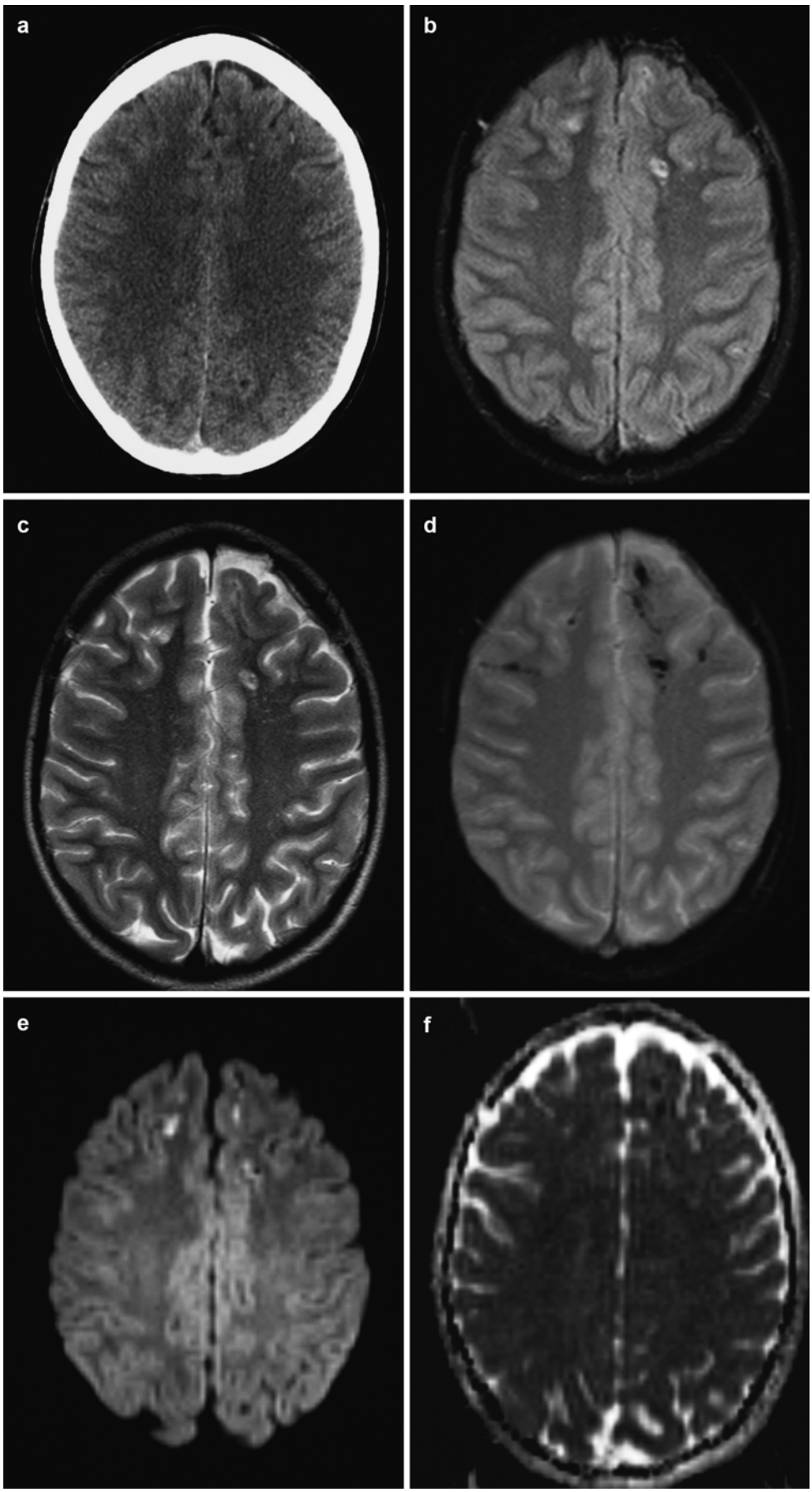

Fig. 10 (**a**–**f**) Diffuse axonal injuries in a 14-year-old boy, 4 days after a motor vehicle accident: (**a**) axial noncontrast CT scan; (**b**) axial turbo-FLAIR image; (**c**) axial TSE T2-weighted image; (**d**) axial gradient-echo FLASH T2*-weighted image (TE = 25 ms); (**e**) axial diffusion-weighted image (DWI) with $b = 1{,}000$; (**f**) axial apparent diffusion coefficient (ADC) map. The noncontrast CT-scan shows several punctate petechial hemorrhages at the gray-white matter junction of the frontal lobes. These lesions are hyperintense on turbo-FLAIR and T2-weighted images. On the T2*-weighted image, multiple hypointense hemosiderin deposits are seen at the gray-white matter junction and in the corpus callosum. The appearance, multiplicity, and topographical distribution are typical of hemorrhagic shearing injuries. On the DWI scan, the lesions are hyperintense, and on the ADC maps, the lesions are hypointense, indicating restricted diffusion

Traumatic Vascular Dissection

Traumatic vascular dissections are unusual complications of brain injury. The injury is caused by a tear in the intimal layer of an artery, resulting in several potential findings, including a "false" lumen within the media. Dissection occurs as a consequence of the contact with the skull in blunt head trauma or less frequently with penetrating trauma [41]. The incidence in blunt trauma victims is 0.86 % for ICA and 0.53 % for traumatic vertebral artery dissections.

Again, different techniques may provide a diagnosis of vessel dissection. Conventional angiography remains a useful examination. Although the intramural hematoma cannot be visualized, the "string sign" and a "flame-shaped tapering" are common radiological features [42]. Ultrasound examinations, especially B-mode and color-flow Doppler, are also increasingly used in detection of traumatic dissections. To detect subtle luminal abnormalities or wall abnormalities in dissection, both CT and MRI, as well as CTA and MRA, are superior to catheter angiography.

Secondary Lesions

Definition

Secondary brain damage results from the posttraumatic pathophysiologic cascade that follows the initial injury and contributes to delayed tissue injury and neuronal loss.

Intracranial Hypertension

Intracranial hypertension may occur after severe cerebral injury and can be a significant finding, resulting in progressive neural dysfunction. After traumatic brain injury, intracranial hypertension may be caused by cumulative edema, hemorrhage, or swelling after contusion. The presence of any of these signs is suspicious: loss of gray-white junction indicating cerebral edema, midline shift, a significant hematoma, herniation, or change in ventricular shape or size [28].

Brain Herniation (Table 4)
Cerebral herniation is the most common and dangerous secondary effect of increased ICP [8]. Cerebral herniations are the most common secondary effect of an expanding intracranial mass. Due to the herniation, the subarachnoid spaces and basal cisterns become obliterated, hydrocephalus develops, vascular compression may result in brain ischemia, and compression on vital brain tissue may cause profound neurological deficits.

Secondary Brainstem Hemorrhage (Duret Hemorrhage)

Secondary brainstem hemorrhage (also known as "Duret hemorrhage") can occur in craniocerebral trauma patients with rapidly evolving descending cerebral herniation [43]. It is evident on CT as a hyperdense brainstem lesion, typically found in lower mesencephalon and ventral pons (Fig. 6). It is not clear whether the origin is arterial or venous, but in the majority of cases, the outcome is fatal [8, 43].

Ischemic Lesions and Infarction

Posttraumatic ischemic lesions are common craniocerebral trauma complications with poor clinical outcome. MRI plays an important role in diagnosing this condition by demonstrating multiple areas of abnormal signal intensity on T2-weighted and FLAIR images [8]. On diffusion-weighted scans, these lesions are seen in the acute phase as hyperintense signal with corresponding hypointense signal on ADC [44]. Of all posttraumatic ischemic lesions, the classic lesion is an ipsilateral posterior cerebral artery infarction in the setting of significant supratentorial mass effect, secondary to any traumatic lesion with mass effect. The causative lesion may be an extra-axial hemorrhage or intracranial hemorrhage associated with edema and mass effect. The posterior cerebral artery may be compressed and transiently occluded between the brain and the free edge of the tentorium. Other intracranial arteries may be occluded or compromised secondary to herniation, including the middle and anterior cerebral arteries [45].

Infections

The risk of local wound infections, meningitis, ventriculitis, or cerebral abscess is particularly high among penetrating head traumas because of the presence of contaminated foreign objects, skin, hair, and bone fragments driven into the brain tissue along the projectile track [46]

Posttraumatic Sequelae

Posttraumatic Encephalomalacia

The term "posttraumatic encephalomalacia" refers to loss of brain tissue after craniocerebral trauma. Gross pathology shows weakening or cystic cavitation of brain tissue, with blurred cortical margins and surrounded by gliotic scar tissue. The basal part of the temporal lobes and anterior pole of the temporal lobes are most frequently affected. CT scans show hypodense areas of tissue loss, particularly in

Table 4 Cerebral herniation types

Type of cerebral herniation	Subfalcial herniation (cingulate herniation)	Tonsillar herniation	Descending transtentorial herniation	Ascending transtentorial herniation	Uncal herniation	External herniation
Definition	Medial displacement of cingulate gyrus under inferior free margin of the falx	Inferior displacement of cerebellar tonsil(s) through foramen magnum	Downward shift of diencephalon, mesencephalon, and upper brainstem	Superior displacement of the vermis through the tentorial incisura	Herniation of medial temporal lobe through tentorial notch	Brain tissue extrudes externally through a skull defect
Cause	Supratentorial mass (e.g., EDH, SDH, hemispheric mass lesion, etc.)	Posterior fossa mass lesions or supratentorial mass effect	Increasing supratentorial mass effect	Posterior fossa mass lesion (tumor)	Temporal lobe mass lesion, e.g., focal hematoma	Increased ICP in association with a traumatic or surgical skull defect
Imaging	Mass lesion Bowing of falx Compression of ipsilateral lateral ventricle Contralateral ventricle Enlarges due to obstruction of the foramen of Monro	Downward displacement of cerebellar tonsils below level of foramen magnum Obliteration of cisterna magna	Obliteration of peri-mesencephalic cisterns with complete plugging of tentorial incisura Downward shift of pineal calcification Brainstem is foreshortened (sagittal plane) and compressed (axial plane)	Fourth ventricle becomes obliterated Effacement of the superior cerebellar and quadrigeminal cisterns	Obliteration of the suprasellar cistern Shift of mesencephalon to opposite side Widening of ipsilateral CPA cistern Obstructive hydrocephalus (due to aqueductal obstruction)	Extracranial displacement of brain tissue Bone defect visible
Compression of vascular structures	ACA infarction (pericallosal and callosomarginal arteries)	PICA infarction	PCA compression leads to occipital lobe ischemia or infarction	SCA compression may result in cerebellar infarction	Compression of the contralateral PCA against the tentorial edge	Venous obstruction may result in venous infarction (propensity to hemorrhage)
Other complications	Intracranial hypertension may cause descending transtentorial herniation	Hydrocephalus and syringomyelia	"Duret" brainstem hemorrhage (disruption of perforating arteries to brainstem)	Hydrocephalus due to compression of the aqueduct	Can progress to descending transtentorial herniation Obstructive hydrocephalus	Pressure necrosis with swelling of the adjacent brain at the margins of the defect

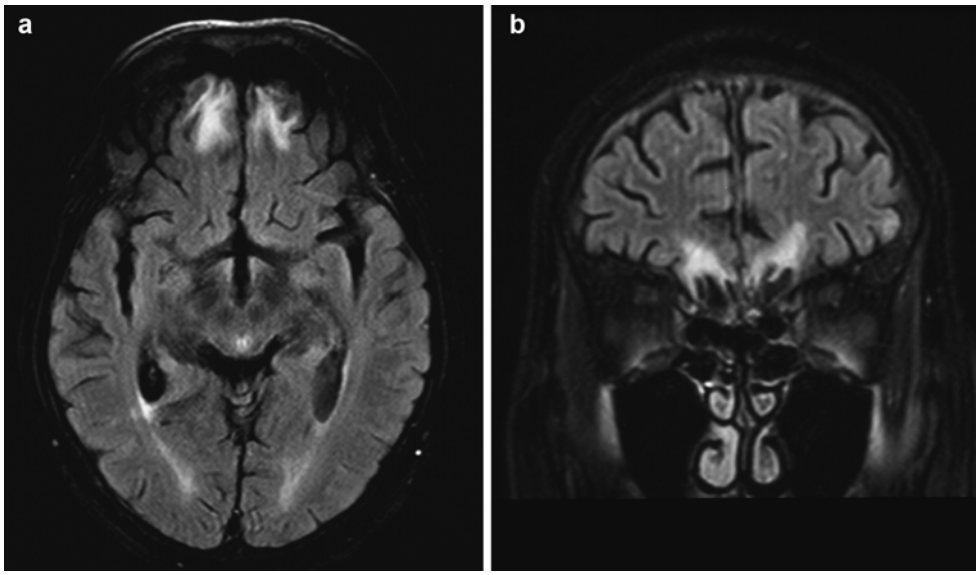

Fig. 11 (**a**, **b**) Posttraumatic encephalomalacia and gliosis. Axial (**a**) and coronal (**b**) turbo-FLAIR images with spectral fat saturation. MRI performed 4 years after severe head injury. There are areas of posttraumatic tissue loss in the basal part of the frontal lobes bilaterally. The areas of tissue loss are surrounded by gliosis, which is hyperintense on the FLAIR images. In addition, there are old diffuse axonal injuries, seen as gliotic foci at the gray-white matter interface, e.g., in the upper part of the left frontal lobe

these parts of the brain. On MRI, encephalomalacia is identified as (multi)cystic areas of tissue loss, surrounded by an irregular rim of gliosis, best seen on FLAIR images as a hyperintense rim (Fig. 11). Posttraumatic encephalomalacia is a very serious condition, resulting in lifelong disability, neurological dysfunction, epilepsy, or even death in some cases.

Growing Skull Fracture

A growing skull fracture is a rare but well-known complication of pediatric head trauma [47]. Its incidence ranges from less than 0.05 to 1.6 % [48]. CT and MRI findings include a diastatic fracture and brain herniation through the skull defect; it can also be accompanied by cystic lesions (meningocele) within the fracture and encephalomalacia [48].

Traumatic CSF Leaks

Traumatic cerebrospinal leakage is a complication seen in 2 % of all head-injured patients and in 12–30 % of cases of basilar skull fractures [49]. The most common locations are the cribriform plate (forming the roof of the ethmoid) and the walls of the frontal sinus [50]. Intracranial air may be an important sign. Careful evaluation of fractures that are contiguous to sinuses is key to making a correct diagnosis. Persistent opacification of sinuses contiguous to a fracture is of particular suspicion. Suggesting the presence of a CSF leak will usually result in testing of fluid in the contiguous sinus for the presence of beta-2 transferrin, a dependable marker of CSF.

Diabetes Insipidus

The prevalence of central diabetes insipidus (DI) after TBI is 1.7–26 %, often resulting from injury or transection of the infundibulum. MRI is the technique of choice for pituitary imaging. A sagittal T1-weighted image demonstrates a posterior pituitary "bright spot" in healthy individuals. The absence of this "bright spot" in diabetes insipidus is a nonspecific sign of DI [51]. In addition to the absence of this sign, an ectopic "bright spot" in the proximal stump of the transected, retracted proximal stalk or hypothalamus may be identified. If there is clinical suspicion of trauma-related DI, a dedicated pituitary examination is the appropriate examination.

Quantitative Imaging in Patients with Traumatic Brain Injury

Diffusion-Weighted Imaging (DWI) with ADC Maps

Diffusion-weighted imaging measures the motion of water molecules and thus helps visualize the physiologic state in the brain [8]. There are physiologic phase shifts or signal loss due to this normal semi-random motion of water molecules. In distinction, areas with abnormal diffusion reflect alterations in the normal water diffusion and appear bright on DWI [29]. The apparent diffusion coefficient (ADC) values indicate the decrease in the diffusion with corresponding hypointense signal on ADC maps [29]. DWI has become an important tool in diagnosing TBI, acute stroke, and white matter diseases [8].

Diffusion Tensor Imaging (DTI) and Diffusion Kurtosis Imaging (DKI)

Diffusion tensor imaging (DTI) is derived from specialized DWI with multiple directions and can measure not only the degree but also the direction of water diffusion [52]. It allows in vivo visualization of the integrity of white matter tracts. The main application is in diffuse axonal injury.

Diffusion kurtosis imaging (DKI) is an extended technique, derived from DTI, and allows diffusional kurtosis to be evaluated using diffusion-weighted imaging techniques [53]. With DKI, both gray and white matter can be evaluated.

Outcome Prediction with Imaging Parameters

Imaging is a very important clinical tool for diagnosis, prognosis, and visualizing therapy outcomes following TBI. Although structural imaging techniques such as CT or MRI offer a rapid evaluation of the brain status and may help predict survival, more information is necessary. Detailed information of cerebral perfusion has also proven useful in management and in assessing outcomes [29].

Several imaging techniques are available to visualize the brain physiology: CT perfusion, MR perfusion, SPECT, fMRI (functional MRI), PET, and MRS (MR spectroscopy).

MRI sequences like DTI, FLAIR, GRE/SWI, and DWI are increasingly used in predicting outcome [54].

Conclusion

Imaging studies represent an essential element in the management of patients with significant neurologic trauma. Diagnosis of the extent of the initial injury is critical to triage patients to surgical or nonsurgical management. Repeated follow-up to determine potential secondary injury patterns and also determine the success of management schemes is of significant value and improves patient outcomes. Imaging techniques have shown considerable promise in improving our knowledge of the patterns and significance of intracranial injury and in suggesting and monitoring therapies to treat these patients and determine their prognosis.

References

1. Maas AI, Stocchetti N, Bullock R (2008) Moderate and severe traumatic brain injury in adults. Lancet Neurol 7(8):728–741
2. Tagliaferri F, Compagnone C, Korsic M, Servadei F, Kraus J (2006) A systematic review of brain injury epidemiology in Europe. Acta Neurochir (Wien) 148(3):255–268
3. Le TH, Gean AD (2009) Neuroimaging of traumatic brain injury. Mt Sinai J Med 76(2):145–162
4. Jones TR, Kaplan RT, Lane B, Atlas SW, Rubin GD (2001) Single- versus multi-detector row CT of the brain: quality assessment. Radiology 219(3):750–755
5. Langford S, Panigrahy A, Narayanan S, Hwang M, Fitz C, Flom L, Lee VK, Zuccoli G (2015) Multiplanar reconstructed CT images increased depiction of intracranial hemorrhages in pediatric head trauma. Neuroradiology 57(12):1263–1268
6. Bykowski J, Wong W (2012) Angiographic evaluation and treatment for head and neck vascular injury. Appl Radiol 41(3): 10–16
7. Provenzale J (2010) Imaging of traumatic brain injury: a review of the recent medical literature. AJR Am J Roentgenol 194(1):16–19
8. Parizel PM, Van Goethem JW, Ozsarlak O, Maes M, Phillips CD (2005) New developments in the neuroradiological diagnosis of craniocerebral trauma. Eur Radiol 15(3):569–581
9. Yen K, Vock P, Tiefenthaler B, Ranner G, Scheurer E, Thali MJ, Zwygart K, Sonnenschein M, Wiltgen M, Dirnhofer R (2004) Virtopsy: forensic traumatology of the subcutaneous fatty tissue; multislice computed tomography (MSCT) and magnetic resonance imaging (MRI) as diagnostic tools. J Forensic Sci 49(4):799–806
10. Malli N, Ehammer T, Yen K, Scheurer E (2013) Detection and characterization of traumatic scalp injuries for forensic evaluation using computed tomography. Int J Legal Med 127(1):195–200
11. Hofman PA, Nelemans P, Kemerink GJ, Wilmink JT (2000) Value of radiological diagnosis of skull fracture in the management of mild head injury: meta-analysis. J Neurol Neurosurg Psychiatry 68(4):416–422
12. Nakahara K, Shimizu S, Utsuki S, Oka H, Kitahara T, Kan S, Fujii K (2011) Linear fractures occult on skull radiographs: a pitfall at radiological screening for mild head injury. J Trauma 70(1): 180–182
13. Tallon JM, Ackroyd-Stolarz S, Karim SA, Clarke DB (2008) The epidemiology of surgically treated acute subdural and epidural hematomas in patients with head injuries: a population-based study. Can J Surg 51(5):339–345
14. Parizel PM, Phillips CD (2012) Neuroradiological diagnosis of craniocerebral trauma: current concepts. In: Hodler J, Von Schulthess GK, Zollikofer ChL (eds) Diseases of the brain, head & neck, spine 2012-2015.
15. Al-Nakshabandi NA (2001) The swirl sign. Radiology 218(2):433
16. Gean AD, Fischbein NJ, Purcell DD, Aiken AH, Manley GT, Stiver SI (2010) Benign anterior temporal epidural hematoma: indolent lesion with a characteristic CT imaging appearance after blunt head trauma. Radiology 257(1):212–218
17. Senturk S, Guzel A, Bilici A, Takmaz I, Guzel E, Aluclu MU, Ceviz A (2010) CT and MR imaging of chronic subdural hematomas: a comparative study. Swiss Med Wkly 140(23-24):335–340
18. Honda Y, Sorimachi T, Momose H, Takizawa K, Inokuchi S, Matsumae M (2015) Chronic subdural haematoma associated with disturbance of consciousness: significance of acute-on-chronic subdural haematoma. Neurol Res 37(11):985–992
19. León-Carrión J, Domínguez-Morales Mdel R, Martín JM BY, Murillo-Cabezas F (2005) Epidemiology of traumatic brain injury and subarachnoid hemorrhage. Pituitary 8(3-4):197–202
20. Fainardi E, Chieregato A, Antonelli V, Fagioli L, Servadei F (2004) Time course of CT evolution in traumatic subarachnoid haemorrhage: a study of 141 patients. Acta Neurochir (Wien) 146(3): 257–263
21. Verma RK, Kottke R, Andereggen L, Weisstanner C, Zubler C, Gralla J, Kiefer C, Slotboom J, Wiest R, Schroth G, Ozdoba C, El-Koussy M (2013) Detecting subarachnoid hemorrhage: comparison of combined FLAIR/SWI versus CT. Eur J Radiol 82(9): 1539–1545
22. LeRoux PD, Haglund MM, Newell DW, Grady MS, Winn HR (1992) Intraventricular hemorrhage in blunt head trauma: an analysis of 43 cases. Neurosurgery 31(4):678–684

23. Sohn CH, Baik SK, Lee HJ, Lee SM, Kim IM, Yim MB, Hwang JS, Lauzon ML, Sevick RJ (2005) MR imaging of hyperacute subarachnoid and intraventricular hemorrhage at 3T: a preliminary report of gradient echo T2*-weighted sequences. AJNR Am J Neuroradiol 26(3):662–665
24. Wu Z, Li S, Lei J, An D, Haacke EM (2010) Evaluation of traumatic subarachnoid hemorrhage using susceptibility-weighted imaging. AJNR Am J Neuroradiol 31(7):1302–1310
25. Toyama Y, Kobayashi T, Nishiyama Y, Satoh K, Ohkawa M, Seki K (2005) CT for acute stage of closed head injury. Radiat Med 23(5):309–316
26. Alahmadi H, Vachhrajani S, Cusimano MD (2010) The natural history of brain contusion: an analysis of radiological and clinical progression. J Neurosurg 112(5):1139–1145
27. Kurland D, Hong C, Aarabi B, Gerzanich V, Simard JM (2012) Hemorrhagic progression of a contusion after traumatic brain injury: a review. J Neurotrauma 29(1):19–31
28. Lee B, Newberg A (2005) Neuroimaging in traumatic brain imaging. NeuroRx 2(2):372–383
29. Coles JP (2007) Imaging after brain injury. Br J Anaesth 99(1): 49–60
30. Besenski N (2002) Traumatic injuries: imaging of head injuries. Eur Radiol 12(6):1237–1252
31. Drew LB, Drew WE (2004) The contrecoup-coup phenomenon: a new understanding of the mechanism of closed head injury. Neurocrit Care 1(3):385–390
32. Hammoud DA, Wasserman BA (2002) Diffuse axonal injuries: pathophysiology and imaging. Neuroimaging Clin N Am 12(2): 205–216
33. Li XY, Feng DF (2009) Diffuse axonal injury: novel insights into detection and treatment. J Clin Neurosci 16(5):614–619
34. Parizel PM, Ozsarlak, Van Goethem JW, van den Hauwe L, Dillen C, Verlooy J, Cosyns P, De Schepper AM (1998) Imaging findings in diffuse axonal injury after closed head trauma. Eur Radiol 8(6):960–965
35. Niogi SN, Mukherjee P, Ghajar J, Johnson C, Kolster RA, Sarkar R, Lee H, Meeker M, Zimmerman RD, Manley GT, McCandliss BD (2008) Extent of microstructural white matter injury in postconcussive syndrome correlates with impaired cognitive reaction time: a 3T diffusion tensor imaging study of mild traumatic brain injury. AJNR Am J Neuroradiol 29(5):967–973
36. Hurley RA, McGowan JC, Arfanakis K, Taber KH (2004) Traumatic axonal injury: novel insights into evolution and identification. J Neuropsychiatry Clin Neurosci 16(1):1–7
37. Chan JH, Tsui EY, Peh WC, Fong D, Fok KF, Leung KM, Yuen MK, Fung KK (2003) Diffuse axonal injury: detection of changes in anisotropy of water diffusion by diffusion-weighted imaging. Neuroradiology 45(1):34–38
38. Hulkower MB, Poliak DB, Rosenbaum SB, Zimmerman ME, Lipton ML (2013) A decade of DTI in traumatic brain injury: 10 years and 100 articles later. AJNR Am J Neuroradiol 34(11): 2064–2074
39. Larson PS, Reisner A, Morassutti DJ, Abdulhadi B, Harpring JE (2000) Traumatic intracranial aneurysms. Neurosurg Focus 8(1):e4
40. Mao Z, Wang N, Hussain M, Li M, Zhang H, Zhang Q, Zhang P, Zhi X, Ling F (2012) Traumatic intracranial aneurysms due to blunt brain injury - a single center experience. Acta Neurochir 154(12): 2187–2193
41. Schievink WI (2001) Spontaneous dissection of the carotid and vertebral arteries. N Engl J Med 344(12):898–906
42. Caplan LR (2008) Dissections of brain-supplying arteries. Nat Clin Pract Neurol 4(1):34–42
43. Parizel PM, Makkat S, Jorens PG, Ozsarlak O, Cras P, Van Goethem JW, van den Hauwe L, Verlooy J, De Schepper AM (2002) Brainstem hemorrhage in descending transtentorial herniation (Duret hemorrhage). Intensive Care Med 28(1):85–88
44. Parizel PM, Demey HE, Veeckmans G, Verstreken F, Cras P, Jorens PG, De Schepper AM (2001) Early diagnosis of cerebral fat embolism syndrome by diffusion-weighted MRI (starfield pattern). Stroke 32(12):2942–2944
45. Server A, Dullerud R, Haakonsen M, Nakstad PH, Johnsen UL, Magnaes B (2001) Post-traumatic cerebral infarction. Neuroimaging findings, etiology and outcome. Acta Radiol 42(3):254–260
46. Kazim SF, Shamim MS, Tahir MZ, Enam SA, Waheed S (2011) Management of penetrating brain injury. J Emerg Trauma Shock 4(3):395–402
47. Drapkin AJ (2006) Growing skull fracture: a posttraumatic neosuture. Childs Nerv Syst 22(4):394–397
48. Ersahin Y, Gülmen V, Palali I, Mutluer S (2000) Growing skull fractures (craniocerebral erosion). Neurosurg Rev 23(3):139–144
49. Friedman JA, Ebersold MJ, Quast LM (2001) Post-traumatic cerebrospinal fluid leakage. World J Surg 25(8):1062–1066
50. Hofmann E, Behr R, Schwager K (2009) Imaging of cerebrospinal fluid leaks. Klin Neuroradiol 19(2):111–121
51. Makulski DD, Taber KH, Chiou-Tan FY (2008) Neuroimaging in posttraumatic hypopituitarism. J Comput Assist Tomogr 32(2): 324–328
52. Xiong KL, Zhu YS, Zhang WG (2014) Diffusion tensor imaging and magnetic resonance spectroscopy in traumatic brain injury: a review of recent literature. Brain Imaging Behav 8(4):487–496
53. Jensen JH, Helpern JA (2010) MRI quantification of non-Gaussian water diffusion by kurtosis analysis. NMR Biomed 23(7):698–710
54. Huisman TA, Schwamm LH, Schaefer PW, Koroshetz WJ, Shetty-Alva N, Ozsunar Y, Wu O, Sorensen AG (2004) Diffusion tensor imaging as potential biomarker of white matter injury in diffuse axonal injury. AJNR Am J Neuroradiol 25(3):370–376

Nontraumatic Neuroemergencies

John R. Hesselink

Several clinical presentations require emergent neuroimaging to determine the cause of the neurological deficit and to institute appropriate therapy. Time is critical because neurons that are lost cannot be replaced. Generally, the clinical symptoms are due to ischemia and compression or destruction of neural elements. The two primary imaging modalities for the CNS are CT and MRI. CT is fast and can readily visualize fractures, hemorrhage, and foreign bodies. Otherwise, in patients who can cooperate for the longer imaging study, MRI provides better contrast resolution and has higher specificity for most CNS diseases. The five major categories of nontraumatic neuroemergencies are discussed below [1].

Acute Focal Neurological Deficit

Arterial Thrombosis/Occlusion

Thrombotic strokes may occur abruptly but the clinical picture often shows gradual worsening over the first few hours. Primary causes of arterial thrombosis include atherosclerosis, hypercoagulable states, arteritis, and dissection. Secondary compromise of vascular structures can result from traumatic injury, intracranial mass effect, neoplastic encasement, meningeal processes, and vasospasm (Fig. 1).

Arterial Embolism

Embolic strokes characteristically have a very abrupt onset. After a number of hours, there may be sudden improvement in symptoms as the embolus lyses and travels more distally. The source of the embolus is usually either the heart (patients with atrial fibrillation or previous myocardial infarction) or ulcerated plaques at the carotid bifurcation in the neck.

J.R. Hesselink
Department of Radiology, UC San Diego, San Diego, CA, USA
e-mail: jhesselink@ucsd.edu

Arterial Dissection

Relatively minor trauma is sufficient to cause a dissection, or it can be spontaneous. The MRA may demonstrate complete occlusion or only narrowing of the arterial lumen. Spin-echo images, especially T1-weighted with fat suppression, should also be obtained because they are very sensitive for detecting the intramural hemorrhage. The typical appearance is an oval-shaped hyperintensity with an eccentrically placed flow void. The MRA is also very useful for following a dissection to look for recanalization of a complete occlusion, resolution of the vascular compromise caused by the intramural thrombus, or development of a pseudoaneurysm.

Brain Hemorrhage

Localized hemorrhages into the brain may present with a focal neurological deficit. Most of these are caused by vascular malformations. The four types of vascular lesions include AV malformation, cavernous angioma, capillary telangiectasia, and venous malformation. AV malformations are more likely to present acutely. Hemorrhage into tumors or infarcts is not uncommon, but patients usually have symptoms related to the underlying lesion. Hypertensive hemorrhages are often large and deep within the brain and produce more global neurological deficits.

Hypotension/Hypoxia

Hypotension can be cardiac in origin or result from blood volume loss or septic shock. Anoxia/hypoxia events are usually related to respiratory compromise from severe lung disease, perinatal problems, near drowning, high altitude, carbon monoxide inhalation, or CNS-mediated effects.

J. Hodler et al. (eds.), *Diseases of the Brain, Head and Neck, Spine 2016–2019*: *Diagnostic Imaging*, DOI 10.1007/978-3-319-30081-8_12

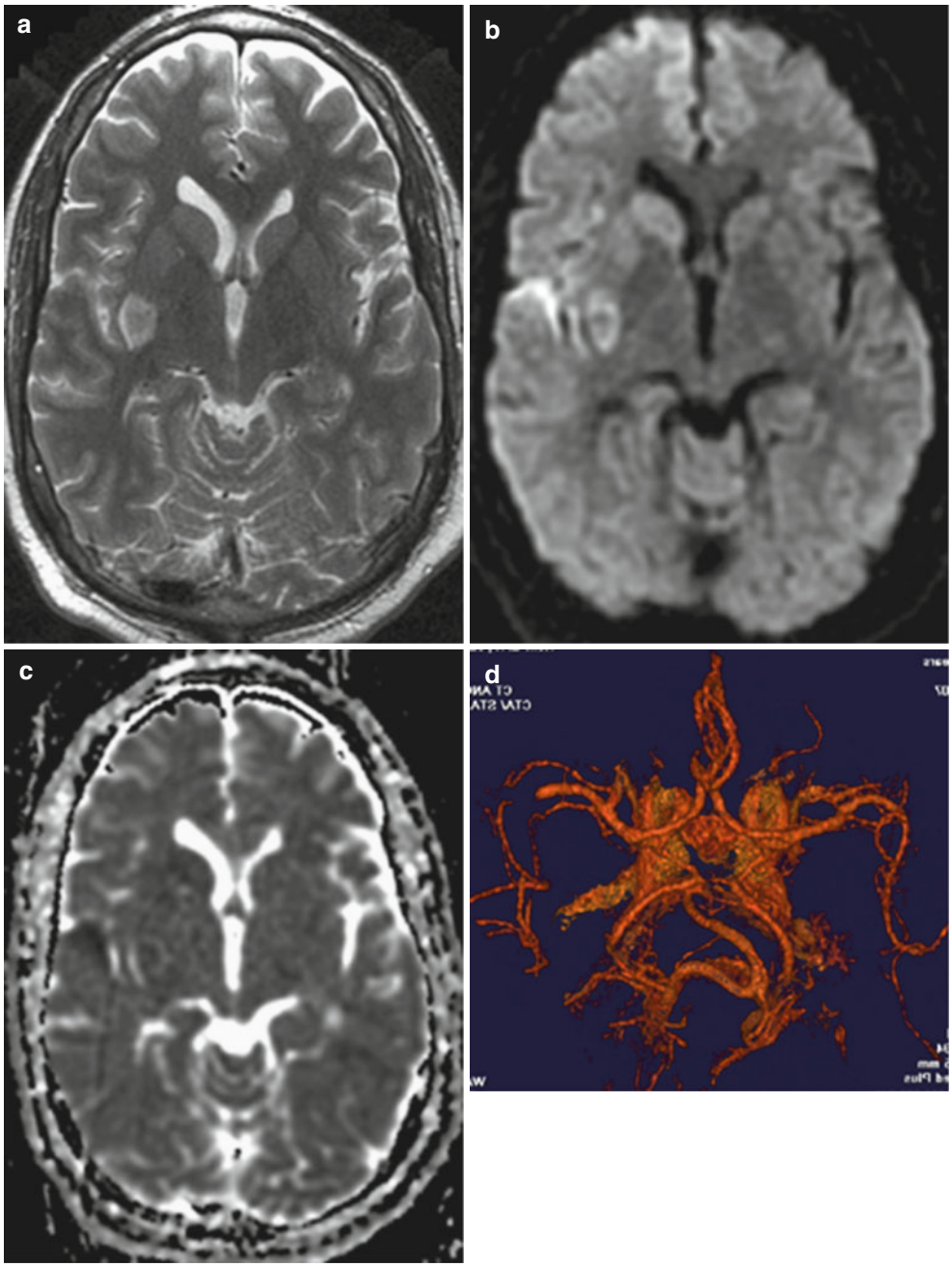

Fig. 1 Acute cerebral infarct secondary to a right MCA embolic occlusion. (**a**) Axial T2 image shows focal hyperintensity in the posterior right putamen and external capsule. (**b**, **c**) Restricted diffusion on the DWI (**b**) is confirmed by hypointensity on the ADC map (**c**). The infarct extends laterally into the peri-sylvian cortex. (**d**) CT angiogram reveals occlusion of the right middle cerebral artery

Venous/Sinus Occlusion

Thrombosis of the cerebral venous sinuses has multiple etiologies, including hypercoagulable states, pregnancy, sepsis, dehydration, paranasal sinus infection, and neoplastic invasion. Occlusion of the venous sinuses results in cerebral venous engorgement, brain swelling, and increased intracranial pressure. If the thrombosis extends retrograde and involves the cortical veins, secondary cerebral infarction can occur.

Acute thrombus is hyperdense on CT and may be detected within one of the major sinuses or cortical veins. The other classic sign is the "empty delta" sign due to nonfilling of the superior sagittal sinus on a contrast scan. Nonetheless, MR is far superior for diagnosing abnormalities of the cerebral veins and sinuses. Normally, the dural sinuses have sufficient flow to exhibit a flow void. If that flow void is missing or if the sinuses are hyperintense, thrombosis should be suspected. One must be careful to exclude the possibility of any inflow enhancement effect. The diagnosis must be confirmed with gradient-echo techniques or MR angiography. Phase-contrast or Gd-enhanced time-of-flight MRAs are the preferred techniques because they are not adversely affected by intraluminal clot [2].

Associated parenchymal infarcts are found in the areas of venous abnormalities, and the infarcts are often hemorrhagic because arterial perfusion is maintained to the damaged tissue. In cases of superior sagittal sinus thrombosis, the infarcts are typically bilateral and in a parasagittal location.

Cortical Mass Lesion

Any lesion that irritates the cortical neurons can be a source of seizures. Neoplasia, encephalitis, meningitis, abscess, and hemorrhage are the more common causes of new onset seizures.

Worst Headache of Life

Subarachnoid Hemorrhage

The incidence of congenital aneurysms in the general population is about 1–2 %. Clinically, a ruptured aneurysm presents as sudden onset of severe headache. In cases of subarachnoid hemorrhages, the most common aneurysms are posterior communicating, 38 %; anterior communicating, 36 %; and middle cerebral, 21 %. These three locations account for 95 % of all ruptured aneurysms. The basilar artery accounts for only 2.8 % and posterior fossa aneurysms are even less common.

The CT scan is important, first of all, to document the subarachnoid hemorrhage and to assess the amount of blood in the cisterns (Fig. 2). Detection of subarachnoid blood is very dependent on how early the scan is obtained. Data in the literature vary from 60 to 90 %. If the scan is obtained within 4–5 days, the detection rate is very high. Secondly, the CT helps localize the site of the aneurysm. This can be done by the distribution of blood within the cisterns. If conventional angiography is not available or is not planned immediately, CT angiography is very good for detecting and characterizing intracranial aneurysms. Thirdly, the CT is important to evaluate complicating factors such as cerebral hematoma, ventricular rupture, hydrocephalus, cerebral infarction, impending uncal herniation, and rebleed.

Conventional MR sequences are very insensitive for detecting subarachnoid hemorrhage. Clots within cisterns can be detected, but in general, MR is not the procedure of choice in the work-up of patients with subarachnoid hemorrhage. Due to the flow void phenomenon, aneurysms about the circle of Willis can be identified on spin-echo MR images [3]. With fluid-attenuated inversion recovery (FLAIR) sequences, the CSF is dark, so that subarachnoid hemorrhage can be seen more easily. These sequences may be helpful for detecting subarachnoid blood in the posterior fossa where CT has difficulty [4].

Acute Meningitis

Bacterial meningitis is an infection of the pia and arachnoid and adjacent cerebrospinal fluid. The most common organisms are *Haemophilus influenza*, *Neisseria meningitidis* (*meningococcus*), and *Streptococcus pneumoniae*. Patients present with fever, headache, seizures, altered consciousness, and neck stiffness. The overall mortality rate ranges from 5 to 15 % for *H. influenza* and meningococcal meningitis and as high as 30 % with streptococcal meningitis. In addition, persistent neurological deficits are found in 10 % of children after *H. influenza* meningitis and in 30 % of patients with streptococcal meningitis.

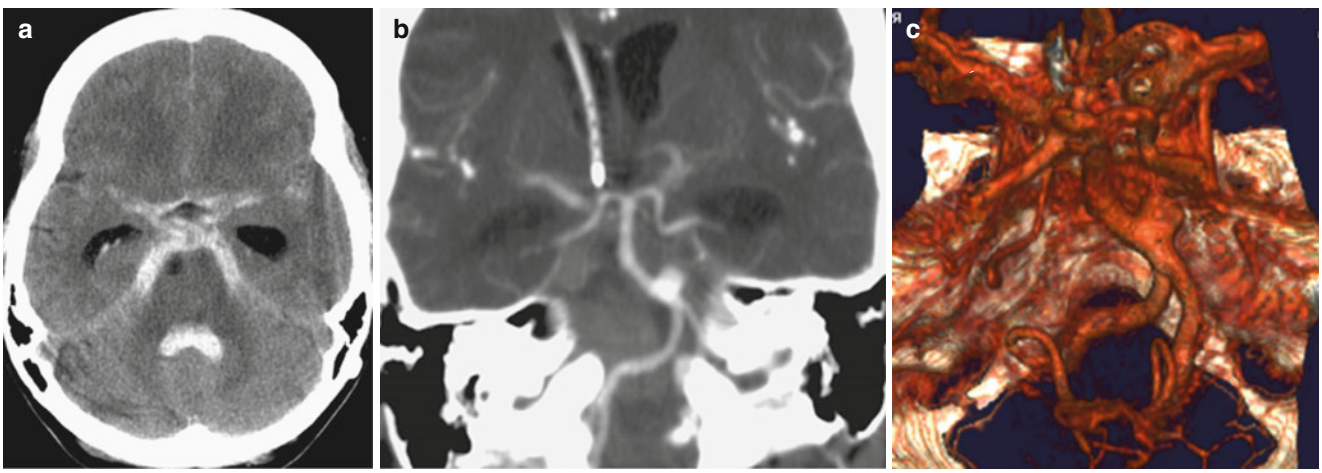

Fig. 2 Subarachnoid hemorrhage due to basilar aneurysm. (**a**) Axial CT scan reveals acute blood in the basal cisterns and fourth ventricle. Temporal horn dilatation indicates hydrocephalus. (**b**, **c**) CT angiography and a surface-shaded reconstruction demonstrate a wide-necked aneurysm at the left vertebrobasilar junction

The ability of nonenhanced MR to image meningitis is extremely limited, and a majority of cases is normal or has mild hydrocephalus. In severe cases, the basal cisterns may be completely obliterated, with high signal intensity replacing the normal CSF signal on FLAIR images. Intermediate signal intensity may be seen in the basal cisterns on T1-weighted images in these cases. Meningeal enhancement often is not present, unless a chronic infection develops [5].

Fungal organisms can start as a meningitis or cerebral abscess or can invade directly from an extracranial compartment. Coccidioidomycosis is endemic to the central valley regions of California and desert areas of the southwestern United States. Infection occurs by inhalation of dust from soil usually heavily infected with arthrospores. Primary coccidioidomycosis, a pulmonary infection, is followed by dissemination in only about 0.2 % of immunocompetent patients. Central nervous system involvement most often represents a meningitis, but cerebral abscess and granuloma formation can also occur [6]. Other fungal infections are primarily found in immunocompromised hosts.

Migraine

Migraine headaches can be severe and unrelenting. At presentation, the severity of the headache may raise the clinical question of possible subarachnoid hemorrhage or acute meningitis. Also, patients with known migraine may develop atypical headaches.

Acute/Increasing Confusion and Obtundation

Obstructive Hydrocephalus

Acute obstructive hydrocephalus is caused by compression of the ventricular system to the point of obstructing the outflow of CSF. The common locations of blockage are at the foramina of Monroe, the cerebral aqueduct, and the outlets of the fourth ventricle. Possible causes include tumor, abscess, ventriculitis, and hemorrhage. Brain injury or cerebral infarction with massive vasogenic edema can also cause obstructive hydrocephalus.

Brain Stem or Basal Ganglia Hemorrhage

Most large deep hemorrhages in the brain are associated with hypertension. The criteria for hypertensive hemorrhage include a hypertensive patient, 60 years of age or older, and a basal ganglia or thalamic location of the hemorrhage. A CT or MR scan is the procedure of choice for evaluating these patients. Arteriography is necessary only if one of these criteria is missing. Hypertensive hemorrhages are often large and devastating. Since they are deep hemorrhages and near ventricular surfaces, ventricular rupture is common. One-half of hypertensive hemorrhages occur in the putamen; the thalamus in 25 %; pons and brain stem, 10 %; cerebellum, 10 %; and cerebral hemispheres, 5 %.

Brain Herniation

As with hydrocephalus, any large mass lesion or process with prominent vasogenic edema can produce brain herniation. With large frontal or parietal lesions, subfalcine herniation is common. Also, any large hemispheric lesion can result in medial migration of the temporal lobe and subsequent inferior herniation through the tentorial incisura. Subfalcine herniation can compress the ipsilateral anterior cerebral artery, leading to brain infarction, whereas temporal lobe herniation commonly compresses the contralateral posterior cerebral artery, causing an occipital infarct. Diffuse brain swelling or posterior fossa masses can result in herniation of the cerebellar tonsils and brain stem inferiorly through the foramen magnum.

Encephalitis

Encephalitis refers to a diffuse parenchymal inflammation of the brain. Acute encephalitis of the non-herpetic type presents with signs and symptoms similar to meningitis but with the added features of any combination of convulsions, delirium, altered consciousness, aphasia, hemiparesis, ataxia, ocular palsies, and facial weakness. The major causative agents are arthropod-borne arboviruses (Eastern and Western equine encephalitis, St. Louis encephalitis, California viral encephalitis). Eastern equine encephalitis is the most serious but fortunately also the least frequent of the arbovirus infections. The enteroviruses, such as Coxsackie virus and echoviruses, can produce a meningoencephalitis, but a mild aseptic meningitis is more common with these organisms. MR reveals hyperintensity on T2-weighted scans within the cortical areas of involvement, associated with subcortical edema and mass effect.

Herpes simplex is the commonest and gravest form of acute encephalitis with a 30–70 % fatality rate and an equally high morbidity rate. It is almost always caused by Type 1 virus except in neonates where Type 2 predominates. Symptoms may reflect the propensity to involve the inferomedial frontal and temporal lobes – hallucinations, seizures, personality changes, and aphasia. MR demonstrates positive findings in viral encephalitis as soon as 2 days after symptoms, more quickly and definitively than CT. Early involvement of the limbic system and temporal lobes is characteristic of herpes simplex encephalitis. The cortical abnor-

malities are first noted as ill-defined areas of high signal on T2-weighted scans, usually beginning unilaterally but progressing to become bilateral. Edema, mass effect, and gyral enhancement may also be present [7].

Meningitis

As describe above, in addition to severe headache, patients with acute meningitis commonly present with fever, seizures, altered consciousness, and neck stiffness. Most of these cases are bacterial in origin, but tuberculosis and fungal infections can also present acutely (Fig. 3).

Metabolic/Toxic Disorders

Whenever a patient presents to the emergency department, the possibility of ingestion of drugs or other toxic substances must be considered. The narcotics and sedatives generally produce respiratory depression, which can lead to global cerebral hypoxia. Some toxic agents specifically target the basal ganglia or the white matter. In diabetic patients, the possibility of an insulin overdose and hypoglycemia must be considered. Cocaine and methamphetamine also cause vasospasm, so these patients may present with an acute focal neurological deficit.

Acute/Progressive Visual Deficit

Monocular Deficit

Monocular visual loss can be caused by anything anterior to the optic chiasm that blocks light from the retina or compresses the optic nerve. Ocular diseases, such as retinal detachment and ocular hemorrhage, are generally first evaluated by direct visualization with fundoscopy or by ultrasound. A mass compressing the optic nerve or causing severe proptosis can cause a visual deficit. Severe proptosis and stretching of the optic nerve can compromise the arterial supply to the nerve. Finally, intrinsic optic nerve lesions, such as tumors, ischemia, and inflammation, are other causes of visual loss. Intraorbital diseases are evaluated equally well by CT or MRI (Fig. 4). For intracranial disease MRI is the imaging procedure of choice.

Bitemporal Hemianopsia

This visual deficit is caused by chiasmatic compression, usually by a mass in the suprasellar cisterns. Differential diagnosis includes all tumors and inflammatory conditions that can occur in the suprasellar region.

Homonymous Hemianopsia

The most common cause of a homonymous hemianopsia is ischemia in the distribution of the posterior cerebral artery that supplies the calcarine cortex of the occipital lobe. Also, mass lesions can compress the geniculate ganglion or the optic radiations in the temporal-occipital region.

Acute/Progressive Myelopathy

Epidural Hemorrhage

Most epidural hemorrhages are post-traumatic or postoperative. Also, patients who are anticoagulated are at greater risk for epidural hemorrhage. The introduction or presence of an epidural catheter also increases the risk of both hemorrhage and infection.

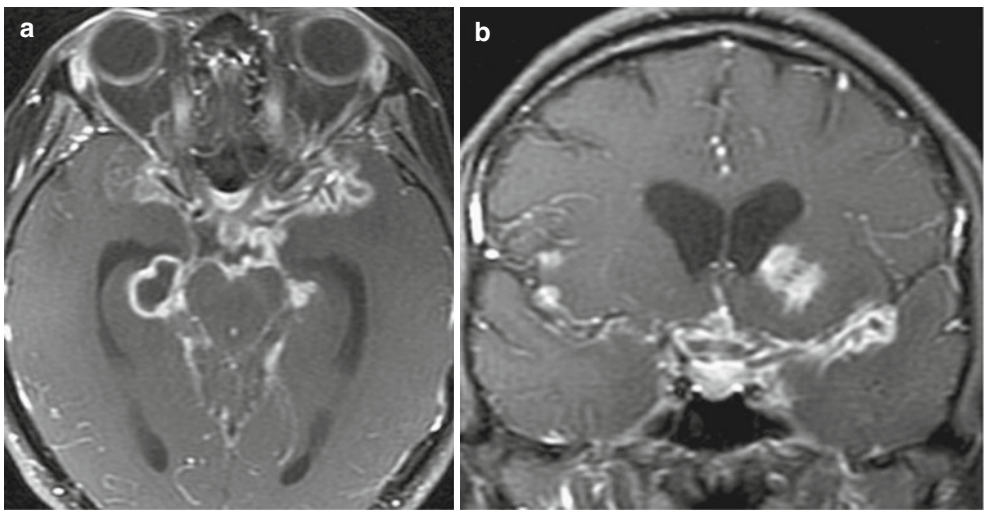

Fig. 3 Tuberculous meningitis. (**a**, **b**) Axial and coronal Gd-enhanced T1-weighted images show diffuse meningeal enhancement in the suprasellar, sylvian, and peri-mesencephalic cisterns. An enhancing mass is also present in the left basal ganglia

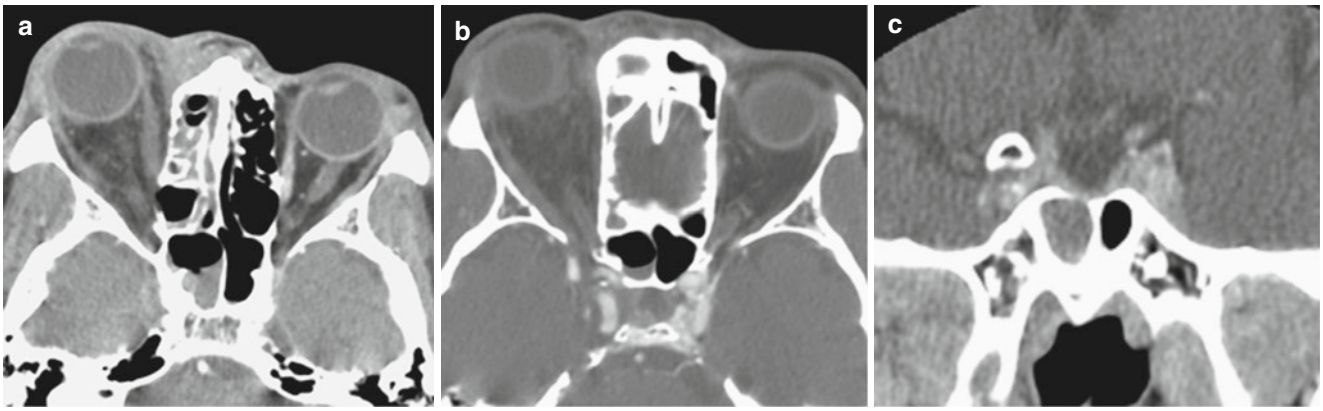

Fig. 4 Aspergillosis with cavernous sinus thrombosis. Contrast-enhanced CT scans. (**a**) The right ethmoid and sphenoid air cells are partially opacified. Right proptosis is present, and abnormal soft tissue has infiltrated the extraconal and intraconal compartments and the preseptal tissues. (**b**, **c**) Axial and coronal scans show no enhancement of the right cavernous sinus, due to septic thrombosis

Epidural Abscess

Most epidural abscesses are associated with diskitis or osteomyelitis; however, isolated infections of the epidural space can occur. The diagnosis of epidural abscess can be a challenge for both the clinician and radiologist. Patients may present with back pain or radicular pain. Fever and leukocytosis may be mild. Early diagnosis and prompt therapy are critical for favorable patient outcomes.

The imaging findings can be quite subtle on plain T1- and T2-weighted images. During the cellulitis stage, the first sign of infection is thickening of the epidural tissues, which is initially isointense on T1-weighted images and moderately hyperintense on T2-weighted images. When liquefaction occurs, the abscess cavity becomes hypointense and more hyperintense on T1- and T2-weighted images, respectively. Detection of the infectious process is easier on gadolinium-enhanced scans. The inflamed tissues (phlegmon) are highly vascular and enhance with gadolinium. On both the T2-weighted images and the enhanced T1-weighted images, fat suppression increases the contrast between the infectious process and normal tissues. The abscess cavity does not enhance and appears as a linear or elongated region of hypointensity surrounded by the enhancing cellulitis on sagittal images. The abscess cavity has an oval configuration on axial images [8].

Tumor

Epidural tumor usually extends from the spine, and the vast majority of spine tumors are metastases. The common primaries are lung, breast, and prostate. Occasionally, the epidural space may be directly seeded by lymphoma or leukemia (Fig. 5).

Spinal cord tumors and other intradural tumors (schwannoma and meningioma) may present with a progressive myelopathy.

Inflammatory Diseases

Several demyelinating diseases are associated with a transverse myelitis and acute myelopathy. In addition to classic multiple sclerosis, post-viral syndromes and Guillain-Barré are in the differential diagnosis. In HIV patients the two primary diseases to consider are epidural abscess and CMV polyradiculopathy.

Ischemia

Spinal cord ischemia is rare. It is usually associated with spinal and paraspinal tumors or surgical procedures on the spine and aorta that may compromise the blood supply to the cord.

Cervical or Thoracic Disk Extrusion

Disk extrusions in the cervical and thoracic spine, if sufficiently large, can compress the spinal cord and produce a myelopathy. Accompanying cord edema can exacerbate the problem. Emergent laminectomy and diskectomy may be necessary to relieve the cord compression.

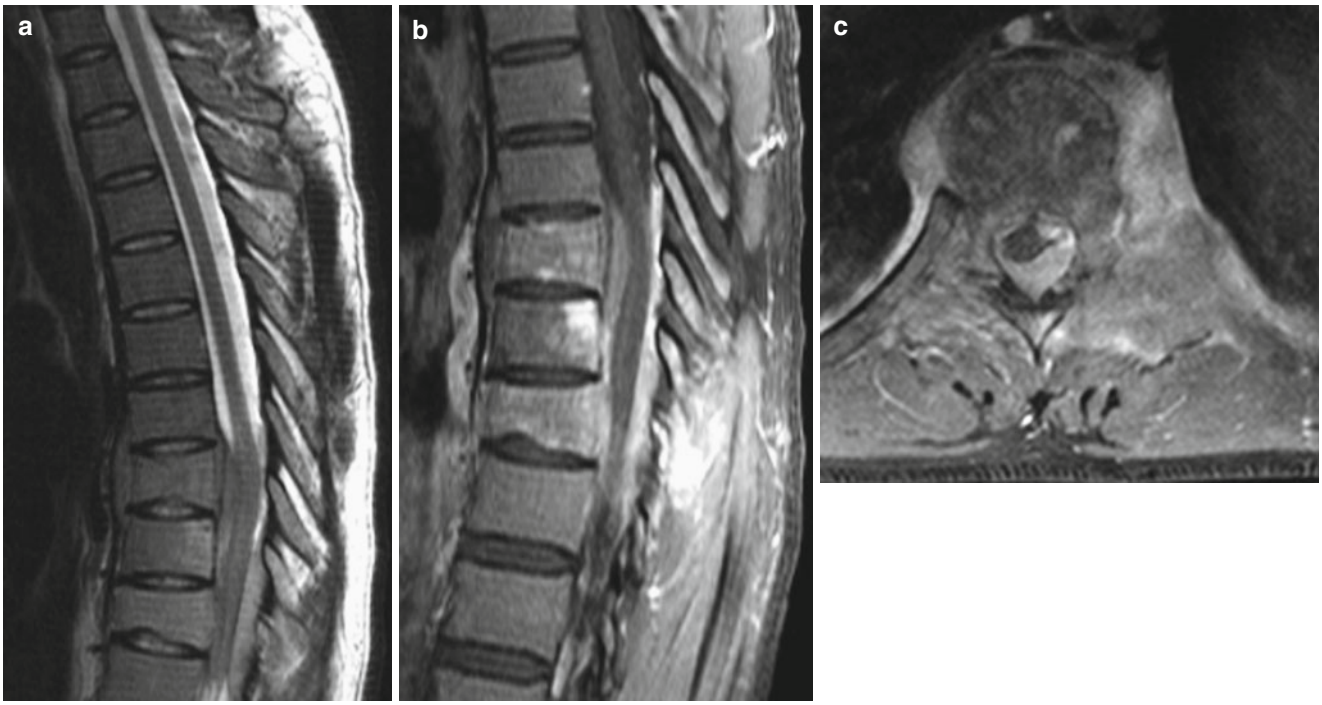

Fig. 5 Epidural spinal lymphoma. (**a**) Sagittal T2-weighted image shows epidural mass compressing the thecal sac. (**b**, **c**) Sagittal and axial Gd-enhanced T1-weighted scans reveal enhancing epidural and paraspinal masses, as well as involvement of three lower thoracic vertebrae

References

1. Gean AD (ed) (2010) Neuroimaging Emergencies. Neuroimag Clin N Am 20(4):455–690
2. Meckel S, Reisinger C, Bremerich J et al (2010) Cerebral venous thrombosis: diagnostic accuracy of combined, dynamic and static, contrast-enhanced 4D MR venography. AJNR 31:527–535
3. Chepuri NB, Perl J II, Masaryk TJ, Turski PA (2006) Aneurysms and central nervous system vascular malformations. In: Edelman RR, Hesselink J, Zlatkin M, Crues J (eds) Clinical magnetic resonance imaging, 3rd edn. Saunders-Elsevier, Philadelphia, pp 1414–1453
4. Fink KR, Benjert JL (2015) Imaging of nontraumatic neuroradiology emergencies. Radiol Clin N Am 53:871–890
5. Kanamalla US, Ibarra RA, Jinkins JR (2000) Imaging of cranial meningitis and ventriculitis. Neuroimaging Clin N Am 10:309–332
6. Mullins M (2011) Emergent neuroimaging of intracranial infection/inflammation. Radiol Clin N Am 49:47–62
7. Sämann PG, Schlege J, Müller G et al (2003) Serial proton MR spectroscopy and diffusion imaging findings in HIV-related herpes simplex encephalitis. AJNR 24:2015–2019
8. Khan SH, Hussain MS, Griebel RW, Hattingh S (2003) Comparison of primary and secondary spinal epidural abscesses: a retrospective analysis of 29 cases. Surg Neurol 59:28–33

Nontraumatic Neuroemergencies

Patrick A. Brouwer

Introduction

Due to the large number of causes, it is hard to give a comprehensive yet effective overview of the diseases responsible for nontraumatic neuroemergencies, let alone an overview of the imaging of these pathologies. The diseases covered in this text will focus on the most frequent *vascular* neuroemergencies, which will be illustrated with their usual presentation, characteristic imaging findings, and available treatment options, during the workshops.

It is well known that patients that suffer from acute neurovascular problems can present with a variety of complaints ranging from chemosis to coma and from dementia to paralysis. In a large proportion of cases is the clinical picture in itself enough to limit the differential diagnosis and therefore choose the most applicable imaging method. Since the brain and spine have only limited ability, if at all, to regenerate after damage, the accurate diagnostic work-up and speed of management is essential and will eventually determine the outcome.

It is wise, if in clinical practice an approach is chosen in which the patient is analyzed based on four important questions that apply to all diseases. These questions will show you that it is necessary that your knowledge should not just concern the radiology of the patient with the disease, but also the natural history and options for medical and/or surgical management.

The four questions to be asked are:

1. What is the cause of the presenting symptom?
2. What are the direct risks for the patient?
3. What is the underlying disease?
4. What is the prognosis and what are the treatment options?

P.A. Brouwer
Department of Neuroradiology/Neurointervention, Karolinska University Hospital, Stockholm 171 76, Sweden
e-mail: neurovascular0@gmail.com

Presenting Symptom

As stated earlier, a patient with a neuroemergency can present with a multitude of symptoms which are often not disease specific. By definition the underlying pathology has an impact on the central nervous system and the causes can, just as much as the symptoms, be numerous ranging from hemorrhage to ischemia and from mass effect to hydrocephalus. It is necessary to analyze the cause of the symptoms first, in order to come to a differential diagnosis and subsequent-targeted imaging.

Direct Risks

Addressing the acute clinical situation of the patient should be the first objective. Nevertheless, we should not ignore obvious or obscure but important secondary risks. It is of importance to recognize a hydrocephalus or a tight stenosis at the carotid bifurcation, before rushing to the angiosuite for endovascular treatment of a ruptured aneurysm. When one focuses too much on getting to the diagnosis, it is easy to overlook simple findings that can save the patient's life or prevent further harm. Many of those will only be recognized if the reading radiologist actively looks for them.

Underlying Disease

Finding "the cause of the presenting symptom" is quite often not synonymous with finding "the underlying disease." A patient presenting with an acute headache (symptom) can be diagnosed with a subarachnoid hemorrhage (cause of symptom) which in fact is an expression of a berry aneurysm (underlying disease). Finding the cause of the symptom can be just as important as finding the underlying disease since both have implications. In this example, the subarachnoid hemorrhage will necessitate treatment with a vasospasm

J. Hodler et al. (eds.), *Diseases of the Brain, Head and Neck, Spine 2016–2019: Diagnostic Imaging*, DOI 10.1007/978-3-319-30081-8_13

agent such as nimodipine. However, finding an unruptured aneurysm will not lead to this treatment.

What Is the Prognosis and What Are the Treatment Options

This is where a clinically involved radiologist can make a real difference. By mastering a helicopter view, the radiologist is capable of suggesting treatment options from a multidisciplinary perspective to the clinician. Wherein some cases the findings on imaging warrant a more conservative approach in the acute phase, it is sometimes necessary to do emergent treatment for the same disease. An example is an intraparenchymal hemorrhage due to an AVM with in one case no target for the bleeding and in another case a clear false/intra-nidal aneurysm. The operator has to rely on the knowledge of the radiologist providing the characteristics and prognostic features of the underlying disease. Furthermore, the radiologist is also responsible for supplying essential information for planning the intervention.

Vascular Neuroemergencies

Many classifications of vascular neuroemergencies can be used, but for the purpose of this text, a subdivision into hemorrhagic and ischemic pathology will be chosen which represents the majority of cases of the workshops.

Hemorrhagic Neuroemergencies

By definition a hemorrhagic neuroemergency is characterized by an intracranial or spinal bleed. The cause of the hemorrhage can be, however contradictory it may sound, nonvascular in origin too. These causes, such as tumors, infection, etc., will not be addressed here. The vascular causes can, for practical purposes, be subdivided into aneurysms and fistulous lesions.

Aneurysms

The most common aneurysm found in the CNS is the saccular or berry aneurysm. These bulging portions of the vessel wall are commonly found on bifurcations and may have a genetic and/or familial background. A number of associated diseases are recognized, of which the most well known are the polycystic kidney disease (PCKD), Marfan syndrome, and Ehlers-Danlos types II and IV. There is a difference in prevalence based on geographic location with a higher penetration in Finland and Japan. The prevalence can be as high as 6 % with multiplicity in 20–30 % of cases. The rate of aneurysm rupture, most often resulting in a subarachnoid hemorrhage, is estimated to be between 4 and 20 patients per 100,000. In some cases the hemorrhage can be intraparenchymal, ventricular, or even subdural. The acute presentation of patients with an aneurysmal hemorrhage is with the well known "thunderclap headache." The proportion of the patients, experiencing a hemorrhage, that will die before reaching the hospital is estimated to be between 20 and 30 %. Another 10–20 % will die due to secondary problems such as vasospasm, raised intracranial pressure, or pneumonia.

Other types of aneurysms that may present with hemorrhage include dissecting and mycotic aneurysms. Giant aneurysms and dolichoectasia or "serpentine" aneurysms are different entities that usually present with mass effect rather than hemorrhage.

Imaging work-up of a patient presenting with a thunderclap headache should consist of a non-contrast CT scan directed at finding a hemorrhage. To facilitate detection of small amounts of blood, one can use a window/level setting of 150/75. If a hemorrhage is found, the scan will be directly followed by a CT angiography (CTA). Postprocessing techniques such as volume rendering and 3D MIP reconstructions may facilitate detection of the bleeding source. Decision taking regarding the treatment strategy and treatment modality can often be done based on this investigation alone. Only in case of doubt, poor quality of the CTA, or negative findings in the presence of an aneurysmal distribution of blood (i.e., a nonperimesencephalic distribution), a catheter angiography is indicated. Follow-up for hemorrhages with an aneurysmal distribution and negative investigations with both CTA and catheter angiography should be done after 7–10 days. An MR of the spinal axis can be considered to exclude a spinal arteriovenous malformation or spinal dural arteriovenous fistula as the source of the hemorrhage.

Routine imaging by MR or MRA is not indicated in the acute phase, although there may be some evidence that vessel wall imaging may be of help in sporadic cases, e.g., with multiple aneurysms and an uncertain source of bleeding.

Imaging of the so-called "perimesencephalic" hemorrhage, in which the distribution of blood is not aneurysmal but defined as blood in the perimesencephalic cistern, no intraventricular blood and no more than one-third of the proximal sylvian fissure filled with blood, is based on CT and CTA alone. If in such a case no aneurysm is visible and the patient is in good clinical condition, no additional imaging by catheter angiography is needed since the recurrence rate is believed to be close to zero and the clinical outcome is invariably excellent.

Fistulous Lesions

The fistulous lesions are the second most common cause of intracranial hemorrhages. The fistulous lesions, comprising arteriovenous malformations (AVMs), dural arteriovenous fistulae (dAVF), and pial fistulae, are characterized by a direct connection between the arterial system and the

draining venous system without a normal capillary network. This short circuit is also the mainstay in the diagnosis of the lesions since in dynamic imaging the venous structures will fill in the arterial phase and are therefore "too early."

AVMs consist of a network, with arterioles that connect to venules, which is called the nidus. Feeding arteries can be enlarged due to the high flow through the lesion. Presentation of AVMs is not exclusively with hemorrhages since patients may also present with seizures, steal phenomena, or mass effect. Hemorrhages are often caused by rupture of flow-related aneurysms, intra-nidal aneurysms, venous pouches, or weak portions of the nidus. In the analysis of AVMs, angiography is of the utmost importance since only dynamic imaging will show the lesion with certainty. Current evolution of 4D CTA and TRICKS MR creates options of using other modalities than catheter angiography to do the analysis. To date the limitations are mostly the lower temporal and spatial resolution of those techniques. Analysis of the AVM should be done in a standard fashion, and it makes sense to perform this from the arterial side to the venous side. Many of the properties of an AVM, such as venous stenoses, deep venous drainage, and location, do have an impact on the prognosis and therefore on the treatment strategy. Treatment can consist of surgery, radiosurgery, embolization, or a combination of any of those. Randomized trials were started, but none of the trials was brought to a conclusive end leading to evidence for decisions on treatment. There seems to be a tendency to only treat AVMs that are symptomatic, i.e., that have bled. Treatment of an AVM to manage seizures is very seldom effective.

Dural arteriovenous fistulae are lesions that exhibit a direct connection between dural vessels and the venous system, and they do not exhibit a nidus. These lesions may present clinically with symptoms that are not easily connected to the underlying disease. For example, spinal dAVF can present with symptoms mimicking a disc herniation, whereas some intracranial dAVF may present with dementia. Hemorrhagic presentation can be with subdural, epidural, but also parenchymal hemorrhage. Besides those serious presentations, the most common complaint with these fistulae is a pulsatile tinnitus.

The fistulous point of the dAVF can be single hole but also multi-hole on a larger part of, e.g., the transverse sinus. Depending on the pressure gradient over the fistulae, the venous system can exhibit retrograde filling (venous congestion) with subsequent disturbance of the normal venous drainage of the brain. The result thereof will in many cases be visible as edema in the affected area on CT imaging or more clearly on MR imaging. This cortical venous reflux is one of the parameters that should be used in the decision to treat a dAVF.

Pial fistulous lesions are direct connections of pial arteries and pial veins on the surface of the brain. These lesions are often seen in hereditary hemorrhagic telangiectasia (HHT/Rendu-Osler-Weber) and other syndromes. Treatment of these lesions is not always indicated and is highly dependent on the underlying disease and the hemorrhagic presentation.

Ischemic Neuroemergencies

Ischemic stroke is the most prevalent nontraumatic neuroemergency and has by far the highest impact on the population as a whole. The list of stroke causes is immense, and getting to the correct underlying disease can be a very difficult task. To date, the role of the radiologist is of importance for both diagnosis and treatment strategy. The presenting symptoms will point the neurologist to the differential diagnosis of an ischemic stroke, and this will trigger the sense of emergency for acute treatment. Since this direct treatment is essential, the first part of the imaging process should be directed to excluding an intracranial hemorrhage as the cause of the symptoms. The normal work-up to this goal would consist of performing a non-contrast CT scan. If a bleeding is excluded, the diagnostic work-up should be focused on showing the stroke. In case of a clear "dense vessel sign," in which a clot is visible in the artery, the diagnosis can be straightforward. If the signs are less clear, particular attention needs to be given to the loss of gray-white matter differentiation, effacement of the surface of the brain, the insular ribbon sign, focal edema, and loss of detail in the basal ganglia. If this is not the case, other causes which are less time sensitive such as seizures, infection, etc., can be analyzed. If however an ischemic stroke is considered to be responsible for the symptoms, intravenous thrombolysis should be started as soon as possible and in any case within 4 h of stroke onset.

Many studies are being performed to get a better idea about the prognosis of a patient suffering an ischemic stroke. These range from classification systems on plain CT to scan protocols on CT and MR providing us with perfusion and diffusion images.

One of the classification systems on CT is the "ASPECT score" (Alberta Stroke Program Early CT score) [1]. This score recognizes ten areas in the brain that each represents one point on a ten-point scoring scale. If the plain CT shows manifest infarction in that area, one point is deducted from the total. If a score is seven points or less, there is a correlation with both poor functional outcome and symptomatic intracerebral hemorrhage. An ASPECTS of 8–10 is associated with a greater extent of benefit from IV thrombolysis.

Perfusion imaging using contrast-enhanced CT scanning will render images of the time to peak (TTP), mean transit time (MTT), cerebral blood flow (CBF), and cerebral blood volume (CBV). The latter two are most commonly used to determine the so-called penumbra and infarct core. A

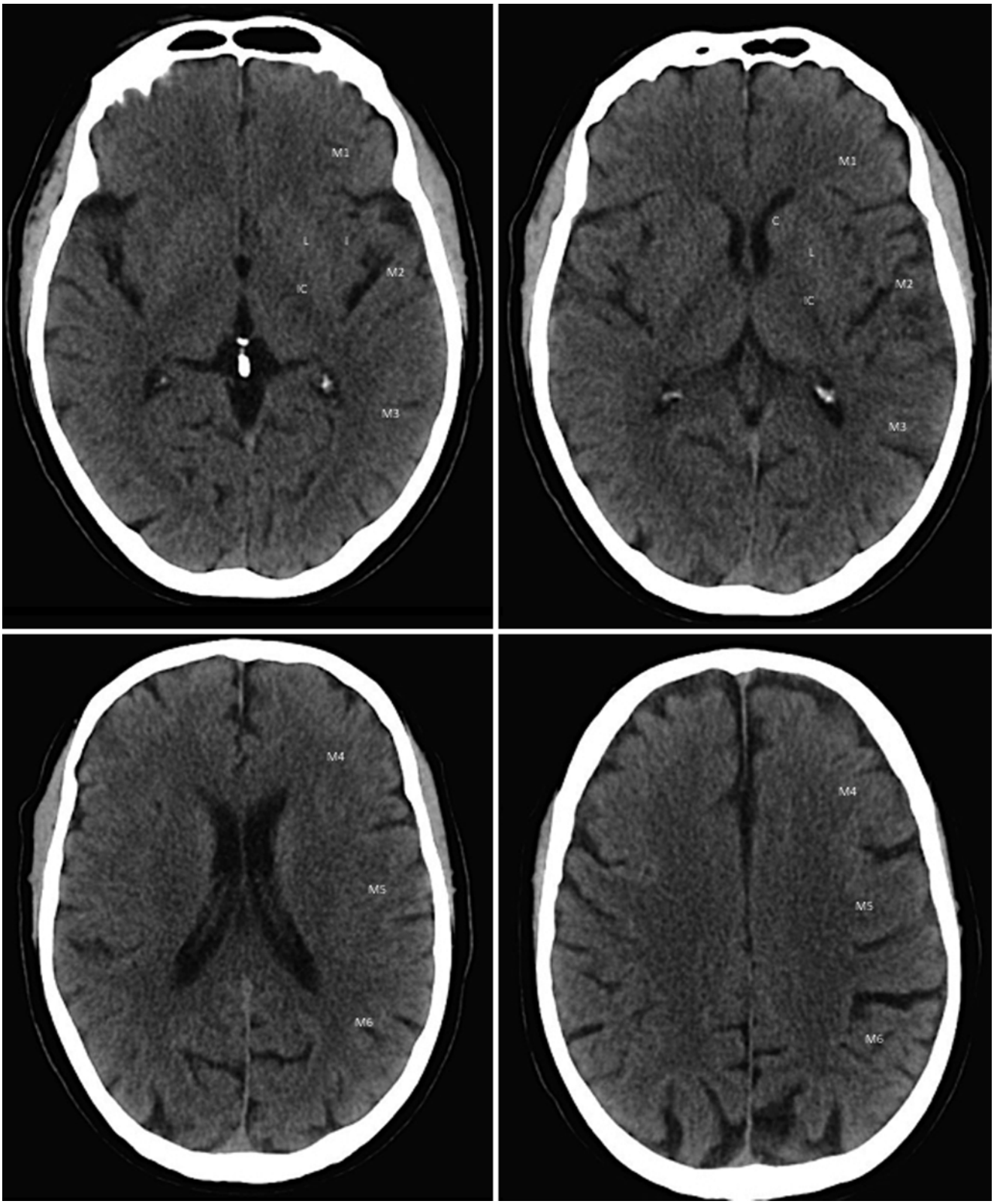

restricted CBF shows the tissue at risk due to limited blood flow, whereas the CBV shows the area of tissue that has already infarcted or can potentially be salvaged. Perfusion imaging has not yet found full acceptance in the field. This is mainly due to the fact that the interpretation of the images is very much dependent on the software used. Different vendors seem to have different output functions, which makes comparison difficult. Furthermore it has been shown that the

perfusion images are not predictive of the outcome of treatment.

The use of diffusion imaging in conjunction with perfusion imaging on MR is currently investigated. Unfortunately, MR does not seem to be the most readily available modality for stroke patients in the majority of centers, and this has a major implication for the clinical applicability. MR should be the first modality of choice in posterior fossa stroke. CT is notoriously unable to show extensive infarction in the posterior fossa, and treatment should be reserved for patients with a fair chance of survival and recovery. There is no sadder outcome than a patient with fully patent arteries suffering from a locked-in syndrome.

In February 2013, during the International Stroke Conference in Honolulu, three trials were presented that showed that there was no benefit of endovascular therapy in ischemic stroke. The conclusions of these trials, IMSIII, MR RESCUE, and SYNTHESIS, were considered to be level 1 evidence, and physicians suggesting intra-arterial treatment after the publications were frowned upon by the neurologists in charge of the patients. It is always hard to argue against level 1 evidence, no matter how many arguments against the trial design one brings up. Fortunately, with the recent publication of the MR CLEAN trial [2], the opinion on intra-arterial treatment techniques, as being valuable alternatives, tipped. After MR CLEAN, other trials performed interim analysis on their patient cohorts, and ESCAPE, EXTEND-IA, SWIFT PRIME, REVASCAT, THERAPY, and THRACE were halted prematurely. Based on the current evidence, thrombectomy is considered to be the treatment of choice in selected patients. To be eligible for intra-arterial treatment, the patient needs to have a large-vessel occlusion (internal carotid, anterior cerebral artery, or middle cerebral artery). Distal obstructions (M2 and A2) are currently being investigated, but direct intra-arterial treatment has not been proven beneficial yet.

Evidence is still lacking for the ischemic stroke in the posterior fossa. The BASICS trial is a multicenter trial focusing on thrombectomy in the posterior fossa, but the results will have to be awaited before any conclusions can be drawn. Nevertheless, the common opinion in posterior fossa stroke seems to be that the natural history is so bad that aggressive treatment is warranted. There are currently various techniques that one can employ to perform intra-arterial treatment ranging from thrombus retrieval to thrombosuction/aspiration and local thrombolysis. A combination of these techniques may be used if deemed necessary.

Intra-arterial stroke treatment should be performed in comprehensive stroke centers with multidisciplinary 24/7 coverage and only by adequately (being) trained physicians (neurointerventionalists). It is of the utmost importance to understand the anatomy, anatomical variations, physiology, and challenging comorbidities of this highly complex end organ. Furthermore, a large number of problems can arise during the treatment that need to be solved by a combination of understanding the circulation and potential collaterals of the end organ and being able to manage all neurointerventional devices in this sensitive area when forced to do so. Training guidelines and charters on standards of practice have already been published by the UEMS (European Union of Medical Specialists) in order to assure good patient care. These guidelines on training are unanimously approved by the division of neuroradiology and the sections of radiology, neurosurgery, neurology, and cardiology [3, 4].

This text is nowhere near a complete overview of nontraumatic neuroemergencies and neither for vascular neuroemergencies. It only serves as background information for the workshops at the IDKD 2016. For more detailed information, you are encouraged to read any of the books in the references [5, 6].

References

1. Hill MD, Rowley HA, Adler F et al (2003) Selection of acute ischemic stroke patients for intra-arterial thrombolysis with pro-urokinase by using ASPECTS. Stroke 34(8):1925–1931
2. Berkhemer OA, Fransen PS, Beumer D et al (2015) A randomized trial of intraarterial treatment for acute ischemic stroke. N Engl J Med 372(1):11–20. Erratum in: N Engl J Med. 2015;372(4):394
3. Rodesch G, Picard L, Berenstein A et al (2013) Editorial: «Interventional neuroradiology: a neuroscience sub-specialty? Interv Neuroradiol 19(4):521–523
4. http://neuro.uemsradiology.eu/charter-cnr-and-inr/uems-charter-on-clinical-neuroradiology-and-interventional-neuroradiology.aspx
5. Lasjaunias P, Berenstein A, Ter Brugge KG (eds) (2006) Surgical neuroangiography, 2nd edn. Springer Berlin, Heidelberg/New York. ISBN 978-3-540-68320-9
6. Caplan LR (ed) (2008) Uncommon causes of stroke. Cambridge University Press, Cambridge. ISBN 978-0-521-87437-3

Imaging the Patient with Epilepsy

Timo Krings and Lars Stenberg

Introduction

Approximately 4 % of the general population will experience a seizure during their lifetime. Imaging in these "first-ever" seizure patients is in most cases normal, and abnormalities are only present in approximately 15 % of patients as seizures can be provoked by fever, sleep deprivation, stroboscopic lights, or drugs. However, an underlying lesion will lower the seizure threshold and thus make a patient more susceptible to experience a seizure. As "first-ever seizures" are a medical emergency, the treatment modality of choice in these cases is an unenhanced CT to exclude acute medical emergencies that may go along with seizures prior to a more extensive workup depending on clinical history and presentation. Imaging abnormalities encountered in patients experiencing their first-ever seizures include (but are not restricted to) virtually all diseases affecting the brain. As such you may find vascular abnormalities (such as microangiopathy, arteriovenous malformations (AVM), sinus thrombosis, hemorrhage, cavernomas, or stroke), tumors (metastases, primary tumors), infections (encephalitis, meningitis, abscess), sequelae of previous head injury, and toxic or metabolic conditions (e.g., PRES) in these patients.

In contrast to the "first-ever seizure," patients diagnosed with "epilepsy" have recurrent and unprovoked seizures. Approximately 1 % of the general population will be diagnosed with this condition, and as seizures are recurrent and unprovoked, an underlying lesion is far more common as compared to patients with their first-ever seizure. Being "unprovoked," lesions that can irritate the brain (i.e., are "epileptogenic") may be present. On brain imaging, lesions will be seen in nearly 50 % of patients; however, these are nonspecific and can encompass a wide variety of underlying conditions that can provoke the recurrent seizure attacks. Imaging findings in patients with epilepsy include but are not restricted to vascular conditions such as microangiopathy, previous ischemia, vascular malformations, previous hemorrhage or cavernomas, tumors (metastases, primary tumors), remote infections (encephalitis, abscess), previous head injury, congenital malformations, or toxic metabolic conditions. Imaging of choice in patients with epilepsy is MRI, given the larger variety of potential underlying diseases.

The vast majority of patients with epilepsy can be treated satisfactorily with antiepileptic drugs. However, 0.4 % of the general population will have recurrent and unprovoked seizures that do not respond to medication. These patients are potentially treatable with surgery, and surgical intervention is an appropriate consideration for 3 % of people who develop epilepsy [1]. The major focus of this chapter will be on the imaging findings in those patients who are diagnosed with "medication-refractory" epilepsy, i.e., patients where the seizure focus is too strong to be controlled by medication which indicates that the underlying lesion has to have a strong epileptogenic potential. In these patients, structural imaging will find a large proportion of abnormalities reaching up to 85 % of patients. Lesions with a strong epileptogenic potential are either close to epileptogenic structures or consist of abnormal neurons. Lesions that are often involved in medication refractory epilepsy are mesial temporal lobe sclerosis (MTS) (primary or secondary to a long-standing seizure disorder), malformations of cortical development, certain epileptogenic tumors (e.g., dysembryoplastic neuroepithelial tumors (DNET), temporal lobe glioma or

T. Krings, MD, PhD, FRCP(C)
Division of Neuroradiology, Toronto Western Hospital, Toronto, ON, Canada

Joint Department of Medical Imaging, University Health Network, Toronto, ON, Canada

Neuroradiology, University of Toronto, Toronto, ON M5T2S8, Canada
e-mail: timo.krings@uhn.ca

L. Stenberg, MD, PhD (✉)
Section of Neuroradiology, Department of Medical Imaging and Physiology, Skåne University Hospital, Lund, Sweden

Department of Diagnostic Radiology, Lund University, Lund SE 221 85, Sweden
e-mail: Lars.Stenberg@skane.se

J. Hodler et al. (eds.), *Diseases of the Brain, Head and Neck, Spine 2016–2019: Diagnostic Imaging*, DOI 10.1007/978-3-319-30081-8_14

ganglioglioma), vascular malformations, post-traumatic, post-infectious, and certain phakomatoses. Imaging findings in some of these conditions will be subtle which necessitate both a dedicated imaging protocol (as compared to a standard MR) and an "expert" experienced in reading these types of scans. In a landmark study of von Oerzten et al. [2], the sensitivity of "nonexpert" reports of standard MRI for focal lesions was 39 %, while sensitivity of "expert" reports of standard MRI increased to 50 %. "Expert" reports of epilepsy-dedicated MRI further increased the sensitivity in detecting subtle lesions to 91 %. Dedicated MRI showed focal lesions in 85 % of patients with "nonlesional" standard MRI. Neuropathological diagnoses were predicted correctly in 22 % of "nonexpert" standard MRI reports but by 89 % of dedicated MRI reports. Thus, the combination of dedicated MRI protocols and dedicated radiologists trained in evaluating patients with medication refractory seizures increases significantly the sensitivity of MRI in this subgroup of patients. A multidisciplinary approach that involves close communication between epilepsy neurology, neuroradiology, EEG, nuclear medicine, neuropsychology, and neurosurgery is an important feature of modern epilepsy imaging.

The necessity of expert MR reading with a dedicated imaging protocol is further highlighted by the fact that postsurgical seizure freedom is achieved significantly more often when a circumscribed, resectable epileptogenic lesion can be identified on MRI preoperatively compared to patients that are rated nonlesional [3]. As pointed out by Wellmer et al. in [4], the possible reasons for undetected epileptic lesions in standard outpatient MRI are insufficient clinical information from the referring clinician, routine MR protocols not optimized for the spectrum of epileptogenic lesions, and unfamiliarity with the spectrum of epileptogenic lesions. Wellmer pointed out that "because even the best focus hypothesis and most profound knowledge of epileptogenic lesions do not permit the detection of lesions when they are invisible on the MRI scan, the starting point for any improvement of outpatient MRI diagnostics should be defining an MRI protocol that is adjusted to common epileptogenic lesions."

This indicates that a specific imaging protocol to identify these lesions is necessary. This protocol should take into account that – as small epileptogenic lesions are usually those that provide the best chance for postoperative seizure freedom – slice thickness should be adjusted to detect small lesions, and multiple (coronal, axial, sagittal) cut planes are acquired to ensure that physiologic structures or partial volume effects within the folded cortex are not taken for pathology and vice versa. Coronal sequences have to be angulated perpendicular to the hippocampal axis to allow hippocampal volume estimation, and caution has to be taken that they are oriented in a plane that ensures direct comparison with the contralateral hemisphere. In our practice, we employ this coronal angulation for both T2/FLAIR and T1 IR sequences. High-resolution T1-weighted sequences with isotropic voxel sizes allow for multiplanar reformation and further evaluation (including 3D reformats, "pancake" views, surface rendering, and volumetric assessments). T2 gradient echo or susceptibility-weighted sequences are highly sensitive to detect blood products or calcifications and should therefore be part of a seizure imaging protocol (Fig. 1).

In a recent analysis performed by Wellmer et al. on the prevalence of epileptogenic lesions among 2740 patients, the following pathologies were found: mesial temporal lobe sclerosis in 32 % of patients; tumors (including low- and high-grade tumors as well as malformative tumors and benign epilepsy associated tumors) in approximately 17 %; cortical dysplasias in 11 %; glial scars (including posttraumatic, postischemic, posthemorrhagic, postinfectious/abscess, ulegyria, and postsurgical scars) in 11 %; vascular diseases (cavernoma, AVM, pial angiomatosis) in 5 %; malformations of cortical development including nodular heterotopia, subcortical band heterotopia, polymicrogyria, lissencephaly, pachygyria, agenesis of corpus callosum, craniocephalic malformations, hemiatrophy, lobar dysgenesis, hemimegalencephaly, or hamartomas in 3 %; and sequelae of encephalitis in 1 %, while in approximately 20 %, no lesion could be detected.

Lesion location – presumably related to the different epileptogenic potentials in different brain regions – demonstrates preponderance for the temporal lobes (60 %) followed by the frontal lobe (20 %), the parietal lobe (10 %), the periventricular white matter (5 %), and the occipital lobe (5 %).

The suitability of MR imaging to detect these findings varies between different sequences. It is generally recommended that for an epilepsy-specific protocol, T2/FLAIR, T2/STIR in two parallel planes, T2 gradient echo/SWI sequences, and an isotropic 3D-T1 are necessary. We strongly recommend these imaging sequences to be done on a 3 T scanner given the higher spatial resolution [5, 6]. The use of even higher field strengths (7 T) (Fig. 2) will probably further increase the detection rate of epileptogenic substrates such as mesial temporal lobe sclerosis (MTS), focal cortical dysplasia (FCD), and polymicrogyria [7–10].

Functional MRI (fMRI) can map eloquent cortex and provide information regarding language lateralization [11] (Fig. 3), and the use of diffusion tensor imaging (DTI) and tractography may help to avoid injury to the optic radiation during temporal lobe resection [12].

Radionuclide imaging can add useful information in selected cases [13]. Subtraction of ictal and interictal SPECT coregistered to MRI (SISCOM) can show a seizure-induced hyperperfusion (Fig. 4), whereas ^{18F}FDG PET may show hypometabolism in the seizure onset zone. This is particularly

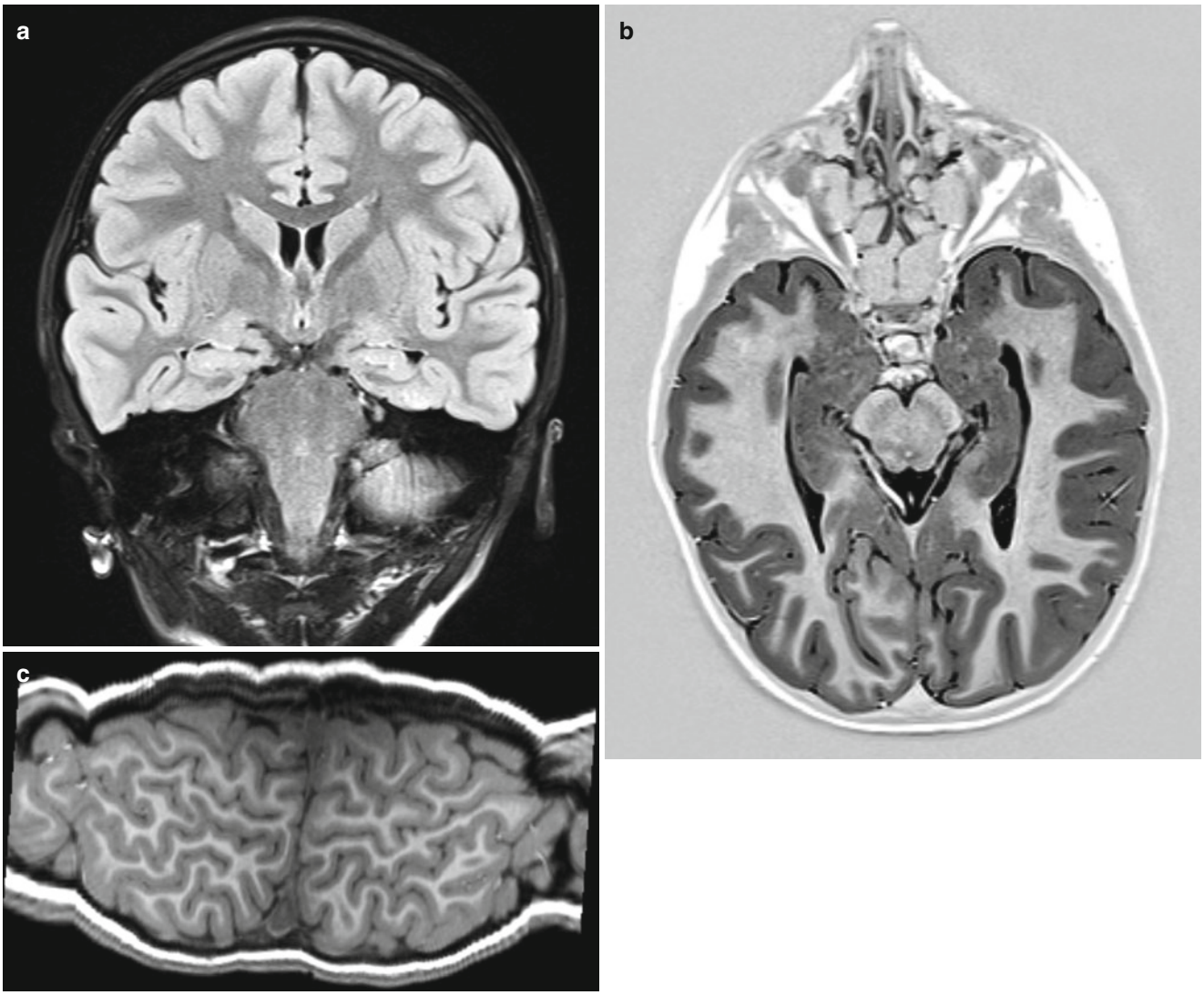

Fig. 1 (**a**–**c**): Some examples of good sequences in a dedicated epilepsy protocol: (**a**) coronal T2/FLAIR, perpendicular to the hippocampal axis; (**b**) axial T1 inversion recovery (IR) parallel to the hippocampal axis; (**c**) T1 3D image set presented as "pancake view" for a better overview of the gyral pattern

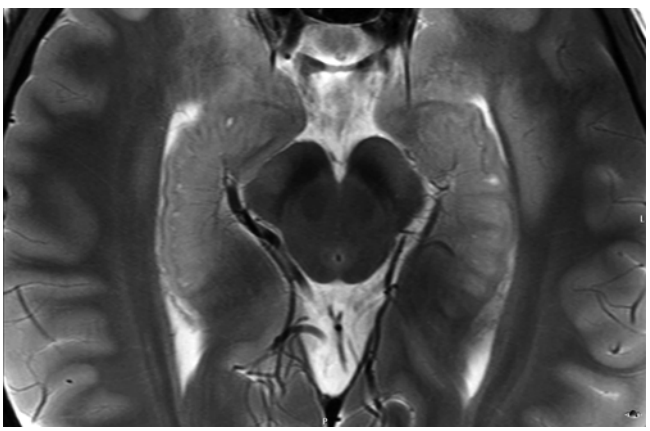

Fig. 2 Axial T2 at 7 T parallel to the hippocampal axis. Excellent in-plane resolution provides detailed imaging of the hippocampus

useful in lateralization of temporal lobe epilepsy in the MR-negative patient.

Imaging evaluation should be standardized using a stepwise approach to evaluate the hippocampus and mesial temporal lobe structures, the ventricular outline, and the gyral and the sulcal anatomy (Table 1). Particular emphasis should be paid upon the T2/FLAIR signal within the cortex and hippocampus, its similarity to other regions of neo- and archicortex, the internal architecture of the hippocampus, the indentations of the pes hippocampi, the fornix and mammillary bodies, and the gray-white matter interface of the neocortex (blurring, gray matter thinning or thickening).

In the following, we will discuss the imaging features of epileptogenic lesions, highlighting imaging pearls and pitfalls.

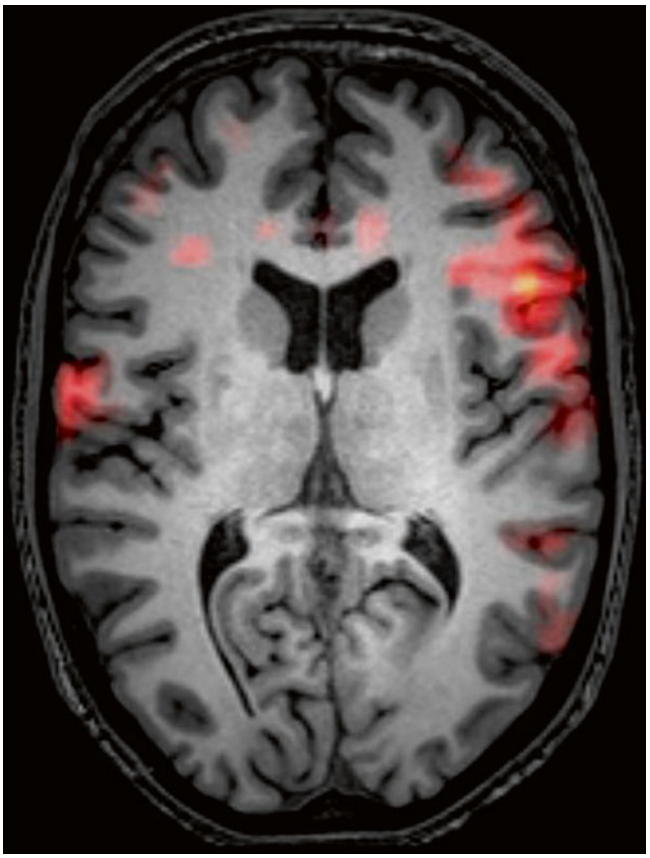

Fig. 3 Functional MRI. *Red* areas indicate activation during a simple word generation task. Activation is seen predominantly in the left hemisphere in the frontal language region; typical language lateralization

Mesial Temporal Lobe/Hippocampal Sclerosis

Patients with mesial temporal sclerosis (MTS) harbor complex partial seizures with a seizure semiology that is characterized by déjà vu sensations, epigastric auras, lip smacking, or other oral automatisms and often have in their past medical history febrile seizures as a child with progressive worsening of seizure frequency and severity over time. On MR imaging, you will find atrophy of the hippocampus as well as signs for gliosis/sclerosis within the hippocampus that will manifest itself as T2/FLAIR hypersignal (Fig. 5). The atrophy will lead to loss of the indentations of the pes hippocampi and widening of the temporal horn and atrophy of the white matter of the temporal lobe. As a consequence of Wallerian degeneration, there will be atrophy of the projecting pathways of the hippocampus, i.e., the Papez cycle, with

Table 1 Checklist for a structured, stepwise approach to evaluate MRI in the patient with epilepsy

Hippocampus, fornices, and mamillary bodies
Ventricular outline
Sulcal morphology, CSF clefts
Gray matter thickening or thinning
Blurring of gray-white matter junction
T2 prolongation
Paramagnetic artifact
Atrophy

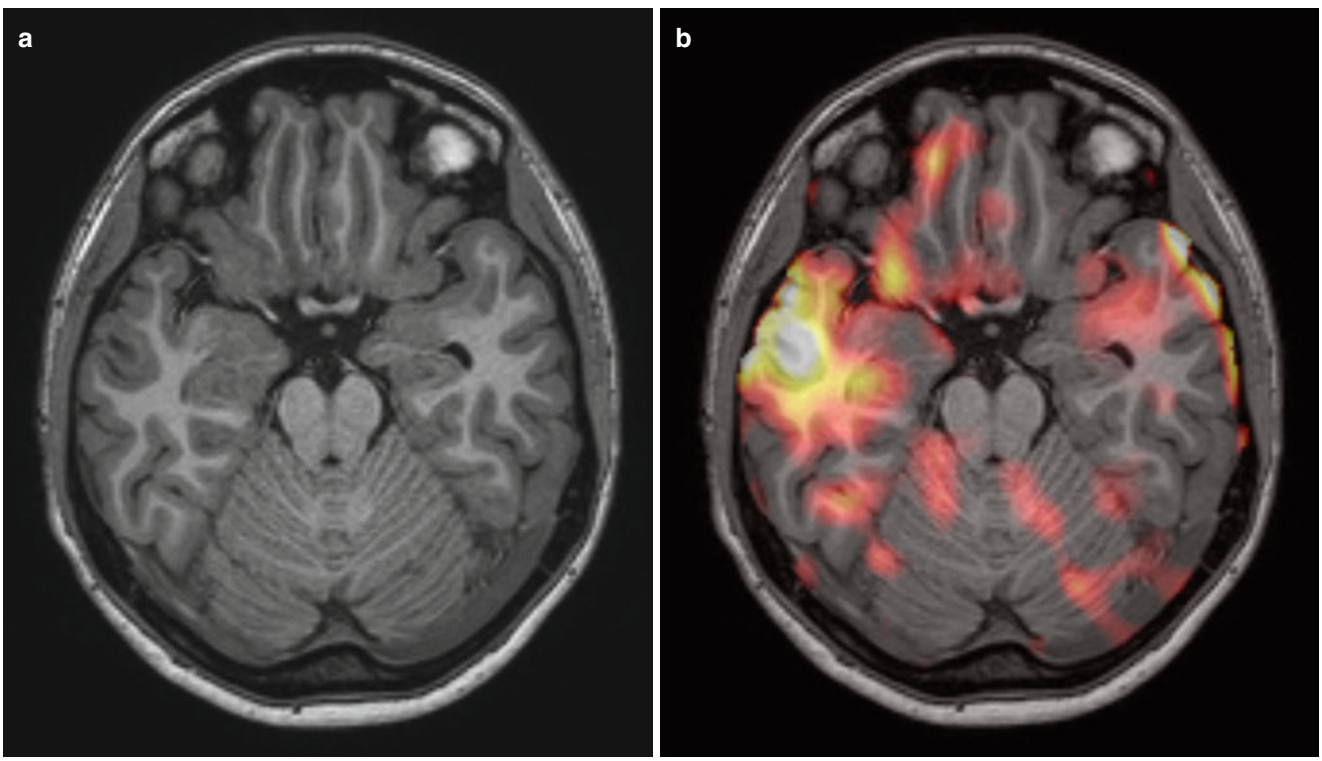

Fig. 4 (**a**, **b**) SISCOM: (**a**) axial T1 with small subcortical area in the right temporal lobe with prolonged T1; (**b**) coregistration of SPECT on MR images shows ictally hyperperfused area exactly in the same spot as the suspected lesion

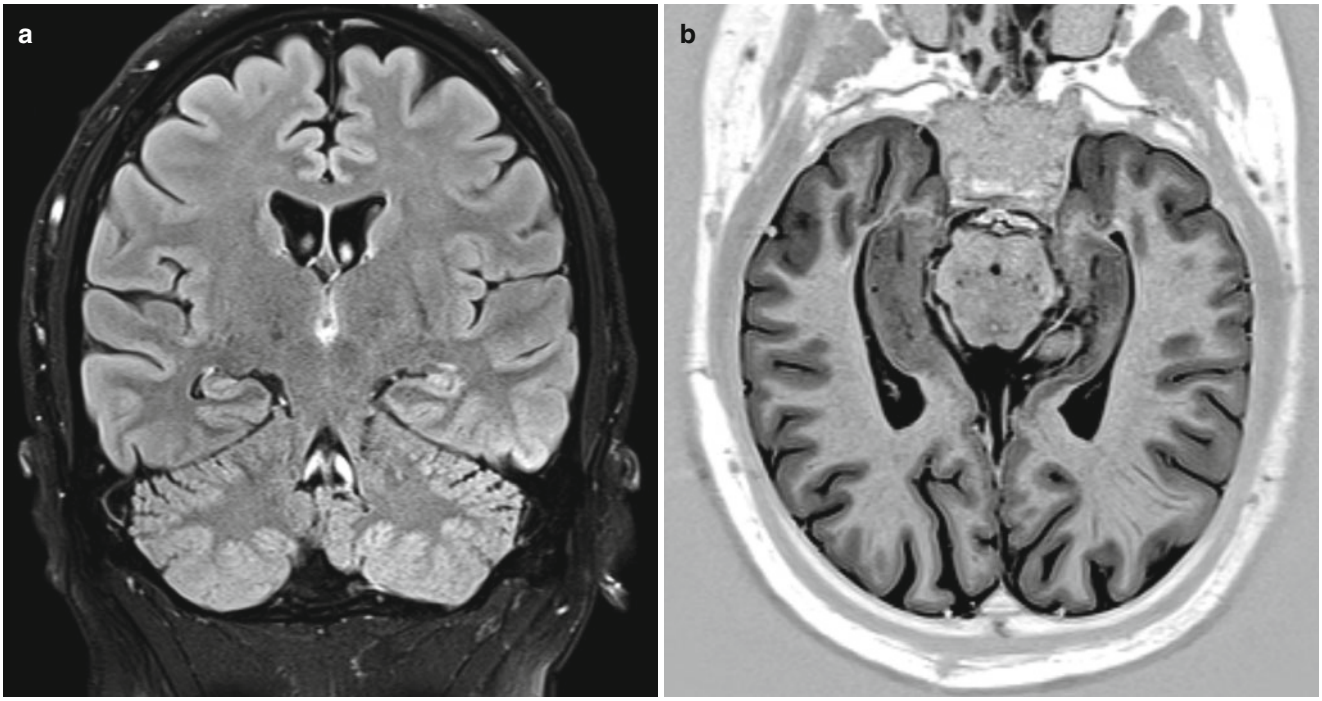

Fig 5 (**a**, **b**) Mesial temporal sclerosis (MTS): (**a**) coronal T2/FLAIR shows increased signal in the left hippocampus; (**b**) axial T1 IR demonstrates volume loss in the left hippocampus. The findings shown are relatively subtle. MRI fails to recognize pathologically detected mesial temporal lobe sclerosis in up to 20 % of the cases

atrophy of the fornix and the ipsilateral mammillary body. In the early stages of mesial temporal lobe sclerosis, the imaging findings are subtle and involve loss of the granular cell layer symmetry (i.e., the internal architecture of the hippocampus) without associated FLAIR signal changes. Hard windowing of the FLAIR-weighted sequences will make identification of the diseased hippocampus easier. In nearly 20 % of patients with mesial temporal lobe sclerosis, dual pathology is present with a second epileptogenic focus. It is believed that in these cases, the other epileptogenic lesion triggered the mesial temporal lobe sclerosis (similar to febrile seizures as a child can trigger or "kindle" a mesial temporal lobe sclerosis). Identification of the second focus is of great importance as failure to do so may result in surgical failure if only a selective amygdalohippocampectomy is performed, thus leaving the "primary" focus behind. On the other hand, failure to identify MTS in patients with other lesions may also lead to surgical failure following lesionectomy. Dual pathology may consist also of bilateral mesiotemporal lobe sclerosis as one hemisphere may trigger the other hippocampus to become sclerotic thus constituting bilateral abnormalities. As the internal reference (i.e., the contralateral hippocampus) is similarly affected, comparison of the signal with other regions of archicortex (three-layered cortex) can identify whether a mesial temporal lobe sclerosis is present bilaterally. Thus, if the T2/FLAIR signal of the hippocampus is bilaterally symmetrical but higher as compared to the cingulum or insula, you have to consider bilateral mesial temporal lobe sclerosis.

Malformations of Cortical Development

In order to understand the different types of malformations of cortical development, it is important to briefly review the embryological development of the cortex: During the 7th week of gestation, neuronal proliferation in the subependymal germinal matrix occurs. After the 8th week, these cells migrate outward in multiple waves of radial outward migration aided by radial glial cell guidance in a process coined as chemotaxis. The third and last part of the cortical development, the lamination, is the organization of the cells within different cortical layers a process that is orchestrated by the subplate (the lowest layer of cortex). Chromosomal mutations, destructive events (ischemia/infections) or toxins may inhibit either of these three processes (proliferation, chemotaxis, or cortical organization) which will lead to abnormalities in stem cell development, migration or lamination [14].

Malformations of cortical development are present in up to 25 % of patients with intractable childhood epilepsy. They are associated with chromosomal alterations, congenital infections, or in utero ischemia. In addition to epilepsy, these patients will have developmental delay and focal neurological deficits.

Malformations related to abnormal stem cell development include the focal or transmantle cortical dysplasias (balloon cell or type II FCDs) and the hemimegalencephalies.

FCD type II is characterized on histology by enlarged (balloon) cells without dendrites or axons and are identical to cortical hamartomas in tuberous sclerosis. The abnormal cells extend from the ventricle to the cortex; thus, a linear hyperintensity from the ventricle toward the cortex (the radial band or foot) can be seen in association with a subcortical FLAIR hyperintensity. The abnormal FLAIR hypersignal is again better seen with a hard window that will exaggerate the abnormal T2 signal. The junction between the cortex and white matter is indistinct, and the gray matter may be focally thickened (Fig. 6).

In hemimegalencephaly, a diffuse hamartomatous overgrowth as a result of abnormal stem cell proliferation is present, resulting in broad gyri, shallow sulci, and a blurred gray-white matter junction. The ipsilateral ventricle is often enlarged and demonstrates an abnormal straight course of the frontal horn (Fig. 7). Clinically, patients present with macrocephaly, hemiplegia, developmental delay, and seizures. The affected hemisphere has no function and thus hemispherectomy can be proposed to these patients. However, hemispherectomy is contraindicated if there are cortical malformations in the contralateral hemisphere which have to be specifically sought after.

Malformations related to abnormal migration are the lissencephalies, the agyria-pachygyrias, and the heterotopias.

In the lissencephalies, there has been a global halt in the migration due to an impaired last phase of neural migration leading to paucity of the gyral and sulcal development with a smooth brain surface and diminished white matter. Patients present with global developmental delay and seizures. Two different types of lissencephaly can be distinguished: the posterior agyria (related to an alteration on chromosome 17) and the anterior agyria which is an x-linked disease (Fig. 8).

Female carriers of the affected x-chromosome present with band heterotopias that is more present in the frontal lobes compared to the parietal lobes. Thus, if females present with band heterotopias, genetic counseling may be indicated. The band may be thin or thick depending on the amount of arrested migration. Patients with a thick band have less normal cortex (that can be thinned) and present with a more severe developmental delay.

In addition to the "band heterotopia," focal subcortical heterotopia can be present. On imaging, swirling, curvilinear bands of gray matter as well as thin cortex, and paucity of the white matter are seen. The ipsilateral ventricle may be distorted, and there can be an associated callosal hypogenesis.

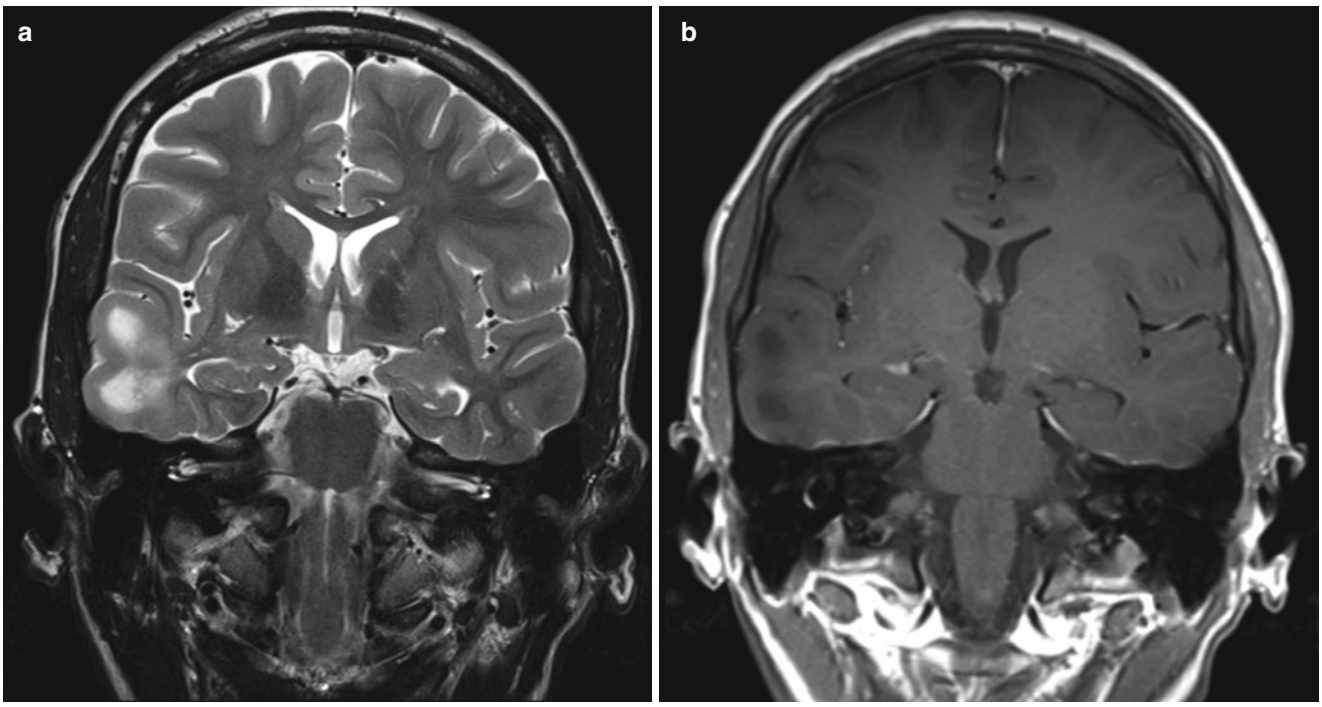

Fig 6 Three cases of focal cortical dysplasia type II. (**a**, **b**) patient 1; (**a**) coronal T2 with large subcortical area in the right temporal lobe with prolonged T2. The increased signal stretches in to the temporal horn of the right ventricle; (**b**) coronal T1 with gadolinium. The corresponding area has decreased signal on T1-weighted image. No enhancement. (**c**, **d**) patient 2; (**c**) axial T1 IR with very subtle signal changes at the bottom of a sulcus lateral in the frontal lobe; (**d**) coronal T2/FLAIR shows increased signal in the same area with a faint band stretching toward the lateral ventricle. (**e**) patient 3, boy, 3 months old, axial T1 IR shows a region with thickened cortex in the right frontal lobe. Notice the premature myelination of the white matter tracts involved in the seizures

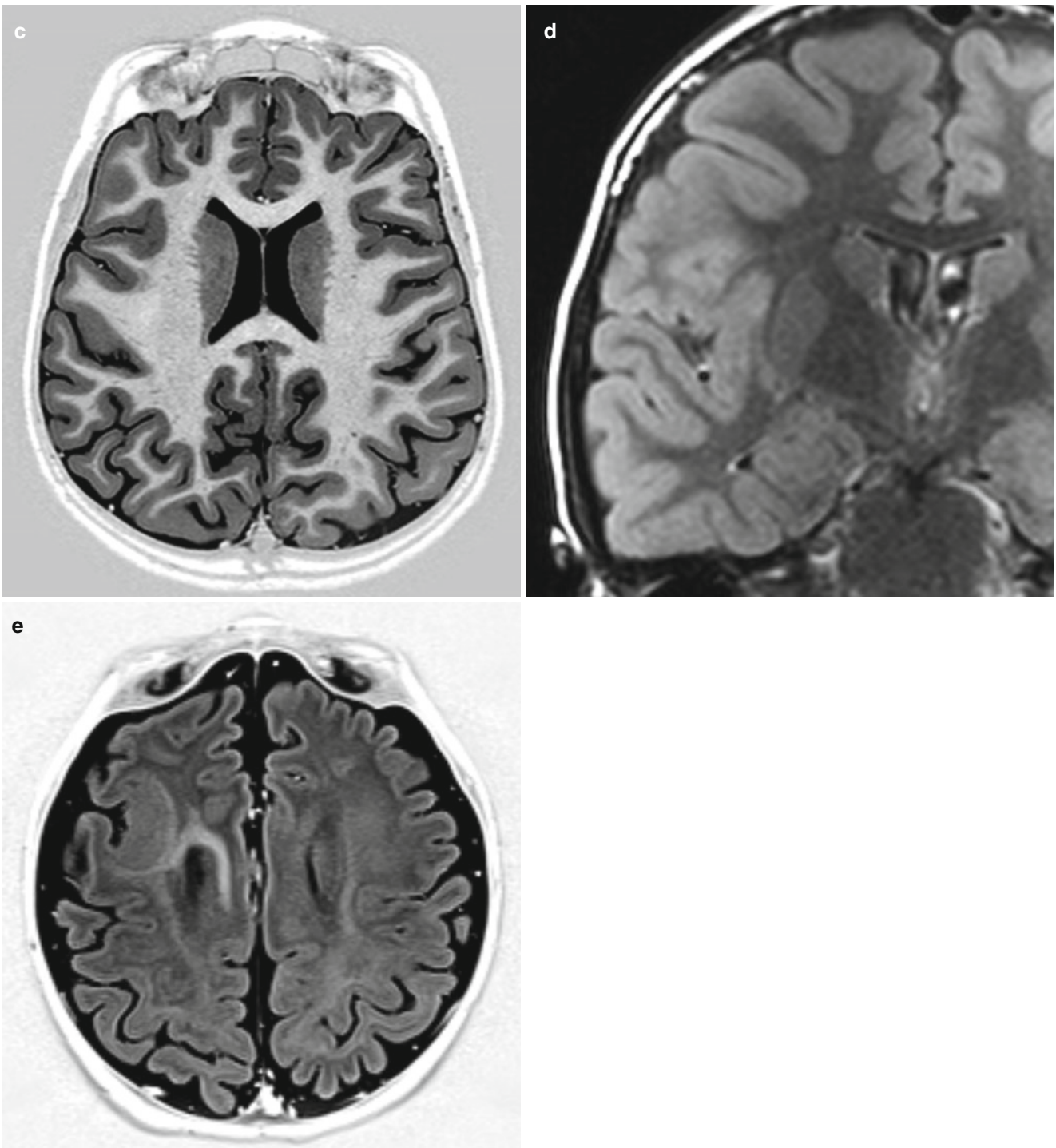

Fig. 6 (continued)

The third type of heterotopia is called perventricular nodular heterotopia or subependymal heterotopia. On imaging, an exophytic smooth ovoid mass in the residual germinal matrix, i.e., along the ventricle, is seen (Fig. 9). Again you may have associated anomalies including Chiari malformations, cephaloceles, corpus callosum agenesis, or a Dandy-Walker syndrome. In contrast to the other malformations of abnormal migration, the periventricular nodular heterotopia may exhibit quite mild symptoms with normal development and late onset of seizures. If the periventricular heterotopia completely lines the walls of both ventricles, a familiar form has to be considered, and genetic counseling may be indicated.

Malformations related to abnormal cortical organization encompass polymicrogyria, schizencephaly, and FCD type

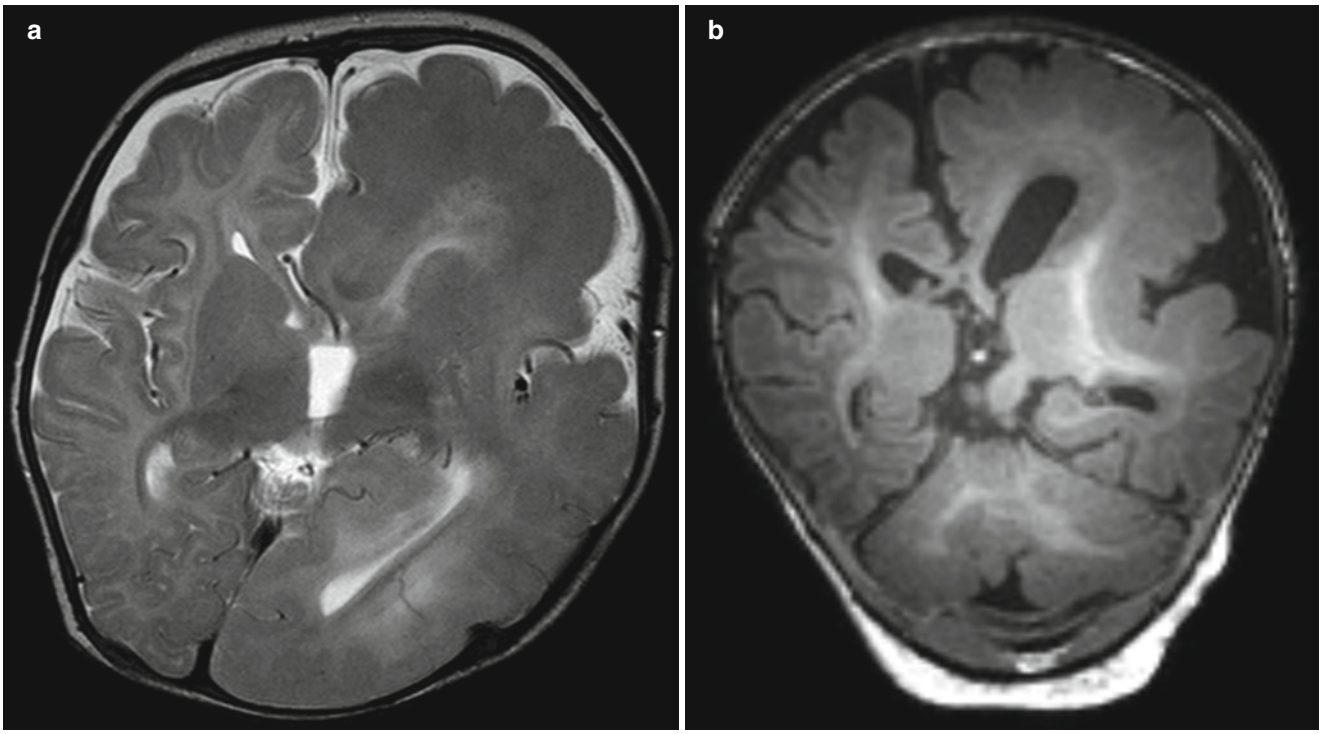

Fig. 7 (**a**, **b**) Boy, 6 months old. Hemimegalencephaly. (**a**) axial T2; (**b**) coronal T1. The left hemisphere is enlarged with broad gyri and shallow sulci. The ipsilateral ventricle is enlarged with an abnormal shape of the frontal horn. Indistinct gray-white matter junction

I (non-balloon cell). In polymicrogyria, neurons reach the cortex but distribute abnormally; thus, multiple small gyri are formed (Fig. 10). Polymicrogyria is most commonly found around the posterior sylvian fissures; when bilaterally present in the perisylvian region, patients present with pseudobulbar palsy.

In open-lip schizencephaly, a cleft that is lined by gray matter reaches from the periphery to the ventricle, while in the closed-lip schizencephaly, gray matter is reaching from the periphery to the ventricle, and a dimple is seen in the ventricular wall. Schizencephaly can be multifocal and bilateral. The cortex lining the defect is polymicrogyric with ill-defined margins to the white matter. Finally, FCD type I (non-balloon cell) is a disorder of lamination. Imaging features are very subtle, and only mild focal blurring of the gray-white matter junction may be present. This type of dysplasia is often undetectable on MRI.

Epileptogenic Tumors

While virtually all tumors may cause epilepsy, there are certain tumors that have a very high propensity of eliciting medication refractory seizures. As most of these are benign and just by means of location (i.e., within the cortical white matter interface and with temporal lobe predilection) cause the seizures, these are often very good candidates for surgery. As a general discussion of all tumors is beyond the scope of this chapter, we will focus only on three tumors that are commonly associated with seizures: the ganglioglioma, the DNETs, and the tuber cinereum hamartomas.

Gangliogliomas are cortically based, partly cystic tumors that may calcify and that harbor an enhancing nodule (Fig. 11). Gangliogliomas occur in young adults and older children; when present under the age of ten, they are often larger with more cystic components. They are mainly located in the temporal lobes but can also occur in parietal and frontal lobes. Cortical dysplasias (coined type III) can be associated with a ganglioglioma. Top differential diagnoses for gangliogliomas are DNETs, pilocytic astrocytomas, pleomorphic xanthoastrocytomas, gliomas, and neurocysticercosis.

DNETs are well-demarcated, bubbly, intracortical masses that also are most common in the temporal, parietal, and frontal lobes (Fig. 12). They may calcify, but enhancement is very rare and if present should lead to more intensive follow-up, as the enhancing portion of a DNET may recur following surgery. Top differential diagnoses for DNETs are cortical dysplasia, ganglioglioma, pilocytic astrocytoma, glioma, neuroepithelial cysts, and dilated VR spaces.

Tuber cinereum hamartoma presents with the combination of gelastic seizures and precocious puberty. They are located at the floor of the third ventricle (i.e., the tuber cinereum) and do not enhance and are isointense to the cortex

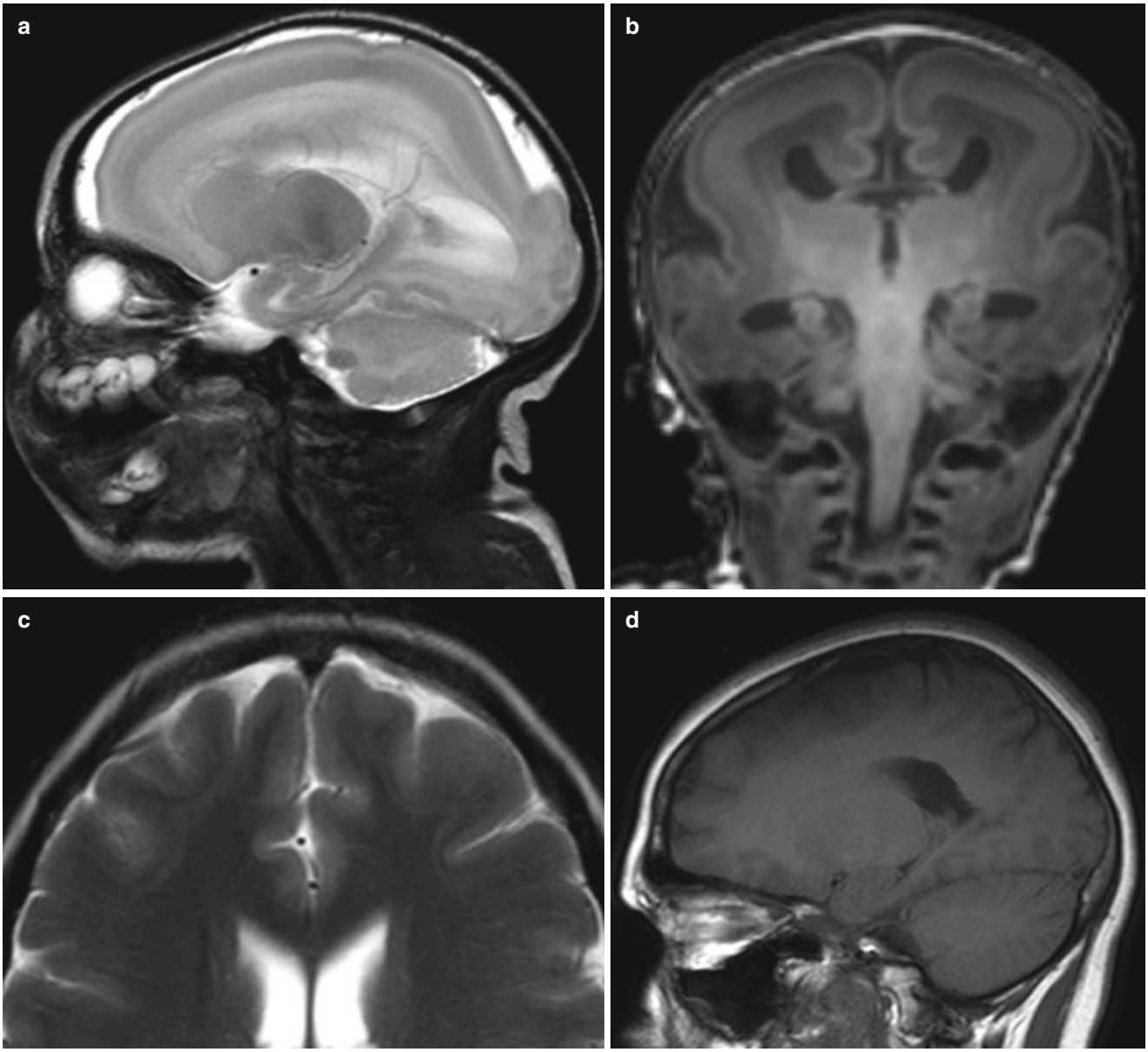

Fig. 8 (**a**, **b**) X-linked lissencephaly, boy, 2 weeks old. (**a**) sagittal T2; (**b**) coronal T1. Lissencephaly with agyria more pronounced in the anterior part of the brain. In addition callosal hypogenesis. (**c**, **d**) the mother of the boy in (**a**) and (**b**), female carrier. **c**: axial T2 (detail); (**d**) sagittal T1; Subtle subcortical band heterotopia in both frontal lobes

(Fig. 13). They are nonneoplastic tumors with disorganized collection of neurons and glia.

Miscellaneous: Vascular Malformations/ Trauma/Infection/Phakomatoses

Similar to the previous paragraph, it is beyond the scope to in detail describe imaging features of vascular malformations, infections, or trauma that can go along with seizures, and most of the entities are described in other chapters of this syllabus. We therefore only want to highlight few epilepsy-relevant facts and features of these miscellaneous conditions.

Brain AVMs can cause seizures due to previous hemorrhage and scarring, hemosiderin deposits (especially when close to the cortex), or gliosis. AVMs in the temporal lobe have a higher likelihood of producing seizure due to interference of the normal blood supply and drainage of potentially epileptogenic structures such as the hippocampus.

While cavernomas that are deeply located in the white matter rarely cause seizures, those that are cortically located and have hemosiderin staining reaching the cortex, and in particular the mesial temporal lobe structures, are very often associated

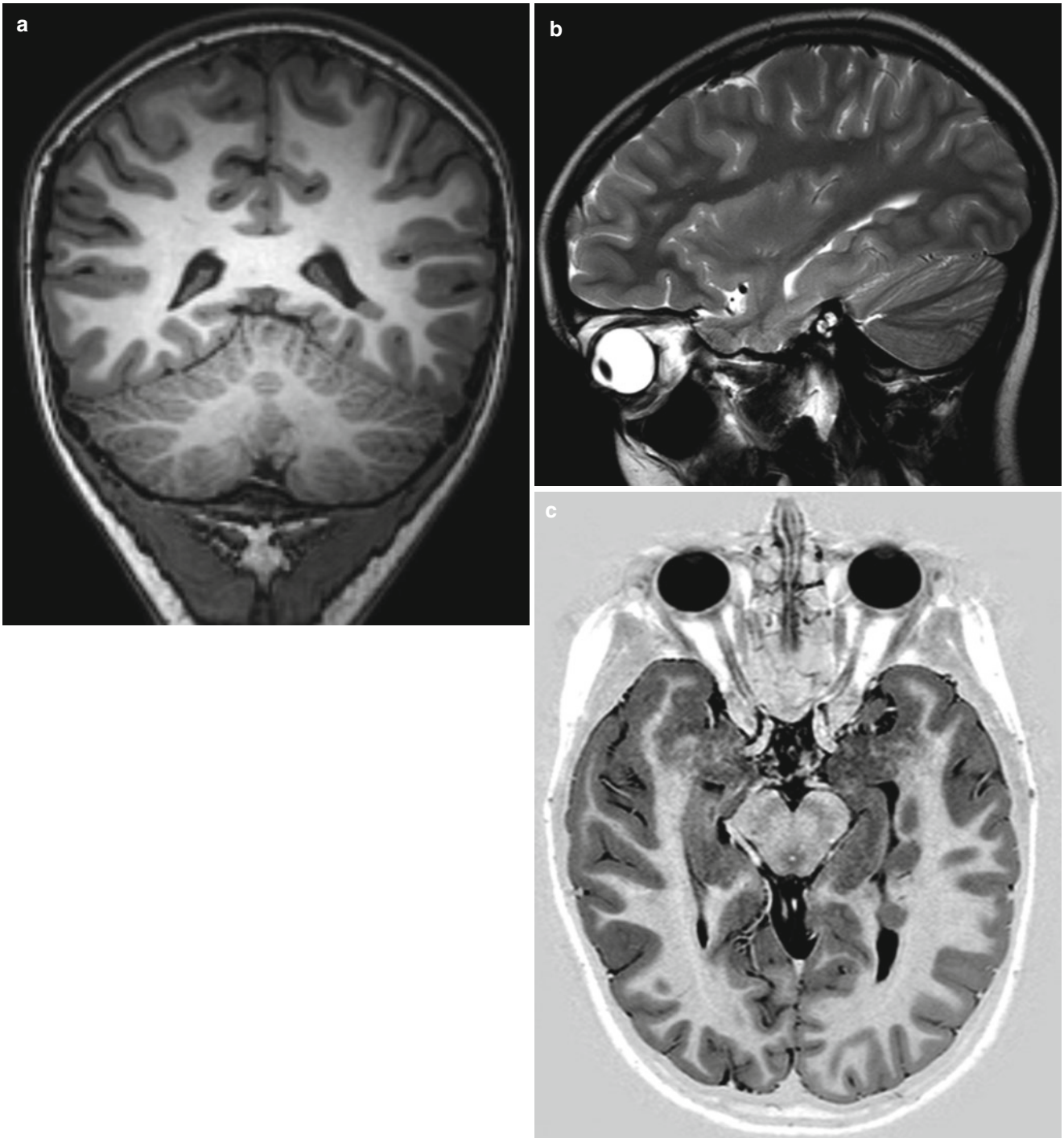

Fig. 9 (**a**–**c**) Periventricular nodular heterotopia: (**a**) coronal T1; (**b**) sagittal T2; (**c**) axial T1 IR. Well-delineated smooth ovoid masses lateral to the trigone and temporal horn of the left ventricle. Note that the signal is identical to that of cortex in all sequences

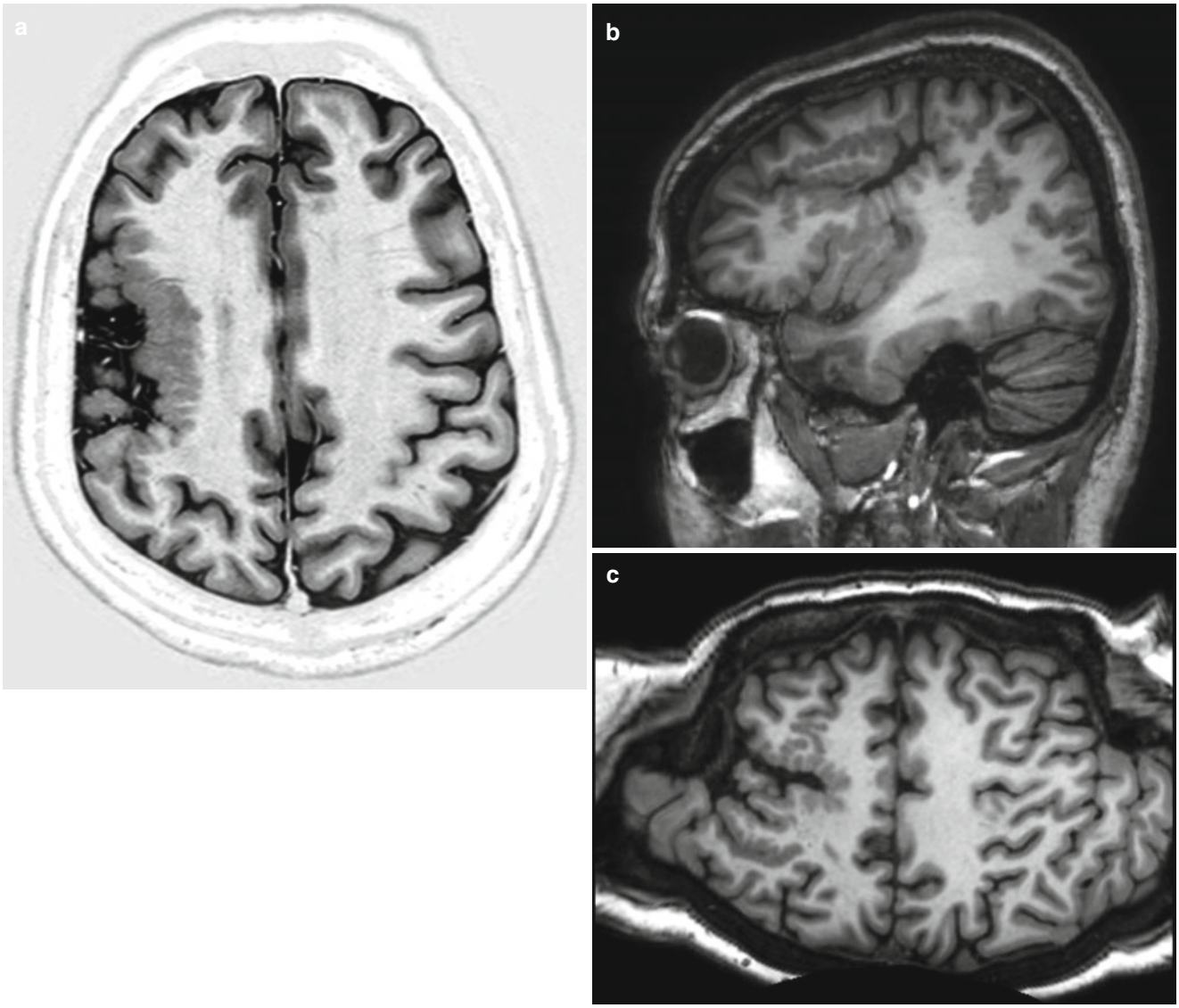

Fig. 10 (**a**–**c**) Two patients with polymicrogyria. (**a**) axial T1 IR; (**b**) sagittal T1. Patient 1. Abnormal gyration in the right hemisphere with a large region with polymicrogyria. (**c**) Patient 2, "pancake view" from a 3D T1 sequence gives a very good overview of the migration anomalies in the right hemisphere. It also increases the chance to detect subtle changes – see small area with polymicrogyria in the *left* hemisphere!

with seizures as the hemosiderin stain is believed to have a strong irritative potential for neurons. They are best visualized on T2 gradient echo or SWI sequences where they demonstrate with the classical blooming artifact (Fig. 14). Cavernomas may be multiple, and they can be associated with developmental venous anomalies (DVA). New intracavernomatous thrombosis or hemorrhage may lead to change in seizure frequency.

Patients with previous trauma can experience posttraumatic seizure disorder, especially after having sustained contusional hemorrhages of their temporal lobes as gliosis and

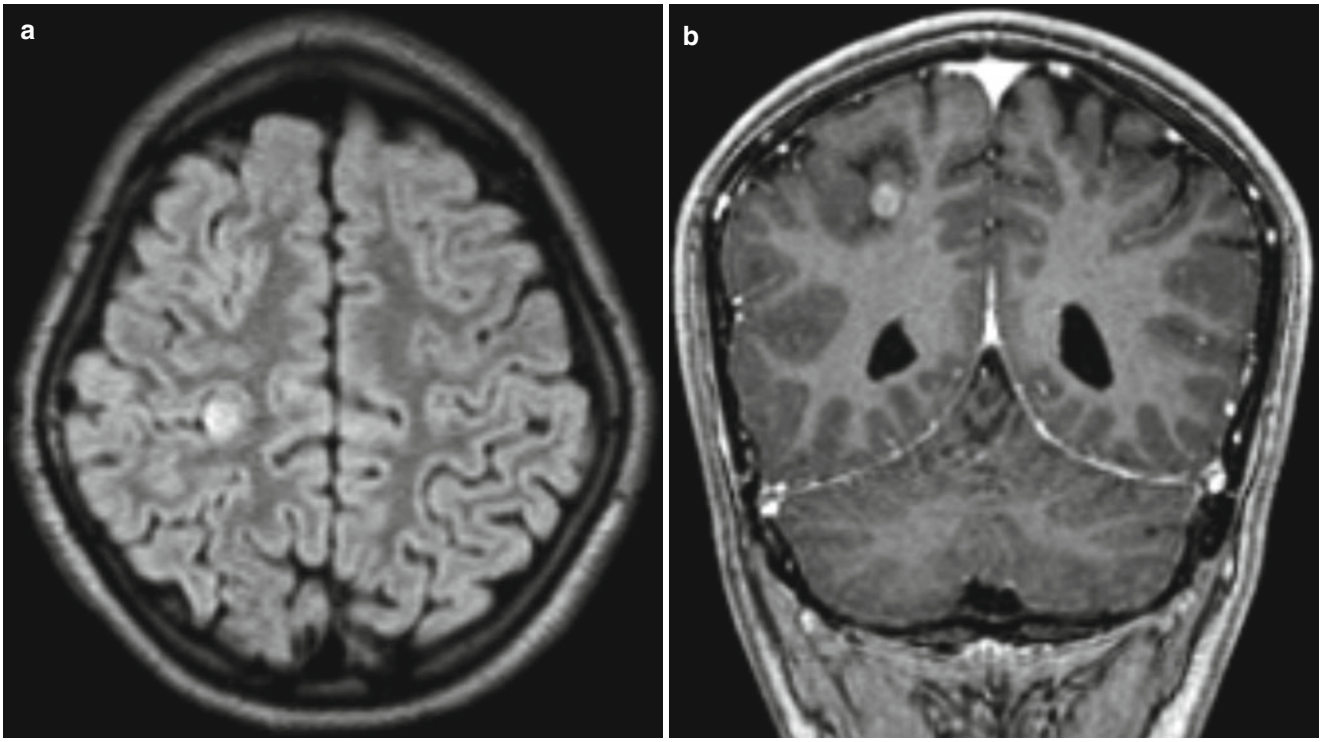

Fig. 11 (**a**, **b**) Ganglioglioma close to the right postcentral sulcus. (**a**) axial T2/FLAIR with a small, cortical/subcortical, nodular high-signal area in the right parietal lobe close to the postcentral sulcus; (**b**) coronal T1 with gadolinium shows contrast enhancement in the nodulus

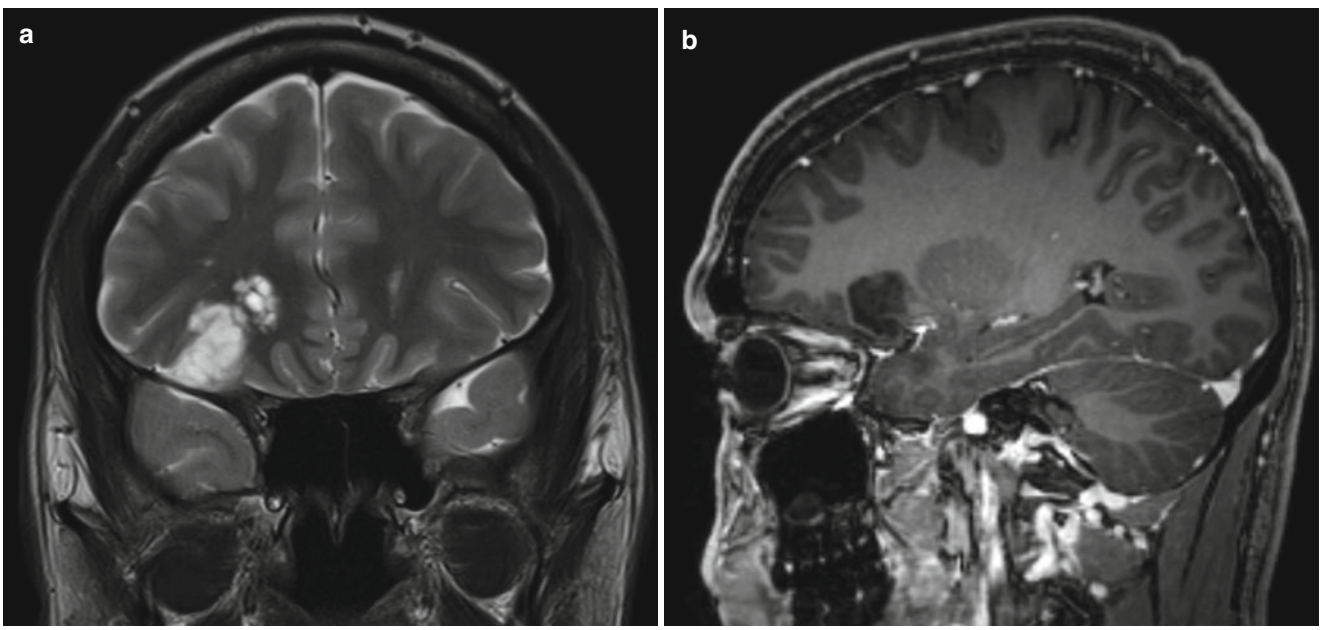

Fig. 12 Two patients with DNET. (**a**, **b**) patient 1. (**a**) coronal T2; (**b**) sagittal T1 with gadolinium; well-delineated cortical/subcortical bubbly mass in the right frontal lobe with prolonged T2 and no contrast enhancement typical of a DNET. (**c**, **d**) patient 2: (**c**) sagittal T1; (**d**) coronal T2/FLAIR. This DNET in the left parietal lobe is associated with a FCD type II. Notice the streak with signal changes which stretches toward the lateral ventricle

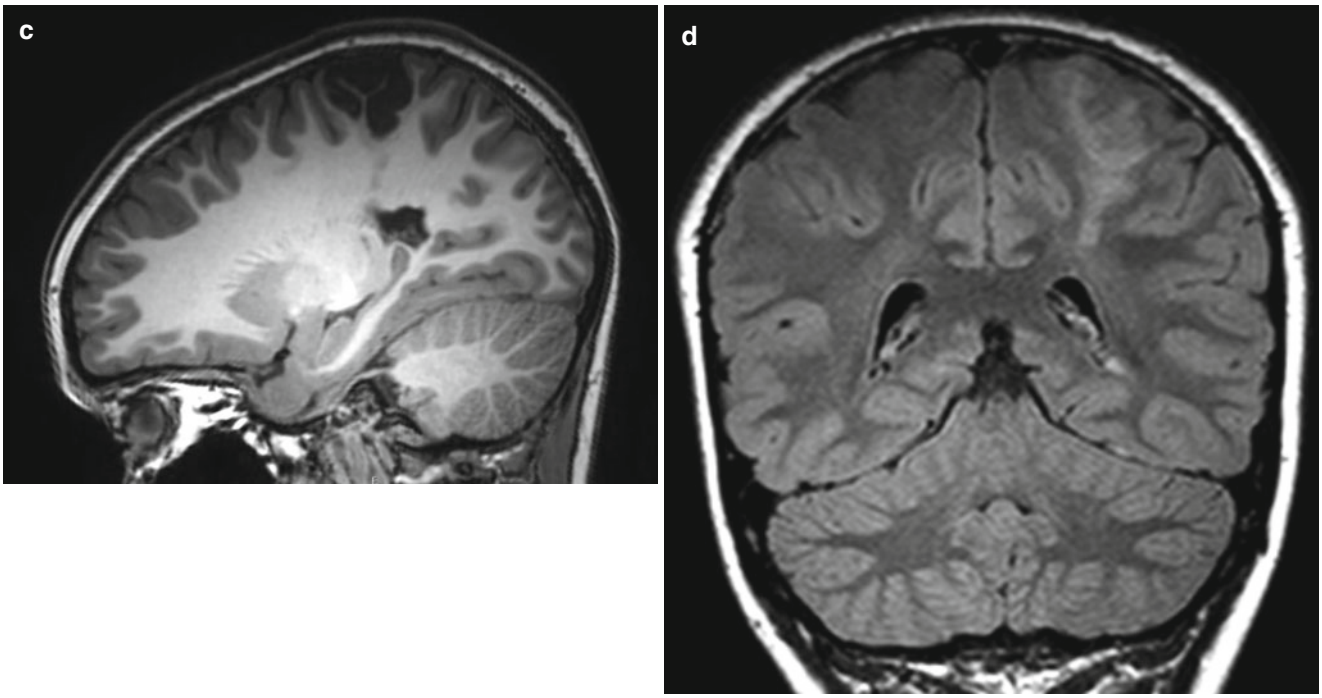

Fig. 12 (continued)

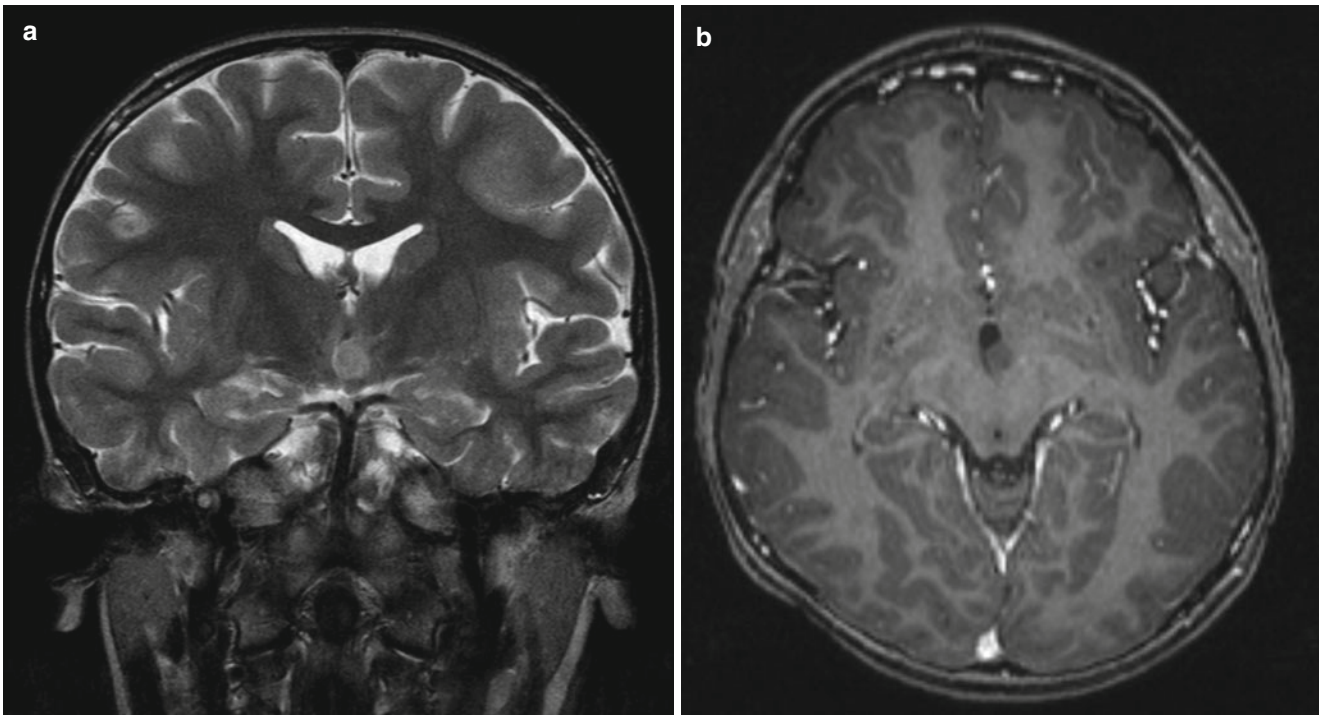

Fig 13 (**a**, **b**) Hypothalamic hamartoma. (**a**): Coronal T2 with a lobular mass close to the left wall of the third ventricle. (**b**): Axial T1 with gadolinium detects no contrast enhancement in the mass

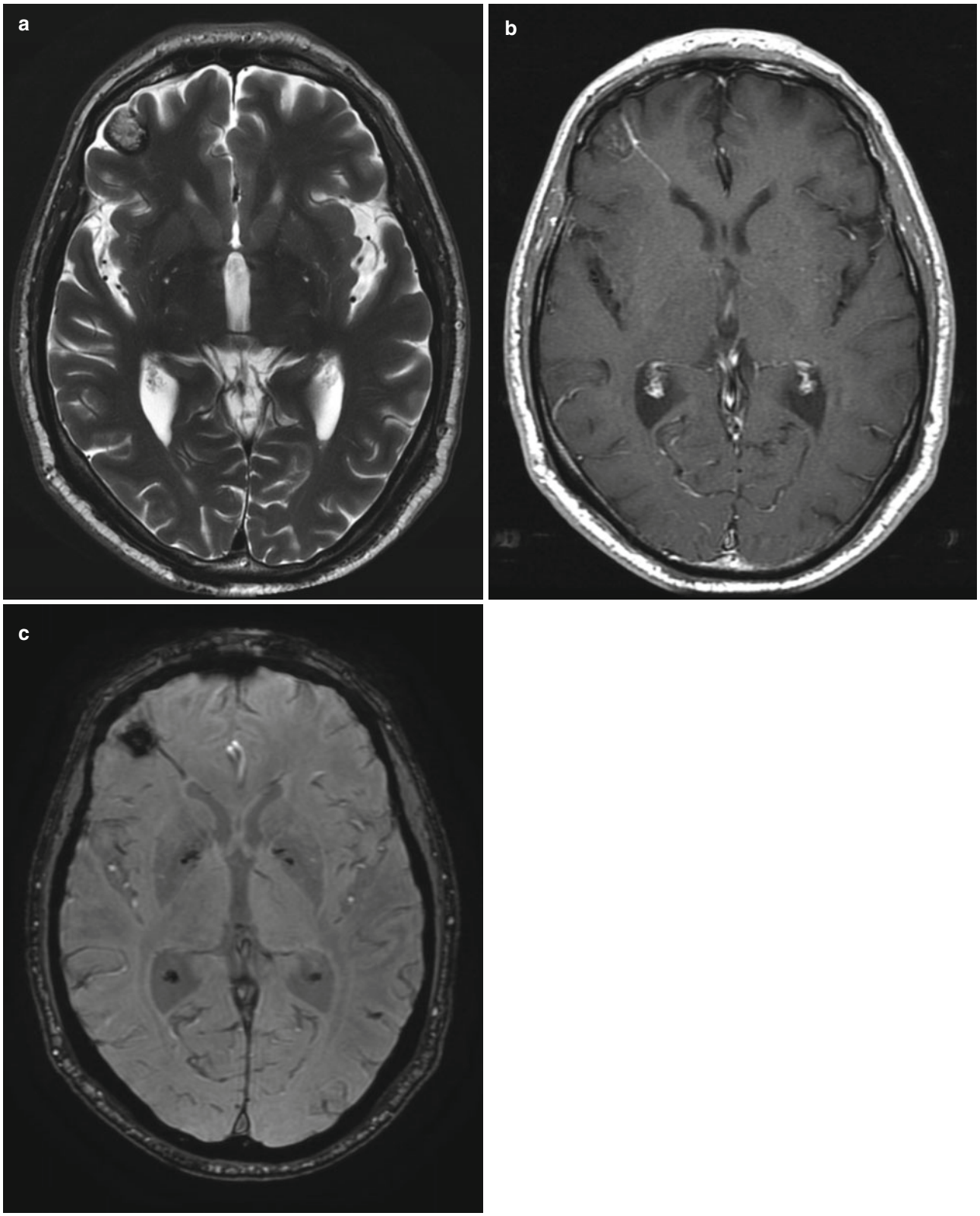

Fig. 14 (**a**–**c**) Cavernoma in the right frontal lobe with an associated DVA. (**a**): axial T2 shows the superficial lesion with heterogeneous signal; (**b**): axial T1 with gadolinium shows an associated vascular structure, a DVA; (**c**): axial SWAN sequence. This susceptibility sensitive sequence shows the classical blooming effect of the cavernoma

hemosiderin staining can cause irritation of the surrounding cortex.

Neonatal anoxic ischemia or hypoxemia can cause ulegyria – i.e., a scar/defect of the cerebral cortex that mainly involves the cortex in the depth of the sulcus – whereas the cortical crowns remain relatively unaffected. This peculiar pattern can be explained by the vascular supply of the gyri in the newborn that leads to a better perfusion of the apices of the gyri as compared to the depth of the sulci. There will be paucity of the white matter and, as the lesion occurred prior to complete myelination, a relatively mild gliosis. If the perinatal ischemia has only involved one hemisphere (perinatal stroke), a Dyke-Davidoff-Masson syndrome will ensue where stable hemiatrophy is present with hypertrophy of the skull and the sinuses, paucity of white matter, ventricular enlargement, and mild gliosis.

Virtually any infection (bacterial, fungal, parasitic) can produce epileptogenic lesions, and worldwide infections are the leading cause of epilepsy. A typical example is neurocysticercosis which in the late nodular phase is a very common cause of focal epilepsy in the developing world.

Antero-basal temporal lobe encephaloceles are lesions that are either related to a congenital defect of the bone or to previous trauma. Brain tissue can extend into the pterygopalatine fossa through the bony defect at the base of the greater sphenoid wing in the region of the foramen rotundum and pterygoid process. The herniated brain demonstrates high T2/FLAIR signal in the area believed to be the epileptogenic focus. Following resection of the abnormal brain tissue, seizure freedom can be obtained in a very large proportion of cases.

Rasmussen's encephalitis is a presumably autoimmune-mediated chronic inflammation of the brain that presents with progressive gliosis and volume loss. Patients experience seizures and a progressive hemiparesis.

The two phakomatoses commonly associated with seizures are tuberous sclerosis and Sturge-Weber syndrome. In tuberous sclerosis, multiple hamartomas are present within the cortical/subcortical region (Fig. 15). These are similar in histology to the FCD type II and are therefore believed to be epileptogenic. In addition, patients may develop subependymal calcification as well as a subependymal giant cell astrocytoma; however, the latter two lesions are not believed to be epileptogenic. In Sturge-Weber syndrome, the cortical calcification and the pial angiomatosis along the cortex are presumably related to the seizures. In addition, patients may present with choroid plexus hypertrophy and brain hemiatrophy as well as a facial port-wine stain (Fig. 16).

Conclusion

Neuroimaging in patients with refractory epilepsy will find abnormalities in as high as 85 % of cases and therefore plays a crucial role in the identification of epileptogenic lesions and their possible surgical removal. A dedicated epilepsy protocol is necessary to identify these lesions, and the MR should be interpreted in conjunction with EEG, neuropsychological testing, and clinical semiological data to increase the likelihood of identifying these often very subtle lesions.

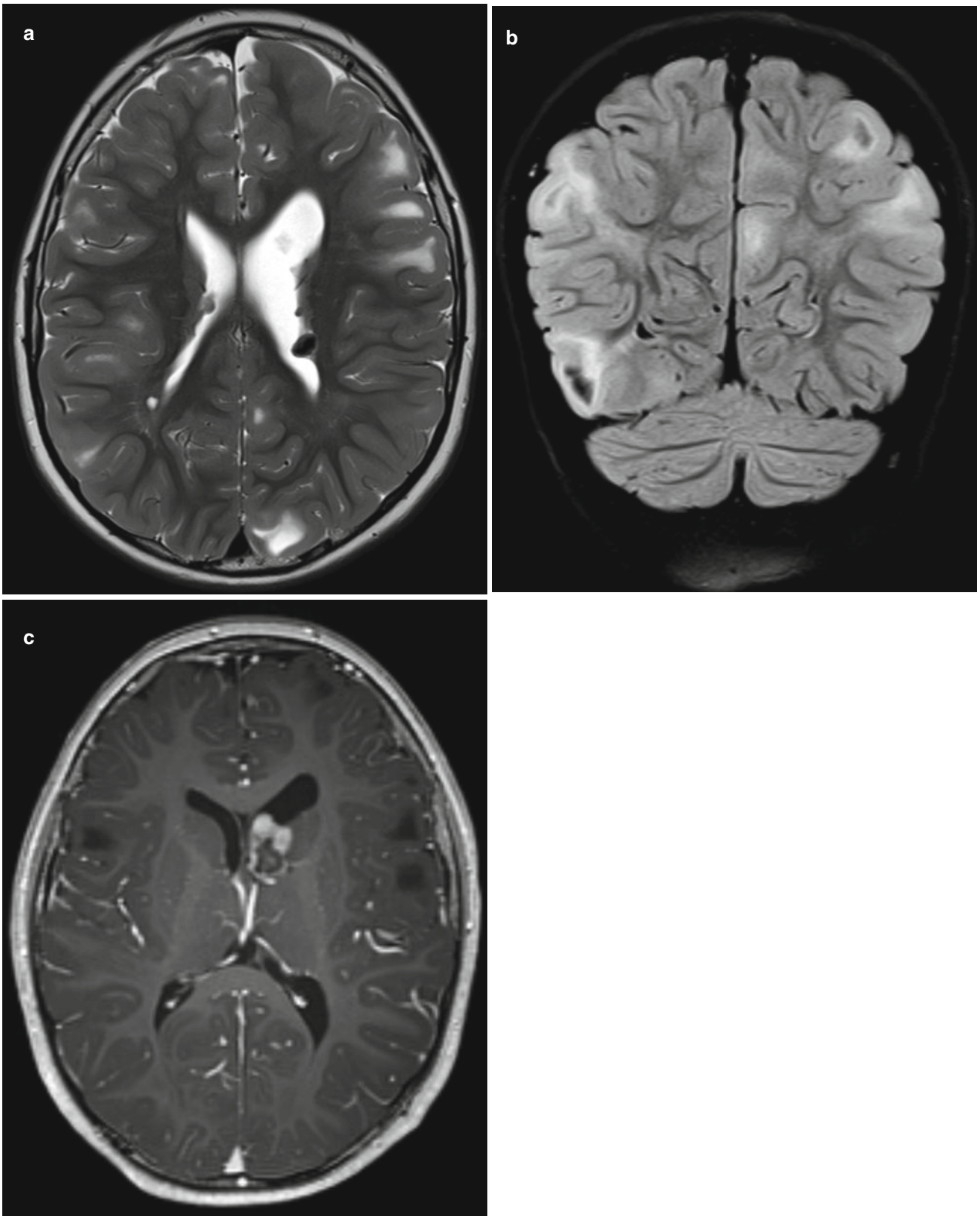

Fig. 15 (**a**–**c**) Tuberous sclerosis; (**a**) axial T2 and (**b**): coronal T2/FLAIR show subependymal hamartomas and widespread cortical and subcortical signal changes; (**c**) axial T1 with gadolinium with a large giant cell astrocytoma in a classical position, close to the foramen of Monro in the left lateral ventricle

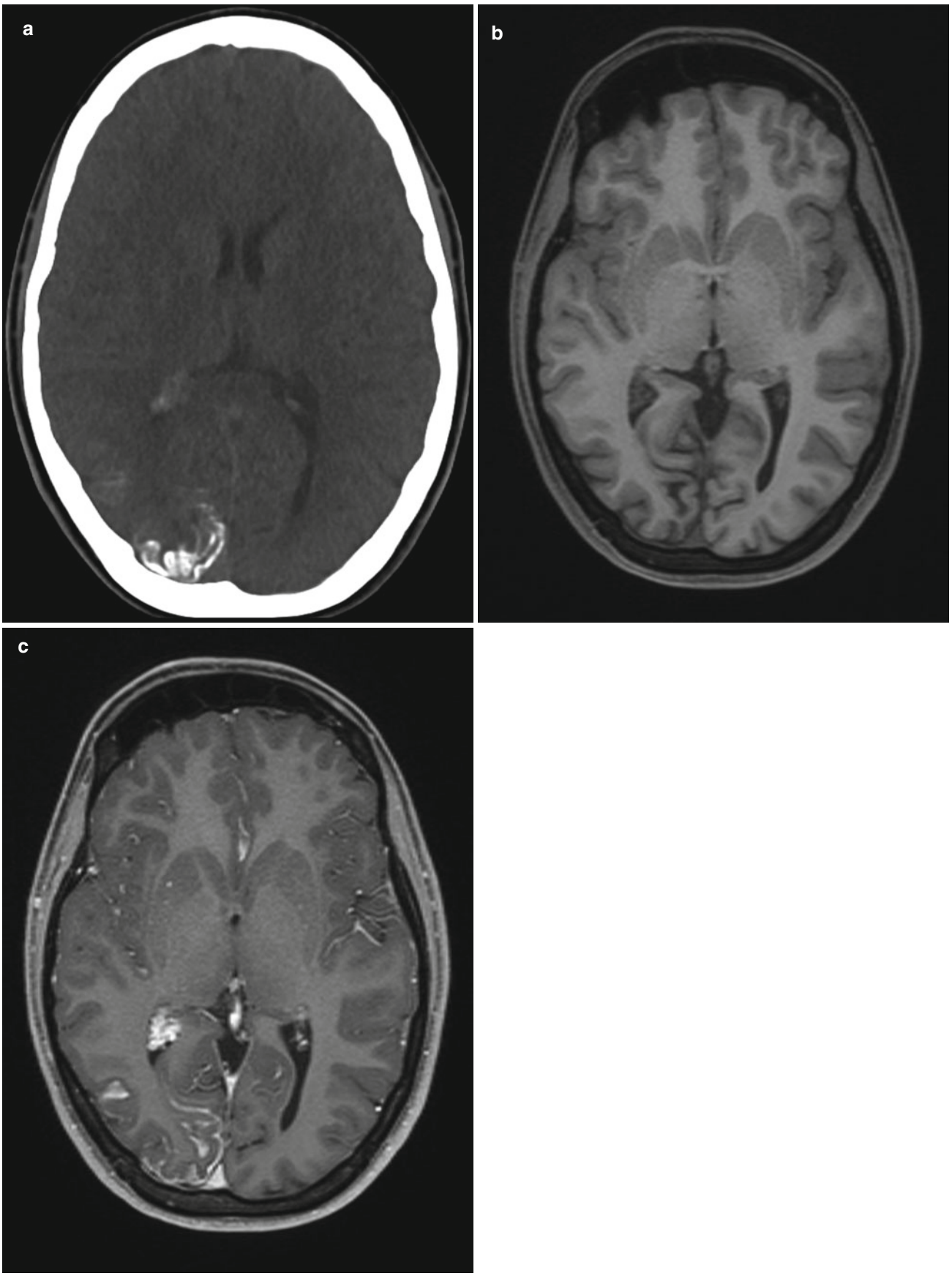

Fig. 16 (**a**–**c**) Sturge-Weber syndrome; (**a**) axial CT shows curvilinear cortical calcifications in the right occipital lobe; (**b**) axial T1 without and **c**: with gadolinium shows contrast enhancement caused by pial angiomatosis. Note also hypertrophy of the ipsilateral choroidal plexus, typical for this syndrome

References

1. Duncan JS (2010) Imaging in the surgical treatment of epilepsy. Nat Rev Neurol 6:537–550
2. von Oertzen J, Urbach H, Jungbluth S et al (2002) Standard magnetic resonance imaging is inadequate for patients with refractory focal epilepsy. J Neurol Neurosurg Psychiatry 73:643–647
3. Téllez-Zentenoa JF, Ronquilloa H, Moien-Afshari F et al (2010) Surgical outcomes in lesional and non-lesional epilepsy: a systematic review and meta-analysis. Epilepsy Res 89:310–318
4. Wellmer J, Quesada CM, Rothe L et al (2013) Proposal for a magnetic resonance imaging protocol for the detection of epileptogenic lesions at early outpatient stages. Epilepsia 54:1977–1987
5. Strandberg M, Larsson EM, Backman S et al (2008) Pre-surgical epilepsy evaluation using 3T MRI. Do surface coils provide additional information? Epileptic Disord 10:83–92
6. Winstona GP, Micallef C, Brian E, Kendell BE (2013) The value of repeat neuroimaging for epilepsy at a tertiary referral centre: 16 years of experience. Epilepsy Res 105:349–355
7. Balchandani P, Naidich TP (2015) Ultra-high-field MR neuroimaging. Am J Neuroradiol 36:1204–1215
8. De Ciantis A, Barkovich AJ, Cosottini M et al (2015) Ultra-high-field MR imaging in polymicrogyria and epilepsy. Am J Neuroradiol 36:309–316
9. Breyer T, Wanke I, Maderwald S et al (2010) Imaging of patients with hippocampal sclerosis at 7 tesla: initial results. Acad Radiol 17:421–426
10. Neel Madan N, Grant PE (2009) New directions in clinical imaging of cortical dysplasias. Epilepsia 50:9–18
11. Bauer PR, Reitsma JB, Bernard M, Houweling BM et al (2014) Can fMRI safely replace the Wada test for preoperative assessment of language lateralisation? A meta-analysis and systematic review. J Neurol Neurosurg Psychiatry 85:581–588
12. Piper RJ, Yoong MM, Kandasamy J et al (2014) Application of diffusion tensor imaging and tractography of the optic radiation in anterior temporal lobe resection for epilepsy: a systematic review. Clin Neurol Neurosurg 124:59–65
13. Desai A, Bekelis K, Thadani VM et al (2013) Interictal PET and ictal subtraction SPECT: sensitivity in the detection of seizure foci in patients with medically intractable epilepsy. Epilepsia 54:341–350
14. Barkovich AJ, Guerrini R, Kuzniecky RI et al (2012) A developmental and genetic classification for malformations of cortical development: update. Brain 135:1348–1369

Suggested Reading

Gaitanis JN, Donahue J (2013) Focal cortical dysplasia. Pediatr Neurol 49:79–87

Guerrini R, Duchowny M, Jayakar P et al (2015) Diagnostic methods and treatment options for focal cortical dysplasia. Epilepsia 56:1669–1686

Pohlmann-Eden B, Crocker CE, Matthias H, Schmidt MH (2013) A conceptual framework for the use of neuroimaging to study and predict pharmacoresistance in epilepsy. Epilepsia 54:75–79

Ryvlin P, Cross JH, Rheims S (2014) Epilepsy surgery in children and adults. Lancet Neurol 13:1114–1126

Vattoth S, Manzil FFP, Singhal A et al (2014) State of the art epilepsy imaging an update. Clin Nucl Med 39:511–526

Cerebral Infections

David J. Mikulis and Majda M. Thurnher

Introduction

The broad categories of infectious diseases that affect the central nervous system (CNS) continue to present diagnostic challenges. Although imaging patterns of disease are well established, overlap between categories can occur. For example, the differentiation of cysticercosis, a parasitic infection from a tuberculous abscess, a bacterial infection, can be difficult. Additional challenges are posed by the increasing probability of encountering non-endemic pathogens secondary to the "globalization" of infections brought on by the expansion of international travel, transportation, and immigration. Additionally, increasing numbers of patients are undergoing treatments and therapies that compromise the immune system, leading to altered host responses that no longer express the expected patterns of tissue injury.

Imaging plays a central role in the detection and differentiation of CNS infections with conventional MRI serving as the modality of choice by virtue of its superior tissue contrast. This enables a more selective differential diagnosis, accurate "staging" of the infection, and can provide an objective measure of treatment response. Functional/physiological MRI methods can also add useful information increasing diagnostic confidence. Perhaps the best example of this is the detection of restricted water diffusion in a ring-enhancing lesion that must then be considered to be an abscess until proven otherwise. Proton magnetic resonance spectroscopy (MRS) can then be applied for confirmation if conducted prior to antibiotic administration.

D.J. Mikulis
Department Medical Imaging, The University Health Network, The Toronto Western Hospital, The University of Toronto, Toronto, ON, Canada
e-mail: mikulis@mac.com

M.M. Thurnher (✉)
Department of Biomedical Imaging and Image-Guided Therapy, University Hospital Vienna, Medical University Vienna, Vienna, Austria
e-mail: Majda.thurnher@meduniwien.ac.at

In view of these considerations, the information provided here will focus on each of the broad categories of infectious diseases that affect the brain and its coverings. Emphasis will be placed on pathophysiology since the evolving response of the host to the pathogen will be reflected in the imaging findings providing clues for establishing an accurate diagnosis. It is important to understand how these infections express themselves in the normal host before attempting to assess similar infections in the immunocompromised host since the host response can and will be altered. Finally, certain atypical infectious agents will be mentioned when appropriate to highlight the need for awareness of the spectrum of pathogens that may be encountered in modern practice.

Bacterial Infections

Pyogenic Meningitis

Although viruses are the most common cause of meningitis including enteroviruses, varicella, herpes, coxsackievirus, EBV, CMV, mumps, etc., the pyogenic infections are most feared. Mortality can be as high as 30 % (pneumococcus) even with antibiotic treatment but is typically on the order of 15 % [1, 2]. The most common bacterial causes of meningitis are *Streptococcus pneumoniae*, *Neisseria meningitidis*, and *Haemophilus influenzae* type b. These bacteria can colonize the nasopharynx, and if the local vasculature is invaded, dissemination to the CNS vasculature can occur. Access to the subarachnoid space is achieved through interaction and penetration of the endothelium. The choroid plexus vasculature lacks blood-brain barrier endothelium and is therefore the most likely point of entry. CSF is an excellent medium for bacterial growth due to low levels of antibodies, complement, and phagocytic cells. Significant multiplication of bacteria occurs before there is an immune response [3].

The diagnosis of bacterial meningitis is almost always based on clinical presentation that consists of high fever, signs of meningismus, and a rapidly decreasing level of

J. Hodler et al. (eds.), *Diseases of the Brain, Head and Neck, Spine 2016–2019: Diagnostic Imaging*, DOI 10.1007/978-3-319-30081-8_15

consciousness. Imaging is usually performed to assess the status of the ventricles prior to lumbar puncture since hydrocephalus is a relative contraindication to this procedure. CT can show evidence of increased attenuation in the basal cisterns and sulci due to high concentrations of inflammatory cells. MRI will also show increased signal in these areas due to an elevation in CSF protein becoming abnormal earlier in the infection compared to CT. This must not be confused with subarachnoid hemorrhage since CT and MR can show increased attenuation in the basal cisterns [4, 5]. Vessels in the subarachnoid space can become directly involved in the inflammatory process leading to necrotizing panarteritis and septic thrombophlebitis causing ischemic injury to the brain. In addition, the inflammatory process can extend directly into the brain resulting in encephalitis. Hydrocephalus occurs in most patients secondary to impaired CSF absorption resulting in increased intracranial pressure that further compromises blood flow. The presence and extent of ischemic manifestations of the meningeal infection are well demonstrated with diffusion imaging. However, direct infection of the brain parenchyma resulting in cerebritis has also been associated with restricted water diffusion as well [6].

Although MRI is not generally performed for the diagnosis of acute meningitis, it is useful in assessing the complications that can occur secondary to the meningeal infection including subdural effusions and empyemas, hydrocephalus, ventriculitis, septic thrombophlebitis, infarcts, and labyrinthitis. In pediatric cases, 44 % of survivors will develop sensorineural hearing loss with more than a third (38 %) having severe or profound deficits [7]. In fact, labyrinthine gadolinium enhancement on MRI performed at presentation is 87 % sensitive and 100 % specific for permanent hearing loss [8].

Imaging can play a significant role in the detection and management of less fulminant forms of meningitis. Tuberculous (TB) meningitis, for example, can initially be quite indolent in patients presenting with headache and cranial neuropathies. There is a predilection for involvement of the basal cisterns. Untreated, the disease can progress rather suddenly with high mortality. Lumbar puncture may show no growth of the bacillus, but there is usually an elevation in the white cell count and protein level. Pre-contrast MRI can be normal although FLAIR images may show increased signal in the sulci when CSF protein is sufficiently elevated [9]. Gadolinium-enhanced acquisitions can show striking enhancement of the leptomeninges. Tuberculous pachymeningeal involvement can also occur [10].

Patients with immune deficiencies are also susceptible to TB meningitis, but in addition, fungal, viral, and treponemal etiologies must be considered including cryptococcal infection and neurosyphilis. Although these other agents can be associated with leptomeningeal enhancement [11, 12], TB typically produces a very intense diffuse and/or nodular pattern of enhancement in the basal cisterns. This pattern, however, can be seen with carcinomatous meningitis as well. Meningeal enhancement is uncommon in viral meningitis with MRI appearing normal unless an encephalitic component develops with signal changes in the parenchyma.

Cerebral Abscess

In the pre-antibiotic era, brain abscesses were most commonly caused by direct extension from infected paranasal sinuses. Now, the most common source is blood-borne bacterial seeding originating from infections elsewhere in the body.

Four stages of abscess formation have been described [13]:

- Stage 1 – Early cerebritis (Days 1–3)
  - Perivascular infiltration of inflammatory cells including neutrophils, lymphocytes, and plasma cells
  - Reactive astrocytes
  - Visible bacteria
  - Developing necrotic center
  - Surrounding edema
  - *Partial ringlike enhancement on CT with surrounding edema*
- Stage 2 – Late cerebritis (Days 4–9)
  - Well-formed necrotic center containing tissue debris and inflammatory cells
  - Macrophages, fibroblasts, and reticulin deposition seen at periphery of necrotic center
  - Maximum extent of cerebritis and necrotic core
  - *Thick ring enhancement on CT with surrounding edema*
- Stage 3 – Early capsule formation (Days 10–13)
  - Increased numbers of fibroblasts and macrophages
  - Mature collagen capsule (less well developed on ventricular side)
  - Decreased surrounding cerebritis but maximum degree of neovascularity
  - Decreasing edema
  - *Thin ring enhancement on CT with surrounding edema*
- Stage 4 – Late capsule formation (Days 14 and later)
  - Increased fibroblasts
  - High-density collagen in capsule
  - Decreased cerebritis and edema
  - Marked gliosis in adjacent brain
  - *Strong contrast enhancement in thin smooth ring with little surrounding edema*

The abscess initially begins as a region of cerebral inflammation or cerebritis, which progresses to form a pus-filled cavity with a fibroglial capsule. The typical abscess will have a relatively thin, smooth wall showing intense contrast enhancement on CT or MRI. Edema in the adjacent white

matter is common. The abscess wall can appear bright on T1-weighted images. This is thought to be the result of T1 shortening related to reactive oxygen species derived from an oxidative burst in neutrophils as well as accumulation of collagen fibers [14, 15]. The critical imaging issue, however, concerns similarities between brain abscesses and neoplastic diseases especially metastases. Both commonly show ring enhancement following contrast administration. How then can they be distinguished? In general, the enhancing ring of an abscess is thin and quite smooth as opposed to a neoplasm where some irregularity or nodularity is present. The deepest portion of the abscess wall that "points" to the ventricular system is typically thinner than other portions of the rim. However, these features are not reliable as metastases can have thin smooth-enhancing rims, and abscesses can often have irregular margins.

Increases in diagnostic specificity can be gained through application of diffusion methods and MRS. Abscess cavities on MR diffusion imaging typically show restricted water movement similar to that seen with acute ischemic stroke. Although the reason for this restriction has not been established, it is tempting to assume that it is related to dead or dying white cells "absorbing" any available extracellular water analogous to the proposed mechanism for ischemic neurons and glia in ischemic stroke. Recent work has shown that the degree of restricted diffusion is linearly correlated with the number of "viable" inflammatory cells in the abscess with viability determined by "intact cell membranes and nuclei" [16, 17]. Clearly cell density plays a role as it does in certain metastases such as small cell lung cancer. Even mucin-producing metastases usually from the gastrointestinal tract can show restricted water diffusion as increasing protein concentrations will reduce water mobility. Interestingly, increasing fractional anisotropy from diffusion tensor acquisitions directly correlates with an increase in inflammatory cells in the abscess [18, 19]. Effective treatment of the abscess is also associated with a decrease in FA and increase in apparent diffusion coefficient (ADC) [15]. Recently, susceptibility-weighted MR imaging (SWI) has been suggested as a useful discriminator between pyogenic abscess and other ring-enhancing lesions by virtue of the "dual rim" sign consisting of "two concentric rims surrounding the central cavity at lesion margins, with the outer one being hypointense and the inner one hyperintense compared with the cavity content on SWI" seen with bacterial abscesses [20].

Perhaps the most important contribution that MRS has made in the diagnosis of cerebral diseases is the ability to detect bacteria by their metabolic signatures. Certain byproducts of bacterial metabolism are not seen in mammals in spectroscopically significant concentrations (millimolar range). Bacterial fermentation leads to the production of lactate, acetate, and succinate (an important metabolite in anaerobic abscesses). Proton MRS is capable of detecting the distinct spectral peaks of each of these substances. However, pretreatment with antibiotics prior to MRS may reduce these metabolites to undetectable levels. Amino acids, produced by proteases released by white cells as part of the inflammatory response, can also be detected. This is relevant since large amounts of free amino acids are not seen in the normal brain or in other disease processes. They can be present even if antibiotics have been administered since the proteolytic enzymes generated by the inflammatory response remain. Table 1 lists these peaks and their resonant frequencies in parts per million (ppm).

By noting the presence or absence of these metabolites, it may even be possible to determine the class of organism involved in the infection [21]:

A. Lactate, amino acids, alanine, and acetate, with or without succinate at 2.4 indicate obligate anaerobes (fermentation only and killed by atmospheric oxygen) and/or a mixture of obligate and facultative anaerobes (fermentation but can switch to respiration)
B. Lactate and amino acids with/without lipids representing mostly obligate aerobes or facultative anaerobes
C. Lactate alone (usually streptococcus)

The expected utility of MRS should therefore be quite high in screening patients suspected of having brain abscesses. However, in modern practice, most patients are under treatment with antibiotics by the time MRI is performed, undermining the ability to detect bacterial metabolites diminishing the value of MRS in this setting. However, as opposed to diagnosis, it has been suggested that MRS can monitor therapeutic efficacy. Declines in acetate and pyruvate have been reported 1 week following antibiotic treatment correlating with positive responses to treatment [22].

Tuberculoma/tuberculous abscess – Parenchymal infection of the brain by mycobacterium can take the form of the classic bacterial abscess but can also form a tuberculoma. Tuberculous abscesses contain more lymphocytes and virtually no proteolytic enzymes compared to the conventional bacterial abscess [23]. The tuberculoma by definition is a parenchymal infection in which granulomas are found, whereas a tuberculous abscess contains mostly pus. Both may show ring enhancement. Tuberculomas usually have decreased T2 signal but can be variable and even hyperintense with variable ADC as well. Somewhat counter intuitively, the lower the T2 signal in a tuberculoma, the higher is the ADC [24]. The TB abscess is bright on T2 with a hypointense wall and restricted diffusion typical for a bacterial abscess. Both tuberculous abscesses and tuberculomas can be surrounded by T2 bright edema in the adjacent brain. Tuberculous abscesses are very uncommon usually appearing in immunocompromised hosts. MRS has shown that there are differences between bacterial and mycobacterial brain abscesses [23]. Although, both can show elevations in

Table 1 The four stages of abscess evolution

Metabolite	Resonant frequency (ppm)
Broad amino acid peak (valine, leucine, and isoleucine)[a]	0.9
Alanine[b]	1.4 and 1.6 doublet
Succinate	2.4
Acetate	1.9
Pyruvate	2.4

[a]Shows phase reversal (inverted peak) at TE = 135
[b]Shows phase reversal at TE = 135; peak at 1.4 overlaps with peak of lactate doublet; alanine can be seen in meningiomas and demyelination

lipid and lactate, mycobacterial infections show a conspicuous absence of the peaks indicated in Table 1 [25]. Tuberculomas may also show an elevated lipid peak related to caseation. In fact, TB can appear quite similar to tissue necrosis regardless of etiology showing lipid, lactate, and nothing else. In general, it can be difficult to distinguish tumors from TB even with spectroscopy.

Fungal Infections

Fungi are eukaryotes that can exist as single cells (yeasts) or multicellular hyphae (molds) that can organize into complex hyphal structures called mycelia forming large structures such as the common mushroom. Certain fungi (dimorphic) can transform between yeast and mold forms based on environmental conditions including temperature. Primary energy and metabolic substrates are derived from release of enzymes by the fungus enabling decomposition of decaying organic matter into absorbable nutrients. However, living organisms including humans can become such a metabolic substrate. Fortunately, fungal infections of the CNS are rare in healthy individuals. They are unfortunately common in immunocompromised patients. These infections can be difficult to treat in nonimmunocompromised patients but can be life threatening in those with little ability to mount an immune response. Just as with bacterial infections, fungal infections can produce meningitis, cerebritis, and abscesses. When these conditions are seen in immunocompromised patients, a fungal etiology must always be considered high in the differential diagnosis. The most common sources of entry of the infectious agent into the CNS include pulmonary infections with hematogenous dissemination; sinonasal infections with direct, perineural, or vascular spread; and invasive surgery, indwelling lines/catheters, or trauma.

Fungal Meningitis

Pathogens causing fungal meningitis are found in the soil including the yeast fungi *Cryptococcus neoformans* (soil and bird droppings) and *Candida albicans* (found in gut flora); the dimorphic fungi *Histoplasma capsulatum*, *Coccidioides immitis*, *Paracoccidioides brasiliensis*, *Blastomyces dermatitidis* (rare infections); and the hyphal fungi *Aspergillus* species and Zygomycetes, along with others. In terms of pathogenesis, it is known that blood-borne *Cryptococcus* and *Candida* can pass directly through endothelial cells into the meninges via endocytosis. *Cryptococcus* can also live within macrophages that are crossing the endothelium ("TROJAN horse" entry) [26]. The mechanism of entry of the other fungal pathogens has not been clarified but hyphal forms are more likely to enter via direct extension from sinus infections due to size constraints (large hyphae).

Cryptococcus is the most common cause of fungal meningitis involving the basal meninges with extension into the perivascular spaces particularly within the striatum. The fungus produces an external polysaccharide capsule that can coalesce into macroscopic collections forming gelatinous pseudocysts within the subarachnoid space, perivascular space, and ventricular system. These cryptococcal lesions typically do not show restricted diffusion [27]. Meningeal enhancement, which can be minimal in extent or when present linear/nodular in appearance, depends on the ability of the patient to mount an immune response. In a recent review, only 20–30 %of all patients with HIV presenting and cryptococcal meningitis had a positive MRI study, whereas all patients presenting with a recurrence of cryptococcal meningitis, who were also on immune reconstitution therapy, had a positive MRI with multifocal leptomeningeal enhancement [28]. Infection within perivascular spaces can lead to compromise of penetrating arteries with ischemic lacunar infarcts. As with any meningitis, leptomeningeal inflammation can lead to obstructive hydrocephalus.

Parenchymal Fungal Brain Infections

Fungal abscesses can have all the conventional imaging findings typical for a bacterial abscess including restricted diffusion. Similar to bacterial abscesses, succinate and acetate have been reported on MRS [29]. Fortunately, there are atypical features in comparison to bacterial abscesses including (1) signal loss on T2 images or long-TE gradient echo images in the capsule of the abscess indicating iron deposition, a feature usually not seen with bacterial infections (not to be confused with "dual rim sign" seen in bacterial infections on SWI images) but an increasingly recognized feature of fungal abscess (in fact, iron is a necessary component for hyphal growth), (2) intracavitary projections that represent fungal hyphae on histopathologic examination, and (3) the presence of trehalose, a stored disaccharide with peaks at 3.6–3.8 ppm on MRS [30–32].

Another important feature of fungi is the elaboration of enzymes such as elastase that enable hyphal penetration through the walls of blood vessels. *Aspergillus* and Mucor are the prototypical fungi with this ability. These fungi gain access to the vasculature by weakening the elastin-rich arterial wall that can lead to focal dilation of the vessel wall, producing mycotic aneurysms [33, 34]. A common clinical scenario occurs in immunocompromised patients with fungal sinus infections where hyphae grow into the walls of local vessels resulting in vessel wall inflammation and vasculitis. Several adverse events can then develop including (1) mycotic aneurysm formation and or hemorrhage secondary to weakening of the vessel wall, (2) local vascular thrombosis with tissue ischemia, and (3) emboli consisting of blood clots, fungal hyphae, or both resulting in ischemic injury or distant fungal cerebritis or both. Diabetics are particularly susceptible to developing *Mucor* infection as it thrives in acidic hyperglycemic environments, factors that also serve to suppress the immune response. Mortality of angioinvasive fungal infection with these complications is 85–100 % [35, 36]. Other notable fungal infections include Nocardia that forms abscesses said to have the highest mortality rate of any abscess-forming organism; blastomycosis that has been reported to occur equally in healthy and immunocompromised patients causing meningitis, abscesses, or granulomas; and histoplasmosis originating from bird or bat excrement producing meningitis, cerebritis abscesses, or granulomas (histoplasmomas – solid nodular-enhancing lesions) [36].

Viral Infections

The most important virus family causing CNS infection is the herpesvirus family with several neurotropic viruses: HSV-1, HSV-2, cytomegalovirus (CMV), HHV-6, HHV-7, HHV-8, varicella-zoster virus (VZV), and Epstein-Barr virus (EBV). Several others will cause serious life-threatening infections such as human immunodeficiency virus (HIV) and JC virus.

Human Immunodeficiency Virus (HIV)

Human immunodeficiency virus (HIV) infection of the brain can present clinically as HIV-associated dementia (HAD) or minor cognitive-motor disorder (MCMD). Neuropathological correlates of direct cerebral infection by HIV include multinucleated giant cell encephalitis (MGCE) and progressive diffuse leukoencephalopathy (PDL) [37].

The most common reported imaging finding is cerebral atrophy followed by white matter changes. Approximately 80 % of AIDS patients will have white matter lesions (diffuse; patchy; focal; and punctuate) [38]. These can be diffuse, bilateral, and symmetric representing HIV encephalopathy or/and bilateral, patchy high signal intensity lesions in the white and gray matter, which represent HIV encephalitis [38].

Antiretroviral therapy in patients with HAD may result in clinical improvement and stabilization or even regression of white matter signal intensity changes [39, 40].

JC Virus (JCV)

The JC virus was isolated in 1971 and named for the first patient in whom this virus was isolated [41]. Between the ages of 1 and 5 years, approximately 10 % of children demonstrate antibody to JCV, and by age ten, it can be observed in 40–60 % of the population. By adulthood, 70–80 % of the population has been infected.

JCV represents an excellent example of an agent that is normally controlled by an intact immune system but has the potential to cause a severe, potentially fatal neurological disorder if CNS immune surveillance is disturbed.

After initial infection the virus persists in the renal tubular epithelial cells. The reactivation of latent JCV and the entry of the JCV into the brain result in destruction and myelin loss and subsequently progressive multifocal leukoencephalopathy (PML).

On MR imaging, PML lesions are recognized as patchy, scalloped, high T2 and FLAIR signal intensity white matter lesions with extension along the white fibers [42]. Normally, enhancement is not seen; only rarely peripheral, faint enhancement will be observed. On diffusion-weighted imaging (DWI), a typical pattern has been observed, low DWI signal in the central demyelinated areas and high DWI signal at the periphery, representing active demyelination. The final diagnosis is made with the positive PCR to JCV in the CSF.

Clinical and radiological improvement in patients with PML who underwent highly active antiretroviral therapy (HAART) has been described in numerous studies [43, 44]. In some patients, immune reconstitution inflammatory syndrome (IRIS) will develop. PML-IRIS is characterized by the development of new inflammatory changes with an increase of PML lesion size and new areas of contrast enhancement with edema and mass effect.

PML and MS-PML-IRIS have also been described in patients with multiple sclerosis (MS) under natalizumab [45, 46]. Natalizumab is a monoclonal antibody and one of the cutting-edge drugs for relapsing MS [47, 48].

Human Herpes Virus-6 (HHV-6)

HHV-6 is a neurotropic virus, initial infection usually occurs in the first 2 years of life with the persistent latent infection.

HHV-6 encephalitis will occur in immunocompromised patients (especially bone marrow recipients).

Imaging findings include signal abnormalities in one or both hippocampi, medial temporal lobes, olfactory cortex, and insular region. Patients present clinically with signs of limbic system dysfunction.

Herpes Simplex Virus Type 1 (HSV-1)

Herpes simplex encephalitis (HSE) caused by HSV-1 is the most common cause of sporadic lethal encephalitis with high mortality and poor prognosis. Patients present with an acute onset of severe focal neurological deficits, confusion, and seizures.

HSE is a result of the reactivation of latent infection. HSV reaches the brain by direct neuronal transmission of the virus from a peripheral site via the trigeminal or olfactory nerve. The HSE has affinity for the temporal lobes, the orbital surfaces of the frontal lobes, the hippocampus, and the insular cortex. The basal ganglia are usually not involved.

MR is the method of choice in early detection of HSE. On FLAIR high signal intensity abnormalities will be detected in the affected areas. Diffusion-weighted imaging has been reported as highly sensitive in early detection of signal changes, even before FLAIR shows any abnormality [49, 50]. Enhancement will not be present early on, but will be apparent in the subacute stage.

Varicella-Zoster Virus (VZV)

The varicella-zoster virus causes chickenpox (varicella) in childhood, remains latent in the dorsal root ganglia, and may be reactivated decades later to produce shingles (zoster) in adults. Reactivation occurs in individuals with impaired immune status.

CNS infection with VZV is rare (1 %) and may present as meningitis, encephalitis, vasculopathy, and cerebellitis. VZV encephalitis is predominantly a vasculopathy, involving small and large vessels. On MR imaging ischemic or hemorrhagic infarcts will be seen [51].

Parasitic Infections

Toxoplasmosis

Immunocompromised patients, such as HIV-positive patients, and patients after bone marrow or organ transplants are at increased risk for cerebral toxoplasmosis. The incidence of toxoplasmosis in HIV-positive individuals has significantly decreased with the introduction of antiretroviral therapy. Toxoplasmosis is caused by an obligate intracellular parasite *Toxoplasma gondii*.

On MRI in patients with toxoplasmosis, multiple hypo- or hyperintense lesions will be detected on T2WI. They will show nodular or ringlike enhancement, and in 30 %, "eccentric target sign" will be seen [52]. On DWI restricted or elevated diffusion can be seen, ADC values are overlapping with those measured in lymphoma.

The major differential diagnosis remains primary CNS lymphoma (PCNSL). F-18 fluorodeoxyglucose (FDG)-positron emission tomography (PET) has been proven accurate in differentiation of lymphoma from toxoplasmosis in AIDS patients [53].

In patients after BMT, MRI may reveal multiple, non-enhancing toxoplasmosis lesions with no or only mild edema [54]. Hemorrhagic transformation will often be seen.

Bilateral pallidal hemorrhage has recently been described in cerebral toxoplasmosis [55].

References

1. Thigpen MC, Whitney CG, Messonnier NE et al (2011) Bacterial meningitis in the United States, 1998–2007. N Engl J Med 364(21):2016–2025
2. http://emedicine.medscape.com/article/961497-overview
3. http://neuropathologyweb.org/chapter5/chapter5aSuppurative.html
4. Chatterjee T, Gowardman JR, Goh TD (2003) Pneumococcal meningitis masquerading as subarachnoid hemorrhage. Med J Aust 178(10):505–507
5. Mitchell P, Wilkinson I, Hoggard N et al (2001) Detection of subarachnoid haemorrhage with magnetic resonance imaging. J Neurol Neurosurg Psychiatry 70(2):205–211
6. Tung GA, Rogg JM (2003) Diffusion-weighted imaging of cerebritis. AJNR 24(6):1110–1113
7. Karanja BW, Oburra HO, Masinde P, Wamalwa D (2014) Prevalence of hearing loss in children following bacterial meningitis in a tertiary referral hospital. BMC Res Notes 7:138
8. Kopelovich JC, Germiller JA, Laury AM, Shah SS, Pollock AN (2011) Early prediction of post-meningitic hearing loss in children using magnetic resonance imaging. Arch Otolaryngol Head Neck Surg 137(5):441–447
9. Kuwahara S, Kawada M, Uga S (2001) Cryptococcal meningoencephalitis presenting with an unusual MRI appearance–case report. Neurol Med Chir (Tokyo) 41(10):517–521
10. Goyal M, Sharma A, Mishra NK, Gaikwad SB, Sharma MC (1997) Imaging appearance of pachymeningeal tuberculosis. AJR 169(5):1421–1424
11. Erly WK, Bellon RJ, Seeger JF, Carmody RF (1999) MR imaging of acute coccidioidal meningitis. AJNR 20(3):509–514
12. Berkefeld J, Enzensberger W, Lanfermann H (1999) Cryptococcus meningoencephalitis in AIDS: parenchymal and meningeal forms. Neuroradiology 41(2):129–133
13. Britt RH, Enzmann DR (1983) Clinical stages of human brain abscesses on serial CT scans after contrast infusion. Computerized tomographic, neuropathological, and clinical correlations. J Neurosurg 59(6):972–989
14. Haimes AB, Zimmerman RD, Morgello S, Weingarten K, Becker RD, Jennis R, Deck MD (1989) MRI of brain abscesses. AJR 152(5):1073–1085

15. Muccio CF, Caranci F, D'Arco F, Cerase A, De Lipsis L, Esposito G, Tedeschi E, Andreula C (2014) Magnetic resonance features of pyogenic brain abscesses and differential diagnosis using morphological and functional imaging studies: a pictorial essay. J Neuroradiol 41(3):153–167
16. Mishra AM, Gupta RK, Saksena S, Prasad KN, Pandey CM, Rathore D, Purwar A, Rathore RK, Husain N, Jha DK, Jaggi RS, Husain M (2005) Biological correlates of diffusivity in brain abscess. Magn Reson Med 54(4):878–885
17. Tomar V, Yadav A, Rathore RK, Verma S, Awasthi R, Bharadwaj V, Ojha BK, Prasad KN, Gupta RK (2011) Apparent diffusion coefficient with higher b- value correlates better with viable cell count quantified from the cavity of brain abscess. AJNR Am J Neuroradiol 32(11):2120–2125
18. Gupta RK, Nath K, Prasad A et al (2008) In vivo demonstration of neuroinflammatory molecule expression in brain abscess with diffusion tensor imaging. AJNR Am J Neuroradiol 29:326–332
19. Nath K, Ramola M, Husain M et al (2010) Assessment of therapeutic response in patients with brain abscess using diffusion tensor imaging. World Neurosurg 73:63–68
20. Toh CH, Wei KC, Chang CH et al (2012) Differentiation of pyogenic brain abscesses from necrotic glioblastoma with use of susceptibility-weighted imaging. AJNR 33(8):1534–1538
21. Lai PH, Li KT, Hsu SS et al (2005) Pyogenic brain abscess: findings from in vivo 1.5-T and 11.7-T in vitro proton MR spectroscopy. AJNR Am J Neuroradiol 26:279–288
22. Dev R, Gupta RK, Poptani H, Roy R, Sharma S, Husain M (1998) Role of in vivo proton magnetic resonance spectroscopy in the diagnosis and management of brain abscesses. Neurosurgery 42(1):37–43
23. Dusak A, Hakyemez B, Kocaeli H, Bekar A (2012) Magnetic resonance spectroscopy findings of pyogenic, tuberculous, and cryptococcus intracranial abscesses. Neurochem Res 37(2):233–237
24. Gupta RK, Prakash M, Mishra AM et al (2005) Role of diffusion weighted imaging in differentiation of intracranial tuberculoma and tuberculous abscess from cysticercus granulomas – a report of more than 100 lesions. Eur J Radiol 55(3):384–392
25. Gupta RK, Vatsal DK, Husain N, Chawla S, Prasad KN, Roy R, Kumar R, Jha D, Husain M (2001) Differentiation of tuberculous from pyogenic brain abscesses with in vivo proton MRS and magnetization transfer MRI. AJNR 22(8):1503–1509
26. Liu TB, Perlin DS, Xue C (2012) Molecular mechanisms of cryptococcal meningitis. Virulence 3(2):173–181
27. Smith AB, Smirniotopoulos JG, Rushing EJ (2008) From the archives of the AFIP: CNS infections associated with HIV infection: radiologic-pathologic correlation. Radiographics 28(7):2033–2058
28. Katchanov J, Branding G, Jefferys L, Arastéh K, Stocker H, Siebert E (2016) Neuroimaging of HIV-associated cryptococcal meningitis: comparison of magnetic resonance imaging findings in patients with and without immune reconstitution. Int J STD AIDS 27(2):110–117
29. Siegal JA, Cacayorinb ED, Nassif AS, Rizk D, Galambos C, Levy B, Kennedy D, Visconti J, Perman W (2000) Cerebral mucormycosis: proton MR spectroscopy and MR imaging. Magn Reson Imaging 18(7):915–920
30. Andrade AI, Donato M, Previgliano C, Hardjasudarma M (2014) Histoplasmosis brain abscesses in an immunocompetent adult. A case report and literature review. Neuroradiol J 27(3):334–338
31. Yamada K, Zoarski GH, Rothman MI, Zagardo MT, Nishimura T, Sun CC (2001) An intracranial aspergilloma with low signal on T2-weighted images corresponding to iron accumulation. Neuroradiology 43(7):559–561
32. Luthra G, Parihar A, Nath K, Jaiswal S, Prasad KN, Husain N, Husain M, Singh S, Behari S, Gupta RK (2007) Comparative evaluation of fungal, tubercular, and pyogenic brain abscesses with conventional and diffusion MR imaging and proton MR spectroscopy. AJNR Am J Neuroradiol 28(7):1332–1338
33. Lee WK, Mossop PJ, Little AF, Fitt GJ, Vrazas JI, Hoang JK et al (2008) Infected (mycotic) aneurysms: spectrum of imaging appearances and management. Radiographics 28(7):1853–1868
34. Allen LM, Fowler AM, Walker C, Derdeyn CP, Nguyen BV, Hasso AN et al (2013) Retrospective review of cerebral mycotic aneurysms in 26 patients: focus on treatment in strongly immunocompromised patients with a brief literature review. AJNR 34(4): 823–827
35. Norlinah MI, Ngow HA, Hamidon BB (2007) Angioinvasive cerebral aspergillosis presenting as acute ischaemic stroke in a patient with diabetes mellitus. Singapore Med J 48(1):e1–e4
36. Palacios E, Rojas R, Rodulfa J, González-Toledo E (2014) Magnetic resonance imaging in fungal infections of the brain. Top Magn Reson Imaging 23(3):199–212
37. Kleihues P, Lang W, Burger PC et al (1985) Progressive diffuse leukoencephalopathy in patients with acquired immune deficiency syndrome (AIDS). Acta Neuropathol (Berl) 68: 333–339
38. Olsen WL, Longo FM, Mills CM et al (1988) White matter disease in AIDS: findings at MR imaging. Radiology 169:445–448
39. Filippi CG, Sze G, Farber SJ et al (1998) Regression of HIV encephalopathy and basal ganglia signal intensity abnormality at MR imaging in patients with AIDS after initiation of protease inhibitor therapy. Radiology 206:491–498
40. Thurnher MM, Schindler EG, Thurnher SA et al (2000) Highly active antiretroviral therapy for patients with AIDS dementia complex: effect on MR imaging findings and clinical course. AJNR Am J Neuroradiol 21:670–678
41. Padget BL, Walker DL, ZuRhein GM et al (1997) Cultivation of papova-like virus from human brain with progressive multifocal leukoencephalopathy. Neuroradiology 1997;39(9):611–618.
42. Thurnher MM, Thurnher SA, Mühlbauer B et al (1997) Progressive multifocal leukoencephalopathy in AIDS: initial and follow-up CT and MRI. Neuroradiology 39(9):611–618
43. Shapiro RA, Mullane KM, Camras L et al (2001) Clinical and magnetic resonance imaging regression of progressive multifocal leukoencephalopathy in an AIDS patient after intensive antiretroviral therapy. J Neuroimaging 11:336–339
44. Thurnher MM, Donovan Post MJ, Rieger A et al (2001) Initial and follow-up MR imaging findings in AIDS-related progressive multifocal leukoencephalopathy treated with highly active antiretroviral therapy. AJNR Am J Neuroradiol 22:977–984
45. Post MJ, Thurnher MM, Clifford DB, Nath A, Gonzalez RG, Gupta RK, Post KK (2013) CNS-immune reconstitution inflammatory syndrome in the setting of HIV infection, part 2: discussion of neuro-immune reconstitution inflammatory syndrome with and without other pathogens. AJNR Am J Neuroradiol 34(7): 1308–1318
46. Post MJ, Thurnher MM, Clifford DB, Nath A, Gonzalez RG, Gupta RK, Post KK (2013) CNS-immune reconstitution inflammatory syndrome in the setting of HIV infection, part 1: overview and discussion of progressive multifocal leukoencephalopathy-immune reconstitution inflammatory syndrome and cryptococcal-immune reconstitution inflammatory syndrome. AJNR Am J Neuroradiol 34(7):1297–1307
47. Wattjes MP, Warnke C (2016) Guidelines on PML risk stratification and diagnosis in patients with MS treated with natalizumab: so far so good? J Neurol Neurosurg Psychiatry 87(2):115
48. Sinnecker T, Othman J, Kühl M, Mekle R, Selbig I, Niendorf T, Kunkel A, Wienecke P, Kern P, Paul F, Faiss J, Wuerfel J (2015) 7T MRI in natalizumab-associated PML and ongoing MS disease activity: a case study. Neurol Neuroimmunol Neuroinflamm 2(6):e171
49. Küker W, Nägele T, Schmidt F et al (2004) Diffusion-weighted MRI in herpes simplex encephalitis: a report of three cases. Neuroradiology 46:122–125

50. Renard D, Nerrant E, Lechiche C (2015) DWI and FLAIR imaging in herpes simplex encephalitis: a comparative and topographical analysis. J Neurol 262(9):2101–2105
51. Kaewpoowat Q, Salazar L, Aguilera E, Wootton SH, Hasbun R. Herpes simplex and varicella zoster CNS infections: clinical presentations, treatments and outcomes. Infection 2015 Dec 17 [Epub ahead of print].
52. Kumar GG, Mahadevan A, Guruprasad AS, Kovoor JM, Satishchandra P, Nath A, Ranga U, Shankar SK (2010) Eccentric target sign in cerebral toxoplasmosis: neuropathological correlate to the imaging feature. J Magn Reson Imaging 31(6):1469–1472
53. Villringer K, Jager H, Dichgans M et al (1995) Differential diagnosis of CNS lesions in AIDS patients by FDG-PET. J Comput Assist Tomogr 19:532–536
54. Mueller-Mang C, Castillo M, Mang TG, Cartes-Zumelzu F, Weber M, Thurnher MM (2007) Fungal versus bacterial brain abscesses: is diffusion-weighted MR imaging a useful tool in the differential diagnosis? Neuroradiology 49:651–657
55. Finelli PF, Wrubel GL (2015) Bilateral pallidal hemorrhage in toxoplasmosis update of acute symmetric lesions of deep nuclei. Neuroradiol J 28(4):413–417

Disorders of the Sellar and Parasellar Region

Chip Truwit and Walter Kucharczyk

Introduction

While a broad set of lesions can involve the sella and parasellar regions, pituitary adenomas are the most common pathologies in clinical practice. In this syllabus, we discuss pertinent information regarding the imaging of pituitary adenomas, as well as many less common disorders that are included in the differential diagnosis.

Pituitary Adenomas

Magnetic resonance imaging (MRI) is the imaging modality of choice in the investigation of pituitary pathology. Patients are referred for MR imaging of the pituitary most commonly on the basis of clinical and laboratory findings, although given the frequency of MR imaging of the brain, it is also not uncommon to discover sellar and parasellar lesions as serendipitous findings. Computed tomography (CT) remains a complementary diagnostic exam for special cases where intralesional calcifcations, bone destruction, or anatomic variants are suspected.

Despite the many advances in MR imaging over the past decade, the imaging work-up of the pituitary remains largely unchanged. Specifically, precontrast T1-weighted images are obtained in the sagittal and coronal planes, and at least one of these planes is obtained following the administration of paramagnetic contrast. In addition, it is common to obtain a heavily T2-weighted sequence in the coronal (occasionally sagittal) plane to identify potential signal intensity changes of an adenoma and to identify small pars intermedia cysts, many of which exhibit T2 prolongation. Many investigators also perform dynamic contrast-enhanced T1-weighted imaging, particularly in the unoperated pituitary. While this is of little value in the case of macroadenomas, the dynamic sequence can be valuable in the identification of microadenomas, some of which will exhibit mild enhancement, potentially obscuring their presence.

Pituitary microadenomas commonly exhibit hypointensity to the normal adenohypophysis on T1-weighted images. Occasionally, however, they may be isointense to the anterior pituitary, making them a bit more difficult to identify on the basis of signal characteristics. The lesions are round or oval in shape; more commonly than not, the pituitary infundibulum is deviated away from the side of the lesion. Sometimes, there is no such mass effect. Rarely, the adenoma appears to "torque" the gland, appearing to retract the infundibulum toward the lesion. Occasionally, pituitary adenomas may exhibit hyperintensity on T1-weighted images, generally reflecting internal hemorrhage. Such hemorrhage is more common in prolactinomas, often times spontaneous or following pharmacotherapy.

The T2 signal intensity of microadenomas is variable, although if focal hyperintensity to the normal gland is seen, a microadenoma is likely. The adenoma may be larger than the focus of hyperintensity. Commonly, the adenoma is a prolactinoma, as 80 % of microprolactinomas exhibit T2 hyperintensity. T2 hypointensity is also a helpful feature; in the clinical and laboratory scenario of excess growth hormone, a mass of focal T2 hypointensity is highly correlated with a diagnosis of a densely granulated GH-secreting adenoma. T2-weighted imaging also occasionally reveals very small foci of hyperintensity; these 3 mm or less lesions may reflect picoadenomas, usually inapparent on T1-weighted images, with or without contrast.

In many cases of prolactinoma, unenhanced T1- and T2-weighted imaging is dispositive. Occasionally, however, the lesion is not obvious, and contrast enhancement is

C. Truwit, MD (✉)
Radiology, Hennepin County Medical Center,
Minneapolis, MN, USA
e-mail: Chip.Truwit@hcmed.org

W. Kucharczyk, MD
Department of Medical Imaging,
University Health Network – Toronto General Hospital,
Toronto, ON, Canada
e-mail: w.kucharczyk@utoronto.ca

J. Hodler et al. (eds.), *Diseases of the Brain, Head and Neck, Spine 2016–2019: Diagnostic Imaging,* DOI 10.1007/978-3-319-30081-8_16

indicated. As the pituitary is a circumventricular organ and not subject to the blood–brain barrier, a half dose of paramagnetic contrast is generally sufficient. Following the administration of contrast, a hypointense lesion either surrounded by or superiorly capped by normal avidly enhancing pituitary tissue will reveal a microadenoma or other lesions in the differential diagnosis. In cases where a full dose of contrast is administered (e.g., cases which are serendipitously discovered on routine brain imaging), small lesions may be obscured by the avidity of the enhancement. Adjusting the window/level parameters may be required to reveal the microadenoma. As well, delayed contrast-enhanced imaging may inadvertently obscure microadenomas by virtue of their slower "wash-in" curve, relative to normal pituitary. Uncommonly, a small tuft of intralesional enhancement may be seen within an otherwise hypointense (lesser enhancing) microadenoma. Finally, as noted above, dynamic contrast-enhancing imaging may be useful for some microadenomas, especially ACTH-secreting tumors.

In contradistinction to the microadenoma, pituitary macroadenomas (defined as tumors greater than 10 mm in size) often extend beyond the confines of the sella. Most commonly, such tumors extend cephalad toward the optic chiasm and hypothalamus or laterally into the cavernous sinus. While the delineation of such extension has always been important to the surgeon, with the increasing adoption of transnasal endoscopic surgical approaches to the sella and parasellar regions, the description of such extension has become a routine component of the preoperative neurosurgical checklist. As will be discussed below, this preoperative checklist is extremely important to a successful surgical outcome. Likewise, stereotactic CT angiography instead of either unenhanced or routine contrast-enhanced CT is becoming a staple of the preoperative work-up. In addition to the anatomic description of the tumoral confines, declarations of the tumor's physical characteristics (firmness, cystic, necrotic, hemorrhagic, calcification) are all useful additions to the presurgical evaluation.

Macroadenomas that extend cephalad are commonly bilobed in shape, constrained at the waist by the diaphragma sellae. Unlike their microadenoma counterparts which are more commonly of one signal intensity, macroadenomas offer multiple signal intensities due to the mixed slid and cystic nature of these lesions. Solid components tend to be slightly hypointense on T2 and T2-weighted images and exhibit some contrast enhancement. Cystic and/or necrotic components exhibit variable signal but often contain proteinaceous debris which may show some hyperintensity on T1-weighted images. On T2-weighted images, hyperintensity within the cystic or necrotic components of an adenoma is common. Occasionally, an intratumoral, intracystic component may reveal a fluid–fluid level, perhaps reflecting intralesional hemorrhage or separation of proteinaceous components.

While contrast administration is not necessary to identify the lesion, contrast is useful to the neurosurgeon in many ways. First, it is common to see relatively hyperenhancing normal pituitary tissue between the tumor and the cavernous sinus, unless the tumor has grown laterally. Second, it is common to see a curvilinear component of normal, enhancing pituitary, asymmetrically capping the tumor. This normal tissue forms a pseudocapsule around the adenoma, most commonly above the lesion, less frequently behind, in front of, or beneath the tumor. Again, this information is important to include in the presurgical checklist for the endoscopic neurosurgeon in particular.

In the normal situation, the posterior lobe hyperintensity sits slightly behind the adenohypophysis, often within a cup-shaped depression of the dorsum sellae. In the case of a microadenoma, the posterior lobe is unlikely to be disturbed. In the macroadenoma, however, the normal neurohypophysis may be compressed, laterally displaced, or completely absent from the normal location. In many cases, compression of the infundibulum is disruptive enough that the neurohypophyseal function is displaced upstream, with a "new" bright spot more cephalad along the infundibulum.

With significant upward extension, normal landmarks may become obscured; identification of the chiasm may be problematic. Heavily T2-weighted images may be helpful in such cases, as the normal hypointensity of the prechiasmatic optic nerves and the chiasm may be more readily distinguished. Contrast enhancement in patients with macroadenomas may also reveal subtle meningeal enhancement where the tumor and meninges are in contact. Occasionally, a non-specific dural tail may be noted.

Cavernous sinus involvement may be due to compressive growth and consequent medial and occasionally lateral dural reflection or due to true invasion of the sinus. On imaging, invasion is suggested by tumor appearing to encircle the cavernous internal carotid artery. Invasion is excluded if normal pituitary tissue is seen between the mass and the sinus.

Other Considerations: Gender, Age, Hormone Secretion, and Pregnancy

Prolactin-secreting microadenomas are common in young women. Some may spontaneously remain dormant over long periods. They do not develop after menopause. When prolactin-secreting adenomas are discovered in male patients, they have usually reached the stage of macroadenomas. This is probably due in part to the fact that clinical signs are less obvious in men than in women and in part to the fact that their development is probably different. Cavernous sinus involvement is far from exceptional. Pediatric pituitary adenomas are not only exceptional but also potentially active. Prolactin-secreting adenomas can be responsible for late

puberty. Prolactinomas are usually discovered at the stage of microadenomas owing to distinctive clinical signs found in young women, including amenorrhea, galactorrhea, and hyperprolactinemia (over 30 or 40 µg/l). When imaging the pituitary in the clinical setting of elevated prolactin alone, a bit of caution is recommended. A broad list of pharmacological agents, minor traumas, and even transient vasovagal events or seizures can cause elevations of prolactin into the ranges seen in the setting of microadenoma. In such cases, care is recommended not to overcall findings on the MRI. Most of the time, the prolactinoma is hypointense on T1-weighted images, while it is hyperintense on T2-weighted images in four cases out of five. Moreover, this high signal may only be exhibited by a portion of the adenoma.

Correlation between prolactin levels and adenoma size is usually good. However, given two prolactinomas of equal size, the hypointense tumor on T2-weighted images secretes more than its counterpart. Medical treatment based on bromocriptine decreases adenoma volume drastically; occasionally, bromocriptine-induced hemorrhage can be seen. As a result, diagnosis becomes difficult, either because of morphology or because of the potential to mimic a Rathke's cleft cyst. We strongly recommend MRI documentation before instituting the medical treatment. In some cases when prolactinomas are imaged long after medical treatment with bromocriptine is started, peculiar scarred tissue can be seen, which is evocative of a former pituitary adenoma: it is due to the local remodeling of the pituitary gland, forming a "V" on its superior aspect.

While prolactinomas and growth hormone (GH)-secreting adenomas are usually located laterally in the sella turcica, ACTH-secreting adenomas in Cushing's disease, usually smaller in size, are more often located in the midline. Because of the severe prognosis of this disease and the surgical possibilities, ACTH-secreting lesions require the most detailed and exhaustive imaging.

GH-secreting adenomas have the unique characteristic of exhibiting hypointensity on T2-weighted images in two-thirds of cases, usually the densely granulated subtype. Spontaneous infarction or necrosis of GH-secreting adenomas is far from exceptional. Some cases of acromegaly that were detected late in the course of the disease exhibited an enlarged, partially empty sella turcica, lined with adenomatous tissue that proved difficult to analyze. Medical treatment based on octreotide analogs (somatostatin) decreases the size of the adenoma by an average of 35 % and brings the level of somatomedin C back to normal in 50 % of cases. It is useful before surgery.

Macroadenomas can be nonfunctioning, but they can also be prolactin-secreting adenomas, gonadotrope adenomas, and growth hormone-secreting adenomas. The greater their size, the more heterogeneous they are, as areas of cystic necrosis are caused by poor tumoral blood supply. Gonadotrope adenomas are often massive and have a strong tendency to recur.

Hemorrhage occurs in all or parts of 20 % of all pituitary adenomas, but it is usually occult. Pituitary apoplexy, with the usual headache, pseudomeningeal syndrome, cranial nerve paralysis, and severe hypopituitarism, is generally caused by massive hemorrhage within a pituitary macroadenoma. Smaller-scale hemorrhage occurs much more often and can be seen within pituitary adenomas. Bromocriptine is held responsible, to a certain degree, for intratumoral hemorrhages in prolactinomas, although the phenomenon is sometimes revealed on MR images before the treatment has been instituted. Recurrent hemorrhage is possible and can cause repeated headaches.

Intratumoral hemorrhages are revealed by hyperintensity on the T1-weighted image, sometimes with a blood–fluid level in the mass; it is worth remembering that patients lay supine in the scanner, and therefore the blood–fluid level will be oriented along the coronal plane, i.e., vertically, on sagittal scans. Normal pituitary tissue has a shorter T1 in women during pregnancy. Normal pituitary tissue also increases in height during pregnancy (0.08 mm per week, i.e., almost 3 mm during the whole pregnancy). Pituitary adenomas also increase in volume, especially prolactinomas. The increased volume of the prolactinoma is especially visible when medical treatment has been interrupted. Vision and tumor size should be closely monitored during this period.

Preoperative Considerations

Surgery of the sella and parasellar region is undertaken via one or more of three approaches: cranial, transsphenoidal, and transnasal endoscopic. As noted above, a surgical checklist is extremely valuable for the neurosurgeon, as such checklists are elsewhere in medicine and surgery. In general, classical neurosurgical approaches via craniotomy offer broad exposure to the suprasellar region, albeit less exposure to the intrasellar region. The transsphenoidal approach via a surgical speculum placed in the midline offers a good alternative to approaching the intrasellar pituitary but is limited in the ability of the neurosurgeon to "see" let alone operate beyond the confines of the central channel. More recently, the previously developed transnasal endoscopic approach to the sella has been more widely adopted for a number of reasons. First, multiple instruments can be utilized, including angled endoscopes. Second, a transnasal mucosal flap can be created at the time of surgery. This flap has been very successful at limiting the unfortunate complication of CSF leak. Third, the exposure can be lateralized to extend to parasellar lesions, as well as extended posteriorly through the clivus to reach the prepontine cistern, the basilar artery, and the anterior brainstem.

With the renewed enthusiasm for the versatile transnasal endoscopic approach comes an increased responsibility of the radiologist: imaging as part of presurgical planning. In particular, these cases are performed with frameless stereotactic systems and thus require preoperative CT (for bony landmarks) and MR (typically with contrast) to identify the lesion.

We encourage clinicians to include contrast on the CT study and to perform it as a circle of Willis CT angiogram. We suggest this for a few reasons: first, the CTA exquisitely delineates pertinent cerebral vasculature. By performing the study as a CTA, the cavernous and supraclinoid internal carotid arteries are well seen. In addition, parasellar aneurysms of the internal carotid, posterior communicating, and even the anterior choroidal artery origin can be identified with great reliability. This may be particularly important in patients with somatotopic adenomas. In 2011, Manara et al. reported that 17 % (one in six) of patients with GH adenomas harbored intracranial aneurysms.

Second, this study will reveal bony anatomy including the number and location of instrasphenoidal septa and their insertions, the presence of Onodi cells, and the degree of aeration of the sphenoid sinus, all of which will influence the surgical approach, patient safety, and, ultimately, the patient outcome. Third, it is relatively straightforward to color-code the tumor volume, the cerebrovasculature, and the skull base on modern 3D workstations, which show not only the lesion but the adjacent vascular landmarks and landmines and the underlying bony confines of the surgical corridor. Finally, it is now common to prepare preoperative image batches or videos that show the lesion from the sphenoid floor, "looking up" at the eroded sellar floor, affording the surgeon a preoperative video tour of the upcoming surgical procedure.

Postoperative Sella Turcica and Pituitary Gland

The surgical cavity is often filled with packing material after transsphenoidal resection of a pituitary adenoma. Surgicel is frequently used and is impregnated with blood and secretions. The presence of packing material, secretions, and peri-adenomatous adhesions usually keeps the cavity from collapsing in the days and weeks that follow surgery. Blood, secretions, and packing material slowly involute over the following 2–3 months. Even after a few months, fragments of blood-impregnated Surgicel can still be found in the surgical cavity. If the diaphragm of the sella turcica is torn in the course of surgery, fat or muscle implants are inserted by the surgeon to prevent the occurrence of a cerebrospinal fluid fistula. Their resorption takes much longer. Implanted fat involutes slowly and may exhibit hyperintensity on the T1-weighted image up to 2–3 years after surgery. Postoperative MRI 2–3 months after surgery is useful to monitor further development of a resected adenoma. An earlier MRI examination performed 48 h after surgery checks for potential complications and may visualize what appears to be residual tumor, i.e., a mass of intensity identical to that of the adenoma before surgery that commonly occupies a peripheral portion of the adenoma. This early investigation is extremely helpful to interpret the follow-up MR images. At this stage, the remaining normal pituitary tissue can be characterized: it is usually asymmetrical, and a hyperintense area is frequently observed at the base of the deviated hypophyseal stalk, due to an ectopic collection of neurohypophyseal secretory vesicles. The 2-month follow-up MRI examination is essential to check for residual tumor. Late follow-up MRI, after 1–2 years or more, usually demonstrates adenoma recurrence as a rounded or convex mass that is isointense with the initial tumor.

3 T MRI and DWI for Pituitary Imaging

The improved SNR of 3 T scanners relative to 1.5 T can be traded-off for thinner image slices and smaller voxels, thereby offering improved spatial resolution at comparable SNR. Hence, some microadenomas may be detected at 3 T that are invisible at 1.5 T. Also, the cavernous sinus wall can be depicted more consistently. These facts have led us to preferentially schedule our pituitary exams on our 3 T MRI. FSE T2-weighted images are especially useful. On the negative side of 3 T imaging, there are the issues of worse T1 weighting at 3 T due to the lengthening of T1, greater motion artifacts, and exaggerated susceptibility effects. DWI and ADC images have been applied to pituitary imaging as aids to determining tumor consistency and thereby aiding surgical planning. Early evidence suggests that soft adenomas with high cellularity and scant fibrous stroma have low ADCs, whereas firm adenomas, with low cellularity and abundant fibrous stroma, have high ADCs. DWI obtained without echoplanar imaging offers improved imaging at the skull base. Such TSE-based DWI, therefore, is increasingly supplanting echoplanar DWI in head and neck, pediatric, and pituitary imaging.

Craniopharyngioma

Craniopharyngiomas are epithelial-derived neoplasms that occur exclusively in the region of the sella turcica and suprasellar cistern or in the third ventricle. Craniopharyngiomas account for approximately 3 % of all intracranial tumors and show no gender predominance. Craniopharyngiomas are hormonally inactive lesions, although compression of the stalk may result in diabetes insipidus. They have a bimodal age distribution; more than half occurs in childhood or

adolescence, with a peak incidence between 5 and 10 years of age. There is a second smaller peak in adults in the sixth decade. The tumors vary greatly in size, from a few millimeters to several centimeters in diameter. The center of most tumors is in the suprasellar cistern. Infrequently, the lesions are entirely within the sella or in the third ventricle.

Most discussions of craniopharyngiomas in the literature are confined to the most frequent form, the classic *adamantinomatous* type, but a distinct squamous or *papillary* type is also recognized. Typically, adamantinomatous craniopharyngiomas are identified during the first two decades of life. These children most often present with symptoms and signs of increased intracranial pressure: headache, nausea, vomiting, and papilledema. Visual disturbances due to compression of the optic apparatus are also frequent but difficult to detect in young children. Others present with pituitary hypofunction because of compression of the pituitary gland, pituitary stalk, or hypothalamus. Occasionally, lesions rupture into the subarachnoid space and evoke a chemical meningitis. Rarely, adamantinomatous craniopharyngiomas are found outside the suprasellar cistern, including the posterior fossa, pineal region, third ventricle, and nasal cavity (sphenoid sinus).

Adamantinomatous tumors are almost always grossly cystic and usually have both solid and cystic components. Calcification is seen in the vast majority (~90 %) of these tumors. Commonly, these calcifications can be identified on MR scans as nodular excrescences of the wall of the primary lesion. Occasionally, the calcifications are difficult to discern; in these cases, CT will prove helpful. Extensive fibrosis and signs of inflammation are often found with these lesions, particularly when they are recurrent, so that they adhere to adjacent structures, including the vasculature at the base of the brain. Optic tract edema on T2-weighted images is a common associated finding that is not commonly seen with other suprasellar masses. Due to the inflammatory and fibrotic nature of this lesion, recurrence is common, typically occurring within the first 5 years after surgery.

The most characteristic MRI finding is a suprasellar mass that is itself heterogeneous but contains a cystic component that is well defined, internally uniform, and hyperintense on both T1- and T2-weighted images. Almost always, an adamantinomatous craniopharyngioma that presents with large cystic components in the middle cranial fossa and elsewhere can be traced back to the suprasellar region, where a more solid, enhancing component of the lesion can be seen. The lesions often encase nearby cerebral vasculature. The solid portion, which is frequently partially calcified, is represented as the heterogeneous region. On rare occasions, the cyst is absent and the solid component is completely calcified. These calcified types of tumors can be entirely overlooked on MRI unless close scrutiny is paid to subtle distortion of the normal suprasellar anatomy. Contrast medium administration causes a moderate degree of enhancement of the solid portion of the tumor, which otherwise may be difficult to see.

Papillary craniopharyngiomas are typically found in adult patients. These lesions are solid, without calcification, and often found within the third ventricle. Although surgery remains the definitive mode of therapy for all craniopharyngiomas, as papillary variants are encapsulated and are readily separable from nearby structures and the adjacent brain, they are generally thought to recur much less frequently than the adamantinomatous type. On pathologic examination, papillary lesions do not show the features characteristic of the adamantinomatous variant. In papillary lesions, there is extensive squamous differentiation.

In distinction from their adamantinomatous counterpart, MRI typically shows papillary craniopharyngiomas as solid lesions. Occasionally, cysts may be seen, although they are unlikely to be dominant cysts as in the adamantinomatous variety. As noted previously, they are often situated within the third ventricle. These lesions demonstrate a nonspecific signal intensity pattern, without the characteristic hyperintensity on T1-weighted images of the cystic component of adamantinomatous tumors. Like all craniopharyngiomas, papillary lesions typically enhance.

Rathke's Cleft Cyst

Symptomatic cysts of Rathke's cleft are less frequent than craniopharyngiomas, although asymptomatic Rathke's cysts are a common incidental finding at autopsy. In a recent evaluation of 1000 nonselected autopsy specimens, 113 pituitary glands (11.3 %) harbored incidental Rathke's cleft cysts. These cysts are predominantly intrasellar in location. Of incidental Rathke's cysts larger than 2 mm in a large autopsy series, 89 % were localized to the center of the gland, whereas the remaining 11 % extended to show predominant lateral lesions. In that series, of all incidental pituitary lesions localized to the central part of the gland, 87 % were Rathke's cysts. Others may be centered in the suprasellar cistern, usually midline and anterior to the stalk. Rathke's cysts are found in all age groups. They share a common origin with some craniopharyngiomas in that they are thought to originate from remnants of squamous epithelium from Rathke's cleft. The cyst wall is composed of a single cell layer of columnar, cuboidal, or squamous epithelium on a basement membrane. The epithelium is often ciliated and may contain goblet cells. The cyst contents are typically mucoid, less commonly filled with serous fluid or desquamated cellular debris. Calcification in the cyst wall is rare.

As noted above, most Rathke's cleft cysts are small and asymptomatic, discovered at autopsy. Symptoms occur if the cyst enlarges sufficiently to compress the pituitary gland or

optic chiasm and, rarely, secondary to hemorrhage. The cysts with mucoid fluid are often indistinguishable from purely cystic craniopharyngiomas on MRI: both are hyperintense on T1- and T2-weighted images. The serous cyst matches the signal intensity of the cerebrospinal fluid (CSF) and is the only subtype that has the typical imaging features of benign cysts. Those containing cellular debris pose the greatest difficulty in differential diagnosis for they resemble solid nodules. The surgical approaches to Rathke's cleft cyst and craniopharyngioma differ. Because of infrequent postoperative recurrences, partial removal or aspiration is sufficient. Rathke's cleft cysts do not typically enhance. However, occasionally there may be thin marginal enhancement of the cyst wall. This feature can be used to advantage in difficult cases to separate these cysts from craniopharyngiomas. CT may reveal calcification, frequently found in craniopharyngiomas, helping to distinguish the mass from a Rathke's cleft cyst.

Meningioma

Approximately 10 % of meningiomas occur in the parasellar region. These tumors arise from a variety of locations around the sella including the tuberculum sellae, clinoid processes, medial sphenoid wing, and cavernous sinus. Meningiomas are usually slow-growing lesions that present because of compression of vital structures. Patients may suffer visual loss because of ophthalmoplegia due to cranial nerve involvement, proptosis due to venous congestion at the orbital apex, or compression of the optic nerves, chiasm, or optic tracts.

Meningiomas are most frequently isointense – and less commonly hypointense – to gray matter on unenhanced T1-weighted sequences. Approximately 50 % remain isointense on the T2-weighted sequence, whereas 40 % are hyperintense. Since there is little image contrast to distinguish meningiomas from brain parenchyma, indirect signs such as a mass effect, thickening of the dura, buckling of adjacent white matter, white matter edema, and hyperostosis are important diagnostic features. Other diagnostic signs include visualization of a cleft of CSF separating the tumor from the brain (thus denoting that the tumor has an extra-axial location) and a clear separation of the tumor from the pituitary gland (thus indicating that the tumor is not of pituitary gland origin). The latter sign is particularly well assessed on sagittal views of planum sphenoidale meningiomas. A peripheral black rim occasionally noted at the edges of these meningiomas is thought to be related to surrounding veins. Hyperostosis and calcification are features that may be apparent on MRI but are better assessed with CT. Vascular encasement is not uncommon, particularly with meningiomas in the cavernous sinus. The pattern of encasement is of diagnostic value. Meningiomas commonly constrict the lumen of the encased vessel. This is rare with other tumors. As on CT, the intravenous administration of contrast medium markedly improves the visualization of basal meningiomas. They enhance intensely and homogeneously, often with a trailing edge of thick surrounding dura (the "dural tail sign").

Chiasmatic and Hypothalamic Gliomas

The distinction between chiasmatic and hypothalamic gliomas often depends on the predominant position of the lesion. In many cases, the origin of large gliomas cannot be definitively determined, as the hypothalamus and chiasm are inseparable; therefore, hypothalamic and chiasmatic gliomas are discussed as a single entity. The vast majority (75 %) of these tumors occur in the first decade of life, with equal prevalence in males and females. There is a definite association of optic nerve and chiasmatic gliomas with neurofibromatosis, more so for tumors that arise from the beginning optic nerve rather than from the chiasm or hypothalamus.

Tumors of chiasmal origin are also more aggressive than those originating from the optic nerves and tend to invade the hypothalamus and floor of the third ventricle and cause hydrocephalus. Patients suffer from monocular or binocular visual disturbances, hydrocephalus, or hypothalamic dysfunction. The appearance of the tumor depends on its position and direction of growth. It can be confined to the chiasm or the hypothalamus; however, because of its slow growth, the tumor usually attains a considerable size by the time of presentation, and the site of origin is frequently conjectural. Smaller nerve and chiasmal tumors are visually distinct from the hypothalamus, and their site of origin is more clear-cut. From the point of view of differential diagnosis, these smaller tumors can be difficult to distinguish from optic neuritis, which can also cause optic nerve enlargement. The clinical history is important in these cases (neuritis is painful; tumor is not), and, if necessary, interval follow-up of neuritis will demonstrate resolution of optic nerve swelling.

On T1-weighted images, the tumors are most often isointense, while on T2-weighted images, they are moderately hyperintense. Calcification and hemorrhage are not features of these gliomas, but cysts are seen, particularly in the larger hypothalamic tumors. Contrast enhancement occurs in about half of all cases. Because of the tumor's known propensity to invade the brain along the optic radiations, T2-weighted images of the entire brain are necessary. This pattern of tumor extension is readily evident as hyperintensity on the T2-weighted image; however, patients with neurofibromatosis (NF) present a problem in differential diagnosis. This relates to a high incidence of benign cerebral hamartomas and atypical glial cell rests in NF that can exactly mimic glioma. These both appear as areas of high signal intensity on T2-weighted images within the optic radiations. Lack of interval growth and possibly the absence of contrast

enhancement are more supportive of a diagnosis of hamartoma while enhancement suggests glioma.

Metastases

Symptomatic metastases to the pituitary gland are found in 1–5 % of cancer patients. These are primarily patients with advanced, disseminated malignancy, particularly breast and bronchogenic carcinoma. The vast majority will succumb to their underlying disease before becoming symptomatic of pituitary disease. Autopsy series have demonstrated a much higher incidence, but these by and large are small and asymptomatic lesions. Intrasellar and juxtasellar metastases arise by hematogenous seeding to the pituitary gland and stalk, by CSF seeding, and by direct extension from head and neck neoplasms. There are no distinctive MRI characteristics of metastases, although infundibular involvement is common, and bone destruction is a prominent feature of lesions that involve skull base. Occasionally, leptomeningeal enhancement of posterior fossa sulci may be visualized on the postcontrast images which lends credence to the diagnosis in those cases of CSF tumor seeding, although this finding also invokes the differential diagnosis of sarcoidosis and tuberculosis.

Infections

Infection in the suprasellar cistern and cavernous sinuses is usually part of a disseminated process or occurs by means of intracranial extension of an extracranial infection. The basal meninges in and around the suprasellar cistern are susceptible to tuberculous and other forms of granulomatous meningitis. The cistern may also be the site of parasitic cysts, in particular (racemose and subarachnoid) neurocysticercosis. In infections of the cavernous sinus, many of which are accompanied by thrombophlebitis, the imaging findings on CT and MRI consist of a convex lateral contour to the affected cavernous sinus with evidence of a filling defect after contrast administration. The intracavernous portion of the internal carotid artery may also be narrowed secondary to surrounding inflammatory change.

Infections of the pituitary gland itself are uncommon. Direct viral infection of the hypophysis has never been established and bacterial infections are unusual. There has been speculation that cases of acquired diabetes insipidus may be the result of a select viral infection of the hypothalamic supraoptic and paraventricular nuclei. Tuberculosis and syphilis, previously encountered in this region because of the higher general prevalence of these diseases in the population, are now uncommon. Gram-positive cocci are the most frequently identified organisms in pituitary abscesses. Pituitary abscesses usually occur in the presence of other sellar masses such as pituitary adenomas, Rathke's cleft cysts, and craniopharyngiomas, indicating that these mass lesions function as predisposing factors to infection.

There are a few reports on CT of pituitary abscesses. These indicate that the lesion is similar in appearance to an adenoma. As a result of the frequent coincidental occurrence of abscesses with adenomas, and because of their common clinical presentations, the correct preoperative diagnosis of abscess is difficult and rarely made. Noncontrast MRI demonstrates a sellar mass indistinguishable from an adenoma. With intravenous administration of contrast medium, there is rim enhancement of the mass with persistence of low intensity in the center. Occasionally, pituitary abscesses are unrelated to primary pituitary lesions. In these cases, erosion of the bony sella from an aggressive sphenoid sinusitis may be the route of infection.

Noninfectious Inflammatory Lesions

Lymphocytic hypophysitis is a rare, noninfectious inflammatory disorder of the pituitary gland. It occurs almost exclusively in women and particularly during late pregnancy or in the postpartum period. The diagnosis should be considered in a peripartum patient with a pituitary mass, particularly when the degree of hypopituitarism is greater than that expected from the size of the mass. It is believed that, if untreated, the disease results in panhypopituitarism. Clinically, the patient complains of headache, visual loss, failure to resume menses, inability to lactate, or some combination thereof. Pituitary hormone levels are depressed. CT and MRI demonstrate diffuse enlargement of the anterior lobe without evidence of any focal abnormality or change in internal characteristics of the gland. The distinction between simple pituitary hyperplasia and lymphocytic hypophysitis may be difficult on MRI alone.

Sarcoid afflicting the hypothalamic–pituitary axis usually manifests itself clinically as diabetes insipidus or occasionally as a deficiency of one or more anterior lobe hormones. Low signal intensity on T2-weighted images is one finding that occurs in sarcoid with some frequency, but rarely in other diseases, with few exceptions (other granulomatous inflammatory diseases, lymphoma, some meningiomas). This low-signal finding may aid in differential diagnosis. Also, the presence of multiple, scattered intraparenchymal brain lesions should raise the possibility of the diagnosis, as should diffuse or multifocal lesions of the basal meninges. The latter are best defined on coronal contrast-enhanced T1-weighted images.

Tolosa–Hunt syndrome (THS) refers to a painful ophthalmoplegia caused by an inflammatory lesion of the cavernous sinus that is responsive to steroid therapy. Pathologically, the

process is similar to orbital pseudotumor. Imaging in this disorder is often normal or may show subtle findings such as asymmetric enlargement of the cavernous sinus, enhancement of the prepontine cistern, or abnormal soft tissue density in the orbital apex. The lesion resolves promptly with steroid therapy. Hypointensity on T2-weighted images may be observed; since this observation is uncommon in all but a few other diseases (e.g., meningioma, lymphoma, and sarcoid), it may be helpful in diagnosis. Clinical history allows further precision in differential diagnosis: meningioma does not respond to steroids while lymphoma and sarcoid have evidence of disease elsewhere in almost all cases.

Vascular Lesions

Saccular aneurysms in the sella turcica and parasellar area arise from either the cavernous sinus portion of the carotid artery or its supraclinoid segment. These are extremely important lesions to identify correctly. Confusion with a solid tumor can lead to surgical catastrophes. Fortunately, their MRI appearance is distinctive and easily appreciated. Aneurysms are well defined and lack any internal signal on spin-echo (SE) images, the so-called signal void created by rapidly flowing blood. This blood flow may also cause substantial artifacts on the image, usually manifest as multiple ghosts in the phase-encoding direction, and in itself is a useful diagnostic sign.

Thrombus in the aneurysm lumen fundamentally alters these characteristics, the clot usually appearing as multilamellated high signal on T1-weighted SE images, partially or completely filling the lumen. Hemosiderin from superficial siderosis may be visible in the adjacent brain, evident as a rim of low signal intensity on T2-weighted SE images or on gradient-echo (GE) or susceptibility-weighted images. If confusion exists as to the vascular nature of these lesions, MR or CT angiography is used to confirm the diagnosis, define the neck of the aneurysm, and establish the relationship of the aneurysm to the major vessels.

Carotid cavernous fistulas are abnormal communications between the carotid artery and cavernous sinus. Most cases are due to trauma; less frequently they are "spontaneous." These spontaneous cases are due to a variety of abnormalities, including atherosclerotic degeneration of the arterial wall, congenital defects in the media, or rupture of an internal carotid aneurysm within the cavernous sinus. Dural arteriovenous malformations (AVMs) of the cavernous sinus are another form of abnormal arteriovenous (AV) communication in this region.

On MRI, the dilatation of the venous structures, in particular the ophthalmic vein and cavernous sinus, is usually clearly visible. The intercavernous venous channels dilate in both direct and indirect carotid cavernous fistulas and may also be seen on MR images. Furthermore, the internal character of the cavernous sinus is altered; definite flow channels become evident secondary to the arterial rates of flow within the sinus. The fistulous communication itself is most often occult on MRI. The pituitary gland has been noted to be prominent in cases of dural arteriovenous fistula without evidence of endocrine dysfunction. The exact mechanism of pituitary enlargement is not known; however, venous congestion is a postulated cause.

Cavernous hemangiomas are acquired lesions and not true malformations. However, there have been reports of extra-axial cavernous hemangiomas occurring in the suprasellar cistern. Of importance is that one of these hemangiomas did not have the features usually associated with, and so highly characteristic of, cavernous hemangiomas in the brain. The atypical appearance of extra-axial cavernous hemangiomas indicates that some caution must be exercised in the differential diagnosis of parasellar masses, because even though cavernous hemangiomas in this location are rare, failure of the surgeon to appreciate their vascular nature can lead to unanticipated hemorrhage. Cavernous hemangiomas should at least be considered in the differential diagnosis of solid, suprasellar masses that do not have the classic features of more common lesions, in particular craniopharyngiomas or meningiomas. Furthermore, T2-weighted images should be a routine part of the MRI protocol for suprasellar masses because visualization of a peripheral dark rim may be the only sign of the nature of the lesion.

Other vascular abnormalities of the sella include unilateral tortuous or bilateral "kissing" internal carotid arteries and medial trigeminal artery. While the former are relatively straightforward on imaging, the medial trigeminal artery is worth remembering. Much like with the intrasellar aneurysm, with the medial trigeminal artery, neurosurgical catastrophes can occur if the presence of an intrasellar artery is not identified. This artery will arise from the medial aspect of the cavernous carotid artery and will course directly posteriorly through the gland and through the dorsum sellae to reach the basilar artery. Approximately 40 % of trigeminal arteries arise medially. In addition, patients with trigeminal arteries are at increased risk of associated intracranial aneurysm. Finally, congenital absence of the internal carotid artery and asymmetric pneumatization of the sphenoid and sella can pose confusing images.

Other Conditions

Many other lesions may involve the sella turcica and parasellar region. These include mass lesions such as germinoma, epidermoid, dermoid, teratoma, schwannoma, chordoma, ecchordosis, choristoma, arachnoid cyst, hamartoma, and Langerhans cell histiocytosis. Also, there are several important metabolic conditions that may cause pituitary dysfunction or MRI-observable abnormalities in and around the

sella. These include diabetes insipidus, growth hormone deficiency, hemochromatosis, hypermagnesemia, and hypothyroidism. Space limitations preclude their further discussion in this synopsis.

Finally, not all that seems abnormal is indeed abnormal: specifically, two normal, physiologic conditions can be seen on MR imaging of the pituitary that should be kept in mind. First, during the initial 7 weeks of life, all pituitary glands exhibit hyperintensity of the adenohypophysis. This should not be interpreted as abnormal. After 7 weeks, the pituitary will assume its normal appearance, as at this time, maternal and fetal mechanisms will have subsided. Second, the gland in girls and young women is commonly enlarged with menarche and often through the teen years. This, too, is a normal phenomenon, a sort of hyperplasia. Occasionally, heterogeneity of enhancement may be seen and may suggest underlying pathology. Wisdom calls for the absence of haste in diagnosing potential surgical conditions in this age group, as follow-up examinations may prove normal.

Suggested Reading

Bonneville JF, Cattin F, Gorczyca W, Hardy J (1993) Pituitary microadenomas: early enhancement with dynamic CT-implications of arterial blood supply and potential importance. Radiology 187: 857–861

Dietemann JL, Portha C, Cattin F, Mollet E, Bonneville JF (1983) CT follow-up of microprolactinomas during bromocriptine-induced pregnancy. Neuroradiology 25:133

Kucharczyk W, Peck WW, Kelly WM, Norman D, Newton TH (1987) Rathke cleft cysts: CT, MR imaging and pathologic features. Radiology 165:491–495

Lum C, Kucharczyk W, Montanera WJ (2002) The sella turcica and parasellar region. In: Atlas SW (ed) MRI of the brain and spine, 3rd edn. Lippincott Williams & Wilkins, Philadelphia

Lundin P, Bergström K, Nyman R, Lundberg PO, Muhr C (1992) Macroprolactinomas: serial MR imaging in long term bromocriptine therapy. AJNR Am J Neuroradiol 13:1279–1291

Manara R, Maffei P, Citton V et al (2011) Increased rate of intracranial saccular aneurysms in acromegaly: an MR angiography study and review of the literature. J Clin Endocrinol Metab 96(5):1292–1757

Nagahata M, Hosoya T, Kayama T, Yamaguchi K (1998) Edema along the optic tract: a useful MR finding for the diagnosis of craniopharyngiomas. AJNR Am J Neuroradiol 19:1753–1757

Naylor MF, Scheithauer BW, Forbes GS, Tomlinson FH, Young WF (1995) Rathke cleft cyst: CT, MR, and pathology of 23 cases. J Comput Assist Tomogr 19(6):853–859

Oka H, Kawano N, Suwa T, Yada K, Kan S, Kameya T (1994) Radiological study of symptomatic Rathke's cleft cysts. Neurosurgery 35(4):632–636

Steiner E, Knosp E, Herold CJ et al (1992) Pituitary adenomas: findings of postoperative MR imaging. Radiology 185:521–527

Teramoto A, Hirakawa K, Sanno N, Osamura Y (1994) Incidental pituitary lesions in 1,000 unselected autopsy specimens. Radiology 193:161–164

Voelker J, Campbell R, Muller J (1991) Clinical, radiographic, and pathological features of symptomatic Rathke's cleft cysts. J Neurosurg 74:535–544

Diseases of the Temporal Bone

Jan W. Casselman and Timothy John Beale

Imaging of the Temporal Bone Anatomy

High-resolution CT is best suited to look at the external and middle ear but can also provide information about 'the inner ear'. For many years multi-detector CT (MDCT) was the method of choice [1, 2], but recently high-end cone beam CT (CBCT) started to challenge MDCT. CBCT not only provides similar information at a substantially lower dose but high-end CBCTs are also able to produce images with a spatial resolution down to 125 μm. Subtle bone structures like the footplate, crura of the stapes, walls of the tympanic segment of the facial nerve canal, tegmen tympani, etc. can be visualised in a more reliable way at this resolution and open possibilities to more accurately depict pathology associated with these structures. An additional advantage is that images can be displayed in any plane without quality loss which is not the case on reformatted MDCT images. Therefore the difference between MDCT and CBCT even becomes more obvious on coronal or double-oblique images.

The inner ear is best studied on T2-weighted gradient-echo (CISS) or turbo spin-echo driven equilibrium (DRIVE), three dimensional turbo spin-echo (3D TSE), fast imaging employing steady state acquisition (FIESTA) MR images. The intralabyrinthine fluid can be seen as high signal intensity on these images, and the bony (modiolus and bony septa) and membranous (soft-tissue structures or membranes) have a low signal intensity on these images making it possible to distinguish, for instance, the scala tympani and scala vestibuli. For the same reasons, the facial nerve and the three-end branches of the cochleovestibular nerve can be distinguished in the fundus of the internal auditory canal (IAC) [3]. Even smaller structures like the macula utriculi, the ganglion of Scarpa and the posterior ampullar nerve can be visualised when the spatial resolution is high enough (0.3 × 0.3 × 0.7 mm, with the overlapping slices of 0.7 mm made every 0.35 mm) (Fig. 1).

The cause of deafness can also be located along the auditory pathway, and this can only be depicted on MR images. MR is able to visualise lesion at the level of the cochlear nuclei, trapezoid body, lateral lemniscus, inferior colliculus, medial geniculate body and auditory cortex [4]. The myelinated structures of the auditory and vestibular pathway can be seen as low signal intensity structures on multi-echo sequences like m-FFE, MEDIC and MERGE.

Choice Between CT and MR Depends on Clinical Presentation

CT is the preferred technique in patients with conductive hearing loss (CHL), and MR is the modality of choice in case of sensorineural hearing loss (SNHL), vertigo or tinnitus. However, both techniques can often contribute as is the case in trauma of the inner ear or cholesteatoma of the middle ear.

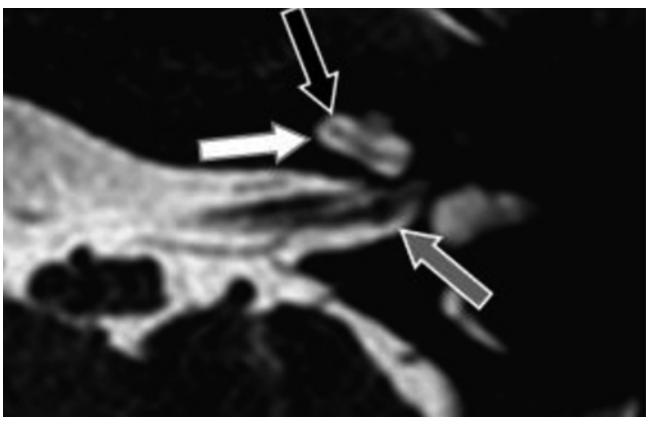

Fig. 1 3.0 T 0.7 mm thick DRIVE image with an in-plane resolution of 0.3×0.3 mm showing ganglion of Scarpa located on the superior vestibular branch of the VIIIth nerve (*grey arrow*). The separation in scala vestibuli (*black arrow*) and tympani (*white arrow*) inside the cochlea can also be seen

J.W. Casselman, MD, PhD (✉)
Radiology and Medical Imaging, AZ St-Jan Brugge-Oostende AV, Campus Bruges, Bruges, Belgium
e-mail: jan.casselman@azsintjan.be

T.J. Beale
Imaging Department, University College London, London, UK
e-mail: tim.beale@uclh.nhs.uk

J. Hodler et al. (eds.), *Diseases of the Brain, Head and Neck, Spine 2016–2019: Diagnostic Imaging*, DOI 10.1007/978-3-319-30081-8_17

In the paragraphs below, the value of CT and MR in the diagnosis of the most frequent diseases of the temporal bone will be discussed.

Pathology

Congenital External and Middle Ear Malformations

The embryology of the middle and external ear is linked, and this explains why external and middle ear malformations often occur together. In case of external auditory canal 'fibrous' or 'osseous' atresia, the middle ear cannot be evaluated by the ear surgeons, and in these cases they even totally depend on the imaging findings. In case of congenital CHL, it is crucial for the surgeons to know which ossicles or parts of the ossicles are present and available for the reconstruction of a functioning ossicular chain and whether the round and oval windows are open [5, 6]. Subtle malformations of the stapes, footplate and oval window can be the cause of congenital CHL and are today visualised in a more reliable way on high-resolution 125 μm cone beam CT images (Fig. 2). The course of the facial nerve will often shift anteriorly in the presence of external and middle ear malformations. Therefore one of the major tasks of the radiologist is to warn the surgeon for an abnormal course of the facial nerve which can be running through the middle, can split in two or more branches at the level of the mastoid segment of the nerve, etc. An abnormal course of the facial nerve and also a dehiscence of the facial nerve canal can be better visualised since high-resolution 125 μm CBCT is available.

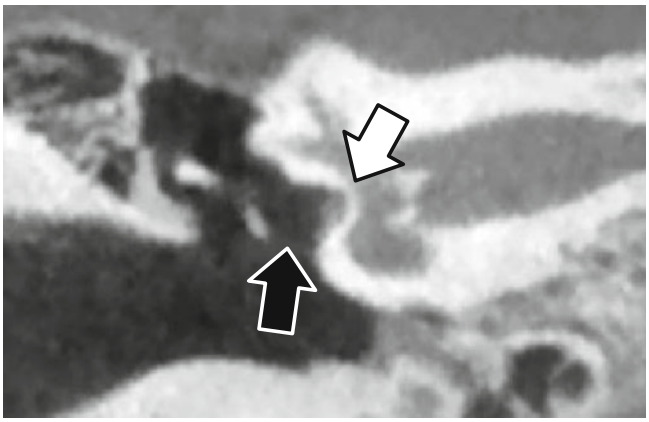

Fig. 2 Congenital conductive hearing loss caused by absent stapes (*black arrow*) and a thickened oval window or footplate (*white arrow*). Notice that the facial nerve is lying over the closed oval window and descended from its normal position under the lateral semicircular canal

Trauma

Longitudinal fractures along the long axis and transverse fractures perpendicular on the long axis of the temporal bone are best depicted on CT images with bone window settings. Longitudinal fractures most often run through the middle ear where they can cause fractures or luxation of the ossicles (Fig. 3a) and resulting CHL and they often end at the level of the geniculate ganglion where they can be at the origin of facial nerve palsy. Although CT remains the initial imaging technique in trauma of the temporal bone, [7] MR must be considered when the post-traumatic SNHL remains unexplained on CT.

Post-traumatic intralabyrinthine haemorrhage or inner ear concussion is best seen on unenhanced T1-weighted images (Fig. 3b) (DRIVE, CISS, 3D TSE, FIESTA). The high signal intensity of the fluid will disappear in case of fibrosis or cloth formation, and this is best seen on heavily T2-weighted images of the inner ear like CISS, 3D TSE, DRIVE, FIESTA, etc. However when the fluid is mixed with fresh blood, it can retain its normal high signal intensity for some time.

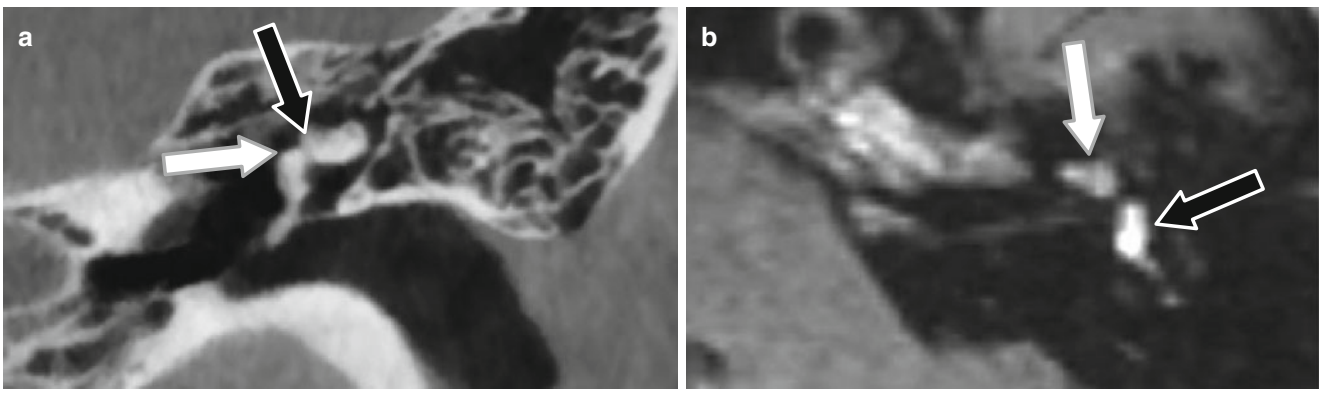

Fig. 3 (**a**) Cone beam CT. Coronal image showing an incudo-mallear luxation malleus (*white arrow*), incus (*black arrow*). (**b**): Axial unenhanced T1-weighted image showing high signal intensity blood in the labyrinth: labyrinthine concussion cochlea (*white arrow*), vestibule (*black arrow*)

Meningoceles or encephaloceles can be the result of tegmen fractures and can be distinguished from middle ear blood or inflammation on MR images [8].

Trauma to the brainstem and auditory pathways and cortex can also be the cause of SNHL or deafness. In case of haemorrhagic concussion the most frequently involved structures of the auditory pathways are the inferior colliculi and the auditory cortex. CT sometimes remains normal in patients with post-traumatic facial nerve palsy. In these patients the labyrinthine segment of the facial nerve should be checked. The labyrinthine segment occupies 95 % of the available space of the canal. Therefore post-traumatic concussion and resulting retrograde oedema can easily cause ischaemia and secondary necrosis of the labyrinthine segment itself as there is no remaining space for swelling. This can be seen as enhancement of the labyrinthine segment and enhancement near the fundus of the internal auditory canal, which is always abnormal [9]. In such a case, decompression of the nerve should be considered in order to save the facial nerve function.

Otosclerosis

The dense ivory-like endochondral bone layer around the labyrinthine capsule is replaced by foci of spongy vascular irregular new bone and causes mixed hearing loss in otosclerosis patients. Otosclerosis/otospongiosis can be fenestral and retrofenestral.

Fenestral otosclerosis is in the first place causing CHL, and hypodensities or even hypodense masses can be found on the promontory, near the facial nerve canal and close to the oval and round window. The fissula ante fenestram, just anterior to the footplate, is most frequently involved. At the level of the oval window, the footplate can be thickened, or the anterior crus of the stapes can be fixed or overgrown by otospongiosis so that the stapes can no longer move freely. This can explain the CHL in these patients. Subtle otospongiosis lesions near the footplate cannot be visualised in a strict axial or coronal plane as the footplate is angled in space. Only high-resolution double-oblique reformatted images can visualise both branches of the stapes and the footplate in one plane (Fig. 4). These double-oblique images can only be acquired when 0.1-mm thick reformatted MDCT or high-resolution 0.125 mm CBCT images are used. Successful surgery in otosclerosis is only possible when the round window is still (partially) open, and therefore these structures should always be checked preoperatively.

Retrofenestral otosclerosis is predominantly responsible for the SNHL component of the mixed hearing loss and involves the bone around the membranous labyrinth, most frequently around the cochlea. In severe case a hypodense ring can develop around the complete cochlea, but retrofenestral otosclerosis can also be limited to a small hypodense spur anterior to the antero-inferior wall of the fundus of the internal auditory canal [10, 11].

Chronic Middle Ear Inflammation

Retraction and thickening of the drum and disturbed middle ear aeration are the hallmarks of chronic middle ear inflammation. Other signs are mucosal thickening, replacement of the middle ear aeration by fluid and/or glue-like thickened material, demineralisation of the ossicles, luxation of the ossicles by inflammatory tractions, etc. However, clear destruction or displacement of the ossicles is not seen. The middle ear inflammation often follows pre-existing structures like the plicae and ligaments which form the tympanic diaphragm. This explains why the inflammation will stop at these structures and is visible as a straight barrier with the aerated part of the rest of the middle ear, a sign confirming that one is dealing with inflammation and not cholesteatoma. In completely non-aerated middle ears and mastoids, the differential diagnosis becomes more tricky as a small

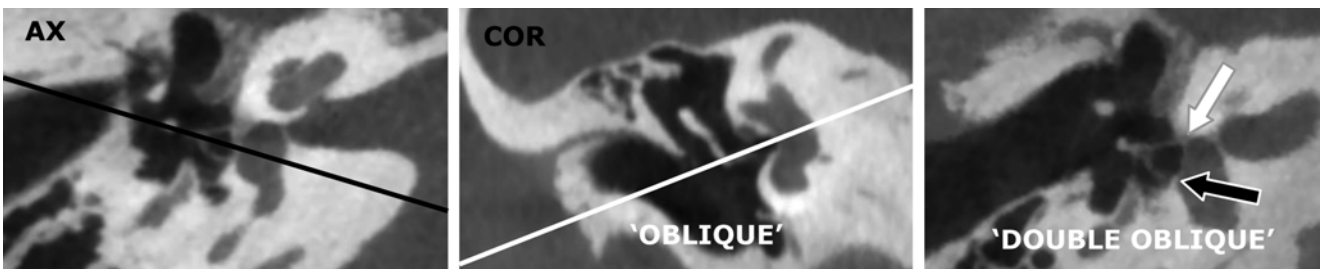

Fig. 4 The only reliable way to evaluate fenestral otosclerosis is the double-oblique technique. Para-coronal images are made on the axial image through the incudostapedial joint and perpendicular on the footplate (*black line*). Then double-oblique images are produced when reconstructions are made parallel to the incudostapedial junction on the para-coronal '*oblique*' images (*white line*). The resulting *double-oblique* images show the subtle otospongiosis at the fissula ante fenestram (*white arrow*), fixing the anterior branch of the stapes and the posterior otosclerotic footplate plaque (*black arrow*), narrowing the footplate opening

cholesteatoma can be hidden somewhere in the inflammation. In order to exclude a cholesteatoma, one should exclude displacement or erosion/destruction of the ossicles and erosion or destruction of the bony septa and/or middle ear, antrum and mastoid walls.

Finally one is dealing with tympanosclerosis (Fig. 5) when the thickened drum or inflammatory tissue in the middle ear is calcified. It is clear that CT is the imaging technique of choice to depict these middle ear changes in a reliable way.

Cholesteatoma

Cholesteatoma develops when ectoderm tissue gets trapped in the middle or inner ear (during embryology or later in life) and consists of a sac lined by keratinising stratified squamous epithelium. The diagnosis of a cholesteatoma is made when a convex soft-tissue mass is seen in the middle ear; when the ossicles are displaced, eroded and destroyed; when tympanic wall structures like the lateral wall and tegmen are eroded and destroyed; and when the scutum is amputated. The soft-tissue lesion itself will only be visible when it is surrounded by normal middle ear aeration. There is suspicion for a cholesteatoma when only one side of the lesion is convex, and the probability of a cholesteatoma becomes very high when it is completely convex. However it becomes often impossible to distinguish post-surgery changes, inflammation (recurrent), cholesteatoma, etc. when the middle ear and mastoid are completely non-aerated. This even becomes more difficult in a postoperative ear where landmarks as the integrity of the ossicles and walls of the middle ear cavity can no longer be used.

This explains why MR is today replacing CT in the diagnosis and follow-up of cholesteatoma patients. Cholesteatoma has specific signal intensities on MR: high signal intensity on T2, low signal intensity on unenhanced T1, low signal intensity on Gd-enhanced T1 but with a thin rim of enhancement around the lesion and a very high signal intensity on non-echoplanar diffusion-weighted MR images (b = 1000). Even in a completely non-aerated middle ear, the diagnosis can now be made on MR. The very high signal on echo-planar imaging diffusion-weighted imaging (non-EPI DWI) images is most specific and even allows differentiation with cholesterol granuloma and inflammation which both have a low signal intensity on non-EPI DWI. Calculated ADC maps should always be used to confirm the diagnosis as only cholesteatoma has a low signal on ADC images. It goes without saying that this technique is even more valuable in the postoperative ear and has provided us for the first time with a reliable imaging technique to rule out recurrent or residual cholesteatoma. The result is that expensive, time-consuming and for the patient unpleasant routine second-look surgery could be abolished. Partial volume still poses a problem as it is difficult to acquire diffusion-weighted MR images with a slice thickness below 2–3 mm. As a consequence very small recurrences can still be overlooked. On the other hand, there are no false positives on the non-EPI DWI MR images, which means that when a high signal is present on the b-1000 images, a cholesteatoma will be found (Fig. 6). The remaining role of CT and especially low-dose CBCT is now to provide the surgeon with a preoperative road map once a cholesteatoma or residual/recurrent cholesteatoma is found on MR [12–14].

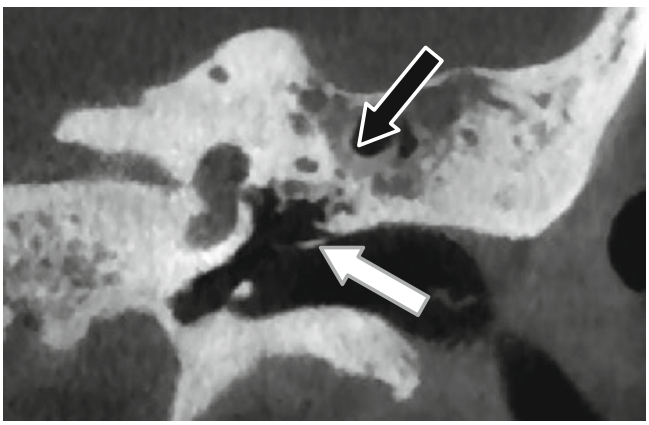

Fig. 5 Coronal cone beam CT image. Tympanosclerosis with perforation and calcification of the drum (*white arrow*) and calcifications in non-aerated part of the antrum (*black arrow*)

Cochleovestibular Schwannoma

Cochleovestibular schwannomas (CVS) are the most frequent tumours found inside the IAC and cerebellopontine angle, and the most frequent symptoms at presentation are SNHL, vertigo and tinnitus [15]. Gd-enhanced T1-weighted images are the most sensitive images to detect them. Although many of these schwannomas can also be seen on submillimetric T2-weighted images, gadolinium (Gd) administration is still needed as a schwannoma cannot be distinguished from a normal ganglion of Scarpa on these T2-weighted images, and many CVS start in the ganglion of Scarpa [16].

Once a CVS is found, the most important task of the radiologist is to exclude contralateral pathology. The detection of a contralateral schwannoma or other important middle and inner ear pathology will make the surgeon much more reluctant to remove the initially detected schwannoma. Removal of the initial schwannoma can result in a deaf ear, a risk the surgeon will not likely take when he is aware that the presence of a contralateral schwannoma or even intralabyrinthine schwannoma [17] or other middle/inner ear pathology can eventually result in bilateral deafness. In these patients the

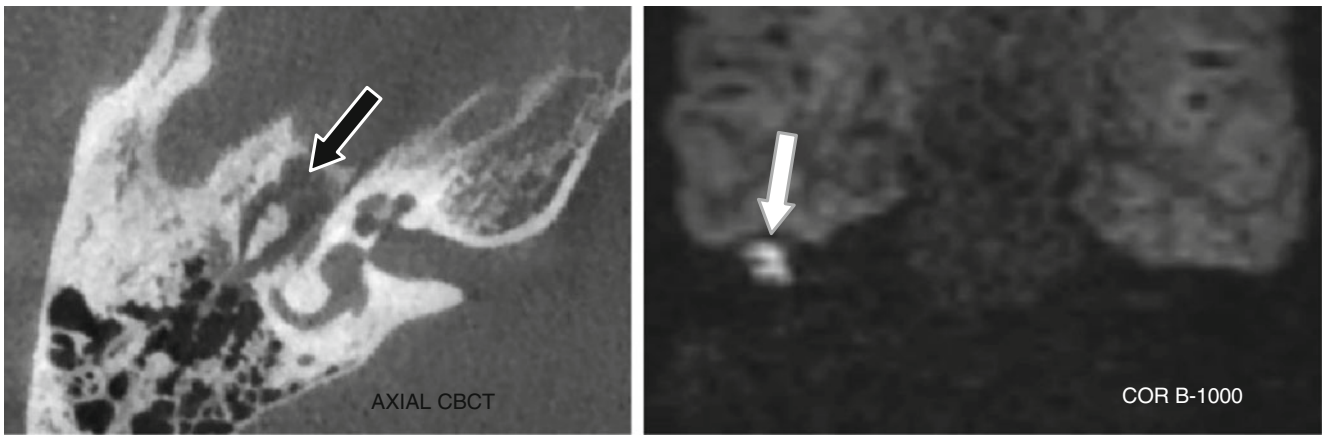

Fig. 6 *Axial CBCT* showing a completely non-aerated middle ear; a cholesteatoma cannot be ruled out. A cholesteatoma can be seen on the *B-1000* non-EPI DWI image (*white arrow*) and corresponded with the non-aerated region in the pro-epitympanum on CBCT (*black arrow*)

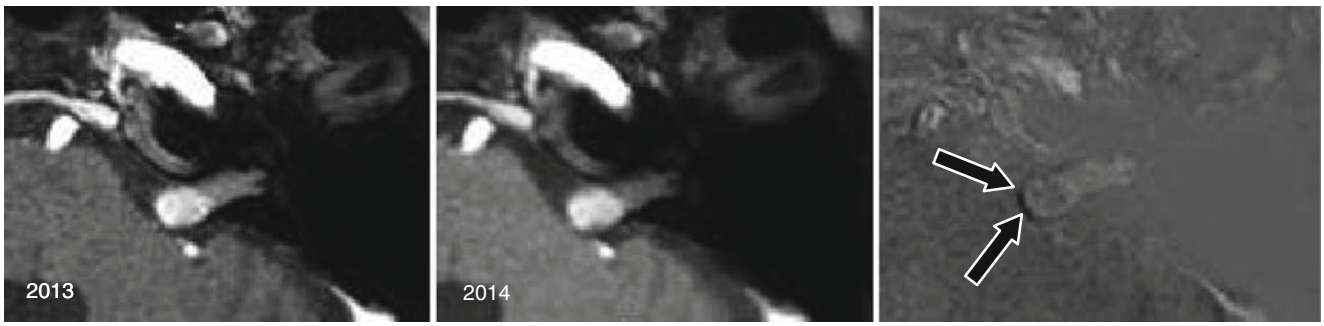

Fig. 7 Gadolinium-enhanced axial 0.6-mm thick GE T2-weighted image made in *2013* and *2014* shows a schwannoma on the left side. Volume measurements showed no growth; however subtle growth towards the cerebellopontine angle could be seen as a black rim on the subtraction images (*black arrows*)

surgeon will prefer to "follow-up and scan" until there is an important reason to remove one of the lesions.

The most important reason to remove a CVS is when it grows, and therefore its 'growth potential' must be assessed. High-resolution submillimetric T1-weighted gradient-echo images (e.g. 3DFT-MPRAGE) are best suited and can be used for volume measurements. In the first year, the follow-up studies should be acquired every 6 months and subsequently annually in case the schwannoma is not growing fast. Image subtraction is today the most sensitive technique to detect CVS growth (Fig. 7).

Submillimetric T2-weighted images are also best suited to predict whether hearing preservation surgery will be successful or not. The absence of fluid between the schwannoma and the base of the cochlea and the decrease of the signal intensity of the intralabyrinthine fluid are two bad indicators for hearing preservation [18, 19]. Hence, in such a case, the less invasive translabyrinthine approach is chosen. However, when MR indicates that hearing preservation is possible, then the surgeon will go for a suboccipital or middle cranial fossa approach.

Labyrinthitis

The calcifications in end-stage ossifying labyrinthitis are only visible on CT, while the intralabyrinthine enhancement in acute labyrinthitis (Gd enhancement) and fibrosis formation in subacute labyrinthitis are only detectable on MR (Fig. 8). In the latter case, it is not possible to distinguish fibrosis from calcifications on T2-weighted TSE or GE images. Therefore both MR and CT should be used to study patients with labyrinthitis.

Gd enhancement can be seen in viral labyrinthitis, and fibrosis formation or calcification only rarely occurs in these patients. On the contrary, fibrosis can develop quickly, and calcification can already appear in 3–4-week time in patients with bacterial meningitis (e.g. pneumococcus or meningococcus). Meningitis is more frequent in children and can result in complete deafness when both ears are affected. Urgent MR and CT imaging is needed in these children so that the surgeon has an idea about the cochlear fibrosis and/or calcification. Depending on the imaging results, the surgeon will be able to decide whether a cochlear implant can

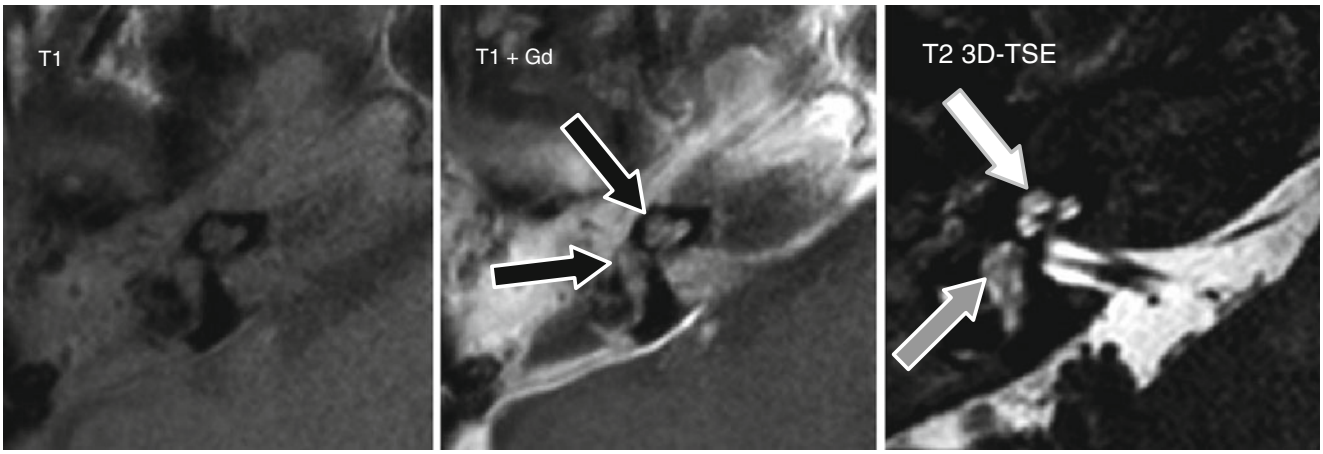

Fig. 8 Middle ear infection with secondary labyrinthitis. Low signal intensity is seen in the labyrinth on the unenhanced image. Clear enhancement is seen in the cochlea and labyrinth after intravenous Gd administration, confirming the presence of acute labyrinthitis (*black arrows*). The *T2* image shows normal fluid in the cochlea (*white arrow*), while the signal in the vestibule decreased, confirming vestibular fibrosis formation (*grey arrow*)

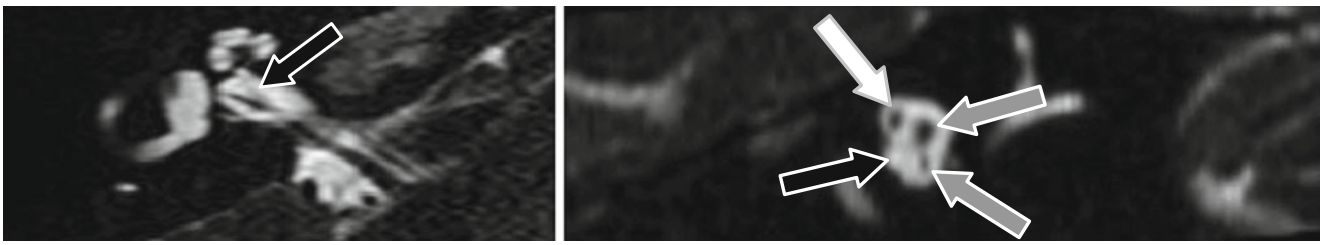

Fig. 9 Axial- and parasagittal-reformatted image through the fundus of the right internal auditory canal. The cochlear branch is absent (*black arrows*) and there is no connection with the otherwise normal cochlea. Notice the normal facial nerve (*white arrow*) and superior and inferior vestibular branches (*grey arrows*) on the parasagittal image

be installed or not and this before complete calcification sets in and makes cochlear implantation impossible. Anaesthesia is needed to examine young children, and to avoid the risks of a second anaesthesia, it is wise to perform CT and MR during the same initial imaging session [11, 20, 21].

Congenital Inner Ear Malformations

Congenital malformations of the inner ear are best studied on MR although the bony malformations can also be seen on CT. Subtle changes inside the cochlea like the absence or incomplete development of the inter- or intrascalar separations and the presence of normal fluid inside the cochlea can only be evaluated on MR. These patients present with congenital SNHL or deafness and are today best classified by using the Sennaroglu classification. A large vestibular aqueduct (CT) or enlarged endolymphatic duct and sac (MR) is the most frequent inner ear malformation. The diagnosis should not be overlooked as repetitive trauma in these patients can result in complete deafness. The second most frequent malformation is a saccular lateral semicircular canal or duct, and this malformation is most often an incidental finding without any clinical consequence. The danger of a gusher ear is always present in patients with congenital inner ear malformations. In a gusher ear, the CSF pressure is transmitted to the perilymph by defects at the base of the cochlea or fundus of the IAC. Demonstration of such a defect, a large vestibular aqueduct or an abnormal convex shape of the angle between the labyrinthine and tympanic segment of the facial nerve should warn the surgeon; however sometimes the inner ear can look completely normal on MR and CT. Surgery in such a patient will almost always result in a deaf ear and should be avoided. Finally the facial nerve can have an abnormal cause in case of inner ear malformations, and the radiologist should warn the surgeon when this is the case [5, 11, 22]! MR is also needed to demonstrate the presence of a cochleovestibular nerve or cochlear branch of the VIIIth nerve in congenital deaf cochlear implant candidates. Cochlear implantation is not possible in the absence of the VIIIth nerve or its cochlear branch (Fig. 9), and unnecessary expensive surgery and implantation can be avoided in these patients [23].

Menière's Disease: Labyrinthine Hydrops

One of the fastest growing new indications is the demonstration of endolymphatic hydrops, which is also causing the SNHL, vertigo and tinnitus in Menière's patients. The confirmation of the hydrops makes the clinicians more certain of the diagnosis, a diagnosis which is not always certain and must be confirmed when more aggressive treatment is considered. Today the hydrops can be demonstrated in a non-invasive way by using high-resolution 3D-FLAIR images made 4 h after intravenous gadolinium injection [24]. The gadolinium only has access to the perilymphatic space, and hence the scala media will remain black. This non-enhancing (black) endolymphatic utricle/saccule and scala media will enlarge in case of hydrops and will push away the surrounding enhancing perilymph in the vestibule and the enhancing perilymph in the scala vestibuli (Fig. 10).

Pathology Involving the Central Auditory Pathways

The cause of SNHL can be located along the auditory pathway, and therefore an MR study of the brainstem and auditory cortex should be performed when selective CT and MR studies of the temporal bone remain normal. Infarctions (older patients), multiple sclerosis (younger patients), trauma, tumour and inflammation located at the level of the cochlear nuclei, the trapezoid body, the lateral lemniscus, the inferior colliculus, the medial geniculate body and the auditory cortex can all cause SNHL. The SNHL will be unilateral up to the level of the cochlear nuclei and bilateral up to the level of the medial geniculate bodies, and auditory agnosia will occur when the auditory cortex gets involved. Congenital cortical pachygyria or polymicrogyria can also affect the auditory cortex and should be excluded in all cochlear implant candidates [4, 25, 26].

Tinnitus

Today patients with tinnitus can be examined in a non-invasive way using MR, with the highest sensitivity in patients with 'pulsatile' and 'objective' tinnitus. The yield is much lower in subjective and non-pulsatile tinnitus. Neurovascular conflicts near the root entry zone of the VIIIth nerve can best be recognised on gradient-echo or turbo spin-echo T2-weighted images (showing the nerves), unenhanced MRA TOF images (showing the arteries) and selective contrast-enhanced T1-weighted images (showing veins and arteries) of the temporal bone. Matching of the three sequences allows to distinguish nerves, arteries and veins in all cases. Nevertheless a neurovascular conflict is not frequently the cause of pulsatile tinnitus, and this diagnosis is often questioned. Far more frequent causes of tinnitus are paragangliomas, dural arteriovenous fistulas, idiopathic venous tinnitus and benign intracranial hypertension. Only the first two can be shown on MR.

Early venous drainage (high flow in veins) can be seen on the non-enhanced MRA TOF images in case of dural fistulas. Unenhanced and Gd-enhanced MRA TOF images are also suited to detect glomus tumours, arteriovenous malformations, aberrant vessels running through the middle ear, high or dehiscent jugular bulbs, tortuous carotid arteries near the skull base, fibromuscular dysplasia, carotid dissection, etc. Vascularised tumours like meningiomas cause a higher arte-

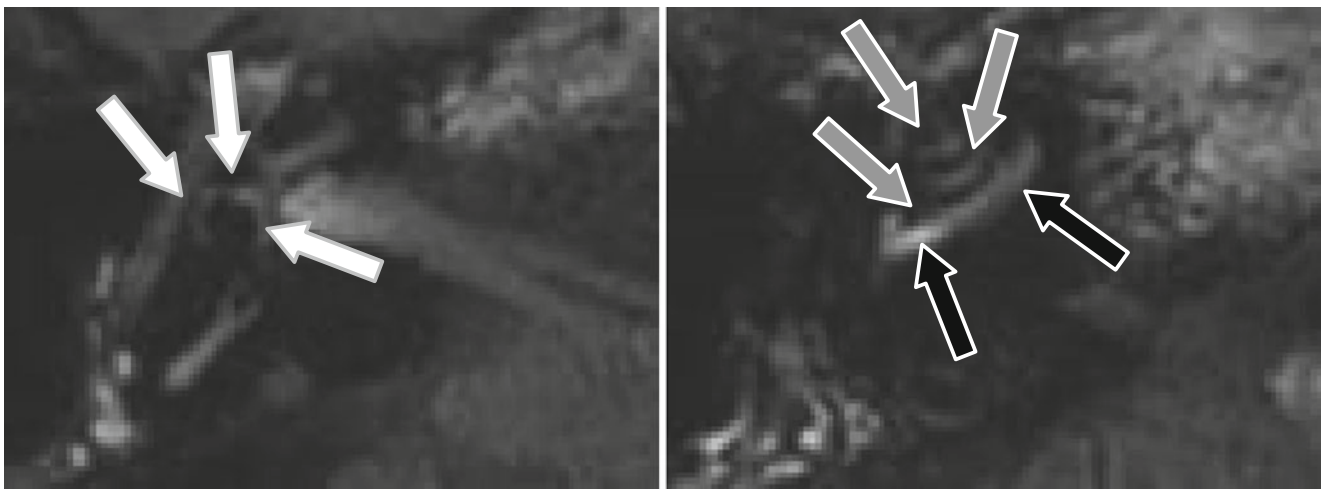

Fig. 10 Axial 3D-FLAIR images 4 h after intravenous gadolinium injection. The enlarged black saccule and utricle are confluent and compress the enhancing perilymph (*white arrows*) against the walls of the bony vestibule. The perilymph in the scala vestibuli is completely compressed by the black enlarged scala media (*grey arrows*). Normal enhancing perilymph in the scala tympani (*black arrows*) which cannot be compressed by the scala media as a bony lamina separates them

rial and venous flow in their surroundings and therefore can cause tinnitus. Hence tumours in the neighbourhood of the temporal bone must be excluded in tinnitus patients. MRA clearly became the method of first choice and detects much more causes of tinnitus than CT. However in rare cases, like Paget's disease, CT can still have its value when MRA remains negative. Today the place of angiography is limited to the treatment of tinnitus (embolisation); it will only be used for diagnostic purposes when MR and CT remain negative and the pulsatile tinnitus renders a normal life impossible [27–29].

Bibliography

1. Alexander AE, Caldemeyer KS, Rigby P (1998) Clinical and surgical application of reformatted high-resolution CT of the temporal bone. Neuroimaging Clin N Am 8:31–50
2. Nayak S (2001) Segmental anatomy of the temporal bone. Semin Ultrasound CT MR 22:184–218
3. Casselman JW, Mermuys K, Delanote J et al (2008) MRI of the cranial nerves – more than meets the eye: technical considerations and advanced anatomy. Neuroimaging Clin N Am 18:197–231
4. Casselman JW, Safronova MM (2014) Imagerie des voies auditives et vestibulaires. In: Veillon F, Casselman JW, Meriot P et al (eds) Imagerie de l'oreille et de l'os temporal. Lavoisier, Paris, pp 227–238
5. Casselman JW, Delanote J, Kuhweide R et al (2015) Congenital malformations of the temporal bone. In: Lemmerling M, De Foer B (eds) Temporal bone imaging. Springer, Berlin/Heidelberg, pp 119–154
6. Veillon F, Riehm S, Emachescu B et al (2001) Imaging of the windows of the temporal bone. Semin Ultrasound CT MR 22:271–280
7. Veillon F, Baur P, Dasch JC et al (1991) Traumatismes de l'os temporal. In: Veillon F (ed) Imagerie de l'oreille. Médecine-Sciences Flammarion, Paris, pp 243–281
8. Casselman JW, Safronova MM (2014) IRM des traumatismes de l'os temporal et des régions adjacentes. In: Veillon F, Casselman JW, Meriot P et al (eds) Imagerie de l'oreille et de l'os temporal. Lavoisier, Paris, pp 747–760
9. Sartoretti-Schefer S (1997) Gadolinium-DTPA enhanced MRI of the facial nerve in patients with posttraumatic facial nerve palsy. AJNR Am J Neuroradiol 18:1115–1125
10. Swartz JD, Harnsberger HR (1998) The otic capsule and otodystrophies. In: Swartz JD, Harnsberger HR (eds) Imaging of the temporal bone. Thieme, New York, pp 240–317
11. Casselman JW, Mark AS, Butman JA (2009) Anatomy and diseases of the temporal bone. In: Atlas S (ed) Magnetic resonance imaging of the brain and spine, 4th edn. Lippincott Williams & Wilkins a Walters Kluwer Business, Philadelphia, pp 1193–1257
12. De Foer B, Vercruysse J-P, Pouillon M et al (2007) Value of high-resolution computed tomography and magnetic resonance imaging in the detection of residual cholesteatoma in primary bony obliterated mastoids. Am J Otolaryngol 28:230–234
13. De Foer B, Vercruysse J-P, Bernaerts A et al (2010) Value of non echo-planar diffusion-weighted MR imaging versus delayed post-gadolinium T1-weighted MR imaging for the detection of middle ear cholesteatoma. Radiology 255:866–872
14. De Foer B, Nicolay S, Vercruysse JP et al (2015) Imaging of cholesteatoma. In: Lemmerling M, De Foer B (eds) Temporal bone imaging. Springer, Berlin/Heidelberg, pp 69–88
15. Juliano AFT, Maya M, Lo WW et al (2011) Temporal bone tumors and cerebellopontine angle lesions. In: Som PM, Bergeron RT (eds) Head and neck imaging, 5th edn. Mosby Inc-affiliate of Elsevier Inc, St-Louis, pp 1449–1531
16. Casselman JW, Lu CH, De Foer B et al (2014) Schwannomes du nerf vestibulocochléaire. In: Veillon F, Casselman JW, Meriot P (eds) Imagerie de l'oreille et de l'os temporal. Lavoisier, Paris, pp 921–958
17. Tieleman A, Casselman JW, Somers T et al (2008) Imaging of intralabyrinthine schwannomas: a retrospective study of 52 cases with emphasis on lesion growth. AJNR Am J Neuroradiol 29:898–905
18. Somers T, Casselman J, de Ceulaer G et al (2001) Prognostic value of MRI findings in hearing preservation surgery for vestibular schwannoma. Am J Otol 22:87–94
19. Dubrulle F, Ernst O, Vincent C et al (2000) Enhancement of the cochlear fossa in the MR evaluation of vestibular schwannoma: correlation with success at hearing preservation surgery. Radiology 215:458–462
20. Mark AS (1994) Contrast-enhanced magnetic resonance imaging of the temporal bone. Neuroimaging Clin N Am 4:561–578
21. Kenis C, De Foer B, Casselman JW (2015) Inner ear pathology. In: Lemmerling M, De Foer B (eds) Temporal bone imaging. Springer, Berlin/Heidelberg, pp 219–235
22. Casselman JW, Kuhweide R, Ampe W et al (1996) Inner ear malformations in patients with sensorineural hearing loss: detection with gradient-echo (3DFT-CISS) MR imaging. Neuroradiology 38:278–286
23. Casselman JW, Offeciers FE, Govaerts PJ et al (1997) Aplasia and hypoplasia of the vestibulocochlear nerve: diagnosis with MR imaging. Radiology 202:773–781
24. Barath K, Schuknecht B, Monge Naldi B et al (2014) Detection and grading of endolymphatic hydrops in Menière disease using MR imaging. AJNR Am J Neuroradiol 35:1387–1392
25. Deplanque D, Godefroy O, Guerouaou D et al (1998) Sudden bilateral deafness: lateral inferior pontine infarction. J Neurol Neurosurg Psychiatry 64:817–818
26. Sasaki O, Ootsuka K, Taguchi K et al (1994) Multiple sclerosis presented acute hearing loss and vertigo. ORL J Otorhinolaryngol Relat Spec 56:55–59
27. Moonis G, Lo WWM, Maya M (2011) Vascular tinnitus of the temporal bone. In: Som PM, Curtin HD (eds) Head and neck imaging, 5th edn. Mosby Inc – affiliate of Elsevier Inc, St.-Louis, pp 1409–1422
28. Swartz JD, Harnsberger HR (1998) Temporal bone vascular anatomy, anomalies, and diseases, emphasizing the clinical-radiological problem of pulsatile tinnitus. In: Swartz JD, Harnsberger HR (eds) Imaging of the temporal bone. Thieme, New-York, pp 170–239
29. Casselman JW (2014) Imagerie des acouphènes. In: Veillon F, Casselman JW, Meriot P et al (eds) Imagerie de l'oreille et de l'os temporal. Lavoisier, Paris, pp 1523–1564

Oral Cavity, Larynx, and Pharynx

Martin G. Mack and Hugh D. Curtin

Imaging of the oral cavity, the larynx, and the pharynx must be coordinated with the clinical exam [1, 2]. The information acquired at imaging usually emphasizes the deeper tissues as the superficial assessment is done by direct visualization. The description of the anatomy is key to description of any lesion.

Anatomy

Oral Cavity

The oral cavity extends from the lips and oral fissure to the oropharyngeal isthmus. It is bounded anteriorly and laterally by the lips and cheeks. The roof of the oral cavity consists of the hard and soft palate, and its floor is formed by the muscular oral floor and the structures it supports.

The tongue occupies almost all of the oral cavity when the mouth is closed, its upper surface lying against the palate. The musculature of the tongue consists of intrinsic muscles as well as extrinsic muscles that are inserted into the tongue. The posterior limit of the oral cavity is made up of the anterior tonsillar pillars and the circumvallate papillae along the dorsum of the tongue.

The floor of the mouth is inferior to the tongue. Immediately inferior to the mucosal is the sublingual gland in the sublingual pace. The mylohyoid muscle supports the floor of the mouth with the geniohyoid/genioglossal muscle complex vertically segmenting the soft tissues above the mylohyoid.

M.G. Mack
Radiologie München, Munich, Germany
e-mail: m.mack@radiologie-muenchen.de

H.D. Curtin (✉)
Department of Radiology, Massachusetts Eye and Ear Infirmary, Harvard Medical School, Boston, MA, USA
e-mail: hdcurtin@meei.harvard.edu

Pharynx

The pharynx consists of the nasopharynx, the oropharynx, and the hypopharynx.

Nasopharynx

The nasopharynx is the upper portion of the pharynx. The sphenoid bone forms the roof of the nasopharynx, while the floor and junction with the oropharynx are at the level of the soft palate. These anatomic relationships are best seen on sagittal and coronal sections. The pharyngeal recess (fossa of Rosenmüller) is a pouch-like recess in the lateral wall of the nasopharynx directed toward the parapharyngeal space and lying directly adjacent to the torus tubarius and the eustachian tube orifice. Many nasopharyngeal malignancies have their origin in the fossa.

Oropharynx

The oropharynx extends from the soft palate/uvula to the margin of the epiglottis. The palatine tonsils are located along the lateral walls of the oropharynx. The anterior and posterior pillars converge superiorly at a sharp angle to form the supratonsillar fossa. Portions of the tongue base and valleculae belong to the oropharynx. The principal superficial structures are the paired palatine tonsils.

Hypopharynx

The hypopharynx extends from the oropharynx to the supraglottic portion of the larynx. It is bounded superiorly by the free margin of the epiglottis and the lateral pharyngoepiglottic folds that form the valleculae. The left and right piriform sinuses and post-cricoid region represent the lower part of the hypopharynx.

J. Hodler et al. (eds.), *Diseases of the Brain, Head and Neck, Spine 2016–2019: Diagnostic Imaging*, DOI 10.1007/978-3-319-30081-8_18

Larynx

The larynx opens from the anterior wall of the hypopharynx and extends to the trachea.

Important Mucosal Landmarks

Several key anatomic structures are important to the radiological assessment of the larynx. Perhaps the most important relationship in the larynx is that of the false vocal fold, true vocal fold, and ventricle complex. The ventricle is a crucial reference point. Much imaging of tumors is aimed at defining the location of a lesion relative to this key landmark. Another important landmark is the upper margin cricoid cartilage. This cartilage is the only complete ring of the cartilage framework and thus is key to the integrity of the airway.

The true vocal folds (cords) play a major role in speech. The cords stretch across the lower larynx and are in the horizontal or axial plane. The small crease just above the true vocal fold is called the ventricle. Immediately above the ventricle and again parallel to both the ventricle and true fold are the false vocal folds. The mucosa curves out laterally from the false vocal folds to the upper edges of the larynx at the aryepiglottic folds.

These structures are the basis for anatomic localization within the larynx. The glottic larynx refers to the true vocal folds. The glottis has been defined as extending from the ventricle to a plane approximately 1 centimeter below the ventricle. Here, the glottis merges with the subglottis (the lower part of the larynx). The subglottis extends from the lower margin of the glottis to the inferior margin of the cricoid cartilage. Everything above the ventricle of the larynx is part of the supraglottis.

Another important anatomic term is the anterior commissure. This is the point where the true folds converge anteriorly and the vocal ligaments insert into the thyroid cartilage.

Cartilage Framework

The cartilages make up the framework of the larynx and give it structure (Fig. 1). The cricoid cartilage is the foundation of the larynx. The arytenoid cartilages perch upon the posterior edge of the cricoid at the cricoarytenoid joint. Above the cricoid is the thyroid cartilage. This shield-like cartilage provides protection to the inner workings of the larynx. The epiglottis is a fibrocartilage extending behind the thyroid cartilage in the supraglottic larynx.

In axial imaging the cartilages can help orient us to the mucosal levels in the larynx (Fig. 2). The cricoid is at the level of the glottis and subglottis. The upper posterior edge of the cricoid cartilage is actually at the level of the true folds and ventricle. The lower edge of the cricoid cartilage represents the lower boundary of the larynx and, therefore, the lower edge of the subglottis.

The arytenoid cartilage spans the ventricle. The upper arytenoid is at the level of the false fold, whereas the vocal process defines the position of the vocal ligament and, therefore, the true fold. The epiglottis is totally within the supraglottic larynx.

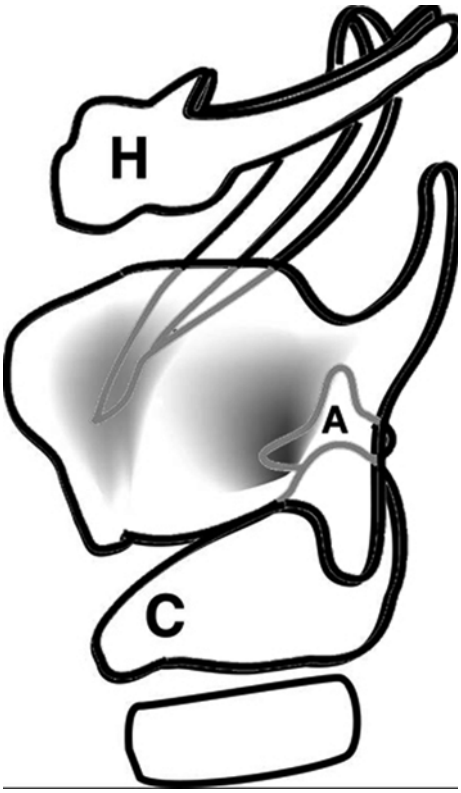

Fig. 1 Line diagram showing the relationships of larynx cartilages. The thyroid cartilage attaches to the signet-ring-shaped cricoid cartilage (*C*). The arytenoid cartilages (*A*) perch on the posterior aspect of the cricoid cartilage. The epiglottis is protected by the hyoid bone (*H*) and the thyroid cartilage

Deep Soft Tissues

Muscles There are many muscles within the larynx. The key muscle for the radiologist is the thyroarytenoid muscle. This forms the bulk of the true fold or cord and extends from the arytenoid to the anterior part of the thyroid cartilage at the anterior commissure. The radiologist should be familiar with this muscle because identifying this muscle identifies the level of the true vocal fold.

Paraglottic Space The paraglottic space refers to the major part of the soft tissue between the mucosa and the cartilaginous framework of the larynx. At the supraglottic or false fold level, the space predominantly contains fat, whereas at the level of the true fold, the paraglottic region is filled by the thyroarytenoid muscle (Fig. 2). Again, this concept is helpful in orienting one to the level within the larynx. The level of the ventricle is identified as the transition between the fat and muscle. At the level of the subglottis, the paraglottic space essentially disappears.

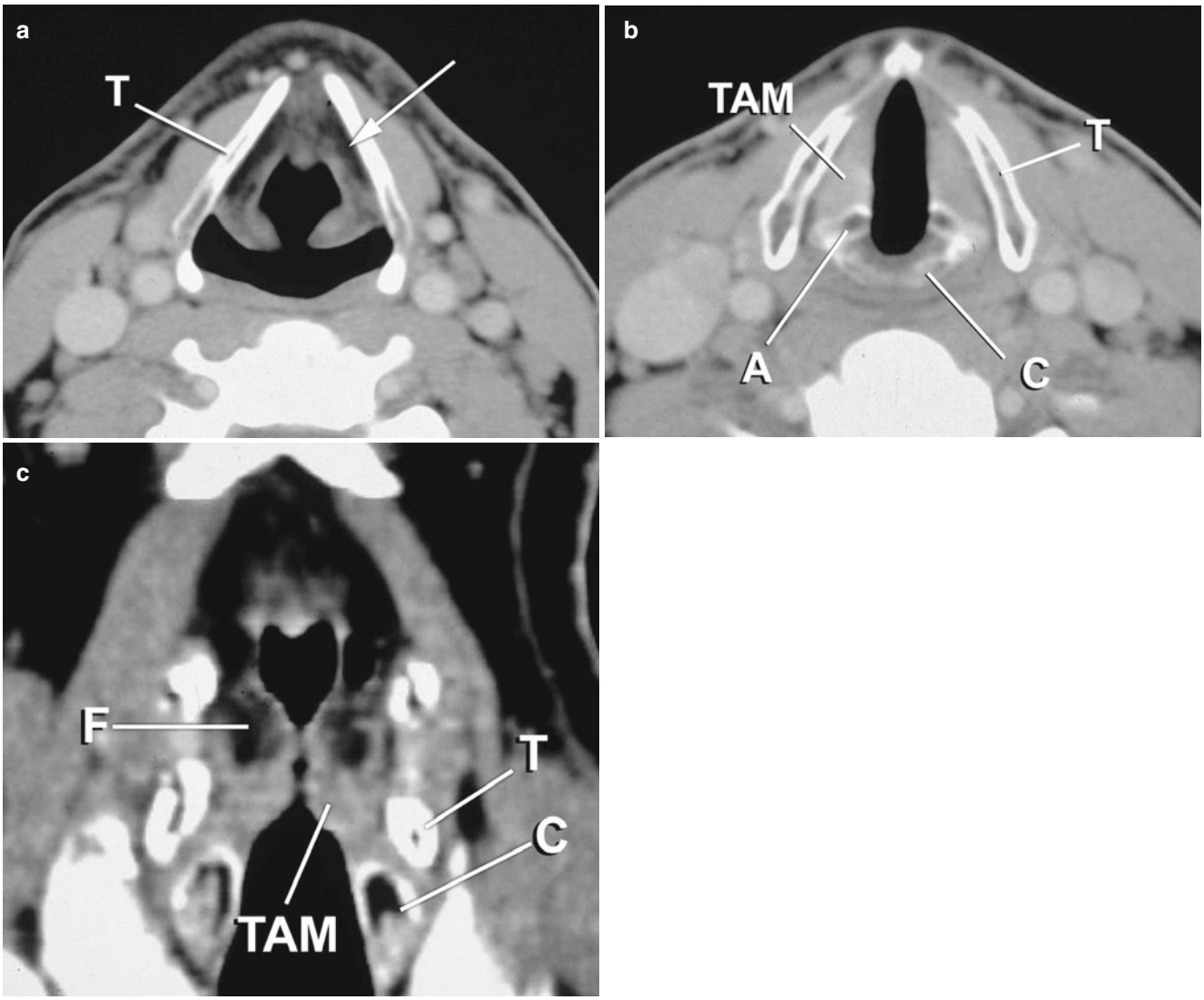

Fig. 2 Normal CT. (**a**) Axial image through the supraglottis. Notice the fat (*arrow*) in the paraglottic space of the lateral larynx. (*T*) Thyroid cartilage. (**b**) Axial image through the level of the true cord. The thyroarytenoid muscle (*TAM*) makes up the bulk of the true cord. Other structures seen at this level include the thyroid cartilage (*T*), the upper edge of the posterior cricoid cartilage (*C*), and the arytenoid cartilage (*A*). The vocal ligament attaches to the anterior margin or vocal process of the arytenoid cartilage. (**c**) Coronal image through larynx. The thyroarytenoid muscle (*TAM*) makes up the bulk of the true cord or fold. Note the fat (*F*) in the paraglottic space of the supraglottis. The ventricle is not seen but can be predicted to be at the level of the transition of fat to muscle. (*C*) Cricoid cartilage; (*T*) thyroid cartilage

The pre-epiglottic space is the fat-filled region anterior to the epiglottis in the supraglottic larynx.

Pathology and Imaging

Nasopharynx

Five percent of all malignant tumors of the head and neck originate in the nasopharynx, and more than 90 % of these are carcinomas. The most common nasopharyngeal malignancies in adults are squamous cell carcinoma and lymphoepithelial neoplasms. Lymphomas and rhabdomyosarcomas are more common in children and tend to undergo early, extensive lymphogenous spread.

Benign nasopharyngeal tumors are rare. However, cystic lesions within the mucosa of the nasopharynx (e.g., retention cyst, Tornwaldt cyst) are quite common. Detection and the evaluation of the infiltration pattern are the main goal of imaging. MR imaging is the method of choice for the evaluation of the nasopharynx [3].

Oropharynx and Oral Cavity

Most tumors of the oropharynx and the oral cavity are detected during clinical examination. However, the infiltration pattern (e.g., tongue base, perineural spread, infiltration of the pterygopalatine fossa, and contiguous tissues) is

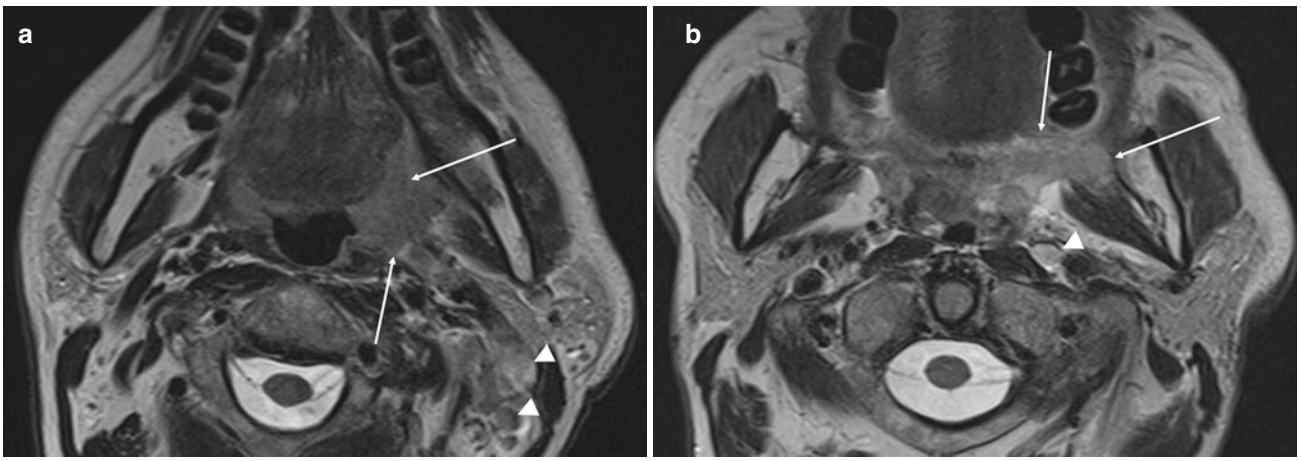

Fig. 3 Carcinoma of the tonsil. (**a**) Level of the tonsil. The tumor (*arrows*) infiltrates of the constrictor muscles and the parapharyngeal space. Metastatic lymph node, level 2 (*arrowhead*). (**b**) Level of the retromolar trigone shows tumor (*arrows*). There is infiltration of the masticator space. Metastatic retropharyngeal node – *arrowhead*

critical and has significant influence in the management of the patient (Fig. 3). In addition the increase in human papillomavirus (HPV)-associated head and neck squamous cell carcinoma plays an important role [4, 5]. MR imaging is usually preferred for the evaluation of the oropharynx and the oral cavity as it is less affected by dental artifacts and is providing a better evaluation of the infiltration pattern [6–8].

The floor of the mouth is immediately inferior to the tongue. Squamous cell carcinoma can invade the deeper soft tissues and can invade the inner cortex of the mandible. Imaging plays a role in defining the extension of cancers and also plays a role in evaluation of submucosal masses in the floor of the mouth. Ranulas and sublingual gland tumors tend to arise off midline, while dermoid complex lesions tend to be midline within the genioglossus/geniohyoid complex. The relationship of a lesion to the mylohyoid muscle is key to surgical planning as well as to diagnosis (Fig. 4).

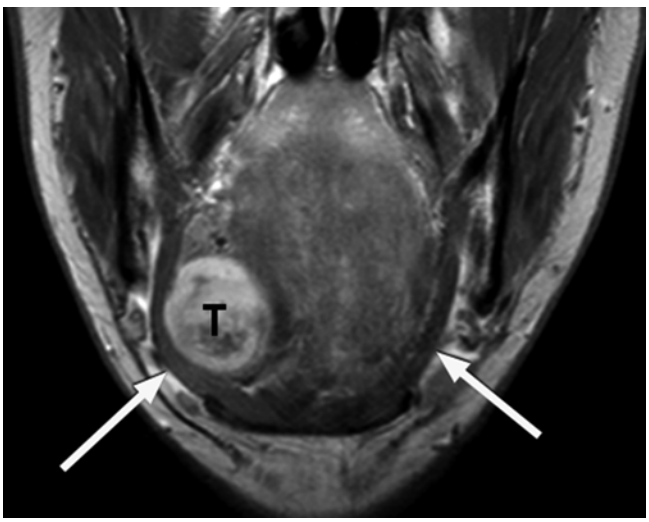

Fig. 4 Schwannoma arising in the sublingual space. The tumor (*T*) fills much of the sublingual space. Note the lesion is superior to the mylohyoid muscle (*arrows*)

Hypopharynx and Larynx

Hypopharyngeal and laryngeal disorders can cause a variety of symptoms, depending on the site of origin as well as the type of disease. In neonates laryngeal abnormalities such as tracheomalacia, tracheoesophageal fistula, or congenital cysts are the most common causes of congenital lower airway obstruction. Another frequent congenital laryngeal abnormality is vocal cord paralysis due to peripheral or central neurologic deficits. Laryngeal infections are the most common diseases of the larynx, related to an upper respiratory tract infection. Hoarseness is a main complaint of patients suffering from a variety of laryngeal diseases including laryngeal infection.

For the clinician, the rapidity of the progression as well as associated symptoms and risk factors (nicotine abuse) is important to be able to develop an adequate diagnostic and therapeutic approach. Normally, an acute infection of the larynx should not last for more than 3 or 4 weeks. If a hoarseness of unclear origin lasts longer, it must be seen by the otorhinolaryngologist to exclude a malignancy.

Imaging of the larynx and upper airway is done in many situations. At our institution, most laryngeal imaging studies relate to tumor evaluation or to trauma.

Tumors of the Larynx

Most tumors of the larynx are squamous cell carcinomas and arise from the mucosa [1, 2, 9]. A few tumors arise from the cartilaginous skeleton or from the other submucosal tissues [10].

The endoscopist almost always detects and diagnoses the mucosal lesions. Indeed, imaging should not be used in an attempt to "exclude" squamous cell carcinoma of the larynx. In squamous cell carcinoma, the role of the radiologist is almost always determination of depth of spread and the inferior limit of spread. Submucosal tumors are, however, somewhat different. The endoscopist can usually visualize, but since they are covered by mucosa, there may be considerable difficulty in making the diagnosis, and in these cases the clinician relies on the radiologist to determine the identity of the lesion.

Squamous Cell Carcinoma Much of imaging is determination depth of extension. Radiologists can see submucosal disease which can make a difference in the choice of therapy. It is important to know some of the indications and contraindications of various alternatives to total laryngectomy. The following represents the standard classic partial laryngectomies [11]. Most surgeries are now done via endoscopic approaches [11]. However, if the information needed for these classic procedures is gathered through imaging, then there is more than enough information for radiotherapists and other clinical specialists as well.

Supraglottic Laryngectomy This procedure, done for supraglottic tumors, removes everything above the level of the ventricle. Tumor may obstruct the endoscopist's view of the lower margin of the tumor or tumor can cross the ventricle by "tunneling" beneath the mucosal surface. Such submucosal spread can travel along the paraglottic pathway around the ventricle. Such extension is a contraindication to supraglottic laryngectomy, and since it can be missed by direct visualization, the radiologist must try to detect this phenomenon (Fig. 5).

Cartilage involvement is another contraindication, but this is extremely rare in supraglottic cancers unless the lesion has actually crossed the ventricle to become transglottic. Other contraindications include significant extension into the tongue or significant pulmonary problems. These mostly relate to difficulty in learning how to swallow once the key part of the laryngeal protective mechanism has been removed.

Vertical Hemilaryngectomy The vertical hemilaryngectomy was designed for lesions of the true vocal fold. The aim is to remove the tumor but to retain enough of one true fold so that the patient can still create speech using the usual mechanism. Actually, the lesion can extend onto the anterior part of the opposite fold and there can still be a satisfactory removal. In these areas, the radiologist looks most closely at inferior extension. Does the tumor reach the upper margin of the cricoid cartilage (see Fig. 5c)? In most institutions such extension would mean that the patient is not a candidate for vertical hemilaryngectomy but rather should have a total laryngectomy or alternative therapies. However, recently some surgeons have taken a part or even a section of the cricoid with secondary reconstruction.

Lesions of the anterior commissure may extend anteriorly into either the thyroid cartilage or through the cricothyroid membrane into the soft tissues of the neck. This may be invisible to the examining clinician and is again a key point to evaluate.

Radiotherapy or Combination Rads/Chemotherapy Radiation, with or without chemotherapy, is another speech conservation treatment. Here the therapist wants to know the extent of the lesion using the same landmarks used for potential surgical planning. Cartilage invasion and the volume of the tumor are also important [12]. Many tumors previously treated with advanced surgery are now treated with organ preservation radiation chemotherapy protocols.

Imaging Laryngeal Squamous Cell Cancer At this institution we begin with CT. CT scanners give excellent resolution and give good coronal and sagittal plane image reformats. Modern scanners can perform the entire study during a single breath hold. Magnetic resonance is reserved for evaluation of lesions close to the cartilage or ventricle. A limited study may be done to clarify a particular margin and to evaluate the cartilage.

Imaging of cartilage involvement is controversial [13–18]. Some favor CT and some MRI. At CT, sclerosis of the cartilage and obliteration of the low-density fat in the medullary space can indicate involvement. The negative finding, intact fat in the medullary space, with a normal cortex is considered reliable. On MRI, one begins with the T1-weighted image. If there is high signal (fat) in the medullary space, the cartilage is considered normal. If the area is dark, then one examines the T2-weighted image. Nonossified cartilage remains dark where tumor is usually brighter. High signal on T2-weighted images can mean tumor or edema related to tumor. More research is needed to determine the significance of signal changes to prognosis. Dual energy may give the ability to evaluate the cartilage more easily than previously possible.

Submucosal Tumors Submucosal tumors may arise from the cartilages or from minor salivary glands or the other soft tissue structures and can be of neural, vascular, adipose, muscular, or fibrous tissue origin [9, 10].

CT with intravenous contrast can be very helpful. Chondromatous lesions can arise from any cartilage and often have demonstrable cartilage matrix [19]. The lesions

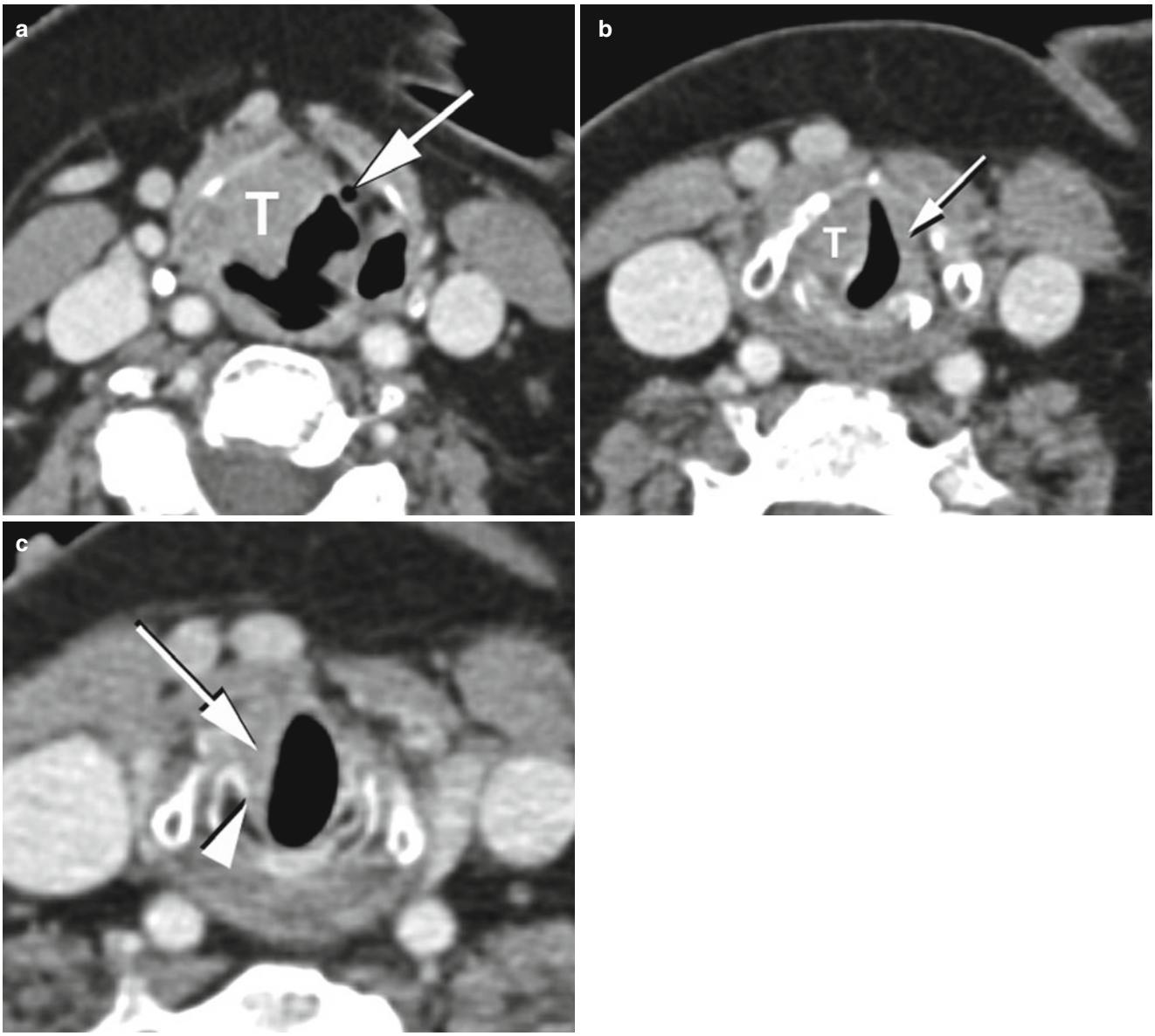

Fig. 5 Carcinoma of the larynx crossing the laryngeal ventricle (transglottic). (**a**) Axial image; supraglottic level. Tumor (*T*) is seen obliterating the right supraglottic fat in the paraglottic and pre-epiglottic areas. Note the small amount of air in the ventricular appendix (*arrow*) in the normal paraglottic fat on the left. (**b**) Axial image; true cord (glottic) level. Tumor (*T*) enlarges the cord on the right side. Note the typical appearance of the thyroarytenoid muscle (*arrow*) on the left indicating that the image is at the level of the cord. (**c**) Axial image; subglottic level. The tumor (*arrow*) spreads along the inner cortex of the cricoid cartilage (*arrowhead*)

tend to expand the parent cartilage. Hemangiomas enhance intensely as do the very rare glomus (paraganglioma) tumors. There are other lesions which arise in the submucosal region but do not enhance as avidly and do not involve the cartilage. In these cases, the identity cannot be made precisely, but it is very helpful to the clinician if one has excluded a very vascular lesion or a chondroid lesion.

Another submucosal lesion which is very important is the laryngocele or saccular cyst. Both represent dilatation of the ventricular appendix but the latter does not communicate with the lumen of the larynx and is filled with mucus. Terminology varies and some refer to the saccular cyst as a fluid-filled laryngocele. Laryngoceles usually occur later in life and can be classified in three subtypes (internal laryngocele, external laryngocele, combined internal). A laryngocele is a benign lesion; however, relationships between laryngoceles or saccular cysts and laryngeal carcinomas at the level of the ventricle have been described. The lesions can be thought of as a supraglottic, paraglottic cysts.

Trauma

Trauma to the airway can obviously be life-threatening. Most patients that have a demonstrable fracture of the larynx have endoscopy looking for mucosal tears. If there is a fragment of cartilage exposed to the airway, then chondritis and eventual chondronecrosis can be expected. One should carefully evaluate the integrity of the thyroid cartilage and the cricoid ring. These fractures are associated with edema or hemorrhage of the endolarynx, and this can be very helpful especially when, as in a young patient, the cartilages are not completely calcified.

Fractures

Fractures of the cricoid usually involve "collapse" of the ring. The anterior arch of the cricoid is pushed posteriorly into the airway, and there is usually swelling indicated by fluid/soft tissue density within the cricoid ring. The thyroid can fracture vertically or horizontally. Hemorrhage in the adjacent pre-epiglottic fat may be a clue to the horizontal type of fracture. The arytenoid does not commonly fracture but can be dislocated.

Summary

For the nasopharynx, the oropharynx, and the oral cavity, MRI is usually preferred for the evaluation of benign and malignant lesions. For the hypopharynx and larynx, we begin with CT and use MRI for additional evaluation of cartilage.

The detailed knowledge of the anatomy is crucial for the radiological assessment of this area.

For trauma we use CT looking for fractures or dislocations.

References and Suggested Reading

1. Curtin HD (2011) Anatomy, imaging, and pathology of the larynx. In: Som PM, Curtin HD (eds) Head and neck imaging. Mosby Elsevier, St. Louis, pp 1905–2039
2. Becker M, Burkhardt K, Dulguerov P, Allal A (2008) Imaging of the larynx and hypopharynx. Eur J Radiol 66:460–479
3. King AD, Vlantis AC, Yuen TW, et al (2015) Detection of Nasopharyngeal Carcinoma by MR Imaging: Diagnostic accuracy of MRI compared with endoscopy and endoscopic biopsy based on long-term follow-up. AJNR Am J Neuroradiol 36:2380–2385
4. Nesteruk M, Lang S, Veit-Haibach P, Studer G, Stieb S, Glatz S, Hemmatazad H, Ikenberg K, Huber G, Pruschy M, Guckenberger M, Klöck S, Riesterer O (2015) Tumor stage, tumor site and HPV dependent correlation of perfusion CT parameters and [18F]-FDG uptake in head and neck squamous cell carcinoma. Radiother Oncol 117:125–31
5. Whang SN, Filippova M, Duerksen-Hughes P (2015) Recent progress in therapeutic treatments and screening strategies for the prevention and treatment of HPV-associated head and neck cancer. Viruses 7(9):5040–65
6. Garcia MR, Passos UL, Ezzedine TA, Zuppani HB, Gomes RL, Gebrim EM (2015) Postsurgical imaging of the oral cavity and oropharynx: what radiologists need to know. Radiographics 35(3): 804–18
7. Meesa IR, Srinivasan A (2015) Imaging of the oral cavity. Radiol Clin North Am 53(1):99–114
8. Arya S, Rane P, Deshmukh A (2014) Oral cavity squamous cell carcinoma: role of pretreatment imaging and its influence on management. Clin Radiol 69(9):916–30
9. Pilch BZ (2001) Larynx and hypopharynx. In: Pilch BZ (ed) Head and neck surgical pathology. Lippincott Williams & Wilkins, Philadelphia, pp 230–283
10. Becker M, Moulin G, Kurt AM et al (1998) Non-squamous cell neoplasms of the larynx: radiologic-pathologic correlation. Radiographics 18:1189–1209
11. Bailey BJ (2006) Early glottic and supraglottic carcinoma: vertical partial laryngectomy and laryngoplasty. In: Bailey BJ, Johnson JT, Newlands SD (eds) Head & neck surgery–otolaryngology. Lippincott Williams & Wilkins, Philadelphia, pp 1727–1741
12. Mancuso AA, Mukherji SK, Schmalfuss I et al (1999) Preradiotherapy computed tomography as a predictor of local control in supraglottic carcinoma. J Clin Oncol 17:631–637
13. Ljumanovic R, Langendijk JA, van Wattingen M M et al (2007) MR imaging predictors of local control of glottic squamous cell carcinoma treated with radiation alone. Radiology 244:205–212
14. Ljumanovic R, Langendijk JA, Schenk B et al (2004) Supraglottic carcinoma treated with curative radiation therapy: identification of prognostic groups with MR imaging. Radiology 232:440–448
15. Curtin HD (2008) The "evil gray": cancer and cartilage. Radiology 249:410–412
16. Castelijns JA, van den Brekel MW, Tobi H et al (1996) Laryngeal carcinoma after radiation therapy: correlation of abnormal MR imaging signal patterns in laryngeal cartilage with the risk of recurrence. Radiology 198:151–155
17. Castelijns JA, van den Brekel MW, Smit EM EM et al (1995) Predictive value of MR imaging-dependent and non-MR imaging-dependent parameters for recurrence of laryngeal cancer after radiation therapy. Radiology 196:735–739
18. Becker M, Zbaren P, Casselman JW, Kohler R, Dulguerov P, Becker CD (2008) Neoplastic invasion of laryngeal cartilage: reassessment of criteria for diagnosis at MR imaging. Radiology 249:551–559
19. Franco RA Jr, Singh B, Har-El G (2002) Laryngeal chondroma. J Voice 16:92–95

Extramucosal Spaces of the Head and Neck

Laurie A. Loevner and Jenny K. Hoang

Introduction

The extramucosal head and neck consists of several distinct spaces bounded by fascia [1, 2]. Knowing the anatomy of these spaces and their contents helps the radiologist to describe and correctly diagnose pathology. Some neck diseases are incidental findings while others are large enough to present as a palpable mass. Other diseases are not large, but in a location that leads to symptoms of ear pain, ear pressure/fullness, tinnitus, dysphagia, or cranial nerve palsies.

This article will discuss the rationale for evaluating these lesions and provide an approach in the radiologic assessment of extramucosal spaces of the head and neck with an emphasis on pertinent anatomy and correct localization of lesions. The spaces include the parapharyngeal space, carotid space, parotid space, masticator space, submandibular space, retropharyngeal space, and visceral space (Fig. 1). The perivertebral space will be discussed in another article.

Approach and Differential Diagnoses

When a radiologist encounters neck pathology, a systematic approach can help to diagnose the abnormality as well as provide information relevant to the patient's management. The steps in evaluating head and neck diseases are:

1. Localize the finding to the space of origin.
2. Describe the lesion characteristics including margins and morphology.
3. Describe the involvement or invasion of surrounding structures especially bones, muscles, vessels, and nerves.
4. Consider the differential diagnoses for the neck space along with the clinical history, and give the most likely differential first.

The differential diagnoses can be grouped into (1) space-specific diagnoses and (2) general neck diagnoses. Space-specific diagnoses are those that are unique to the space because it contains a structure that is not present in other neck spaces, for example, a major salivary gland, teeth, and carotid body. These space-specific differentials will be discussed in the following section. General neck diagnoses can arise in any neck space, although their frequency may differ depending on contents of the space. General neck diagnoses include nodal metastasis, lymphoma, mesenchymal tumors (sarcomas and lipomas), and vascular malformations. The most common primary tumors that metastasize to the neck are squamous cell cancer (SCC), thyroid cancer, and melanoma.

Extramucosal Spaces: Anatomy and Pathology

A thorough knowledge of the cross-sectional anatomy of the neck and skull base is essential in identifying pathology on imaging, in generating a succinct list of differential diagnoses based on lesion location and imaging appearance, and in determining the subsequent management.

Parapharyngeal Space

The parapharyngeal space (also known as the pre-styloid parapharyngeal) contains predominantly fat and is, therefore, easily identified on CT and MR imaging [3]. It extends from the skull base to the hyoid bone, merging with the submandibular space inferiorly. It is bordered by four spaces: anteriorly by the masticator space, laterally by the parotid space, medially by the pharynx, and posteriorly by the carotid space (post-styloid parapharyngeal space).

L.A. Loevner, MD
Radiology, Division of Neuroradiology, University of Pennsylvania Health System, 3400 Spruce Street, Philadelphia, PA 19104, USA
e-mail: laurieloevner@aol.com

J.K. Hoang (✉)
Radiology, Division of Neuroradiology, Duke University Medical Center, Erwin Road, Box 3808, Durham, NC 27710, USA
e-mail: jennykh@gmail.com

J. Hodler et al. (eds.), *Diseases of the Brain, Head and Neck, Spine 2016–2019: Diagnostic Imaging*, DOI 10.1007/978-3-319-30081-8_19

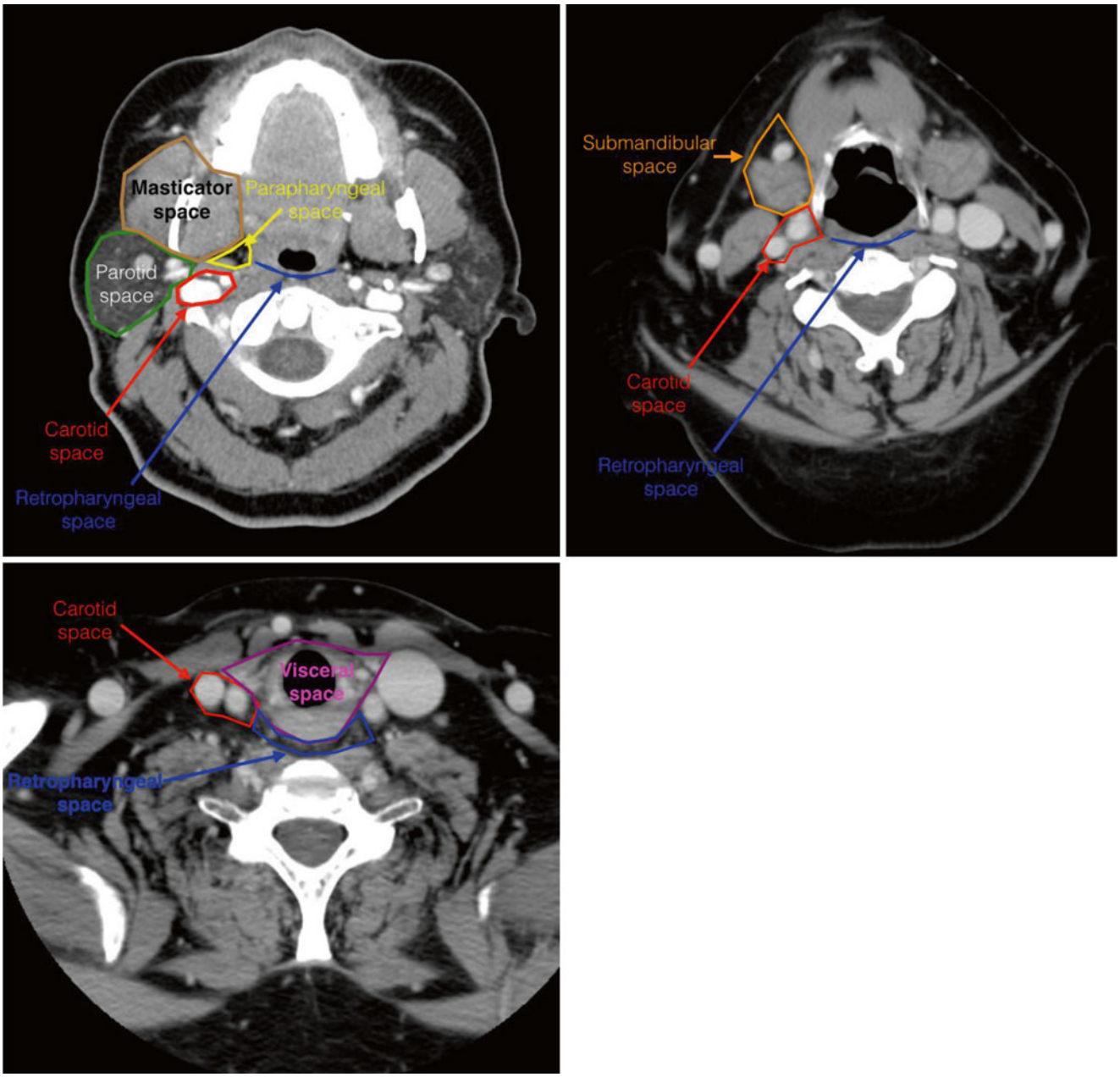

Fig. 1 Extramucosal spaces of the head and neck. The spaces are labelled on (**a**) contrasted CT of the suprahyoid neck, (**b**) contrasted CT at the level of the hyoid bone, and (**c**) contrasted CT of the infrahyoid neck

In addition to fat, the parapharyngeal space contains branches of the mandibular nerve (third division of the trigeminal nerve), branches of the external carotid artery (internal maxillary, middle meningeal, and ascending pharyngeal), the pterygoid venous plexus, minor salivary gland tissue, a lobule of the deep lobe of the parotid gland, and lymph nodes.

Pathology in the parapharyngeal space is usually due to extension of tumor or infection from the pharyngeal mucosa, the palatine tonsils, and/or an adjacent deep extramucosal space. Of the lesions arising primarily from the parapharyngeal space, the two main differentials are salivary tumors and schwannomas. Salivary gland tumors arise from the deep lobe of the parotid gland (Fig. 2) or from minor salivary rests. The majority of these salivary neoplasms are benign mixed tumors (pleomorphic adenomas), with the rest representing mucoepidermoid, adenoid cystic, and adenocarcinomas. It is important for the radiologist to attempt to distinguish whether a salivary neoplasm in the parapharyngeal space is arising from the deep lobe of the parotid gland or minor salivary tissue as this can affect surgical approach. Other less common lesions include

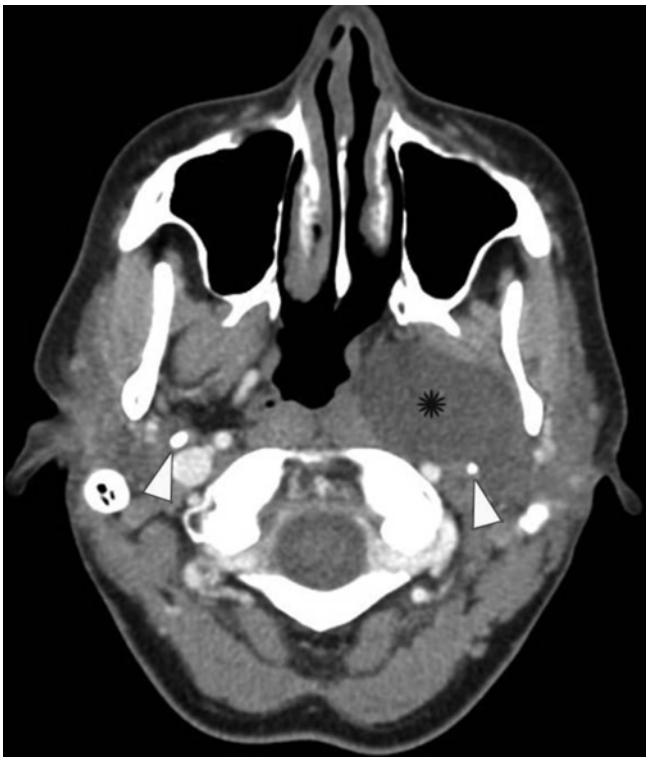

Fig. 2 Benign mixed tumor (pleomorphic adenoma). Axial contrast CT shows a low-attenuation mass (*asterisk*) in the left parapharyngeal space. The stylomandibular tunnel (styloid process [*arrowheads*] to mandible distance) is widened indicating that this parapharyngeal space arises from the deep lobe of the parotid gland

lymph nodes and cysts (retention and the rare branchial cleft cyst).

Tip Expansion of the stylomandibular tunnel indicates that the parapharyngeal mass arises from the deep lobe of the parotid (Fig. 2) [4].

Tip Direction of displacement of parapharyngeal fat can help to localize masses to one of the four surrounding spaces. A mass arising primarily from the parapharyngeal space will have a complete rim of surrounding fat.

Carotid Space (Post-styloid Parapharyngeal Space)

The carotid space (also referred to as the post-styloid parapharyngeal space) extends from the skull base to the aortic arch and contains the common and internal carotid arteries (ICAs), the internal jugular vein (IJV), deep cervical lymph nodes, cranial nerves IX–XII, and the cervical sympathetic plexus. In the suprahyoid neck, the carotid space is bordered anteriorly by the parapharyngeal space, and it sits anterior to the prevertebral space. The carotid sheath is comprised of all layers of the deep cervical fascia. The sheath is complete below the carotid bifurcation; however, it is often incomplete in the suprahyoid neck.

Lesions in the carotid space displace the parapharyngeal space/fat anteriorly. Since most pathology in this compartment arises behind the carotid artery, in the suprahyoid neck, most lesions in the carotid space displace the ICA anteriorly. Lesions here also tend to be radiologically characteristic. The most common carotid space lesion is an inflammatory or neoplastic jugular chain lymph node [5, 6]. Space-specific differential diagnoses of carotid space include schwannoma (Fig. 3), paraganglioma (Fig. 4), and pseudomass (jugular vein thrombosis, vascular ectasia, internal carotid artery pseudoaneurysm).

Tip Relationship of vessels to the mass helps to localize the mass within the carotid space. Masses arising from the vagus nerve will displace the ICA and IJV anteriorly or splay the ICA anteromedially and IJV posterolaterally (Fig. 3). Sympathetic chain masses displace the ICA and IJV anteromedially or posterolaterally. Carotid body masses splay the ICA and ECA (Fig. 4).

Tip In adults always consider metastatic disease in addition to a congenital cyst for a cystic neck mass in the carotid space. Cystic metastases may occur with thyroid cancer and SCC.

Parotid Space

The parotid space is bounded by the masticator space anteriorly, the parapharyngeal and carotid space medially, and the prevertebral space posteriorly. The facial nerve (CNVII) divides the parotid gland into the larger superficial and smaller deep lobes. The normal facial nerve is usually not seen on imaging, but the course can be mapped from the stylomastoid foramen to the lateral aspect of the retromandibular vein. Other contents of the parotid space include lymph nodes (intra- and extraparotid) and branches of the external carotid artery.

The most common tumor in the parotid space is a pleomorphic adenoma followed by Warthin tumor, mucoepidermoid carcinoma, and adenoid cystic carcinoma. However, given that the parotid gland contains lymph nodes, a parotid mass differential also includes lymphoma and metastasis. Nonneoplastic diseases in the parotid space include parotiditis, lymphoepithelial cysts, and branchial cleft cysts.

Tip Consider a primary parotid tumor in sites around the main parotid gland. The parotid can extend inferiorly below the mandible as the parotid tail and anteriorly over the masseter muscle as accessory parotid, and the deep lobe can extend into the parapharyngeal space (Fig. 2).

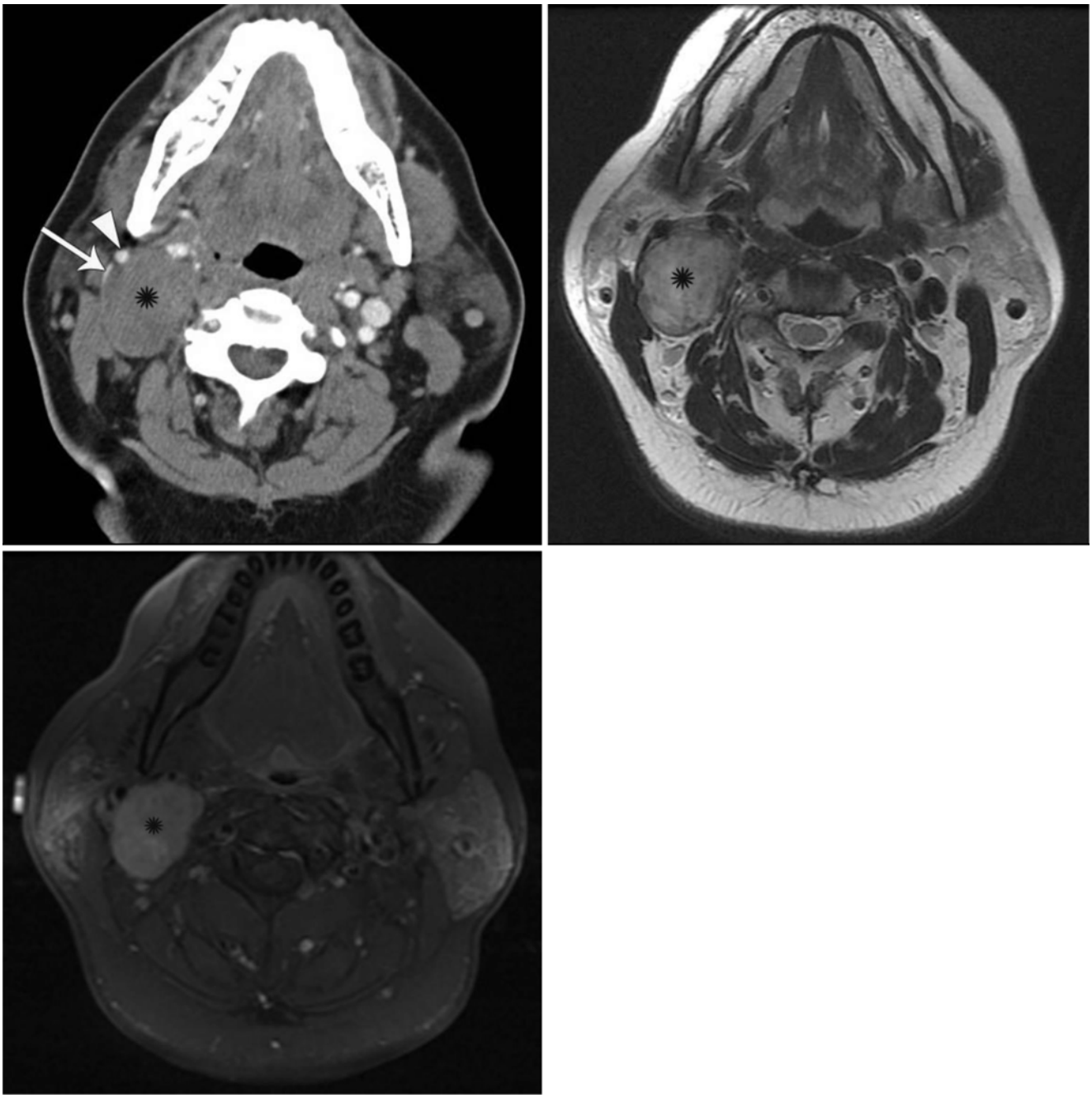

Fig. 3 Vagal schwannoma. (**a**) Axial contrast shows a low-attenuation mass (*asterisk*) in the right carotid space displacing the ICA (*arrowhead*) and IJV (*arrow*) anterolateral. (**b**) Axial T2-weighted and (**c**) enhanced fat suppressed T1-weighted image shows the mass (*asterisks*) has hyperintense T2 signal and homogenous enhancement

Tip It is particularly important to review the facial nerve to the stylomastoid foramen and within the temporal bone in patients with parotid malignancies since the facial nerve can be a path of perineural spread of tumor (Fig. 5).

Masticator Space

The inferior extent of the masticator space is the bottom of the mandible. Superiorly, the masticator space extends to the temporal fossa where the temporalis muscle inserts. It is bordered anteriorly by the buccal space, posteromedially by the parapharyngeal space, and posterolaterally by the parotid space. The masticator space contains the muscles of mastication (medial and lateral pterygoid, masseter, and temporalis muscles), the ramus and posterior body of the mandible, inferior alveolar arteries and veins, and masticator and inferior alveolar nerves. It may be divided into the infra-

temporal fossa and temporal fossa demarcated by the zygomatic arch. The investing fascia of the masticator space is the superficial layer of the deep cervical fascia. When lesions in the masticator space are large, the parapharyngeal space is displaced posteriorly or posteromedially.

Fig. 4 Carotid body paragangliomas. Axial contrast CT image shows vividly enhancing masses (*arrowheads*) in the carotid space bilaterally that between the ICA and ECA

The differential diagnosis of masticator space masses includes congenital/developmental lesions such as hemangiomas, lymphangiomas, and venolymphatic malformations, which frequently have radiologically characteristic appearances and are also frequently transpatial involving one or more of the extramucosal spaces as well as the mucosal surface of the adjacent pharynx. Infection in the masticator space secondary to odontogenic infections is also very common (Fig. 6). Finally, a mass in the masticator space could be a mesenchymal tumor. The role of the radiologist in this setting is to determine soft tissue versus bone origin and to look for findings that distinguish benign from malignant processes. The radiologist should be assessing for bone remodeling versus destruction, perineural spread along the trigeminal nerve, and the presence of matrix formation within the mass. In children malignant sarcomas are most common. In adults, schwannomas and metastatic disease are more common than primary sarcomas.

Tip Most masticator infections arise from the teeth, but sinus origin for infection should also be considered (Fig. 6).

Tip It is essential to review the bone windows for bony changes for any masticator space pathology.

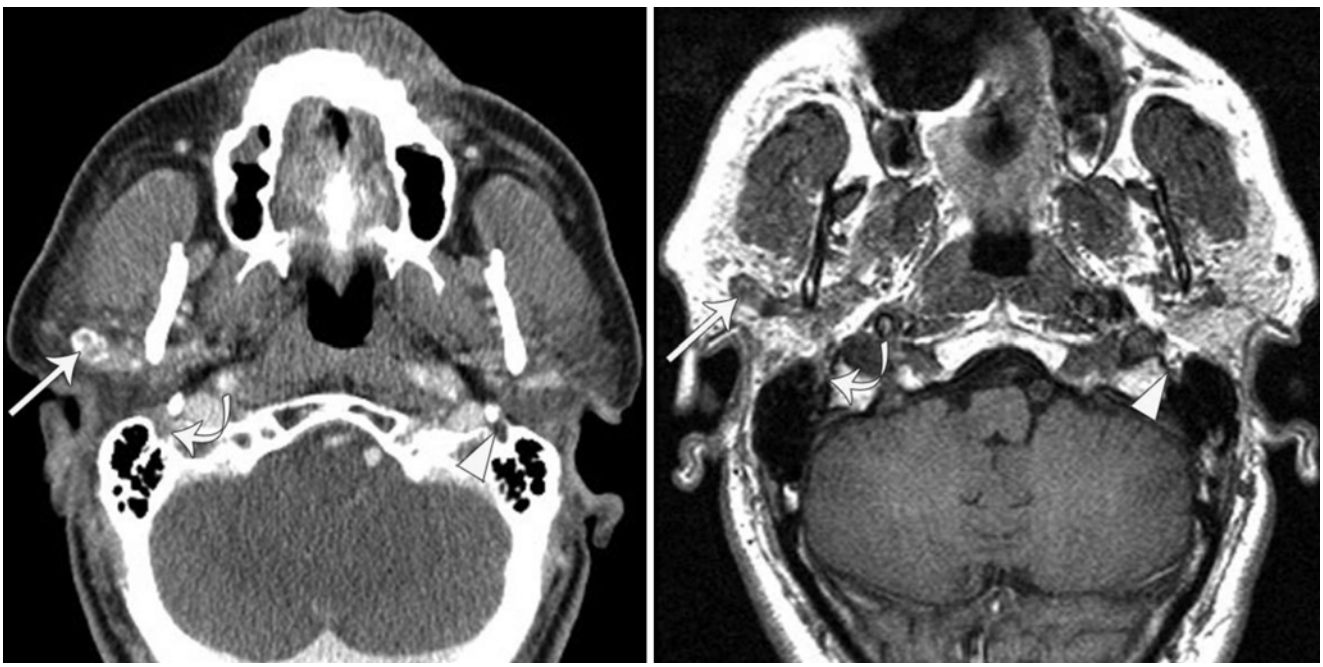

Fig. 5 Parotid ductal carcinoma with perineural spread of tumor. (**a**) Axial-enhanced CT and (**b**) T1-weighted MRI show partially calcified mass in the right parotid gland (*arrow*). The right stylomastoid foramen has soft tissue attenuation/signal (*curved arrow*) in contrast to the normal fat seen on the left side (*arrowhead*). This was due to perineural spread of tumor along CNVII

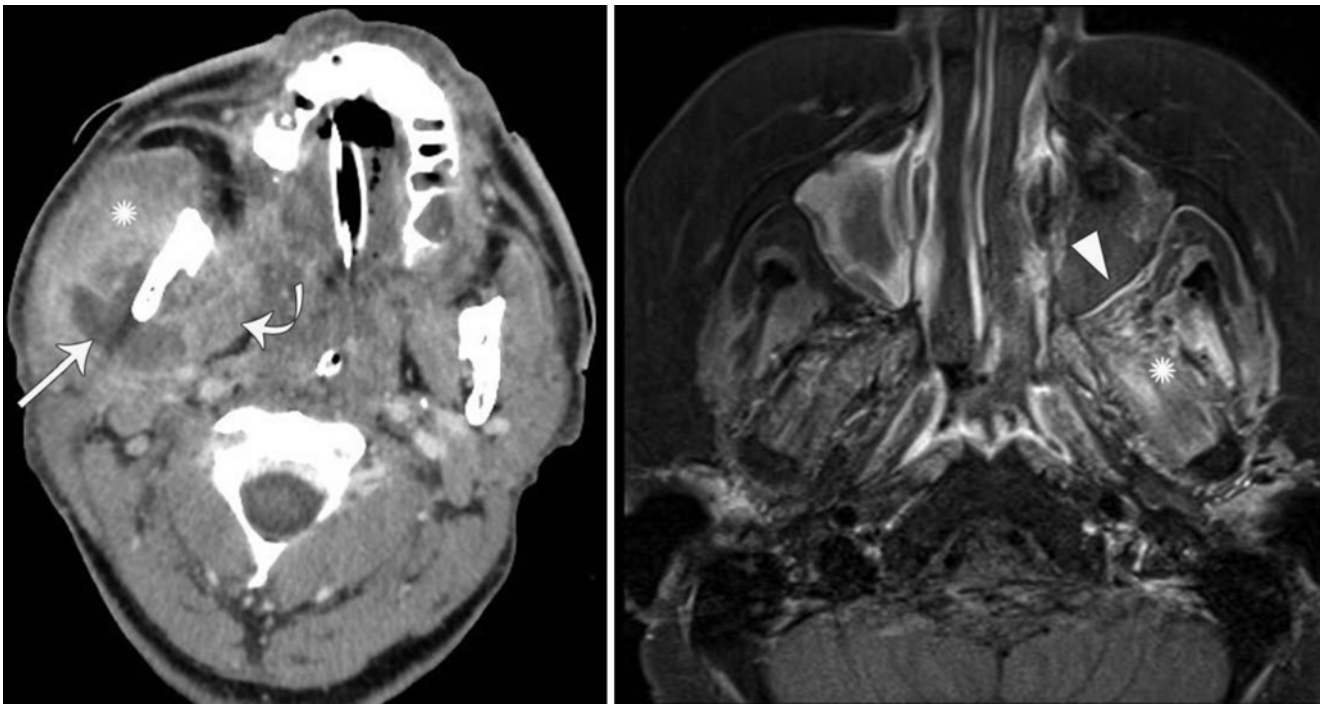

Fig. 6 Masticator space infections. (**a**) Bacterial abscess in the right masticator space (*arrow*) from odontogenic infection. The masseter (*asterisk*) and medial pterygoid (*curved arrow*) muscles are enlarged due to myositis. (**b**) Acute invasive fungal sinusitis with extension into the left masticator space (*asterisk*) resulting in increased enhancement. The left maxilla has lack of mucosal enhancement (*arrowhead*) in keeping with invasive fungal disease

Submandibular Space

The submandibular space is below the mylohyoid muscle and bordered by the carotid, sublingual, and masticator space [7]. The contents are the submandibular gland, submandibular nodes, facial vein and artery, and inferior loop of the facial nerve. The sublingual space lies above the mylohyoid muscle and is part of the oral cavity.

Like the parotid space, neoplastic differentials of the submandibular space include metastases, lymphoma, and primary tumors of the salivary gland. Pleomorphic adenoma is the most common benign primary tumor, but malignant tumors account for more than half of submandibular gland primary neoplasms [8]. The most common malignancies are adenocarcinoma and adenoid cystic carcinoma. Given the close proximity to the base of the tongue and floor of the mouth, there can also be direct extension of SCC to the submandibular space. Nonneoplastic pathologies of the submandibular space include sialoadenitis (viral or calculi) and diving ranula (Fig. 7).

Fig. 7 Diving ranula. Axial-enhanced CT shows a cystic mass (*asterisk*) in the left sublingual space and submandibular space. The left submandibular gland is displaced inferiorly relative to the right submandibular gland (*arrowhead*)

Retropharyngeal Space

The retropharyngeal space (RPS) is frequently seen on imaging as only a small 1–2 mm fat plane behind the pharynx (Fig. 1) [1, 9]. The RPS is divided into the true RPS anteriorly and danger space posteriorly. The true RPS extends from the skull base superiorly to the thoracic inlet inferiorly, but the "danger space" continues inferiorly to

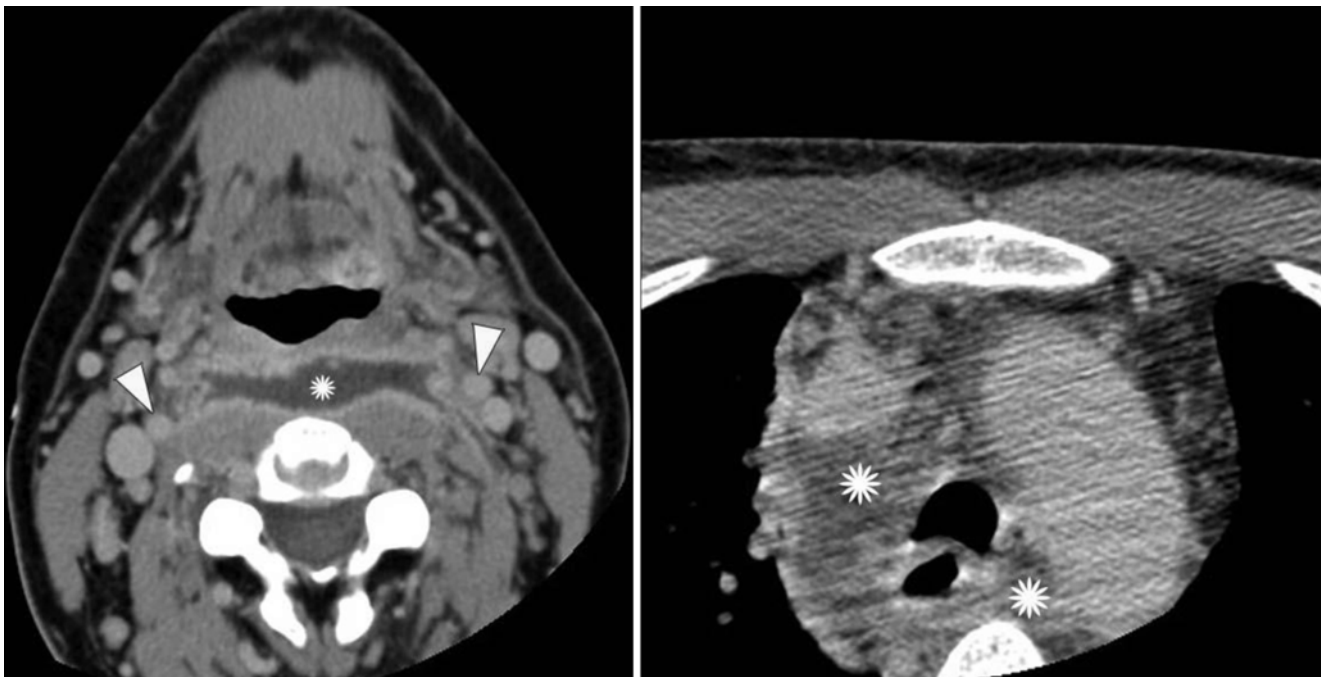

Fig. 8 Retropharyngeal abscess and mediastinitis. (**a**) Axial-enhanced CT demonstrates a rim-enhancing collection (*asterisk*) in retropharyngeal space spanning ICA-to-ICA (*arrowheads*). (**b**) Axial-enhanced image of the mediastinum shows fat stranding in keeping with mediastinitis

the crura of the diaphragm. The RPS is situated between the pharyngeal constrictor muscles that are anterior, the longus colli and capitis muscles that are posterior to this compartment, and the carotid space laterally. The RPS contains fat, lymph nodes, mesenchymal tissue, nerves, and lymphatics. In the suprahyoid neck, the RPS has abundant lymph nodes.

The differential diagnosis of retropharyngeal space pathology includes collections (effusion and abscess) (Fig. 8), adenopathy (inflammatory and nodal metastases), and neoplasms including schwannomas and the less common mesenchymal tumors (lipoma, rhabdomyoma, and sarcomas).

Tip RPS abscess spans the RPS from side to side is a surgical emergency that requires immediate drainage because of potential for spread of infection to the mediastinum (Fig. 8). A small unilateral collection in the RPS is usually a suppurative lymph node and not at immediate risk of spreading to the mediastinum.

Visceral Space

The visceral space is a single midline space surrounded by the middle layer of the deep cervical fascia and extends from the hyoid to the mediastinum. It contains the thyroid and parathyroid glands, hypopharynx and esophagus, larynx and trachea, paraesophageal nodes, and recurrent laryngeal nerves. The most common visceral space lesions are benign thyroid nodules and multinodular goiter [10, 11]. Preoperative imaging of thyroid carcinoma requires careful review of the structures that could be locally invaded such as the trachea, esophagus, vessels, and recurrent laryngeal nerve [12, 13].

Tip Not all incidental thyroid nodules seen on CT or MRI require workup. If there are no suspicious imaging findings or clinical history, the American College of Radiology (ACR) White Paper recommends ultrasound for nodules ≥1.5 cm in patients aged ≥35 years and ≥1 cm for patients aged <35 years [10].

Conclusion

A systematic approach to diagnosing diseases in the extramucosal head and neck first starts with understanding the boundaries and contents of the spaces. This is essential in order to generate a succinct list of differential diagnosis based on lesion location and imaging appearance and to identify important anatomy that may affect management. The differential diagnoses can be grouped into space-specific diagnoses and general neck diagnoses.

References

1. Harnsberger HR, Osborn AG (1991) Differential diagnosis of head and neck lesions based on their space of origin. 1. The suprahyoid part of the neck. AJR Am J Roentgenol 157(1):147–154
2. Smoker WR, Harnsberger HR (1991) Differential diagnosis of head and neck lesions based on their space of origin. 2. The infrahyoid portion of the neck. AJR Am J Roentgenol 157(1):155–159

3. Shin JH, Lee HK, Kim SY, Choi CG, Suh DC (2001) Imaging of parapharyngeal space lesions: focus on the prestyloid compartment. AJR Am J Roentgenol 177(6):1465–1470
4. Abrahams JJ, Culver RR, Kalra VB (2014) Stylomandibular tunnel widening versus narrowing: a useful tool in evaluating suprahyoid mass lesions. Clin Radiol 69(11):e450–e453
5. Hoang JK, Vanka J, Ludwig BJ, Glastonbury CM (2013) Evaluation of cervical lymph nodes in head and neck cancer with CT and MRI: tips, traps, and a systematic approach. AJR Am J Roentgenol 200(1):W17–W25
6. Gor DM, Langer JE, Loevner LA (2006) Imaging of cervical lymph nodes in head and neck cancer: the basics. Radiol Clin North Am 44(1):101–110, viii
7. Law CP, Chandra RV, Hoang JK, Phal PM (2011) Imaging the oral cavity: key concepts for the radiologist. Br J Radiol 84(1006):944–957
8. Rapidis AD, Stavrianos S, Lagogiannis G, Faratzis G (2004) Tumors of the submandibular gland: clinicopathologic analysis of 23 patients. J Oral Maxillofac Surg 62(10):1203–1208
9. Hoang JK, Branstetter BF, Eastwood JD, Glastonbury CM (2011) Multiplanar CT and MRI of collections in the retropharyngeal space: is it an abscess? AJR Am J Roentgenol 196(4):W426–W432
10. Hoang JK, Langer JE, Middleton WD et al (2015) Managing incidental thyroid nodules detected on imaging: white paper of the ACR Incidental Thyroid Findings Committee. J Am Coll Radiol 12(2):143–150
11. Loevner LA, Kaplan SL, Cunnane ME, Moonis G (2008) Cross-sectional imaging of the thyroid gland. Neuroimaging Clin N Am 18(3):445–461, vii
12. Hoang JK, Branstetter BF, Gafton AR, Lee WK, Glastonbury CM (2013) Imaging of thyroid carcinoma with CT and MRI: approaches to common scenarios. Cancer Imaging 13: 128–139
13. Hoang JK, Sosa JA, Nguyen XV, Galvin PL, Oldan JD (2015) Imaging thyroid disease: updates, imaging approach, and management pearls. Radiol Clin North Am 53(1):145–161

Degenerative Spinal Disease

Johan Van Goethem, Marguerite Faure,
and Michael T. Modic

Introduction

Back pain is one of the most common disorders worldwide. A global burden of disease study from 2010 [1] ranks it sixth between HIV and malaria in terms of its impact on disability-adjusted life years. Degenerative disease of the spine is considered the most common etiologic cause. Mechanical, traumatic, nutritional, and genetic factors all play a role in the cascade of disk degeneration. The presence of degenerative change is by no means an indicator of symptoms, and there is a very high prevalence in asymptomatic individuals. The etiology of pain as the symptom of degenerative disease is complex and appears to be a combination of mechanical deformation and the presence of inflammatory mediators. The role of imaging is to provide accurate morphologic information and influence therapeutic decision making. A necessary component, which connects these two purposes, is accurate natural history data. This is critical because the justification of an intervention, whether diagnostic or therapeutic, requires the intervention to have a more favorable outcome than the untreated natural history of the disease process. In order to fully understand the value of imaging findings on therapeutic thinking, the following five considerations are critical: first, the reliability and reproducibility of imaging findings; second, the prevalence of findings in asymptomatic and symptomatic populations; third, the natural history and behavior over time; fourth, the prognostic value of the findings; and fifth, the treatability of the condition.

In terms of the reliability and reproducibility of the imaging findings, standard nomenclature is crucial and has been much discussed in the literature [2]. The morphologic changes one can identify in imaging are myriad and variable. These include degenerative disk changes such as narrowing, signal intensity loss on T2-weighted images, fissures, vacuum phenomena, annular disruption, bulge, and herniation. Adjacent changes in the soft tissues, bone, and ligament are also important as are morphologic changes such as canal and foraminal narrowing, nerve root compression, etc. Facet changes are also considered to be important. Even in the presence of standardized nomenclature, there is significant variability between and within readers. For instance, the reliability of interpretation based on interobserver reliability is quite good for morphology and kappa of .81 [3], yet only fair for the degree of stenosis, the presence of spondylolisthesis, marrow change, or facet disease [4].

Any study looking at the natural history of degenerative disk disease, prognostic value of imaging, or its effect on therapeutic decision making will be confounded by the high prevalence of morphologic change in the asymptomatic population [5–7]. 20–28 % of asymptomatic patients demonstrate disk herniations and the majority have evidence of additional degenerative disk disease [5–7]. These findings are not only non-predictive in the moment, but prospectively as well. In a 7-year follow-up of a patient group with back pain [8], the original MR findings were not predictive of the development or duration of low back pain.

The natural history and behavior of degenerative changes over time are important to appreciate. Degenerative disk space narrowing, facet disease, and stenosis tend to slowly progress over time. Eventual stabilization of the three-joint discovertebral complex is thought to be part of the natural history of degenerative disease, and it is assumed to be accompanied by a decrease in pain. These impressions,

J. Van Goethem (✉)
Department of Radiology, AZ Nikolaas,
Moerlandstraat 1, Sint-Niklaas 9100, Belgium

Department of Radiology, University Hospital Antwerp,
Wilrijkstraat 10, Edegem 2650, Belgium
e-mail: Johan.vangoethem@uantwerpen.be

M. Faure
Department of Radiology, University Hospital Antwerp,
Wilrijkstraat 10, Edegem 2650, Belgium

M.T. Modic
Neurological Institute, Cleveland Clinic,
9500 Euclid Ave. NA4, Cleveland, OH 44195, USA
e-mail: Modicm1@ccf.org

J. Hodler et al. (eds.), *Diseases of the Brain, Head and Neck, Spine 2016–2019: Diagnostic Imaging*, DOI 10.1007/978-3-319-30081-8_20

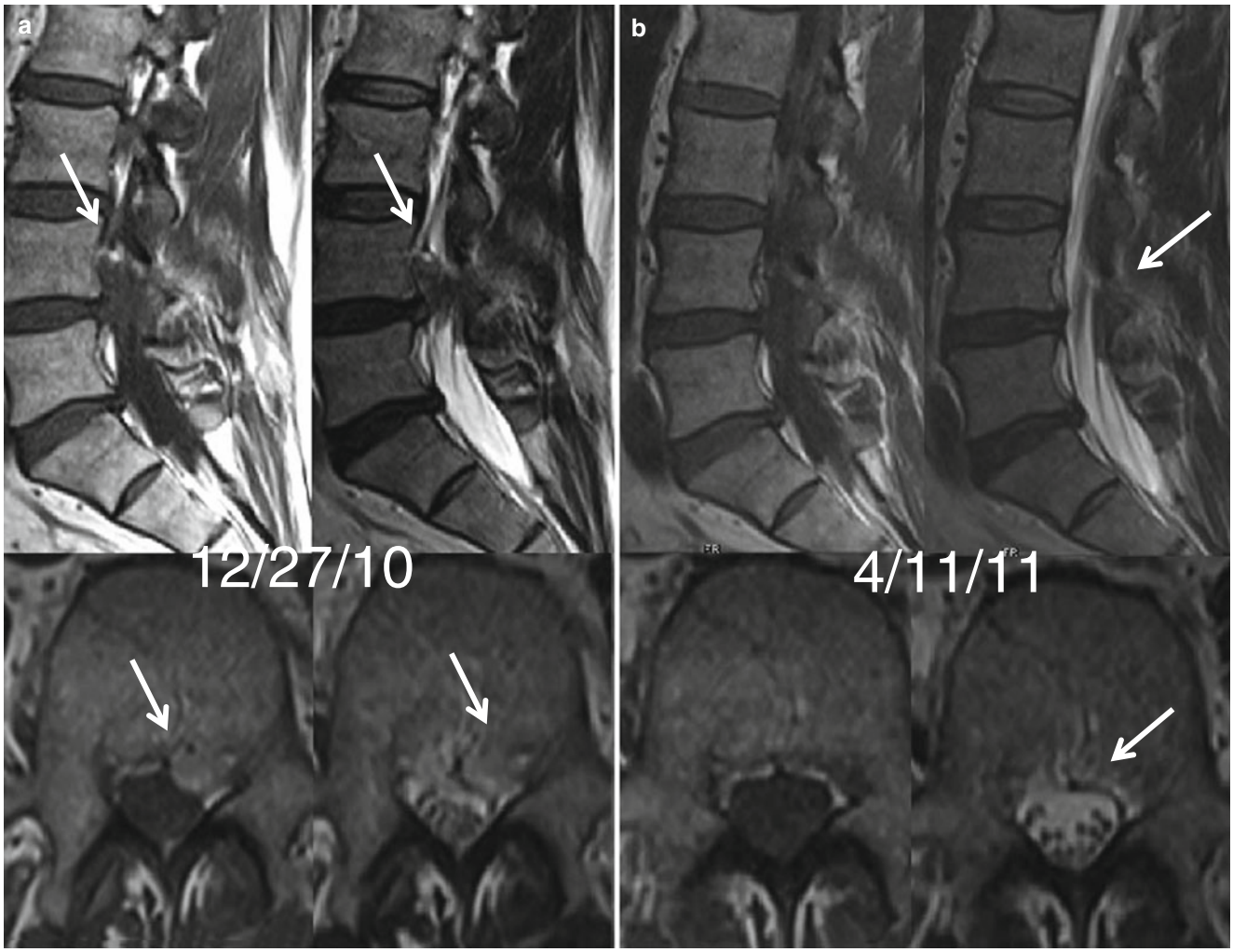

Fig. 1 46-year-old male with left leg radicular symptoms. (**a**) is a composite of sagittal and axial T1 and T2 images of the lumbar spine. (**a**) is from the initial MR performed on 27 December 2010. This study demonstrates a large disk extrusion (*arrows*) in the left anterior epidural space at the L4/L5 level. (**b**) is a composite of the follow-up MR performed 12 weeks later and demonstrates complete resolution of the previously described disk extrusion (*arrows*)

however, are anecdotal and have not been tested by a formal natural history study. Some findings, such as disk herniation and degenerative marrow changes, are known to change. Multiple studies in which computed tomography or MR imaging has been used have shown that the size of disk herniations, especially larger ones, can reduce dramatically in patients undergoing conservative treatment [9, 10].

The prognostic value of these findings is important in computing this information's effect on therapeutic thinking. In a study of symptomatic patients, the prevalence of disk herniation in patients with low back pain and those with radiculopathy at presentation was similar [11]. There was a higher prevalence of herniation, 57 % in patients with low back pain and 65 % in patients with radiculopathy, than the 20–28 % prevalence reported in asymptomatic series [6, 7]. In general, one-third of patients with disk herniation at presentation had significant resolution or disappearance by 6 weeks and two-thirds by 6 months (Fig. 1) [10, 11]. The type, size, and location of herniation at presentation and changes in herniation size and type over time did not correlate with outcome. Knowledge of imaging findings did not affect outcome or impact treatment. In a similar study, by Gilbert et al., earlier imaging did not affect conservative management. A systematic review and meta-analysis by Chou [12] showed that routine lumbar spine imaging in patients with low back pain and no features suggesting serious underlying conditions did not improve clinical outcomes compared with usual clinical care without immediate imaging. The reason these considerations are important is that the rates of spinal surgery are increasing, and there is a moderate to strong correlation between changes in the rates between CT and MR use and spine surgery [13]. This lack of prognostic value also appears to apply to the conservative management of spinal stenosis. There do not appear to be reliable

prognostic imaging findings that would correlate with surgical success or even whether patients would benefit from surgery and spinal stenosis [14, 15].

Interestingly, one imaging variable that did have positive predictive value was the presence of disk herniation at presentation. Patients who presented with a disk herniation were three times more likely to do well than those without a discernible disk herniation [11]. The reason for this is thought to be related to the favorable natural history of patients with disk herniations. That is, the overwhelming majority of these patients recover without significant intervention, and in fact we know from the morphologic data that the majority of these disk herniations regress or disappear over time. Therefore, the presence of a herniation is actually a good sign, that is, likely to have a more favorable natural history.

Intervertebral Disk

Intervertebral disk pathology is thought to be one of the causative factors of low back pain [16]. Studies that demonstrate innervation to the intervertebral disk provide evidence that may account for instances of discogenic low back pain [17]. It was revealed that innervation of the inner disk was observed only in painful disks, not in normal control disks [18, 19]. Based on these observations, nerve ingrowth into the inner disk may be a cause of nonspecific discogenic low back pain. MR imaging findings that correlate with painful disks on discography are those typical for disk degeneration, mainly signal loss of the disk on T2–WI, but also loss of disk height, the presence of a hyperintensity zone (HIZ), and modic changes [20].

The hyperintensity zone (HIZ) is a localized region of high signal intensity on T2–WI within the annulus fibrosus. Histopathologically these lesions represent replacement of the normal lamellar structure by a disorganized, vascularized granulation tissue consisting of small round cells, fibroblasts, and newly formed blood vessels around tears that extend from the nucleus pulposus to the outer region of the annulus fibrosus [21]. Originally the presence of an HIZ was strongly correlated with a painful disk on discography [22]. This correlation was confirmed in multiple later studies, but was also questioned in a few other studies. In general, the association between an annular tear on MR images and low back pain is unclear.

Bone Marrow Changes

Signal intensity changes of the vertebral body marrow adjacent to the end plates of degenerated disks are a long recognized and common observation on MR images of the lumbar spine [23, 24]. However, despite a growing body of literature on this subject, their clinical importance, etiology, and relationship to symptoms remain unclear [25]. These marrow changes appear to take three main forms on MR imaging. Type I changes demonstrate decreased signal intensity on TI-weighted images and increased signal intensity on T2-weighted images. They have been identified in approximately 4 % of patients scanned for lumbar disease [17], approximately 8 % of patients after diskectomy [26], and in 40–50 % of chymopapain-treated disks, which may be viewed as a model of acute disk degeneration [27]. Histopathologic sections of disks with type I changes show disruption and fissuring of the end plate and vascularized fibrous tissues within the adjacent marrow, prolonging T1 and T2. Enhancement of type I vertebral body marrow changes is seen with administration of gadolinium that at times extends to involve the disk itself and is presumably related to the vascularized fibrous tissue within the adjacent marrow. Type II changes are represented by increased signal intensity on T1-weighted images and isointense or slightly hyperintense signal on T2-weighted images. They have been identified in approximately 16 % of patients at MR imaging. Disks with type II changes also show evidence of end plate disruption, with yellow (lipid) marrow replacement in the adjacent vertebral body resulting in a shorter T1. Type III changes are represented by decreased signal intensity on both T1- and T2-weighted images and correlate with extensive bony sclerosis on plain radiographs. The lack of signal in the type III change no doubt reflects the relative absence of marrow in areas of advanced sclerosis. Unlike type III, types I and II changes show no definite correlation with sclerosis at radiography [28].

This is not surprising when one considers the histology; the sclerosis seen on plain radiographs is a reflection of dense woven bone within the vertebral body, whereas the MR changes are more a reflection of the intervening marrow elements. While the aforementioned histologic changes appear to describe the underlying anatomic substrate for the MR signal changes, they by no means describe the etiology of the underlying causative process. The marrow changes are likely epiphenomena and are a consequence of the biomechanical, cellular, and immunological factors that are primarily responsible for symptomatology.

Similar marrow changes have also been noted in the pedicles. While originally described as being associated with spondylolysis, they have also been noted in patients with degenerative facet disease and pedicle fractures [29, 30]. We do not know the exact mechanism by which these marrow changes occur. Their association with degenerative disk disease, facet changes, and pars and pedicle fractures suggests they are a response to biomechanical stress. This then suggests the first and likely most common etiology – mechanical.

Of these three types, type I changes appear to be more fluid and variable, a reflection of some ongoing underlying

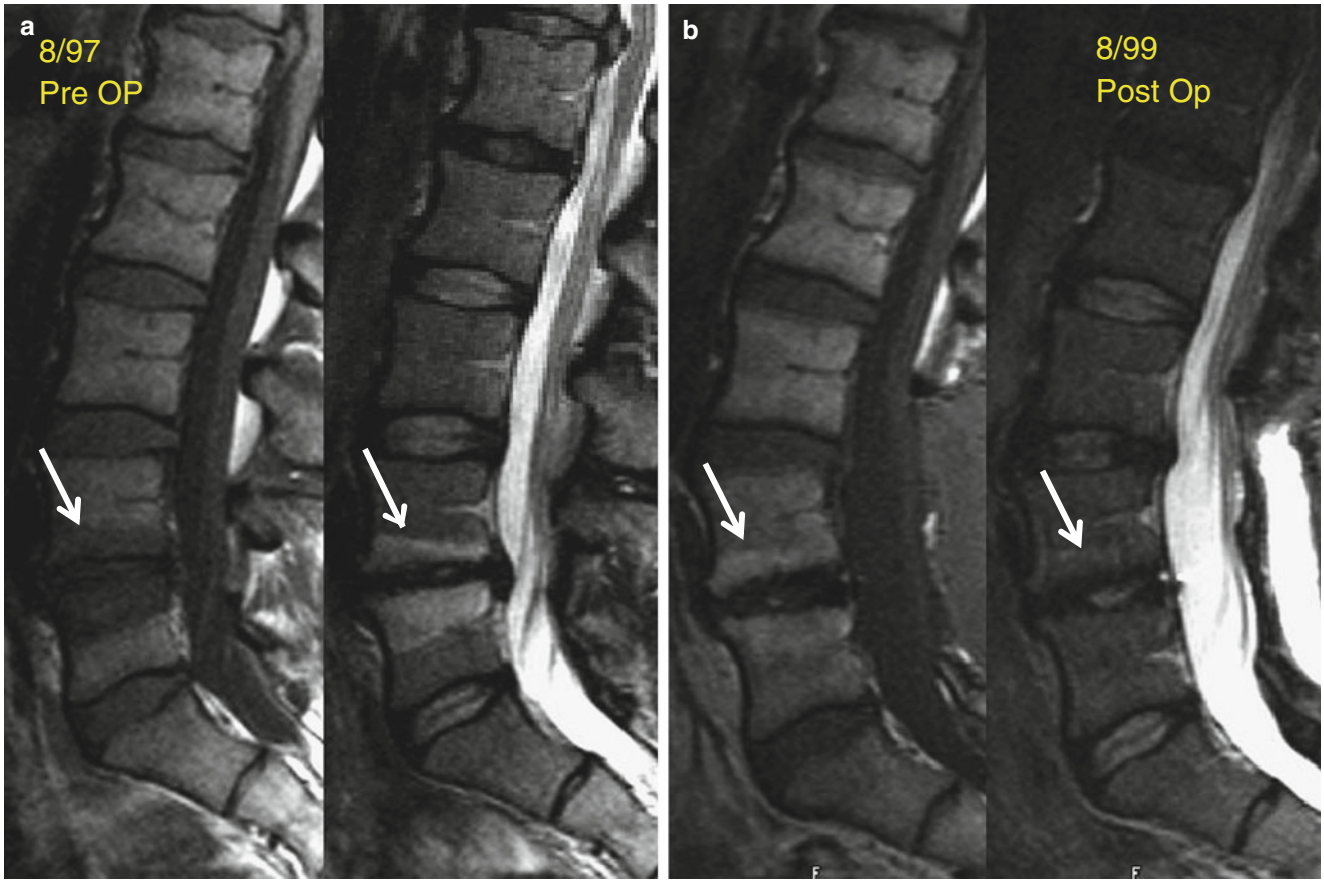

Fig. 2 (**a**) is a composite of sagittal T1- and T2-weighted images in a patient with severe low back pain. (**a**) (*arrows*) demonstrates degenerative type I marrow changes at the L4/L5 level with decreased signal intensity on T1 and increased signal intensity on T2 of the adjacent vertebral body margins. (**b**) is a composite of sagittal T1- and T2-weighted images obtained 2 years later. The patient had undergone a posterior lateral fusion in the interim. Note the laminectomy defect posteriorly. The type I degenerative marrow changes at L4/L5 have now converted to type 2 marrow changes with increased signal intensity on the T1 and normal signal intensity on T2 (*arrows*)

pathological process such as continuing degeneration with resulting changing biomechanical stresses. Of the three types, type I is most often associated with ongoing low back symptomatology [31–35]. In most cases, type II degenerative changes appear to be associated with a more stable state. Type II changes, however, are not always permanent and conversion between type II and I has been demonstrated. In general, when type II marrow changes convert to type I, there is usually a superimposed process such as continued or accelerated degeneration or vertebral osteomyelitis.

Some authors have suggested that mixed lesions are more common than originally thought and indicative of overlap and progression of one type to another [26, 36, 37]. In most studies of marrow changes, type II is the most prevalent and the prevalence increases with age [26].

The available data would support type I marrow changes are more strongly associated with symptomatology than type II and more fluid, and their resolution or change is more common and associated with clinical improvement. The greatest support for suggesting these marrow changes, particularly type I, is related to biomechanical instability which is based on observations following fusion (Fig. 2). Chataigner [38] has suggested that type I marrow changes have much better outcomes with surgery than those with isolated degenerative disk disease and normal or type II marrow changes. In addition, resolution of type I marrow changes to either normal or type II was associated with higher fusion rates and better outcomes. As further support for these fluid marrow changes reflecting biomechanical stress, we have seen similar marrow conversion in the pedicles of vertebral bodies associated with symptomatic pars and pedicle fractures as well as severe degenerative facet joint disease (Fig. 3). Self-reported pain scores tended to improve over time with concordant resolution of marrow signal intensity.

While the data is strong that there is a mechanical etiology to many of these marrow changes, there is a growing body of literature that suggests that in some there is a true infectious or inflammatory cause [39]. In patients with the low back pain and type I marrow changes, an important differential consideration is vertebral osteomyelitis. While

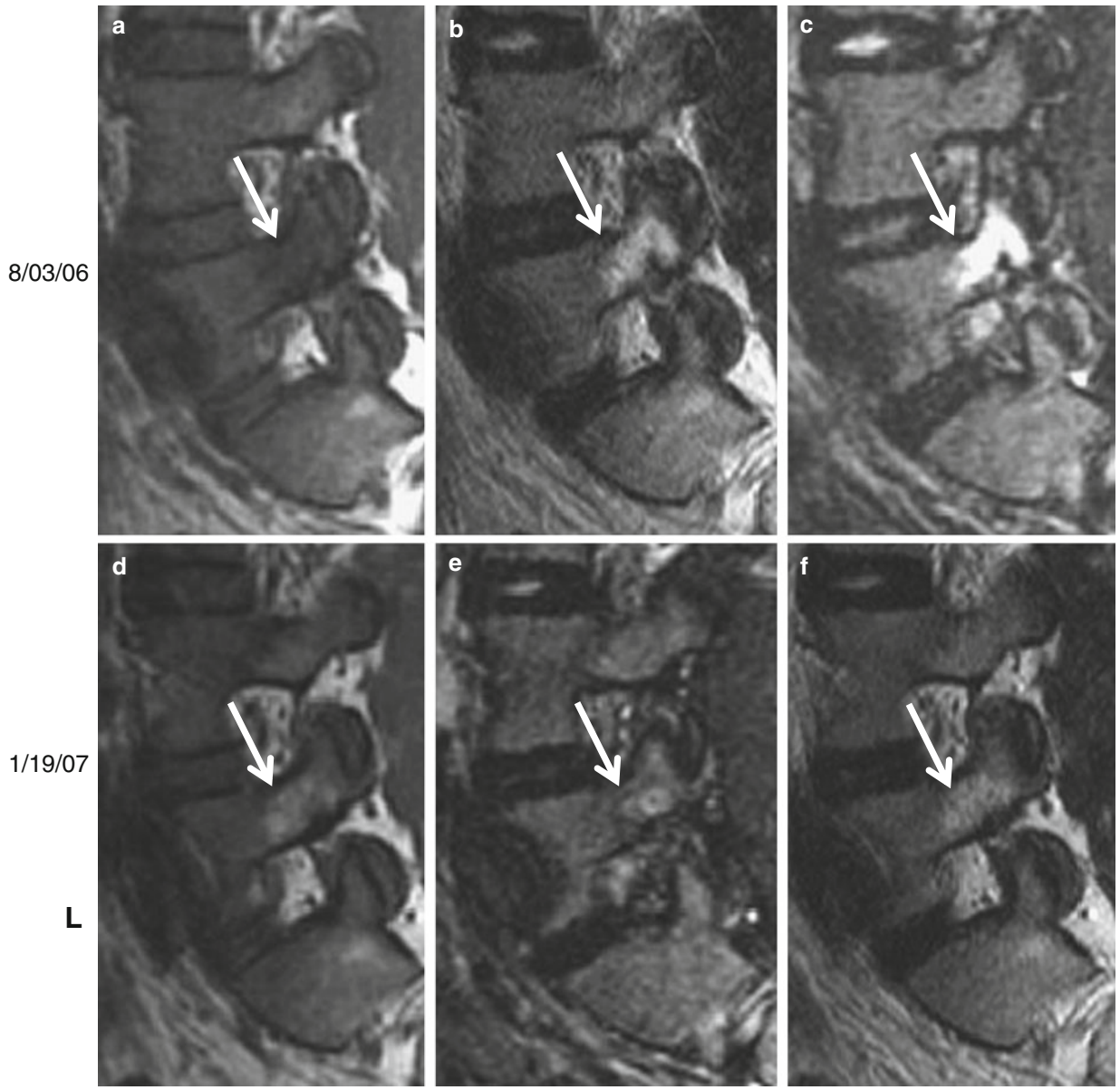

Fig. 3 (**a**–**c**) Left parasagittal T1, T2 and STIR weighted sequences obtained at the time of presentation with back pain. (**d**–**f**) are parasagittal T1-, T2-, and STIR-weighted images obtained 14 weeks after the initial study. Note the conversion of the type I marrow signal intensity change on the previous examination to a type 2 marrow signal. The decreased signal intensity on T1 has converted to an increased, more lipid marrow signal. The high signal intensity on T2 and STIR has for the most part resolved. The *arrows* denote the pedicles

classic pyogenic and fungal osteomyelitis may, in their earliest stages, overlap in appearance on MR with type I marrow degenerative changes, classic osteomyelitis has a distinctly different clinical and more rapidly changing imaging picture. More recently, it has been proposed that some type I marrow changes which heretofore have been presumed to be degenerative may in fact be secondary to a low virulent anaerobic bacterial process [40]. The authors hypothesize that the marrow changes are a side effect of the cytokine propionic acid production from the bacteria entering the adjacent marrow space, presumably through degenerative changes related to disk herniation and underlying degenerative disk disease.

Degenerative Facet Disease

The zygapophysial joint aka "facet" joints in the spinal column is located posterior to the vertebral body. Each vertebra has two facet joints. They are surrounded with a fibrous capsule and connect the superior and inferior articular facets of the vertebrae. Unlike the intervertebral disk, they are true

synovial joints. The joint produces synovial fluid, the prime lubricant for the joint and the nutritional source for the joint surface cartilage. Facet joints are an important part of the posterior column and provide structural stability to the vertebral column. The posterior ligamentous complex (facet joint capsule, ligamentum flavum, interspinous ligament, and supraspinous ligament) keeps the facet joints and the vertebrae in a fixed position with each other. Injury of this complex can result in subluxation or dislocation of the facet.

Most literature focuses on the intervertebral disks; however it is increasingly apparent that facet joints also play a major role in low back pain. Degenerative facet disease is the most frequent form of facet pathology, but degenerative disk and degenerative facet disease often go along [41]. Like in all synovial lined joints, arthrosis in facet joints is a continuum between loss of joint space narrowing, loss of synovial fluid, and cartilage and bony overgrowth. High-grade cartilage necrosis arises quite rapidly in facets. It is mainly a disease affecting the elderly population, present in virtually everyone after the each of 60 and in varying degrees affecting the majority of adults. No sex difference is noted. It is probably related to mechanical loading, minor repetitive trauma, and/or a form of predisposition [42]. The L4–L5 facet joints are more prone to degeneration than any other level, because of their more horizontal position in the sagittal plane. Facet joint osteoarthritis is intimately linked to the distinct but functionally related condition of degenerative disk disease and disk degeneration usually proceeds facet joint osteoarthritis [41].

Diagnosing pain as deriving from the facet joints can be challenging. History and physical examination may suggest, but cannot confirm, the facet joint as the source of pain [43]. Although radiologists are commonly asked by clinicians to determine the degree of facet joint osteoarthritis, the published radiological studies report no correlation between the clinical symptoms of low back pain and degenerative spinal changes observed on radiological imaging studies [44]. Specifically, the association between degenerative changes in the lumbar facet joints and symptomatic low back pain remains unclear and is a subject of ongoing debate. Current standard criteria for the diagnosis of facet joint pain are reduction in symptoms following the direct introduction of local anesthetic into the facet joint or block of local innervation [45]. The procedure is considered diagnostic if there is pain relief of more than 50 %.

In imaging studies more and more the emphasis lies on the visualization of inflammation of the facet joint and the surrounding soft tissues. It is believed that this inflammation is the cause of local, i.e., non-irradiating pain. Not all changes are inflammatory, especially bony overgrowth is a protective reaction to inflammation, diminishing inflammatory response. However bony overgrowth can be an important cause of neuroforaminal narrowing, giving rise to irradiating pain.

Table 1 Meyerding classification for spondylolisthesis

1	<25 % displacement of vertebral body
2	25–50 % displacement of vertebral body
3	50–75 % displacement of vertebral body
4	>75 % displacement of vertebral body
5	Spondyloptosis (vertebral body displaced completely anteriorly, with inferior displacement to level of vertebral body below)

Adult degenerative scoliosis (spinal deformity or curvature in the coronal plane) and degenerative spondylolisthesis (displacement of one vertebra relative to another in the sagittal plane) are also thought to be related to facet joint degeneration and failure of the motion segment. In degenerative scoliosis, asymmetric deformity and asymmetric loading lead to asymmetric degeneration, which in turn leads to more scoliotic deformity and further increased force transmission through the facet joint on the concave side of the curve. In degenerative spondylolisthesis, progressive loss of cartilage and articular remodeling lead to subluxation of the facet joint. Facet joints at spinal levels affected by degenerative spondylolisthesis have been found to be more sagittally oriented than those at levels without spondylolisthesis. Spondylolisthesis most often occurs at L4–L5, the same level that is most often affected by arthrosis [34].

Plain radiographs are of only limited use in investigating chronic back pain. Arthrosis of the facet joints is a frequent radiographic finding, particularly among the elderly. Oblique radiographs are the best projections to demonstrate the facet joints of the lower lumbar spine because of the oblique position and curved configuration of the facet joints. Even on oblique views, however, only the portion of each joint that is oriented parallel to the X-ray beam is clearly visible.

Typical findings in facet joint degeneration on plain radiographs include joint space narrowing, sclerosis, bone hypertrophy, and osteophytes. Intra-articular gas ("vacuum phenomenon") may be present and spondylolisthesis is not uncommon. Conventional radiography is insensitive in the detection of mild facet joint disease and becomes slightly more sensitive for detecting severe disease. The degree of degeneration tends to be underestimated. The literature reports a 55 % sensitivity and 69 % specificity in identifying the presence of degenerative change in the L3–4 and L5–S1 facet joints on plain radiography [46]. Therefore, standard radiographs can best be used for screening for facet joint osteoarthritis and grading spondylolisthesis according to the Meyerding classification (table 1) [47]. It is particularly useful for evaluating motion-related abnormalities in flexion or extension. This can be very important for assessing instability in case of spondylolisthesis. As mentioned before, the clinical relevance of detecting osteoarthritis of the facet joints remains unclear and controversial [39, 48]. They also have little value in being able to predict response to facet joint interventions.

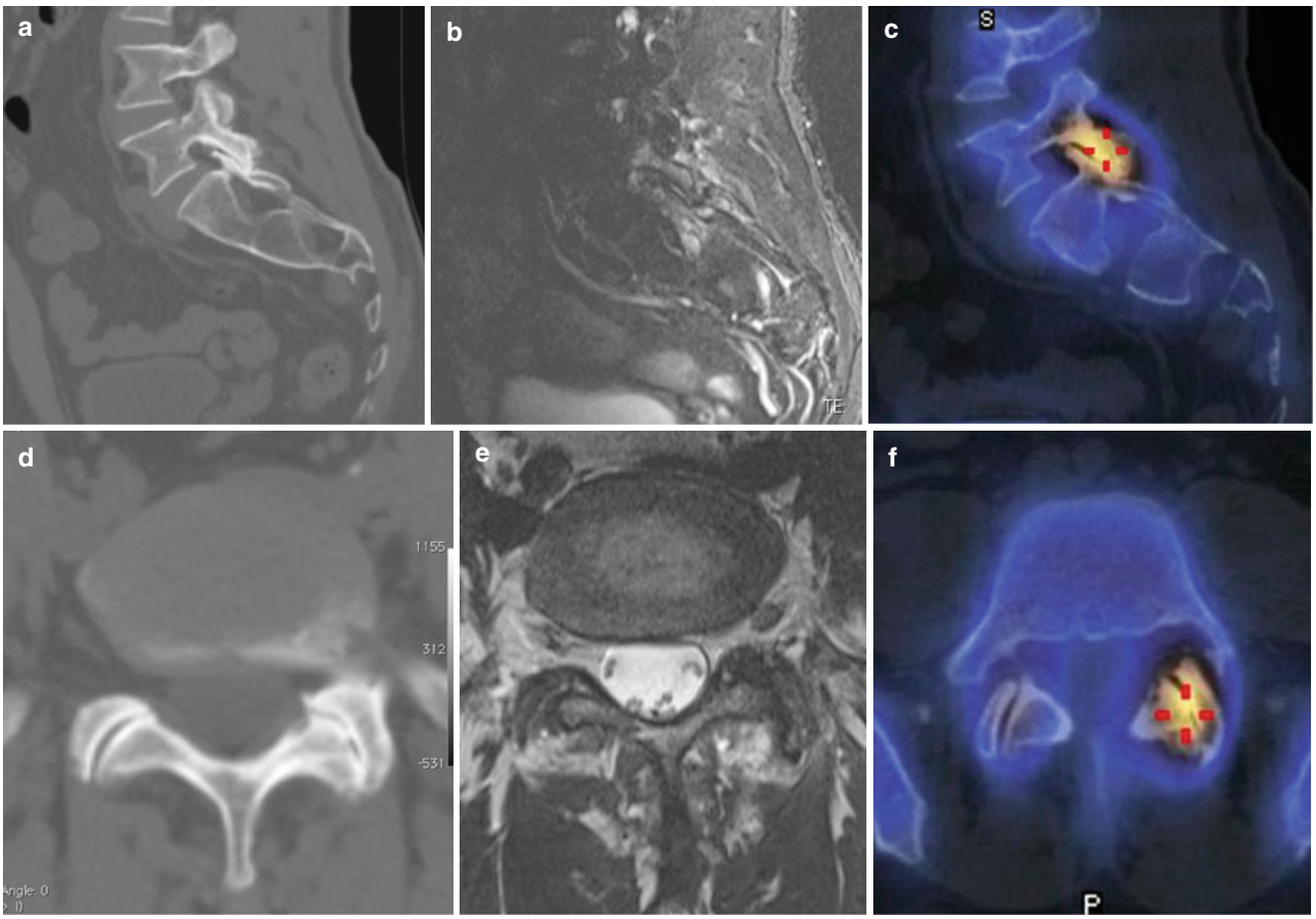

Fig. 4 Grade 3 facet degeneration (see also Table 2) and grade 4 facet joint synovitis (see also Table 3). Note the good correspondence of severe degenerative changes on CT (**a**, **d**) with narrowing of the joint, large osteophytes, severe hypertrophy of the articular process, and severe subarticular bone erosions and subchondral cysts, with inflammatory changes on STIR T2-weighted MRI (**b**) with extensive bone edema, which is not visible on regular T2-weighted imaging (**e**). Same facet joint shows marked increased uptake on SPECT (**c**, **f**). The *red cross* denotes the center of SPECT activity

In comparison with plain radiographs, CT is better in delineating the facet joints due to its capability to image the joint in multiple planes and the high contrast between bony structures and the surrounding soft tissue. Therefore, CT has the ability to detect degenerative changes in the facet joints earlier than plain radiographs. On CT scan we can see articular joint space narrowing with subchondral sclerosis and erosions, osseous overgrowth, and/or hypertrophy of the ligamentum flavum, causing impingement of the foramina (Fig. 4). Also secondary signs including intra-articular gas, joint effusion, and spondylolisthesis can be detected. Synovial cysts can arise, extending posterior of the facet joint but also anterior in the spinal canal or neuroforamen. Joint traction during subluxation may produce intra-articular gas (vacuum). These abnormalities associated with arthrosis can be categorized by CT [49]. Four grades of osteoarthritis of the facet joints were defined by Weishaupt, adapting the criteria published by Pathria (grade 0, normal; grade 1, mild degenerative disease; grade 2, moderate degenerative disease; and grade 3, severe degenerative disease) (table 2) [39, 41]. This grading system aids objective assessment of disease severity and progression. On the other hand, CT has a poor differentiation of soft tissues within the spine, and it is not that good in demonstrating cartilage abnormalities which may indicate early facet degeneration. In the presence of an MR examination, CT is not required for the assessment of facet joint degeneration due to relative good interobserver agreement [41]. But once again, abnormal morphology may not necessarily reflect underlying pathology.

Table 2 Grade criteria for facet degeneration (Pathria, adapted by Weishaupt)

0	Normal facet joint space (2±4 mm width)
1	Narrowing of the facet joint space (<2 mm) and/or small osteophytes and/or mild hypertrophy of the articular process
2	Narrowing of the facet joint space and/or moderate osteophytes and/or moderate hypertrophy of the articular process and/or mild subarticular bone erosions
3	Narrowing of the facet joint space and/or large osteophytes and/or severe hypertrophy of the articular process and/or severe subarticular bone erosions and/or subchondral cysts

Table 3 Grade criteria for facet joint synovitis

0	No signal abnormality
1	Signal abnormality confined to joint capsule
2	Periarticular signal abnormality involving less than 50 % of the perimeter of the joint[a]
3	Periarticular signal abnormality involving more than 50 % of the perimeter of the joint[a]
4	Grade 3 with extension of signal abnormality into the intervertebral foramen, ligamentum flavum, pedicle, transverse process, or vertebral body

[a]Signal abnormality may extend into the articular pillar or lamina, but does not contribute to the definition of the grade

Magnetic resonance imaging is a noninvasive investigation that is not associated with exposure to ionizing radiation. MRI is the preferred imaging technique for the diagnosis of most spinal diseases as it has a superior delineation of soft tissues compared to other imaging modalities. T2-weighted sequences are useful in identifying fluid in facet joint effusions, periarticular cysts, and also better delineate cartilage defects. As mentioned before CT and MR are consistent in demonstrating morphologic aberrances of the facet joint, but MRI is better to demonstrate compression of the thecal sac and the fat-filled neuroforamen, compressing the nerve roots. However, MRI is less sensitive for evaluating cortical anatomy, calcified structures, and subchondral sclerosis [41, 42]. The role of MR imaging in the evaluation of facet joint degeneration, however, is not that clear. Osteoarthritis of these joints may be demonstrated in patients who present with back pain with or without pain irradiating into the legs [50], but is also a frequent observation in a large percentage of asymptomatic patients. Moreover facet joint arthropathy defined anatomically on MRI and CT does not seem to be a significant predictor for the outcome of patients undergoing facet joint blocks [51]. Recent studies suggest that the facet joint (unlike the intervertebral disk) is perhaps better examined in the context of the scientific literature on other synovial joints. Normal facet joints with intact capsules may hold between 1 and 2 ml of fluid. A larger effusion may indicate a loss of capsular function with subsequent abnormal facet joint motion. A positive correlation is found between the amount of facet joint fluid present and the degree of lumbar instability [52]. Chronic degenerative processes in facet joints involve active synovial inflammation, which can be detected using MRI with a fat-saturation technique. Facet synovitis can be graded, using a grading system (Table 3). Facet synovitis appears to correlate with the patient's pain [53]. Moreover synovial abnormalities seem to correlate with SPECT findings [54] (Fig. 4).

The detection of inflammation in the facet joint may be more useful than imaging of joint morphology. Radionuclide bone scintigraphy can depict bone areas with increased osteoblastic activity, and it can depict synovial changes caused by inflammation or hyperemia. Bone scintigraphy also can depict degenerative changes, particularly those that demonstrate a high degree of remodeling. The induced radiopharmaceutical uptake can vary from subtle to pronounced, depending on the metabolic activity and size of the lesions. Osteophytes that are in the process of growing exhibit a high uptake, whereas mature osteophytes tend to have a normal or slightly increased uptake. Abnormalities can be detected earlier with bone scintigraphy than they can be with radiographic methods, and joints observed as abnormal at scintigraphy eventually show the most progressive radiographic changes. Joints that are radiographically abnormal but normal at bone scintigraphy do not show additional deterioration.

Anatomic co-localization with computed tomography (SPECT/CT) is important because facet joints are anatomically juxtaposed, the number of vertebral bodies is variable, and transitional lumbosacral vertebral bodies are present in 4–30 % of patients (Fig. 4).

Several studies show that strictly targeting facet joints with increased 99mTc MDP activity instead of using clinical localization for percutaneous treatment is predictive of a positive response and that use of bone scans can decrease the number of treated facet joints [55–57].

Thus SPECT/CT is emerging as an ideal modality for imaging the facet joint due to the detail of information it provides, the ability to accurately localize the site of pain, and the possibility to differentiate pars defects or other degenerative changes from facet joint disease. However, its use as an appropriate imaging modality should be considered carefully given the increased radiation dose in young individuals with the benign disease and altered low-dose CT protocols should be considered.

Radicular Pain

Acute lumbar disk herniations are the most common cause of acute radicular leg pain. After excluding emergent causes, such as cauda equina syndrome, epidural abscess, fracture, or malignancy, a 6-week trial of conservative management is indicated [58]. Patients should be advised to stay active. If symptoms persist after 6 weeks, or if there is worsening neurologic function, imaging and invasive procedures may be considered. Most patients with lumbar disk herniations improve over 6 weeks.

If a disk herniation is identified that correlates with physical findings, surgical discectomy may improve symptoms more quickly than continued conservative management. Epidural steroid injections can also provide short-term relief [58].

Herniated disks are more easily detected with MRI than with CT for a number of reasons. Firstly, MR imaging allows visualization of the complete lumbar (or cervical or thoracic)

spine in one examination. Secondly, sagittal images also depict the spinal canal in between intervertebral disk spaces. It is not unusual for a disk fragment to migrate (or extend) into the area behind the vertebral body. Some of these migrated disks can be missed on CT if axial slices are limited to the intervertebral disk spaces examined. Finally, the intrinsic tissue contrast is usually better on MR. Especially the lumbosacral region can be hard to assess on CT due to beam hardening, especially in larger patients.

Chronic radicular pain can be caused by a disk herniation, but also vertebral osteophytic spurs, degenerative osteophytic facet spurs and facet hypertrophy, and degenerative foraminal stenosis are an important cause of nerve root irritation. Foraminal nerve root entrapment is best visualized on T1-weighted MRI where the high contrast between fat tissue and the nerve root sheath is of great help. Usually a combination of hypertrophic degenerative facets with osteophytic spurs posteriorly, and vertebral osteophytes and/or disk herniation anteriorly, diminishes the anteroposterior diameter of the foramen. Foraminal height is lessened by degenerative disk disease and subsequent disk height loss. Whenever the normal rounded (oval) appearance of the nerve root sheath is lost in combination with loss of the surrounding fat tissue, nerve root compression should be considered.

References

1. Murray CJL, Vos T, Lozano R et al (2012) Disability-adjusted life years (DALYs) for 291 diseases and injuries in 21 regions, 1990–2010: a systematic analysis for the Global Burden of Disease Study 2010. Lancet 380:2197–2223
2. Fardon DF et al (2014) Lumbar disc nomenclature: version 2.0: Recommendations of the combined task forces of the North American Spine Society, The American Society of Spine Radiology and the American Society of Neuroradiology. Spine J 14(11):2525–2545
3. Lurie Jon D MD, MS (2008) Reliability of Magnetic Resonance Imaging Readings for Lumbar Disc Herniation in the Spine Patient Outcomes Research Trial (SPORT). Spine 33:991–998
4. Carrino JA, Lurie JD, Tosteson AN, Tosteson TD, Carragee EJ, Kaiser J, Grove MR, Blood E, Pearson LH, Weinstein JN, Herzog R (2009) Lumbar spine: reliability of MR imaging findings. Radiology 250(1):161–170
5. Wiesel SW, Tsourmas N, Feffer HL, Citrin CM, Patronas N (1984) A study of computer-assisted tomography. I. The incidence of positive CAT scans in an asymptomatic group of patients. Spine 9:549–551
6. Boden SD, Davis DO, Dina TS, Patronas NJ, Wiesel SW (1990) Abnormal magnetic-resonance scans of the lumbar spine in asymptomatic subjects: a prospective investigation. J Bone Joint Surg Am 72:403–408
7. Jensen MC, Brant-Zawadzki MN, Obuchowski N, Modic MT, Malkasian D, Ross JS (1994) Magnetic resonance imaging of the lumbar spine in people without back pain. N Engl J Med 331:69–73
8. Borenstein DG, O'Mara JW Jr, Boden SD et al (2001) The value of magnetic resonance imaging of the lumbar spine to predict low back pain in asymptomatic subjects: a 7-year follow-up study. J Bone Joint Surg Am 83-A:1306–1311
9. Saal JA, Saal JS, Herzog RJ (1990) The natural history of lumbar intervertebral disc extrusions treated nonoperatively. Spine 15: 683–686
10. Modic MT, Ross JS, Obuchowski NA, Browning KH, Cianflocco AJ, Mazanec DJ (1995) Contrast-enhanced MR imaging in acute lumbar radiculopathy: a pilot study of the natural history. Radiology 195:429–435
11. Modic MT, Obuchowski NA, Ross JS et al (2005) Acute low back pain and radiculopathy. Radiology 237:597–604
12. Chou R, Fu R, Carrino JA, Deyo RA (2009) Imaging strategies for low-back pain: systematic review and meta-analysis. Lancet 373(9662):463–472
13. Verrilli D, Welch HG (1996) The impact of diagnostic testing on therapeutic interventions. JAMA 275(15):1189–1191
14. ECRI. Treatment of degenerative lumbar spinal stenosis. I. Evidence report. Agency for Healthcare Research and Quality publication no. 01-E048 #32. Plymouth Meeting, Pa: ECRI, 2001
15. Benoist M (2002) The natural history of lumbar degenerative spinal stenosis. Joint Bone Spine 69(5):450–457
16. Takahashi K, Aoki Y, Ohtori S (2008) Resolving discogenic pain. Eur Spine J 17(Suppl 4):428–31
17. Troyanovich SJ, Harrison DD, Harrison DE (1999) Low back pain and the lumbar intervertebral disk: clinical considerations for the doctor of chiropractic. J Manipulative Physiol Ther 22(2):96–104
18. Coppes MH, Marani E, Thomeer RT, Oudega M, Groen GJ (1990) Innervation of annulus fibrosus in low back pain. Lancet 336: 189–190
19. Freemont AJ, Peacock TE, Goupille P, Hoyland JA, O'Brien J, Jayson MIV (1997) Nerve ingrowth into diseased intervertebral disc in chronic back pain. Lancet 350:178–181
20. O'Neill C, Kurgansky M, Kaiser J, Lau W (2008) Accuracy of MRI for diagnosis of discogenic pain. Pain Physician 11(3):311–326
21. Peng B, Hou S, Wu W, Zhang C, Yang Y (2006) The pathogenesis and clinical significance of a high-intensity zone (HIZ) of lumbar intervertebral disc on MR imaging in the patient with discogenic low back pain. Eur Spine J 15(5):583–587
22. Aprill C, Bogduk N (1992) High-intensity zone: a diagnostic sign of painful lumbar disc on magnetic resonance imaging. Br J Radiol 65:361–369
23. DeRoss A, Kressel H, Spritzer C et al (1987) MR imaging of marrow changes adjacent to end plates in degenerative lumbar disc disease. AJR Am J Roentgenol 149:531–534
24. Modic MT, Steinbert PM, Ross JS et al (1988) Degenerative disc disease; assessment of changes in vertebral body marrow with MR imaging. Radiology 166:193–199
25. Rahme R, Moussa R (2008) The modic vertebral endplate and marrow changes: pathologic significance and relation to low back pain and segmental instability of the lumbar spine. AJNR 29:838–842
26. Ross JS, Obuchowski N, Zepp R (1998) The postoperative lumbar spine: evaluation of epidural scar over a 1-year period. AJNR Am J Neuroradiol 19:183–186
27. Masaryk TJ, Boumphrey F, Modic MT, Tamborrello C, Ross JS, Brown MD (1986) Effects of chemonucleolysis demonstrated by MR imaging. J Comput Assist Tomogr 10:917–923
28. Modic MT, Masary TJ, Ross JS et al (1988) Imaging of degenerative disk disease. Radiology 168:177–186
29. Ulmer JL, Elster AD, Mathews VP, Allen AM (1995) Lumbar spondylolysis: reactive marrow changes seen in adjacent pedicles on MR images. AJR Am J Roentgenol 164:429–433
30. Morrison JL, Kaplan PA, Dussault RG, Anderson MW (2000) Pedicle marrow signal intensity changes in the lumbar spine: a manifestation of facet degenerative joint disease. Skelet Radiol 29:703–707, 2002;69:450–457
31. Toyone T, Takahashi K, Kitahara H et al (1994) Vertebral bone marrow changes in degenerative lumbar disc disease: an MRI study of 74 patients with low back pain. J Bone Joint Surg (Br) 76:757–764

32. Mitra D, Cassar-Pullicino VN, McCall IW (2004) Longitudinal study of vertebral type-1 end-plate changes on MR of the lumbar spine. Eur Radiol 14:1574–1581
33. Kuisma M et al (2006) A three-year follow up of lumbar spine endplate (Modic) changes. Spine 31(15):1714–1718
34. Albert HB, Manniche C (2007) Modic changes following lumbar disc herniation. Eur Spine J 16:977–982
35. Modic MT (2007) Modic type I and type 2 changes. J Neurosurg Spine 6:150–151
36. Karchevsky M, Schweitzer ME, Carrino JA et al (2005) Reactive endplate marrow changes: a systematic morphologic and epidemiologic evaluation. Skelet Radiol 34:125–129
37. Boos N, Weissbach S, Rohrbach H et al (2002) Classification of age-related changes in lumbar intervertebral discs: 2002 Volvo Award in basic science. Spine 27:2631–2644
38. Chataigner H, Onimus M, Polette A (1998) Surgery for degenerative lumbar disc disease: should the black disc be grafted (in French)? Rev Chir Orthop Reparatrice Appar Mot 84:583–589
39. Albert H et al (2008) Modic changes, possible causes and relation to low back pain. Med Hypotheses 70:361–368
40. Albert H et al (2013) Antibiotic treatment in patients with chronic low back pain and vertebral bone edema (Modic type 1 changes): a double-blind randomized controlled trial of efficacy. Eur Spine J 22:697–707
41. Fujiwara A, Tamai K, Yamato M, An HS, Yoshida H, Saotome K et al (1999) The relationship between facet joint osteoarthritis and disc degeneration of the lumbar spine: an MRI study. Eur Spine J 8:396–401
42. Gellhorn AC, Katz JN, Suri P (2013) Osteoarthritis of the spine: the facet joints. Rheumatology 9(4):216–224
43. Hancock MJ, Maher CG, Latimer J, Spindler MF, McAuley JH, Laslett M, Bogduk N (2007) Systematic review of tests to identify the disc, SIJ or facet joint as the source of low back pain. Eur Spine J 16:1539–1550
44. Schwarzer AC, Wang SC, O'Driscoll D, Harrington T, Bogduk N, Laurent R (1995) The ability of computed tomography to identify a painful zygapophysial joint in patients with chronic low back pain. Spine 20:907–912
45. Makki D, Khazim R, Zaidan AA, Ravi K, Toma T (2010) Single photon emission computerized tomography (SPECT) scan-positive facet joints and other spinal structures in a hospital-wide population with spinal pain. Spine J 10:58–62
46. Pathria M, Sartoris DJ, Resnick D (1987) Osteoarthritis of the facet joints: accuracy of oblique radiographic assessment. Radiology 164:227–230
47. Meyerding HW (1932) Spondylolisthesis. Surg Gynecol Obstet 54:371–377
48. Weishaupt D, Zanetti M, Boos N, Hodler J (1999) MR imaging and CT in osteoarthritis of the lumbar facet joints. Skeletal Radiol 28(4):215–219
49. Carrino JA et al (2008) Lumbar spine: reliability of MR imaging findings. Radiology 250:161–170
50. Resnick D, Niwayama G (1995) Degenerative diseases of the spine. In: Resnick D (ed) Diagnosis of bone and joint disorders. Saunders, Philadelphia, pp 1396–1462
51. Gorbach C, Schmid MR, Elfering A, Hodler J, Boos N (2006) Therapeutic efficacy of facet joint blocks. AJR Am J Roentgenol 186:1228–1233
52. Rihn JA, Lee JY, Khan M, Ulibarri JA, Tannoury C, Donaldson WF et al (2007) Does lumbar facet fluid detected on magnetic resonance imaging correlate with radiographic instability in patients with degenerative lumbar disease? Spine (Phila Pa 1976) 32:1555–1560
53. Czervionke LF, Fenton S (2008) Fat-saturated MR imaging in the detection of inflammatory facet arthropathy (facet synovitis) in the lumbar spine. Pain Medicin 9:400–406
54. Kim KY, Wang MY (2006) Magnetic resonance image-based morphological predictors of single photon emission computed tomography-positive facet arthropathy in patients with axial back pain. Neurosurgery 59:147–156
55. Pneumaticos SG, Chatziioannou SN, Hipp JA, Moore WH, Esses SI (2006) Low back pain: Prediction of short-term outcome of facet joint injection with bone scintigraphy. Radiology 238:693–698
56. Lehman VT, Murphy RC, Kaufmann TJ, Diehn FE, Murthy NS, Wald JT et al (2014) Frequency of discordance between facet joint activity on technetium Tc99m methylene diphosphonate SPECT/CT and selection for percutaneous treatment at a large multispecialty institution. AJNR Am J Neuroradiol 35:609–614
57. Matar HE, Navalkissoor S, Berovic M, Shetty R, Garlick N, Casey AT et al (2013) Is hybrid imaging (SPECT/CT) a useful adjunct in the management of suspected facet joints arthropathy? Int Orthop 37:865–870
58. Gregory DS, Seto CK, Wortley GC, Shugart CM (2008) Acute lumbar disk pain: navigating evaluation and treatment choices. Am Fam Physician 78(7):835–842

Spinal Trauma and Spinal Cord Injury

Pia C. Sundgren and Adam E. Flanders

Introduction

The majority of the spinal injuries (60 %) affect young healthy males between 15 and 35 years of age with cervical spine injuries to be most common. The main cause for spinal injuries is blunt trauma most commonly due to motor vehicle accidents (48 %), followed by falls (21 %), and sport injuries (14.6 %). Assault and penetrating trauma account for approximately 10–20 % of the cases. Injuries to the spinal column and the spinal cord are a major cause of disability, affecting predominately young healthy individuals with important socioeconomic consequences, and the costs of lifetime care and rehabilitation exceed one million US dollars per patient excluding financial losses related to wages and productivity. Over the past several decades, the mean age of the spinal cord-injured patient has increased which is attributed to a substantially greater proportion of injuries related to falls in the elderly.

Cervical spine injuries, of which approximately one-third occur in the craniocervical junction (CCJ) [1], account for the majority of the spinal injuries followed by thoracolumbar fractures diagnosed. Almost half of the spinal injuries result in neurological deficits, often severe and sometimes fatal [2]. Survival is inversely related to the patient's age and neurological level of injury, with lower overall survival for high quadriplegic patients compared to paraplegic injuries. Mortality rate during the initial hospitalization is reported to be almost 10 % [3].

P.C. Sundgren, MD, PhD (✉)
Department of Diagnostic Radiology,
Institution for Clinical Sciences/Radiology, Lund University,
Getingevägen 4, Lund, NA 221 85, Sweden
e-mail: Pia.sundgren@med.lu.se

A.E. Flanders
Department of Radiology, Thomas Jefferson University Hospital,
Suite 1080B Main Building 132 S. Tenth St,
Philadelphia, PA 19107-5244, USA
e-mail: adam.flanders@jefferson.edu

Injury to the spinal cord occurs in 10–14 % of spinal fractures and dislocations with injuries of the cervical spine being by far the most common cause of neurological deficits (40 % of cervical injuries) [4, 5]. The majority of injuries to the spinal cord (85 %) occur at the time of trauma, whereas 5–10 % of injuries to the spinal cord occur in the immediate post-injury period [6].

The imaging methods for evaluating patients with acute spinal trauma have dramatically changed in the last decade especially with the development of more advanced computed tomography (CT) scanner such as the use of thin-section multi-detector computed tomography (MDCT) that with sagittal and coronal reformats allows for the evaluation of extent of the injury of the spinal column. In addition, magnetic resonance imaging (MRI) has become the method of choice for evaluation of spinal cord, soft tissue, and ligamentous injury or when a reliable neurological examination cannot be performed.

Imaging Modalities

In the emergency setting, one of the critical decisions to make is determining which patients require imaging of the spine and/or cord and what type of imaging is required. The appropriate selection of imaging depends upon several factors such as availability of the different imaging modalities, the patient's clinical and neurological condition, type of trauma (blunt, single, or multi-trauma), and other associated injuries to the brain, thorax, or abdomen. Clinical factors to consider also include the quality and severity of pain, limitations in motion, or the presence of permanent or transient neurological deficits. MRI is reserved for those patients with post-traumatic myelopathy (spinal cord dysfunction) or in the instance whereupon a patient's symptoms cannot be explained by findings on plain films or CT and when a reliable neurological exam cannot be obtained.

J. Hodler et al. (eds.), *Diseases of the Brain, Head and Neck, Spine 2016–2019: Diagnostic Imaging*, DOI 10.1007/978-3-319-30081-8_21

Plain-Film Radiography

In the rare circumstance where MDCT is not available, the initial imaging modality is radiography. A minimum of three set of views must be obtained: lateral, anteroposterior, and an open-mouth odontoid view to clear the cervical spine. Often additional views such as oblique views and/or the swimmer's view are performed in an attempt to clear the cervicothoracic junction. With the exception of pediatric trauma, in most settings, radiography has been supplanted by MDCT.

Computed Tomography (CT)

Thin-section multi-detector computed tomography (MDCT) is the initial method of choice when evaluating the cervical spine for bone injuries after blunt trauma allowing for whole-spine examination in a very short time, and fast reformatting of images in multiple planes allows for better and more exact diagnosis of bone and soft tissue abnormalities [7–13]. Moreover in the instance of polytrauma, spine images can be reconstructed directly from the chest, abdomen, and pelvis datasets with sensitivity that is equivalent to a dedicated CT study. This has the added benefit of minimizing radiation dose.

With the introduction of these new MDCT imaging techniques, most trauma centers have set up dedicated acute (multi-)trauma protocol(s) which include CT of the brain, cervical spine, thorax and abdomen, and pelvis, with subsequent reformatting of images of the thoracic and lumbar spine. This both expedites the data acquisition for medically unstable patients and serves to minimize radiation dose since the body imaging data can be reconstructed offline into targeted spine reconstructions. CT has a higher sensitivity to fractures (especially involving the posterior elements) than radiography. This rapid digital assessment of the spinal axis has been shown to be more efficient and safer by virtually eliminating the need for repeat radiographs and unnecessary patient transfers in the setting of an unstable spine. Moreover, the diagnostic quality of radiography varies considerably, is more time-consuming to acquire, and may be difficult to perform in a medically unstable patient. While MDCT excels at delineating bony injury, it also can detect many soft tissue abnormalities such as disc herniation, paravertebral soft tissue, and epidural hematoma. A high-resolution CT imaging protocol begins with submillimeter overlapping partitions to create an isotropic dataset that yields identical spatial resolution in any reconstructed plane. Axial data can be reformatted into thicker sections for diagnostic display, with reformatted 1.25–2-mm thin slices in the C1–C2 region, 2–3-mm thin slices in the rest of the cervical spine, and 3–4-mm thin slices in the thoracic and lumbar spine that are typically chosen for axial presentation. Reformatted sagittal and coronal images of the entire spine are produced from contiguous submillimeter (0.3–0.75 mm) axial images or, on the older scanners, from thicker slices that have been reconstructed with overlapping (e.g., at 1.5 mm). Multiplanar reformatted (MPR) sagittal and coronal images of the entire spine are typically produced automatically from the scanning console or from a nearby workstation. Reconstructions are performed with both bone and soft tissue algorithms.

Magnetic Resonance Imaging (MRI)

The greatest impact that MRI has made in the evaluation of spinal trauma has been in assessment of the soft tissue component of injury. MRI is today considered the method of choice for assessing the spectrum of soft tissue injuries associated with spinal trauma. This includes damage to the intervertebral discs, ligaments, vascular structures, and spinal cord [14–16]. No other imaging modality has been able to faithfully reproduce the internal architecture of the spinal cord, and it is this particular feature that is unique to MRI. Any patient who has a persistent neurological deficit after spinal trauma should undergo an MRI in the acute period to exclude direct damage/compression to the spinal cord. MRI provides unequivocal evidence of not only spinal cord injury but will also reliably demonstrate disc injuries/herniations, paraspinal soft tissue edema (ligament strain/failure), epidural hematomas, and vascular injury. In addition, MRI provides the most reliable assessment of chronic spinal cord injury and the imaging analogs of post-traumatic progressive myelopathy (PTPM) which is often manifested with imaging as syrinx formation, myelomalacia, and cord atrophy (Fig. 1). The extent with which MRI is able to determine spinal instability is overstated as MRI is unable to provide a reliable assessment of ligamentous integrity in most cases. In fact, MRI falsely overestimates the soft tissue component of injury.

An acute spinal trauma MR imaging protocol of the cervical spine shall include 3-mm thick sagittal T1- (T1W) and T2-weighted (T2W) and short tau inversion recovery (STIR) sequences and 3-mm thick axial T2*- weighted gradient recalled echo (GRE) images without contrast. In the thoracic and lumbar spine, 4-mm thick sagittal T1W, T2W, and STIR sequences and axial 4-mm thick T1W, T2W, and T2*GRE images without contrast are recommended. 3D volumetric axial GRE or T2-weighted partitions at 1–2-mm thickness are useful in the cervical region. Fat-saturated T2W images are valuable to evaluate for ligamentous and soft tissue injuries and T2* GRE to evaluate for small hemorrhage or blood products in the spinal cord.

Fig. 1 Post-traumatic syringomyelia. There is a large cystic cavity located within the lower cervical spinal cord extending into the upper thoracic spine

Different Grading Systems to Evaluate Spinal Injuries

There are different classic grading scales for determining spinal instability of thoracolumbar injuries based upon the McAfee (two column) and Denis three-column concept [17, 18], which relies only on CT findings of the Magerl classification [19]. In recent years a new grading scale that is based on CT and magnetic resonance (MR) imaging findings, like the thoracolumbar injury classification and severity score (TLICS), has been developed by the Spine Trauma Group [20] to overcome some of the perceived difficulties regarding the use of other thoracolumbar spinal fracture classification systems for determining treatment. Also for the grading of the cervical spine, a new grading scale and score system – the cervical spine Subaxial Injury Classification and Scoring (SLIC) system [21] – has been developed and is gaining acceptance among spine surgeons.

Injuries to the Vertebral Column

Classically, injuries to the spinal column are categorized by mechanism of injury and/or by instability. *Instability* is defined by White and Punjabi as abnormal translation between adjacent vertebral segments with normal physiologic motion. Unrecognized instability after trauma is a potential cause of delayed spinal cord injury. This is why early stabilization of the initial injury is an imperative to appropriate clinical management. The simplest method to test for instability in a controlled environment is by performing flexion and extension lateral radiography to produce a visible subluxation at a suspected level.

From an imaging point of view and for the evaluation of the thoracolumbar spine, the spine can be divided into three osteo-ligamentous columns: anterior, middle, and posterior column [17]. The anterior column includes the anterior longitudinal ligament and anterior two-thirds of the vertebral body and disc including annulus fibrosus. The middle column is composed of the posterior third of the vertebral body and disc including annulus fibrosus and posterior longitudinal ligament. Finally, the posterior column is composed of the pedicles, articular processes, facet capsules, laminae, ligamenta flava, spinous processes, and the interspinous ligaments. The mechanism of injury will result in several different types of traumatic injuries to the cervical, thoracic, and lumbar vertebral column and spinal cord, which may result in stable or unstable spine injuries. Although this model is often inferred for cervical injuries, there is no similar established model in the cervical spine.

Because of the distinct anatomic differences and the resultant injury patterns, injuries to the cervical spine are divided into subaxial injuries (cranial base to axis) and lower cervical injuries (C3–C7). The mechanism of injury to the cervical column can be divided into four major groups: hyperflexion, hyperextension, rotation, and vertical compression with frequent variations that include components of the major groups (e.g., flexion and rotation). Hyperflexion injuries include anterior subluxation, bilateral interfacetal dislocation, simple wedge fracture, fracture of the spinous process, teardrop fracture, and odontoid (dens) fracture. Of these the simple wedge fractures and isolated spinous process fractures are considered initially stable, while the other fractures are considered unstable such as the bilateral interfacetal dislocation and the teardrop fracture. The odontoid fracture can be considered stable or unstable depending on the type of fracture type.

Hyperextension injuries are less frequent than the hyperflexion injuries and result in the following types of fractures and injuries: dislocation, avulsion fracture, or fracture of the posterior arch of C1, teardrop fracture of C2, laminar fracture, and traumatic spondylolisthesis of C2 (Hangman's fracture). Most of these injuries with the exception of Hangman's fracture are defined as stable fractures; however, this does not imply that these injuries should go untreated. The hyperextension injuries are often associated with central cord syndrome especially in patients with preexisting cervical spondylosis and usually produce diffuse prevertebral soft tissue swelling. Vertical compression results in the Jefferson fracture which involves atlas and is considered unstable or burst fractures. A common site for injuries is the craniocervical junction (CCJ) and the atlantoaxial joint, which is the most mobile portion of the spine as it predominantly relies on the ligamentous framework for stability. The imaging findings of important CCJ injuries, such as atlantooccipital dissociation, occipital condyle fractures, atlas fractures with transverse ligament rupture, atlantoaxial distraction, and traumatic rotatory subluxation, are important to recognize in the acute setting as for the patient management

Fractures in the lower thoracic and lumbar spine differ from those in the cervical spine. The thoracic and lumbar fractures are often complex and due to a combination of mechanisms. The thoracic cage confers substantial biomechanical protection to the thoracic spine. Therefore, statistically, most injuries occur where the thoracic cage ends, the thoracolumbar junction. When injuries occur in the upper or middle thoracic spine, it is usually a result of major trauma, e.g., high-velocity trauma such as motor vehicular accidents. The most common fracture, at the thoracolumbar junction, is the simple compression or wedge fracture (50 % of all fractures) which is considered stable. The remaining types of fractures among those the so-called seat belt injury, which can be divided into three subtypes, type I (Chance fracture) that involves the posterior bony elements, type II (Smith fracture) that involves the posterior ligaments, and type III where the annulus fibrosus is ruptured allowing for subluxation, are considered unstable fractures [22]. The most common of all thoracolumbar fracture – the burst fractures – accounts for 64–81 % of all thoracolumbar fractures. The burst fracture, which can be divided into five subtypes, is associated with high incidence of injuries to the spinal cord, conus medullaris, cauda equina, and nerve roots [23]. It is important to remember that a burst fracture involving anterior and middle column can be misdiagnosed as mere compression fracture on plain films and, therefore, may be misinterpreted as a simple compression or mild wedge fracture that involves only anterior column. CT has improved characterization of these injuries.

Traumatic Disc Herniation and Ligamentous Injury

Traumatic disc injuries are caused by distraction and shearing in sudden hyperflexion or extension. A direct injury to the disc is more common than post-traumatic disc extrusion. Traumatic disc herniation should be considered when the disc exhibits high signal on T2-weighted images especially when traumatic vertebral body fractures and/or ligamentous injury is present at the same level [13]. Extruded disc material may extend into the epidural or prevertebral space. When there is a gap between parts of the vertebrae or by increased signal in the ligament or adjacent structures on T2W and STIR images, a ligamentous injury is suspected. Up to 25 % of all cervical injuries will demonstrate signal changes in the posterior ligamentous complex. This finding does not equate with instability. Ligamentous injury without underlying fracture in the cervical spine is rare [24]. Disruption of the anterior longitudinal ligament is associated with hyperextension mechanisms with associated injury to the prevertebral muscles and intervertebral discs and can be identified as interruption of the normal linear band of hypointense signal of the ligament on T1W images. Hyperflexion and distraction forces may cause disruption of the posterior ligament complex which is manifested by increased distance between spinous processes on lateral radiography and increased signal in the interspinous region on MRI sagittal STIR sequences. Abnormal angulation, distraction, and subluxation are often recognized on initial CT study.

Injuries to the Spinal Cord

A majority of patients with spinal cord injury (80 %) harbor multisystem injuries [25]; typically associated injuries include other bone fractures (29.3 %) and brain injury (11.5 %) [26]. Nearly all spinal cord injuries damage both upper and lower motor neurons because they involve both the gray matter and descending white matter tracts at the level of injury. The American Spinal Injury Association (ASIA) has suggested a comprehensive set of standardized clinical measurements which are based upon a detailed sensory and motor examination of all dermatomes and myotomes. The neurological deficit that results from injury to the spinal cord depends primarily upon the extent of damage at the injury site and the cranial-caudal location of the damage (i.e., the neurological level of injury or NLI); anatomically higher injuries produce a greater neurological deficit (e.g., cervical injury=quadriparesis, thoracic injury=paraparesis). These comprehensive set of standardized clinical measurements have been adopted worldwide. While functional transection of the spinal cord is relatively frequent in spinal cord injury, true mechanical transection is relatively rare and is

confined to penetrating type injuries or extensive fracture-dislocations/translocations. The neurological deficits associated with spinal cord injuries are further categorized into anterior cord syndrome, Brown-Sequard syndrome, central cord syndrome, conus medullaris syndrome, and cauda equina syndrome. Spontaneous neurological recovery after spinal cord injury overall is relatively poor and largely depends upon the degree of neurological deficit identified at the time of injury. Of the different cord syndromes, the anterior cord syndrome has the worst prognosis of all cord syndromes, especially, if no recovery is noticed during the first 72 h after injury.

Spinal Cord Hemorrhage

Post-traumatic spinal cord hemorrhage or hemorrhagic contusion is defined as the presence of a discrete area of hemorrhage within the spinal cord after an injury. The most common location for hemorrhage to accumulate is within the central gray matter of the spinal cord and centered at the point of mechanical impact [14, 27, 28]. Experimental and autopsy pathologic studies have shown that the underlying lesion most often will be hemorrhagic necrosis of the spinal cord while true hematomyelia will rarely be found [29]. There are significant clinical implications if there is identification of frank hemorrhage in the cervical spinal cord following trauma on an MRI examination. Originally it was thought that detection of intramedullary hemorrhage was predictive of a complete injury. However, the increased sensitivity and spatial resolution of current MRI techniques has shown that even small amounts of hemorrhage are identifiable in incomplete lesions. Therefore, the basic construct has been altered such that the detection of a sizable focus of blood (>4 mm in length on sagittal images) in the cervical spinal cord is often indicative of a complete neurological injury [30]. The anatomic location of the hemorrhage closely corresponds to the neurological level of injury, and the presence of frank hemorrhage implies a poor potential for neurological recovery (Fig. 2) [14, 27, 28, 31–33].

Fig. 2 Acute hemorrhagic spinal cord injury. There is a flexion type injury of C5 with acute ventral angulation. The spinal cord is markedly swollen with edema spanning the entire length of the spinal cord. There is a central hemorrhagic focus which is of low signal intensity that spans from C4 to C6. Note the disruption of the posterior spinal soft tissues

Spinal Cord Edema

Spinal cord edema is defined as a focus of abnormal high signal intensity seen on MRI T2-weighted images [28]. Presumably, this signal abnormality reflects a focal accumulation of intracellular and interstitial fluid in response to injury [14, 28, 34, 35]. Edema is usually well defined on the mid-sagittal T2-weighted image, while the axial T2-weighted images offer additional information in regard to involvement of structures in cross section (Fig. 2). Spinal cord edema involves a variable length of spinal cord above and below the level of injury, with discrete boundaries adjacent to uninvolved parenchyma, and is invariably associated with some degree of spinal cord swelling. The length of spinal cord affected by edema is directly proportional to the degree of initial neurological deficit [27, 36]. Notable is that spinal cord edema can occur without MRI evidence of intramedullary hemorrhage. Cord edema alone connotes a more favorable prognosis than cord hemorrhage.

Injuries to the Pediatric Spine and Spinal Cord

Spinal injuries are generally less common in the pediatric population compared to adults with cervical spine injuries being most frequent spine injury of all spine injuries occurring in up to 40–60 % of all injuries in children. The etiology varies depending on the age of the child. The most common cause of pediatric cervical spine injury is a motor vehicle accident, but also obstetric complication, fall, and child abuse are known causes. In the adolescent sports and diving

accidents are other well-known causes. The specific biomechanics of the pediatric cervical spine leads to a different distribution of injuries and distinct radiological features and represents a distinct clinical entity compared to those seen in adults. Young children have a propensity for injuries to the CCJ, upper cervical injuries (i.e., cranial base to C2), whereas older children are prone to lower cervical injuries similar to those seen in adults. The spinal cervical injuries in children less than 8 years of age demonstrate a high incidence of subluxation without fractures. The biomechanical differences are explained by the relative ratio of the size of the cranium to the body in the young child, lack of ligamentous stability, poor muscle strength, and increased forces relative to the older child and adult. Children are also more prone to spinal cord injury with otherwise normal radiographs, the so-called SCIWORA (spinal cord injury without radiographic abnormality), compared to adults. This is especially evident in children younger than 9 years of age where there is a high incidence of reported complete cord injuries associated with SCIWORA. Suggested mechanisms of the SCIWORA include hyperextension or flexion injuries to the immature and the inherently elastic spine, which is vulnerable to external forces and allows for significant intersegmental movement and transient soft disc protrusion, resulting in distraction injuries, and/or ischemic injury of the spinal cord [37]. The elasticity of the spine allows it to stretch up to 5 cm before rupture, whereas the spinal cord, which is anchored to the brachial plexus superiorly and the cauda equina inferiorly, ruptures after 4–6 mm of traction [38]. As MRI is readily capable of detecting the soft tissue injury component, the concept of SCIWORA is less relevant.

The imaging algorithm for pediatric spinal trauma is somewhat different than that for adults. MDCT is used more judiciously due to radiation exposure considerations, and at many places lower-dose radiography is often utilized initially. MRI is always used if there is a consideration of a pure soft tissue injury or neurological deficit.

Neurological Recovery After Spinal Cord Injury

Although there are no pharmacologic "cures" for spinal cord injury, spontaneous neurological recovery after injury can occur, and it largely depends upon the severity of the initial neurological deficit, the neurological level of injury, patient age, and comorbidities. Very few patients with a neurologically complete injury (i.e., no motor or sensory function below the injury level) actually regain any useful function below the injury level although most patients will spontaneously improve by one neurological level (e.g., a C5 level spontaneously descends to a C6 level). Even these small improvements can have a substantial impact on a patients' capacity to function independently.

The role of MRI to predict capacity for spontaneous neurological recovery after cervical SCI has been evaluated. Although there is considerable overlap in results, some general characterizations about the MRI appearance of SCI and neurological recovery are evident. Intramedullary hemorrhage four millimeters or greater is equated with a severe neurological deficit and a poor prognosis. Cord edema alone is indicative of a mild to moderate initial neurological deficit and a better capacity for spontaneous neurological improvement. The length of the cord lesion may also correlate with the initial deficit and in the neurological outcome. As novel pharmacologic therapies for SCI are developed and tested, MRI will likely play a more essential role in characterizing the injury and helping to select patients for clinical trials.

References

1. Riascos R, Bonfante E, Cotes C, Guirguis M, Hakimelahi R, West C (2015) Imaging of Atlanto-Occipital and Atlantoaxial Traumatic Injuries: What the Radiologist Needs to Know. Radiographics 35(7):2121–2134. doi:10.1148/rg.2015150035
2. Hill MW, Dean SA (1993) Head injury and facial injury: is there an increased risk of cervical spine injury? J Trauma 34:549–554
3. Pope AM, Tarlov AR (1991) Disability in America: toward a national agenda for prevention. National Academy Press, Washington
4. Riggins RS, Kraus JF (1997) The risk of neurological damage with fractures of the vertebrae. J Trauma 17:126–130
5. Castellano V, Bocconi FL (1970) Injuries of the cervical spine with spinal cord involvement (myelic fractures): statistical considerations. Bull Hosp J Dis Orthop Inst 31:188–198
6. Rogers WA (1957) Fractures and dislocations of the cervical spine; an end-result study. J Bone Joint Surg 39:341–351
7. Diaz JJ Jr, Gillman C, Morris JA Jr et al (2003) Are five-view plain films of the cervical spine unreliable? A prospective evaluation in blunt trauma in patients with altered mental status. J J Trauma 55:658–663
8. Griffen MM, Frykberg KAJ et al (2003) Radiographic clearance of blunt cervical spine injury: plain radiograph or computed tomography scan? J Trauma 55:222–226
9. Holmes JF, Mirvis SE, Panacek EA, NEXUS Group (2002) Variability in computed tomography and magnetic resonance imaging in patients with cervical spine injuries. J Trauma 53:524–529
10. Kligman M, Vasili C, Roffman M (2001) The role of computed tomography in cervical spine injury due to diving. Arch Orthop Trauma Surg 121:139–141
11. Schenarts PJ, Diaz J, Kaiser C et al (2001) Prospective comparison of admission computed tomographic scan and plain films of the upper cervical spine in trauma patients with altered mental status. J Trauma 51:663–668
12. Berne JD, Velmahos GC, El Tawil Q et al (1999) Value of complete cervical helical computed tomographic scanning in identifying cervical spine injury in the unevaluable blunt trauma patient with multiple injuries: a prospective study. J Trauma 47:896–902
13. Van Goethem JW, Maes M, Ozsarlak O et al (2005) Imaging in spinal trauma. Eur Radiol 15(3):582–590
14. Flanders AE, Schaefer DM, Doan HT et al (1990) Acute cervical spine trauma: correlation of MR imaging findings with degree of neurological deficit. Radiology 177(1):25–33
15. Sliker CW, Mirvis SE, Shanmuganathan K (2005) Assessing cervical spine stability in obtunded blunt trauma patients: review of medical literature. Radiology 234:733–739
16. Wilmink JT (1999) MR imaging of the spine: trauma and degenerative disease. Eur Radiol 9:1259–1266

17. Denis F (1983) The three column spine and its significance in the classification of acute thoracolumbar spinal injuries. Spine 8(8):817–831
18. Mcafee PC, Yuan HA, Fredrickson BE et al (1983) The value of computed tomography in thoracolumbar fractures. An analysis of one hundred consecutive cases and a new classification. J Bone Joint Surg Am 65(4):461–473
19. Magerl F, Aebi M, Gertzbein SD et al (1994) A comprehensive classification of thoracic and lumbar injuries. Eur Spine J 3(4):184–201
20. Lee JY, Vaccaro AR, Lim MR et al (2005) Thoracolumbar injury classification and severity score: a new paradigm for the treatment of thoracolumbar spine trauma. J Orthop Sci 10(6):671–675
21. Dvorak MF, Fischer CG, Fehlings MG, Rampersaud YR, Oner FC, Aarabi B, Vaccaro AR (2007) The surgical approach to subaxial cervical spine injuries: an evidence-based algorithm based on the classification system. Spine 32(23):2620–2629
22. Rogers LF (1971) The roentgenographic appearances of transverse or chance fractures of the spine: the seat belt fracture. Am J Roentgenol 111:844–849
23. Gertzbein SD (1992) Scoliosis Research Society: multicenter spine fracture study. Spine 17:528–540
24. Diaz JJ, Aulino JM, Collier B et al (2005) The early work-up for isolated ligamentous injury of the cervical spine: does computed tomography scan have a role. J Trauma 59:897–904
25. Burney RE, Maio RF, Maynard F et al (1993) Incidence, characteristics, and outcome of spinal cord injury at trauma centers in North America. Arch Surg 128:596–599
26. Dawodu ST (2009) Spinal cord injury–definition, epidemiology, pathophysiology. Medscape Reference. http://emedicine.medscape.com/article/322480-overview
27. Bondurant FJ, Cotler HB, Kulkarni MV et al (1990) Acute spinal cord injury. A study using physical examination and magnetic resonance imaging. Spine 15(3):161–168
28. Kulkarni MV, McArdle CB, Kpanicky D et al (1987) Acute spinal cord injury: MR imaging at 1.5 T. Radiology 164(3):837–843
29. Schouman-Claeys E, Frija G, Cuenod CA et al (1990) MR imaging of acute spinal cord injury: results of an experimental study in dogs. AJNR Am J Neuroradiol 11(5):959–965
30. Ramon S, Dominguez R, Ramirez L et al (1997) Clinical and magnetic resonance imaging correlation in acute spinal cord injury. Spinal Cord 35(10):664–673
31. Cotler HB, Kulkarni MV, Bondurant FJ (1988) Magnetic resonance imaging of acute spinal cord trauma: preliminary report. J Orthop Trauma 2(1):1–4
32. Sato T, Kokubun S, Rijal KP et al (1994) Prognosis of cervical spinal cord injury in correlation with magnetic resonance imaging. Paraplegia 32(2):81–85
33. Marciello MA, Flanders AE, Herbison GJ et al (1993) Magnetic resonance imaging related to neurologic outcome in cervical spinal cord injury. Arch Phys Med Rehabil 74(9):940–946
34. Goldberg AL, Rothfus WE, Deeb ZL et al (1988) The impact of magnetic resonance on the diagnostic evaluation of acute cervicothoracic spinal trauma. Skeletal Radiol 17(2):89–95
35. Wittenberg RH, Boetel U, Beyer HK (1990) Magnetic resonance imaging and computer tomography of acute spinal cord trauma. Clin Orthop Relat Res 260:176–185
36. Schaefer DM, Flanders A, Northrup BE et al (1989) Magnetic resonance imaging of acute cervical spine trauma. Correlation with severity of neurologic injury. Spine 14(10):1090–1095
37. Kriss VM, Kriss TC (1996) SCIWORA (spinal cord injury without radiographic abnormality) in infants and children. Clin Pediatr (Phila) 35:119–124
38. Manary MJ, Jaffe DM (1996) Cervical spine injuries in children. Pediatr Ann 25:423–428

Spinal Cord Inflammatory and Demyelinating Diseases

Philippe Demaerel and Jeffrey S. Ross

Introduction

The etiopathogenesis of acute transverse myelopathy can be of inflammatory (viral, postviral), demyelinating/autoimmune, infectious, (para)neoplastic, and vascular origin. When no underlying cause can be found despite extensive search, the myelopathy is classified as idiopathic.

In the appropriate clinical setting and in the presence of signs of inflammation on CSF examination, the term acute transverse myelitis can be used. Inflammatory and demyelinating (often autoimmune) spinal cord pathology usually presents as myelitis and/or (meningo)radiculitis. Multiple sclerosis and transverse myelitis are the most common inflammatory/demyelinating spinal cord diseases.

MR imaging is the modality of choice in the diagnostic workup and plays a crucial role in excluding compressive disorders or spinal cord ischemia and in narrowing the diagnosis in a patient with suspected myelitis. The protocol should include sagittal and axial T2-weighted images as well as pre- and post-gadolinium T1-weighted images. Diffusion tensor imaging has been shown to provide additional information on degree of demyelination (decreased fractional anisotropy) or axonal injury (increased mean diffusivity) but does not yet play a significant role in daily clinical practice.

P. Demaerel (✉)
Department of Radiology, University Hospitals KU Leuven, Herestraat 49, Leuven 3000, Belgium
e-mail: Philippe.Demaerel@uzleuven.be

J.S. Ross
Neuroradiology Department, Barrow Neurological Institute, St Joseph's Hospital and Medical Center, 350 West Thomas Road, Phoenix, AZ 85013, USA
e-mail: jstuartr@aol.com

Multiple Sclerosis (MS)

MS is a multiphasic disease and most patients present in the second or third decade of life.

Transverse myelitis is an uncommon initial presentation but can be seen at some stage in up to 90 % of the patients with MS. In a minority of the patients (<10 %), spinal cord plaques can be seen in the absence of cerebral lesions. The risk of developing clinically definite MS in these patients is 20 % over a period of 20 years.

Up to one third of patients presenting with clinically isolated syndrome have asymptomatic spinal cord lesions, associated with an increased risk of developing clinically definite MS.

According to the McDonald criteria, spinal cord lesions can be used to demonstrate dissemination in space [1]. Demonstration of dissemination in time is more difficult because of the less reliable detection of new spinal cord plaques and the difficulty of detecting contrast enhancement in spinal cord plaques.

Indications for spinal cord imaging in MS are (1) clinically isolated syndrome and normal or nonspecific brain abnormalities, (2) partial myelitis in order to exclude non-demyelinating pathology, and (3) transition to a progressive phase of MS [2].

Lesions in the spinal cord often affect the pyramidal and spinothalamic tract and the dorsal column system leading to more severe physical disability, but correlation with the clinical symptomatology remains poor. This could at least partly be explained by the more challenging imaging approach of the spinal cord. Imaging is more prone to artifact from motion and from cerebrospinal fluid pulsation, and detection of plaques depends on the technique used.

In spinal cord MS, usually more than one rather small lesion (about the length of a vertebral body on sagittal image and involving less than half the spinal cord on axial images) is seen on MR imaging, without swelling of the spinal cord (Fig. 1). Most plaques are located in the cervical spinal cord.

J. Hodler et al. (eds.), *Diseases of the Brain, Head and Neck, Spine 2016–2019: Diagnostic Imaging*, DOI 10.1007/978-3-319-30081-8_22

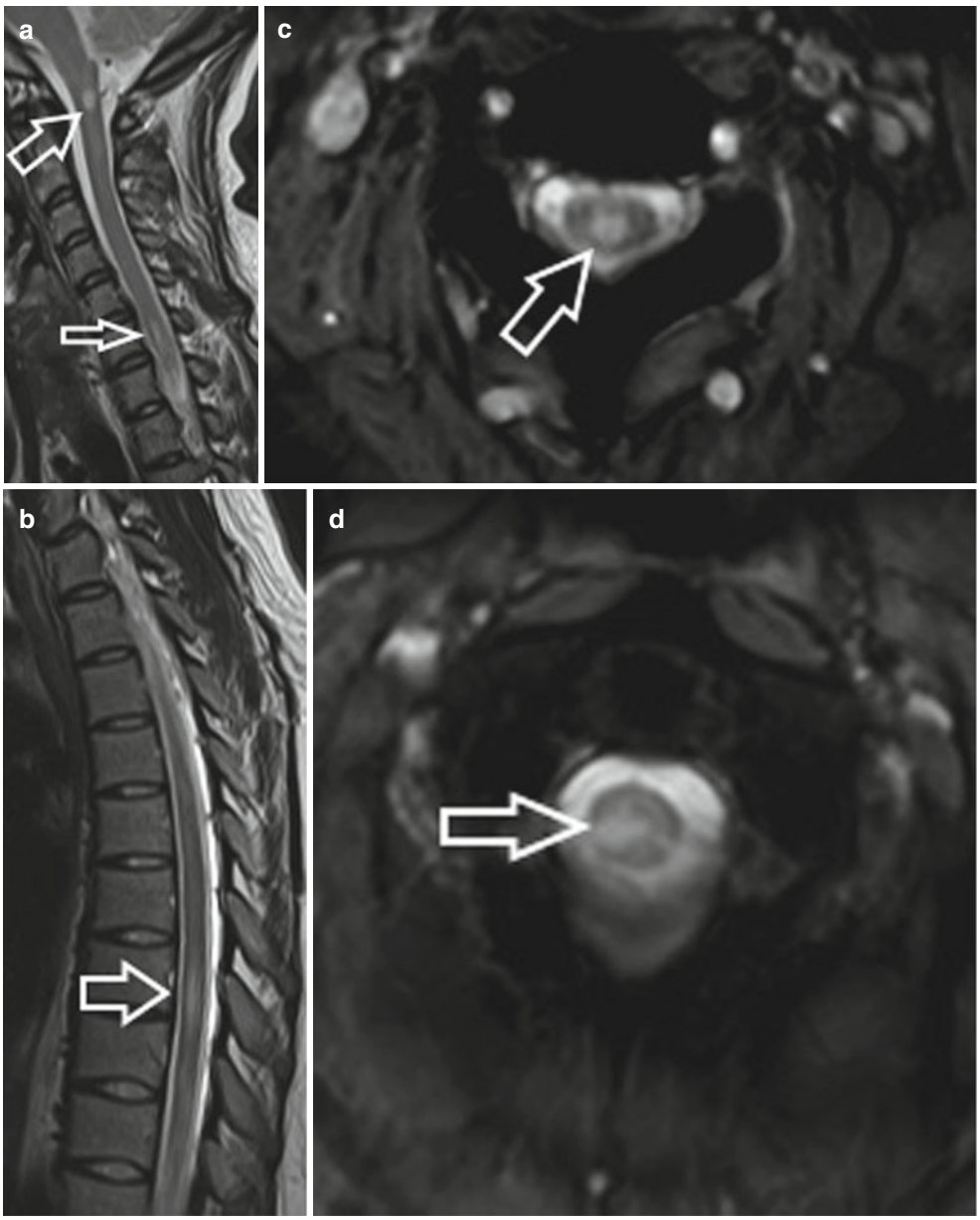

Fig. 1 (**a**, **d**) Multiple sclerosis. (**a**, **b**) Sagittal T2-weighted images show two small intramedullary lesions. (**c**, **d**) On axial T2-weighted images, the plaques are located in the dorsal and lateral columns

Gadolinium uptake may be seen in the acute stage but is now considered to be a rather insensitive marker of blood–brain barrier breakthrough [3]. After the acute stage, plaques tend to be well-defined and oval in shape along the long axis of the venous system. Enhancement has been observed in inactive plaques too and can be absent in progressive MS.

In primary progressive MS, diffuse abnormalities can be seen in the spinal cord.

In relapsing remitting MS, atrophy mainly involves the dorsal columns of the cervical spinal cord. In secondary progressive MS, more generalized atrophy is seen involving the lateral and dorsal columns.

A high number of spinal cord plaques and atrophy are two imaging findings associated with a worse clinical outcome. Atrophy of the thoracic cord is less common and should raise the suspicion of other diseases such as human T lymphocyte virus type 1-associated myelopathy [4].

Quantitative MR imaging of the spinal cord has demonstrated novel associations with disability and disease progression [2]. 7 T imaging and improved coil design will allow a more detailed analysis of spinal cord gray and white matter.

Acute Transverse Myelitis

Generally speaking, acute transverse myelitis is a monophasic disease typically presenting with rapidly progressing paraplegia, a sensory disturbance and bowel/bladder disturbance.

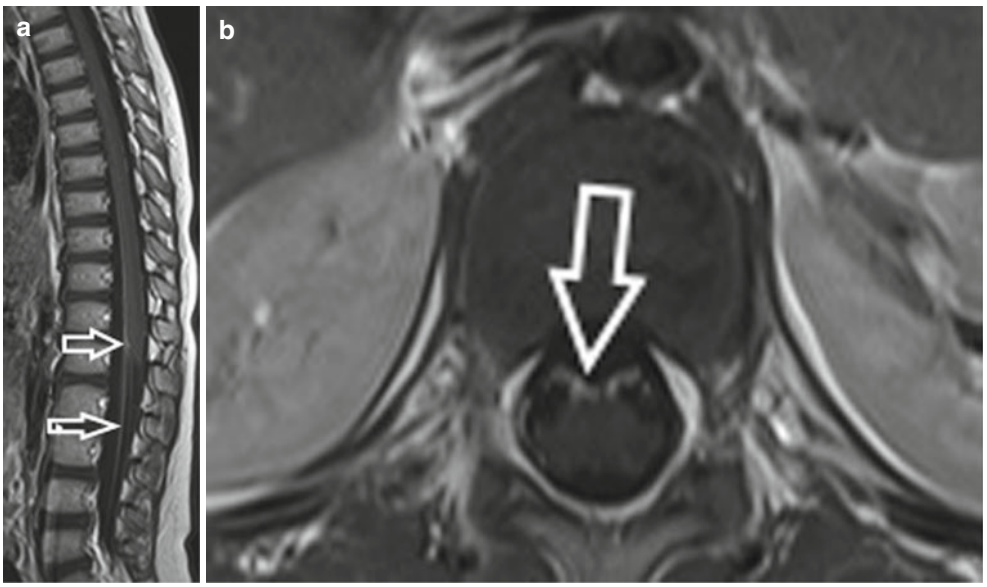

Fig. 2 (**a**–**c**) Guillain-Barré syndrome. Sagittal (**a**) and axial (**b**, **c**) postcontrast T1-weighted demonstrate pial enhancement along the conus and cauda equina. Note the selective involvement of the anterior nerve roots

A variety of viral agents has been reported. Increased serological titer and increased CSF protein and positive CSF PCR for viral genome can support the diagnosis, but etiological diagnosis is not always obtained, and the myelitis is then classified as "idiopathic."

Up to 40 % of pediatric transverse myelitis is preceded by an, often viral, infection [5]. The risk of developing MS is very low. Postvaccination myelitis can occur too. The pathogenesis in acute transverse myelitis and in ADEM is resembling each other.

The spinal cord lesion typically extends over three to four vertebral segments and usually involves more than two thirds of the cross-sectional area of the spinal cord at the cervical and/or thoracic level. The central location of the pathology is a useful finding in the differential diagnosis with demyelination (more eccentric location). Diffuse, peripheral, and patchy gadolinium enhancement can occur and is more frequent in the subacute stage than in the acute stage.

Guillain-Barré syndrome involves the peripheral nerves and acute inflammatory demyelinating polyradiculopathy is considered a subtype. Leptomeningeal and/or nerve root enhancement has been reported in Guillain-Barré syndrome and more commonly involves the ventral nerve roots (Fig. 2).

According to the Transverse Myelitis Consortium Working Group, the role of imaging in the diagnosis of transverse myelitis is limited to the exclusion of compressive pathology and the demonstration of spinal inflammation by gadolinium enhancement (or CSF pleocytosis or elevated IgG) [6].

Neuromyelitis Optica Spectrum Disorder (NMOSD)–Autoimmune Aquaporin-4 (AQP4) Channelopathy

Historically neuromyelitis optica (NMO, Devic's disease) was considered to be an inflammatory disease, characterized by bilateral optic neuritis and myelitis (predominantly involving the cervical and thoracic cord). The interval between the optic neuritis and the myelitis is usually days or weeks, but longer intervals are possible too. The clinical presentation may resemble multiple sclerosis but is more common in females, and most patients present in the fourth decade of life. Neurological symptoms and physical disability are more severe in NMO than in MS, and recovery is less good.

Later, the major criteria for NMO were redefined and included (1) (bilateral) optic neuritis mainly involving the posterior part of the optic nerve and the optic chiasm, (2) transverse myelitis extending over more than three vertebral segments, and (3) no evidence of sarcoidosis, vasculitis, SLE, Sjögren's syndrome. In addition one of the following should also be present: (1) brain abnormalities not fulfilling Barkhof criteria or (2) positive test in serum or CSF for AQP4 antibodies [7].

The term NMOSD was introduced in 2007 and consists of (1) NMO, (2) limited/partial/inaugural form of NMO, (3) Asian optic–spinal myelitis, (4) optic neuritis or longitudinal extensive transverse myelitis (LETM) associated with autoimmune disease, and (5) optic neuritis or myelitis with brain lesions typical of NMO [7]. In NMOSD, the AQP4 is always positive.

Fig. 3 (**a**–**f**) Neuromyelitis optica. Sagittal T2 (**a**)- and T1 (**b**)- and postcontrast T1 (**c**)-weighted images show an extensive spinal cord lesion ranging from level C7 to Th8 with high signal on T2 (**a**) and low signal on T1 (**b**). The low T1 signal is another helpful finding in the differentiation with MS. There is predominantly peripheral enhancement after contrast administration. Coronal T2-weighted images (**d**, **e**), obtained 2 months earlier, show evidence of chiasmitis

More recently the international consensus diagnostic criteria for NMOSD were published [8]. A distinction is made between AQP4IgG+ NMOSD and AQP4IgG- NMOSD. Six clinical characteristics have been defined, i.e., acute myelitis, optic neuritis, acute brainstem syndrome, area postrema syndrome, acute diencephalic syndrome (with MR abnormalities), and symptomatic cerebral syndrome (with typical MR lesions). The criteria for AQP4IgG+ NMOSD require at least one clinical characteristic and the exclusion of alternative diagnoses. For AQP4IgG- NMOSD, at least two clinical characteristics are required, at least one of them being optic neuritis, LETM myelitis, or area postrema syndrome, as well as dissemination in space. In a single episode of LETM, up to 40 % of the patients have NMOSD, while in case of relapse, this increases to 70 % [9, 10].

The discovery of AQP4 opened a whole new research area which led to the definition of autoimmune AQP4 channelopathy, representing diseases in which the AQP4-IgG biomarker is always true positive. Cell-based serum assays have improved the sensitivity of auto-antibody detection, but they are not yet widely available.

AQP4IgG+ is an astrocytopathy and is more often seen in female patients presenting at an older age. The myelin oligodendrocyte glycoproteinopathy (MOG) is an oligodendrocytopathy with a different immunopathogenic mechanism (10–15 % of the AQP4IgG–patients). This monophasic disease more frequently hits men at a younger age, and outcome appears to be more favorable. Optic neuritis is more common than transverse myelitis, and cord lesions (gray matter often conus involvement) can resolve following treatment. A recent paper reported on a cohort of 33 children with ADEM, 19 of them having serum MOG antibodies. Those children more often had spinal cord involvement with lesion extending over more than three vertebral levels and had a better outcome [11].

On imaging usually one spinal cord lesion is seen, extending over three or more vertebral segments of the spinal cord, predominantly involving the gray matter (Fig. 3). The low T1 signal reflects the extensive parenchymal damage and is a helpful differential diagnostic sign compared with MS. Gadolinium enhancement can be observed. Cerebral lesions are absent or nonspecific in most cases. However, lesions

in the circumventricular organs (e.g., area postrema, lamina terminalis), brainstem, and corpus callosum have been reported, corresponding to regions with high expression of AQP4.

Patients with NMOSD are at high risk (approximately 40 %) of developing autoimmune diseases (e.g., rheumatoid arthritis, SLE, antiphospholipid syndrome) and are clearly more frequently seen in AQP4IgG+ patients (see systemic autoimmune diseases).

Differential diagnosis with MS is important because other treatment options are available, e.g., plasmapheresis and intravenous gammaglobulins.

Sarcoidosis

Sarcoidosis is a noninfectious granulomatous immune disorder with primarily involvement of the lungs, lymph nodes, and skin. Central nervous system involvement occurs in approximately 10 % of patients with sarcoidosis. Primary involvement of the spinal cord is uncommon and more frequently concerns the cervical level and the cervicothoracic junction. Cerebrospinal fluid abnormalities are nonspecific and can even remain normal in patient with spinal cord involvement only [12]. Elevated serum and CSF angiotensin-converting enzyme (ACE) can be helpful in reaching a diagnosis. It is important to know the imaging appearances of spinal cord sarcoidosis in order to suggest the possible diagnosis and to avoid delay of adequate therapy.

In neurosarcoidosis granulomatous infiltrates can be seen in the meninges, pituitary gland, hypothalamus, and cranial nerves. Leptomeningeal infiltrates along the spinal cord and cauda equina can be observed (Fig. 4). Infectious granulomatous diseases such as tuberculosis and brucellosis can yield similar imaging findings. A corset-like neuropathy may raise the suspicion of neurosarcoidosis, especially if cranial nerve palsy is observed too [12].

Systemic Autoimmune Diseases

Myelitis has been reported to occur occasionally (1–3 %) in a large number of autoimmune disorders, e.g., SLE, antiphospholipid syndrome, Sjögren's syndrome, Behçet's disease,

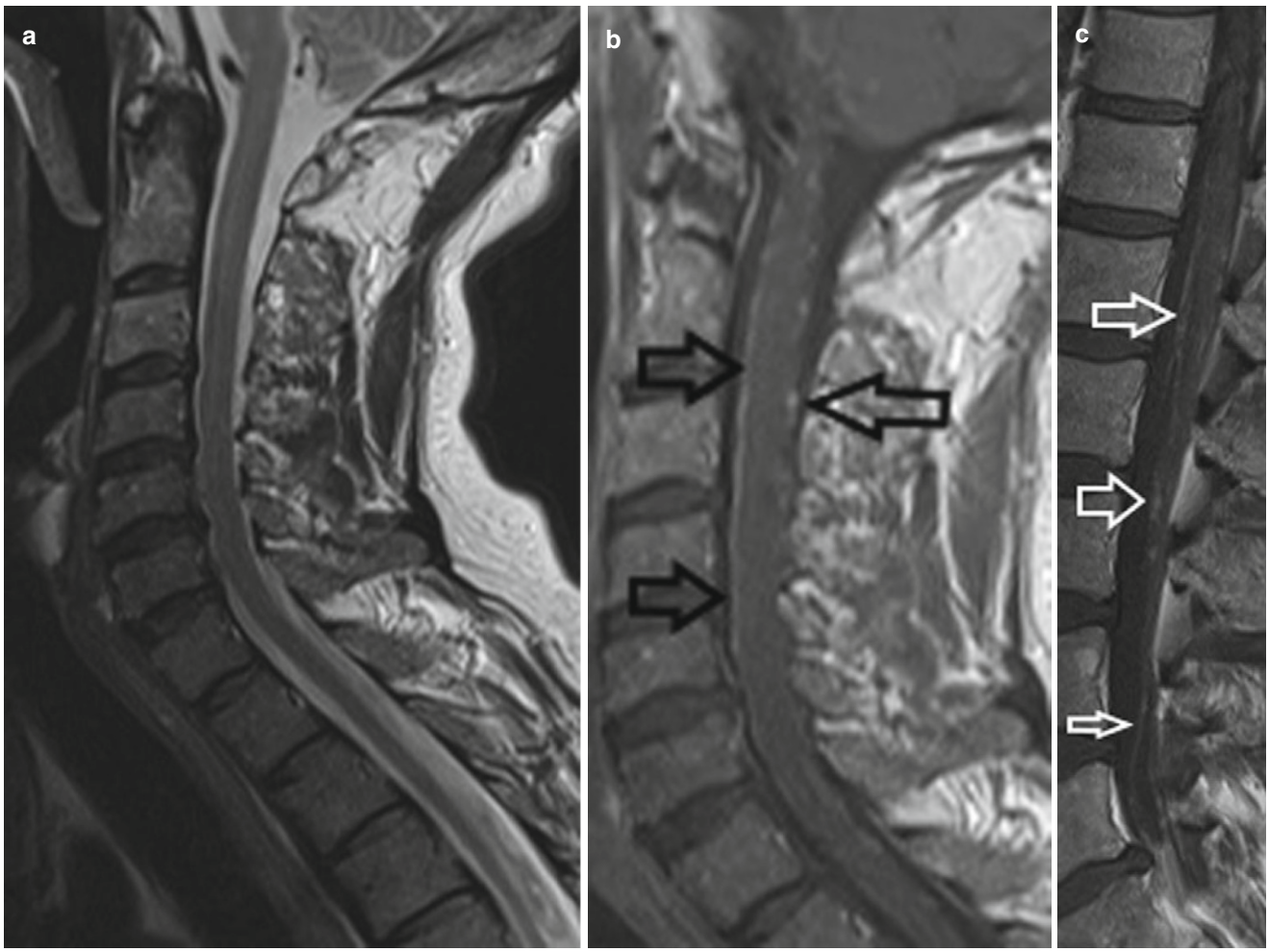

Fig. 4 (**a**–**c**) Neurosarcoidosis. Sagittal T2 (**a**)- and postcontrast T1 (**b**, **c**) -weighted images. There are no intramedullary abnormalities (**a**). Postcontrast images show pial enhancement along the cervical spinal cord and cauda equina (**b**, **c**)

mixed connective tissue disease, rheumatoid arthritis, ankylosing spondylitis, etc. Myelitis can be the first event leading to the diagnosis of an autoimmune disease or can occur during the course of an autoimmune disease. A recent review of the literature has identified 22 autoimmune diseases which can be seen in association with NMO [13].

The pathogenesis is not fully clear, and it is likely that different theories might be possible. Myelitis could be due to a coexistent NMO spectrum disorder or due to a vasculitic process with inflammation and myelomalacia [14]. An underlying vasculitic process is associated with an acute onset, and prognosis is less good than in patients presenting with coexistent NMO.

Although new CSF autoimmune markers are being developed, etiological diagnosis is not always obtained, and the myelitis is still classified as "idiopathic."

Imaging may reveal LETM as well as multifocal small lesions with symmetrical gray matter involvement (Fig. 5).

Differential Diagnosis

Inflammatory and demyelinating (autoimmune) diseases have been reviewed, but MR plays an important role in ruling out other pathologies, e.g., infectious (bacterial and TB) myelitis and myelitis in immunosuppressed patients, ischemia, vascular malformations, cobalamin/copper deficiency, and radiation myelitis [15, 16].

Disk space infections on MR typically produced confluent decreased signal intensity of the adjacent vertebral bodies and the involved intervertebral disk space on T1-weighted images as compared to the normal vertebral body marrow. A well-defined end plate margin between the disk and adjacent vertebral bodies cannot be defined. T2-weighted images show increased signal intensity of the vertebral bodies adjacent to the involved disk and an abnormal morphology and increased signal intensity from the disk itself, with absence or irregularity of the normal intranuclear cleft.

The incidence of spinal epidural abscess ranges from 0.2 to 1.96 cases per 10,000 [17]. Risk factors for the development of epidural abscess include altered immune status, renal failure requiring dialysis, alcoholism, and malignancy. Although intravenous drug abuse is a risk factor for epidural abscess, HIV infection does not appear to play a role in the overall increasing incidence of the disease.

Staphylococcus aureus is the organism most commonly associated with epidural abscess, constituting approximately 60 % of the cases. It is ubiquitous, tends to form abscesses, and can infect compromised as well as normal hosts. Clinical acute symptomatology classically includes back pain, fever, obtundation, and neurologic deficits. Chronic cases may have less pain and no elevated temperature. The classic course of epidural abscess consists of four stages: spinal ache, root pain, weakness, and paralysis. Acute deterioration from spinal epidural abscess, however, remains unpredictable. Patients may present with abrupt paraplegia and anesthesia. The cause for this precipitous course is unknown but is likely related to a vascular mechanism (epidural thrombosis and thrombophlebitis, venous infarction).

Bacterial spinal cord meningitis and myelitis is relatively rare but can be seen after spinal surgery, in complicated meningitis, or in septicemia [15]. Cord swelling and peripheral enhancement are usually seen (Fig. 6). *Staphylococcus* and *Streptococcus* are the most common pathogens.

The clinical presentation of spinal cord ischemia is usually more abrupt than in myelitis although occasionally it can be difficult to differentiate both entities. The thoracic gray matter cord is more vulnerable. In the first hours, MR imaging can remain normal, and diffusion-weighted imaging can be helpful. Gadolinium enhancement can be observed in the subacute stage.

Bilateral anterior horn infarct results in the so-called snake eyes (Fig. 7). Spinal dural arteriovenous fistula can present with spinal cord expansion and high signal on T2, and usually numerous vascular flow voids can be seen representing venous congestion.

In cobalamin (vitamin B12) deficiency, T2 signal in the dorsal parts of the spinal cord is seen leading to loss of proprioception and vibration sense.

Fig. 5 (**a**–**c**) Perinuclear anti-neutrophil cytoplasmic antibody (pANCA)-positive myelitis. Sagittal (**a**, **b**) and axial (**c**) T2-weighted images show a diffuse hyperintensity of the spinal cord. More than two thirds of the spinal cord is involved on axial images with a predominant central and gray matter involvement (**c**)

Fig. 6 (**a**–**c**) Bacterial myelitis and meningitis. Sagittal T2 (**a**)- and postcontrast sagittal (**b**) and axial (**c**) T1-weighted images. There is a diffuse high signal in a swollen cervical and thoracic spinal cord (**a**). On postcontrast images, a peripheral and patchy enhancing pattern is noted (**b**, **c**)

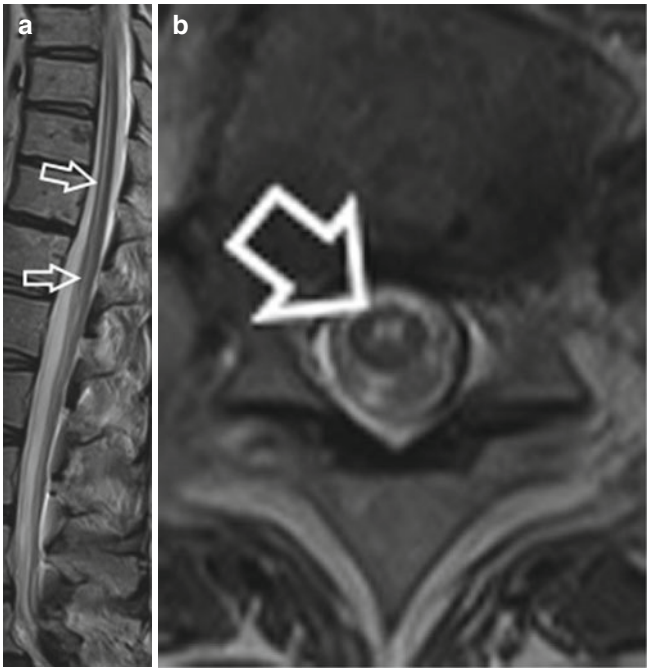

Fig. 7 (**a**, **b**) Spinal cord ischemia. Sagittal (**a**) and axial (**b**) T2-weighted images. Bilateral anterior horn ischemia is seen, with the typical "snake eye" imaging appearances

References

1. Polman CH, Reingold SC, Banwell B et al (2011) Diagnostic criteria for multiple sclerosis: 2010 revisions to the McDonald criteria. Ann Neurol 69:292–302
2. Kearney H, Miller DH, Ciccarelli O (2015) Spinal cord MRI in multiple sclerosis–diagnostic, prognostic and clinical value. Nat Rev Neurol 11:327–338
3. Lassmann H (2011) A dynamic view of the blood-brain barrier in active multiple sclerosis lesions. Ann Neurol 70:1–2
4. Liu W, Nair G, Vuolo L (2014) In vivo imaging of spinal cord atrophy in neuroinflammatory diseases. Ann Neurol 76:370–378
5. Alper G, Petropoulou KA, Fitz CR et al (2011) Idiopathic acute transverse myelitis in children: an analysis and discussion of MRI findings. Mult Scler 17:74–80
6. Transverse Myelitis Consortium Working Group (2012) Proposed diagnostic criteria and nosology of acute transverse myelitis. Neurology 59:499–505
7. Kim W, Kim SH, Kim HJ (2011) New insights into neuromyelitis optica. J Clin Neurol 17:115–127
8. Wingerchuk DM, Banwell B, Bennett JL (2015) International consensus diagnostic criteria for neuromyelitis optica spectrum disorders. Neurology 85:177–189
9. Iorio R, Pittock SJ (2014) Neuromyelitis optica and the evolving spectrum of autoimmune aquaporin-4 channelopathies. Clin Exper Neuroimmunol 5:175–187
10. Pittock SJ, Lucchinetti CF (2015) Neuromyelitis optica and the evolving spectrum of autoimmune aquaporin -4 channelopathies: a decade later. Ann N Y Acad Sci Ann N Y Acad Sci. doi:10.1111/nyas.12794. [Epub ahead of print].
11. Baumann M, Sahin K, Lechner C (2015) Clinical and neuroradiological differences of paediatric acute disseminating encephalomyelitis with and without antibodies to the myelin oligodendrocyte glycoprotein. J Neurol Neurosurg Psychiatry 86:265–272
12. Lidar M, Dori A, Lidar Z, Chapman J, Langevitz P (2010) Sarcoidosis presenting as "corset-like" myelopathy: a description of six cases and literature review. Clinic Rev Allerg Immunol 38:270–275
13. Iyer A, Elsone L, Appleton R et al (2014) A review of the current literature and a guide to the early diagnosis of autoimmune disorders associated with neuromyelitis optica. Autoimmunity 47:154–161
14. Birnbaum J, Petri M, Thompson R et al (2009) Distinct subtypes of myelitis in systemic lupus erythematosus. Arthritis Rheum 60:3378–3387
15. DeSanto J, Ross JS (2011) Spine infection/inflammation. Raiol Clin N Am 49:105–127
16. Goh C, Desmond PM, Phal PM (2014) MRI in transverse myelitis. J Magn Reson Imaging 40:1267–1279
17. Hlavin ML, Kaminski HJ, Ross JS, Ganz E (1990) Spinal epidural abscess: a ten-year perspective. Neurosurgery 27(2):177–184

Fetal MRI of the Brain and Spine

Marjolein H.G. Dremmen, P. Ellen Grant,
and Thierry A.G.M. Huisman

Introduction

Fetal magnetic resonance imaging (MRI) is nowadays an established second-line imaging modality next to prenatal ultrasound (US) [1–3]. Ultrafast fetal MR sequences allow to "picture freeze" the fetus in utero without the need for sedation. The goal of fetal MRI is to offer an enhanced visualization and characterization of the pathologies detected by routine prenatal sonography, and it is therefore used as a problem-solving technique in a selected patient population. Prenatal sonography remains the imaging modality of choice for evaluating disorders related to the fetus and pregnancy; however, occasionally fetal MRI can identify subtle lesions that remained uncovered by US but may be essential for accurate diagnosis. Furthermore, fetal MRI contributes to selection of intrauterine treatment options and obstetric management, determines immediate postnatal care, and enhances parental counseling.

MRI of the fetal brain and spine provides a higher sensitivity and specificity compared to prenatal US, because of several inherent US limitations. Depending on the maternal habitus, maternal bowel gasses, amount of amniotic fluid (e.g., oligohydramnios), and positioning of the child in utero (e.g., fetal head descended in the maternal bony pelvis), visualization of the fetal central nervous system (CNS) may be limited by US. Furthermore, the progressing development of the fetal cartilaginous/osseous calvarium and spinal canal during pregnancy may obscure lesions close to the skull or vertebral bodies on US examination [4–6].

The goals of this manuscript are to become familiar with the imaging protocol and indications for fetal MRI of the CNS, enhance your expertise about interpreting fetal MRI of the brain and spine, and become familiar with developmental variants of the fetal brain and spine.

Clinical Indications of Fetal MRI of the Brain and Spine

In general, fetal MRI is indicated in the case of sonographic visualization or suggestion of a CNS pathology of which the etiology or exact constellation of findings remains uncertain [7]. In addition, fetal MRI should be considered if an unexplained spontaneous abortion occurred in a previous pregnancy or if there is a positive family history for CNS abnormalities. Recent studies show that in 30–50% of fetuses undergoing second-line fetal MRI, additional abnormalities of variable clinical significance can be diagnosed [1, 2, 8]. Table 1 summarizes accepted clinical indications for fetal MRI of the CNS. A few specific congenital spinal abnormalities (e.g., non-skin-covered spinal dysraphia) are potentially treatable by means of fetal surgery. In those cases, fetal MRI has become the gold standard for confirming the diagnosis and guides the decision-making for the various surgical options [9, 10].

The appropriate gestational age for fetal MR imaging of the brain and spine is depending on the clinical indication.

M.H.G. Dremmen, MD (✉)
Division of Pediatric Radiology and Pediatric Neuroradiology,
Department of Radiology and Radiological Science,
Johns Hopkins Hospital, 1800 Orleans Street,
Baltimore, MD 21231, USA

Division of Pediatric Radiology, Department of Radiology,
Erasmus MC – University Medical Center,
1800 Orleans Street, Rotterdam 21231, The Netherlands
e-mail: marjolein.dremmen@gmail.com

P. Ellen Grant
Department of Radiology, Children's Hospital Boston and Harvard
Medical School, 300 Longwood Ave, Boston, MA 02115, USA
e-mail: ellen.grant@childrens.harvard.edu

T.A.G.M. Huisman
Division of Pediatric Radiology and Pediatric Neuroradiology,
Department of Radiology and Radiological Science,
Johns Hopkins Hospital, 1800 Orleans Street,
Baltimore, MD 21231, USA
e-mail: thuisma1@jhmi.edu

J. Hodler et al. (eds.), *Diseases of the Brain, Head and Neck, Spine 2016–2019: Diagnostic Imaging*, DOI 10.1007/978-3-319-30081-8_23

Table 1 Clinical indications of fetal MRI of the brain and spine [3, 10]

Brain	*Congenital anomalies of the brain or skull*
	Ventriculomegaly Callosal anomalies Posterior fossa anomalies Cerebral cortical malformations or migrational anomalies Cavum septum pellucidum abnormalities Holoprosencephaly Solid or cystic masses Cephalocele
	Acquired abnormalities of the brain
	Infarction Hemorrhage Congenital infection Vascular malformations Hydranencephaly Monochorionic twin pregnancy complications
	Identified risk factor for brain abnormalities
	Family history of genetic disorders Maternal infection Tuberous sclerosis or other phakomatoses Complex extracerebral malformations
Spine	Congenital anomalies of the spine
	Neural tube defects Sacrococcygeal teratoma Caudal regression/sacral agenesis Sirenomelia Vertebral anomalies
	Fetal surgery assessment
	Open, non-skin-covered spinal dysraphia (myelomeningocele) Sacrococcygeal teratoma

MR imaging of the fetus prior to 18 weeks of gestational age is of limited diagnostic value because of small fetal size and high fetal mobility. In general, fetal MR imaging of the CNS is performed between 20 and 23 weeks of gestational age to be able to adjust clinical decision-making during pregnancy and prenatal counseling. Fetal MR imaging later than 24 weeks of gestational age can contribute to decisions on treatment options, delivery modus, and prenatal counseling.

Finally, it should never be forgotten that fetal MRI should not only focus on the CNS. Many pathologies may affect multiple functional systems and organs in the fetus simultaneously. Identification of the complete entirety of fetal pathology may not only facilitate final diagnosis but may also have a significant impact on fetal prognosis, obstetric management, and parental counseling. Imaging the fetus should also include evaluation of the umbilical cord, amniotic fluid, placenta, and maternal uterus. Fetal MRI should be performed by experts on fetal pathology combining expertise on fetal CNS and non-CNS pathology.

Imaging Technique of Fetal MRI of the Brain and Spine

Standard MRI Sequences

Typically, fetal MRI is performed at 1.5 T magnetic field strength; 3 T MR units are however progressively used. Multichannel phased array surface coils are used for data collection. Imaging is done without fetal or maternal sedation. Ultrafast single-shot T2-weighted half-Fourier sequences serve as the backbone sequence of fetal MRI. The ultrashort acquisition times per slice (<800 msec) and single-shot approach allow to image the fetal anatomy in exquisite detail. In particular, the fetal brain and spinal cord can be well evaluated due to their high water content which guarantees a strong MR signal. In addition, the T2 hyperintense cerebrospinal fluid which surrounds the fetal brain and spinal cord enhances depiction of the neuroanatomy. Depending on the suspected or encountered pathology (e.g., hemorrhage, fat), additional sequential T1-weighted imaging may be added. Unfortunately, currently no similar ultrafast T1-weighted sequences are available. Consequently, T1-weighted imaging still suffers from some motion artifacts. Triplanar imaging adapted to the fetal brain is collected to facilitate diagnoses.

Advanced MRI Techniques

The application of advanced MRI techniques can serve as problem solver in selected cases and is mainly applied to imaging of the fetal brain. Nevertheless, the use of advanced MRI techniques in assessing the fetal brain and spine needs to be studied more comprehensively before standard application is possible. The relative long acquisition times of advanced MRI techniques result in the principal use of these techniques in the last trimester of pregnancy because of descending of the fetal head and therefore reduced fetal motion.

Diffusion-weighted imaging in general is used to evaluate water motion and tissue characteristics. Including DWI sequences in imaging of the fetal brain provides information about developmental, metabolic, or ischemic brain processes. Diffusion tensor imaging is typically used for fetal CNS malformations.

^{1}H MR spectroscopy is sporadically used to detect the presence of normal or abnormal metabolites in the fetal brain parenchyma. Similar to the DWI/DTI sequences, ^{1}H MRS is due to its longer acquisition time susceptible for fetal motion.

Depending on your local settings and suspected pathology, the imaging protocols will vary combining standard anatomical sequences with a variety of advanced, functional sequences. We refer here to the extensive literature available.

Finally, fetal MRI studies should always be correlated with the prenatal US imaging findings. Fetal MRI should avoid to be considered a "stand-alone" imaging. In many institutions, prenatal US will be either revisited if available by the reading radiologist or will be repeated prior to the fetal MRI study.

Safety of Fetal MRI of the Brain and Spine

The available research studies investigating the safety and potential risks of routine clinical fetal MRI have not been able to determine any adverse effects affecting the mother or developing fetus. The American College of Radiology has published a practice guideline for the safe and optimal performance of fetal MRI in 2010. This guideline was revised collaboratively by the American College of Radiology (ACR) and the Society for Pediatric Radiology (SPR) in 2015. In the guideline is stated that no special consideration is recommended for any trimester in pregnancy to undergo MRI examination involving 3T or weaker magnetic fields if, in the determination of a level 2 MR personnel-designated attending radiologist, the risk-benefit ratio to the patients warrants that the MRI study should be performed [3]. The radiologist should review the indications and document them in the radiology report or the patient's medical record. The radiologist should be cognizant of the increased power deposition (long exposure times, high specific absorption rate) typically accompanying some higher magnetic field studies and ensure that they do not exceed established guidelines [3]. MRI contrast agents should not be routinely administered to pregnant patients. Gadolinium is a pregnancy class C drug, meaning that the safety in humans has not been proven [3]. In addition due to recirculation phenomena, gadolinium-based contrast agents will remain for an extended period in the fetal circulation if injected to the mother.

In consideration of the possible side effects to the developing fetus as well as the present limitations of fetal MRI of the brain and spine at an early gestational age, fetal MRI examination is preferably not performed prior to 18 weeks of gestation.

Normal Development of the Fetal Brain and Spine

The development of the fetal brain encompasses multiple programmed, interacting, and complex processes including neuronal cell proliferation and migration (histogenesis), cortical sulcation/gyration, and white matter myelination to mention a few key processes. The brain development does not stop postnatally but extends well into the first and partially second decade of life. Familiarity with the normal and abnormal brain embryology and subsequent maturation is a sine qua non to each radiologist for correct identification of pathologies on fetal MRI.

Neuronal Proliferation and Migration

The migration of neurons begins during the sixth week of embryologic development. Neuroectodermal elements proliferate within and migrate from the germinal matrix in the direction of the surface of the brain, developing cortical ribbon. The high cellular germinal matrix is a low T2 signal intensity band surrounding the walls of the lateral ventricles (pronounced at the level of the frontal and temporal horns). During the migration process, the germinal matrix involutes gradually (Fig. 1). The germinal matrix persists in the caudothalamic groove until several months after birth [11–14]. The earliest migrating neurons give rise to the deep primitive cerebral cortex (inner layer) followed by neurons creating the outer superficial layer of the cortex. The next arriving neurons will build op the four intermediate cortical layers in an inside-out manner [7]. The migration process reaches completion around the 24th week of embryologic development. The cortical plate is extremely cellular and is identified as a smooth low T2 signal intensity band. Furthermore, an additional layer of neuroectodermal elements migrates toward the surface of the brain and discontinues their outward migration in the white matter before reaching the peripheral cortex (intermediate layer). This high cell density intermediate layer is seen as a low T2 signal intensity band between developmental weeks 20 and 28. The low cell density adjacent white matter shows high T2 signal intensity [13]. The advancing distribution of glial cells throughout the white matter after the 28th–30th week causes the multilayered pattern to be no longer visible on fetal MRI (Fig. 1). Likewise, by weeks 26–27 of embryologic development, the cerebellar hemispheres show a three-layered pattern matching the high cell density and low T2 signal intensity cerebellar cortex and dentate nuclei alternated with the intervening low cellularity, high T2 signal intensity cerebellar white matter [15].

Cortical Sulcation and Gyration

In the supratentorial brain, the primary lateral fissure and primary parieto-occipital sulcus are the first sulci visible on fetal MRI around the 18th week of embryologic development (Fig. 1). The primary calcarine sulcus, cingulate sulcus, and central sulcus are identified at, respectively, week 24, week 25, and week 27 of development. Cortical sulcation

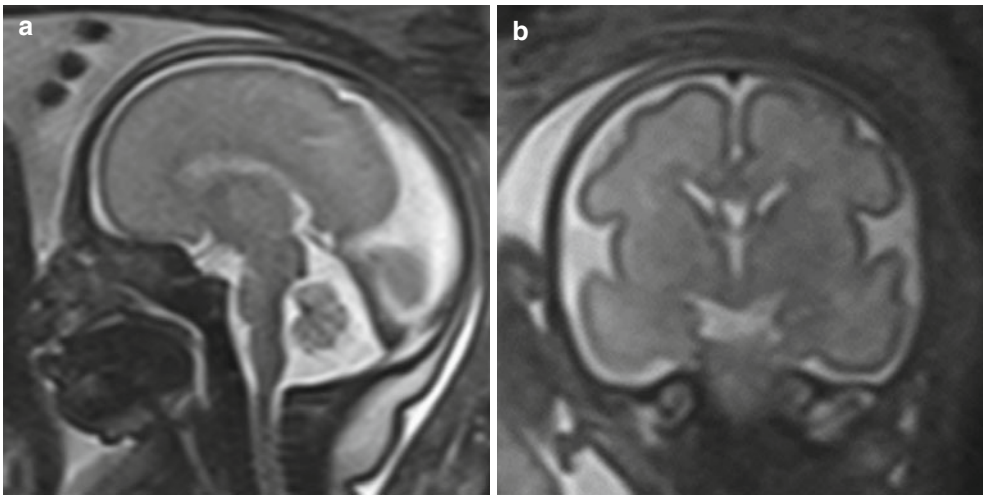

Fig. 1 Sagittal and coronal T2-weighted fetal magnetic resonance images of a normal developing fetal brain at 29 weeks of gestational age. The sagittal image (**a**) illustrates the normal development of the midline structures and vermis. The T2 hypointense signal in the posterior brain stem is related to the normal myelination process. The parieto-occipital fissure is clearly visible. The coronal image (**b**) demonstrates the germinal matrix as a thin residual T2 hypointense band lining the lateral ventricles. The low cellularity white matter reveals a T2 hyperintense signal intensity. The T2 hypointense signal of the cortical layer is caused by the high cell density in the cortex. Asymmetry in the closure of the Sylvian fissures is noted as normal variance; the left Sylvian fissure is more advanced in its closure than the right

and gyration follow a specific pattern and serve as an indicator for cortical maturation. The number and depth of the primary sulci progress with fetal age, and they gradually mature into secondary and tertiary sulci. The process of sulcation and gyration will reach final contours in the 34th–35th developmental week.

In the infratentorial brain, the primary fissure of the cerebellar vermis can be identified in week 20 of embryologic development, followed by the horizontal fissure at the 21th developmental week. The volume of the fetal cerebellum is relatively small compared to the volume of the supratentorial brain [7, 16].

The appearance of sulci on fetal MRI demonstrates an approximate 2 week time delay compared to anatomic-pathologic identification of sulci in the fetal brain, because of the somewhat limited spatial resolution of fetal MRI of the brain compared to pathological-anatomical studies [17]. Proper knowledge of the temporal/sequential appearance of the sulci and neuronal migration is essential to identify subtle cortical and migrational anomalies.

Myelination

Brain myelination is visualized first in the sensory tracts of the posterior brain stem at week 20 of embryologic development (Fig. 1). The myelination process causes a decrease in water content and increase in cell density and lipid-containing myelin (intensely binding water molecules and thus decreasing the quantity of free water molecules) of the white matter and white matter tracts. Therefore, the myelinated regions of the brain convert to lower T2 signal intensity and higher T1 signal intensity on fetal MRI. Myelination is a strictly programmed process following a specific pattern from the spinal cord to the brain and in any portion of the brain from central to peripheral, caudal to cephalic, and occipital to temporal/frontal [11–13]. The posterior limb of the internal capsule appears myelinated on T1-weighted images in the 33th developmental week. In the subcortical perirolandic white matter, myelination is observed at week 35 of embryologic development on T1-weighted images.

Corpus Callosum

The formation of the corpus callosum starts in the eighth week of embryologic development. As of the 20th week, the completely formed corpus callosum should be detectable at fetal MRI as a low T2 signal intensity midline structure of global uniform thickness [7]. If the intended midline sagittal view is obtained a little off midline (because of fetal motion), the coronal images are helpful in assessing the integrity of the corpus callosum.

Cerebrospinal Fluid (CSF) Spaces

The lateral ventricles, particularly the trigones and occipital horns, as well as the extra-axial CSF spaces are relatively large till about week 24 of embryologic development.

Because of increase in brain volume and brain surface, the lateral ventricles and extra-axial CSF spaces appear less prominent with increasing fetal age. The ventricular dimensions are rather stable during fetal brain development, with an upper limit of 10–12 mm measured at the level of the atria in the axial plane [11]. Furthermore, the vacuolization of the primary meninges progresses from ventral to dorsal and posterior to anterior potentially causing accumulation of CSF in temporal and parieto-occipital regions resulting in persistent prominent CSF spaces in some fetuses [16].

Many review articles and textbooks are nowadays available summarizing the normal fetal brain development. In the author's opinion, it is advisable to consult these documents while reading fetal brain studies. In many cases, "eyeballing" based upon experience may be sufficient; however, subtle deviations from normal development may easily be missed or remain under recognized.

Abnormalities of the Fetal Brain and Spine

Abnormalities of the developing brain and spine involve both so-called "true" congenital brain malformations (programmed maldevelopment) and acquired or secondary brain anomalies (resulting from injuries to already developed fetal brain structures). Between both groups there is however some overlap. A destructive event or injury early during gestation may not only injure already developed structures but may also induce an abnormal subsequent development. For example, a focal stroke early during gestation may result in a focal brain defect, but the concomitant injury to, e.g., the germinal matrix may result in an abnormal or impaired migration of surviving neuronal progenitors. In addition, there is a well-known occasionally confusing overlap between etiologies. Migrational abnormalities may be inherited (e.g., X-linked band heterotopia), part of syndromes (e.g., Aicardi syndrome), and secondary to metabolic disorders (Zellweger syndrome) or result from an infectious process (CMV infection), to mention a few. High-end fetal MRI may identify many abnormalities; however, final recognition of the etiology may be limited.

In the current review, we cannot cover all abnormalities that can be diagnosed by fetal MRI. We will focus on several well-known and more frequently fetal abnormalities that you may see in your daily practice.

Ventriculomegaly

Ventriculomegaly identified on prenatal US is one of the most frequent indications for fetal MRI. The goal is to differentiate between isolated ventriculomegaly (incidental ventriculomegaly due to, e.g., aqueductal stenosis (Fig. 2) or secondary ventriculomegaly due to intraventricular hemorrhage) and syndromal ventriculomegaly in which the observed widening of the ventricles only represents the tip of the iceberg of findings [12, 18]. Differentiation is especially important because of a significant difference in functional prognosis between isolated and syndromal ventriculomegaly. The widespread used definition of fetal ventriculomegaly is a transtrigone diameter of ≥10 mm in the axial plane at any stage of embryologic development [18]. The ventriculomegaly is categorized as mild (10–12 mm), moderate (13–15 mm), or severe (≥16 mm) based on the transtrigone diameter. Isolated ventriculomegaly may be secondary to a congenital aqueductal stenosis, postinfectious

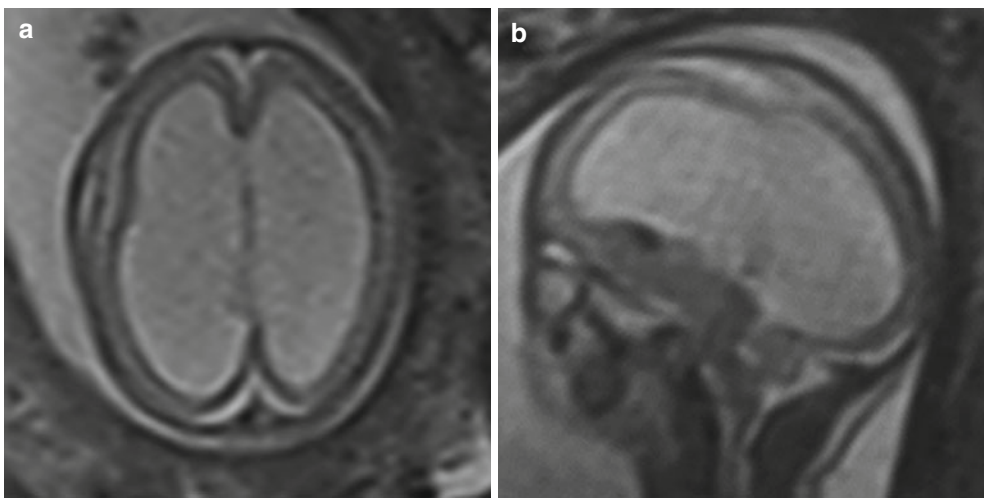

Fig. 2 Axial and sagittal T2-weighted fetal magnetic resonance images of a fetus with isolated ventriculomegaly due to aqueductal stenosis. The axial image (**a**) shows severe supratentorial ventriculomegaly. The T2 hypointense band along the ventricles represents the germinal matrix. The midline sagittal T2-weighted MR image (**b**) reveals a normal-sized fourth ventricle. Normal anatomy and development of the posterior fossa structures are noted

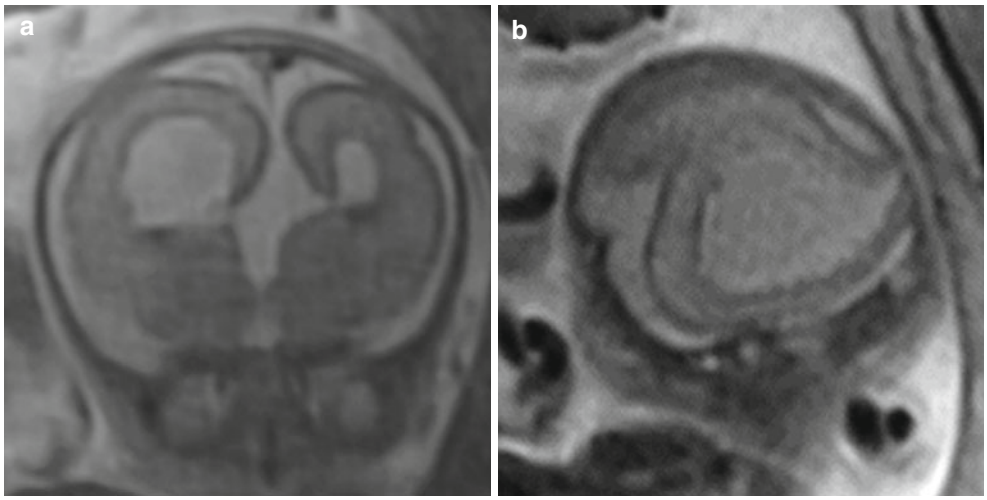

Fig. 3 Coronal and sagittal T2-weighted fetal magnetic resonance images of a fetus with corpus callosum agenesis and associated schizencephaly and periventricular heterotopia. The coronal image (**a**) shows the absence of the corpus callosum with the typical configuration of the moderate enlarged lateral ventricles. Associated periventricular heterotopia is noted. The sagittal T2-weighted MR image (**b**) reveals an additional unilateral open-lip schizencephaly in the parietal region. Incidental finding of a two-vessel umbilical cord

or posthemorrhagic obstruction of the Sylvian aqueduct, or arachnoid cysts blocking the normal CSF flow dynamics. Syndromal ventriculomegaly may be seen in a wide range of abnormalities including, e.g., Chiari II malformation, Dandy-Walker malformation, rhombencephalosynapsis, commissural anomalies, and migrational abnormalities. Furthermore, ventriculomegaly may be secondary to vascular anomalies like, e.g., a vein of Galen aneurysmal malformation in which the Sylvian aqueduct may be compressed by the dilated vein of Galen and in addition the increased (arterial) pressure in the venous system impairs CSF resorption and the chronic venous hypertension with venous ischemia induces a ventriculomegaly ex vacuo by progressive tissue loss ("melting brain").

Commissural Anomalies

Commissural anomalies represent a complex spectrum of malformations in which the various major commissures (corpus callosum, anterior commissure, and hippocampal commissure) may be absent, hypoplastic, malformed, or injured/destructed. Corpus callosum malformations are usually obvious on prenatal US. However, similar to the diagnostic workup of fetal ventriculomegaly, the corpus callosum pathology may just be the most obvious tip of the iceberg. Associated lesions, which may occur in up to 85% of cases, have to be excluded for decision-making and counseling [19]. The number of related abnormalities is extensive and includes Chiari II malformation, Dandy-Walker malformation, septo-optic dysplasia, gray matter heterotopia, gyration abnormalities, holoprosencephaly, schizencephaly, and encephaloceles (Fig. 3). Isolated corpus callosum anomalies are associated with delayed sulcation and encompass a possibility of altered neurodevelopment outcome.

Indirect evidence of abnormalities of the corpus callosum are the absence of cavum septum pellucidum, dilated ventricular atria and occipital horns (colpocephaly), high-riding third-ventricle radiating medial hemispheric sulci, and the classic staghorn configuration of the lateral ventricles on coronal imaging [11, 19].

Differentiation between "syndromal" corpus callosum agenesis and thinned or destructed corpus callosum due to high-grade ventriculomegaly or adjacent white matter injury (e.g., stroke) is essential for prediction of outcome as well as risk stratification for recurrence in a future pregnancy.

Posterior Fossa Anomalies

A variety of abnormalities of the posterior fossa can be accurately assessed with fetal MRI. Fetal MRI frequently outperforms prenatal US in the correct identification and characterization of posterior fossa pathologies. For the correct identification, a high-resolution evaluation of the various components of the cerebellum, vermis, and brain stem is essential. Fetal MRI typically allows to identify and differentiate Dandy-Walker malformations (Fig. 4), Blake's pouch cyst, posterior fossa arachnoid cysts, Chiari II/III malformations (Fig. 6), Joubert syndrome, rhombencephalosynapsis, cerebellar hypoplasia/aplasia, and rarer disorders like, e.g., muscle-eye-brain disease with ease. In addition, fetal MRI may identify posterior fossa hemorrhages and stroke. Many posterior fossa anomalies are associated with additional supratentorial brain anomalies (commissural abnormalities, ventriculomegaly, cortical

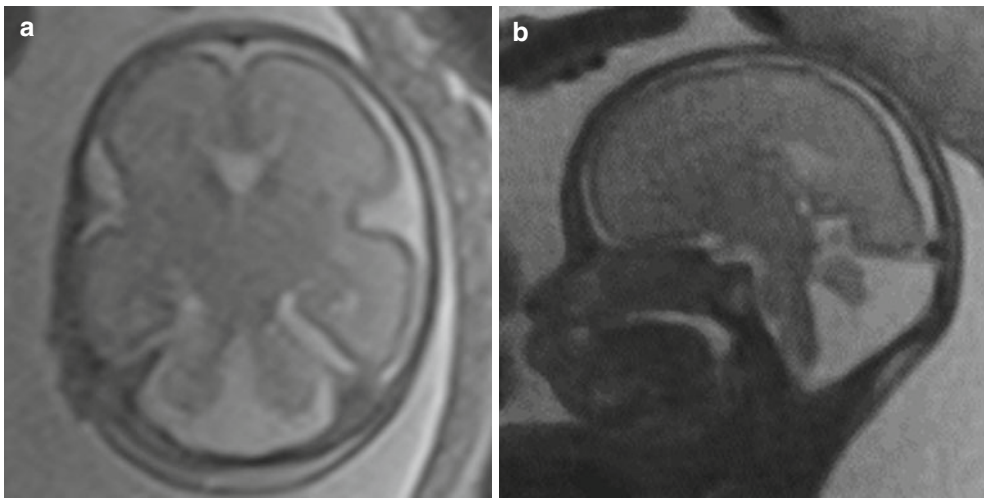

Fig. 4 Axial and sagittal T2-weighted fetal magnetic resonance images. The axial image (**a**) shows significant enlargement of the fourth ventricle. The midline sagittal T2-weighted MR image (**b**) reveals an enlarged posterior fossa with high insertion of the torcular Herophili and tentorium. The vermis is hypoplastic and rotated upward. The fourth ventricle is widened

malformations, or migrational disorders), and several entities are related to abnormalities of the spine (open, non-skin-covered spinal dysraphia) [20]. Fetal MRI of the posterior fossa may be limited early in gestation due to the small size of the infratentorial structures which can result in false-positive imaging findings [21]. Therefore, follow-up fetal MRI in case of apparent isolated anomalies of posterior fossa structures should be considered.

Cerebral Cortical Malformations or Migrational Anomalies

Fetal MRI is able to demonstrate sulcation/gyration disorders and neuronal migration disorders in better detail than prenatal US. The fetal skull may obscure detection of subtle cortical abnormalities on US. Sulcation/gyration and neuronal migration anomalies may originate from (a combination of) ischemic, infectious, metabolic, or genetic causes. Several more common cortical malformations include focal or diffuse polymicrogyria, focal cortical dysplasia, lissencephaly, and schizencephaly (Fig. 3) [20]. Periventricular or subcortical nodular gray matter heterotopia and band heterotopia are among the relative frequent migrational anomalies (Fig. 3) [22]. Additional associated findings consist of shallow sulci, focal atrophy, and white matter abnormalities [11]. The imaging characteristics of cortical malformations or migrational anomalies are similar to the characteristics described in detail for the postnatal period. The likelihood of detecting cortical malformations and migrational anomalies is determined by fetal age and the severity of the malformation. Identification of the malformation is potentially extremely difficult or impossible before the 20th–21th week of gestation. Subtle shape anomalies of the ventricular system or cerebral sulci may suggest adjacent migrational anomalies.

Ischemia and Hemorrhage

Focal or diffuse ischemia of the fetal brain can be the consequence of maternal hypoxic-ischemic conditions, placental abnormalities, or congenital vascular malformations of the fetal brain [12].

The potential causes of hemorrhage of the fetal brain include fetal stress, focal ischemia, congenital infections, coagulation disorders (congenital or drug induced), or congenital vascular malformations of the fetal brain [12]. Germinal matrix hemorrhage can occur in the intrauterine period with similar features as in premature neonates and likewise result in porencephalic cysts or periventricular leukomalacia. As a result of pronounced volume loss of the germinal matrix with high fibrinolytic activity, there is a significantly increased risk of germinal matrix hemorrhage in developmental weeks 26 to 28 [11]. Intraventricular hemorrhage is a risk factor for developing obstructive hydrocephalus. Cerebellar hemorrhage raises the possibility of an infectious etiology with possible additional extracranial abnormalities [20].

Ischemia as well as hemorrhage of the fetal brain attributes to abnormalities of the developing white matter, for instance, reduced parenchymal thickness, irregular ventricular margins, or destructive white matter lesions. An indicator for white matter damage early in embryologic development is nonappearance of the intermediate layer at fetal age less than 30 weeks [11, 15]. Furthermore, ischemia and hemorrhage in the fetal brain may derange the normal development of the brain, manifested as ventricular dilatation, cortical malformations, and abnormal sulcation [11, 12].

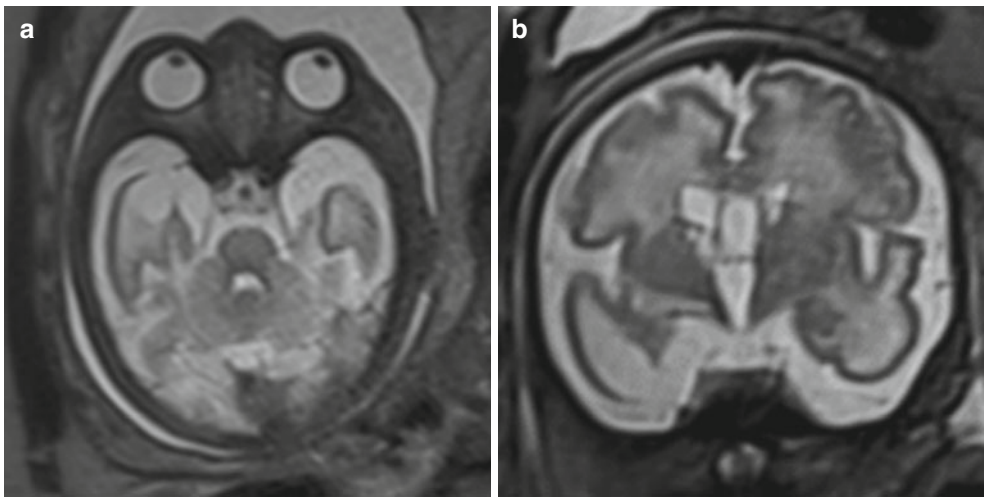

Fig. 5 Axial and coronal T2-weighted fetal magnetic resonance images of a fetus with congenital cytomegalovirus infection. The axial image (**a**) shows cystic changes of the right anterior temporal lobe involving the cortical and subcortical region. The coronal image (**b**) reveals diffuse increase in T2 signal intensity of the cerebral white matter and mild widening of the bilateral Sylvian fissures. Additional subependymal cysts in the bilateral caudothalamic region are identified

Congenital Infection

Cytomegalovirus is the most common congenital viral infection followed by varicella zoster virus and rubella (Fig. 5) [23]. A frequent parasitic infectious agent is *Toxoplasma gondii*. The associated effects of congenital infections on the developing fetal brain may be mild or extensive depending on the time point of infection in relation to the gestational age. The earlier, the more extensive the resultant destructive and malformative features are which may include migrational and cortical abnormalities, parenchymal calcifications, hemorrhages, white matter de-/dysmyelination, ventriculomegaly, microcephaly, cerebellar hypoplasia, and ocular anomalies. Several extracranial manifestations include intrauterine growth retardation, echogenic bowel, and fetal hydrops [19].

Congenital Anomalies of the Spine

Fetal MRI has proven to be especially helpful for the detailed diagnostic workup of a wide range of spinal malformations including open and closed spinal dysraphias (Fig. 6), diastematomyelia, caudal regression syndrome, sacrococcygeal teratomas, segmentation and formation anomalies of the vertebral column, and several rare anomalies including terminal myelocystoceles or neuroenteric fistulas [19]. In addition, associated brain abnormalities (posterior fossa anomalies, Chiari II malformation (Fig. 6)) and assessment and planning of fetal surgery of neural tube defects benefit from high-resolution fetal MRI of the brain and spine [15]. In addition, fetal MRI of the spine serves as a confirmative imaging technique after prenatal US has suggested diagnosis.

Conclusion

Prenatal sonography and fetal MRI are complimentary imaging techniques for the evaluation of the normal and abnormal development of the fetal CNS. Furthermore, fetal MRI can serve as a confirmative diagnostic tool to validate sonographically detected abnormalities. Definitive and complete knowledge of fetal pathologies is essential for prenatal, perinatal, and postnatal decision-making and for parental counseling.

The technical improvements of fetal MRI of the brain and spine have significantly contributed to the current detailed knowledge of normal fetal development and etiologic factors and pathogenic processes of congenital and acquired abnormalities of the CNS. Additional technical advances and ongoing research allow application of advanced imaging techniques (diffusion tensor imaging, magnetic resonance spectroscopy) in fetal neuroimaging, facilitating a better understanding of fetal pathologies.

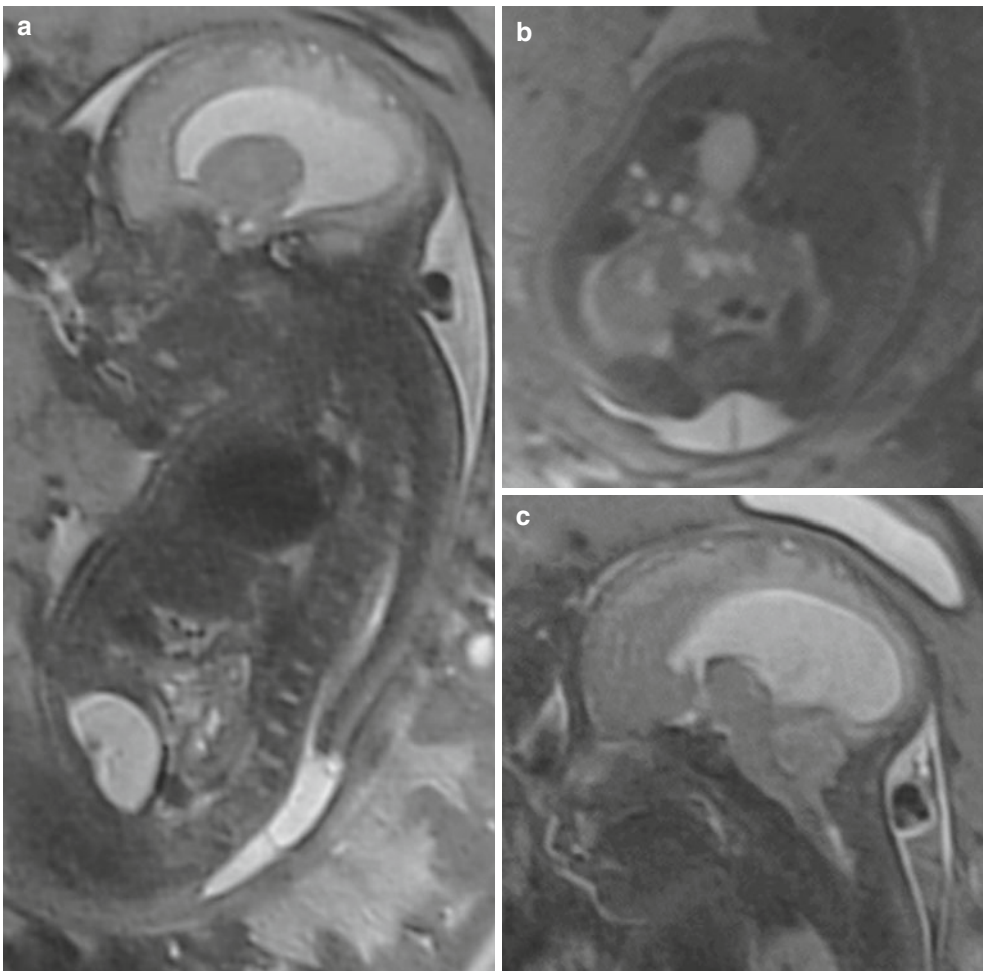

Fig. 6 Sagittal and axial T2-weighted fetal magnetic resonance images of a fetus with a Chiari II malformation and associated non-skin-covered lumbar myelomeningocele. The sagittal image of the spine (**a**) shows the spinal defect in the lumbar region with a protruding cystic myelomeningocele. The axial image at the level of the lumbar spinal defect (**b**) demonstrates the stretched T2 hypointense nerve roots coursing from the widened spinal canal to the neural placode. Incidental finding of a horseshoe kidney. The sagittal image of the craniocervical junction (**c**) reveals a small posterior fossa and herniation of vermian and cerebellar structures into the upper cervical canal. Additional moderate to severe supratentorial ventriculomegaly is noted [1]

References

1. Breysem L, Bosmans H, Dymarkowski S et al (2003) The value of fast MR imaging as an adjunct to ultrasound in prenatal diagnosis. Eur Radiol 13(7):1538–1548
2. Frates MC, Kumar AJ, Benson CB, Ward VL, Tempany CM (2004) Fetal anomalies: comparison of MR imaging and US for diagnosis. Radiology 232(2):398–404
3. Bulas DI, Levine D, Barth RA, Cassady CI, Estroff JA, Victoria D (2015) ACR-SPR practice parameter for the safe and optimal performance of fetal magnetic resonance imaging (MRI). Am College Radiol
4. Raybaud C, Levrier O, Brunel H et al (2003) MR imaging of fetal brain malformations. Childs Nerv Syst 19:455–470
5. Coakley FV, Glenn O, Qayyum A et al (2004) Fetal MRI: a developing technique for the developing patient. Am J Roentgenol 182:243–252
6. Aubry MC, Aubry JP, Dommergues M (2003) Sonographic prenatal diagnosis of central nervous system abnormalities. Childs Nerv Syst 19:391–402
7. Glenn OA, Barkovich AJ (2006) Magnetic resonance imaging of the fetal brain and spine: an increasing important tool in prenatal diagnosis, part 1. Am J Neuroradiol 27:1604–1611
8. Levine D, Barnes PD, Madsen JR et al (1997) Fetal central nervous system anomalies: MR imaging augments sonographic diagnosis. Radiology 204:635–642
9. Saleem SN (2014) Fetal MRI: an approach to practice: a review. JARE 5:507–523
10. Coakley FV (2001) Role of magnetic resonance imaging in fetal surgery. Top Magn Reson Imaging 12(1):39–51
11. Girard NJ, Chaumoitre K (2012) The brain in the belly: what and how of fetal neuroimaging? J Magn Reson Imaging 36(4): 788–804
12. Huisman TAGM (2008) Fetal magnetic resonance imaging. Semin Roentgenol 43(4):314–336

13. Huisman TAGM, Martin E, Kubik-Huch R, Marincek B (2002) Fetal magnetic resonance imaging of the brain: technical considerations and normal brain development. Eur Radiol 12(8):1941–1951
14. Fogliarini C, Chaumoitre K, Chapon F, Fernandez C, Lévrier O, Figarella-Branger D, Girard N (2005) Assessment of cortical maturation with prenatal MRI. Part I: normal cortical maturation. Eur Radiol 15(8):1671–1685
15. Huisman TAGM, Martin E, Kubik-Huch R, Marincek B (2002) Fetal magnetic resonance imaging of the central nervous system. Eur Radiol 12(8):1952–1961
16. Girard NJ, Raybaud CA (2001) Ventriculomegaly and pericerebral CSF collections in the fetus: early stage of benign external hydrocephalus? Childs Nerv Syst 17:239–245
17. Garel C, Chantrel E, Brisse H et al (2001) Fetal cerebral cortex: normal gestational landmarks identified using prenatal MR imaging. Am J Neuroradiol 22:184–189
18. Griffiths PD, Reeves MJ, Morris JE, Mason G, Russell SA, Paley MNJ, Whitby EH (2010) A prospective study of fetuses with isolated ventriculomegaly investigated by antenatal sonography and in utero MR imaging. Am J Neuroradiol 31:106–111
19. Glenn OA, Barkovich AJ (2006) Magnetic resonance imaging of the fetal brain and spine: an increasing important tool in prenatal diagnosis, part 2. Am J Neuroradiol 27:1807–1814
20. Glen OA (2010) MR imaging of the fetal brain. Pediatr Radiol 40:68–81
21. Limperopoulos C, Robertson RL, Estroff JA et al (2006) Diagnosis of inferior vermian hypoplasia by fetal magnetic resonance imaging: potential pitfalls and neurodevelopmental outcome. Am J Obstet Gynecol 194:1070–1076
22. Fogliarini C, Chaumoitre K, Chapon F, Fernandez C, Lévrier O, Figarella-Branger D, Girard N (2005) Assessment of cortical maturation with prenatal MRI. Part II: abnormalities of cortical maturation. Eur Radiol 15(8):1781–1789
23. Hollier LM, Grissom H (2005) Human herpes viruses in pregnancy: cytomegalovirus, Epstein-Barr virus, and varicella zoster virus. Clin Perinatol 32:671–696

Children with Acute Neurologic Deficits: What Has to Be Ruled Out Within Two to Three Hours

W.K. 'Kling' Chong and Andrea Rossi

Introduction

Compared to the illnesses encountered in the ageing populations of the developed world, illness in children is relatively uncommon. Basic societal hygiene and healthcare provision is supportive of paediatric populations which are mostly healthy. When illness occurs, some of the diseases may be unusual or only rarely encountered. This has led to the impression that the neuroimaging of children is found to be challenging for many general radiologists.

This syllabus contribution aims to dispel some of these myths and concerns by taking a practical approach to the problem solving of acute neurological illness in children.

The Acute Neurological Presentation in Children

There are few conditions which require diagnosis within 2–3 h, where an immediate change in management which may take place could result in an improvement in outcome. There are, however, many conditions where the exclusion of which, by neuroimaging, could help with the efficient clinical management of the patient and direct patient care.

The timescale of clinical illness in the presentation provides a good guide to the required speed of response by the radiology team. Children respond to illness in a different timescale compared to adults. By one's own experience with children, one may already be aware that children may fall ill very quickly, but they also recover from illness quickly.

W.K. 'Kling' Chong (✉)
Radiology, Great Ormond Street Hospital for Children, Great Ormond Street, London WC1N 3JH, UK
e-mail: kling.chong@gosh.nhs.uk

A. Rossi
Neuroradiology Unit, Istituto Giannina Gaslini, Via Gerolamo Gaslini 5, Genoa 16147, Italy

Rapidly changing illness over a few hours is typically encountered in cases of trauma, stroke, haemorrhage, overwhelming infection or inflammation, neurotoxins, poisons and encephalopathic syndromes.

For all of these, a clinical hallmark will be that of a change in conscious level or behaviour which is noticeable to a carer. Additional clinical diagnostic clues may be obtained from a detailed history of the onset of illness or on clinical examination. These may include the presence or absence of a clinical prodrome, pyrexia, focal or generalised seizures; the disturbances of vision, hearing, motor control or coordination and sensation; as well as the involvement or not of other non-CNS organ systems. This clinical information provides an opportunity for the radiologist to optimise the neuroimaging to address the clinical problem.

Acute Neuroimaging Modalities in Practice

Essentially, the choices are limited to CT and MRI; and for both of these, whether or not contrast agent needs to be administered. In the neonatal period and early infancy, there is also the very effective option of ultrasound, but this syllabus contribution is focused on diseases in children.

When speed is of the essence, the main consideration will be access to the modality and the best method of keeping the child still for the examination. The aim should always be to provide the most diagnostically efficient result with the lowest burden of clinical risk and ionising radiation [4]. A general anaesthetic will be required for the majority of cases. In the practical setting, access will vary between centres and at times of the day. However, the personal experience of the authors will confirm that a clinically useful result will always be obtainable. The variation will only be in the degree of confidence with which that result is delivered. In many situations, CT and MRI are

J. Hodler et al. (eds.), *Diseases of the Brain, Head and Neck, Spine 2016–2019: Diagnostic Imaging*, DOI 10.1007/978-3-319-30081-8_24

complementary modalities, although MRI is considered the definite modality for diagnostic neuroimaging.

The rest of this manuscript will focus on specific topics by clinical presentation.

Trauma

An obvious and essential element of the clinical presentation is that of a child who is completely well prior to the event. Anything else should raise suspicions and open questions.

In most clinical practices, CT will be the first imaging modality with MRI providing additional information as required. The imaging is aimed at documenting the extent of injury and identifying those which require specific early surgical intervention, for example:

- Fractures: requiring elevation and stabilisation, interfering with nerves, blood supply or venous drainage (Fig. 1).
- Haematomas: these are instantaneous space-occupying lesions which may require decompression.
- Foreign bodies: may require extraction and antimicrobial cover.

There is controversy on the extent of spinal imaging that may be required following uncomplicated head trauma. It is the author's view that this should not be routine and judged on a case by case basis, as the added value is judged to be

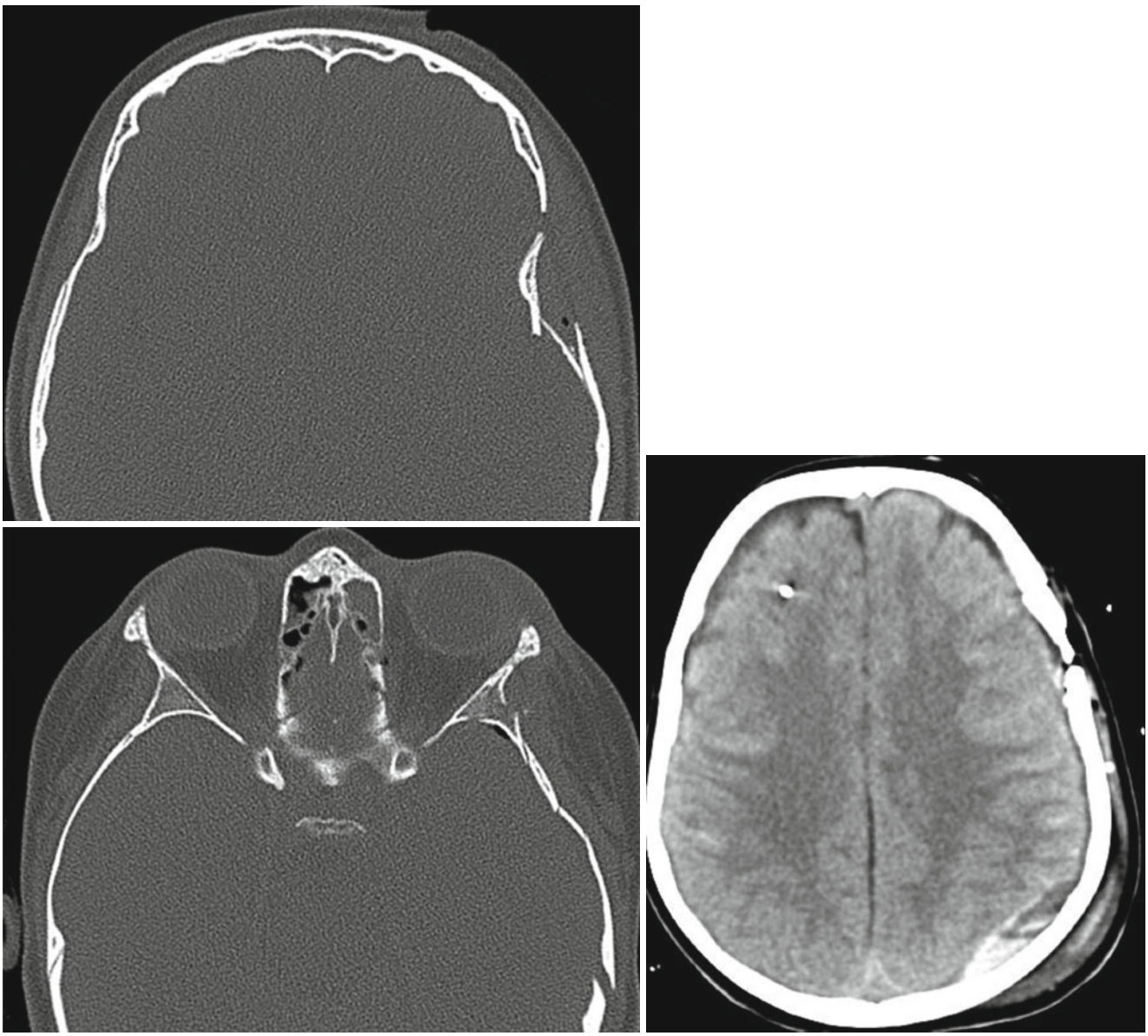

Fig. 1 Severe head trauma with an epidural collection, depressed fracture and fracture line running across the apex of both orbits

extremely low given the very low incidence of paediatric spinal injury in head trauma cases.

The issues of child protection are inevitable in paediatric practice, and so radiologists are encouraged to embrace and prepare for them rather than trying to avoid them [2]. This should be triggered if any radiology indicates trauma which is unexplained. A detailed forensic analysis may be left for experts in the field. In the acute setting, it is not important to determine 'who did it', but to raise the concern for team discussion and to initiate additional tests such as skeletal surveys. This is not common in children as abusive head trauma is more often seen in infancy.

Clinical Stroke and Stroke Mimics

The most diagnostically efficient modality will be MRI although CT is often applied first in most practical settings. It is an unfortunate practical reality that in many modern practices, it is still very difficult to avoid the scenario of the CT head followed by an MRI head in the following days. Radiologists are encouraged to try to provide an 'MRI first' service whenever possible.

The immediate imperative on diagnosis of an arterial ischaemic stroke (infarct) is to complete the imaging of the entire cerebrovascular supply (from aortic arch to cranium) at the same time. Whilst specific outcome measures are not available, there is a consensus that anticoagulant and antiplatelet therapies are most effective when delivered early. Currently, thrombolysis and thrombectomy are not recommended in the paediatric setting unless part of a clinical trial.

Very large infarcts or posterior fossa haemorrhages may require elective surgical craniectomy for decompression [3].

Haemorrhagic stroke is a feature of venous thrombosis and venous stroke, so if there are features of haemorrhage, then additional imaging of the cerebral venous structures may be needed to provide diagnostic confidence. With any haemorrhage, an attempt should be made to identify any potential structural cause for haemorrhage even allowing for the fact that cerebral aneurysms and arteriovenous malformations are relatively rare in children.

Overwhelming Sepsis or Inflammation

The clinical hallmark here is of a pyrexial illness. The onset is more gradual than for a vascular insult but more rapid than for tumours. MRI is the imaging modality of choice. Intravenous contrast agents are invaluable in these situations, and there should be a low threshold for using these whenever possible.

The aim of imaging is to demonstrate the anatomical compartments which may be involved and require specific surgical intervention. Epidural, subdural and parenchymal collections may need to be drained. Obstructive hydrocephalus is a neurosurgical emergency and may require urgent CSF diversion.

Recall that arteries that supply and veins that drain the brain have to pass through the meninges, so arterial stroke and venous thrombosis are complications which may require specific identification, management and treatment (Fig. 2).

Seizures

By definition, the electrical disturbance from complex seizures results in an alteration in conscious level. This should not necessarily be taken as an indication for immediate imaging in a matter of hours. Seizures should be controlled, particularly prolonged seizures (status epilepticus), before neuroimaging is performed.

Urgent neuroimaging is indicated if there is a persisting encephalopathy or neurological illness after the seizure has stopped. In other words, urgent neuroimaging is performed for the acute unexplained encephalopathy and not actually for the seizure. The seizure is considered a symptom or feature of the encephalopathy. A corollary of this is that if the patient has returned to his/her normal pre-ictal state with no new clinical neurology after the seizure is controlled, then there is no indication for urgent or emergency neuroimaging. Such imaging may be performed, if required on discussion, electively.

MRI is the modality of choice for the investigation of seizures or epilepsy. When applied appropriately in the emergent setting, the commonest causes of 'a seizure presentation with persisting encephalopathy' demonstrated on imaging are encephalitis, venous thrombosis and PRES (see later). In the author's own series of consecutive paediatric intracranial haemorrhage presenting to neurosurgery over 6 years (1997–2003), none presented with a seizure alone without encephalopathy.

Acute Paraparesis or Suspected Cord Compression

This requires MRI and, if contraindicated, CT myelography. The aim is to exclude a surgically treatable cause. The surgical imperative arises because the best results follow decompression if performed in a matter of hours. However, in clinical practice, medical causes far outweigh surgical cases, and the vast majority of cases turn out to be Guillain-Barré syndrome or myelitis. A good clinical assessment may help avoid unnecessarily invasive neuroimaging.

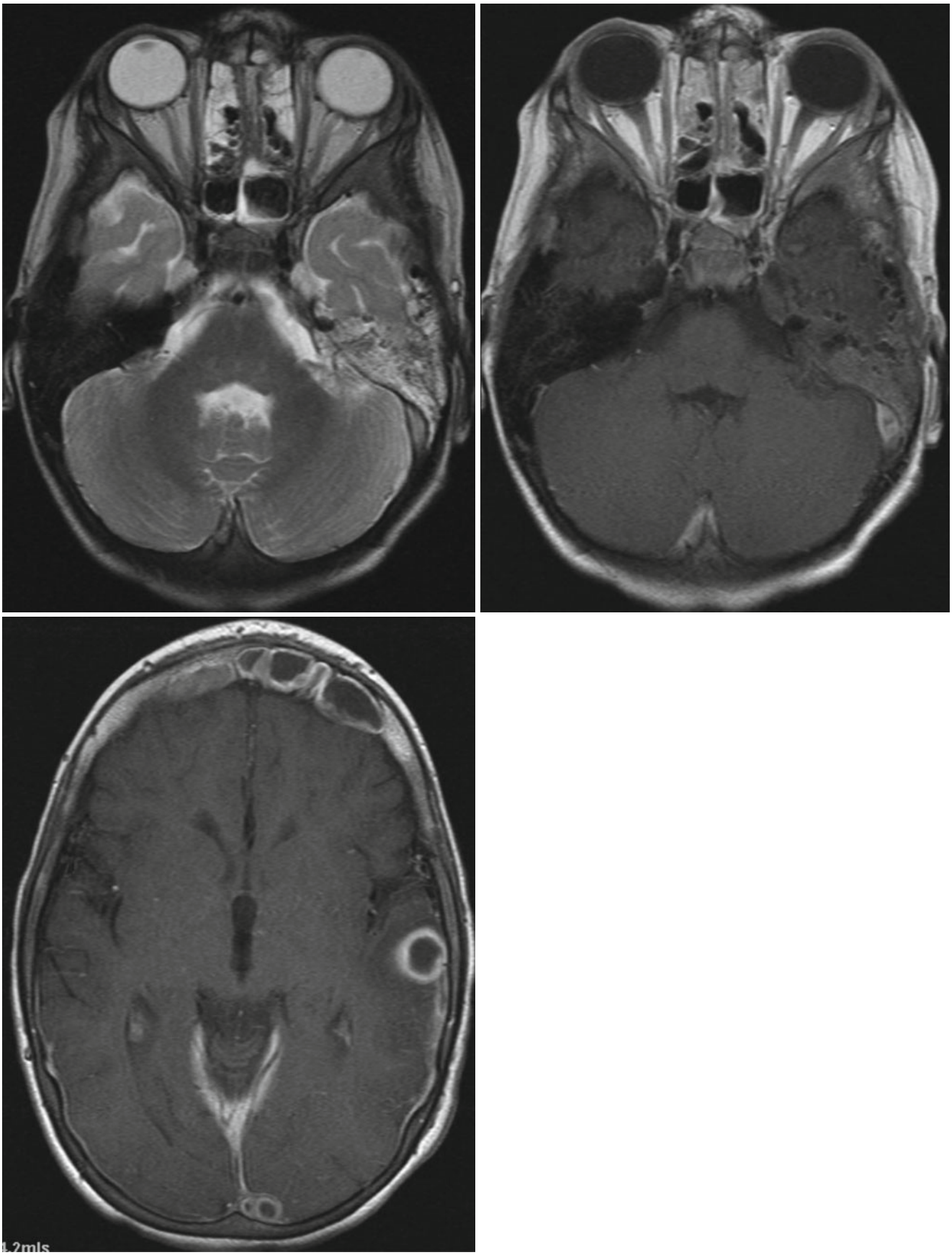

Fig. 2 Sinusitis and mastoiditis complicated by epidural empyema, brain abscess and venous sinus thrombosis

Other Acute Unexplained Encephalopathy

The following are radiological diagnoses with distinct radiological features which, when identified, can provide important clinical guidance and direct management.

- PRES – posterior reversible encephalopathy syndrome, also known as reversible posterior leukoencephalopathy syndrome (RPLS). A condition that is memorable as much as it is a misnomer because the condition is not always posterior nor always reversible nor confined to the white matter. The syndrome is the same as hypertensive encephalopathy and can also result from an idiosyncratic reaction to immunosuppressive therapy, such as cyclosporine and tacrolimus (Fig. 3).
- ADEM – acute demyelinating encephalomyelitis. The tumefactive form may present acutely with significant

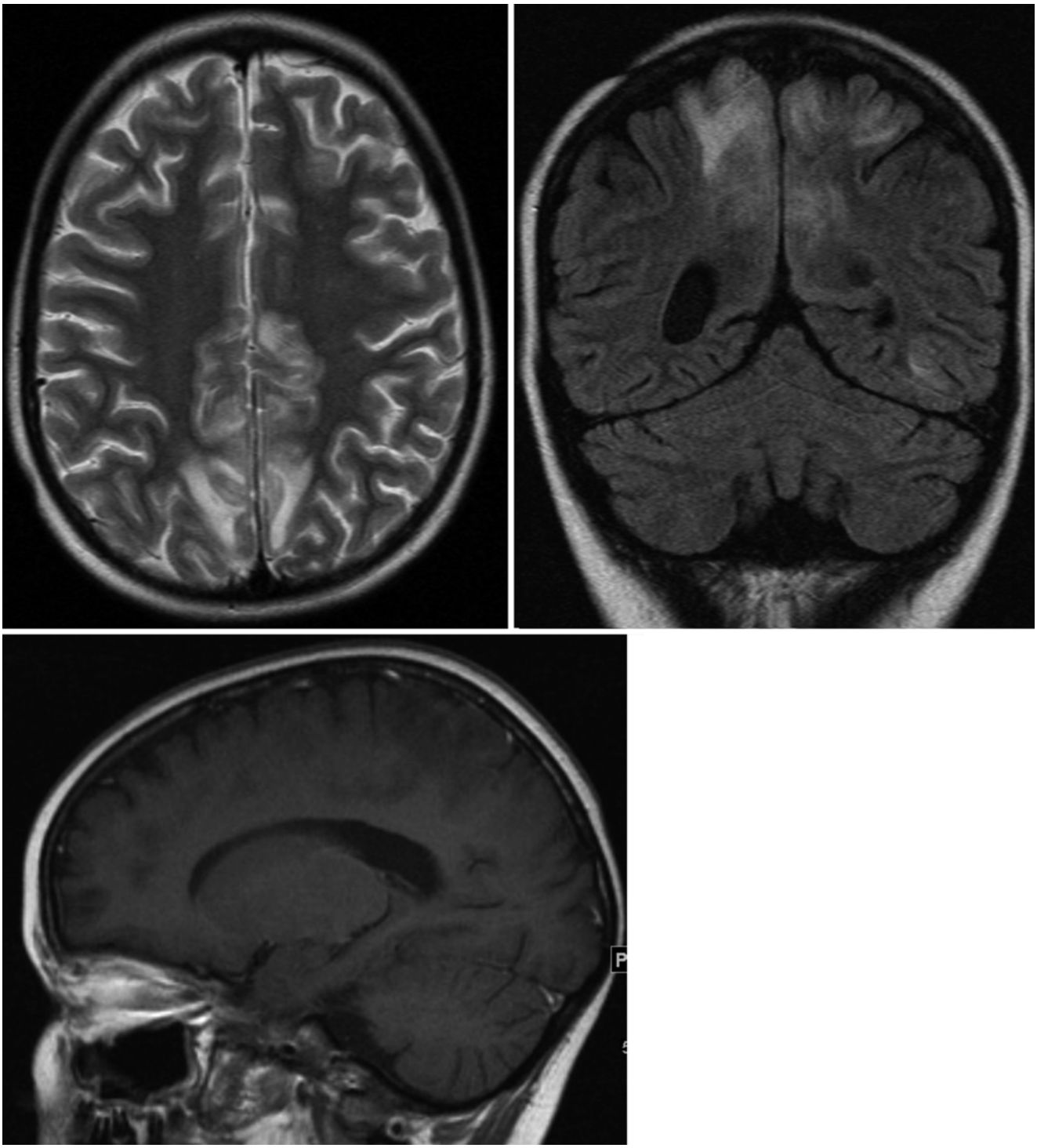

Fig. 3 Typical posterior location of cortical and subcortical non-enhancing lesions of PRES in a patient on cyclosporine therapy for acute leukaemia

mass effect. Clues may be obtained from the identification of multiple lesions or from distinctive patterns of enhancement.
- Neurotoxicity and poisons. These are often diagnoses of exclusion and should be considered when there are atypical or unexpected findings. For example, when there is clinical-radiological discordance such as a patient in deep coma but with normal imaging.

Summary and Conclusions

What to rule out in 2–3 h, in children?

Answer 1: Conditions that present over a few hours
Answer 2: Mass (space-occupying) lesions, hydrocephalus and cord/brain compression

In other words:

- Not that different from adults
- Not that difficult radiologically (acute neuroimaging should be a basic skill)

To make it easier – *think like a doctor; and think 'paediatric'*.

References

Good General Reading and Reference Text

1. Barkovich AJ, Raybaud C (2011) Pediatric neuroimaging. 5th edn. ISBN/ISSN: 9781605477145. http://www.amazon.com/Pediatric-Neuroimaging-Barkovich/dp/1605477141

Some Related Peer Reviewed Papers

2. Roy AA, Mankad K, Chong WK, Saunders D (2015) Neuroimaging of non-accidental injury. Curr Pediatr Rev 11(4):262–277
3. Liu AC, Segaren N, Cox TS, Hayward RD, Chong WK, Ganesan V, Saunders DE (2006) Is there a role for magnetic resonance imaging in the evaluation of non-traumatic intraparenchymal haemorrhage in children? Pediatr Radiol 36(9):940–946
4. Saunders DE, Thompson C, Gunny R, Jones R, Cox T, Chong WK (2007) Magnetic resonance imaging protocols for paediatric neuroradiology. Pediatr Radiol 37(8):789–797

Part II

Nuclear Medicine Satellite Course “Diamond”

Integrated Imaging of Brain Tumours

Ian Law

Introduction

The incidence rate of all primary malignant and non-malignant brain and CNS tumours is 21 cases per 100,000. Gliomas are a broad term, which includes all tumours arising from glia and represents 30 % of all brain tumours and 80 % of all malignant brain tumours. Gliomas are the second leading cause of cancer mortality in people under the age of 35.

Pathoanatomically gliomas are graded from grade I to grade IV using the World Health Organisation (WHO) criteria. Grades I and II are considered low-grade glioma (LGG) and grades III and IV are classified as high-grade glioma (HGG). LGG have a malignant potential and usually all will transform before or later to HGG. The risk of transformation is in the order of 10–25 %/year, but there are patients with LGG that have lived for 20 years before transformation. Thus, a low-grade glioma that gives significant clinical symptoms or appears to have a malignant potential will usually be operated on, while "wait and scan" will be the strategic choice for the more indolently appearing tumours.

Glioblastomas (GBM), the most aggressive variant, represent 15–20 % of all primary brain tumours and 50 % of all gliomas. The standard GBM treatment today consists of maximal surgical resection, but the tumour's ability to infiltrate into the ambient tissue makes it challenging. Postoperatively patients are offered radiotherapy in combination of concomitant and adjuvant chemotherapy with temozolomide yielding a median overall survival of 14–16 months in clinical trial populations [1].

Magnetic resonance imaging (MRI) is the primary imaging modality in the management of primary brain tumours including initial diagnosis, tumour grading, treatment planning prior to surgery and radiotherapy planning, postoperative evaluation, monitoring treatment response and progression. The most important clinical sequences are T1-weighted imaging without and with contrast medium and T2-weighted as well as fluid-attenuated inversion recovery (FLAIR) sequences.

Although MRI is a very useful and powerful technique, it has its shortcomings. These are the whole raison d'être for performing positron emission tomography (PET) scanning in brain tumours. PET scanning is a molecular imaging method, which uses various tracers to visualise biological processes. In clinical PET of brain tumours, the most established and available radiotracers deal with glucose metabolism (^{18}F-2-fluoro-2-deoxy-D-glucose (FDG)), amino acid transport ([^{11}C-methyl]-methionine (MET), O-(2-[^{18}F]-fluoroethyl)-L-tyrosine (FET) and 3,4-dihydroxy-6-[^{18}F]-fluoro-L-phenylalanine (FDOPA)) and somatostatin receptor II binding ligands such as ^{68}Ga-DOTA(0)-Phe(1)-Tyr(3)octreotide (DOTATOC).

FDG

Mechanism Many tumours overexpress the glucose transporters (GLUT) and hexokinase enzymes leading to an increased accumulation and metabolic fixation of FDG in the tissue.

The advantages:

1. *Availability*. Ease of use and a widely distributed availability as a result of the acceptance of whole-body FDG PET scanning within oncology in general.
2. *Short scan duration*. A 10 min static PET scan about 40 min postinjection makes FDG PET brain scanning a cost-effective technique.
3. *Delayed or dual-time-point imaging*. Potential improvement in diagnostic quality by supplementing with late FDG scans 3–6 h postinjection. The metabolically active tumour area is enhanced because of a differential clearance of FDG in healthy and malignant tissue [2].

I. Law
Department of Clinical Physiology, Nuclear Medicine & PET, Rigshospitalet, 9, Blegdamsvej, Copenhagen 2100, Denmark
e-mail: ilaw@pet.rh.dk

J. Hodler et al. (eds.), *Diseases of the Brain, Head and Neck, Spine 2016–2019: Diagnostic Imaging*, DOI 10.1007/978-3-319-30081-8_25

The disadvantages:

1. *High physiological uptake in healthy brain tissue*. Thus, it may be very difficult to differentiate active tumour tissue from physiological uptake with the present limitations in scanner resolution. Some of these limitations can be overcome by fusing the FDG PET image to recent MRI scans of the patient – particularly T1-weighted MRI scans with contrast – and the FLAIR sequences are mandatory in this context (Figs. 1 and 4).
2. *No uptake in LGG*. This makes PET FDG tumour delineation impossible (Fig. 1a).
3. *Tumour-associated epileptiform activity*. Almost all patients with brain tumours are in antiepileptic treatment. Epileptic seizure activity that is present during the uptake phase of FDG will give rise to a two- to tenfold increase in FDG uptake. Epileptic seizures need not be clinically manifest. This depends on the localisation and the extent of the seizure. Particularly seizures in the frontal lobes may be clinically silent. Thus, a regional signal change in FDG may be the only sign of the event and may be confused with active tumour tissue. This condition can be identified as hypermetabolic areas of varying extend in normally appearing cortex particularly on the T2-weighted MRI sequences.

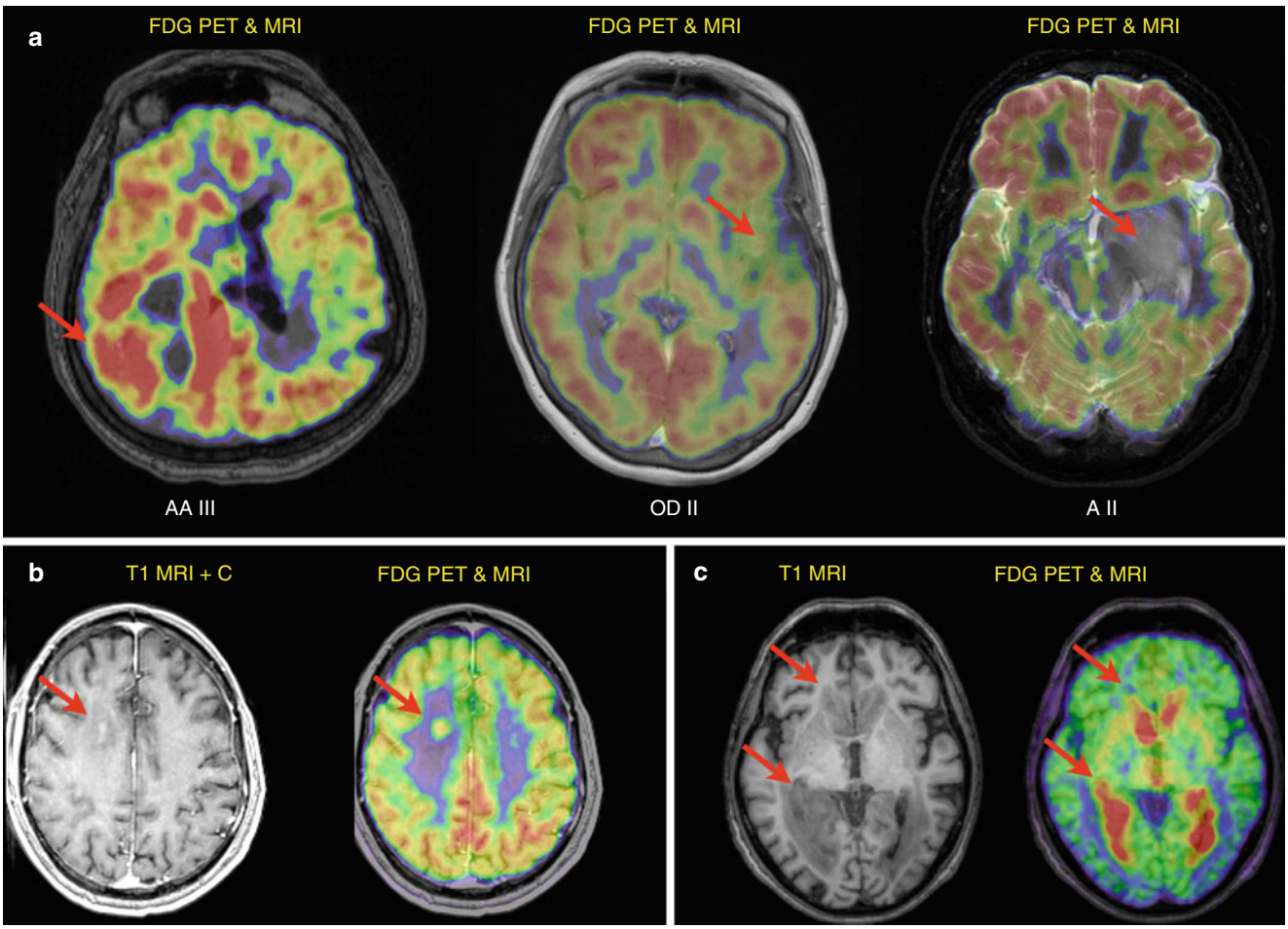

Fig. 1 Co-registered FDG PET to MRI images showing typical examples of uptake in brain tumours. (**a**) *FDG uptake in high- and low-grade glioma*. From *right to left*: Anaplastic glioma (*AA III*) in the right parieto-occipito-temporal region with invasion of the central area and a cystic/necrotic area, oligodendroglioma (*OD II*) in the left insula and anterior temporal region and astrocytoma (*A II*) in the left insula and inferior temporal region. High-grade gliomas (III, IV) typically have uptake above healthy white matter, and low-grade gliomas (II) have uptake below healthy white matter. Oligodendroglioma II (*centre*) may deviate from this pattern with uptake larger than white matter. Note the relatively difficult tumour delineation in areas bordering to the high physiological uptake in healthy grey matter. (**b**) *Recurrence of glioblastoma multiforme or treatment damage*? Focal FDG uptake in slightly contrast-enhancing area in right mesial centrum semiovale indicating recurrent tumour. (**c**) *FDG uptake in primary CNS lymphoma* (*PCNSL*). Immunocompetent patient showing FDG PET fused with axial non-contrast T1 MRI prior to treatment showing highly avid FDG uptake extending along the ependymal surfaces of the lateral ventricles indicative of liquoral spread. This is a common feature of PCNSL. In the differential diagnosis between PCNSL and high-grade glioma, a very high FDG uptake supports PCNSL. PCNSL should be biopsied and not resected. *Red arrows* point to tumours. Left is to the right of the image

4. *FDG uptake modification of other causes*:
   (a) *Inflammation/infection* (abscesses, parasitoses, sarcoidosis, TB, hematoma, histiocytosis, recent stereotactic radiation).
   (b) *Drug effects*: High doses of cortisol are administered to patients with clinically significant tumour oedema. Cortisol decreases the uptake of FDG across the blood-brain barrier (BBB) and increases noise. However, the uptake is reduced more in healthy tissue than in tumour tissue, thus, somewhat counteracting the deteriorating noise effects. There is a marked cytolytic and FDG-reducing effect on primary CNS lymphoma, so preferably patients should be scanned before treatment initiation. It is not indicated to pause with cortisol prior to scanning.
   (c) *Effects of blood glucose*: As in other tissue, a high blood glucose concentration will compete with and reduce the uptake of FDG. In glioma the reduction in uptake is more pronounced in healthy tissue than in glioma, thus increasing the ability to identify malignant tissue.

Amino Acid/Amino Acid Analogue PET Tracers (MET, FET, DOPA)

To overcome some of the FDG disadvantages, there is a growing interest in the use of more specific tracers, particularly amino acid or amino acid analogue PET tracers (MET, FET, FDOPA). The best known is MET with a 30-year history of use. However, in larger-scale routine clinical use, FET (Figs. 1, 2, 3 and 4) or FDOPA [3] predominates.

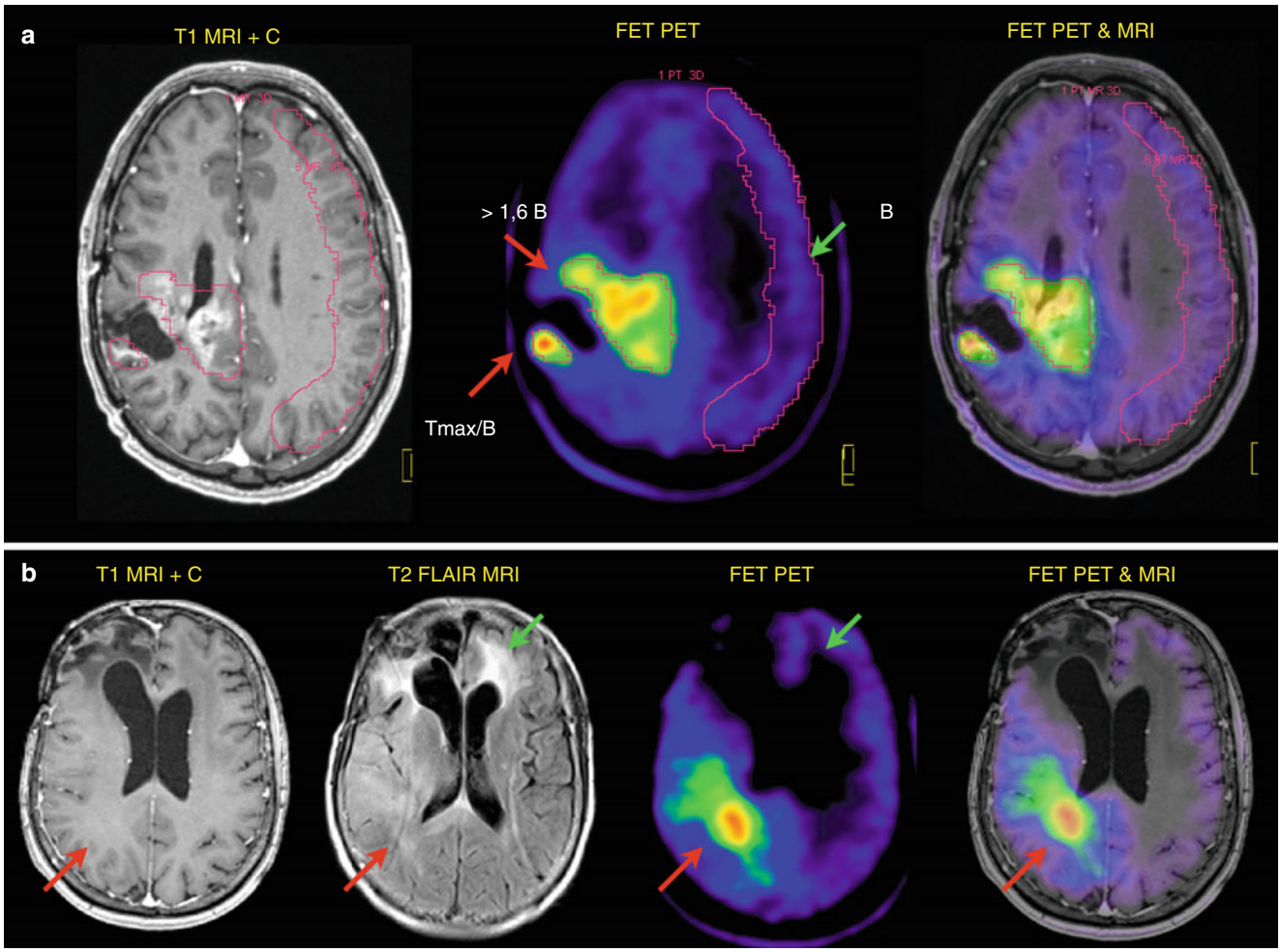

Fig. 2 (**a**) *Data analysis using FET PET*. The biological tumour volume (BTV) is defined as FET uptake in a scan 20–40 min after injection with values above 1.6 times the activity in a region (*B*) of healthy-appearing cortical grey and white matter in the contralateral hemisphere [9]. The maximal uptake (Tmax/B) is calculated and defined as the biopsy target. (**b**) *Recurrence of glioblastoma*: After antiangiogenic treatment a glioblastoma may transform into a diffusely infiltrating gliomatose phenotype predominantly coopting existing vasculature instead of stimulating new vascular growth. The metabolically active tumour in the right subcortical parieto-occipito-temporal region (*red arrows*) is not visualised on post-contrast MRI, but can be seen as a diffuse signal change and architectural disruption on T2 FLAIR. This sequence, however, also shows unspecific signal changes in the frontal lobes without increased activity (*green arrows*) possibly ischemia, demyelination, oedema or gliosis

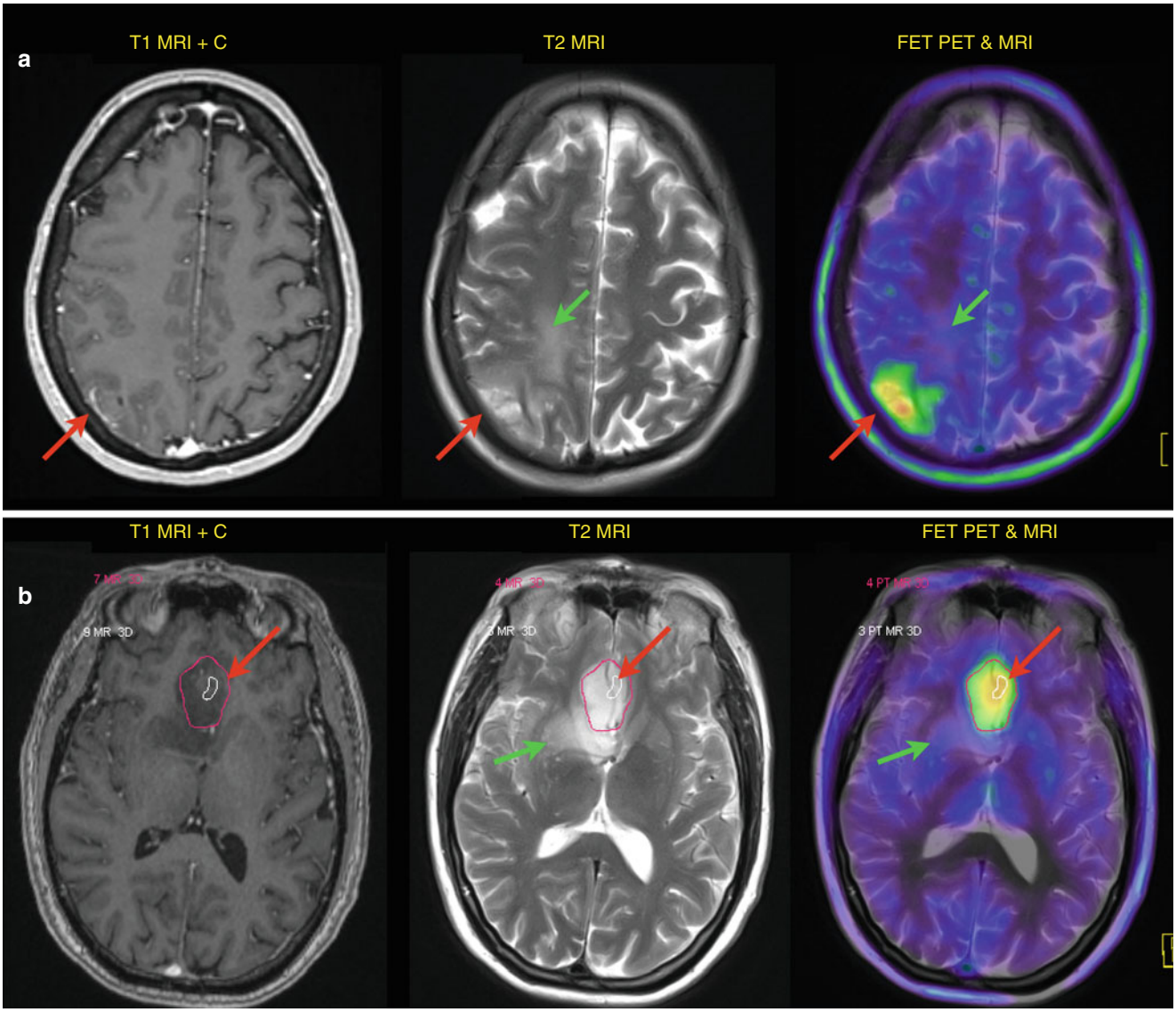

Fig. 3 Biopsy guidance. (**a**) Diffusely infiltrating tumour on T2 MRI with uncertain contrast enhancement. Focally increased FET uptake in right parietal cortex (*red arrow*). No uptake in subcortical T2 signal changes (*green arrow*). Histology showed oligodendroglioma II. (**b**) Diffusely infiltrating tumour (red arrow) on T2 MRI in mesial frontal lobe and right anterior striatum without contrast enhancement on T1 MRI. The borders of the metabolically active tumour (*magenta*) and peak area (*white*) suggested for biopsy trajectory are indicated. No uptake in subcortical T2 signal changes in right anterior striatum (*green arrow*). Histology showed glioblastoma multiforme

MET, FET and FDOPA

Mechanism Gliomas overexpress the L-amino transporters (LAT). MET and FDOPA are transported via LAT1 and LAT2, and FET predominantly via LAT2. LAT1 is overexpressed in inflammation, while LAT2 is more tumour selective [3]. These tracers are not fixed and will be cleared from the brain and tumour.

The advantages:

1. *Image contrast*: There is very little uptake in healthy tissue. There is, thus, a high target to background ratio (Fig. 4).
2. *Uptake in LGG*: LGG can be delineated (Fig. 3a).
3. *Tumour grading*: Glioma can be graded (only FET) based on the shape of the time activity curve [3, 4].
4. *Better specificity than FDG* (Fig. 4). However, there may still be an uptake in astrogliosis (FET) or microglia (MET) caused by inflammatory lesions, such as multiple sclerosis and treatment damage [5–7].
5. *F18-labelled radio synthesis* (FET, FDOPA): The F18 half-life is 2 h. This is essential for the broad clinical acceptance of the technique for routine clinical use. One production can supply 20 patients or more depending on the number of scanners used. The shelf life is up to 8 h, so they can be transported to neighbouring PET centres.

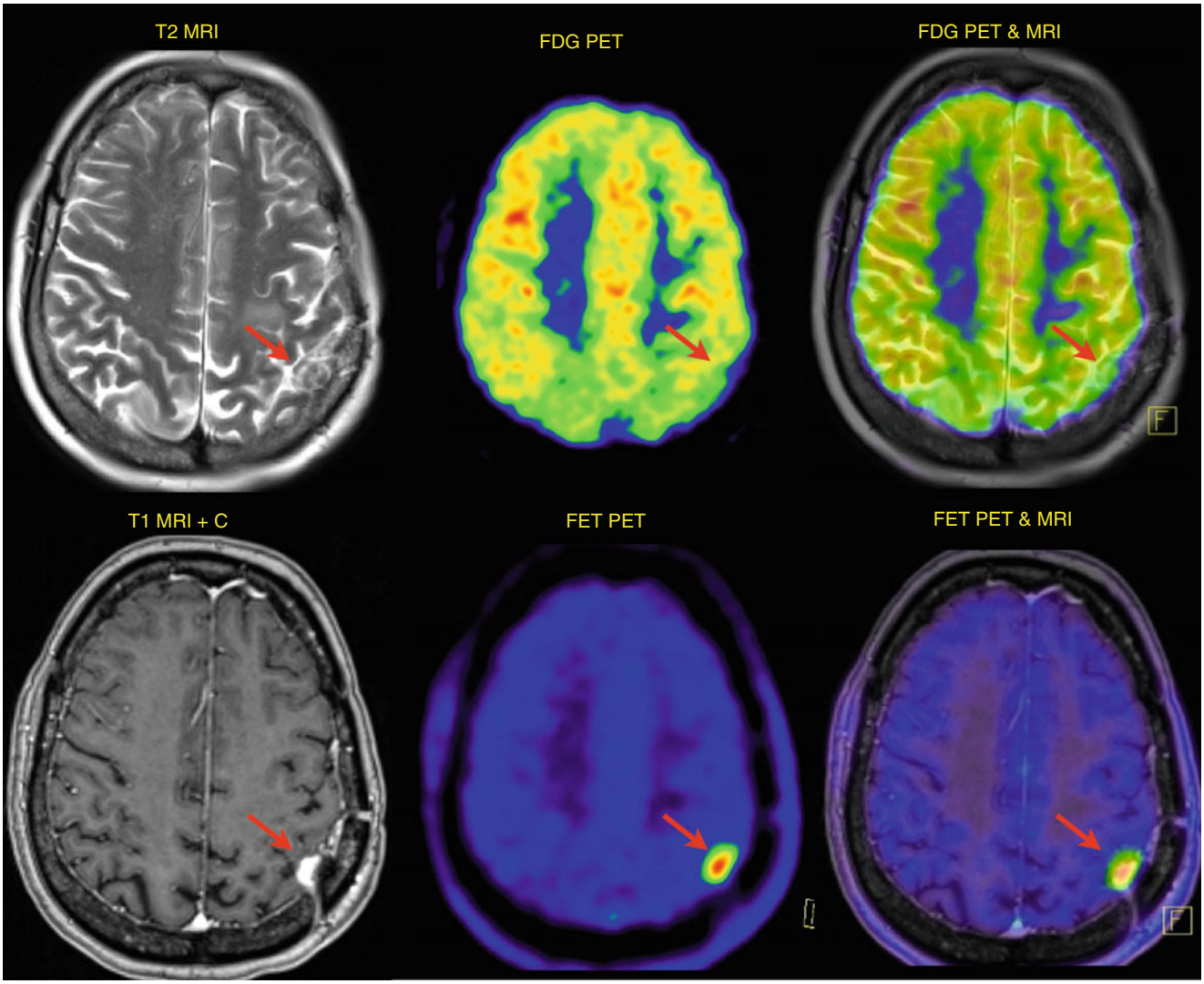

Fig. 4 Recurrence of glioblastoma multiforme or treatment damage? Comparison of tumour uptake using FDG (*top*) or FET (*bottom*) in the same patient with glioblastoma multiforme in postoperative follow-up. The metabolic activity in contrast-enhancing area (*red arrows*) is difficult to evaluate using FDG because of the high physiological uptake in adjacent healthy cortex. FET shows focal increase. Recurrence confirmed on re-resection

6. *Can identify both solid and infiltrative tumour components*. Thus, the tumour margins defined by T1 contrast enhancement will often exceed these tracers [8] (Figs. 2 and 3).

The disadvantages:

1. *C11-labelled radio synthesis* (only MET): C11 half-life is only 20 min. Capacity limitation to 1–2 patients per production.
2. *Blood volume background* (*only FET*): FET is only slowly excreted in the kidneys, so there is moderate activity in the blood vessels that in selected case can confuse the image reading.
3. *Longer scan duration* (only FET): Glioma grading requires a 40 min dynamic scan, reducing cost-effectiveness [4].
4. *High striatal uptake* (*only FDOPA*): Difficult delineation of tumours infiltrating into central areas [3].
5. *Lack of biopsy proven threshold for tumour tissue* (*only FDOPA*): For MET and FET, the threshold of uptake is 1.3 [8] and 1.6 times (Fig. 2) [9] relative to healthy cortex, respectively.
6. *Pretreatment with carbidopa to inhibit metabolism* (*only FDOPA*) [3].

PET Brain Tumour Indications

Glioma Grading and Malignant Transformation

There are clinically important implications associated with the ability to differentiate between LGG and HGG. This distinction can be difficult with MRI. Usually contrast

enhancement would be a characteristic that would be emphasised. However, about 40–50 % of non-enhancing lesions with an MR presentation that would be identified as LGG are found subsequently to be HGG [10] (Fig. 3) and LGG can be contrast enhancing. Usually, it is the distinction between grade II and grade III that proves to be most difficult.

PET scanning can be used in support of either a "wait and scan" strategy in the metabolically inactive tumours or an aggressive surgical strategy in the active tumours. None of the tracers, however, can obviate the need for tissue verification, but it can change the time point for sampling.

FDG

The regional FDG uptake correlates to cellular density and regional anaplasia. FDG is trapped metabolically and is only removed slowly. As a rule LGG has low uptake and HGG has increase uptake. In a retrospective study of 333 patients, tumour grading could be done using the metabolic activity in white matter as a visual threshold. Of all HGG 84 % had uptake above this level and only 7 % of the LGG (Fig. 1). It should be noted that a number of LGG, such as grade I glioma (pilocytic astrocytoma), and hamartomas (dysplastic gangliocytoma) are characterised with a very large FDG uptake. However, these have a characteristic appearance on MRI, so usually clinical PET scanning is not required. The FDG uptake is prognostic for overall survival and a better prognosticator of WHO grade. If an LGG increases its metabolism during the cause of observation, this can be indicative of malignant transformation and should be followed by histological verification.

FET

About 60–70 % of the LGG show uptake [11, 12] and close to 100 % for HGG [13]. Hence, no grading information can be derived from the uptake itself. Nevertheless, the FET uptake can possibly prognosticate progression in LGG. A lack of FET uptake in a circumscribed tumour predicts slow progression, while increased uptake in a diffuse tumour predicts faster progression [11]. This has, however, recently been disputed [12].

Several studies have shown that the 40 min dynamic uptake curve in the most active regions can be used to grade glioma [4]. Thus, LGG has typically a steadily increasing curve, while HGG have a typically fast uptake and washout or a plateau. The mechanism behind has not been clarified, but it does not seem to be related to the presence or absence of a BBB defects. This allows for a sensitivity and a specificity of 80–90 % [4, 14]. Both tumour-to-brain uptake and kinetic parameters of FET PET uptake can provide valuable diagnostic information for the noninvasive detection of malignant progression of LGG [15].

Primary Intracerebral Lymphoma (PCNSL)

Primary CNS lymphoma (PSNSL) is a rare form of extranodal non-Hodgkin's lymphoma (NHL) confined to the brain and account for 1–6 % of all intracranial tumours. PCNSLs are highly proliferative tumours and usually show high FDG uptake (Fig. 1c). FDG PET is useful for the differentiation between lymphomas and infectious lesions in AIDS patients [16]. However, with improved HIV treatments, these are rarely seen. The major MRI differential diagnosis of PCNSL is GBM. This is clinically important for correct preoperative planning. PCNSL should be biopsied and treated with chemotherapy, while GBM should be resected. PCNSL has significantly larger FDG uptake than GBM and is useful for this indication [17, 18].

Optimising Tumour Biopsy

FDG, MET and FET can be used to optimise the diagnostic quality of a tumour biopsy (Fig. 3) by directing sampling at the most metabolically active areas [19]. This may be used both in grading and in confirmation of tumour recurrence. In a prospective study, MRI yielded a sensitivity of 96 % for the detection of tumour tissue but a specificity of only 53 %, and combined use of MRI and FET PET yielded a sensitivity of 93 % and a specificity of 94 % [9]. Simulations indicate that FET PET may be cost-effective if used in biopsy planning [20].

Postoperative Monitoring

After surgical intervention and concomitant radiochemotherapy, the patients are monitored for recurrent tumour, which can lead to additional surgical intervention, second- and third-line chemotherapy and re-irradiation. Using MRI to distinguish recurrent tumour from treatment damage is difficult. As a rule PET HGG are metabolically very active while treatment damage is inactive or less active (Figs. 1, 2 and 4). However, tumour tissue and treatment damage can coexist, and reactive tissue changes will increase activity. The best diagnostic accuracy with reference to histology has been found with MET/FET. For FET the ratio of maximal tumour uptake to average background in normally appearing cortical tissue (Tmax/B) is calculated (Fig. 2a). A Tmax/B threshold above 2.4 will have a specificity of 90–100 %, while the sensitivity would be approximately 75 % [4]. A Tmax/B of 2.0–2.4 with a focal uptake would be interpreted

as recurrence, while crescent-shaped diffuse uptake around the resection cavity is more likely reactive changes. Sensitivity and specificity at this cut-off are 100 % and 78–100 %, respectively. It should be noted that the patients in some of these studies receive unusual and experimental treatment, such as radioimmunotherapy (RIT). This may lead to a high level of local tissue damage and reaction and, thus, influence the specificities calculated. Furthermore, the thresholds are dependent on a close duplication of the scan set-up used in these studies. If the pattern is equivocal, a fast rescan <6 weeks can be recommended.

The diagnostic accuracy of FDG (Fig. 1) is worse than MET/FET with an overall sensitivity of 80–90 % and a specificity of 50–90 % [21]. One caveat of these studies, however, is that the studies are performed on older generations of PET scanners with lower resolution, not all studies have used MRI co-registration and they are often subject to sampling bias.

Meningiomas and Somatostatin Receptor-Based Tracers

Meningiomas represent 34 % of all primary brain tumours, making them the most common primary brain tumour. Almost all meningiomas show high expression of somatostatin receptors subtype 2 (SSTRII) that may be efficiently visualised with PET using DOTATOC. This is particularly useful in meningiomas at the skull base, because of postoperative changes and tumour infiltration into cavities, sinuses (Fig. 5a) and bone. DOTATOC PET/CT for target volume delineation for intensity modulated RT, fractionated stereotactic RT or proton therapy has been shown to change the planning target volume significantly in several publications [22]. On average the target volume was modified in 80 % and reduced in 54 % of patients, but the clinical impact remains to be documented in long-term follow-up. DOTATOC PET is likely to be useful

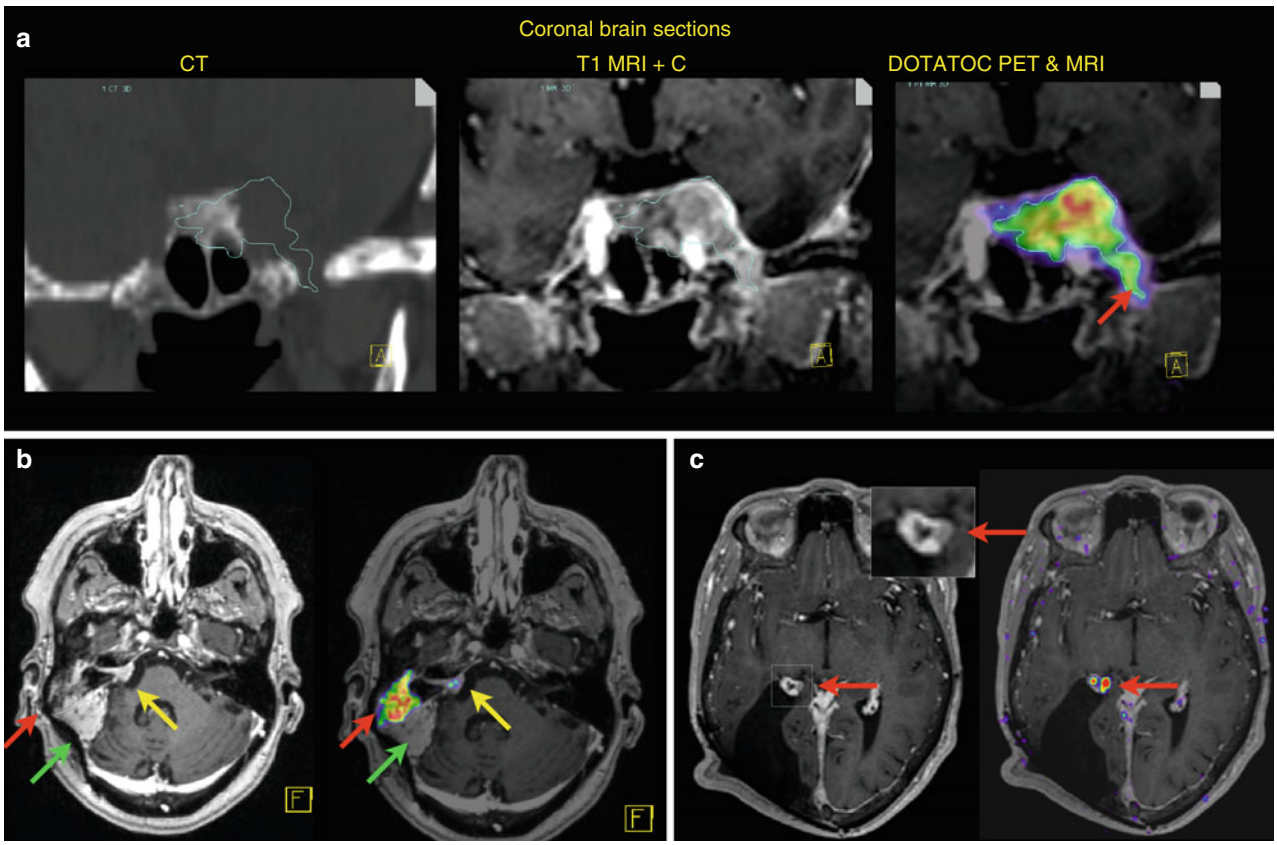

Fig. 5 Examples of DOTATOC PET use in meningioma management. (**a**) *Recurrent meningioma* (*WHO I*) *referred for radiotherapy planning*. The patient suffered from trigeminus neuralgia and was treated without effect with dilation of the foramen ovale unaware that the tumour is infiltrating into the same opening (*red arrow*). Coronal CT shows an increased foramen ovale and tumour contours in *blue*. The tumour invading the ethmoidal sinuses is hard to delineate on post-contrast T1 MRI, but can easier be detected on DOTATOC PET scanning. (**b**) *Recurrent meningioma* (*WHO I*) *referred for radiotherapy planning*. Previous resection for a meningioma in the anterior right cerebellar hemisphere with fat tissue inserted to support the organ (*green arrow*). The patient was referred for radiotherapy planning of small relatively inactive tumour lateral to the right pons (*yellow arrow*). The MR signal changes in the right pars petrosa (*red arrow*) were originally interpreted as reactive changes, but DOTATOC PET scanning indicated bone invasion, and the planning field was subsequently modified. (**c**) *Staging DOTATOC PET scan prior to surgery of recurrent malignant meningioma* (*WHO III*). The finding of an additional 3 mm in diameter recurrence (*red arrow*) not identified initially on MRI and hidden in the right choroid plexus (*insert*) changed the treatment from surgery to radiation therapy [23]

in biopsy planning, in differentiating active tumour tissue from posttreatment damage (Fig. 5b) and in selection of treatment strategies, e.g. operative vs. radiation therapy (Fig. 5c) [23]. Furthermore, DOTATOC might be used in dosimetry planning of peptide receptor radionuclide therapy (PRRT) using ^{90}Y-DOTATOC, ^{177}Lu- DOTATATE or ^{177}Lu-DOTATOC in non-resectable locally recurring, progressive or symptomatic meningiomas, but the clinical effects need to be documented in randomised clinical trials [24].

Simultaneous PET/MRI Imaging

At our institution, we have implemented our hybrid PET/MR system for routine clinical MRI and FET PET imaging of patients with gliomas. This provides simultaneous structural and metabolic evaluation under identical physiological condition with the addition of various advanced MRI techniques in a single examination of 20–40 min [25], e.g. combined FET and tumour blood volume (BV) imaging using T2* dynamic susceptibility contrast (DSC) (Fig. 6). DSC has been suggested as a cost-effective substitute for PET scanning. However, in postoperative glioma patients, we found that the spatial congruence of BV and FET was remarkably poor. MRI susceptibility artefacts affected the ability to evaluate BV DSC in FET-avid tumour areas in 56 % of patients [25]. T1 dynamic contrast enhanced (DCE) has a higher resolution, is not subject to susceptibility artefacts and may be a more attractive alternative to explore [26, 27].

As PET scanning is a quantitative technique, good attenuation correction is essential. This has been the primary technical limitation of the present PET/MRI systems [28]. Thus, at our unit patients presently receive a low-dose CT scanning of the head for this purpose, while other strategies are being considered [29].

PET/MR may increase the overall diagnostic quality, decrease clinical decision time and increase acceptance of PET imaging with patients and treating clinicians in clinical

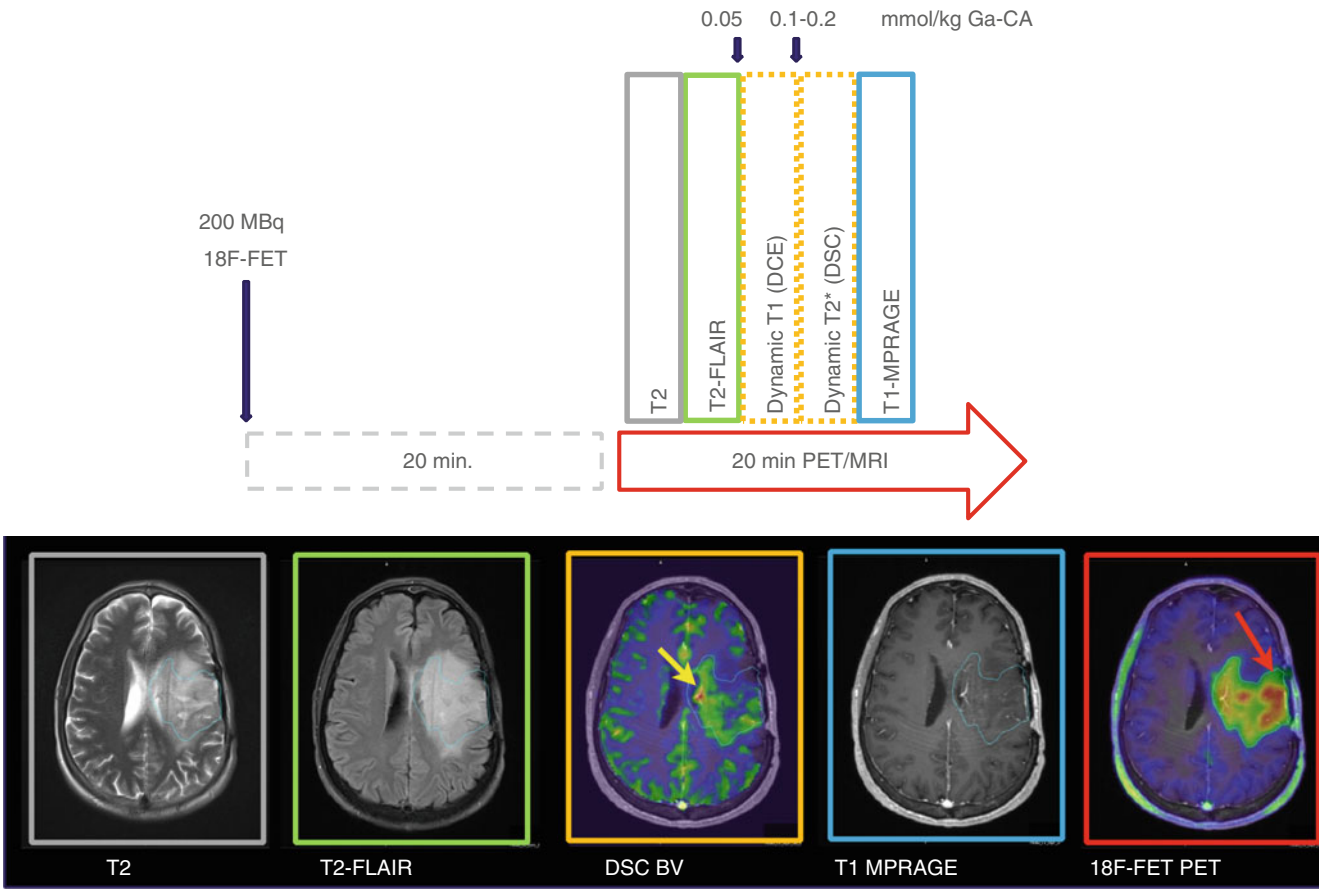

Fig. 6 Integrated multiparametric brain tumour imaging using PET/MRI and FET. Workflow illustrating a combined 20 min FET PET/MRI and tumour blood volume (*DSC BV*) scanning session of a patient with non-contrast-enhancing oligodendroglioma III. Intravenous injection of 200 MBq FET is performed 20 min prior to simultaneous FET PET and standard MRI scanning. T2* dynamic susceptibility contrast (*DSC*) or T1 dynamic contrast-enhanced (DCE) MRI imaging after contrast injection will supply measurements of tumour blood volume. Notice the areas of increased blood volume (*yellow arrow*) and metabolic activity (*red arrow*) are not congruent [25]

management and in trials. This might be particularly important in paediatric neurooncology requiring the use of anaesthesia only once. CNS tumours are the leading cause of cancer-related deaths from solid tumours in children under age 20, and the clinical use of PET scanning in this patient group is not fully developed [6, 30].

References

1. Stupp R, Mason WP, van den Bent MJ et al (2005) Radiotherapy plus concomitant and adjuvant temozolomide for glioblastoma. N Engl J Med 352(10):987–996
2. Prieto E, Marti-Climent JM, Dominguez-Prado I et al (2011) Voxel-based analysis of dual-time-point 18F-FDG PET images for brain tumor identification and delineation. J Nucl Med 52(6):865–872
3. Kratochwil C, Combs SE, Leotta K et al (2014) Intra-individual comparison of (1)(8)F-FET and (1)(8)F-DOPA in PET imaging of recurrent brain tumors. Neuro Oncol 16(3):434–440
4. Popperl G, Kreth FW, Herms J et al (2006) Analysis of 18F-FET PET for grading of recurrent gliomas: is evaluation of uptake kinetics superior to standard methods? J Nucl Med 47(3):393–403
5. Floeth FW, Pauleit D, Sabel M et al (2006) 18F-FET PET differentiation of ring-enhancing brain lesions. J Nucl Med 47(5):776–782
6. Law I, Borgwardt L, Højgaard L (2015) Pediatric hybrid imaging of the brain. In: von Schulthess GK (ed) Clinical molecular anatomic imaging – PET/CT, PET/MR and SPECT/CT. Wolters Kluwer Health, Philadelphia, pp 218–229
7. Hutterer M, Nowosielski M, Putzer D et al (2013) [18F]-fluoroethyl-L-tyrosine PET: a valuable diagnostic tool in neuro-oncology, but not all that glitters is glioma. Neuro Oncol 15(3):341–351
8. Kracht LW, Miletic H, Busch S et al (2004) Delineation of brain tumor extent with [11C]L-methionine positron emission tomography: local comparison with stereotactic histopathology. Clin Cancer Res 10(21):7163–7170
9. Pauleit D, Floeth F, Hamacher K et al (2005) O-(2-[18F] fluoroethyl)-L-tyrosine PET combined with MRI improves the diagnostic assessment of cerebral gliomas. Brain 128(Pt 3): 678–687
10. Jansen NL, Graute V, Armbruster L et al (2012) MRI-suspected low-grade glioma: is there a need to perform dynamic FET PET? Eur J Nucl Med Mol Imaging 39(6):1021–1029
11. Floeth FW, Pauleit D, Sabel M et al (2007) Prognostic value of O-(2-18F-fluoroethyl)-L-tyrosine PET and MRI in low-grade glioma. J Nucl Med 48(4):519–527
12. Jansen NL, Suchorska B, Wenter V et al (2013) Dynamic 18F-FET PET in newly diagnosed astrocytic low-grade glioma identifies high-risk patients. J Nucl Med 55(2):198–203
13. Jansen NL, Suchorska B, Wenter V et al (2015) Prognostic significance of dynamic 18F-FET PET in newly diagnosed astrocytic high-grade glioma. J Nucl Med 56(1):9–15
14. Lohmann P, Herzog H, Rota Kops E et al (2015) Dual-time-point O-(2-[F]fluoroethyl)-L-tyrosine PET for grading of cerebral gliomas. Eur Radiol 25(10):3017–3024
15. Galldiks N, Stoffels G, Ruge MI et al (2013) Role of O-(2-18F-fluoroethyl)-L-tyrosine PET as a diagnostic tool for detection of malignant progression in patients with low-grade glioma. J Nucl Med 54(12):2046–2054
16. Westwood TD, Hogan C, Julyan PJ et al (2013) Utility of FDG-PETCT and magnetic resonance spectroscopy in differentiating between cerebral lymphoma and non-malignant CNS lesions in HIV-infected patients. Eur J Radiol 82(8):e374–e379
17. Kosaka N, Tsuchida T, Uematsu H et al (2008) 18F-FDG PET of common enhancing malignant brain tumors. AJR Am J Roentgenol 190(6):W365–W369
18. Law I, Højgaard L (2015) Brain tumors: other primary brain tumors, metastases and radiation injury. In: von Schulthess GK (ed) Clinical molecular anatomic imaging – PET/CT, PET/MR and SPECT/CT. Wolters Kluwer Health, Philadelphia, pp 169–179
19. Pirotte B, Goldman S, Massager N et al (2004) Combined use of 18F-fluorodeoxyglucose and 11C-methionine in 45 positron emission tomography-guided stereotactic brain biopsies. J Neurosurg 101(3):476–483
20. Heinzel A, Stock S, Langen KJ et al (2012) Cost-effectiveness analysis of FET PET-guided target selection for the diagnosis of gliomas. Eur J Nucl Med Mol Imaging 39(7):1089–1096
21. Langleben DD, Segall GM (2000) PET in differentiation of recurrent brain tumor from radiation injury. J Nucl Med 41(11): 1861–1867
22. Combs SE, Welzel T, Habermehl D et al (2013) Prospective evaluation of early treatment outcome in patients with meningiomas treated with particle therapy based on target volume definition with MRI and 68Ga-DOTATOC-PET. Acta Oncol 52(3):514–520
23. Bashir A, Ziebell M, Fugleholm K et al (2015) A potential role of 68Ga-DOTATOC PET in modifying eligibility to surgery in patients with recurrent meningioma. J Nucl Med Radiat Ther 6:256
24. Marincek N, Radojewski P, Dumont RA et al (2015) Somatostatin receptor-targeted radiopeptide therapy with 90Y-DOTATOC and 177Lu-DOTATOC in progressive meningioma: long-term results of a phase II clinical trial. J Nucl Med 56(2):171–176
25. Henriksen OM, Larsen VA, Muhic A et al (2016) Simultaneous evaluation of brain tumour metabolism, structure and blood volume using [F]-fluoroethyl tyrosine (FET) PET/MRI: feasibility, agreement and initial experience. Eur J Nucl Med Mol Imaging 43(1):103–112
26. Larsen VA, Simonsen HJ, Law I et al (2013) Evaluation of dynamic contrast-enhanced T1-weighted perfusion MRI in the differentiation of tumor recurrence from radiation necrosis. Neuroradiology 55(3):361–369
27. Moller S, Lundemann M, Law I et al (2015) Early changes in perfusion of glioblastoma during radio- and chemotherapy evaluated by T1-dynamic contrast enhanced magnetic resonance imaging. Acta Oncol 54(9):1521–1528
28. Andersen FL, Ladefoged CN, Beyer T et al (2014) Combined PET/MR imaging in neurology: MR-based attenuation correction implies a strong spatial bias when ignoring bone. Neuroimage 84:206–216
29. Ladefoged CN, Benoit D, Law I et al (2015) Region specific optimization of continuous linear attenuation coefficients based on UTE (RESOLUTE): application to PET/MR brain imaging. Phys Med Biol 60(20):8047–8065
30. Dunkl V, Cleff C, Stoffels G et al (2015) The usefulness of dynamic O-(2-18F-Fluoroethyl)-l-Tyrosine PET in the clinical evaluation of brain tumors in children and adolescents. J Nucl Med 56(1):88–92

Nuclear Imaging of Dementia

Alexander Drzezga

Introduction

The prevalence of dementia, representing a category of age-associated disorders, is continuously increasing in our aging society. Currently, more than 9 Mio patients are supposed to be affected by this devastating condition in Europe (http://www.alzheimer-europe.org/), not including a presumably high number of patients who have not yet been diagnosed or patients in early stages of disease. Approximately 20 % of persons in an age greater than 80 years are suffering from clinically manifest dementia [1, 2]. With regard to the rising life expectancy, this poses a massive burden not only on patients and their relatives but also on the healthcare/socio-economic systems. These facts appear even more alarming in the light of the very limited therapeutic options which are currently available for most forms of dementia.

In short, dementia itself is defined as an impairment of cognitive abilities sufficient to affect the activities of daily living, which is developing gradually and is not associated with a loss of consciousness [3]. Different causal pathologies can underlie the clinical manifestation of a dementia, the most frequent being Alzheimer's disease which holds responsible for approximately 60 % of all cases, followed by vascular dementia, dementia with Lewy body disease, and the frontotemporal lobar degenerative disorders [4, 5]. A common factor contributing to the development of neurodegenerative forms of dementia appears to be the pathological aggregation of proteins in the brain. For Alzheimer's disease, this includes the deposition of ß-amyloid protein aggregates in the form of extracellular plaques and of tau protein aggregates in the form of intraneuronal neurofibrillary tangles [6]. According to current disease concepts, these aggregates contribute to neuronal dysfunction and later neuronal loss [7]. Modern therapy approaches are directed toward the removal/prevention of these protein aggregation pathologies. However, so far these studies have not resulted in very promising results. As for factors possibly contributing to this limited success, it has been discussed that attempts to treat have been initiated too late in the course of disease, i.e., when irreversible neuronal damage has already occurred. Furthermore, it has been demonstrated that a relevant proportion of patients included in these trials may have been clinically misdiagnosed [8].

These insights underline the need for a reliable and early diagnosis of ongoing neurodegeneration. However, clinical diagnosis of dementia is hampered in many respects. First, it is well accepted that the causal neuropathologies leading to dementia are usually starting to develop years to decades ahead of the symptomatic onset of disease. Consequently, today preclinical and pre-dementia mild clinical stages (the so-called mild cognitive impairment or MCI) are discussed, particularly with regard to Alzheimer's disease [9]. From this perspective, dementia can be considered a late stage of disease and early diagnosis on the basis of the assessment of clinical symptoms is limited per definition. In the same context, biomarker-supported diagnosis of Alzheimer's disease is recently recommended, all the more if early diagnosis of ongoing neurodegeneration is required [10–13]. Also, differential diagnosis of different forms of dementia is difficult, because different causal pathologies can result in similar cognitive deficits. Finally, clinical symptomatology of dementia may not be an optimal parameter for follow-up and therapy monitoring, because of a limited association between neuropathology and extent of symptoms as well as fluctuation of the latter. Consequently, the role of imaging biomarkers in the diagnosis of pathologies underlying the development of dementia may be of growing importance. In this context, nuclear medicine offers particularly promising methods for imaging molecular pathologies and neuronal dysfunction.

A. Drzezga
Nuclear Medicine, University Hospital, University of Cologne, Kerpener Str. 62, Cologne, Northrine-Westfalia 50937, Germany
e-mail: Alexander.drzezga@uk-koeln.de

J. Hodler et al. (eds.), *Diseases of the Brain, Head and Neck, Spine 2016–2019: Diagnostic Imaging*, DOI 10.1007/978-3-319-30081-8_26

[18F]FDG-PET

It is well known that glucose represents the source of energy for the brain and that cerebral neuronal activity is tightly coupled to the uptake and metabolism of glucose, probably mediated by the glial cells [14]. Consequently, regional cerebral uptake of [18F]FDG as a tracer for measuring glucose metabolism reflects neuronal function or dysfunction. It has been demonstrated by numerous studies – including studies with in vivo versus postmortem histopathological cross evaluation – that typical patterns of hypometabolism can be observed in manifest neurodegenerative forms of dementia [15]. In Alzheimer's disease, a characteristic pattern of hypometabolism in the temporoparietal, posterior cingulate, and later also frontal cortex can be observed [16]. The pattern of affected brain regions fits to the functional abnormalities which are usually involving memory, language functions, visual-spatial abilities, and later personality changes. The sensorimotor regions as well as the primary visual cortex and cerebellum are usually spared from metabolic changes, in correspondence with maintained motor and sensory functions in these patients. The topography of these hypometabolic changes is highly specific for Alzheimer's disease, and it has been demonstrated that FDG-PET allows more accurate diagnosis as compared to neuropsychological assessment [17]. Importantly, hypometabolic abnormalities are not only observed in patients with manifest dementia of Alzheimer's type but also in earlier stages of disease. A number of studies analyzed the value of FDG-PET in the early detection of Alzheimer's disease in the stage of MCI. It has been demonstrated that mild hypometabolism in posterior cingulate cortical regions, often accompanied by subtle parietal and temporal hypometabolism, has a high predictive value with regard to later conversion to manifest dementia in these patients [16, 18]. On the other hand, patients with MCI symptoms but without signs of hypometabolism on FDG-PET have a very low risk of conversion to dementia of Alzheimer's type. FDG-PET has also been demonstrated to have a very high value in the differential diagnosis between different forms of neurodegenerative disorders [19]. For non-Alzheimer forms of dementia, disease-specific patterns of hypometabolism have been described. Dementia with Lewy bodies has been shown to be associated with a pattern of temporoparietal hypometabolism similar to Alzheimer's disease, however, extending clearly into the occipital cortex, involving primary visual cortical areas [20]. This goes hand in hand with the known visual hallucinations in these patients. FDG-PET has also been shown to have a high value for differentiation between Alzheimer's-type dementia and the frontotemporal lobar degenerative disorders [21]. Also, for the different subtypes of frontotemporal lobar degeneration (FTLD), specific patterns of hypometabolism have been described [22–27], with the behavioral variant (bvFTD) showing stronger frontal and temporal polar abnormalities [28], the semantic variant of primary progressive aphasia (svPPA) displaying bilateral temporal hypometabolism [25, 29, 30], and the logopenic variant as well as the nonfluent variant (lvPPA, nfvPPA) both demonstrating clearly asymmetric unilateral (usually left-hemispheric) hypometabolism of the temporal and in part frontal and parietal cortex. In nfvPPA, involvement of left frontal cortical regions (often including Broca's area) has been shown [31, 32], and in lvPPA hypometabolic regions have been observed within the left lateral temporal and parietal lobe as well as in the precuneus and posterior frontal lobe [33–36]. It has to be mentioned that the FDG pattern is reflecting the symptomatic appearance of these subtypes of neurodegeneration without allowing a clear distinction of the underlying neuropathology. FTLD has been demonstrated to comprise a number of different causal pathologies which can result in similar clinical phenotypes of disease [37, 39]. This includes tau-positive forms, TDP-43 aggregation-positive forms, and even atypical forms of Alzheimer's disease. In particular the variant of logopenic aphasia has been demonstrated to frequently represent an atypical variant of Alzheimer's disease [31]. However, other neuropathological changes such as TDP-43 may result in the clinical appearance of lvPPA accompanied by a similar hypometabolic pattern in FDG-PET [33]. In addition to the phenotype of logopenic aphasia, Alzheimer's disease can appear in other atypical variants. This includes the so-called posterior cortical atrophy, which is characterized by predominantly visual-constructive deficits in the early phases of disease, often leading the patients to see an ophthalmologist [39]. In the FDG-PET scan these patients exhibit a distinct bilateral occipitoparietal hypometabolism [40, 41]. Another atypical form of Alzheimer's disease is the frontal/executive subtype [42]. Patients may show symptoms more similar to the behavioral variant of frontotemporal dementia in early cases. In the FDG-PET scan, they show frontal cortical hypometabolism, but in contrast to bvFTD usually some involvement of temporoparietal cortices is to be expected. Using amyloid imaging (see below) doubts about the causal pathology in these atypical cases of Alzheimer's disease can be cleared. Finally, FDG-PET represents a valuable tool to differentiate pseudodementia in patients with depression and cognitive symptoms (who will show a rather normal finding on the FDG-PET scan) versus patients suffering from early Alzheimer's disease with depressive symptoms [43].

Amyloid Imaging

Since their first description by Alois Alzheimer himself, amyloid plaques represent one key hallmark for the diagnosis of Alzheimer's disease. Until very recently, definite diagnosis of Alzheimer's disease has only been possible by

means of postmortem histopathological assessment of brain tissue. The advent of tracers for amyloid imaging now allows the detection of this core pathology in vivo. Consequently, for the first time, noninvasive in vivo proof of amyloid deposition in the brain and longitudinal observation of the onset and course of this pathology became possible. A great number of studies on in vivo imaging of amyloid deposits in the brain have been performed with the tracer [11C]PiB [44]. These studies form the basis of our current knowledge on the potential value of amyloid imaging in clinical practice. In addition, for a number of 18F-labeled tracers (with longer half-life), FDA approval has been achieved and they are now also commercially available. This includes [18F]florbetaben (NeuraCeq™), [18F]florbetapir (Amyvid™), and [18F]flutemetamol (Vizamyl™) [45–47]. All tracers had to undergo extensive evaluation before approval, including in vivo versus postmortem evaluation of their properties [48–57].

For all tracers, typically intense tracer uptake is observed in the frontal, temporoparietal, and posterior cingulate cortex, the precuneus, and also the caudate nucleus. Sensorimotor and visual cortices are usually somewhat less affected and the cerebellum is spared of amyloid aggregates and, thus, can serve as a reference region [45, 47, 58, 59].

Regarding early diagnosis, several studies were now able to demonstrate that the proof of amyloid pathology in the brain in patients with MCI has a high sensitivity with regard to prediction of later conversion to manifest Alzheimer's dementia [60–65]. The specificity varied depending on the selected follow-up periods. Importantly, studies consistently demonstrated that in approximately 25–30 % of elderly subjects (>60 years), significant amyloid pathology could be detected using amyloid imaging in the presence of normal cognitive function [58, 66–69]. A recent study demonstrated the rate of amyloid positivity appears to increase exponentially with age in otherwise healthy elderly subjects in dependence of the ApoE genotype, with homozygous carriers of the e4 allele showing the highest risk [69]. It is yet unclear if "amyloid positivity" translates inevitably into symptomatic Alzheimer's disease in all of these subjects. Several studies indicate that amyloid-positive elderly subjects may in fact be suffering from preclinical Alzheimer's disease by demonstrating abnormalities in other imaging tests, comparatively lower cognitive performance and steeper cognitive decline in these subjects as compared to amyloid-negative age-matched controls [70–72]. However, even in this case the information on the potential time to conversion in these subjects is still very limited. It appears possible that amyloid pathology may be detected in the brain 10–20 years ahead of clinical disease onset [63]. Consequently, according to recently published appropriate use criteria for amyloid imaging, it would not be recommended to offer an amyloid PET scan in otherwise healthy elderly subjects [73]. First, the interpretation of a positive amyloid scan in terms of prognosis would be difficult to judge. Second, at this time no therapeutic options would be on hand. Thus, the disclosure of the information of amyloid positivity to an otherwise healthy person would in fact be ethically problematic. On the other hand, in the context of clinical trials, it obviously stands to reason to include subjects with only mild or even no clinical symptoms into studies aiming for the removal or prevention of amyloid deposition in the brain. In fact, large clinical trials have been initiated following this concept [74]. Thus, in summary, there is a value of amyloid imaging with regard to early diagnosis/exclusion of Alzheimer pathology in patients with mild symptoms. However, in asymptomatic stages, amyloid imaging would currently be restricted to systematic clinical trials.

Regarding differential diagnosis, it has been demonstrated that the available amyloid tracers are specific with regard to amyloid pathology, i.e., they would not bind to other forms of protein aggregation such as tau or alpha-synuclein [52, 75–78]. However, it is also known that amyloid plaques do not only develop in Alzheimer's disease but can also be found in up to 80 % of cases of dementia with Lewy bodies [79–81]. Thus, differential diagnosis between AD and DLB cannot be performed using amyloid imaging. For this diagnostic question, it has been demonstrated that dopamine transporter imaging can be applied which reveals normal findings in AD but reduced transporter density in patients with DLB [82]. Amyloid imaging may be of high value to differentiate between the amyloid-negative forms of frontotemporal lobar degeneration and Alzheimer's disease [83]. As mentioned above, atypical clinical variants of Alzheimer's disease may appear in symptomatic forms typically associated with frontotemporal lobar degeneration, e.g., in logopenic aphasia [31, 84, 85]. Inversely, frontotemporal lobar degenerative disorders may mimic Alzheimer's disease as well. Consequently, according to the appropriate use criteria, it can be recommended to clinically employ amyloid imaging in cases of early-onset dementia and in cases with atypical appearance of suspected Alzheimer's disease [73]. Amyloid imaging is currently not recommended in cases of clinically typical Alzheimer's disease. This position can however be challenged with regard to recent insights from clinical trials, indicating that a high proportion (>30 %) of patients clinically diagnosed with Alzheimer's disease by experts in fact do not show amyloid pathology in their amyloid scans [8]. Amyloid imaging may therefore be crucial for inclusion of patients into anti-amyloid therapy trials. Some studies have also employed amyloid imaging to monitor therapy response [86]. It may not be useful for disease follow-up, however, because it has been demonstrated that amyloid deposition shows a stagnation or plateau in the symptomatic stages of disease [87]. Regarding differential diagnosis with amyloid PET, it should be kept in mind that the probability of amyloid positivity increases with age not only in healthy subjects but also in patients suffering from

clinical forms of neurodegeneration other than Alzheimer's disease, as recently demonstrated [88]. Consequently, in elderly subjects, the possibility of amyloid deposition, which is not disease related, or the presence of dual pathology should be taken into account.

Tracers for Tau Imaging

In addition to now established tracers for amyloid imaging, recently introduced experimental tracers are promising to be suitable for imaging tau aggregates [89, 90]. The imaging of tau is considerably more complicated as compared to amyloid imaging, as tracers have to enter not only the brain across the blood-brain barrier but also enter the neurons because tau aggregates occur intracellularly.

For several tracers promising results in humans have already been published. This includes tracers developed at Tohoku University, Japan [91–94], and the tracer [18F]T807 ([18F]AV1451) now licensed by Avid Radiopharmaceuticals [95, 96]. The first studies with these tracers in humans demonstrate an uptake pattern which is different from amyloid deposition in the same patients with Alzheimer's disease and consistent with the distribution of tau pathology, as known from neuropathology. In a first study, the binding behavior of T807 has also been evaluated on human brain tissue [97]. However, for all of these tracers, histopathological in vivo versus postmortem cross evaluation is still pending. A clinical value of tau imaging tracers with regard to early diagnosis of Alzheimer's disease may be discussed [89, 90]. However, according to currently discussed concepts on the order of appearance of biomarkers of Alzheimer's disease, it would be expected that amyloid pathology would be detectable ahead of tau pathology [98]. On the other hand, neuropathological studies suggest that cerebral tau aggregation correlates with the extent of cognitive decline (in contrast to amyloid plaque deposition). Correspondingly, the first tau imaging studies indicate that the uptake of tau correlates closely with the level of cognitive impairment [96]. Thus, tau imaging may represent a suitable biomarker for disease follow-up but rather not for very early detection of Alzheimer pathology in the asymptomatic stages. It may, however, be helpful to detect the onset of neurodegeneration in amyloid-positive subjects. Future studies will need to demonstrate an added value in this context, as compared to markers of neuronal dysfunction such as [18F]FDG. With regard to differential diagnosis, the application of tau imaging may be very complicated, because tau as a target is highly heterogeneous [99, 100]. There are two different haplotypes and 6 isoforms, tau can occur in phosphorylated/non-phosphorylated forms, and there are different structural variants of aggregation (straight filaments, helical filaments/tangles, coiled bodies, etc.). Depending on the disorder, aggregates can occur in neurons and in the glial cells [101]. Tau imaging may be helpful to differentiate between tau-positive and tau-negative forms of syndromes, e.g., tau-positive corticobasal syndrome versus synuclein-positive multiple system atrophies (MSA). However, tau pathology can be found in a number of different neurodegenerative disorders, summarized under the term "tauopathies" [102]. This includes Alzheimer's disease, corticobasal syndrome, progressive supranuclear palsy, Pick's disease, FTLD-MAPT (FTD/parkinsonism, chromosome 17 (FTDP-17)), and also brain trauma. Thus, differential diagnosis between these neurodegenerative disorders on the basis of tau positivity or negativity will not be possible. However, patterns of cerebral tau aggregation are different between the various tauopathies, thus potentially providing information beyond the bare presence of tau pathology. The fact that levels and anatomical distribution of tau aggregation pathology may be detected by tau imaging potentially also represents an added value over CSF tests (Fig. 1).

Summary

Recent guidelines for diagnosis of Alzheimer's disease recommend a three-step biomarker-supported categorization [10]. According to these guidelines, increased levels of amyloid pathology in the brain are coding for a low risk, presence of additional neuronal injury for an intermediate risk, and the additional proof of cognitive decline for a high risk of suffering from Alzheimer's disease. Molecular imaging methods offer the unique opportunity to monitor these parameters in vivo, noninvasively. Amyloid imaging has entered the clinical arena and may allow to detect subjects at risk for Alzheimer's disease in very early stages, to select patients for therapy trials, and (if negative) to exclude Alzheimer's disease as a reason for cognitive decline. FDG-PET as the best established tracer for imaging neurodegeneration can be considered the Swiss Knife in dementia diagnosis. It allows reliable prediction in the stages of mild cognitive impairment and provides information on the pattern and extent of neuronal dysfunction in different forms of neurodegenerative disorders. Novel tau imaging procedures are still in an experimental stage but may allow to detect onset of neurodegeneration in amyloid-positive subjects, select patients for tau trials, and differentiate between tau-positive and tau-negative forms of neurodegeneration in the future.

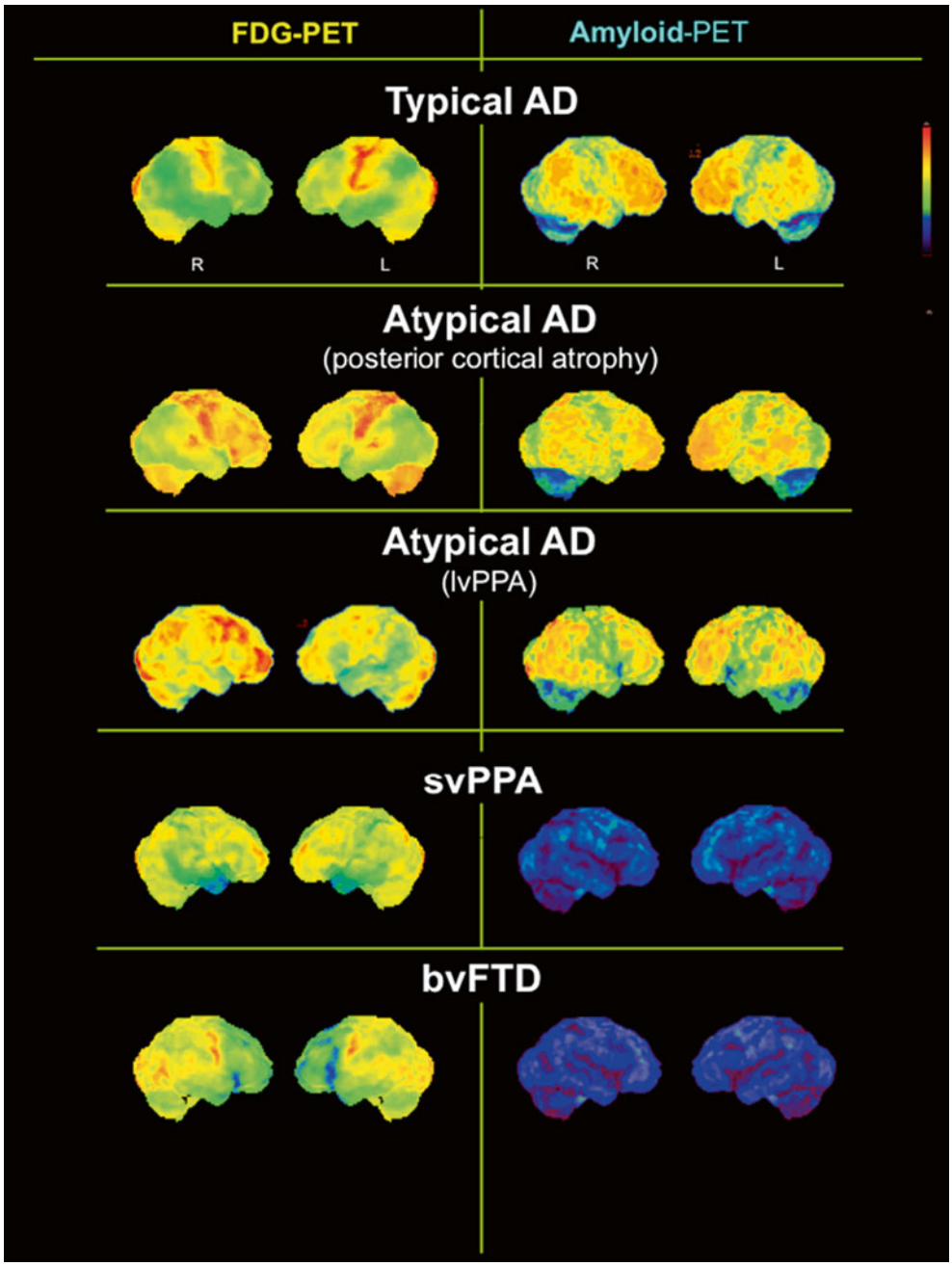

Fig. 1 Exemplary presentation (surface projections, 3DSSP, Neurostat) of [18F]FDG-PET (glucose metabolism) and [11C] PiB-PET (amyloid imaging) in different forms of dementia. Images are displayed in left lateral (*1st and 3rd column*) and right lateral (*2nd and 4th column*) aspects of the brain (*1st two columns*, FDG-PET; *3rd and 4th column*, PiB-PET). *AD* Alzheimer's disease, *lvPPA* logopenic variant of primary progressive aphasia, *svPPA* semantic variant of primary progressive aphasia, *bvFTD* behavioral variant of frontotemporal dementia

References

1. Hebert LE, Weuve J, Scherr PA et al (2013) Alzheimer disease in the United States (2010–2050) estimated using the 2010 census. Neurology 80(19):1778–1783
2. Plassman BL, Langa KM, Fisher GG et al (2007) Prevalence of dementia in the United States: the aging, demographics, and memory study. Neuroepidemiology 29(1–2):125–132
3. American Psychiatric Association. (2013). Diagnostic and statistical manual of mental disorders (5th ed.). Arlington, V.A.P.P
4. Alafuzoff I (1992) The pathology of dementias: an overview. Acta Neurol Scand Suppl 139:8–15
5. Zaccai J, McCracken C, Brayne C (2005) A systematic review of prevalence and incidence studies of dementia with Lewy bodies. Age Ageing 34(6):561–566
6. Braak H, Braak E (1991) Neuropathological stageing of Alzheimer-related changes. Acta Neuropathol (Berl) 82(4): 239–259
7. Selkoe DJ (2003) Folding proteins in fatal ways. Nature 426(6968):900–904
8. Salloway S, Sperling R, Fox NC et al (2014) Two phase 3 trials of bapineuzumab in mild-to-moderate Alzheimer's disease. N Engl J Med 370(4):322–333
9. Petersen RC, Smith GE, Waring SC et al (1999) Mild cognitive impairment: clinical characterization and outcome. Arch Neurol 56(3):303–308
10. Dubois B, Feldman HH, Jacova C et al (2007) Research criteria for the diagnosis of Alzheimer's disease: revising the NINCDS-ADRDA criteria. Lancet Neurol 6(8):734–746
11. Sperling RA, Aisen PS, Beckett LA et al (2011) Toward defining the preclinical stages of Alzheimer's disease: recommendations

from the National Institute on Aging-Alzheimer's Association workgroups on diagnostic guidelines for Alzheimer's disease. Alzheimers Dement 7(3):280–292
12. McKhann GM, Knopman DS, Chertkow H et al (2011) The diagnosis of dementia due to Alzheimer's disease: recommendations from the National Institute on Aging-Alzheimer's Association workgroups on diagnostic guidelines for Alzheimer's disease. Alzheimers Dement 7(3):263–269
13. Albert MS, DeKosky ST, Dickson D et al (2011) The diagnosis of mild cognitive impairment due to Alzheimer's disease: recommendations from the National Institute on Aging-Alzheimer's Association workgroups on diagnostic guidelines for Alzheimer's disease. Alzheimers Dement 7(3):270–279
14. Magistretti PJ, Pellerin L (1996) Cellular mechanisms of brain energy metabolism. Relevance to functional brain imaging and to neurodegenerative disorders. Ann N Y Acad Sci 777:380–387
15. Herholz K (2003) PET studies in dementia. Ann Nucl Med 17(2):79–89
16. Minoshima S, Giordani B, Berent S et al (1997) Metabolic reduction in the posterior cingulate cortex in very early Alzheimer's disease. Ann Neurol 42(1):85–94
17. Silverman, D.H., G.W. Small, C.Y. Chang, et al (2001) Positron emission tomography in evaluation of dementia: Regional brain metabolism and long-term outcome. Jama, 286(17): p. 2120–7.
18. Drzezga A, Lautenschlager N, Siebner H et al (2003) Cerebral metabolic changes accompanying conversion of mild cognitive impairment into Alzheimer's disease: a PET follow-up study. Eur J Nucl Med Mol Imaging 30(8):1104–1113
19. Panegyres PK, Rogers JM, McCarthy M et al (2009) Fluorodeoxyglucose-positron emission tomography in the differential diagnosis of early-onset dementia: a prospective, community-based study. BMC Neurol 9:41
20. Minoshima S, Foster NL, Sima AA et al (2001) Alzheimer's disease versus dementia with Lewy bodies: cerebral metabolic distinction with autopsy confirmation. Ann Neurol 50(3): 358–365
21. Foster NL, Heidebrink JL, Clark CM et al (2007) FDG-PET improves accuracy in distinguishing frontotemporal dementia and Alzheimer's disease. Brain 130(Pt 10):2616–2635
22. Diehl J, Grimmer T, Drzezga A et al (2004) Cerebral metabolic patterns at early stages of frontotemporal dementia and semantic dementia. A PET study. Neurobiol Aging 25(8):1051–1056
23. Diehl-Schmid J, Grimmer T, Drzezga A et al (2006) Longitudinal changes of cerebral glucose metabolism in semantic dementia. Dement Geriatr Cogn Disord 22(4):346–351
24. Diehl-Schmid J, Grimmer T, Drzezga A et al (2007) Decline of cerebral glucose metabolism in frontotemporal dementia: a longitudinal 18F-FDG-PET-study. Neurobiol Aging 28:42–50
25. Drzezga A, Grimmer T, Henriksen G et al (2008) Imaging of amyloid plaques and cerebral glucose metabolism in semantic dementia and Alzheimer's disease. Neuroimage 39(2): 619–633
26. Nestor PJ, Graham NL, Fryer TD et al (2003) Progressive non-fluent aphasia is associated with hypometabolism centred on the left anterior insula. Brain 126(Pt 11):2406–2418
27. Nestor PJ, Fryer TD, Hodges JR (2006) Declarative memory impairments in Alzheimer's disease and semantic dementia. Neuroimage 30(3):1010–1020
28. Schroeter ML, Laird AR, Chwiesko C et al (2014) Conceptualizing neuropsychiatric diseases with multimodal data-driven meta-analyses - The case of behavioral variant frontotemporal dementia. Cortex 57C:22–37
29. Edwards-Lee T, Miller BL, Benson DF et al (1997) The temporal variant of frontotemporal dementia. Brain 120(Pt 6):1027–1040
30. Jagust WJ, Reed BR, Seab JP et al (1989) Clinical-physiologic correlates of Alzheimer's disease and frontal lobe dementia. Am J Physiol Imaging 4(3):89–96
31. Rabinovici GD, Jagust WJ, Furst AJ et al (2008) Abeta amyloid and glucose metabolism in three variants of primary progressive aphasia. Ann Neurol 64(4):388–401
32. Drzezga A, Grimmer T, Siebner H et al (2002) Prominent hypometabolism of the right temporoparietal and frontal cortex in two left-handed patients with primary progressive aphasia. J Neurol 249(9):1263–1267
33. Josephs KA, Duffy JR, Strand EA et al (2014) Progranulin-associated PiB-negative logopenic primary progressive aphasia. J Neurol 261(3):604–614
34. Gorno-Tempini ML, Dronkers NF, Rankin KP et al (2004) Cognition and anatomy in three variants of primary progressive aphasia. Ann Neurol 55(3):335–346
35. Madhavan A, Whitwell JL, Weigand SD et al (2013) FDG PET and MRI in logopenic primary progressive aphasia versus dementia of the Alzheimer's type. PLoS One 8(4):e62471
36. Teichmann M, Kas A, Boutet C et al (2013) Deciphering logopenic primary progressive aphasia: a clinical, imaging and biomarker investigation. Brain 136(Pt 11):3474–3488
37. Mesulam M, Wieneke C, Rogalski E et al (2009) Quantitative template for subtyping primary progressive aphasia. Arch Neurol 66(12):1545–1551
38. Bonner MF, Ash S, Grossman M (2010) The new classification of primary progressive aphasia into semantic, logopenic, or nonfluent/agrammatic variants. Curr Neurol Neurosci Rep 10(6): 484–490
39. Crutch SJ, Lehmann M, Schott JM et al (2012) Posterior cortical atrophy. Lancet Neurol 11(2):170–178
40. Nestor PJ, Caine D, Fryer TD et al (2003) The topography of metabolic deficits in posterior cortical atrophy (the visual variant of Alzheimer's disease) with FDG-PET. J Neurol Neurosurg Psychiatry 74(11):1521–1529
41. Whitwell JL, Jack CR Jr, Kantarci K et al (2007) Imaging correlates of posterior cortical atrophy. Neurobiol Aging 28(7): 1051–1061
42. Back-Madruga C, Boone KB, Briere J et al (2002) Functional ability in executive variant Alzheimer's disease and typical Alzheimer's disease. Clin Neuropsychol 16(3):331–340
43. Videbech P (2000) PET measurements of brain glucose metabolism and blood flow in major depressive disorder: a critical review. Acta Psychiatr Scand 101(1):11–20
44. Klunk WE, Engler H, Nordberg A et al (2004) Imaging brain amyloid in Alzheimer's disease with Pittsburgh Compound-B. Ann Neurol 55(3):306–319
45. Barthel H, Gertz HJ, Dresel S et al (2011) Cerebral amyloid-beta PET with florbetaben (18F) in patients with Alzheimer's disease and healthy controls: a multicentre phase 2 diagnostic study. Lancet Neurol 10(5):424–435
46. Vandenberghe R, Van Laere K, Ivanoiu A et al (2010) 18F-flutemetamol amyloid imaging in Alzheimer disease and mild cognitive impairment: a phase 2 trial. Ann Neurol 68(3): 319–329
47. Fleisher AS, Chen K, Liu X et al (2011) Using positron emission tomography and florbetapir F18 to image cortical amyloid in patients with mild cognitive impairment or dementia due to Alzheimer disease. Arch Neurol 68(11):1404–1411
48. Bacskai BJ, Frosch MP, Freeman SH et al (2007) Molecular imaging with Pittsburgh Compound B confirmed at autopsy: a case report. Arch Neurol 64(3):431–434
49. Burack MA, Hartlein J, Flores HP et al (2010) In vivo amyloid imaging in autopsy-confirmed Parkinson disease with dementia. Neurology 74(1):77–84
50. Cairns NJ, Ikonomovic MD, Benzinger T et al (2009) Absence of Pittsburgh compound B detection of cerebral amyloid beta in a patient with clinical, cognitive, and cerebrospinal fluid markers of Alzheimer disease: a case report. Arch Neurol 66(12):1557–1562

51. Clark CM, Schneider JA, Bedell BJ et al (2011) Use of florbetapir-PET for imaging beta-amyloid pathology. JAMA 305(3):275–283
52. Ikonomovic MD, Klunk WE, Abrahamson EE et al (2008) Post-mortem correlates of in vivo PiB-PET amyloid imaging in a typical case of Alzheimer's disease. Brain 131(Pt 6):1630–1645
53. Kadir A, Marutle A, Gonzalez D et al (2011) Positron emission tomography imaging and clinical progression in relation to molecular pathology in the first Pittsburgh Compound B positron emission tomography patient with Alzheimer's disease. Brain 134 (Pt 1):301–317
54. Leinonen V, Alafuzoff I, Aalto S et al (2008) Assessment of beta-amyloid in a frontal cortical brain biopsy specimen and by positron emission tomography with carbon 11-labeled Pittsburgh Compound B. Arch Neurol 65(10):1304–1309
55. Sojkova J, Driscoll I, Iacono D et al (2011) In vivo fibrillar beta-amyloid detected using [11C]PiB positron emission tomography and neuropathologic assessment in older adults. Arch Neurol 68(2):232–240
56. Villemagne VL, McLean CA, Reardon K et al (2009) 11C-PiB PET studies in typical sporadic Creutzfeldt-Jakob disease. J Neurol Neurosurg Psychiatry 80(9):998–1001
57. Wolk DA, Grachev ID, Buckley C et al (2011) Association between in vivo fluorine 18-labeled flutemetamol amyloid positron emission tomography imaging and in vivo cerebral cortical histopathology. Arch Neurol 68(11):1398–1403
58. Pike KE, Savage G, Villemagne VL et al (2007) Beta-amyloid imaging and memory in non-demented individuals: evidence for preclinical Alzheimer's disease. Brain 130(Pt 11):2837–2844
59. Rowe CC, Ellis KA, Rimajova M et al (2010) Amyloid imaging results from the Australian Imaging, Biomarkers and Lifestyle (AIBL) study of aging. Neurobiol Aging 31(8):1275–1283
60. Forsberg A, Engler H, Almkvist O et al (2008) PET imaging of amyloid deposition in patients with mild cognitive impairment. Neurobiol Aging 29:1456–1465
61. Koivunen J, Scheinin N, Virta JR et al (2011) Amyloid PET imaging in patients with mild cognitive impairment: a 2-year follow-up study. Neurology 76(12):1085–1090
62. Okello A, Koivunen J, Edison P et al (2009) Conversion of amyloid positive and negative MCI to AD over 3 years: an 11C-PIB PET study. Neurology 73(10):754–760
63. Villemagne VL, Pike KE, Chetelat G et al (2011) Longitudinal assessment of Abeta and cognition in aging and Alzheimer disease. Ann Neurol 69(1):181–192
64. Zhang S, Han D, Tan X et al (2012) Diagnostic accuracy of 18 F-FDG and 11 C-PIB-PET for prediction of short-term conversion to Alzheimer's disease in subjects with mild cognitive impairment. Int J Clin Pract 66(2):185–198
65. Nordberg A, Carter SF, Rinne J et al (2013) A European multicentre PET study of fibrillar amyloid in Alzheimer's disease. Eur J Nucl Med Mol Imaging 40(1):104–114
66. Mintun MA, Larossa GN, Sheline YI et al (2006) [11C]PIB in a nondemented population: potential antecedent marker of Alzheimer disease. Neurology 67(3):446–452
67. Villemagne VL, Pike KE, Darby D et al (2008) Abeta deposits in older non-demented individuals with cognitive decline are indicative of preclinical Alzheimer's disease. Neuropsychologia 46(6):1688–1697
68. Villemagne VL, Fodero-Tavoletti MT, Pike KE et al (2008) The ART of loss: Abeta imaging in the evaluation of Alzheimer's disease and other dementias. Mol Neurobiol 38(1):1–15
69. Jansen WJ, Ossenkoppele R, Knol DL et al (2015) Prevalence of cerebral amyloid pathology in persons without dementia: a meta-analysis. JAMA 313(19):1924–1938
70. Hedden T, Van Dijk KR, Becker JA et al (2009) Disruption of functional connectivity in clinically normal older adults harboring amyloid burden. J Neurosci 29(40):12686–12694
71. Sperling RA, Laviolette PS, O'Keefe K et al (2009) Amyloid deposition is associated with impaired default network function in older persons without dementia. Neuron 63(2):178–188
72. Drzezga A, Becker JA, Van Dijk KR et al (2011) Neuronal dysfunction and disconnection of cortical hubs in non-demented subjects with elevated amyloid burden. Brain 134(Pt 6):1635–1646
73. Johnson KA, Minoshima S, Bohnen NI et al (2013) Appropriate use criteria for amyloid PET: a report of the Amyloid Imaging Task Force, the Society of Nuclear Medicine and Molecular Imaging, and the Alzheimer's Association. J Nucl Med 54(3): 476–490
74. Sperling RA, Rentz DM, Johnson KA et al (2014) The A4 study: stopping AD before symptoms begin? Sci Transl Med 6(228):228fs13
75. Fodero-Tavoletti MT, Brockschnieder D, Villemagne VL et al (2012) In vitro characterization of [(18)F]-florbetaben, an Abeta imaging radiotracer. Nucl Med Biol 39:1042–1048
76. Fodero-Tavoletti MT, Smith DP, McLean CA et al (2007) In vitro characterization of Pittsburgh compound-B binding to Lewy bodies. J Neurosci 27(39):10365–10371
77. Lockhart A, Lamb JR, Osredkar T et al (2007) PIB is a non-specific imaging marker of amyloid-beta (Abeta) peptide-related cerebral amyloidosis. Brain 130(Pt 10):2607–2615
78. Thompson PW, Ye L, Morgenstern JL et al (2009) Interaction of the amyloid imaging tracer FDDNP with hallmark Alzheimer's disease pathologies. J Neurochem 109(2):623–630
79. Weisman D, Cho M, Taylor C et al (2007) In dementia with Lewy bodies, Braak stage determines phenotype, not Lewy body distribution. Neurology 69(4):356–359
80. Rowe CC, Ng S, Ackermann U et al (2007) Imaging beta-amyloid burden in aging and dementia. Neurology 68(20):1718–1725
81. Edison P, Rowe CC, Rinne JO et al (2008) Amyloid load in Parkinson's disease dementia and Lewy body dementia measured with [11C]PIB positron emission tomography. J Neurol Neurosurg Psychiatry 79(12):1331–1338
82. McKeith I, O'Brien J, Walker Z et al (2007) Sensitivity and specificity of dopamine transporter imaging with 123I-FP-CIT SPECT in dementia with Lewy bodies: a phase III, multicentre study. Lancet Neurol 6(4):305–313
83. Rabinovici GD, Furst AJ, O'Neil JP et al (2007) 11C-PIB PET imaging in Alzheimer disease and frontotemporal lobar degeneration. Neurology 68(15):1205–1212
84. Formaglio M, Costes N, Seguin J et al (2011) In vivo demonstration of amyloid burden in posterior cortical atrophy: a case series with PET and CSF findings. J Neurol 258(10):1841–1851
85. de Souza LC, Corlier F, Habert MO et al (2011) Similar amyloid-beta burden in posterior cortical atrophy and Alzheimer's disease. Brain 134(Pt 7):2036–2043
86. Rinne JO, Brooks DJ, Rossor MN et al (2010) 11C-PiB PET assessment of change in fibrillar amyloid-beta load in patients with Alzheimer's disease treated with bapineuzumab: a phase 2, double-blind, placebo-controlled, ascending-dose study. Lancet Neurol 9(4):363–372
87. Engler H, Forsberg A, Almkvist O et al (2006) Two-year follow-up of amyloid deposition in patients with Alzheimer's disease. Brain 129:2856–2866
88. Ossenkoppele R, Jansen WJ, Rabinovici GD et al (2015) Prevalence of amyloid PET positivity in dementia syndromes: a meta-analysis. JAMA 313(19):1939–1949
89. Villemagne VL, Okamura N (2014) In vivo tau imaging: obstacles and progress. Alzheimers Dement 10(3 Suppl):S254–S264
90. Okamura N, Furumoto S, Fodero-Tavoletti MT et al (2014) Non-invasive assessment of Alzheimer's disease neurofibrillary pathology using 18F-THK5105 PET. Brain 137(Pt 6):1762–1771
91. Villemagne VL, Okamura N (2015) Tau imaging in the study of ageing, Alzheimer's disease, and other neurodegenerative conditions. Curr Opin Neurobiol 36:43–51

92. Ishiki A, Okamura N, Furukawa K et al (2015) Longitudinal assessment of tau pathology in patients with Alzheimer's disease using [18F]THK-5117 positron emission tomography. PLoS One 10(10):e0140311
93. Harada R, Okamura N, Furumoto S et al (2016) 18F-THK5351: a novel PET radiotracer for imaging neurofibrillary pathology in Alzheimer's disease. J Nucl Med 57:208–214
94. Harada R, Okamura N, Furumoto S et al (2015) [(18)F]THK-5117 PET for assessing neurofibrillary pathology in Alzheimer's disease. Eur J Nucl Med Mol Imaging 42(7):1052–1061
95. Chien DT, Bahri S, Szardenings AK et al (2013) Early clinical PET imaging results with the novel PHF-tau radioligand [F-18]-T807. J Alzheimers Dis 34(2):457–468
96. Johnson KA, Schultz A, Betensky RA et al (2016) Tau PET imaging in aging and early Alzheimer's disease. Ann Neurol 79: 110–119
97. Marquie M, Normandin MD, Vanderburg CR et al (2015) Validating novel tau positron emission tomography tracer [F-18]-AV-1451 (T807) on postmortem brain tissue. Ann Neurol 78(5):787–800
98. Jack CR Jr, Knopman DS, Jagust WJ et al (2010) Hypothetical model of dynamic biomarkers of the Alzheimer's pathological cascade. Lancet Neurol 9(1):119–128
99. Majounie E, Cross W, Newsway V et al (2013) Variation in tau isoform expression in different brain regions and disease states. Neurobiol Aging 34(7):1922 e7–1922 e12
100. Houlden H, Baker M, Morris HR et al (2001) Corticobasal degeneration and progressive supranuclear palsy share a common tau haplotype. Neurology 56(12):1702–1706
101. Wang Y, Mandelkow E (2016) Tau in physiology and pathology. Nat Rev Neurosci 17:22–35
102. Lee VM, Goedert M, Trojanowski JQ (2001) Neurodegenerative tauopathies. Annu Rev Neurosci 24:1121–1159

Nuclear Imaging of Movement Disorders

Klaus Tatsch

Introduction

Movement disorders belong to the most common neurologic illnesses. In typical cases diagnoses are accurately established by clinical means. In early and monosymptomatic stages, however, clinical diagnoses remain uncertain and may benefit from molecular imaging techniques picking up specific metabolic patterns or changes in neurotransmitter systems. Most established for this purpose are the assessment of the metabolic pattern of fluorodeoxyglucose (FDG) and changes in dopaminergic neurotransmission. These techniques generally allow to separate Parkinson's disease (PD) from other neurodegenerative parkinsonian syndromes (PS), to characterize dementia with Lewy bodies (DLB), and to rule out diseases which may mimic neurodegenerative PS such as symptomatic parkinsonism and various tremor syndromes.

Classification of Movement Disorders

Among the movement disorders, the parkinsonian syndromes (PS) play a predominant role. PS are a syndromic umbrella term which comprises at least four etiologically different entities: Parkinson's disease (PD) (synonym: idiopathic parkinsonian syndrome; IPS), familial PS, atypical PS (PS syndromes caused by other neurodegenerative diseases; aPS), and symptomatic (secondary) parkinsonism including common differential diagnoses such as specific tremor syndromes. The group of aPS include multiple system atrophies (MSA-P, parkinsonian type; MSA-C, cerebellar type), progressive supranuclear palsy (PSP), corticobasal degeneration (CBD), spinocerebellar atrophy, and dementia with Lewy bodies (DLB). Vascular, drug-induced, toxic, and metabolic parkinsonism; parkinsonism associated with inflammation, trauma, and tumor; and the normal pressure hydrocephalus (NPH) belong to the category of secondary parkinsonism. Essential tremor and other tremor syndromes (e.g., orthostatic tremor, psychogenic tremor) are further differential diagnoses to neurodegenerative PS.

Well-defined clinical criteria (UK Parkinson's Disease Society Brain Bank clinical diagnostic criteria) are used to establish the diagnosis of PD and atypical PS, as those criteria also provide pointers indicative for other, non-PD types of parkinsonism [1, 2]. In early stages of disease, however, if symptoms are subtle it may be difficult to establish the correct diagnosis clinically. Several publications have addressed the issue of potential clinical misdiagnosis in clinical and postmortem studies [1, 3–5]. Many of the clinically unclear cases might benefit from molecular imaging with nuclear medicine techniques providing a correct diagnosis at an early time point.

Common Molecular Imaging Strategies

Molecular imaging techniques address not only quite specific changes in metabolism but also disturbances of neurotransmitter systems. Two procedures may be considered as accepted routine investigations: (1) assessment of the regional glucose metabolism with FDG-PET and (2) imaging changes of the dopaminergic neurotransmission. Apart from that many further targets have been specifically addressed such as various other neurotransmitter systems (e.g., 5-HT1B serotonin receptors, nicotinic acetylcholine receptors, cannabinoid receptors) or TSPO ligands as biomarker for neuroinflammation. Specific tau and α-synuclein ligands are at the horizon as well. This paper, however, is focused just on the two mentioned widespread routine procedures used in daily practice.

Glucose metabolism: The patterns of altered glucose metabolism investigated with FDG-PET in various neurodegenerative PS have been well established in the past years [6, 7].

K. Tatsch
Department of Nuclear Medicine, Municipal Hospital Karlsruhe Inc., Moltkestr. 90, Karlsruhe 76133, Germany
e-mail: klaus.tatsch@klinikum-karlsruhe.de

J. Hodler et al. (eds.), *Diseases of the Brain, Head and Neck, Spine 2016–2019: Diagnostic Imaging*, DOI 10.1007/978-3-319-30081-8_27

In conjunction with clinical symptoms, FDG-PET is specifically helpful for the differential diagnosis among the neurodegenerative PS, whereas its use is limited in non-neurodegenerative causes of parkinsonian symptoms.

Dopaminergic neurotransmission: Alterations of dopaminergic neurotransmission are involved in almost all neurodegenerative PS [8, 9]. Nigrostriatal (to a lesser extent also mesostriatal) dopaminergic nerve fibers end in caudate and putamen, where the presynaptic dopaminergic terminals communicate with the postsynaptic dopamine receptors. Nigrostriatal fibers originate in the pars compacta of the substantia nigra. PET and SPECT techniques allow by the use of specific ligands to evaluate the integrity and the number and density of presynaptic dopaminergic terminals and postsynaptic dopamine receptors. Three different key functions allow to assess presynaptic nigrostriatal terminals: PET with fluorodopa reflects the aromatic amino acid decarboxylase activity and dopamine storage capacity. The target region for ligands such as dihydrotetrabenazine is the vesicular monoamine transporter type 2. Last, cocaine analogs bind with high affinity and sufficient selectivity to the plasma membrane dopamine transporter (DAT) which is located at the presynaptic nerve terminals. The DAT is responsible for the reuptake of dopamine from the synaptic cleft; thus, DAT investigations allow to in vivo assess the integrity of presynaptic nerve terminals. At the postsynaptic level, the status of the dopamine D1-like receptors (D1, D5) and the D2-like receptor (D2, D3, and D4) may be imaged with suitable SPECT and PET ligands. See Table 1 for an overview of the more widely used tracers for this purpose.

Alternative Imaging Modalities, Hybrid Imaging (PET/CT, PET/MRI)

Conventional CT and MRI techniques contribute rather little to the early diagnosis of PS. Main reasons are that structural abnormalities – when present at all – are reliably depicted only in more advanced disease or may be difficult to assess in individual subjects. Advanced MRI techniques including magnetic resonance volumetry, proton magnetic resonance spectroscopy, diffusion tensor and diffusion-weighted imaging, relaxometry, neuromelanin imaging, and magnetization transfer may further assist in the differential diagnosis of neurodegenerative PS; however, those techniques require further validation and are not routine applications yet [10, 11]. Modern MRI techniques in combination with metabolic PET imaging by the use of hybrid PET/MRI devices might deliver in near future more fascinating novel insights in the differential diagnosis of movement disorders [12].

Nuclear Imaging Findings in Neurodegenerative Parkinsonism

Parkinson's Disease

PD accounts for about 70–80 % of movement disorders. Its predominant pathology is the loss of dopaminergic neurons which mainly project from the substantia nigra in the midbrain to the striatum (putamen and caudate nucleus) in the forebrain. Typically the projections to the posterior putamen

Table 1 Frequently used PET and SPECT radiopharmaceuticals for the evaluation of the dopaminergic system

Targets for assessment of presynaptic functions		
Dopamine synthesis, AADC activity	F-18 fluorodopa	PET
Vesicular monoamine transporter	C-11 DTBZ	PET
Dopamine transporter	C-11 CIT	PET
	F-18 FP-CIT	PET
	F-18 PE2I	PET
	I-123 β-CIT	SPECT
	I-123 FP-CIT	SPECT
	I-123 IPT	SPECT
	I-123 altropane	SPECT
	I-123 PE2I	SPECT
	Tc-99 m TRODAT	SPECT
Targets for assessment of postsynaptic functions		
D2-like receptors	C-11 raclopride	PET
	F-18 fallypride	PET
	F-18 DMFP	PET
	I-123 IBZM	SPECT
	I-123 IBF	SPECT
	I-123 epidepride	SPECT
D1-like receptors	C-11 SCH23390	PET
	C-11 NNC112	PET

are earlier and more affected than those to the caudate [13]. The loss of neurons results in a dopaminergic deficit which is believed to provoke most of the motor symptoms, which include hypokinesia, tremor, and rigidity. The diagnosis of PD is generally established clinically including positive response on dopaminergic medication as an important criterion. However, since PD shares some of the main features with several other disorders, there is evidence that clinically established diagnoses may be inaccurate, particularly in early stages.

Several molecular imaging studies have suggested changes in glucose metabolism (and perfusion) being helpful to establish the diagnosis of PD based on distinct pathologic patterns. In early PD, studies have shown increased regional metabolic rates of glucose in the lentiform nucleus and thalamus, and this finding has been attributed to increased firing in the basal ganglia neurons as a direct consequence of dopamine deficiency (Fig. 1b) [14]. In more advanced stages of PD, decreased caudate nucleus and cortical metabolic activity (parietal, temporal, frontal) has been reported in patients with and without associated dementia [15]. Nowadays processing software with anatomical standardization and pixel-wise evaluation techniques are widely used and have reported accurate results for the discrimination of PD patients from controls and those with atypical PS [6, 7, 16].

The biochemical hallmark of PD is the degeneration of the presynaptic dopaminergic nigrostriatal nerve fibers, whereas the postsynaptic side bearing the striatal receptors remains intact. Functional PET and SPECT imaging with all types of presynaptic dopaminergic terminal measures show reduced radioligand uptake in the striatum of PD patients with more pronounced decrease in the putamen than in the caudate and usually an asymmetry with more severe affection of the striatum contralateral to the side with the predominant clinical symptoms (Fig. 1b). Disease severity is correlated with the reduction of respective presynaptic terminal measures [17–19]. Based on pathologic findings in hemi-PD patients, in asymptomatic subjects in twins, familial PD, parkin, and other inherited PD kindreds, it was concluded that presynaptic imaging markers are not only a sensitive tool for the early diagnosis of PD but might be sensitive enough to even depict preclinical/premotor disease in neurodegenerative PS.

The postsynaptic dopaminergic system can be targeted with radioligands binding to the dopamine receptors (see Table 1). Uniformly, at least in earlier stages of the disease, elevated D_2-like receptor binding has been reported in the striatum contralateral to the more affected limb, greater in the putamen than in the caudate [17, 20]. This upregulation has been interpreted as an attempt to compensate for the dopaminergic deficiency due to presynaptic nerve cell loss (Fig. 1b). Preserved/upregulated postsynaptic receptor binding has been suggested as discriminator against most other neurodegenerative PS (aPS), in which the postsynaptic side is also affected and which therefore display reduced D_2-like receptor binding.

Multiple System Atrophy

MSA is a sporadic progressive neurodegenerative disorder that may account for up to 10 % of patients with movement disorders. In dependency of the predominant phenotype of the motor disorder, MSA is mainly classified into a parkinsonian type (MSA-P) and a cerebellar type (MSA-C). In MSA, glucose metabolism has been reported to be reduced in the lentiform nuclei, cerebellum, and some cortical structures [6, 7]. Particularly the reduced uptake pattern in the striatum/putamen (MSA-P) might help to distinguish MSA-P from PD patients (Fig. 1c). With respect to neurotransmission, MSA is characterized by a degeneration of the pre- and postsynaptic dopaminergic system, which results in pathologic PET and SPECT findings with the respective radioligands (Fig. 1c) [17, 20, 21]. The major difference to PD, therefore, is the presence of pathologic findings on the postsynaptic level. On the presynaptic level differential diagnosis between MSA and PD is hardly possible, even though a different pattern of signal loss with more uniform affection of caudate and putamen in MSA compared to PD has been reported.

Progressive Supranuclear Palsy

PSP is a rapidly progressing degenerative disease belonging to the family of tauopathies. Clinically it is characterized by parkinsonism with bradykinesia and rigidity, postural instability, and pseudobulbar syndrome with dysarthria and dysphagia. Supranuclear palsy of vertical gaze, which is the key feature of this disease, is rarely present at onset of disease and usually appears later. Histopathologic findings show cell loss, gliosis, and accumulation of tau proteins in different brain regions, such as the brainstem and basal ganglia (pallidus, substantia nigra, subthalamic nucleus) with the cortex being usually spared. The neuropathologic changes result in a midbrain atrophy, particularly of the tectum, and the enlargement of the aqueduct of Sylvius, quadrigeminal cistern, and posterior third ventricle. Decrements of glucose metabolism in the midline frontal regions and in the brainstem have been postulated as the main distinguishing features of PSP versus MSA and PD patients. Hypometabolism in superior frontal cortex, insula, and caudate nucleus, together with relative hypermetabolism in cortical motor areas, the parietal cortex, and the thalamus, has also been reported. According to this pattern PSP patients could be differentiated from MSA and PD patients with an accuracy between 85 and 92 % [6]. Since neurodegeneration in PSP affects both, the pre- and postsynaptic dopaminergic

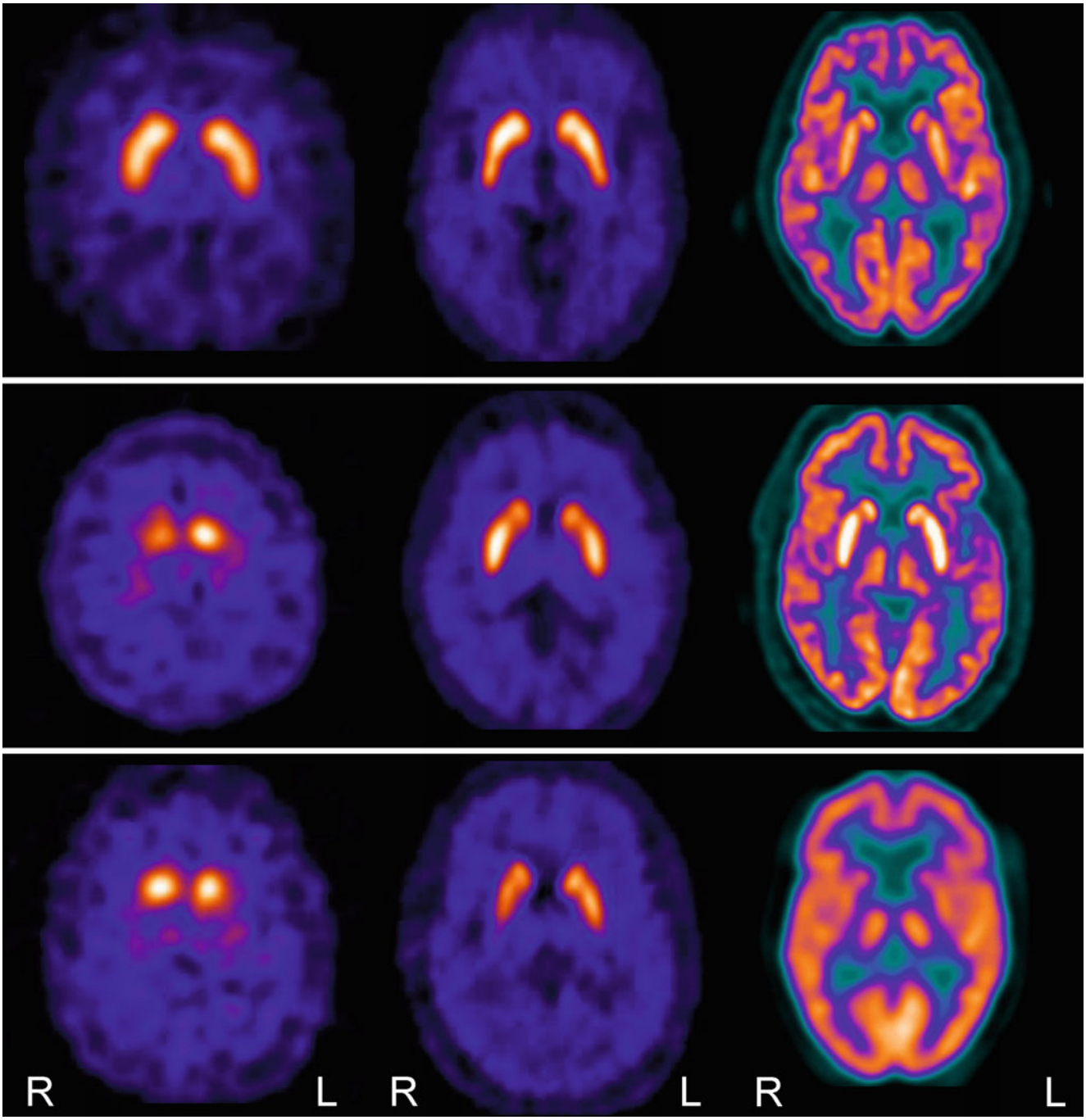

Fig. 1 Presynaptic dopaminergic imaging with [^{123}I]FP-CIT SPECT (*left column*), assessment of postsynaptic D2-like receptors with [^{18}F] DMFP PET (*middle column*), and FDG metabolism (*right column*) in a healthy control (**a**), a patient with Parkinson's disease (**b**), and a patient with MSA-P (**c**). The healthy subject reveals normal pre- and postsynaptic dopaminergic functions and normal cortical and striatal FDG metabolism. In the PD patient a marked presynaptic deficit is evident with more severe reduction of putaminal binding and an asymmetry with more affection of the right striatum corresponding to the clinically more affected left side of the body. Postsynaptic receptors are at least in early stages well preserved, and asymmetry is typically inverse to the presynaptic pattern showing higher binding in the putamen with the more exaggerated presynaptic deficit. This might be interpreted as an upregulation of postsynaptic receptors in an attempt to better compensate for the more severe presynaptic deficit. Note the relative (e.g., in comparison to the cortex and thalamus) preserved/increased FDG metabolism in the striatum. In contrary, patients with atypical PS such as MSA-P concordantly present with a pre- and postsynaptic deficit. This allows to distinguish this category from PD patients at the postsynaptic level. FDG presents with relative reduced striatal FDG metabolism (equal to or even lower as compared to the cortex and thalamus)

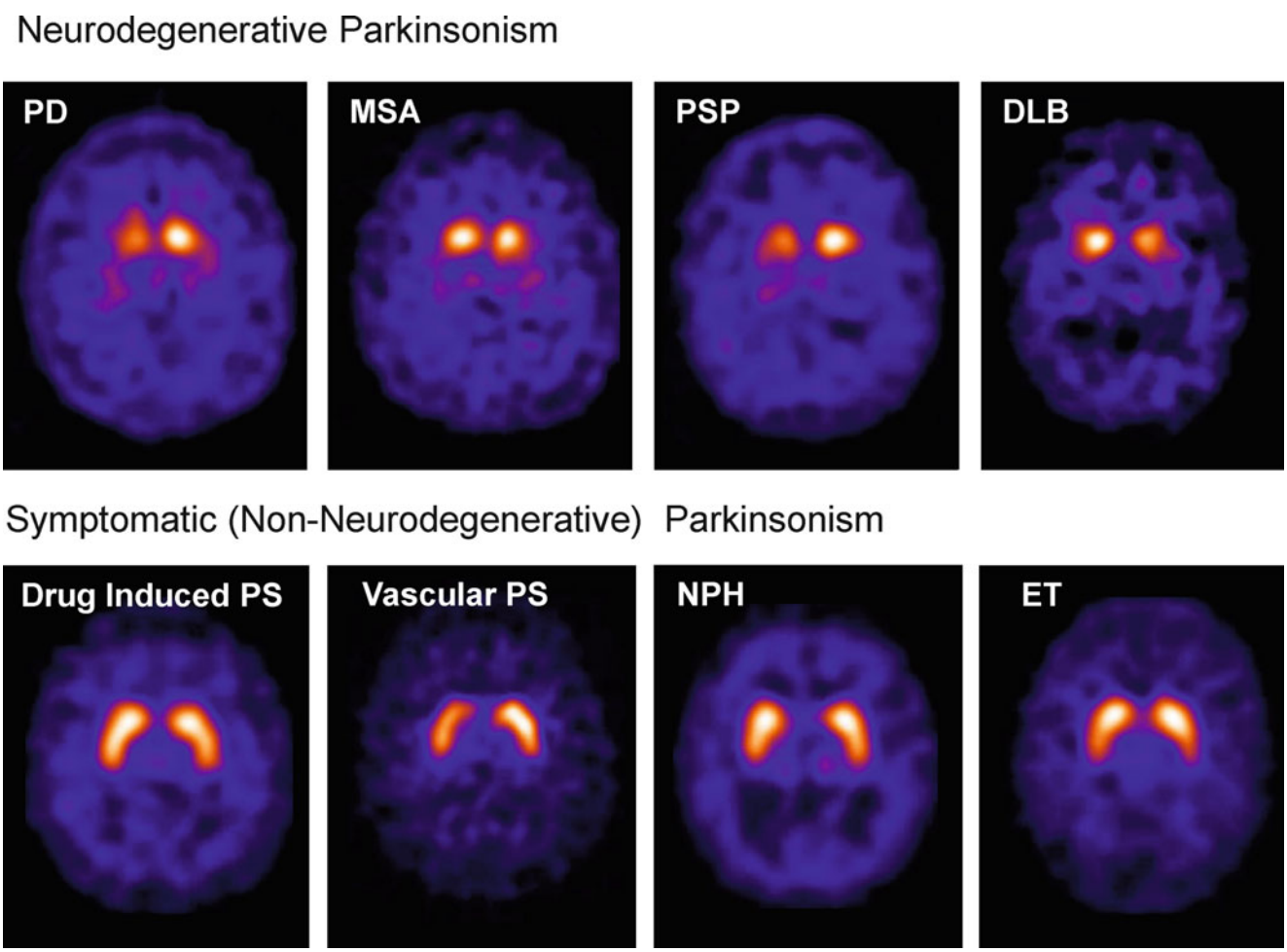

Fig. 2 The *upper panel* shows presynaptic dopaminergic imaging results with [^{123}I]FP-CIT SPECT in various diseases belonging to the category of neurodegenerative parkinsonism. Each of these diseases features a marked presynaptic dopaminergic deficit with affection of the putamen and to some extent also the caudate. Notable asymmetry may be present. The shown pattern indicates presynaptic dopaminergic pathology with high accuracy; however, it does not reliably allow to differentiate between the various diseases. The *lower panel* shows presynaptic dopaminergic imaging results with [^{123}I]FP-CIT SPECT in symptomatic parkinsonism and tremor syndromes, each of the diseases showing normal DAT binding. This allows to highly reliably separate these diseases from those characterized by neurodegeneration. Unfortunately, however, further distinction between the different asymptomatic PS and tremor syndromes based on their normal or only minor compromised [I-123]FP-CIT findings alone is not reliably possible. For this purpose further clinical information and in some instances also morphological imaging results (e.g., in NPH or vascular PS) are needed

system, the respective PET and SPECT findings are similar to those in MSA subjects, mostly showing a marked reduction on both levels (Fig. 2) [13, 17, 20]. Therefore, PSP patients can neither with pre- nor postsynaptic tracers be reliably distinguished from those with MSA. However, like in MSA, the presence of pathologic PET and SPECT findings on the postsynaptic level allows to discriminate between PSP and PD [21].

Corticobasal Degeneration

CBD is an asymmetric progressive neurodegenerative disease characterized by cortical and subcortical involvement with both motor and cognitive dysfunctions. CBD patients often initially present with apraxia and a parkinsonian picture of akinetic rigid type, which usually does not respond to dopaminergic therapy. Further frequently dystonia and alien limb phenomena are observed. Pathologic studies reveal an asymmetric frontoparietal neuronal loss and gliosis, nigral degeneration, and variable subcortical involvement. This results in markedly asymmetric cortical hypometabolism of glucose in PET studies affecting the primary sensorimotor (frontoparietal) cortex, insula, striatum, and thalamus [6]. Corticobasal ganglionic degeneration involves the striatal pre- and possibly also the postsynaptic dopaminergic system. In PET reduction in striatal fluorodopa, uptake has been described, and some SPECT studies have also revealed a marked decrease in dopamine transporter binding [22].

Generally a clear asymmetry with predominant affection of the striatum contralateral to clinical symptoms was observed. Caudate and putamen seem to be similarly affected. Reports on the postsynaptic receptor status in CBD are more controversial describing preserved as well as diminished striatal binding [23].

Dementia with Lewy Bodies

Among the neurodegenerative dementias, DLB plays an increasing role besides Alzheimer dementia (AD) [24]. DLB seems to be more frequent than previously supposed and may account for up to 30 % of dementia cases. Differential diagnosis of DLB versus other dementias based on clinical symptoms may be difficult. However, it is important for the therapeutic management.

The typical metabolic pattern indicative for DLB is an impairment of glucose metabolism of all parts of the visual cortex, while otherwise the pattern is similar to the AD pattern with glucose hypometabolism in lateral temporoparietal association areas. DLB, however, typically does not show a metabolic impairment in the posterior cingulate cortex, which is considered a sensitive marker for AD. Further on, there is a close pathological and clinical relationship between PD and DLB. Autoradiographic studies on DLB postmortem tissue have demonstrated a remarkable loss of presynaptic dopaminergic fibers in the striatum, and several PET and SPECT studies have shown corresponding findings in vivo (Fig. 2). Furthermore, this loss of presynaptic binding excellently separates DLB from AD subjects which present with mostly preserved, not significantly reduced, DAT binding. A recent meta-analysis of four studies reports on a pooled sensitivity of 86.5 % and a specificity of 93.6 % for the differentiation of DLB and non-DLB using [I-123]FP-CIT [25]. Striking is the high correlation between findings of [I-123] FP-CIT examinations in vivo and the corresponding results at autopsy. In such a comparative series of 20 patients, DAT imaging showed a sensitivity of 88 % (7/8) with a respective specificity of 100 % (12/12), while comparing the clinical diagnosis with autopsy results only revealed a sensitivity and specificity of 75 % and 45 %, respectively [24].

Nuclear Imaging in Symptomatic Parkinsonism and Tremor Syndromes

In the case of preserved presynaptic dopaminergic functions, it becomes highly unlikely that the respective patient may suffer from a neurodegenerative PS. Main differential diagnoses are then either symptomatic PS (e.g., drug-induced, psychogenic, and vascular PS) or various tremor diseases which might, for example, clinically mimic a monosymptomatic neurodegenerative PS. Unfortunately metabolic patterns of glucose are often not conclusive in symptomatic PS; thus, this type of imaging is only occasionally helpful.

Drug-Induced PS

During treatment with neuroleptic drugs, parkinsonian symptoms may develop which are mostly attributed to the occupation and blockade of postsynaptic dopamine D2-like receptors. Typical neuroleptics such as haloperidol may lead to an extensive receptor blockade even in relatively low-dose treatments, with the threshold for causing extrapyramidal side effects and herewith parkinsonian symptoms being rather low. In atypical neuroleptics, this threshold is markedly higher; however, also in this class of drugs, dopamine receptors are occupied to some degree, and therefore extrapyramidal symptoms may occur as well. Reports on presynaptic dopaminergic measures have shown that patients with drug-induced PS present with normal findings which allows to highly reliably distinguish these patients from those with neurodegenerative PS (Fig. 2) [26].

Psychogenic PS

As expected, patients suffering from psychogenic PS present with normal striatal DAT binding [27]. Reported findings were indistinguishable from those in healthy controls.

Vascular PS

In the classical type of vascular parkinsonism, the predominant finding is a gait disorder characterized by shuffling short steps. Therefore, it is also referred to as lower-body parkinsonism. Rigidity may be present, tremor is more rare. Hypomimia, swallowing problems, cognitive deficits, and incontinence are further clinical findings. As compared to PD, symptoms in vascular PS mainly show no or only a minor response to anti-parkinsonian drugs. Reports on DAT binding in vascular PS provide heterogeneous results which might indicate that vascular PS is a mixed and yet not well-characterized entity. Some authors report on normal or only slight but no significant reduction of presynaptic dopaminergic measures in patients suspicious for vascular PS; others found significantly reduced binding values. This discrepancy may be attributed to differences in patient populations and relatively small subject numbers. Obviously DAT binding is reduced in striatal subregions directly affected by infarction as demonstrated by corresponding structural defects in CT and MRI examinations ("punched-out" striatum; subgroup of patients with acute begin of symptoms and

a close timely relation to the event) (Fig. 2). Furthermore, another course of vascular PS has been suggested, which is characterized by a slow insidious onset of symptoms in known small vessel disease of the brain and which is associated with pathologic DAT binding. Features like the lack of a pathologic binding gradient from caudate to posterior putamen and also less marked striatal asymmetry permit a good discrimination between vascular PS and PD [28, 29].

Normal Pressure Hydrocephalus

NPH is clinically characterized by the symptom triad of gait disturbance, urinary incontinence, and dementia/cognitive decline. The gait disturbance is most often the first symptom. Even though clinically distinct from the typical parkinsonian shuffling gait, NPH may be misdiagnosed as PD. CT and MRI scans typically show enlarged ventricles and signs of atrophy. As neurodegeneration of presynaptic nigrostriatal nerves is absent in NPH, these patients can be easily differentiated from those with neurodegenerative PS (Fig. 2).

Dopa-Responsive Dystonia

DRD is, like juvenile parkinsonism, a hereditary disease with onset in younger ages. Clinically DRD presents with a dystonic gait disorder, which in some stages may resemble PD with slowness of movements, instability, and occasionally tremor. The disease well responds to dopaminergic medication and in contrast to juvenile parkinsonism presents with normal presynaptic terminal functions [30].

Essential Tremor and Other Tremor Syndromes

Essential tremor (ET) is considered being the most frequent form of a pathologic tremor. Clinically the predominant feature of ET is a bilateral, mostly symmetric kinetic tremor. Frequently affected are the hands and the arms; however, ET may also occur in the head and neck, jaw, voice, or other body regions like the legs. Differential diagnosis of ET versus monosymptomatic (tremor dominant) neurodegenerative PS may be difficult, which emphasizes the role of presynaptic dopaminergic imaging for this purpose. Sensitivity and specificity of discriminating PS from ET have been reported to be 97 % and 100 %, respectively. Findings in patients with ET were not different from those in controls and thus were easily distinguishable from those in neurodegenerative PS (Fig. 2) [31].

Orthostatic tremor (OT) is a rare syndrome which is characterized by unsteadiness in standing caused by a high-frequency tremor of the legs. Most cases of OT are considered being idiopathic; relations of OT with PD and degeneration of the dopaminergic system are discussed. SPECT studies with DAT ligands always reported either normal findings in OT patients [32] or only slightly reduced striatal DAT-binding values, which, however, still allowed highly reliable to differentiate OT from PD. The isolated action tremor (IAT) is a characteristic symptom of ET, however, may also be observed in individuals with PD. Published data in this entity suggest that DAT findings are helpful to correctly assign patients with IAT either in the ET (normal DAT binding) or the PD category (reduced DAT binding) [33].

References

1. Hughes AJ, Daniel SE, Kilford L, Lees AJ (1992) Accuracy of clinical diagnosis of idiopathic Parkinson's disease: a clinico-pathological study of 100 cases. J Neurol Neurosurg Psychiatry 55:181–184
2. Hughes AJ, Daniel SE, Lees AJ (1993) The clinical features of Parkinson's disease in 100 histologically proven cases. Adv Neurol 60:595–599
3. Catafau AM, Tolosa E (2004) Impact of dopamine transporter SPECT using 123I-Ioflupane on diagnosis and management of patients with clinically uncertain Parkinsonian syndromes. Mov Disord 19:1175–1182
4. Hughes AJ, Daniel SE, Ben-Shlomo Y, Lees AJ (2002) The accuracy of diagnosis of parkinsonian syndromes in a specialist movement disorder service. Brain 125:861–870
5. Meara J, Bhowmick BK, Hobson P (1999) Accuracy of diagnosis in patients with presumed Parkinson's disease. Age Ageing 28:99–102
6. Eckert T, Barnes A, Dhawan V et al (2005) FDG PET in the differential diagnosis of parkinsonian disorders. Neuroimage 26: 912–921
7. Zhao P, Zhang B, Gao S (2011) 18F-FDG PET study on the idiopathic Parkinson's disease from several parkinsonian-plus syndromes. Parkinsonism Relat Disord 18(Suppl 1):S60–S62
8. Varrone A, Halldin C (2012) New developments of dopaminergic imaging in Parkinson's disease. Q J Nucl Med Mol Imaging 56:68–82
9. Seibyl J, Russell D, Jennings D, Marek K (2012) The molecular basis of dopaminergic brain imaging in Parkinson's disease. Q J Nucl Med Mol Imaging 56:4–16
10. Cochrane CJ, Ebmeier KP (2013) Diffusion tensor imaging in parkinsonian syndromes: a systematic review and meta-analysis. Neurology 80:857–864
11. Meijer FJ, Bloem BR, Mahlknecht P, Seppi K, Goraj B (2013) Update on diffusion MRI in Parkinson's disease and atypical parkinsonism. J Neurol Sci 332:21–29
12. Barthel H, Schroeter ML, Hoffmann K-T, Sabri O (2015) PET/MR in dementia and other neurodegenerative diseases. Semin Nucl Med 45:224–233
13. Booij J, Tissingh G, Winogrodzka A, van Royen EA (1999) Imaging of the dopaminergic neurotransmission system using single-photon emission tomography and positron emission tomography in patients with parkinsonism. Eur J Nucl Med 26:171–182
14. Dagher A (2001) Functional imaging in Parkinson's disease. Semin Neurol 21:23–32
15. Huang C, Ravdin LD, Nirenberg MJ et al (2013) Neuroimaging markers of motor and nonmotor features of Parkinson's disease: an 18f fluorodeoxyglucose positron emission computed tomography study. Dement Geriatr Cogn Disord 35:183–196

16. Borghammer P, Hansen SB, Eggers C et al (2012) Glucose metabolism in small subcortical structures in Parkinson's disease. Acta Neurol Scand 125:303–310
17. Tatsch K (2010) Extrapyramidal syndromes: PET and SPECT. Neuroimaging Clin N Am 20:57–68
18. Bruck A, Aalto S, Rauhala E, Bergman J, Marttila R, Rinne JO (2009) A follow-up study on 6-[18F]fluoro-L-dopa uptake in early Parkinson's disease shows nonlinear progression in the putamen. Mov Disord 24:1009–1015
19. Hsiao IT, Weng YH, Hsieh CJ et al (2014) Correlation of Parkinson disease severity and 18F-DTBZ positron emission tomography. JAMA Neurol 71:758–766
20. Tatsch K (2016) Movement disorders. In: von Schulthess GK (ed) Molecular anatomic imaging PET/CT, PET/MR and SPECT/CT. Wolters Kluwer, Philadelphia, pp 210–217
21. la Fougere C, Popperl G, Levin J et al (2011) The value of the dopamine D2/3 receptor ligand 18F-desmethoxyfallypride for the differentiation of idiopathic and nonidiopathic parkinsonian syndromes. J Nucl Med 51:581–587
22. Pirker W, Asenbaum S, Bencsits G et al (2000) [123I]beta-CIT SPECT in multiple system atrophy, progressive supranuclear palsy, and corticobasal degeneration. Mov Disord 15:1158–1167
23. Klaffke S, Kuhn AA, Plotkin M et al (2006) Dopamine transporters, D2 receptors, and glucose metabolism in corticobasal degeneration. Mov Disord 21:1724–1727
24. Walker Z, Possin KL, Boeve BF, Aarsland D (2015) Lewy body dementias. Lancet 386:1683–1697
25. Papathanasiou ND, Boutsiadis A, Dickson J, Bomanji JB (2012) Diagnostic accuracy of I-123 FP-CIT (DaTSCAN) in dementia with Lewy bodies: a meta-analysis of published studies. Parkinsonism Relat Disord 18:225–229
26. Diaz-Corrales FJ, Sanz-Viedma S, Garcia-Solis D, Escobar-Delgado T, Mir P (2010) Clinical features and 123I-FP-CIT SPECT imaging in drug-induced parkinsonism and Parkinson's disease. Eur J Nucl Med Mol Imaging 37:556–564
27. Gaig C, Marti MJ, Tolosa E et al (2006) 123I-Ioflupane SPECT in the diagnosis of suspected psychogenic Parkinsonism. Mov Disord 21:1994–1998
28. Zijlmans J, Evans A, Fontes F et al (2007) [123I] FP-CIT spect study in vascular parkinsonism and Parkinson's disease. Mov Disord 22:1278–1285
29. Contrafatto D, Mostile G, Nicoletti A et al (2012) [(123) I]FP-CIT-SPECT asymmetry index to differentiate Parkinson's disease from vascular parkinsonism. Acta Neurol Scand 126:12–16
30. Jeon BS, Jeong JM, Park SS et al (1998) Dopamine transporter density measured by [123I]beta-CIT single-photon emission computed tomography is normal in dopa-responsive dystonia. Ann Neurol 43:792–800
31. Benamer TS, Patterson J, Grosset DG et al (2000) [123I]-FP-CIT SPECT imaging: the [123I]-FP-CIT study group. Mov Disord 15:503–510
32. Trocello JM, Zanotti-Fregonara P, Roze E et al (2008) Dopaminergic deficit is not the rule in orthostatic tremor. Mov Disord 23: 1733–1738
33. Coria F, Gimenez-Garcia M, Samaranch L, Mora FJ, Sampol-Bas C, Pastor P (2012) Nigrostriatal dopaminergic function in subjects with isolated action tremor. Parkinsonism Relat Disord 18:49–53

Imaging of Brain Perfusion

John O. Prior

Introduction

Brain perfusion by SPECT or PET is a well-established and reliable method to measure regional cerebral blood flow (rCBF). The normal adult brain perfusion is symmetrical with higher tracer distribution in the temporal, parietal and occipital (visual) cortices, basal ganglia, thalami and cingulate gyrus than in the white matter and interhemispheric fissure [1]. Depending whether the eyes are open or closed, an increase of ca. 30 % more in the occipital visual cortex can be observed [1]. Motor and sensory stimuli can have asymmetrical effects. In the newborn, perfusion is slightly lowered in the frontal and temporoparietal regions and reaches an "adult" pattern within the first 2 years of life [1]. As the same SPECT pattern may be encountered in several pathologies (Table 1), detailed knowledge of the patient's symptoms and the functional area of the brain likely to be involved is important.

Indications

The human brain has about 130 billion neurons and weights only 2 % of a human body mass, albeit it consumes 20 % of the total body's oxygen supply [2]. The most common indications for rCBF by SPECT and PET are summarized in Table 2, and the following sections will detail these different clinical indications. SPECT is more available and less expensive as PET, but it has a larger radiation burden (Table 2) [3].

Dementia

Both SPECT cerebral perfusion imaging and PET glucose metabolism imaging have been widely used over the last decades to help in the diagnosis of Alzheimer (AD) and Lewy body (DLB) dementias. The main difference with PET using ^{18}F-fluorodeoxyglucose is a better spatial resolution as compared to SPECT. As cerebral glucose metabolism is coupled to neuronal function as the main substrate for energy production, any regional impairment in neuronal function is translated into a reduction of regional glucose metabolism and thus to rCBF [4]. A direct comparison study between ^{99m}Tc-HMPAO SPECT and ^{18}F-FDG PET was performed in 98 patients ($n=38$ AD, $n=30$ DLB, $n=30$ controls) [5]. Visual cues were decreased uptake in the precuneus and lateral parietal lobes in AD and DLB, a relative preservation of the posterior cingulate cortex in DLB, with more occipital loss in DLB, with reduced temporal and frontal uptake more likely in AD. The results showed the superiority of PET over SPECT for the diagnosis of dementia vs. no dementia (area under the curve AUC = 0.93 vs. 0.72, $P=0.001$) as well as for the diagnosis of AD vs. DLB (AUC = 0.80 vs. 0.58, $P=0.005$). Similarly, sensitivity and specificity were significantly better for PET than SPECT (85 and 90 % vs. 71 and 70 %, respectively). Thus, the authors recommended using ^{18}F-FDG PET rather than cerebral perfusion

Table 1 Perfusion pattern and brain disease

Cerebral perfusion pattern	Possible disease
Temporoparietal hypoperfusion	Alzheimer disease dementia
	Parkinson-related dementia
	Lewy body disease
	Normopressure hydrocephalus
Frontal/frontotemporal hypoperfusion	Pick's disease
	Frontotemporal degeneration
	Pseudodepressive dementia
	Progressive supranuclear palsy
	Chronic alcoholism
	Chronic schizophrenia
Multiple distributed defects	AIDS-related dementia
	Creutzfeldt–Jakob disease
	Vascular dementia

Adapted from Catafau [9] originally published in JNM. © Society of Nuclear Medicine and Molecular Imaging, Inc.

J.O. Prior
Department of Nuclear Medicine and Molecular Imaging, Lausanne University Hospital, Lausanne, Switzerland
e-mail: john.prior@chuv.ch

J. Hodler et al. (eds.), *Diseases of the Brain, Head and Neck, Spine 2016–2019: Diagnostic Imaging*, DOI 10.1007/978-3-319-30081-8_28

Table 2 Indication to cerebral perfusion imaging with SPECT or PET

Cerebral perfusion imaging	Clinics	Research
Epilepsy	SPECT, PET	SPECT, PET
Traumatic brain injury	(SPECT)	SPECT, PET
Cerebrovascular disease, Moyamoya disease	SPECT, PET	SPECT, PET
Brain infection, brain inflammation	(SPECT)	SPECT, PET
Dementia	(SPECT)	SPECT, PET
Psychiatric disorder	(SPECT)	SPECT, PET

Rare indications are in parenthesis
Note: Radiation dose SPECT 4.3–8.5 mSv (ECD) or 5.1–10.2 mSv (HMPAO); PET 0.5–2 mSv

SPECT for the differential diagnosis of dementia, if functional imaging is indicated. They recommend adapting national and international guidelines based on these results.

Also, the role of structural and functional imaging techniques for the common dementias (AD, DLB, vascular dementia and frontotemporal lobar degeneration) is changing over time [6]. Anatomical imaging of hippocampal volume loss is not specific to mild cognitive impairment and AD and also present in depression, post-traumatic stress disorder and alcoholism, explaining why functional imaging has better sensitivity and specificity [7].

Traumatic Brain Injury (TBI)

Lesions detected within 72 h of a TBI using SPECT were 40 % more numerous than detected by CT scan and even in regions not detected by MRI; these abnormalities observed up to 1–6 months after the injury [8]. SPECT is a powerful tool for TBI research in the field of cerebrovascular disease and cognitive disorder and can be useful in evaluating patients with neurological and psychiatric sequelae after TBI [8]. SPECT imaging has the potential for estimating rCBF in the acute phase of TBI, but routine clinical implementation is lacking, however. With the newest quantitative SPECT/CT, it has the potential to quantify CBF in absolute value.

TBI imaging with PEt allows detecting regional brain ischaemia [8], and increased ischaemic volume has been shown to correlate with poor outcome. PET logistics for CBF imaging is complex and costly; it is therefore only available in few TBI centres worldwide. However, SPECT and PET suffer from the absence of bedside imaging directly in the neurointensive care unit, and small, xenon CT scanners emerge as an economical imaging technique that can be used directly at the bedside. Also, novel, bedside SPECT and PET scanners are in development and could also be a major game changer in the future.

Trauma impairs neuronal activity and interrupts connections with other brain or cerebellar regions, which become hypoperfused on SPECT at a distance from the injury site. This deafferentiation or diaschisis provides insight into the pathophysiology of the symptoms [9]. However, the most commonly seen corticocerebellar diaschisis has usually no relevance in clinical practice [9].

A special form is the dementia provoked by chronic traumatic head injury (*dementia pugilistica*) [7]. Functional imaging of retired American football players has found diffuse cortical hypoperfusion with extensive involvement of frontal and anterior temporal lobes [7]. It would be expected that amyloid imaging would be negative, as it is uninvolved in chronic traumatic encephalopathy.

Cerebrovascular Disease

Vascular Dementia (VaD) It originates from a multivessel disease (multiple microvascular infarcts) or ischaemic brain injury (sudden onset after initial stroke) [7]. Thus, functional brain imaging of VaD presents diverse patterns ranging from a single large stroke to multiple, small focal defects [7]. To complicate the situation, AD and VaD frequently coexist. There is also more frequently diffuse focal defects seen anteriorly, but this is no way an absolute criterion [7].

Although MRI is the method of choice for investigating VaD, it does not provide useful functional information [10]. SPECT brain perfusion with acetazolamide challenge provides a possible measurement of cerebral hemodynamic reserve for investigating VaD [10]. This underused application could benefit from standardization and long-term follow-up studies [10]. Indeed, SPECT brain perfusion baseline and/or with pharmacological acetazolamide test might have a role in screening, diagnosis and monitoring of patients with VaD [10]. As baseline cerebral SPECT measures rCBF, which reflects the neuronal activity, it would allow earlier detection of functional abnormalities, which precedes clinical symptoms of dementia; SPECT would thus be independent of cognitive reserve allowing highly functional individuals to still perform well on psychometric testing. The acetazolamide test was developed to assess cerebrovascular reserve in relation to chronic cerebrovascular diseases. It tests the ability for the brain vasculature to regulate and maintain adequate rCBF by decreasing

vascular resistance in the presence of chronic vascular disease. Acetazolamide enters the blood–brain barrier and induces increase in rCBF due to carbonic anhydrase blockade leading to acidosis, a very potent stimulus of rCBF. Using same-day, dual studies of baseline rCBF and acetazolamide-induced increase in rCBF, quantitative analysis allows identifying small abnormalities in vasodilation. This cerebrovascular reserve might represent the stroke risk predicting future cognitive complications [10]. Thus, vascular cognitive impairment (VCI) contains large-vessel post-stroke dementia, small-vessel subcortical dementia and brain chronic hypoperfusion [11]. In clinical practice, SPECT might be indicated in subcortical ischaemic vascular dementia for the diagnosis of vascular-associated component (differential diagnosis of frontotemporal dementia [hypoperfusion of frontal and anterior parts of the temporal cortices] vs. subcortical frontal syndromes [slight hypoperfusion of the medial prefrontal and anterior cingulate cortices]) allowing to better manage frontal subcortical syndromes with anticholinesterases [10]. Several studies indicate that vascular pathology affects cerebrovascular reactivity and cerebral metabolism finally leading to cognitive dysfunction, while no link is apparent between microangiopathy on MRI (white matter hyperintensities) and cognitive impairment [10]. SPECT-measured diminution in cerebrovascular reserve identifies the cerebral area of increased risk of stroke as demonstrated in patients with carotid occlusive disease or other diseases such as arterial hypertension, orthostatic hypotension, cardiac failure and dysautonomia [10]. Prevention of vascular episode/stroke by preventive medical therapy of cardiovascular risk factors seems to be the most effective, as well as efficient surgical approaches (carotid stenosis) and anticoagulation (in atrial fibrillation). Waiting for larger studies demonstrating a clear link between cerebral hypoperfusion and cognitive decline, from which a screening strategy would emerge, Farid et al. [10] recommend SPECT brain perfusion imaging in patients with: (i) severe or uncontrolled hypertension and (ii) multiple cardiovascular risk factors and already demonstrated cardiovascular impaction of target organs such as retinopathy or kidney failure. A stricter control of risk factor could then present or slow the evolution from predementia to manifest dementia in these populations.

Arterial Occlusion Patients with aneurysm of the internal carotid may not be suited for surgery and would undergo a balloon occlusion of the artery, in which effect on cerebral blood flow can be demonstrated by brain perfusion SPECT with an injection performed at the 15th min of a 20-min balloon occlusion test [1]. Focal or diffuse hypoperfusion can be seen, and the location and severity of the defects are important in deciding if carotid occlusion can be permanent or a different approach has to be used [1]. An illustrative example is given in Fig. 1.

Identification of Ischaemic Penumbra Cerebral perfusion by PET is the only imaging tool that can identify the presence of ischaemic penumbra (threshold for infarction and irreversible damage) by measuring rCBF, regional metabolic rate for oxygen and the regional oxygen extraction fraction, from which critically perfused but potentially salvageable tissue can be identified [2]. However, the complex logistics and the need for cyclotron-produced O^{15} have kept this modality to a research tool never applicable to clinical routine.

Normal global rCBF is about 45–55 mL/100 g/min (grey matter 80 and white matter 20 mL/100 g/min), and flow is altered by cerebral pulse pressure (50–150 mmHg). The functional threshold for developing paralysis and abolishing the electrocorticogram evoked potential varies from 6 to 22 mL/100 g/min [2]. In PET studies, which are considered as the golden standard for penumbra [12], three regions can be defined after an ischaemic insult: (i) the core of ischaemia transiting to necrosis for rCBF <12 mL/100 g/min; (ii) the penumbra region with flows between 12 and 22 mL/100 g/min, which is still a viable tissue with uncertain chances for infarction or recovery; and (iii) hypoperfused area >22 mL/100 g/min not primarily damaged by lack of blood supply [2]. SPECT equivalent to define penumbra has been defined as 20 % of the activity of the contralateral normal region (corresponding to 20 mL/100 g/min).

As recombinant tissue plasminogen activator (tPA) must be given intravenously within the first 3 h of stroke onset, there is insufficient time to perform SPECT or PET before tPA therapy [12]. However, a patient with stroke more than several hours or in unknown time of onset ("awakening stroke") and those with progressive stroke may be still beneficial in patients not suited for CT or MR imaging [12].

Moyamoya Disease This chronic stenooclusive vasculopathy (also called idiopathic intracranial angiopathy) affects the terminal internal carotid arteries and has been first described in 1969 [13]. Its origin remains unknown, and clinical manifestations are ischaemic stokes and transient ischaemic attack, with a propensity for the fragile collateral network to bleed resulting in haemorrhagic strokes [13]. The measure of the cerebrovascular reserve CVR using a vasodilator (hypercapnia or acetazolamide) is informative in moyamoya disease. Decrease rCBF or increased regional oxygen extraction fraction (rOEF) by PET or decrease of CVR by SPECT may indicate impending ischaemia [13]. These can aid in choosing treatment options, monitoring the disease and evaluating the effect of revascularization surgery [13, 14].

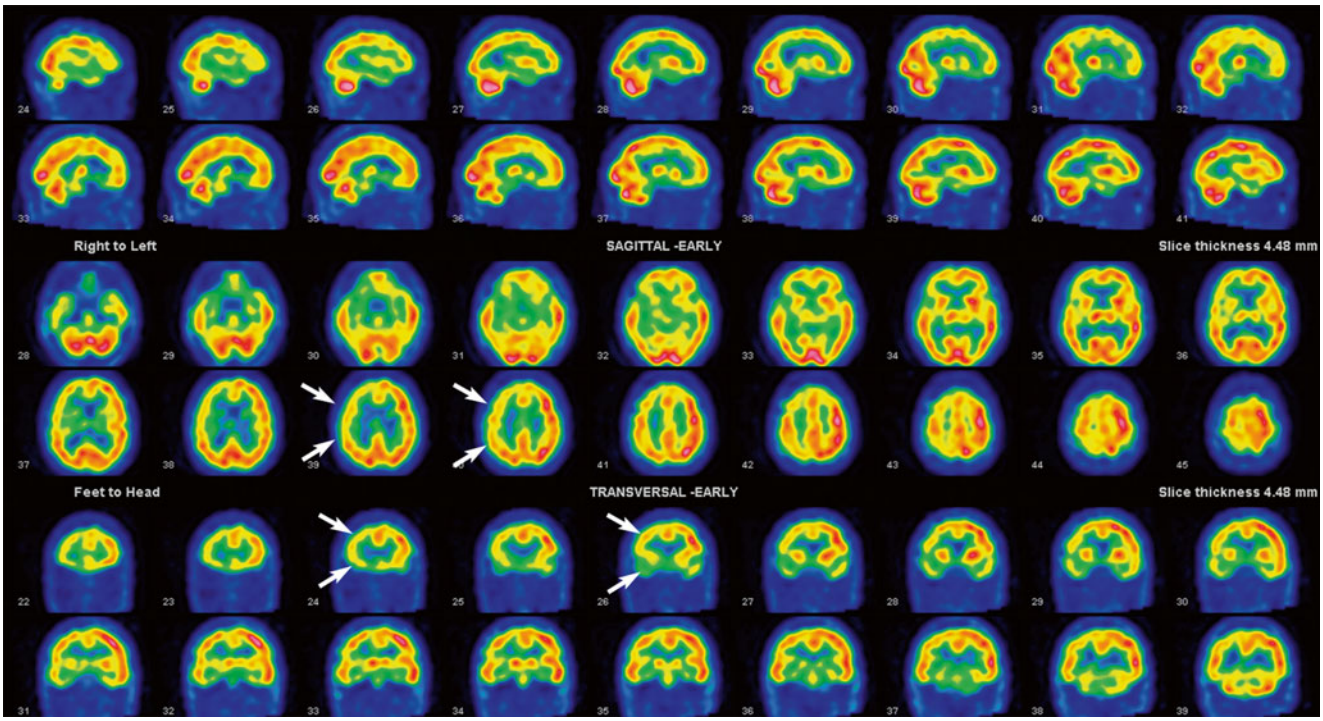

Fig. 1 Case of a 64-year-old woman with a partial thrombosis of the right internal carotid at the origin of the posterior communicant artery. The patient underwent a 37-min balloon-induced right carotid occlusion. The ^{99m}Tc-ECD was injected 5 min before the end of the occlusion, and SPECT imaging study was performed. The sagittal, transversal and coronal slices show an asymmetry in disfavour of the right side (*arrow*) including decreased striatum uptake

Epilepsy

Brain SPECT can localize the origin of the seizures for surgical therapy, especially in temporal epilepsy, which can be cured surgically in more than 70 % of the patients (as compared to extratemporal epilepsy where only 40–50 % have surgically addressable seizures) [1]. SPECT studies are performed ictally (sensibility 97 %, specificity 100 % in temporal lobe epilepsy, with a radiopharmaceutical injection typically within 5–10 s of the seizure onset) under EEG monitoring and interictally, i.e. >24-h seizure-free (sensibility 97 %, specificity 100 %) [1].

The accuracy of ictal SPECT can be enhanced by comparing it to interictal state using co-registration, automated subtraction techniques as "subtraction ictal SPECT co-registered to MRI" (or SISCOM) routinely available (Fig. 2) [15], as well as statistical parametric mapping (SPM) [16]. The SISCOM analysis can be falsely negative due to subclinical seizure activity at the time of injection in the so-called interictal scan [15]. This can be avoided if EEG is always performed during the injection. Concerning the injection, one has to consider that the radiotracer take 15–20 s to reach the brain, so that "ictal" SPECT is actually already showing the start of seizure propagation, which can affect also a different lobe (contra- or ipsilateral), with different patterns that have been described in the literature [15]. What is important is to know that injection delay of less than 20 s after seizure debut is significantly correlated with correct localization and that the largest and most intense cluster is likely to represent the seizure onset [15]. If injection occurs in the immediate post-ictal phase, a post-ictal switch can be observed about 60 s after seizure termination, where the area becomes hypoperfused with poor localizing accuracy due to similar changes in multiple brain regions [15]. Techniques for imaging specific receptor systems with SPECT or PET are in development and likely have increasing importance in better understanding the mechanism of seizure and epilepsy [15]. Usually, brain SPECT imaging of epilepsy requires a specialized team and clinical setting, not only with a dedicated nuclear medicine physician experienced in ictal SPECT and interictal ^{18}F-FDG PET, but also a neurologist specialized in epilepsy, a neurosurgeon, an electrophysiologist, a neuroradiologist, a psychologist and psychiatrist and nurses trained in administering radiopharmaceuticals [16].

PET is being used in epilepsy, but with a different tracer—^{18}F-fluorodeoxyglucose—which is not a perfusion tracer. Traditionally, interictal PET shows hypometabolism in the seizure focus [17]. Interestingly, ictal PET is possible in focal status epilepticus and has proven to be useful [18].

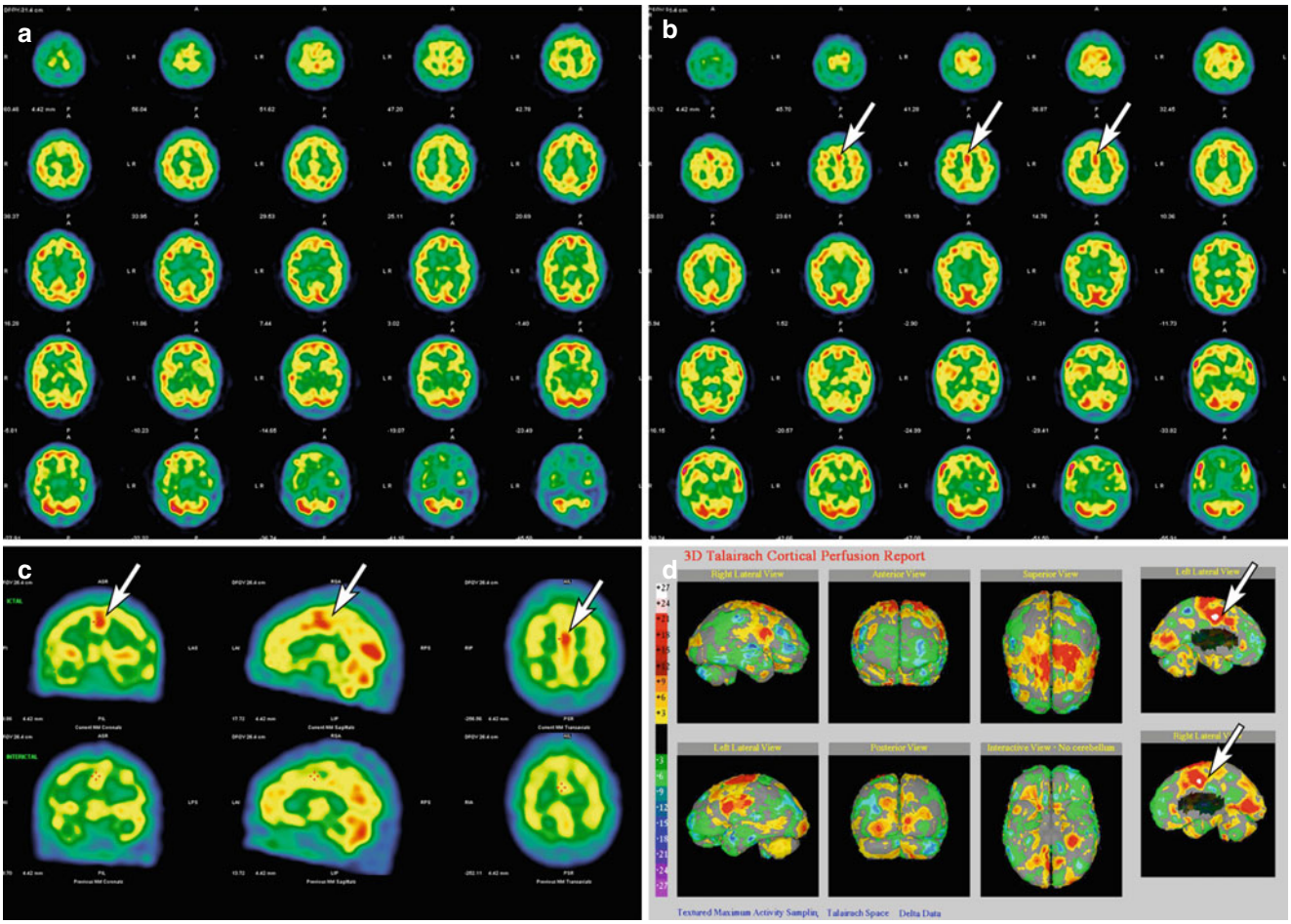

Fig. 2 Case of a 31-year-old man with pharmacoresistant epilepsy with 5–10 seizures per night and up to 4 diurnal seizures. The patient was hospitalized for an interictal (**a**) and ictal (**b**) SPECT rCBF imaging study using ^{99m}Tc-HMPAO. The comparison of both studies revealed a small focal precentral lesion (*arrow*) in the midline (**c**) which lateralization was difficult to precise. The SISCOM analysis (**d**) is also clearly pinpointing the midline cortical precentral localization of the seizure origin. Surgery was performed after electrocorticography and showed type-Ia frontal cortical dysplasia. Since then, the frequency of the seizure greatly regressed (focal seizure 1 every 4 days)

Brain Infection

In HIV encephalopathy, rCBF shows decreases cortical uptake due to microvascular changes in a "moth-eaten" appearance with multifocal defects in the basal ganglia with a decreased white matter rCBF [19]. The pathophysiology might be due to cytokines and macrophages and is correlated to the number of cotton-wool spots [19]. Thus, SPECT may be useful in the presence of psychosis or mild attentional impairment or depression in the presence of normal CT or MRI [19]. This pattern is not specific to HIV encephalopathy and can be observed in chronic cocaine users, chronic fatigue syndrome patients or mild trauma [19].

In brain herpes simplex encephalitis, SPECT rCBF changes with increased temporal lobe activity may be present in the early stage where MR, CT and cerebrospinal fluid might still be negative [19].

Brain Tumors

Cerebral blood flow by $H_2{}^{15}O$-PET has been found to be decreased in adult glioma, with most malignant glioma having the deepest rCBF reduction [16]. There is no correlation between $H_2{}^{15}O$-PET with the glioma grade of brain tumour [16].

Major Psychiatric Disorder

SPECT and PET have been used as a research tool in many studies [1, 20]. However, they are not routinely used in psychiatry and have the potential for individualizing treatment, monitoring response and modifying treatment when warranted. The rest of this section will present evidences for such a use in psychiatry, for a number of major diseases:

- *Attention deficit hyperactivity disorder* (*ADHD*) – Several studies investigated rCBF changes in ADHD, to show decrease in brain perfusion in premotor cortex and prefrontal cortex and hypoperfusion of striatal and periventricular structures [20]. Response to methylphenidate therapy has been investigated and shows prefrontal rCBF normalization, while in one study nonresponders may have increased activity in the anterior cingulate at the baseline [21].
- *Obsessive-compulsive disorders* (*OCD*) – The anterior cingulate cortex is thought to be important in the pathogenesis of OCD [20], and SPECT may identify patients benefiting from anterior cingulotomy for symptom relief in one study [21].
- *Gilles de la Tourette's syndrome* – In this rare, severe tic syndrome, closely related to obsessive-compulsive disorder, hypoperfusion of the frontal lobes, cingulate gyrus and basal ganglia/thalami may be found [1].
- *Schizophrenia* – In schizophrenia (1 % of the population), SPECT-derived rCBF generally shows frontal hypoactivity (especially during a specific task), and perfusion changes in the basal ganglia (eventually due to neuroleptic drugs) and temporal lobes hypoactivity (usually left-sided) frequently associated with ipsilateral frontal hypoperfusion have been observed [20]. Patients that are medication-free may usually present with frontal hyperperfusion and depending on the presence of positive symptoms (auditory, tactile, visual or olfactory hallucination, etc.) present increased precuneus activity or frontal and temporal hypoperfusions if negative symptoms are present (poor eye contact, speech or hygiene, apathy, etc.) [20]. If radiopharmaceutical injection occurs at the time of visual or auditory hallucination, hyperactivity in the associated visual or auditory cortex is observed. With treatment, rCBF improvements in frontal, temporal and basal ganglia, as well as motor cortex, are observed. In chronic or progressive disease, significant hypoactivity has been observed in the inferior parietal cortex, cuneus and posterior temporal lobe [22].
- *Anxiety and depression* – These two illnesses are extremely common nowadays and present a major healthcare problem incurring significant societal losses. Affected people seek actively out a cure, and involved medications can make additional harm due to side effects. SPECT-measured rCBF in medication-free patients shows hypoperfusions in the prefrontal, limbic, paralimbic regions, cingulate gyrus and left caudate nucleus [20]. In both unipolar and bipolar depression, hypoperfusions are seen in prefrontal, limbic and paralimbic regions, and lateral frontal hypoperfusion is involved in the acute depression in the elderly [20]. Increased activity can be seen in the basal ganglia and frontal lobe of the patient with anxiety. Frequently, anxiety and depression coexist. The severity of depression is correlated to hypoperfusion in the left cingulate cortex, lentiform nucleus and parahippocampal gyrus and increase in right posterolateral cortex [20].
- *Substance abuse and addiction* – Disseminated alterations of rCBF can be observed in short- and long-term substance abuse and dependence. Disappearance/improvements after abstinence have been observed in alcohol, cocaine, crack and heroin [20], suggesting that arterial spasms may cause the observed defects. Patients with history of inhalation of industrial solvents (paint, glue, gasoline) present similar perfusion abnormalities [23].
- *Autism* – This early and severe developmental disorder (20–50/100,000 births, M:W = 1.5:1) may induce decreased temporal lobe perfusion, although many cerebral SPECT are normal and each individual might have his unique perfusion pattern. Up to 30 % of autistic children may develop epilepsy [20].
- *Panic disorder* – Decreased rCBF is seen in the frontal lobes of patients with this disorder during a yohimbine challenge, while healthy volunteers did not show this decrease [1, 24].

Clinical Use of Brain SPECT in Psychiatric Diseases The exact use of rCBF for tailoring patient therapy in the clinics is still under investigation, but studies have shown potential use depending on the gross rCBF changes (a more detailed review and references are available in [20]):

- *Frontal hyperactivity*: It predicts a positive response to serotonergic medication in depression and OCD, as well as a response to cingulotomy in OCD or to sleep deprivation or repetitive transcranial magnetic stimulation in depression. It helps also to distinguish OCD from ADHD.
- *Prefrontal hypoperfusion*: It is associated with a negative response to serotoninergic medication in depression and clozapine in schizophrenia. It also predicts relapse in alcoholism and improved response to acetylcholinesterase inhibitors for memory and behaviour in Alzheimer disease. It also predicts poor ketamine response in fibromyalgia and improved response to stimulants in ADHD patients during concentration challenge.
- This pattern is associated with antisocial and impulsive behaviour and murder, as well as chances of completed suicide. When this pattern is observed in depressed patients, the physician should be more vigilant in their care and seek family support, as patients are less likely to respond to typical medication.
- *Temporal lobe abnormalities* (*hyper-/hypoperfusion*): When present in patients with mood instability or temper problems, it provides a rational for anticonvulsants

therapy. In the presence of memory or learning issues and a hypoperfusion pattern, it may show the usefulness of introducing acetylcholine esterase inhibitors.

Although SPECT has been used as a tool for research for in vivo probing of the brain function, it is not used in daily practice of psychiatry. SPECT may have the potential for personalizing treatment based on each patient's brain pathophysiology, but its true value and cost-efficiency need to be evaluated further. Currently, fMRI has superseded SPECT and PET for the real-time evaluation on the effects of drugs on cognition and impulse behaviour because of a better temporal resolution [3]. The true strength of PET and SPECT in psychiatry lies in the emergence of novel radiopharmaceuticals targeting specific receptor systems [3].

Technical Considerations

The current procedure guidelines European Association of Nuclear Medicine and the Society of Nuclear Medicine and Molecular Imaging (SNMMI) were published in 2009 [25, 26]. Relevant history including past drug use or head trauma and results of neurological, psychiatric, mini-mental status or neuropsychological testing [26].

Patient Preparation

The patients should be instructed to avoid substances known to affect CBF (alcohol, caffeine, energy drinks and any drugs know to affect CBF) the day of the examination. The injection of the radiopharmaceutical should be done after a 20-min resting period in a quiet, dark (or dimly lit) room without moving, to avoid any neurological stimulation. Ideally, the same room and preparation should be used uniformly at a given centre.

If sedation is needed for the images, the radiopharmaceutical administration should precede the sedation, as to avoid blood flow changes related to sedation.

Radiopharmaceuticals

Basically two tracers are used for brain perfusion SPECT: ^{99m}Tc-hexamethylpropyleneamineoxime (^{99m}Tc-HMPAO, Ceretec™) and ^{99m}Tc-ethylcysteinate dimer (^{99m}Tc-ECD, Neurolite™) [25, 26]. ^{99m}Tc-HMPAO requires freshly eluted (<2-h old) ^{99m}Tc solution and is less stable in vitro than ^{99m}Tc-ECD, which has a higher grey-matter-to-white contrast contributing to higher image quality. Both tracers present an uptake which is not entirely proportional to rCBF with underestimation of higher blood flows and overestimation at lower blood flows [27, 28]. They enter the brain cells because of their lipophilicity and undergo a lipophilic-to-hydrophilic conversion, which allows them to be trapped within neuronal and glial cells during its first passage and occur within 1 min of tracer injection. There is a small difference between tracers, as ^{99m}Tc-HMPAO reflects blood flow arrival to cerebral regions, while ^{99m}Tc-ECD would measure a more perfusion–metabolic uptake, because of a de-esterification needed for cellular trapping [29]. The more rapid urinary excretion of ECD favours its dosimetry, with about 4–8 mSv (ECD) or 5–10 mSv (HMPAO).

Quality control should be performed according to the manufacturer's instruction, and purity should be >90 % (ECD) and >80 % (HMPAO). After reconstitution, one should respect the delay for stability (HMPAO: 4 h, ECD 6 h) [25]. The activity is 555–1100 MBq (typically 740 MBq) in either radiopharmaceutical; in children, use the EANM dosage card (version 1.2.2014) with the weight-based multiplication with the baseline activity (ECD: 32.0 MBq; HMPAO: 51.8 MBq) with a minimum activity of 110 MBq (ECD) or 100 MBq (HMPAO) [30].

Of note, ECD is not commercially available since summer 2011 due to production. However, a new FDA-approved manufacturing site has been approved for commercial use in early 2015.

For brain perfusion imaging with PET, the short-lived (2-min half-life), cyclotron-produced ^{15}O-positron-emitting radionuclide is incorporated into chemical compounds (carbon monoxide $C^{15}O$, carbon dioxide $C^{15}O_2$, and water $H_2{}^{15}O$) or as a molecular tracer ($^{15}O_2$) and given intravenously or inhaled and is distributed according to physiology, allowing to mathematically quantify CBF, cerebral blood volume (CBV), the oxygen extraction fraction (OEF) and the cerebral metabolic rate of oxygen ($CMRO_2$). The advantage of PET over SPECT is clearly the absolute quantification, but a major drawback is the costly infrastructure and logistics for obtaining the short-lived radioisotope.

Acquisition Protocols

The best image resolution is reached with fan-beam collimators, and CT-based attenuation correction allows improving image quality and anatomical correlation. The ideal SPECT camera is a high-resolution dedicated camera but, alternatively, is a general-purpose camera with fan-beam collimators or high-resolution, parallel collimators; the SPECT camera must follow appropriate quality control programme [9]. Usually at least a 128×128 matrix size is chosen with a pixel size at least half of the camera's FWHM resolution. The acquisition duration should maximize total image count while minimizing patient motion, and the number of projections should be kept close to the number of pixels in the

matrix (e.g. 128 × 128 matrix leads to 3° projections for 360° or 120 projections); higher projection number brings minimal reconstruction benefits, and too low projection number will cause reconstruction artefacts [9]. Total acquisition time should be close to 20–25 min (triple-head camera) or 30 min (dual-head camera) [25].

Attenuation correction should be applied in all cases (Chang method or dedicated CT acquisition in SPECT/CT system) during reconstruction [25]. The number of image counts (ideally >5 million) should guide the filter to be used, with the higher the number of counts, the sharper the filter [9]. Scatter correction should be applied for better signal/noise ratio and lesion detection accuracy [25].

PET may be routinely done in large centres, but it might be more difficult to organize in an emergency setting. Usually CBF, OEF and $CMRO_2$ are measured using ^{15}O-labelled compounds [31].

Pharmacological Interventions

Acetazolamide challenge test—Intravenous injection of acetazolamide (Diamox™, adults 1 g; children 14 mg/kg) induces a vasodilation and increases rCBF by 30–50 % above baseline in 20–30 min, which returns to normal within 2–3 h [1]. Areas with low perfusion will see little changes to the challenge. Side effects include mild vertigo, tinnitus, paresthesia and nausea, and contraindications are allergy to sulfa, skin rash, bronchospasm, anaphylactoid reaction or <3 days after acute stroke or intracranial haemorrhage, as well as sickle cell patient at risk of veno-occlusive crisis) [25]. One-day protocol can be performed with split dose (1st dose = $^1/_3$ of activity, 2nd dose = $^2/_3$ of the total activity) which allows to perform baseline and challenge acquisition [25].

Alternatively, hypercapnia (inhalation of 5 % CO_2), dipyridamole or adenosine can be used and induces the same increase in rCBF [19].

Processing

Slice orientation is also important, and several reference systems are used (fronto-occipital plane similar to canthomeatal line in CT, fronto-cerebellar plane or temporal slices parallel to the longitudinal edge of the temporal lobe, useful for differentiating the mesial and temporal aspects of the temporal lobe for epilepsy or early Alzheimer-type dementia) [9]. The choice of the colour or black-and-white lookup table is arbitrary, but discontinuous scale may overestimate defects or asymmetry, and consistent normalization (e.g. to maximum count in the oblique slices) should be applied to avoid subjective image manipulations [9]. Iterative reconstruction including ordered-subset expectation maximization (OSEM) is available and can improve lesion detectability [25].

Usually images are interpreted visually using standard axial, coronal and sagittal plane [1]. Control groups using a minimum of 30 healthy volunteers can be used to define mean and SD in a semiquantitative approach usually using the cerebellum as a reference (or the pons in presence of cerebellar disease). Prior written patient information and consent is advised for provocation tests [9].

Major vendors have dedicated brain perfusion application to assess and display rCBF for each brain structural region (Fig. 3), with possibility to compare with normal population databases through statistical parameter mapping, and even some are freely available to academic institutions (Neurostat—Neurological Statistical Image Analysis Software, Department of Radiology, University of Washington, Seattle, WA, USA, http://128.208.140.75/~Download/), which runs mostly on older platforms using a DOS-like, cumbersome command language.

With the latest quantitative SPECT/CT scanners (e.g. Intevo xSPECT QUANT, Siemens), absolute quantitation can be obtained for SPECT ^{99m}Tc-tracers in Bq/mL with an accuracy of ±10 %. This may allow measuring absolute rCBF, but no comparison studies have been performed so far. Taking into account the difference in price between PET and SPECT and the fact that SPECT/CT may provide a cost-effective strategy for early identification and monitoring of the AD epidemics, such quantitative research should be encouraged [7].

Interpretation

Usually, brain SPECT interpretation is done stepwise [9]. First read sets of axial (or oblique temporo-occipital slices) and look for basic SPECT patterns, while the other sagittal and coronal slices will be used for confirmation or for additional findings. Identify then cerebral structures within the resolution of the images to identify lobes (eventually use an atlas as a guide). Using a standard regional order, visualize all cerebral regions (e.g. cortical regions in the caudal-to-cranial direction, cerebellum, temporal lobes, frontal lobes, occipital lobes and parietal lobes; mesial and lateral aspects of the brain being evaluated separately, as well as the subcortical regions [striatum, thalami, and white matter] and the pons). Then, global and regional tracer uptake is assessed for abnormalities (check for asymmetry, with attention to pattern due to incorrect tilts, which are easily identified on consecutives slices). Compare SPECT images to morphology (CT or MRI) (Fig. 3), as it is difficult to identify difference in uptake between periventricular white matter and lateral ventricles on SPECT only (e.g. hydrocephalus). When cerebral atrophy is present, partial volume effect may decrease brain uptake in the presence of cerebrospinal fluid within the cerebral cortex atrophy. Thus,

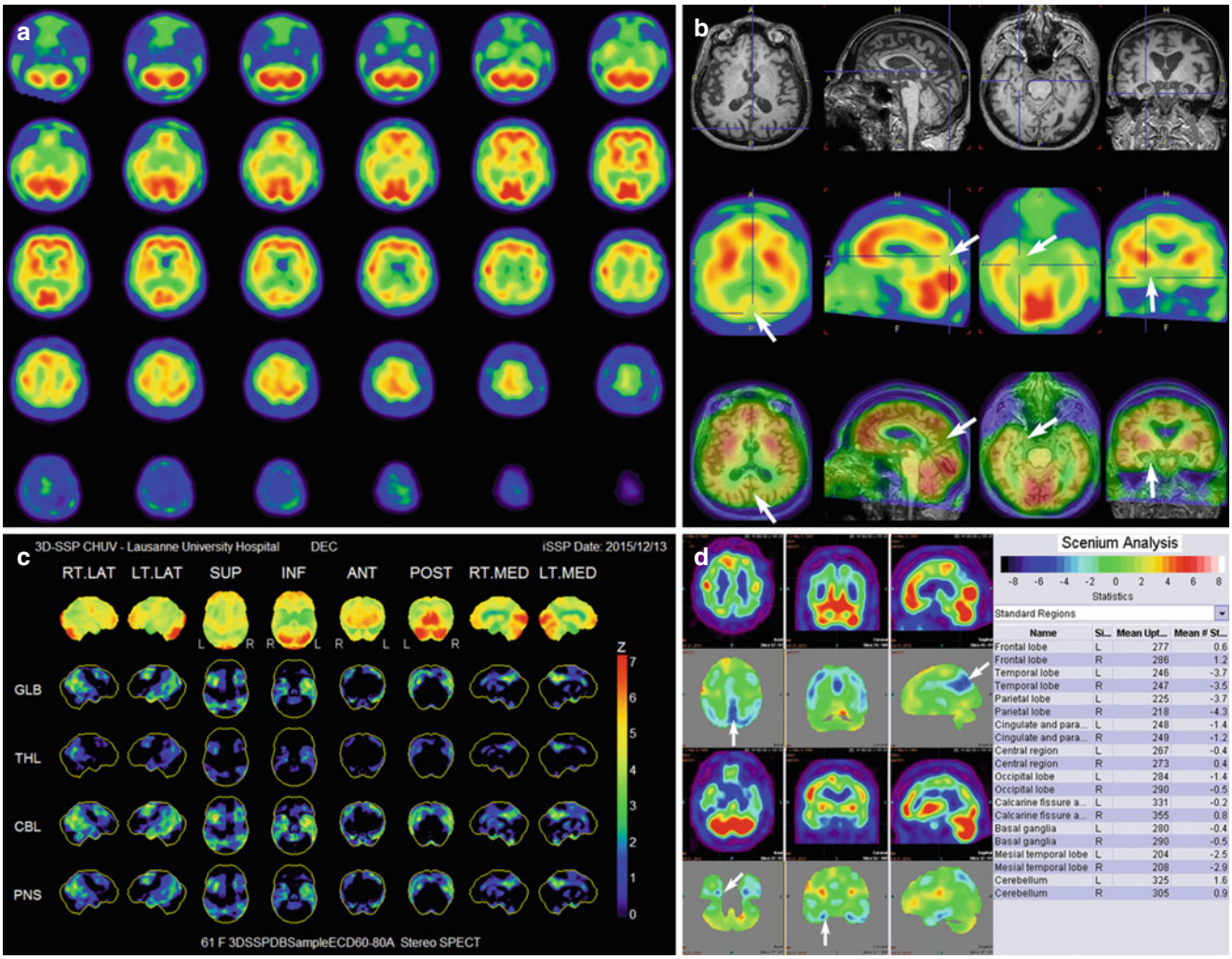

Fig. 3 Case of a 61-year-old woman with memory problems, aggressive behaviour, visual hallucination and agitation, with progressive degradation of symptoms over the last 2 years. The ^{99m}Tc-ECD SPECT (**a**) shows an important decrease of perfusion in the posterior cerebral cortex and temporoparietal cortex, as well as on the mesial side of the temporal lobe. These are accompanied of severe atrophy on the SPECT/MR fusion images (**b**, *arrows*). The comparison with databases of normal volunteers can be seen in (**c**) for *Neurostat* and (**d**) for the Siemens *Scenium* tools. The final diagnosis of posterior cortical atrophy (Benson-type) was retained, which is a rare form of neurodegenerative disorder mostly attributable to Alzheimer disease and characterized by visual deficits and atrophy of the parietal, occipital and occipitotemporal cortices)

indirect signs of cerebral atrophy should be searched for (enlarged interhemispheric fissure and marked separation of the basal ganglia), which should be confirmed by anatomical imaging. Advanced analysis software can correct for partial volume effect helping to define if hypoperfusion more marked than simply due to atrophy exists [9]. Finally distribution patterns should be recognized (hypoperfusion, absence of perfusion or hyperperfusion) taking into account the clinical context and morphology. Hypo- or hyperperfusion can be of vascular or axonal origin. Look for pattern distribution of abnormal perfusion such as vascular territories, diaschisis, dementia patterns, temporal lobe epilepsy or herpetic encephalitis. Such a systematic approach is valuable to define the possible aetiology to observed SPECT uptake.

Reporting

A concise report is appreciated by the referring physician, and the initial paragraph should include the requisite for the study, followed by a technical description of the study technical conditions, including the activity and nature of the radiopharmaceutical used and patient-centred conditions possibly influencing brain perfusion and eventually technical pitfalls important to understand the results and the interpretation [9]. The results should describe the localization and type of the abnormalities with description of the anatomical imaging comparison. The interpretation and conclusion should lead to a diagnosis likelihood if the requisite is about a specific clinical application (dementia, epilepsy,

carotid occlusion, etc.) When the role of brain perfusion has not been studied extensively, such as in behavioural disorders, prudence should be exerted.

Quality Control

Regular SPECT quality control should be run in accordance with the specific country's requirement [25].

Pitfalls

Technical pitfalls include unwanted patient movement or unintended cerebral activation, interaction with drugs acting on rCBF and inappropriate processing (background subtraction, thresholding, inappropriate patient database, discontinuous colour table with discrete scale, etc.) [25].

Sedating medication alters rCBF, and >5 min should be waited between the injection time and induction of the sedation, as not to alter image distribution [26]. Patient motion may degrade reconstruction and quality control on SPECT reprojections [26].

Breastfeeding should be interrupted for 24 h after injection of ^{99m}Tc compounds [25]. Sometimes, lack of cooperation or inability to stay still for 30 min limits the realization of the study; in such cases, conscious sedation with benzodiazepine can be used but it should be administered >5 min after tracer injection [26].

Conclusion

Brain perfusion using SPECT is a well-recognized clinical application routinely available in most nuclear medicine centres with applications in cerebrovascular disease, epilepsy and dementia, although this latter is gradually being replaced with PET. Anatomical correlation and close collaboration with the referring clinician enhances the clinical value of brain perfusion SPECT. Brain perfusion with SPECT and PET is still of great value and often unappreciated for imaging functional abnormalities that have not translated into anatomical abnormalities. Further work is also warranted to see the value of cerebral perfusion and cerebral perfusion reserve by SPECT for the evaluation of patients with cerebrovascular disease and risk factors to prevent or slow down the progression from predementia to dementia.

References

1. Camargo EE (2001) Brain SPECT in neurology and psychiatry. J Nucl Med 42(4):611–623
2. Heiss W-D (2011) The ischemic penumbra: correlates in imaging and implications for treatment of ischemic stroke. Cerebrovasc Dis 32(4):307–320
3. Abraham T, Feng J (2011) Evolution of brain imaging instrumentation. Semin Nucl Med 41(3):202–219
4. Herholz K (2011) Perfusion SPECT and FDG-PET. Int Psychogeriatr 23(S2):S25–S31
5. O'Brien JT, Firbank MJ, Davison C, Barnett N, Bamford C, Donaldson C, Olsen K, Herholz K, Williams D, Lloyd J (2014) 18F-FDG PET and perfusion SPECT in the diagnosis of alzheimer and lewy body dementias. J Nucl Med 55(12):1959–1965
6. Bhogal P, Mahoney C, Graeme-Baker S, Roy A, Shah S, Fraioli F, Cowley P, Jäger HR (2013) The common dementias: a pictorial review. Eur Radiol 23(12):3405–3417
7. Henderson TA (2012) The diagnosis and evaluation of dementia and mild cognitive impairment with emphasis on SPECT perfusion neuroimaging. CNS Spectr 17(04):176–206
8. Rostami E, Engquist H, Enblad P (2014) Imaging of cerebral blood flow in patients with severe traumatic brain injury in the neurointensive care. Front Neurol 5:4–114
9. Catafau AM (2001) Brain SPECT in clinical practice. Part I: perfusion. J Nucl Med 42(2):259–271
10. Farid K, Petras S, Ducasse V, Chokron S, Helft G, Blacher J, Caillat-Vigneron N (2012) Brain perfusion SPECT imaging and acetazolamide challenge in vascular cognitive impairment. Nucl Med Commun 33(6):571–580
11. O'Brien JT, Erkinjuntti T, Reisberg B, Roman G, Sawada T, Pantoni L, Bowler JV, Ballard C, DeCarli C, Gorelick PB, Rockwood K, Burns A, Gauthier S, DeKosky ST (2003) Vascular cognitive impairment. Lancet Neurol 2(2):89–98
12. Oku N, Kashiwagi T, Hatazawa J (2010) Nuclear neuroimaging in acute and subacute ischemic stroke. Ann Nucl Med 24(9):629–638
13. Lee M, Zaharchuk G, Guzman R, Achrol A, Bell-Stephens T, Steinberg GK (2009) Quantitative hemodynamic studies in moyamoya disease. Neurosurg Focus 26(4):E5
14. Kuhn FP, Warnock G, Schweingruber T, Sommerauer M, Buck A, Khan N (2015) Quantitative H2[15O]-PET in pediatric moyamoya disease: evaluating perfusion before and after cerebral revascularization. J Stroke Cerebrovasc Dis 24(5):965–971
15. Goffin K, Dedeurwaerdere S, Van Laere K, Van Paesschen W (2008) Neuronuclear assessment of patients with epilepsy. Semin Nucl Med 38(4):227–239
16. Patil S, Biassoni L, Borgwardt L (2007) Nuclear medicine in pediatric neurology and neurosurgery: epilepsy and brain tumors. Semin Nucl Med 37(5):357–381
17. la Fougère C, Rominger A, Förster S, Geisler J, Bartenstein P (2009) PET and SPECT in epilepsy: a critical review. Epilepsy Behav 15(1):50–55
18. Siclari F, Prior JO, Rossetti AO (2013) Ictal cerebral positron emission tomography (PET) in focal status epilepticus. Epilepsy Res 105(3):356–361
19. Masdeu J, Arbizu J (2008) Brain single photon emission computed tomography: technological aspects and clinical applications. Semin Neurol 28(04):423–434
20. Santra A, Kumar R (2014) Brain perfusion single photon emission computed tomography in major psychiatric disorders: from basics to clinical practice. Indian J Nucl Med 29(4):210–220
21. Cho SC, Hwang JW, Kim BN, Lee HY, Kim HW, Lee JS, Shin MS, Lee DS (2007) The relationship between regional cerebral blood flow and response to methylphenidate in children with attention-deficit hyperactivity disorder: comparison between non-responders to methylphenidate and responders. J Psychiatr Res 41(6): 459–465
22. Kanahara N, Shimizu E, Sekine Y, Uchida Y, Shibuya T, Yamanaka H, Hashimoto T, Asaka T, Sasaki T, Miyatake R, Ohkami T, Fukami G, Fujisaki M, Watanabe H, Shirayama Y, Hayashi H, Hashimoto K, Asano M, Iyo M (2009) Does hypofrontality expand to global brain area in progression of schizophrenia?: a cross-sectional study between first-episode and chronic schizophrenia. Prog Neuropsychopharmacol Biol Psychiatry 33(3):410–415

23. Kucuk NO, Kilic EO, Ibis E, Aysev A, Gencoglu EA, Aras G, Soylu A, Erbay G (2000) Brain SPECT findings in long-term inhalant abuse. Nucl Med Commun 21(8):769–773
24. Devous MD Sr (1992) Comparison of SPECT applications in neurology and psychiatry. J Clin Psychiatry 53(Suppl):13–19
25. Kapucu ÖL, Nobili F, Varrone A, Booij J, Vander Borght T, Någren K, Darcourt J, Tatsch K, Van Laere KJ (2009) EANM procedure guideline for brain perfusion SPECT using 99mTc-labelled radiopharmaceuticals, version 2. Eur J Nucl Med Mol Imaging 36(12):2093–2102
26. Juni JE, Waxman AD, Devous MD, Tikofsky RS, Ichise M, Van Heertum RL, Carretta RF, Chen CC (2009) Procedure guideline for brain perfusion SPECT using 99mTc radiopharmaceuticals 3.0. J Nucl Med Technol 37(3):191–195
27. Friberg L, Andersen AR, Lassen NA, Holm S, Dam M (1994) Retention of 99mTc-bicisate in the human brain after intracarotid injection. J Cereb Blood Flow Metab 14(Suppl 1):S19–S27
28. Lassen NA, Andersen AR, Friberg L, Paulson OB (1988) The retention of [99mTc]-d, l-HM-PAO in the human brain after intracarotid bolus injection: a kinetic analysis. J Cereb Blood Flow Metab 8(6):S13–S22
29. Koyama M, Kawashima R, Ito H, Ono S, Sato K, Goto R, Kinomura S, Yoshioka S, Sato T, Fukuda H (1997) SPECT imaging of normal subjects with technetium-99m-HMPAO and technetium-99m-ECD. J Nucl Med 38(4):587–592
30. Lassmann M, Treves ST, Group ESPDHW (2014) Paediatric radiopharmaceutical administration: harmonization of the 2007 EANM paediatric dosage card (version 1.5.2008) and the 2010 North American consensus guidelines. Eur J Nucl Med Mol Imaging 41(5):1036–1041
31. Maeda Y, Kudomi N, Sasakawa Y, Monden T, Kato K, Yamamoto Y, Kawai N, Nishiyama Y (2015) Applicability of emission-based attenuation map for rapid CBF, OEF, and CMRO2 measurements using gaseous 15O-labeled compounds. EJNMMI Phys 2(1):12

Hybrid Imaging: Local Staging of Head and Neck Cancer

Martin W. Huellner and Tetsuro Sekine

Introduction

This chapter discusses the local staging of mucosal and extramucosal epithelial malignant disease of the head and neck, with the exception of mucosal melanoma and thyroid malignancies.

The head and neck is the only compartment of the body that is widely accessible to radiological imaging, clinical examination, and noninvasive endoscopy at the same time. The accuracy of each examination method, however, is different depending on the location of the disease. While superficial mucosal spread of cancer is best addressed with endoscopy, some anatomical subsites, especially parts of the hypopharynx, represent blind spots to the clinician. Cancer arising there might go undetected both with endoscopy and clinical examination, and clinicians have to rely on radiological imaging. Assessing the tumor extension in depth is another domain of cross-sectional imaging, although palpation might be more accurate in certain instances, e.g., in determining the infiltration of the prevertebral fascia or in addressing superficial invasion of cortical bone by cancer.

Currently, head and neck cancer is still among the top ten of malignant diseases in developed parts of the world [1]. Reliable statistics on the overall survival of head and neck cancer patients were established starting in the 1970s, and since then a steady increase in survival has been observed (Fig. 1) [1]. This is believed to be due to several factors. First, advanced cancer stages benefit from a continuous improvement in chemotherapy regimens and radiation therapy, including the advent of intensity-modulated radiation therapy (IMRT) [2]. Second, there was an increase in human papillomavirus (HPV)-related cancers in the oral cavity and oropharynx. These cancers tend to occur in a younger population, and their cure is comparably facile. Third, the technical progress of cross-sectional imaging modalities led to an increase in the staging accuracy of tumors. And this is where diagnostic radiologists contribute to patient care.

While computed tomography (CT) and magnetic resonance (MR) imaging are mainstays of local T and N staging, ^{18}F-fluoro-2-deoxy-D-glucose (FDG) positron emission tomography (PET) raised the bars in the detection of small nodal metastases, distant metastases, and second primary tumors. False-positive results in PET are typically due to inflammatory changes, while false-negatives may be encountered in organs with a high physiologic FDG activity, such as

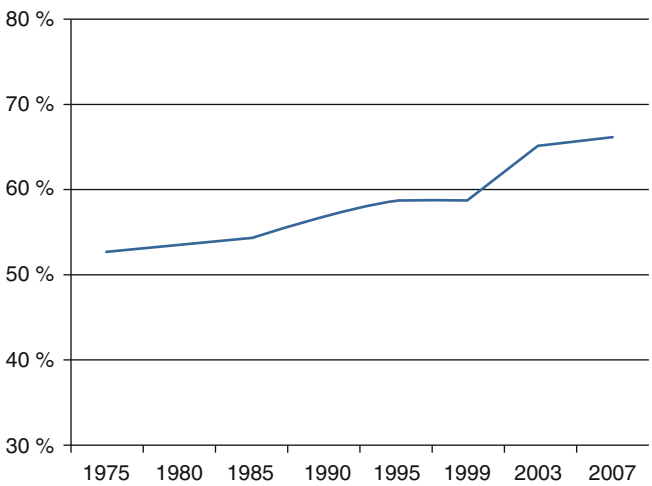

Fig. 1 Five-year relative survival rates in head and neck cancer (Adapted from Pulte et al. [1])

M.W. Huellner (✉)
Division of Nuclear Medicine, Department of Medical Radiology, University Hospital Zurich/University of Zurich, Rämistrasse 100, Zurich 8091, Switzerland

Division of Neuroradiology, Department of Medical Radiology, University Hospital Zurich/University of Zurich, Frauenklinikstrasse 10, Zurich 8091, Switzerland
e-mail: martin.huellner@usz.ch

T. Sekine
Division of Nuclear Medicine, Department of Medical Radiology, University Hospital Zurich/University of Zurich, Rämistrasse 100, Zurich 8091, Switzerland

Department of Radiology, Nippon Medical School, 1-1-5 Sendagi, Bunkyo-ku, Tokyo 113-8603, Japan
e-mail: tetsuro.sekine@usz.ch

J. Hodler et al. (eds.), *Diseases of the Brain, Head and Neck, Spine 2016–2019: Diagnostic Imaging*, DOI 10.1007/978-3-319-30081-8_29

the brain and the liver. Integrated reading of hybrid examinations, either PET/CT or PET/MR, will help classify questionable lesions. Notably, one important pitfall for PET and CT as well as MR exists in the head and neck area: Lymphoepithelial tissue, e.g., in the base of the tongue, takes up both contrast medium and FDG, and indwelling malignant disease might be unnoticed.

Hybrid Imaging of Head and Neck Tumors

The use of FDG-PET in the local staging of head and neck tumors is of limited value. PET activity does not exactly demonstrate the size and extension of a tumor. In larger tumors with high FDG avidity, PET imaging suffers from spillover artifact to surrounding tissues. Smaller tumors (Tis and T1), superficially spreading tumors, or those with low FDG avidity may be missed completely by PET. Therefore, the location and size of a tumor and the depth of invasion need to be accurately identified on contrast-enhanced morphological imaging, using preferably MR, or CT. Small but FDG-avid tumor may hide in regions with high physiologic FDG activity, such as lymphoepithelial tissue, which is found in the nasopharynx, palatine tonsils, and base of the tongue [3]. However, anatomical MR and CT imaging is also limited in this area because lymphoepithelial tissue takes up contrast and is hyperintense on T2-weighted images, and a tumor might be unnoticed therein. One possible solution for this dilemma is the use of diffusion-weighted imaging (DWI) as part of a PET/MR protocol [4–7]. The cellularity of a tumor generates a low apparent diffusion coefficient (ADC), representing a contrast to normal lymphoepithelial tissue (Fig. 2).

The FDG uptake of a tumor is quantified at most institutions as part of clinical routine [3]. This may be helpful for following up the patient after radiation therapy or chemotherapy. No definitive threshold of the standard uptake value (SUV) exists for the differentiation of benign tissue and malignant tumors, for the differentiation of low-grade and high-grade lesions, or for prognostication [3, 8–14].

Due to less interference of artifacts from dental hardware, PET/MR is supposedly advantageous in the suprahyoid neck, whereas PET/CT is less prone to movement and swallowing artifacts occurring in the infrahyoid neck [15]. New MR reconstruction algorithms aiming at metal artifact reduction might further enhance the use of MR in the oral cavity [16].

Hybrid imaging is not routinely performed for the initial staging of patients with small tumors or if there is no clinical suspicion for nodal metastatic disease. Many centers perform sentinel node single-photon emission computed tomography/computed tomography (SPECT/CT) imaging using radiolabeled nanocolloids for the assessment of the nodal stage in patients with oral cavity cancers and oropharyngeal cancers. The radiotracer is injected in peritumoral location, and hybrid lymphoscintigraphic images allow for sentinel node mapping and guide nodal biopsy [3]. Sentinel node biopsy is considered the only reliable presurgical approach for the identification of micrometastatic deposits in lymph nodes [3, 17, 18]. PET may be falsely negative for nodal involvement if metastatic lymph nodes are necrotic and have only a thin rim of viable tumor tissue or if they are cystic [3, 19] (Fig. 2). This is a common situation in patients with squamous cell carcinoma in the oral cavity and oropharynx, with cystic metastases being particularly related to the presence of human papillomavirus (HPV) subtypes 16 and 18, the latter to somewhat less extent. Therefore, the use of contrast-enhanced imaging techniques is advised in the staging of head and neck cancer patients. Cystic metastases may grow rapidly, and response to radiotherapy is sometimes limited (Fig. 3). One

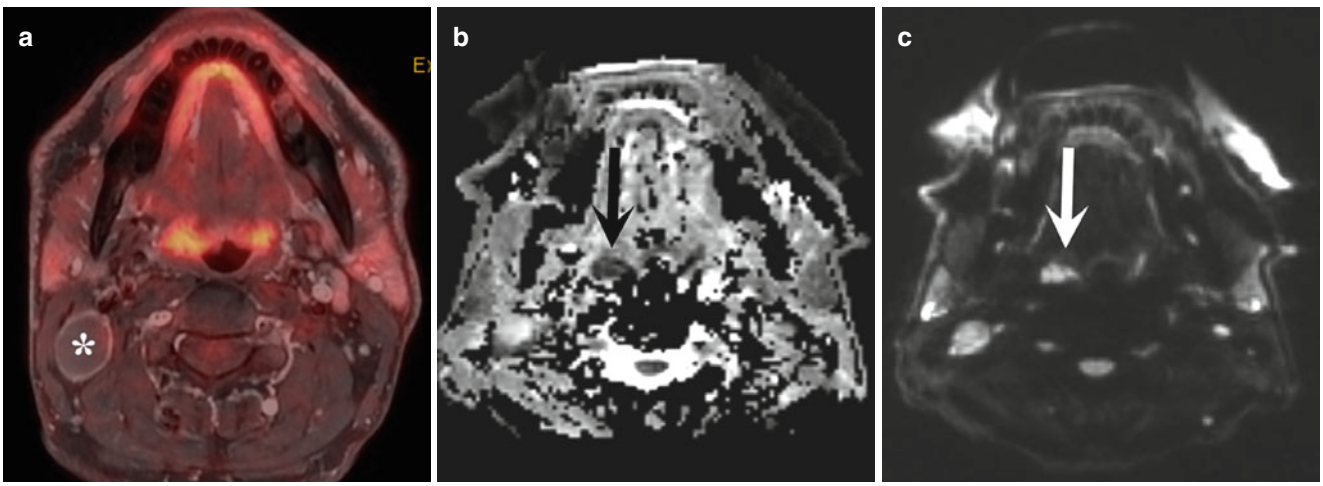

Fig. 2 Patient with palpable lump in the neck on the right side. A cystic lymph node metastasis with contrast enhancement of the rim (**a**, *asterisk*) is seen on FDG-PET/MR, but no obvious tumor. Diffusion-weighted imaging reveals a lesion with low apparent diffusion coefficient (**b**, *arrow*) and high signal on the b800 image (**c**, *arrow*) in the right tonsil. Subsequent tonsillectomy and histopathology confirmed a human papillomavirus (HPV)16-associated squamous cell carcinoma arising from the right tonsil

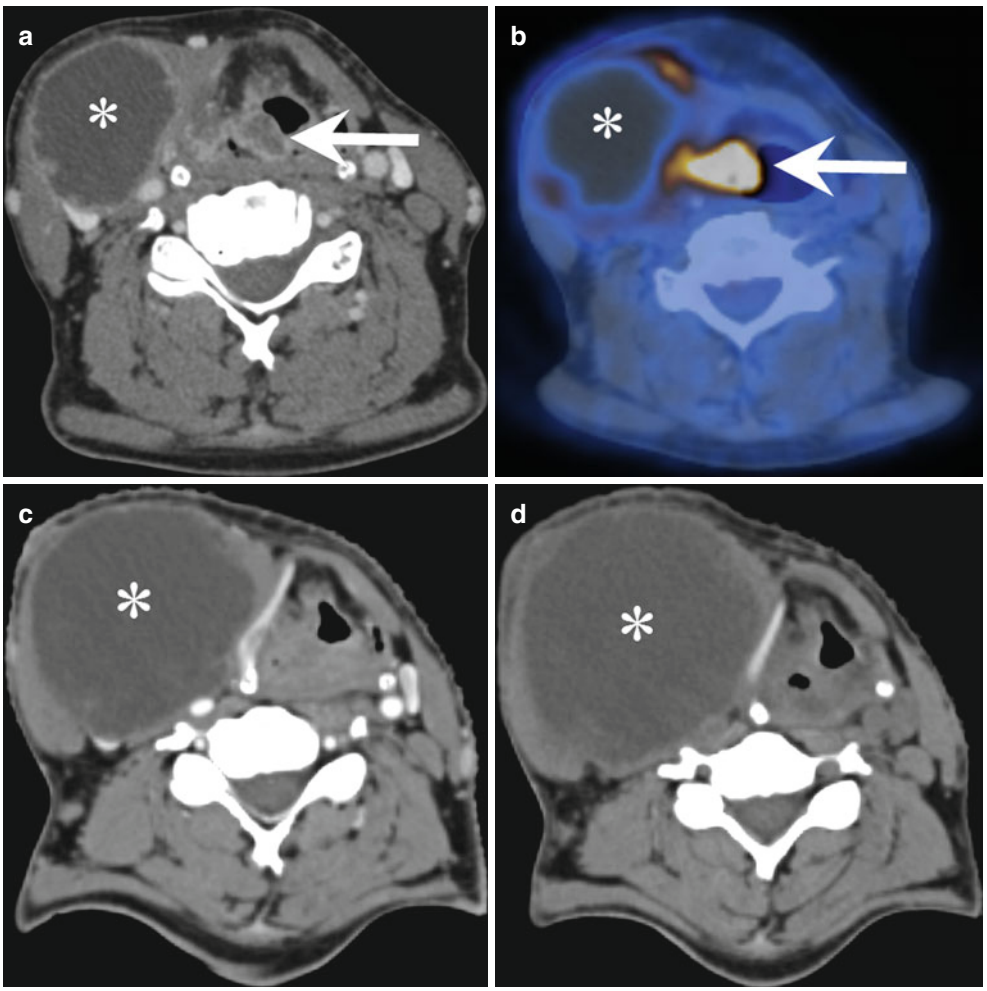

Fig. 3 HPV16-associated right-sided hypopharyngeal carcinoma. The tumor arises in the right piriform sinus and involves the right aryepiglottic fold (*arrows*), as seen on axial contrast-enhanced CT image (**a**) and FDG-PET/CT image (**b**). A large cystic metastasis (*asterisk*) with faintly FDG-avid rim is seen in the neck on the right side. Three weeks later the metastasis has grown in size (*asterisk*), as seen on the contrast-enhanced CT image (**c**). Another 6 weeks later, and after radiotherapy, the metastasis (*asterisk*) has increased even more (**d**)

rare differential diagnosis to cystic lymph node metastases with or without rim-like FDG uptake is branchial cleft cyst, which may be FDG-avid when infected, when containing lymphoid tissue, or when harboring neoplastic tissue [3, 20–22]. In large nodes without evidence of necrotic areas, lymphoma should be considered as a differential diagnosis. Unlike for the T staging, DWI as part of the PET/MR examination seems to offer no additional benefits for the N staging and provides rather redundant information [3, 7].

Extracapsular spread (ECS) on imaging refers to the macroscopic breach of the nodal capsule by tumor [3]. CT and MR may identify contour irregularities of the lymph node capsule (jagged or spiculated margins), stranding of the surrounding tissue, or even direct infiltration of surrounding structures by tumor [3, 23]. The presence of ECS depends on the size of lymph node metastases. ECS occurs in the majority of nodal metastases larger than 3 cm (approximately 75 %), in a significant number of metastatic nodes between 1 and 3 cm (up to 50 %), still in about one fifth of nodes less than 1 cm, and may rarely be present in clinically negative necks as well [3, 24–27]. ECS represents an adverse prognostic indicator, but its presence does not change the nodal stage.

The frequency of distant metastatic disease, mainly to the lung, increases with the T stage and with the N stage [3]. The presence of nodal metastases in the lower neck further increases the possibility of distant metastases. Hybrid PET/CT or PET/MR imaging is considered ideal for whole-body staging. PET/CT is the optimal hybrid modality for addressing the lung parenchyma. Lung imaging is somewhat problematic with PET/MR, because the lung parenchyma basically represents a black hole for MR. Several technical solutions have been suggested to overcome this drawback, e.g., breath-hold sequences and respiration-gated sequences [3, 15, 28]. The current threshold of lung nodule detection in clinical PET/MR ranges between 3 and 5 mm. However,

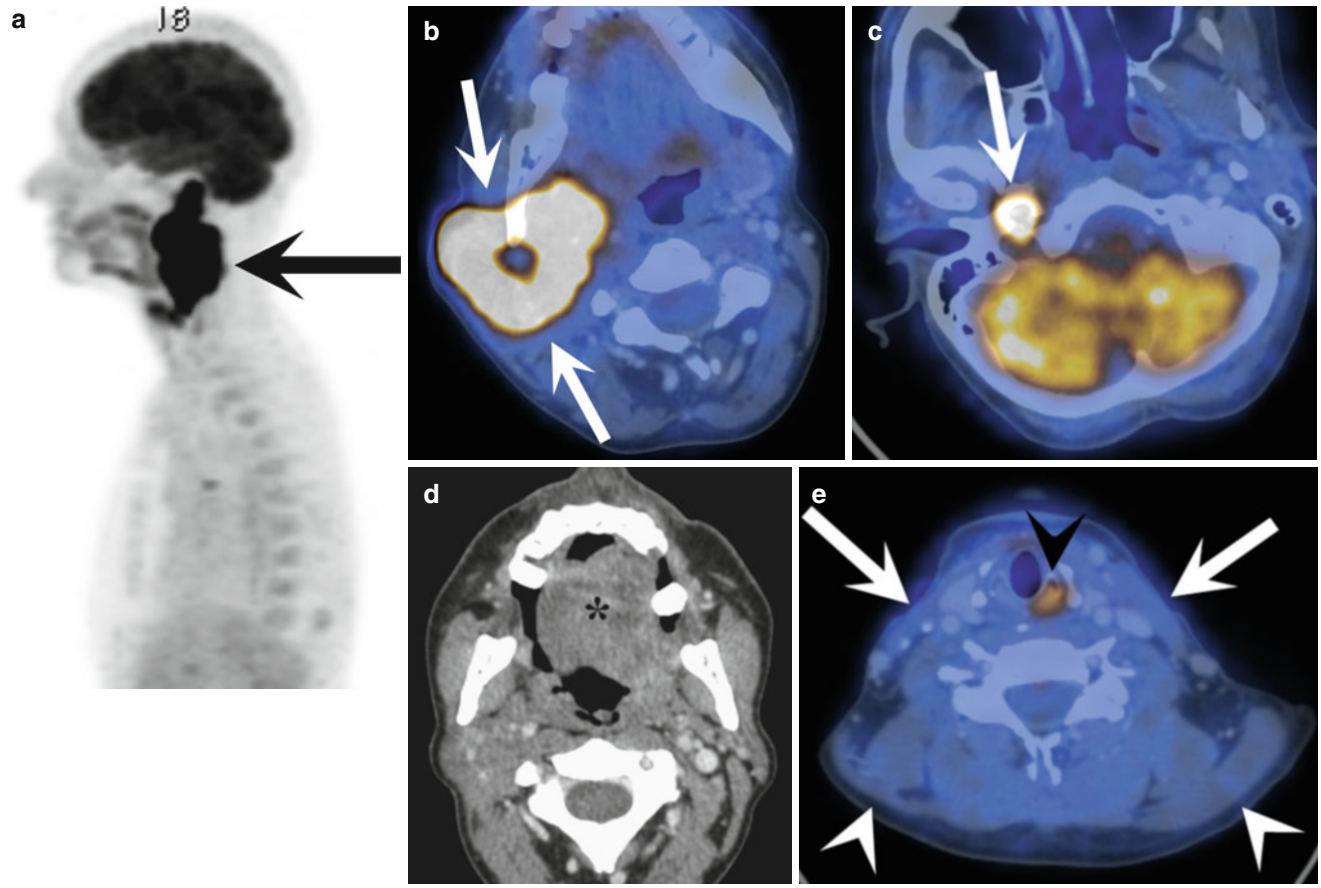

Fig. 4 Patient with cervical lymph node metastasis from an unknown primary tumor. Sagittal FDG-PET maximum intensity projection (MIP) image (**a**) shows an FDG-avid mass (*arrow*) in the neck, extending from the skull base to the level of the hyoid. The centrally necrotic mass (*arrows*) involves the parapharyngeal space, masticator space, and subcutaneous tissue on the right side, as seen on axial contrast-enhanced FDG-PET/CT image (**b**). The top of the mass (**c**, *arrow*) resides below the skull base at the level of the jugular foramen, which is infiltrated. Contrast-enhanced CT image (**d**) reveals an asymmetry of the tongue (*asterisk*), with right-sided atrophy. Contrast-enhanced FDG-PET/CT image (**e**) further reveals asymmetry of the trapezius muscles (*white arrow heads*) and sternocleidomastoid muscles (*arrows*), as well as right-sided loss of FDG uptake in the phonatory muscles (*black arrow head*). These findings are suggestive for combined neuropathy of the vagus nerve, accessory nerve, and hypoglossal nerve (constituents of Collet-Sicard syndrome along with glossopharyngeal nerve palsy)

there appears to be no need for dramatization of the probably somewhat inferior performance of PET/MR in lung nodule detection compared to PET/CT. In oncological patients, more than 98 % of FDG-negative subcentimeter lung nodules are benign, and 97 % of all lung nodules missed by PET/MR do not grow [29, 30]. Other common distant metastatic sites are the brain, the liver, and the bone. There, PET/MR might even offer advantages over PET/CT, particularly in the brain and in the liver, where high physiologic FDG uptake might obscure small metastases.

Several pitfalls need to be avoided in FDG-PET imaging of the head and neck. Physiologic FDG uptake occurs in a number of structures and in certain situations and should not be confused with pathology [3]. In children there is more FDG-avid lymphatic tissue in the adenoids, palatine tonsils, and lingual tonsils than in adults. Of the major salivary glands, the sublingual glands are usually most FDG-avid. Physiologic FDG uptake might also be encountered in the soft palate due to the abundance of salivary gland tissue there. Occasionally, the tip of the tongue appears FDG-avid. Uptake may also be seen in the orbicularis oris muscle and in muscles of mastication if patients were chewing during or shortly before the uptake phase. Depending on previous movement and muscle activity or if patients were positioned uncomfortably, uptake might be seen in the scalene muscles, sternocleidomastoid muscles, and prevertebral muscles. People who talked during the uptake phase have FDG-positive vocal cords and phonatory muscles. Unilateral FDG uptake in vocal cords, however, should raise the question for a lesion of the recurrent laryngeal nerve on the FDG-negative side or even complete vagal nerve palsy (Fig. 4).

Several benign lesions may be FDG-positive (Warthin's tumor, pleomorphic adenoma, schwannoma, branchial cleft cysts, inflammatory pseudotumor). On the other hand, some malignant tumors may be only faintly FDG-avid or even FDG-negative (adenocarcinoma of salivary glands, acinic cell carcinoma, chondrosarcoma, plasmacytoma).

Due to radiogenic inflammatory changes, FDG exams should be postponed to at least 3 months after therapy [3].

Local Staging

The radiological differential diagnosis for mucosal tumors is most often trivial, since the vast majority of tumors (more than 95 %) arising there is of squamous cell origin. The most common exception to that rule is lymphoma, which may arise from lymphoid tissue in Waldeyer's ring and may be accompanied by nodal disease in the neck. Lymphoma may be indistinguishable from squamous cell carcinoma based on morphological imaging characteristics. Its cellularity results in a low signal on T2-weighted images and a low apparent diffusion coefficient (ADC) on diffusion-weighted imaging (DWI). However, unlike carcinomas, lymphoma displaces rather than infiltrates surrounding healthy tissue. One exception to that rule is the somewhat frequent invasion of bone, which is seen in many lymphomas primarily arising in the head and neck. Additionally, lymphoma rarely exhibits intralesional areas of necrosis, appearing hyperintense on T2-weighted images, not even when lesions are large (Fig. 5). One important exception to that rule is posttransplant lymphoproliferative disorder (PTLD), which might show necrotic changes.

However, biopsy oftentimes precedes imaging, and histopathology already revealed the nature of the tumor when the patient is referred for radiological staging.

Throughout the upper aerodigestive tract, the TNM staging system is used to classify malignant tumors [31]. It represents the basis for treatment decisions, for prognostication, and for therapy response assessment.

Besides imaging-based classifications of tumor extent, there are other important factors that warrant consideration when the treatment plan for a patient is laid: patient's will, comorbidites, and life expectancy.

T Staging

The staging of tumor extent basically reverts to the discrimination of stage T4b tumors from tumors with lower T stages. This is because T4b tumors are considered not resectable, while all remaining tumors are generally believed amenable to surgical cure; some important exceptions applying (see below). Certainly, T4b tumors per se are technically resectable, but a surgical approach would result in a very poor outcome and severe functional disabilities of the patient. Items

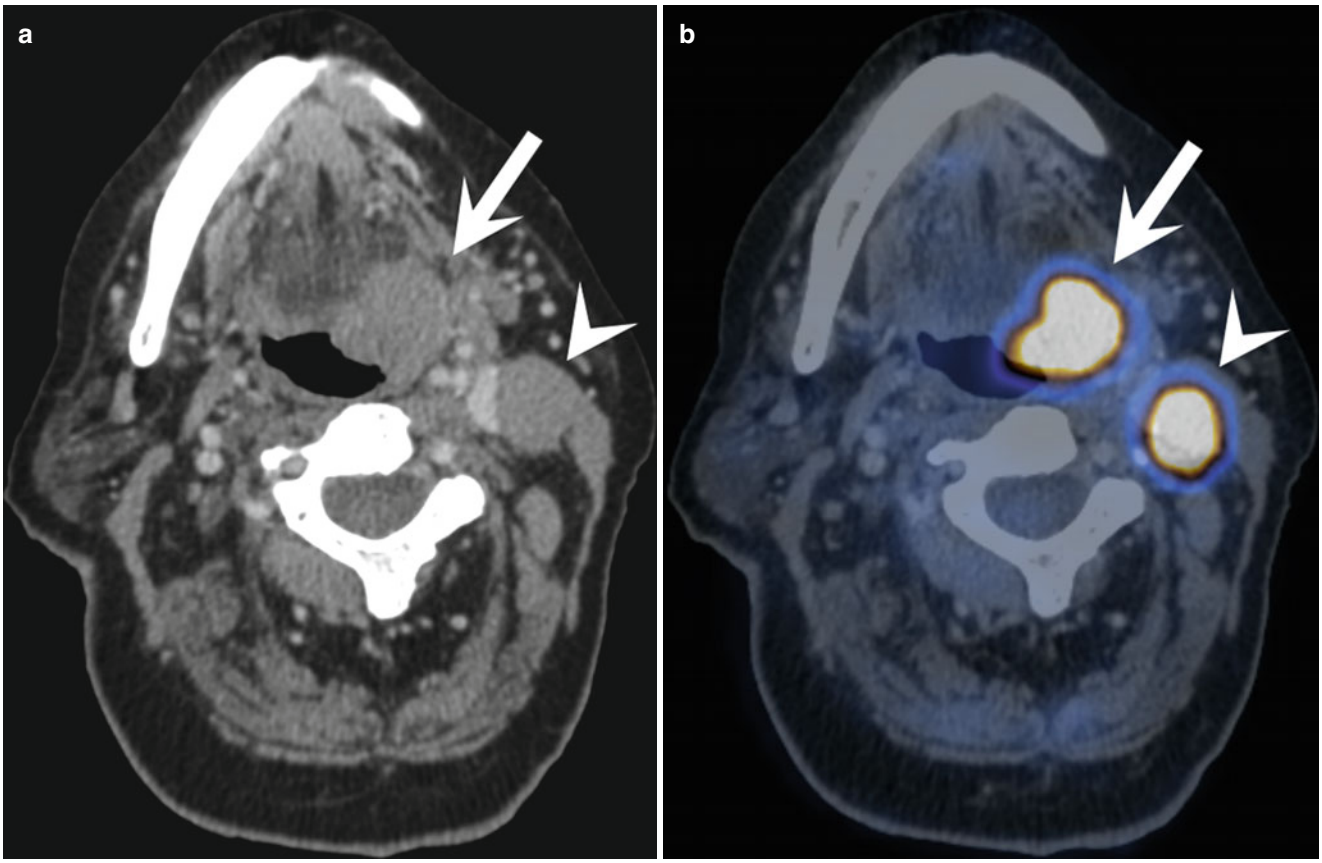

Fig. 5 Lymphoma arising in the left tonsil (**a**, *arrow*), involving the tongue base and the lateral wall of the oropharynx. An enlarged level II lymph node is seen on the left side (**a**, *arrow head*). Both lesions show a homogeneous density without evidence of necrosis, and intense FDG uptake (**b**, *arrow, arrow head*). These imaging features are not specific for lymphoma and may also be seen with squamous cell carcinoma

defining T4b stage are the same for all mucosal and extramucosal cancers of the head and neck, except for nasopharyngeal carcinoma where the T4 stage is not subdivided. Each one of the following three findings defines T4b stage and renders a tumor not resectable: infiltration of the prevertebral fascia and/or prevertebral muscles, encasement of the internal carotid artery or of the common carotid artery, and infiltration of the mediastinum. This general rule is slightly modified depending on the origin of the primary tumor. In the oral cavity and oropharynx, infiltration of the skull base, invasion of the pterygoid plates, and infiltration of the lateral pterygoid muscle are also defined as T4b stage. Additionally in the oropharynx, lateral extension into the nasopharynx is considered T4b. Although infiltration of the prevertebral space and/or the mediastinum is not explicitly mentioned in the T-staging system of oral cavity and oropharyngeal cancers, presence of these factors still would imply T4b stage. There is no breakdown of the T4 stage in T4a and T4b in the nasopharynx. T4 stage in the nasopharynx is defined as intracranial extension, involvement of cranial nerves, or extension into the orbit, masticator space, infratemporal fossa, or hypopharynx.

T4b-Defining Items

Infiltration of the Prevertebral Space

Such is given if the prevertebral fascia and/or muscles are infiltrated by a tumor. The clinical diagnosis is comparably easy, with unhindered motility of the posterior pharyngeal wall and the retropharyngeal contents (or a tumor) against the prevertebral fascial plane on palpation indicating absence of infiltration. The diagnosis on cross-sectional imaging is more difficult most of the time, unless continuous spread of tumor to the vertebral column is seen. The most suggestive feature is a complete obliteration of the prevertebral fat plane, which is better appreciated on non-fat-suppressed MR images than on CT. Other indicators of infiltration are an asymmetric thickening of muscles and contrast enhancement and FDG uptake of muscles (Fig. 6) [32, 33]. Since spillover artifact on PET may mimic tumor extension across the prevertebral fascia, correlation with morphological imaging is necessary.

Mediastinal Invasion

Mediastinal invasion is uncommon in head and neck cancer and if occurring is limited to laryngeal and hypopharyngeal carcinomas. Imaging characteristics of mediastinal invasion are an obliteration of the mediastinal fat with contrast enhancement, or FDG uptake with contiguous tumor. Also, asymmetric thickening, contrast enhancement, and FDG uptake of the wall of the mediastinal vessels and the esophagus should raise the suspicion for mediastinal infiltration by a tumor. Submucosal or mucosal infiltration of the proximal esophagus, which is comparably easy to resect, is difficult to differentiate from deeper invasion on imaging. If only the proximal 2 cm of the esophagus is involved, curative surgery is still considered possible by most surgeons. Such would revert to a stage T3 tumor (hypopharynx) or a stage T4a tumor (larynx).

Vascular Encasement

Vascular infiltration is assumed with circumferential tumor contact of 270° or more or if there is an irregular narrowing of the vessel due to contiguous tumor [34]. An obliteration of the fat plane between the vessel wall and a tumor has also a high positive predictive value [35]. In some instances of vascular infiltration, contrast enhancement and/or focal FDG uptake of the vessel wall is seen. However, these imaging findings may also be seen with peritumoral inflammatory infiltrates [36, 37].

Other T-Stage Issues

The classification of tumors into stages T1 to T4a is somewhat less pivotal than the differentiation of stage T4a and stage T4b tumors. Although the assignment of stages T1 to T4a impacts on the type of curative surgery the patient will undergo if qualifying, it does not primarily preclude surgery as with T4b tumors. Detailed tumor staging classifications by site are provided in Table 1.

There are, however, certain factors that are not necessarily part of the TNM staging system, but still might render a tumor not resectable, independently of its T stage. It is therefore as important as with T4b-defining factors to scrutinize the images for their presence. They consist of the following items: invasion of the laryngeal cartilage, invasion of the preepiglottic adipose tissue, perineural spread, orbital invasion, bone infiltration, skull base invasion, infiltration of the dura, and invasion of the brachial plexus [38].

Invasion of Laryngeal Cartilage

Owing to variable and often asymmetric ossification of the laryngeal cartilage, evaluation of tumor invasion is challenging with any cross-sectional imaging modality [3, 39]. Cartilage invasion is given with visible erosion or osteolysis of the cartilaginous skeleton on CT or MR or with permeative growth of tumor from the paraglottic to the paralaryngeal space (transmural extralaryngeal spread). It may also be assumed with contrast enhancement or focal FDG uptake of the cartilage; however, such might also be seen in chondroradionecrosis in a posttreatment setting, occurring in approximately 5 % of patients [40, 41]. Of note, sclerosis of the cartilaginous skeleton seen on CT does not necessarily indicate tumoral invasion, but might also represent reaction to contiguous tumor or postradiogenic change [3].

Invasion of Preepiglottic Adipose Tissue

Such may be assumed when the preepiglottic is obliterated or with contrast enhancement or focal FDG uptake in the preepiglottic space. The presence of erosion of the hyoid

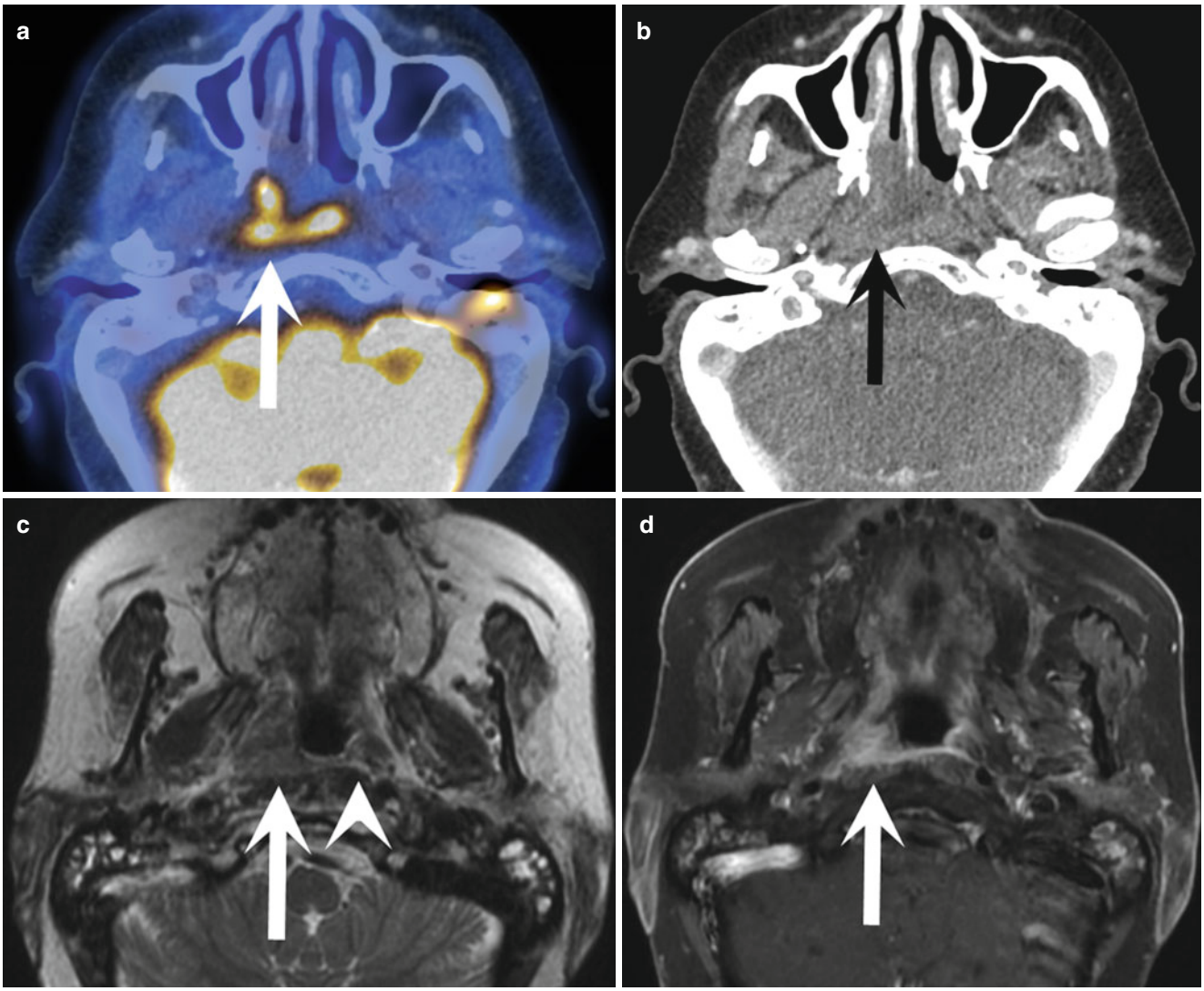

Fig. 6 Squamous cell carcinoma arising from the right-sided pharyngeal recess (fossa of Rosenmüller) with extension across the midline, as seen on contrast-enhanced FDG-PET/CT image (**a**, *arrow*). Presence of prevertebral invasion is difficult to assess on contrast-enhanced CT image because of low density contrast between tumor and prevertebral muscles (**b**, *arrow*). T2-weighted MR image (**c**) displays loss of the prevertebral fat plane on the right side (*arrow*), but preservation on the left side (*arrow head*). Contrast-enhanced T1-weighted fat-suppressed MR (**d**) further reveals a shaggy anterior margin of the right prevertebral muscles with contrast enhancement (*arrow*). MR features are suggestive of prevertebral invasion, which was confirmed with clinical examination

base is also a reliable indicator. Sagittal and/or axial T1-weighted non-fat-suppressed MR images are helpful due to signal intensity contrast between normal and infiltrated adipose tissue [42]. CT also provides reasonable density contrast in this region.

Perineural Spread

The combination of PET with contrast-enhanced MR is probably the best-suited imaging approach to perineural spread [3, 15, 43]. Features indicating perineural spread are thickening of nerves, contrast enhancement or FDG uptake along nerves, and loss of fat close to or within the foramina of the neurocranium or viscerocranium. The latter may be seen both with CT or MR, but MR is more sensitive. Post-gadolinium images with or without fat suppression may be used therefore. The first approach aims at eliminating the T1w-hyperintense signal of adipose tissue in regions below the skull base. However, this is often limited in the vicinity of air-containing spaces (nasal cavity, paranasal sinuses, mastoid air cells) due to field inhomogeneities elicited by local changes in magnetic susceptibility, e.g., paramagnetic properties of oxygen [44–46]. The second approach (without fat suppression) respects the fact that the neural foramina of the skull base are devoid of fat, and any T1w-hyperintense signal on post-gadolinium images should be regarded as potential tumor spread. Notably, enhancing tumor is seen as

Table 1 TNM staging system of head and neck cancers

		Oral cavity	Oropharynx	Hypopharynx	Larynx			Maxillary sinus	Nasal cavity, ethmoid sinus	Major salivary glands	Nasopharynx
					Supraglottis	Glottis	Subglottis				
Primary tumor	TX	Primary tumor cannot be assessed									
	T0	No evidence of primary tumor									
	Tis	Carcinoma in situ									
	T1	Tumor ≤2 cm (greatest dimension) Hypopharynx: and/or limited to 1 subsite of hypopharynx			Limited to 1 subsite of supraglottis, normal vocal cord mobility	Limited to vocal cords (± anterior or posterior commissure), normal vocal cord mobility T1a, 1 vocal cord; T1b, both vocal cords	Limited to subglottis	Limited to maxillary sinus mucosa	Limited to 1 subsite, ± bone invasion	Tumor ≤2 cm (greatest dimension)	Limited to nasopharynx/ extension to oropharynx or nasal cavity without parapharyngeal extension
	T2	Tumor >2 to ≤4 cm (greatest dimension) Hypopharynx: and/or extension to >1 subsite of hypopharynx or adjacent site			Invasion of more ≥1 supraglottic subsite/glottis/ adjacent region (e.g., base of tongue, vallecular, piriform sinus)	Extends to supraglottis and/or subglottis, vocal cord mobility impaired	Extends to vocal cords (normal or impaired mobility)	Invasion of hard palate, middle nasal meatus, anterior wall of maxillary sinus	Limited to 2 subsites, invasion of adjacent region within nasoethmoidal complex, ± bone invasion	Tumor >2 to ≤4 cm (greatest dimension)	Parapharyngeal extension
	T3	Tumor >4 cm (greatest dimension) Oropharynx: and/or extension to lingual surface of epiglottis Hypopharynx: and/or fixation of hemilarynx, extension to esophagus			Limited to larynx with vocal cord fixation Glottis: also invasion of paraglottic space, inner lamina of thyroid cartilage Supraglottis: also all of above + invasion of postcricoid area, preepiglottic space			Invasion of posterior wall of maxillary sinus, floor or medial wall of orbit, pterygoid fossa, ethmoid sinus, subcutaneous fat	Invasion of floor or medial wall of orbit, maxillary sinus, palate, cribriform plate	Tumor >4 cm (greatest dimension), extraparenchymal extension	Invasion of skull base, paranasal sinuses
	T4										Invasion of hypopharynx, orbit, masticator space (infratemporal fossa), intracranial extension, PNS along cranial nerves
	T4a	Invasion of adjacent structures (e.g., cortical bone, floor of mouth, maxillary sinus, skin of face)	Invasion of larynx, deep extrinsic tongue muscles, medial pterygoid muscle, hard palate, mandible	Invasion of thyroid cartilage, cricoid, hyoid, thyroid gland, central compartment (strap muscles, subcutaneous fat)	Invasion of outer lamina of thyroid cartilage, cricoid, invasion beyond larynx (e.g., trachea, deep extrinsic tongue muscles, strap muscles, thyroid, esophagus)			Invasion of anterior orbit, skin of face, pterygoid plates, sphenoid or frontal sinus Maxillary sinus: and/or infratemporal fossa, cribriform plate Nasal cavity, ethmoid sinus: and/or minimal invasion of anterior cranial fossa		Invasion of the skin, mandible, ear canal, PNS along facial nerve	
	T4b	Invasion of masticator space, pterygoid plates, skull base, encasement of ICA	Invasion of lateral pterygoid muscle, pterygoid plates, lateral nasopharynx, skull base, encasement of ICA	Invasion of prevertebral space, mediastinum, encasement of ICA				Invasion of orbital apex, dura, brain, middle cranial fossa, nasopharynx, clivus, PNS along cranial nerves other than $N.V_2$		Invasion of skull base, pterygoid plate, encasement of ICA	

Regional lymph nodes	NX	Regional lymph nodes cannot be assessed	
	N0	No evidence of regional lymph node metastasis	
	N1	1 ipsilateral lymph node metastasis ≤3 cm (greatest dimension)	Unilateral lymph node metastasis ≤6 cm (greatest dimension) above supraclavicular nodes, unilateral or bilateral retropharyngeal lymph node metastasis ≤6 cm (greatest dimension)
	N2	Ipsilateral, contralateral, bilateral lymph node metastasis >3 to ≤6 cm (greatest dimension)	Bilateral lymph node metastases ≤6 cm (greatest dimension) above supraclavicular nodes
	N2a	1 ipsilateral lymph node metastasis >3 cm to ≤6 cm (greatest dimension)	
	N2b	>1 ipsilateral lymph node metastasis ≤6 cm (greatest dimension)	
	N2c	Bilateral/contralateral lymph node metastasis ≤6 cm (greatest dimension)	
	N3	≥1 lymph node metastasis >6 cm (greatest dimension)	N3a: Lymph node metastasis >6 cm N3b: Supraclavicular lymph node metastasis
Distant sites	M0	No distant metastasis	
	M1	Distant metastasis	

Adapted from Edge et al. [31]
Note: TNM staging of mucosal melanoma and thyroid malignancies is not provided. Major salivary glands include parotid, submandibular, and sublingual glands
ICA internal carotid artery, *PNS* perineural spread

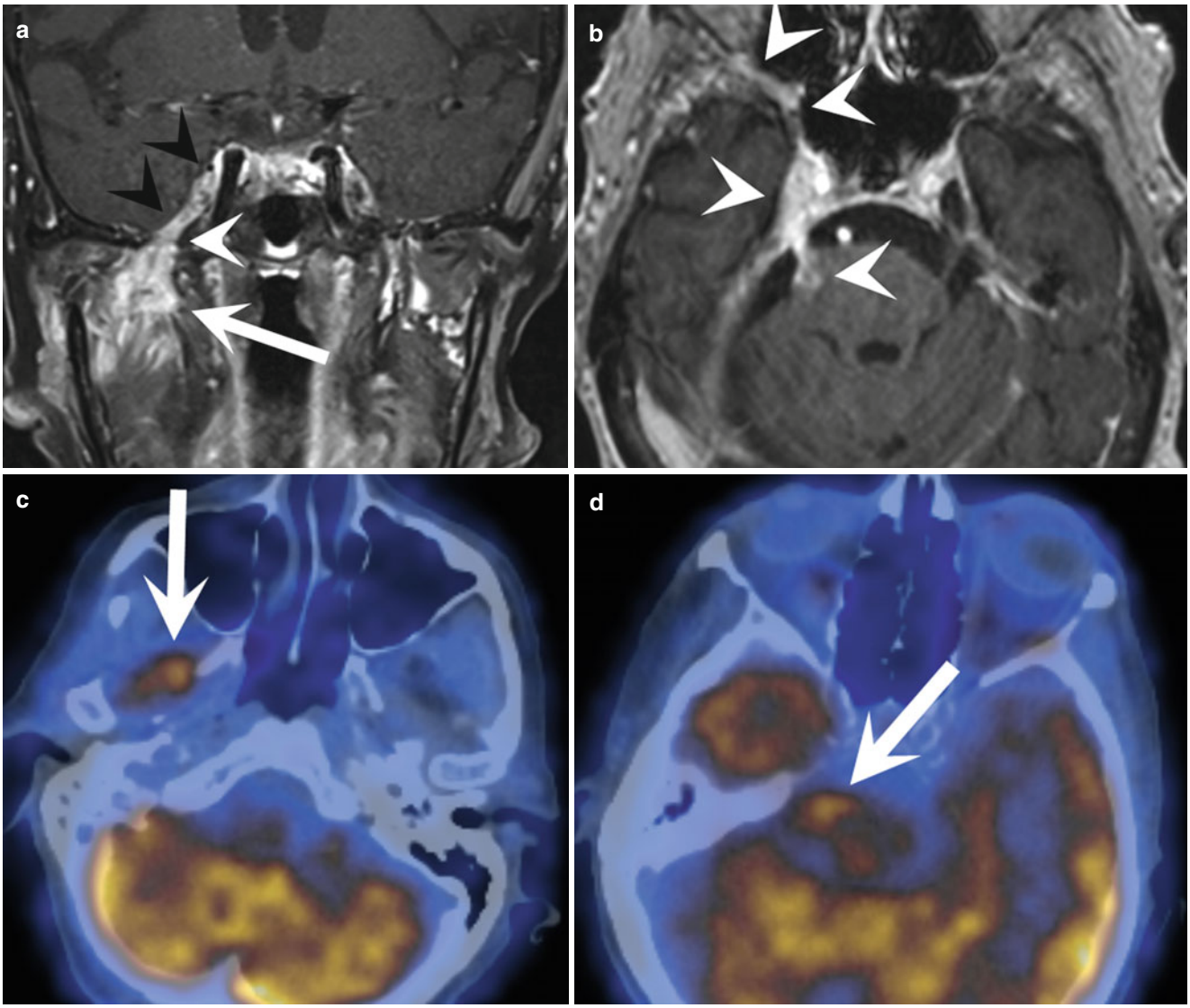

Fig. 7 Patient with right-sided facial nerve palsy and pain in the cheek. Contrast-enhanced T1-weighted fat-suppressed coronal MR image (**a**) shows a tumor in the deep lobe of the right parotid gland (*arrow*). The mandibular nerve is thickened and enhances (*black arrow heads*) along its course from the cavernous sinus via the foramen ovale (white arrow head) to the masticator space. Axial contrast-enhanced T1-weighted coronal MR image (**b**) confirms extensive perineural spread (*arrow heads*) along the trigeminal nerve and its branches, invading the infraorbital canal, foramen rotundum, cavernous sinus, Meckel's cave, prepontine cistern, and mid pons at the level of the root exit zone of the trigeminal nerve. FDG-PET/CT images reveal uptake in the right-sided masticator space, pronounced in the location of the mandibular nerve (**c**, *arrow*), as well as in the right-sided prepontine cistern and pons (**d**, *arrow*)

intermediate to bright signal, and non-infiltrated fat retains its very bright signal, which helps in differentiating both instances despite the absence of fat suppression [44, 45]. Another feature indicating perineural spread is a widening of foramina or canals of the skull base, although this is rather considered a late event [47].

In most patients, perineural spread is already symptomatic by the time it becomes evident on cross-sectional imaging [3, 46]. However, clinically evident perineural spread is often missed by FDG-PET/CT imaging, particularly if the disease burden is relatively small and if the radiologist is not familiar with the anatomy of the skull base and the course of the cranial nerves. The presence of perineural spread in a patient generally predicts a poor outcome (Fig. 7). Although adenoid cystic carcinoma is notorious for its propensity to spread along nerves, due to the overwhelming predominance of squamous cell histology in head and neck cancer (more than 95 %), perineural spread is most commonly seen with squamous cell carcinoma.

Perineural spread refers to the macroscopic extension of tumor along a nerve and does necessarily imply growth along the perineurium itself [3]. The nerve serves as a highway and allows the tumor, representing a hitchhiker, to travel away from its original site, taking an unexpected route that may

lead to distant sites, sometimes far beyond the region of planned surgical resection or irradiation [3, 44, 48]. This may alter or even foil the treatment plan. In the head and neck, perineural spread most often occurs along major branches of the trigeminal nerve (maxillary nerve, foramen rotundum; mandibular nerve, foramen ovale; inferior alveolar nerve, mandibular canal) and facial nerve (stylomastoid foramen), with the auriculotemporal nerve (behind the neck of the mandible) representing a shortcut between the mandibular nerve and the facial nerve as well as the glossopharyngeal nerve. Perineural spread may occur in an antegrade fashion, in a retrograde fashion, or in both fashions at the same time [45, 46, 48]. If advanced perineural spread is encountered, sometimes contiguous meningeal infiltration is seen, starting at the involved skull base foramina, or even direct infiltration of the brainstem at the level of the root entry/exit zones (Fig. 7).

The coexistence of imaging signs of accessory nerve infiltration, such as asymmetry of the sternocleidomastoid muscles and the trapezius muscles, and recurrent laryngeal nerve involvement, such as asymmetry of the vocal cords and lack of FDG uptake in phonatory muscles of the affected side, or vagus nerve involvement, such as unilateral relaxation of the soft palate, should prompt the search for a central lesion that could cause simultaneous accessory nerve and vagus nerve palsy (Fig. 4). Such lesions most of the time are lymph node metastases with extracapsular extension below the skull base. Sometimes, a nasopharyngeal cancer directly infiltrates this deep. Another possibility would be a bone metastasis extending into the jugular foramen. Primary lesions arising at the level of the jugular foramen (glomus tumos, schwannomas, meningiomas) occasionally elicit such symptoms. The constellation of palsies of the accessory nerve, vagus nerve, and glossopharyngeal nerve is termed Vernet syndrome; the latter palsy (N.IX) usually yields no specific imaging signs and is unapparent. If also the hypoglossal nerve is involved, this is then termed Collet-Sicard syndrome. One-sided atrophy and/or fatty degeneration of the tongue represents the imaging correlates for unilateral hypoglossal nerve palsy.

Orbital Invasion

Such is assumed with obliteration of the orbital fat planes or with contrast enhancement or FDG uptake within the orbital adipose tissue. One important pitfall here is spillover of FDG activity from the external ocular muscles, especially if patients did not close their eyes during uptake and acquisition or when a mismatch of PET and CT or MR images is present [3]. Another uncommon pitfall in irradiated or postoperative patients is myositis, which may also lead to a thickening, contrast enhancement and FDG uptake of external ocular muscles (Fig. 8). Lytic destruction of the medial wall or floor of the orbit also suggests orbital invasion, but due to the thin bone there, might be difficult to differentiate from bone atrophy due to tumoral compression, if no soft tissue mass is seen extending beyond the osseous confines into the orbit. Notably, it should be differentiated if only the medial orbital wall is invaded or if there is invasion of the anterior orbit or even tumor extent into the apex, with the latter item indicating T4b stage. Further differentiation into extraconal or intraconal disease and relation of tumor to the optic nerve represent valuable information for the referring clinician.

Bone Infiltration

This is seen by erosion of bone on CT; by loss of fat-equivalent signal intensity or density on MR or CT, respectively; and by contrast enhancement on CT or MR [49]. Focal FDG uptake of bone usually also indicates bone infiltration, but might also be seen in instances of postradiogenic osteonecrosis. Generally, bone infiltration is best assessed with thin-slice CT images, reconstructed with a sharp kernel in bone window display. As said above, bone infiltration by a tumor might be hard to appreciate in regions where the bone is thin and when no soft tissue mass is seen extending beyond the bone. Invasion of the medullary cavity of bone is easily assessed with MR due to its intrinsic high soft tissue contrast that visualizes changes of signal intensity, with fatty marrow being replaced by T1w-hypointense and T2w-hyperintense tumor. However, superficial erosion of bony cortex is difficult to determine with conventional MR pulse sequences due to the paucity of hydrogen molecules in this tissue. The event of PET/MR has stimulated the demand for MR pulse sequences capable of exactly delineating bony cortex for attenuation correction purposes. Such novel MR pulse sequences often use extremely short echo times and are termed ultrashort echo time (UTE) sequences or zero echo time (ZTE) sequences [50–53].

Skull Base Invasion

Both MR and CT are widely used to address skull base invasion, however, with different advantages and disadvantages. Due to the anatomy of the skull base, erosion of the bone is sometimes missed on CT imaging, while MR may be more sensitive and show signal changes in the spongiosa induced by tumor. Another advantage of MR is the absence of beam-hardening artifacts elicited by skull base bones [54–56]. On the other hand, MR might be falsely negative where the skull base is thin and no cancellous bone exists, whereas CT shows lytic changes of the thin cortical bone. Contrast enhancement and FDG uptake of the skull base may also be noted. Spillover of activity from FDG-avid brain is considered an important pitfall here [3]. Other findings indicating skull base invasion are widened foramina and canals.

Infiltration of the Dura

A nodular thickening of the dura, contrast enhancement, or FDG uptake of the dura may indicate dural infiltration by a tumor. Linear thickening or contrast enhancement might also be seen as a reaction to contiguous tumor after radiation therapy, or after surgery in the vicinity of the

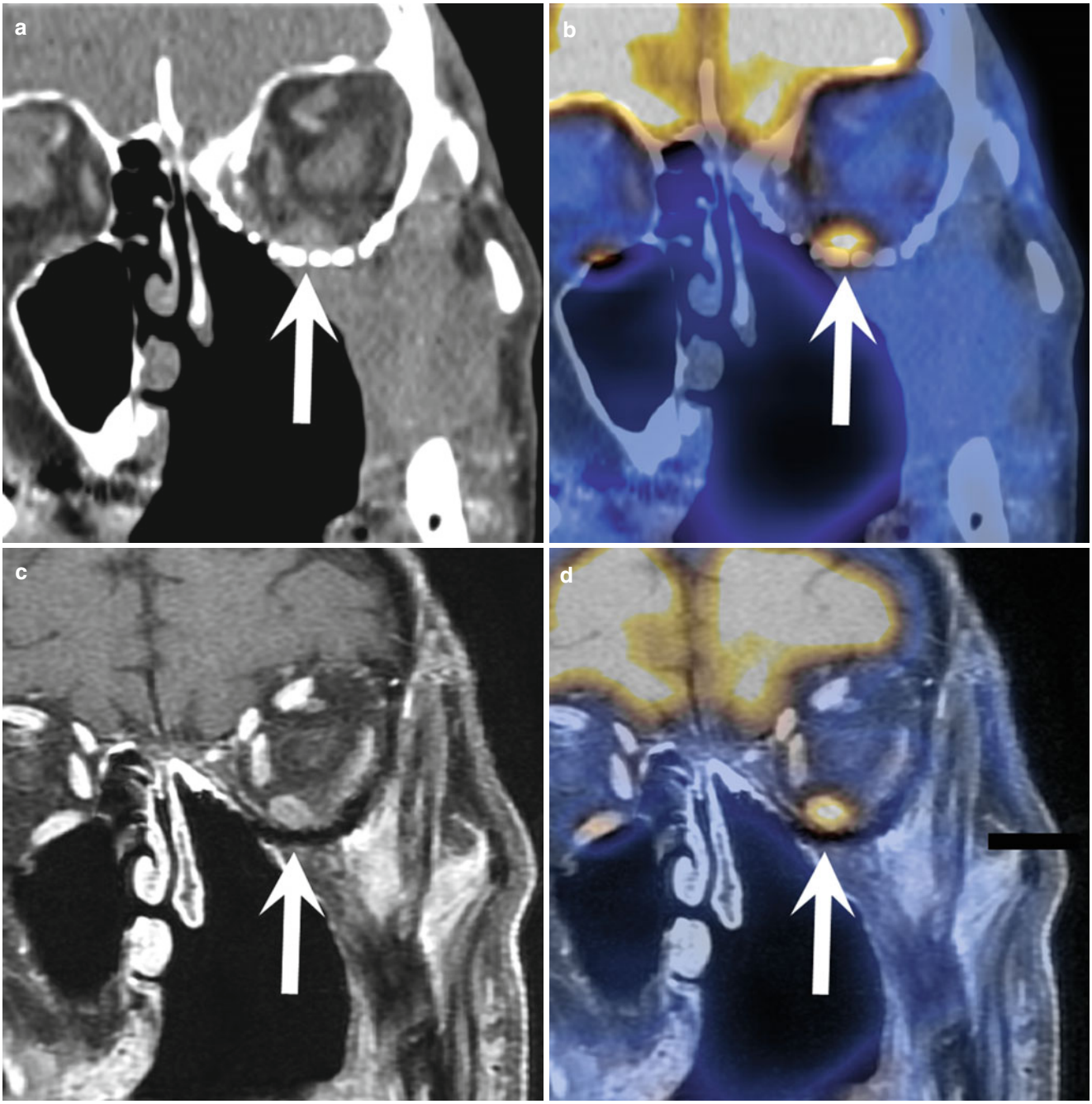

Fig. 8 Follow-up imaging after radiotherapy and reconstruction of the floor of the left orbit, which was infiltrated by a maxillary sinus carcinoma. An FDG-avid mass is seen in the orbit right above the reconstructed floor with surrounding stranding of the intraconal and extraconal adipose tissue on coronal CT image (**a**, *arrow*) and coronal FDG-PET/CT image (**b**, *arrow*). Contrast-enhanced fat-suppressed coronal MR image (**c**, *arrow*) and FDG-PET/MR image (**d**, *arrow*) lead to the diagnosis of myositis of the inferior rectus muscle and no evidence of local tumor recurrence along the reconstructed orbital floor

surgical access path. More widespread nodular dural enhancement is usually seen with infectious, inflammatory, granulomatous, and idiopathic causes of pachymeningitis or with normal pressure hydrocephalus, which might incidentally coexist in head and neck cancer patients and represent a differential diagnosis to dural involvement by a tumor. Dural infiltration is best assessed using contrast-enhanced MR. Due to the close relationship of dura and FDG-avid brain, PET may have difficulties in recognizing increased FDG uptake of the dura (Fig. 9). Close to the skull base, CT is oftentimes limited by beam-hardening artifacts [54–56].

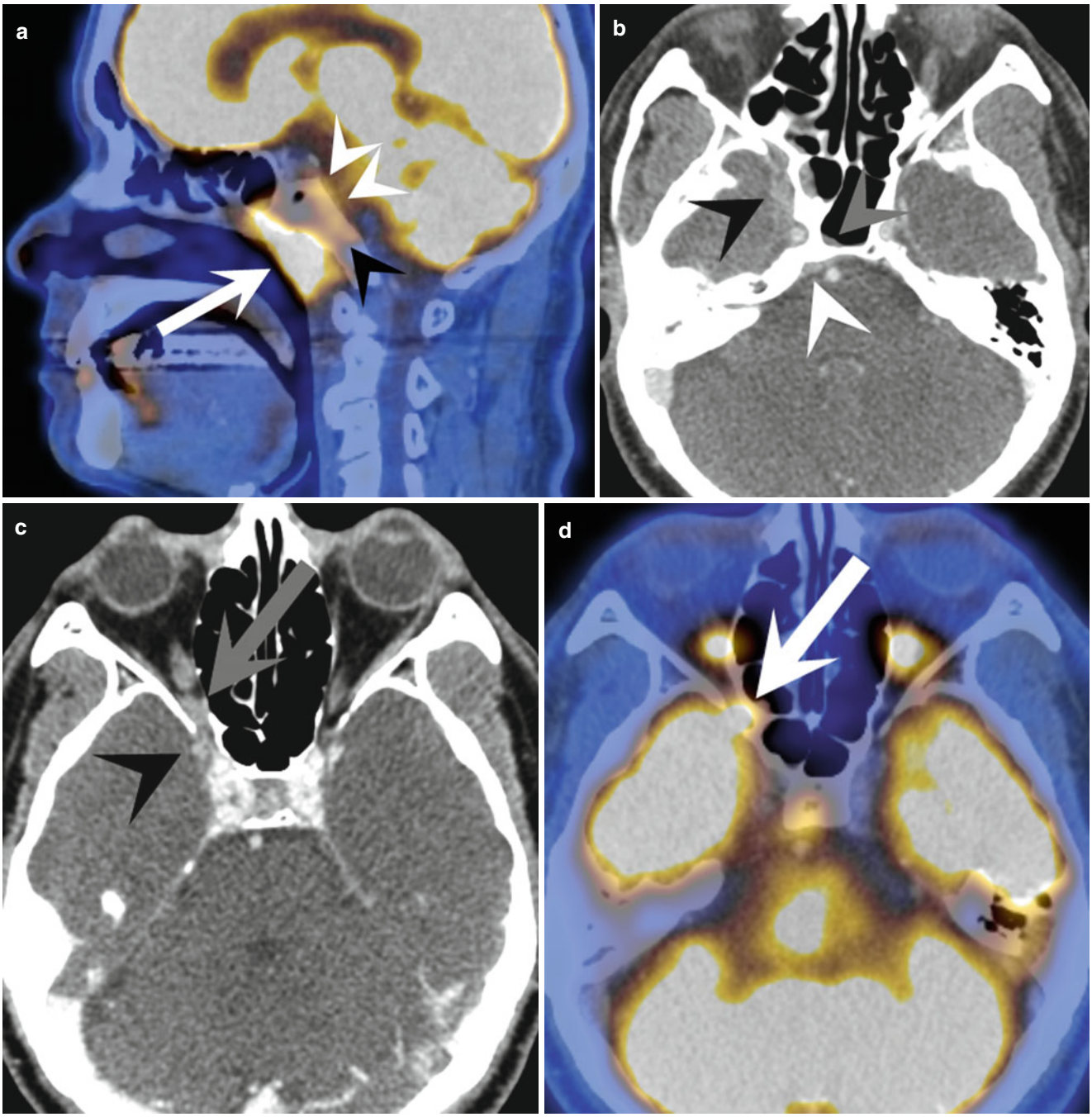

Fig. 9 Patient with EBV-associated poorly differentiated nasopharyngeal carcinoma. Sagittal contrast-enhanced FDG-PET/CT image (**a**) shows the tumor (*arrow*) extending from the nasopharynx via the clivus (*black arrow head*) to the epidural space in retroclival location (*white arrow heads*). Retroclival epidural invasion is also seen on axial contrast-enhanced CT image (**b**, *white arrow head*), as well as extension into the sphenoid sinus (*gray arrow head*) and dural infiltration in the middle cranial fossa (*black arrow head*), lateral and inferior to the cavernous sinus. Axial contrast-enhanced CT image (**c**) (a few slices above the plane of image b) reveals that the temporal dural infiltration (*arrow head*) is in continuation with the foramen rotundum and inferior orbital fissure, where tumor is seen extending into the orbit (*arrow*). Intraorbital extension on the right side is also appreciated on axial contrast-enhanced FDG-PET/CT image (**d**) as FDG-avid mass (*arrow*). However, dural invasion is obscured by activity spillover from FDG-avid brain

Invasion of the Brachial Plexus

Thickening of nerves, obliteration of fat between trunks, divisions, and cords of the plexus, as well as contrast enhancement and FDG uptake along nerves might indicate tumor extending into the brachial plexus. Contrast-enhanced MR (or PET/MR) is the modality of choice.

Sites and Subsites in the Head and Neck

Besides the extension into the deep, i.e., the infiltration of neighboring anatomical structures and spaces, also the longitudinal extension of tumor into other sites or subsites of the head and neck is important for staging and pretherapeutic assessment.

Almost all mucosal sites of the head and neck have subsites, whose infiltration impacts on the T stage (Fig. 10).

The oral cavity has nine distinct subsites: the upper lip, the lower lip, the anterior two thirds of the tongue (posterior one third is an oropharyngeal subsite), the floor of the mouth, the upper alveolar ridge, the lower alveolar ridge, the retromolar trigone, the hard palate, and the buccal mucosa. Some authors address the lips and alveolar ridges as single subsites each, which makes a total of seven subsites. The size of the tumor mainly defines the T stage, whereas the involvement of subsites plays a role in surgical planning (Table 1).

The oropharynx comprises five subsites: the posterior one third of the tongue including the tongue base, the soft palate including the uvula, the palatine tonsils together with the tonsillar pillars, the posterior and lateral oropharyngeal wall, and the valleculae. Some authors also consider the lingual surface of the epiglottis part of the oropharynx. As in the oral cavity, tumor size matters most in the T staging, while the involvement of subsites impacts on surgical planning (Table 1).

The situation is different in the hypopharynx. Here, invasion of subsites is critical for accurate T staging (Table 1). The hypopharynx has six subsites: the left and right piriform sinus, the postcricoid area (the pharyngoesophageal junction), the left and right lateral hypopharyngeal wall, and the posterior hypopharyngeal wall.

The supraglottic larynx has five distinct subsites: the vestibular folds (false vocal cords) and the sinus of Morgagni (upper laryngeal ventricle), the arytenoid cartilages, the suprahyoid portion of the epiglottis, the infrahyoid portion of the epiglottis, and the aryepiglottic folds.

In the glottis, there are three subsites: the true vocal cords together with the glottis muscles, the anterior commissure, and the posterior commissure.

The subglottis is the larynx portion inferior to the true vocal cords, extending from 5 mm below the free margin of the true vocal cords to the inferior margin of the cricoid cartilage. The subglottis has no separate subsites.

In the nasal cavity and paranasal sinuses, subsites are the septum, the floor, the lateral wall and the vestibule of the nasal cavity, the right and left maxillary sinus, and the right and left ethmoid sinus. The lateral wall of the nasal cavity includes the three turbinates, the ostiomeatal complex, and the nasolacrimal duct.

In the nasopharynx, subsites are not important for the T staging, but play a role in presurgical assessment. Subsites of the nasopharynx are the vault, the posterior nasopharyngeal wall, and the lateral nasopharyngeal wall, which consists of the torus tubarius (eustachian tube opening) anteriorly and the pharyngeal recess (fossa of Rosenmüller) posteriorly.

N Staging

Nodal Levels

The presence and extent of nodal metastases directly affect patient management [3].

On cross-sectional imaging, nodal levels in the neck are assigned according to the classification of Som et al., which represents an imaging-based correlation with clinically based nodal classifications [57]. Relevant anatomical structures, which serve as orientation for level borders, are the jugular fossa, the inferior border of the corpus of the mandible, the mylohyoid muscle, the anterior belly of the digastric muscle, the posterior boundary of the submandibular gland, the internal jugular vein, the common carotid artery and internal carotid artery, the lower border of the hyoid bone, the anterior and posterior boundary of the sternocleidomastoid muscle, the anterior boundary of the anterior scalene muscle, the lower margin of the cricoid cartilage, the upper margin of the clavicle, and the top of the manubrium sterni.

Fig. 10 Patient with clinical suspicion of a carcinoma of the tongue on the left side. Sagittal FDG-PET MIP image (**a**) shows an FDG-avid lesion (*arrow*) in the oral cavity. Axial FDG-PET/CT image (**b**) confirms the presence of an FDG-avid tumor (*arrow*) in the sublingual space the left side. The true extent of the tumor (*arrow heads*) is somewhat hard to identify on the contrast-enhanced CT image (**c**). Contrast-enhanced CT (**d**) image at the level of the body of the hyoid bone reveals size asymmetry of the submandibular glands (*arrows*), but no pathologic FDG uptake is seen on corresponding FDG-PET/CT image (**e**, *arrows*). The extent of the tumor in the tongue and sublingual space is clearly better identified on axial fat-suppressed T2-weighted MR image (**f**, *arrow heads*); the lingual septum is preserved. Axial and coronal fat-suppressed T2-weighted MR images (g and h, respectively) at the level of the sublingual glands shows dilation of Wharton's duct on the left side (*arrow*) (**h**). This is suggestive for tumor extension into the floor of the mouth, as seen on coronal fat-suppressed T2-weighted MR image (**i**) which reveals the craniocaudal dimension of the tumor (*arrow heads*) arising from the sublingual space (*arrow*). This was a sublingual carcinoma stage T2, extending into the tongue. Infiltration of the floor of the mouth would render a tongue carcinoma stage T4a

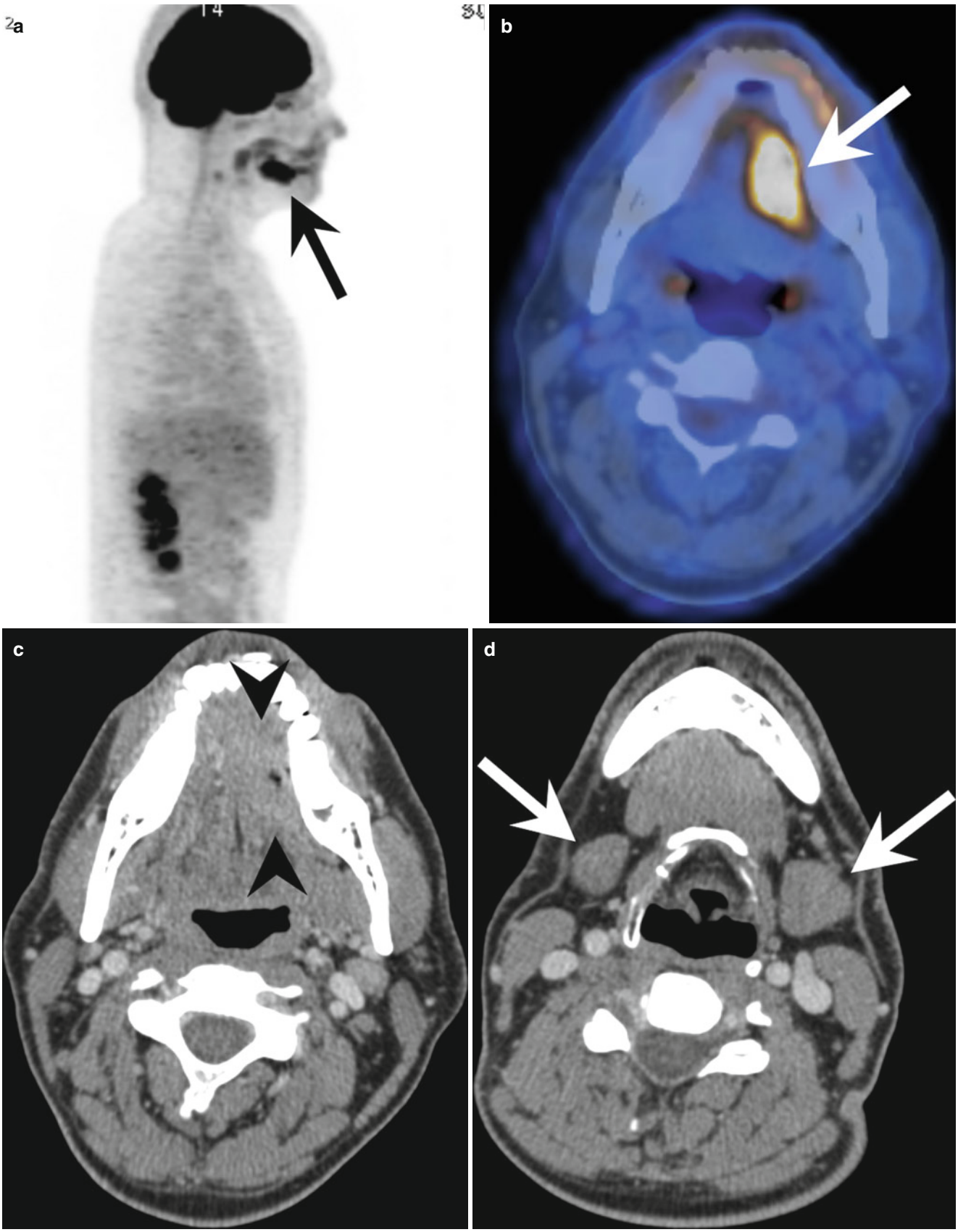
a
b
c
d

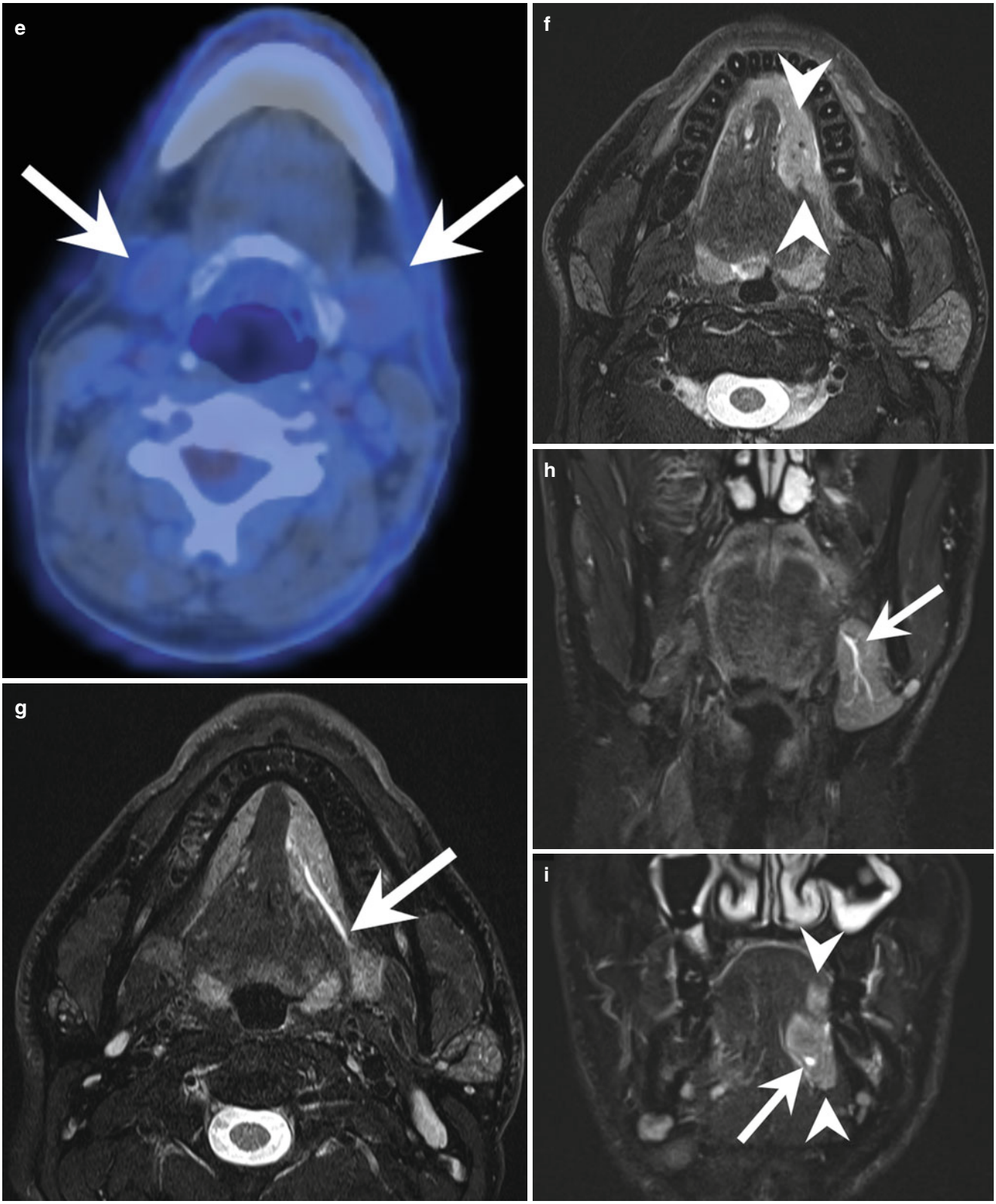

Fig. 10 (continued)

Level I: These nodes are located below the mylohyoid muscle and above the inferior margin of the hyoid. The posterior boundary of the submandibular gland represents the posterior border of level I. Level IA nodes (submental nodes) are found around the midline between the anterior bellies of both digastric muscles. Level IB nodes (submandibular nodes) are located lateral to the anterior bellies of both digastric muscles.

Level II: These nodes are part of the internal jugular chain which is also referred to as deep cervical lymph node chain. Level II extends from the base of the skull unto the inferior border the hyoid bone. The anterior border of level II is the posterior boundary of the submandibular glands, and its posterior border is represented by the posterior boundary of the sternocleidomastoid muscle. Level II is divided into IIA and IIB by the accessory nerve; since this structure is not identified on imaging, the internal jugular vein serves as an alternative. Level IIA nodes are located anteriorly, laterally, or medially to the internal jugular vein. Level IIB nodes are located posteriorly to the internal jugular vein unless inseparable, then being considered level IIA nodes by most authors. Some authors consider retropharyngeal nodes as part of level IIA.

Level III: Between the inferior margin of the hyoid bone and the inferior margin of the cricoid cartilage, the internal jugular chain or deep cervical lymph node chain continues in level III. The posterior boundary of the sternocleidomastoid muscle represents the posterior border of level III, and its medial border is defined by the medial margins of the common carotid artery and internal carotid artery. These two arteries also represent the anterior border of level III.

Level IV: From below the inferior margin of the cricoid cartilage unto the superior border of the clavicle, the internal jugular chain or deep cervical lymph node chain continues in level IV. As with level III, the medial and anterior borders of level IV are defined by the margins of the common carotid artery. The posterior border of level IV is defined by the oblique line extending from the posterior edge of the sternocleidomastoid muscle to the posterior edge of the anterior scalene muscle.

Level V: This level contains the posterior neck triangle lymph nodes. Some authors divide it into VA and VB with respect to the inferior margin of the cricoid cartilage, although this is usually not important for surgery. Level V extends behind levels II–IV from the skull base to the level of the clavicle.

Level VI: This level contains pretracheal, paratracheal and prelaryngeal (Delphian) nodes, which are located anterior to the visceral space. Level VI is located anterior to levels III and IV, being separated by the internal carotid artery and common carotid artery. It extends from the inferior margin of the hyoid bone to the top of the manubrium sterni.

Level VII: Lymph nodes in this level are located in the superior mediastinum between the two common carotid arteries, and below the top of the manubrium sterni.

Some important nodal groups are not included in this system, such as the intraparotid lymph nodes, the preauricular lymph nodes, and the facial lymph nodes.

Implications for Nodal Staging

Nodal levels play an important role in pretherapeutic planning, but are not part of the TNM staging system. With the exception of nasopharyngeal cancer, the exact anatomical distribution of nodal metastases in the neck is not important for the N stage. The presence of supraclavicular (considered level IV by most authors) lymph node metastases indicates an N3 stage in nasopharyngeal cancer. In all other carcinomas, only size (smaller than 3 cm, between 3 and 6 cm, larger than 6 cm), number, and laterality (ipsilateral, contralateral, bilateral) of nodal metastases define the N stage (Table 1).

Oral cavity carcinomas mainly metastasize to lymph nodes in levels I through III. Drainage from the lip is bilateral. Level IA nodes receive lymphatic afferences from the central part of the lower lip, the apex of the tongue, and the floor of the mouth. Their drainage is to level IB nodes and level IIA nodes.

The tributaries of level IB are the cheek, the side of the nose, the region of the canthus, the lips except the medial part of the lower lip, the alveolar ridges, the hard palate, and the anterior two thirds of the lateral aspect of the tongue. Carcinomas arising in the retromolar trigone and floor of the mouth have the highest predilection of nodal involvement (approximately 50 %), followed by the oral part of the tongue (approximately 40 %) [58]. Nodal involvement is least common in cancers of the lip.

Oropharyngeal carcinomas disseminate usually to the internal jugular chain (in levels II and III) and retropharyngeal lymph nodes. Overall, two thirds of patients with oropharyngeal carcinomas present with cervical lymph node metastases, with the base of the tongue having the highest frequency, followed by the palatine tonsils, the oropharyngeal walls, and the soft palate and uvula [3, 58].

The hypopharynx has a rich lympathic network and drains through the thyrohyoid membrane to level IIA and level III nodes and to level V nodes to some less extent. The posterior pharyngeal wall typically tributes to lymph nodes below the jugulodigastric node. If the tumor involves the lowest portion of the hypopharynx, the pharyngoesophageal junction, lymphatic spread may occur to paratracheal (level VI) nodes.

Nodal drainage of the larynx varies by site. The supraglottis is derived from the buccopharyngeal anlage and has a rich lymphatic network. The glottis and subglottis are derived from tracheobronchial buds and have fewer lymphatic vessels [3]. Therefore, lymph node metastases are more often found with supraglottic tumors (more than 50 % have positive nodal stage,

20 % have bilateral nodal involvement), whereas the majority of glottic tumors present with stage N0 (Nodal involvement in stage T1 tumors, <2%; T2, 5% T3, 15–20 %; T4, 20–30 %). The main lymphatic pathway of the supraglottis is to levels II through IV. Since the true vocal cords are vastly devoid of lymphatics, nodal spread generally does not occur until the tumor has extended into the supraglottis or subglottis. In the subglottis there are one anterior lymphatic pedicle and two posterior lymphatic pedicles. The anterior one drains through the cricothyroid membrane into level III and IV or to level VI (prelaryngeal and pretracheal nodes). The posterior chain drains through the cricotracheal membrane to paratracheal lymph nodes (level VI).

Carcinomas in the nasal cavity have an incidence of approximately 10 % of nodal metastases at the initial presentation. Drainage of the vestibule is to level I nodes and facial and preauricular nodes. The paranasal sinuses are poor of lymphatic vessels. Nodal spread occurs usually not until the tumor has invaded the surrounding tissue. The first lymphatic station is the retropharyngeal chain.

In the nasopharynx, the vast majority of tumors present with lymph node metastases (approximately 90 %), which are bilateral in about half of tumors. The main drainage occurs to retropharyngeal lymph nodes.

Tumors arising in the parotid gland metastasize to intraparotid and periparotid lymph nodes, followed by an involvement of levels I through III. Submandibular gland malignancies mainly metastasize to levels I and II, followed by level III.

References

1. Pulte D, Brenner H (2010) Changes in survival in head and neck cancers in the late 20th and early 21st century: a period analysis. Oncologist 15(9):994–1001
2. Studer G, Linsenmeier C, Riesterer O et al (2013) Late term tolerance in head neck cancer patients irradiated in the IMRT era. Radiat Oncol 8:259
3. Huellner MW, Kuhn FP, Curtin HD (2015) FDG-PET/CT and FDG-PET/MR imaging in head and neck cancer. In: von Schulthess GK (ed) Molecular anatomic imaging: PET/CT, PET/MR and SPECT CT. Wolters Kluwer, Philadelphia, pp 341–361
4. Queiroz MA, Huellner MW (2015) PET/MR in cancers of the head and neck. Semin Nucl Med 45(3):248–265
5. Loeffelbein DJ, Souvatzoglou M, Wankerl V et al (2014) Diagnostic value of retrospective PET-MRI fusion in head-and-neck cancer. BMC Cancer 14:846
6. Loeffelbein DJ, Souvatzoglou M, Wankerl V et al (2012) PET-MRI fusion in head-and-neck oncology: current status and implications for hybrid PET/MRI. J Oral Maxillofac Surg Off J Am Assoc Oral Maxillofacial Surg 70(2):473–483
7. Queiroz MA, Hullner M, Kuhn F et al (2014) Use of diffusion-weighted imaging (DWI) in PET/MRI for head and neck cancer evaluation. Eur J Nucl Med Mol Imaging 41(12):2212–2221
8. Allal AS, Slosman DO, Kebdani T, Allaoua M, Lehmann W, Dulguerov P (2004) Prediction of outcome in head-and-neck cancer patients using the standardized uptake value of 2-[18F]fluoro-2-deoxy-D-glucose. Int J Radiat Oncol Biol Phys 59(5):1295–1300
9. Allal AS, Dulguerov P, Allaoua M et al (2002) Standardized uptake value of 2-[(18)F] fluoro-2-deoxy-D-glucose in predicting outcome in head and neck carcinomas treated by radiotherapy with or without chemotherapy. J Clin Oncol Off J Am Soc Clin Oncol 20(5):1398–1404
10. Goerres GW, Haenggeli CA, Allaoua M et al (2000) Direct comparison of F-18-FDG PET and ultrasound in the follow-up of patients with squamous cell cancer of the head and neck. Nuklearmedizin Nucl Med 39(8):246–250
11. Brun E, Kjellen E, Tennvall J et al (2002) FDG PET studies during treatment: prediction of therapy outcome in head and neck squamous cell carcinoma. Head Neck 24(2):127–135
12. Halfpenny W, Hain SF, Biassoni L, Maisey MN, Sherman JA, McGurk M (2002) FDG-PET. A possible prognostic factor in head and neck cancer. Br J Cancer 86(4):512–516
13. Minn H, Lapela M, Klemi PJ et al (1997) Prediction of survival with fluorine-18-fluoro-deoxyglucose and PET in head and neck cancer. J Nucl Med Off Publ Soc Nucl Med 38(12):1907–1911
14. Schwartz DL, Rajendran J, Yueh B et al (2004) FDG-PET prediction of head and neck squamous cell cancer outcomes. Arch Otolaryngol Head Neck Surg 130(12):1361–1367
15. Kuhn FP, Hullner M, Mader CE et al (2014) Contrast-enhanced PET/MR imaging versus contrast-enhanced PET/CT in head and neck cancer: how much MR information is needed? J Nucl Med Off Publ Soc Nucl Med 55(4):551–558
16. Gunzinger JM, Delso G, Boss A et al (2014) Metal artifact reduction in patients with dental implants using multispectral three-dimensional data acquisition for hybrid PET/MRI. EJNMMI Phys 1(1):102
17. Khafif A, Schneebaum S, Fliss DM et al (2006) Lymphoscintigraphy for sentinel node mapping using a hybrid single photon emission CT (SPECT)/CT system in oral cavity squamous cell carcinoma. Head Neck 28(10):874–879
18. Even-Sapir E, Lerman H, Lievshitz G et al (2003) Lymphoscintigraphy for sentinel node mapping using a hybrid SPECT/CT system. J Nucl Med Off Publ Soc Nucl Med 44(9):1413–1420
19. Haerle SK, Strobel K, Ahmad N, Soltermann A, Schmid DT, Stoeckli SJ (2011) Contrast-enhanced (1)(8)F-FDG-PET/CT for the assessment of necrotic lymph node metastases. Head Neck 33(3):324–329
20. Krogdahl AS (1979) Carcinoma occurring in branchial cleft cysts. Acta Otolaryngol 88(3–4):289–295
21. Kendi AT, Magliocca K, Corey A et al (2015) Do 18F-FDG PET/CT parameters in oropharyngeal and oral cavity squamous cell carcinomas indicate HPV status? Clin Nucl Med 40(3):e196–e200
22. Corey AS, Hudgins PA (2012) Radiographic imaging of human papillomavirus related carcinomas of the oropharynx. Head Neck Pathol 6(Suppl 1):S25–S40
23. Puri SK, Fan CY, Hanna E (2003) Significance of extracapsular lymph node metastases in patients with head and neck squamous cell carcinoma. Curr Opin Otolaryngol Head Neck Surg 11(2):119–123
24. Hirabayashi H, Koshii K, Uno K et al (1991) Extracapsular spread of squamous cell carcinoma in neck lymph nodes: prognostic factor of laryngeal cancer. Laryngoscope 101(5):502–506
25. Carter RL, Barr LC, O'Brien CJ, Soo KC, Shaw HJ (1985) Transcapsular spread of metastatic squamous cell carcinoma from cervical lymph nodes. Am J Surg 150(4):495–499
26. Johnson JT, Barnes EL, Myers EN, Schramm VL Jr, Borochovitz D, Sigler BA (1981) The extracapsular spread of tumors in cervical node metastasis. Arch Otolaryngol 107(12):725–729
27. Coatesworth AP, MacLennan K (2002) Squamous cell carcinoma of the upper aerodigestive tract: the prevalence of microscopic

extracapsular spread and soft tissue deposits in the clinically N0 neck. Head Neck 24(3):258–261
28. Stolzmann P, Veit-Haibach P, Chuck N et al (2013) Detection rate, location, and size of pulmonary nodules in trimodality PET/CT-MR: comparison of low-dose CT and Dixon-based MR imaging. Invest Radiol 48(5):241–246
29. Raad RA, Friedman KP, Heacock L, Ponzo F, Melsaether A, Chandarana H (2015) Outcome of small lung nodules missed on hybrid PET/MRI in patients with primary malignancy. J Magn Reson Imaging JMRI. doi:10.1002/jmri.25005
30. Chang ST, Nguyen DC, Raptis C et al (2015) Natural history of preoperative subcentimeter pulmonary nodules in patients with resectable pancreatic adenocarcinoma: a retrospective cohort study. Ann Surg 261(5):970–975
31. Edge SB, American Joint Committee on Cancer (2010) AJCC cancer staging manual, 7th edn. Springer, New York
32. Righi PD, Kelley DJ, Ernst R et al (1996) Evaluation of prevertebral muscle invasion by squamous cell carcinoma. Can computed tomography replace open neck exploration? Arch Otolaryngol Head Neck Surg 122(6):660–663
33. Loevner LA, Ott IL, Yousem DM et al (1998) Neoplastic fixation to the prevertebral compartment by squamous cell carcinoma of the head and neck. AJR Am J Roentgenol 170(5):1389–1394
34. Yousem DM, Hatabu H, Hurst RW et al (1995) Carotid artery invasion by head and neck masses: prediction with MR imaging. Radiology 195(3):715–720
35. Yu Q, Wang P, Shi H, Luo J (2003) Carotid artery and jugular vein invasion of oral-maxillofacial and neck malignant tumors: diagnostic value of computed tomography. Oral Surg Oral Med Oral Pathol Oral Radiol Endodont 96(3):368–372
36. Wagner M, Bjerkvig R, Wiig H et al (2012) Inflamed tumor-associated adipose tissue is a depot for macrophages that stimulate tumor growth and angiogenesis. Angiogenesis 15(3):481–495
37. Manzoor NF, Russell JO, Bricker A et al (2013) Impact of surgical resection on survival in patients with advanced head and neck cancer involving the carotid artery. JAMA Otolaryngol Head Neck Surg 139(11):1219–1225
38. Yousem DM, Gad K, Tufano RP (2006) Resectability issues with head and neck cancer. AJNR Am J Neuroradiol 27(10):2024–2036
39. Kuno H, Onaya H, Fujii S, Ojiri H, Otani K, Satake M (2014) Primary staging of laryngeal and hypopharyngeal cancer: CT, MR imaging and dual-energy CT. Eur J Radiol 83(1):e23–e35
40. Zbaren P, Caversaccio M, Thoeny HC, Nuyens M, Curschmann J, Stauffer E (2006) Radionecrosis or tumor recurrence after radiation of laryngeal and hypopharyngeal carcinomas. Otolaryngol Head Neck Surg Off J Am Acad Otolaryngol Head Neck Surg 135(6):838–843
41. Chu MM, Kositwattanarerk A, Lee DJ et al (2010) FDG PET with contrast-enhanced CT: a critical imaging tool for laryngeal carcinoma. Radiographics Rev Publ Radiol Soc North Am Inc 30(5):1353–1372
42. Loevner LA, Yousem DM, Montone KT, Weber R, Chalian AA, Weinstein GS (1997) Can radiologists accurately predict preepiglottic space invasion with MR imaging? AJR Am J Roentgenol 169(6):1681–1687
43. Paes FM, Singer AD, Checkver AN, Palmquist RA, De La Vega G, Sidani C (2013) Perineural spread in head and neck malignancies: clinical significance and evaluation with 18F-FDG PET/CT. Radiographics Rev Publ Radiol Soc North Am Inc 33(6):1717–1736
44. Curtin HD (2004) Detection of perineural spread: fat suppression versus no fat suppression. AJNR Am J Neuroradiol 25(1):1–3
45. Curtin HD (1998) Detection of perineural spread: fat is a friend. AJNR Am J Neuroradiol 19(8):1385–1386
46. Gandhi D, Gujar S, Mukherji SK (2004) Magnetic resonance imaging of perineural spread of head and neck malignancies. Top Magn Reson Imaging TMRI 15(2):79–85
47. Frunza A, Slavescu D, Lascar I (2014) Perineural invasion in head and neck cancers – a review. J Med Life 7(2):121–123
48. Moonis G, Cunnane MB, Emerick K, Curtin H (2012) Patterns of perineural tumor spread in head and neck cancer. Magn Reson Imaging Clin North Am 20(3):435–446
49. Abd El-Hafez YG, Chen CC, Ng SH et al (2011) Comparison of PET/CT and MRI for the detection of bone marrow invasion in patients with squamous cell carcinoma of the oral cavity. Oral Oncol 47(4):288–295
50. Delso G, Zeimpekis K, Carl M, Wiesinger F, Hullner M, Veit-Haibach P (2014) Cluster-based segmentation of dual-echo ultrashort echo time images for PET/MR bone localization. EJNMMI Phys 1(1):7
51. Delso G, Wiesinger F, Sacolick LI et al (2015) Clinical evaluation of zero-echo-time MR imaging for the segmentation of the skull. J Nucl Med Off Publ Soc Nucl Med 56(3):417–422
52. Wiesinger F, Sacolick LI, Menini A et al (2015) Zero TE MR bone imaging in the head. Magn Reson Med Off J Soc Magn Reson Med Soc Magn Reson Med. doi:10.1002/mrm.25545
53. Cabello J, Lukas M, Forster S, Pyka T, Nekolla SG, Ziegler SI (2015) MR-based attenuation correction using ultrashort-echo-time pulse sequences in dementia patients. J Nucl Med Off Publ Soc Nucl Med 56(3):423–429
54. Rasch C, Keus R, Pameijer FA et al (1997) The potential impact of CT-MRI matching on tumor volume delineation in advanced head and neck cancer. Int J Radiat Oncol Biol Phys 39(4):841–848
55. Sakata K, Hareyama M, Tamakawa M et al (1999) Prognostic factors of nasopharynx tumors investigated by MR imaging and the value of MR imaging in the newly published TNM staging. Int J Radiat Oncol Biol Phys 43(2):273–278
56. Mukherji SK, Wolf GT (2003) Evaluation of head and neck squamous cell carcinoma after treatment. AJNR Am J Neuroradiol 24(9):1743–1746
57. Som PM, Curtin HD, Mancuso AA (1999) An imaging-based classification for the cervical nodes designed as an adjunct to recent clinically based nodal classifications. Arch Otolaryngol Head Neck Surg 125(4):388–396
58. Trotta BM, Pease CS, Rasamny JJ, Raghavan P, Mukherjee S (2011) Oral cavity and oropharyngeal squamous cell cancer: key imaging findings for staging and treatment planning. Radiographics Rev Publ Radiol Soc North Am Inc 31(2):339–354

Integrated Imaging of Thyroid Disease

Michael P. Wissmeyer

Introduction

Since the thyroid and the parathyroid glands can be affected by a variety of different benign and malignant pathologies, both structural and molecular imaging modalities, some of them combined in hybrid modalities, contribute significantly to establish the final diagnosis. Furthermore, they are part of routine follow-up in thyroid disease, especially in differentiated thyroid cancer. However, precise knowledge of the molecular features of the underlying disease is crucial for the correct choice of the imaging modality and the radiopharmaceutical when using molecular imaging such as planar scintigraphy, SPECT/CT, or PET/CT.

Benign Thyroid Disease

Ultrasound

After anamnesis, clinical examination, and assessment of blood levels of the most important thyroid parameters (TSH, free T4), ultrasound is the first imaging modality to be performed, independent whether the diagnosis is normothyroid goiter, hypothyroidism, or hyperthyroidism. It allows for morphologic assessment, for volume measurements, and for analysis of vascularization of the whole thyroid gland and of thyroid nodules when present. Solid nodules can furthermore be assessed for presence of echocomplexity, calcifications, pathologic perfusion patterns, and irregular boundaries which are important attributes in discrimination of probably benign from potentially malignant lesions. Depending on the underlying disease, thyroid or nodular tissue may be iso- (e.g., adenoma), hyper- (e.g., adenoma or scar tissue), or hypoechogenous (liquid, inflammation, carcinoma). Diffuse hypervascularization is observed in inflammatory conditions, especially in Graves' disease. Focal hypervascularization can be found in hyperfunctioning adenomas as well as in lesions suspicious for malignancy. Nowadays, the ultrasound findings of normothyroid nodular goiter should be reported according to the TI-RADS (thyroid imaging reporting and data system) criteria [1, 2]. This reporting system also includes measurement of stiffness of thyroid nodules using strain or shearwaves (ultrasound elastography) [3, 4]. Furthermore, the head and neck lymph node basins should be evaluated routinely, especially in case of suspicious thyroid nodules, since ultrasound may detect macroscopically visible lymph node metastases already in early stages of thyroid carcinoma (Table 1).

Thyroid Scintigraphy

Depending on clinical suspicion, blood samples, ultrasound findings, and potential therapeutic pathways, thyroid scintigraphy is the tool of choice for further functional evaluation of thyroid disease. Due to its excellent sensitivity, in suspected congenital thyroid agenesis, hypothyroidism or ectopic thyroid tissue, thyroid scintigraphy is the exam of first choice, even before ultrasound. In hyperthyroidism, thyroid scintigraphy enables to discriminate between the different

Table 1 TI-RADS scoring system and risk of malignancy

TI-RADS score	Description	Risk of malignancy (%)
1	Normal scan	0
2	Benign lesions	0
3	Very probably benign lesions	0.25
4A	Low suspicion of malignancy	6
4B	High suspicion of malignancy	69
5	Clearly malignant	100

M.P. Wissmeyer
Department of Nuclear Medicine, University Hospital of Geneva (HUG), Rue Gabrielle-Perret-Gentil 4, Geneva, GE 1211, Switzerland
e-mail: michael.wissmeyer@hcuge.ch

J. Hodler et al. (eds.), *Diseases of the Brain, Head and Neck, Spine 2016–2019: Diagnostic Imaging*, DOI 10.1007/978-3-319-30081-8_30

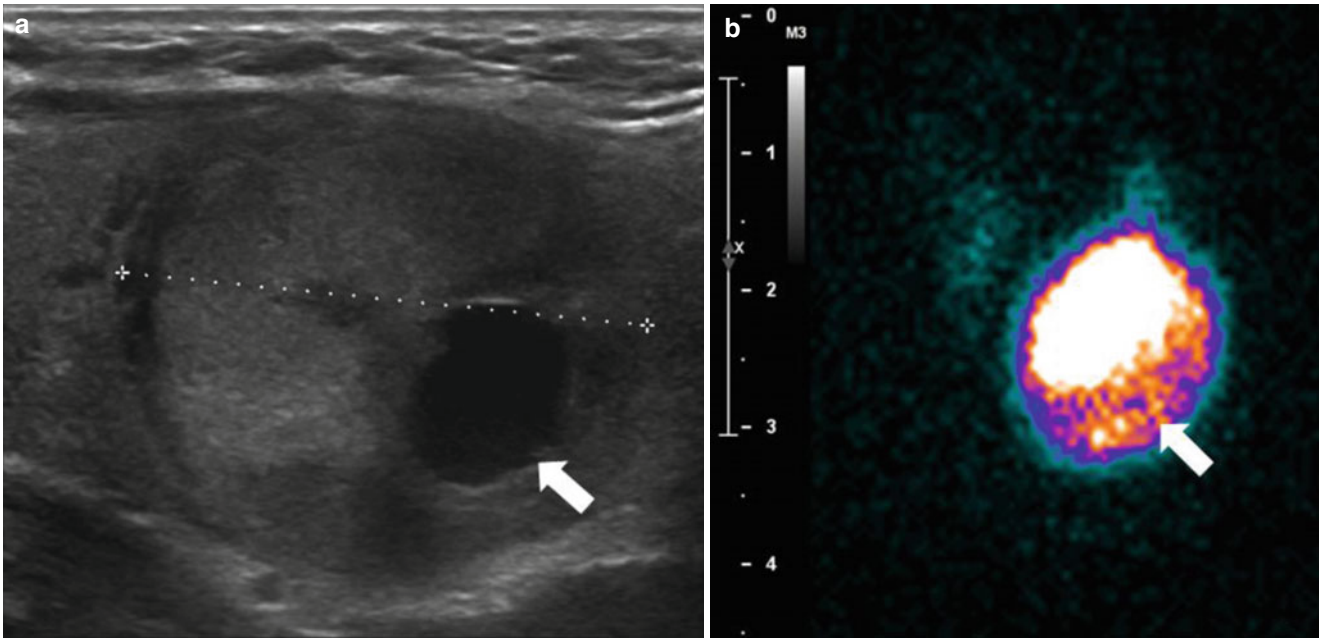

Fig. 1 Sagittal ultrasound (**a**) and planar anterior ^{123}I scintigraphy (**b**) of a hyperfunctioning nodule (adenoma) of the left thyroid gland in a patient presenting with hyperthyroidism. Note the nearly complete functional extinction of the normal thyroid tissue. Furthermore, a liquid part (*arrows*) is present in the inferolateral part of the nodule, visible as an echo-free zone in ultrasound and as "cold" zone in the scintigraphic image

Table 2 Typical scintigraphic patterns of different thyroid conditions

Globally decreased tracer uptake	Focally decreased tracer uptake	Globally increased tracer uptake	Focally increased tracer uptake
Hypothyroidism Thyroiditis Iodine contamination Hyperthyreosis factitia	Nonfunctioning thyroid nodules Thyroid cysts Suppressed normal thyroid in presence of focal autonomy	Disseminated autonomy Graves' disease Lobar autonomy	Uni- or multifocal thyroid autonomy

underlying pathologies such as uni- or multifocal autonomy, disseminated autonomy (Fig. 1), or different presentations of thyroid inflammations which may initially present with hyperthyroid conditions. The typical scintigraphic patterns of the various underlying pathologies are summarized in Table 2. In multinodular goiter, thyroid scintigraphy can be helpful in guidance of fine needle aspiration.

In current clinical practice, thyroid scans are performed using ^{99m}Tc-pertechnetate and ^{123}iodine as specific markers of thyroid function, whereas ^{99m}Tc-MIBI may be used additionally as a nonspecific tumor-seeking agent in patients with normothyroid nodular goiter. Depending on thyroid function, both ^{123}I and ^{99m}Tc-pertechnetate are internalized in the thyroid cells via the Na^+/I^--symporter. ^{123}I is then further metabolized and integrated in the thyroid hormones, whereas ^{99m}Tc-pertechnetate is not metabolized. Usually, images of the thyroid are acquired 20 min after intravenous administration of ^{99m}Tc-pertechnetate and 2 or 24 h after oral administration of very low activities of ^{123}iodine. Ideally, the scans are acquired with a dedicated thyroid gamma camera or, if not available, with a conventional large field of view gamma camera using either pinhole collimators or zoomed images. Most frequently, planar anterior views are acquired. Additionally, right and left oblique views may be obtained for better localization of focally decreased or increased uptake.

In addition to the scintigraphic images, semiquantitative parameters, such as technetium (TcTU) or radioiodine uptake, are routinely calculated. Both parameters are helpful in the differential diagnosis of benign thyroid disease. In case of hyperthyroidism, the maximal thyroid radioiodine uptake in percent of the administered dose is one of the parameters needed to define an individually calculated therapeutic activity of ^{131}I. In case of nodular goiter, nodules presenting with decreased or absent tracer uptake (scintigraphically "cold" nodules), which were classified as solid in ultrasound, can be further evaluated by nonspecific tumor-seeking radiopharmaceuticals (e.g., ^{99m}Tc-MIBI or ^{99m}Tc-tetrofosmin) due to their good sensitivities and negative predictive values for discrimination between benign and malignant lesions [5]. With exception of suspected congenital hypothyroidism (especially suspected ectopic thyroid gland), thyroid scintigraphy should not be performed in hypothyroidism.

PET/CT and SPECT/CT

The value of these hybrid imaging techniques for evaluation of benign thyroid disease is not yet clear and is currently under investigation. First studies showed that PET/CT using ^{18}F-FDG, targeting increased glucose consumption of potentially malignant thyroid nodules, was helpful to better discriminate between benign and malignant lesions and thus avoided non-necessary diagnostic surgery in a significant proportion of the patients [6]. However, there is no role for FDG PET/CT in the assessment of hyper- or hypothyroidism.

Hyperparathyroidism

Once hyperparathyroidism is confirmed by elevated blood levels of parathormone, the standard diagnostic procedure consists from ultrasound of the neck region as well as of planar and tomographic parathyroid scintigraphy. This exam can be performed in double-isotope (^{99m}Tc-pertechnetate or ^{123}I in combination with ^{99m}Tc-MIBI) or single-isotope (dual phase ^{99m}Tc-MIBI) technique. In general, focal ^{99m}Tc-MIBI uptake in the absence of ^{99m}Tc-pertechnetate or ^{123}iodine uptake is diagnostic for parathyroid adenoma or hyperplasia (Fig. 2). However, diagnosis may be difficult in nodular goiter with hypofunctioning, MIBI-positive thyroid nodules or intrathyroid parathyroid adenomas. Independent of the chosen approach, subtraction of the two scans is helpful for better discrimination between normal thyroid tissue and parathyroid adenoma. The use of hybrid SPECT/CT significantly improves precise localization of parathyroid adenomas or hyperplastic parathyroid glands [7]. Additionally, hybrid imaging facilitates planning of the surgical procedure and allows a minimal invasive approach in most cases [8]. In contrary to ultrasound alone, parathyroid scintigraphy allows also for detection and precise localization of ectopic parathyroid adenomas which accounts for up to 8 % of the cases.

Hybrid PET/CT using ^{18}F-fluorocholine, a biomarker of cellular phosphatidylcholine metabolism, appears to be a new and promising diagnostic tool for primary and secondary hyperparathyroidism, especially in patients presenting with negative or discordant ultrasound and scintigraphic results [8–10].

Malignant Thyroid Disease

Differentiated Thyroid Carcinoma (DTC)

Ultrasound

Already in the detection of primary DTC, ultrasound plays an important role. At initial diagnosis, highly suspicious or malignant thyroid nodules typically show the following patterns: the nodules are taller than wide, markedly hypoechogenic, and they present with irregular boundaries, microcalcifications, and a high stiffness in sonoelastography. Besides anamnesis, clinical examination, and determination of blood thyroglobulin levels, ultrasound is an essential part of routine follow-up in DTC. After total thyroidectomy and radioiodine remnant ablation, any vascularized tissue in the thyroid region has to be considered as suspicious for local recurrence. Additionally, any round, hyperechogenic, and hypervascularized lymph node that has lost its typical single sinusoidal vessel has to be considered as suspicious for lymph node metastasis. In doubtful cases, ultrasound-guided fine needle aspiration of suspicious lesions should be performed to confirm the suspicion and initiate adequate treatment (surgery, radioiodine treatment, etc.).

Whole Body Scanning (^{123}I and ^{131}I) Including Hybrid SPECT/CT

Pre-ablative diagnostic whole body scans using low activities of ^{123}I or ^{131}I allow for detection of significant remnant thyroid tissue and occult locoregional and distant metastases. These findings are subject to significantly changing the further management of the patients, e.g., reoperation in order to diminish the amount of remnant thyroid tissue to treat or increase the ^{131}I ablative activity in order to sufficiently treat locoregional and distant metastases [11, 12]. In every case, whole body scans including hybrid SPECT/CT are performed between 4 and 7 days after administration of the ablative activity of ^{131}I. Therefore, ^{131}I can be considered as a theragnostic agent since it its properties allow for a therapeutic and diagnostic use at one time. The post-therapeutic whole body scans are performed in order to determine the definitive amount of remnant thyroid tissue and/or the presence of locoregional or distant metastases. This post-ablation scan serves also for risk stratification and further risk-adapted follow-up and treatments (depending on tumor type and presence or absence of locoregional or distant metastases). Papillary thyroid carcinoma essentially tends to metastasize towards locoregional lymph nodes, whereas follicular thyroid carcinoma additionally tends to spread to distant organs, especially to the lung and to the skeleton. Hybrid SPECT/CT is particularly helpful in discriminating between remnant thyroid tissue, lymph node metastases, and nonspecific radiotracer uptake or retention in the oral cavity, the salivary glands, and the esophagus. Post-therapy whole body scans are repeated after every new radioiodine therapy of iodine-avid tumor manifestations (Fig. 3).

According to ATA (American Thyroid Association) recommendation no. 67, diagnostic whole body scans with a low activity of ^{131}I or, alternatively, ^{123}I may be of value and should be performed 6–12 months after remnant ablation in patients with high or intermediate risk of persistent disease. Furthermore, these diagnostic scans are valuable in patients presenting with antibodies against thyroglobulin or patients who presented extra-thyroid uptake already at the post-ablation whole body scan [13].

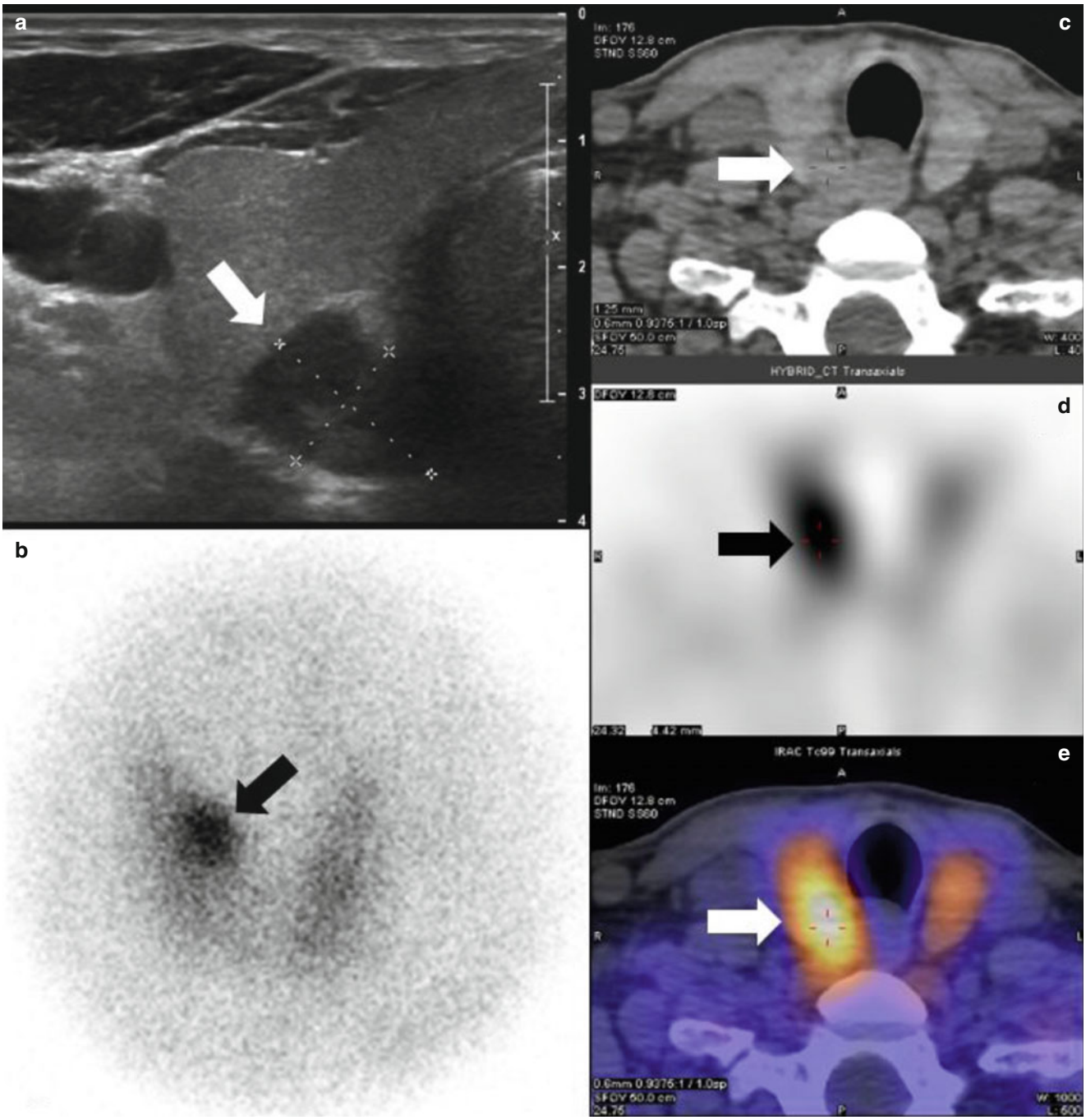

Fig. 2 Ultrasound (**a**), planar ^{99m}Tc-MIBI scintigraphy (**b**), and hybrid ^{99m}Tc-MIBI SPECT/CT (**c**–**e**) of a parathyroid adenoma located behind the right lobe of the thyroid (*arrows*). The transversal ultrasound images demonstrate a hypoechogenous nodular structure; the scintigraphic images show markedly increased tracer uptake in a rather hypodense structure located in between the right thyroid lobe, the trachea, and the esophagus

PET/CT

^{18}F-FDG PET/CT is a very valuable diagnostic tool to assess patients presenting with measurable thyroglobulin, negative neck ultrasound, and negative diagnostic ^{131}I or ^{123}I whole body scan including SPECT/CT, indicating dedifferentiated manifestations of the underlying disease (Fig. 4). Especially, the presence of a low thyroglobulin doubling time is highly predictive of positive FDG PET/CT scans [14]. Also the presence of both differentiated and dedifferentiated manifestations of DTC is possible ("flip-flop phenomenon").

First applications of PET/CT using ^{124}I showed promising results, but due to its limited availability, this tracer is not yet part in the routine workup and follow-up of DTC. The role of PET/MRI in diagnosis and follow-up of thyroid cancer also remains to be investigated.

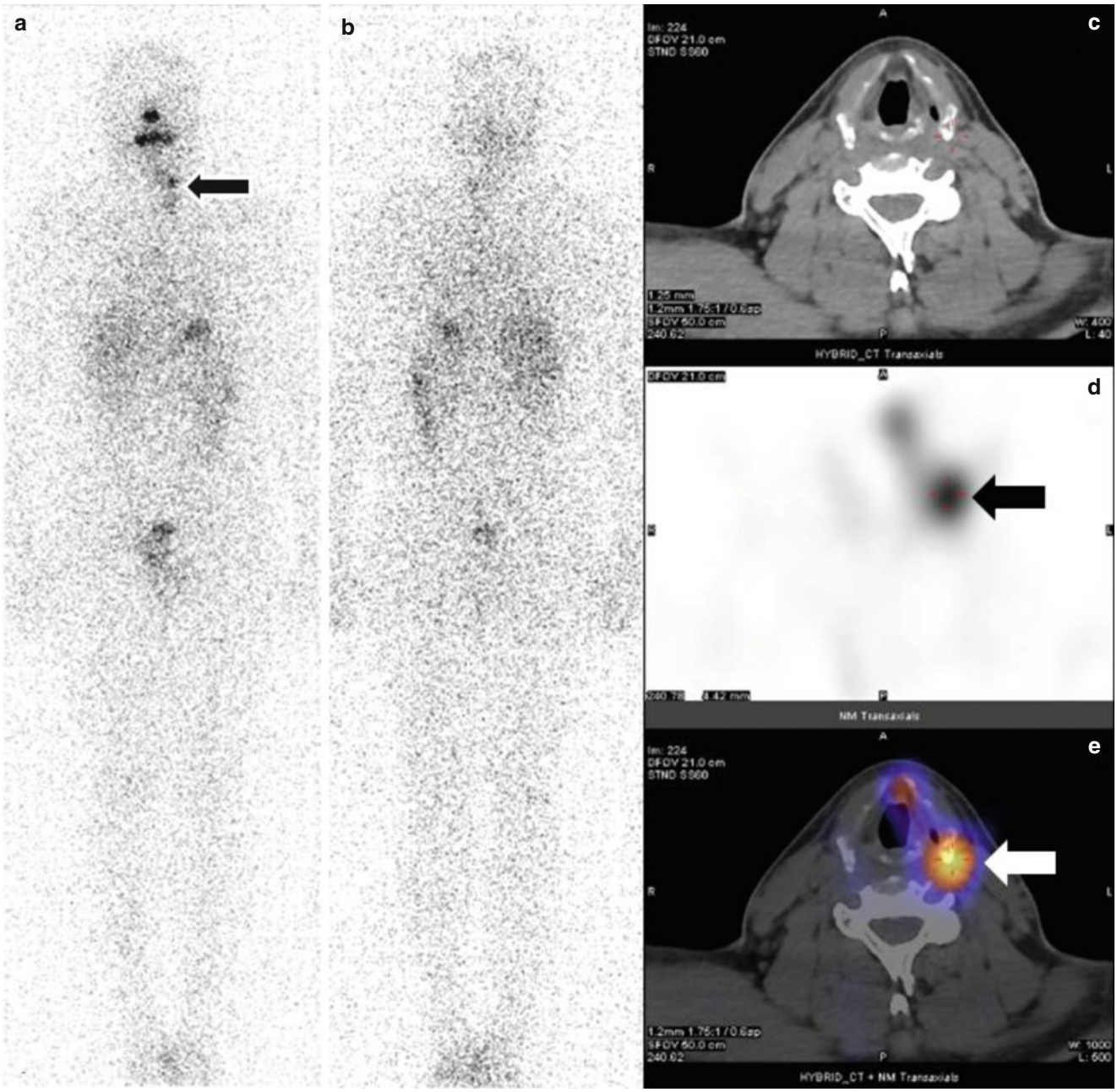

Fig. 3 Diagnostic planar anterior (**a**) and posterior (**b**) ^{131}I whole body images and cervical hybrid SPECT/CT (**c**–**e**) showing local recurrence (*arrows*) in a patient presenting with biochemical relapse of papillary thyroid carcinoma. SPECT/CT enables to discriminate pathologic radiotracer uptake from physiological radiotracer retention in salivary glands, the larynx, and the esophagus

CT and MRI

Since contrast-enhanced CT should not be performed in patients with iodine-avid DTC, native CT does not play a significant role in diagnosis and follow-up. In contrary, native CT is very valuable for attenuation correction and morphologic localization of radiotracer accumulating lesions in hybrid PET/CT and SPECT/CT. In selected cases with nonconclusive findings in hybrid PET/CT and SPECT/CT, the excellent soft tissue contrast of MRI can add valuable additional information. Furthermore, it allows for contrast media administration and thus discrimination of vascular from other structures, especially very small lymph nodes in close proximity of the blood vessels.

Anaplastic Thyroid Carcinoma

Anaplastic thyroid carcinoma is a very aggressive, dedifferentiated entity with a very poor prognosis. Due to its poor grade of differentiation, there is only a very low or even

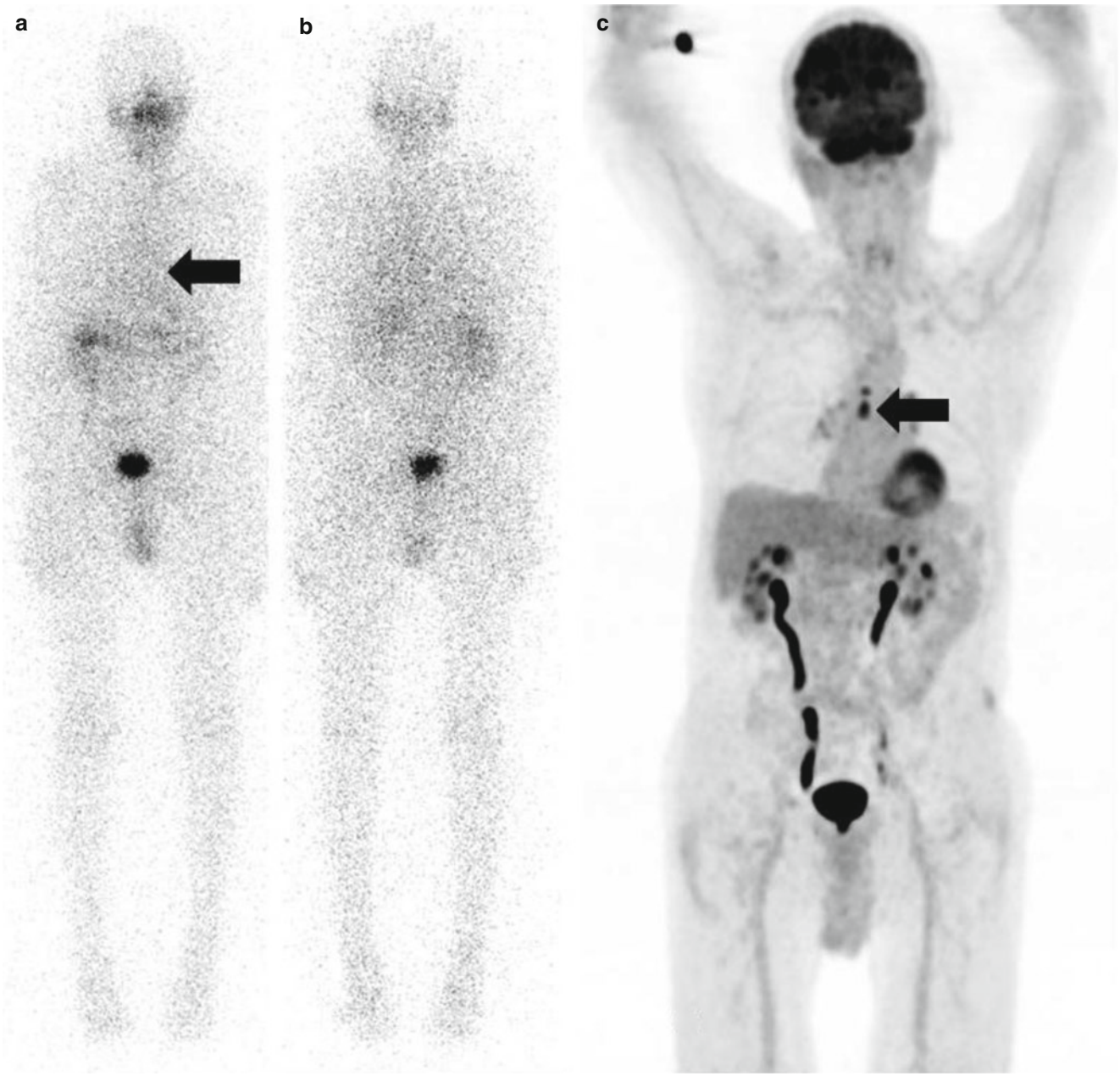

Fig. 4 Planar anterior (**a**) and posterior (**b**) ^{131}I whole body scans and ^{18}F-FDG PET MIP image (**c**) in a patient presenting with biochemical recurrence of papillary thyroid carcinoma. The radioiodine scan is negative, whereas FDG PET shows suspicious tracer uptake in mediastinal lymph nodes (*arrows*)

absent avidity for radioiodine. Remnant ablation using ^{131}I is routinely performed, taking into account the radioiodine avidity of the remnant thyroid tissue and the so-called bystander effect which means an irradiation of non-iodine-avid cells by surrounding iodine-avid cells. However, in the follow-up, neck ultrasound and FDG PET/CT are the imaging modalities of choice. Due to the very low iodine avidity, of the tumor cells even contrast-enhanced CT may be performed in these patients. Whenever possible, surgery is the therapy of choice, followed by external beam irradiation.

Medullary Thyroid Carcinoma (MTC)

Medullary thyroid carcinoma is a rare tumor (accounting for 3% of all thyroid tumors) originating from the calcitonin-producing parafollicular cells of the thyroid. In a significant proportion, especially in hereditary MTC, it is associated with other endocrine neoplasms (especially parathyroid adenoma and pheochromocytoma) which is called multiple endocrine neoplasia type 2. In terms of imaging for the initial diagnostic workup, neck ultrasound plays an important role

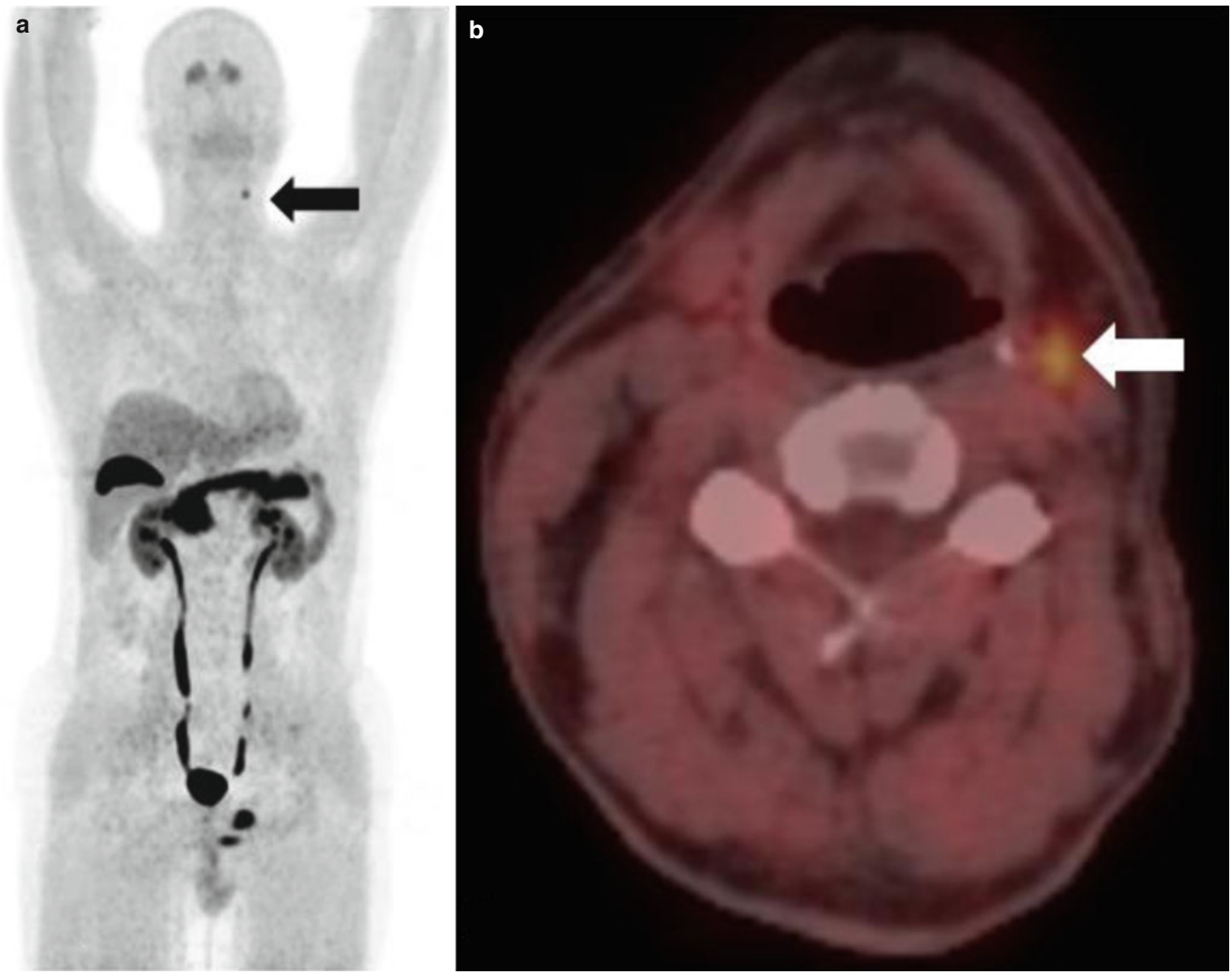

Fig. 5 MIP (**a**) and fused transversal (**b**) ^{18}F-DOPA PET/CT images in a patient presenting with biochemical recurrence of medullary thyroid carcinoma. The PET images nicely show intense tracer uptake a single subcentimetric metastasis in the left cervical lymph node area III

for detection of suspicious thyroid nodules and neck lymph nodes. Structural imaging procedures consist of contrast-enhanced CT and MRI, depending on the body region to scan. Molecular targets for radionuclide imaging are the somatostatin receptors and the APUD (amine precursor uptake and decarboxylation) system which can be addressed with rather low diagnostic performance by hybrid SPECT/CT (^{111}In-octreotide, a somatostatin analogue) and with high diagnostic performance by hybrid PET/CT using ^{68}Ga-DOTA-peptides (somatostatin analogues) or ^{18}F-DOPA (targeting the APUD cell system) [15–17] (Fig. 5). In cases of high-grade tumors, ^{18}F-FDG PET/CT can be used to detect poorly differentiated tumor manifestations.

Conclusion

In addition to clinical and laboratory exams, imaging modalities providing structural (ultrasound), molecular (scintigraphy), and hybrid structural and molecular (SPECT/CT and PET/CT) play an important role in the diagnosis and follow-up of benign and malignant thyroid and parathyroid disease. Ultrasound is a basic imaging modality for any kind of thyroid or parathyroid disorder. Thyroid scintigraphy plays an important role in differential diagnosis and determination of the therapeutic activity of ^{131}I in hyperthyroidism, whereas it is not indicated in most cases of hypothyroidism. In nodular goiter, ^{99m}Tc-MIBI can add useful information and help to advance in diagnostic stratification. Combination of ultrasound and ^{99m}Tc-MIBI scintigraphy represents the standard for localization of orthotopic or ectopic parathyroid adenomas or hyperplastic parathyroid glands. Ultrasound and diagnostic or post-therapeutic whole body scans including hybrid SPECT/CT are the imaging modalities of choice in the follow-up of DTC. Hybrid FDG PET/CT plays an important role in the detection of dedifferentiated manifestations of DTC and in anaplastic

thyroid cancer. New diagnostic molecules for integrated PET/CT are expected to play an important role in the detection of occult parathyroid adenomas (^{18}F-choline) and in the staging and follow-up of medullary thyroid cancer (^{68}Ga-DOTA-peptides, ^{18}F-DOPA). The role of PET/MRI as new integrated imaging modality needs to be investigated. In thyroid ultrasound, the implication of elastography and standardized reporting following the TI-RADS classification are also expected to improve diagnostic accuracy and risk stratification of the patients.

References

1. Horvath E, Majilis S, Rossi R et al (2009) An ultrasonogram reporting system for thyroid nodules stratifying cancer risk for clinical management. J Clin Endocrinol Metab 90:1748–1751
2. Park JY, Lee HJ, Jang HW et al (2009) A proposal for a thyroid imaging reporting and data system for ultrasound features of thyroid carcinoma. Thyroid 19:1257–1264
3. Bamber J, Cosgrove D, Dietrich CF et al (2013) EFSUMB guidelines and recommendations on the clinical use of ultrasound elastography. Part 1: basic principles and technology. Ultraschall Med 34:169–184
4. Cantisani V, Lodise P, Grarhdani H et al (2014) Ultrasound elastography in the evaluation of thyroid pathology. Current status. Eur Radiol 83:420–428
5. Treglia G, Caldarella C, Saggiorato E et al (2013) Diagnostic performance of (99m)Tc-MIBI scan in predicting the malignancy of thyroid nodules: a meta-analysis. Endocrine 44:70–78
6. Vriens D, Adang EM, Netea-Maier RT et al (2014) Cost-effectiveness of FDG-PET/CT for cytologically indeterminate thyroid nodules. J Clin Endocrinol Metab 99:3263–3274
7. Wong KK, Fig LM, Gross MD et al (2015) Parathyroid adenoma localization with 99mTc-sestamibi SPECT/CT: a meta-analysis. Nucl Med Commun 36:363–375
8. Kluijfhout WP, Vorselaars WM, Vriens MR et al (2015) Enabling minimal invasive parathyroidectomy for patients with primary hyperparathyroidism using Tc-99m-sestamibi SPECT-CT, ultrasound and first results of (18)F-fluorocholine PET-CT. Eur J Radiol 84:1745–1751
9. Lezaic L, Rep S, Sever MJ et al (2014) ^{18}F-Fluorocholine PET/CT for localization of hyperfunctioning parathyroid tissue in primary hyperparathyroidism: a pilot study. Eur J Nucl Med Mol Imaging 41:2083–2089
10. Michaud L, Burgess A, Huchet V et al (2014) Is 18F-fluorocholine-positron emission tomography/computerized tomography a new imaging tool for detecting hyperfunctioning parathyroid glands in primary or secondary hyperparathyroidism? J Clin Endocrinol Metab 99:4531–4536
11. Avram AM, Fig LM, Frey KA et al (2013) Preablation 131-I scans with SPECT/CT in postoperative thyroid cancer patients: what is the impact on staging? J Clin Endocrinol Metab 98:1163–1171
12. Chen MK, Yasrebi M, Samii J et al (2012) The utility of I-123 pretherapy scan in I-131 radioiodine therapy for thyroid cancer. Thyroid 22:304–309
13. Alexander EK, Bible KC, Doherty GM et al (2015) American thyroid association management guidelines for adult patients with thyroid nodules and differentiated thyroid cancer. Thyroid. doi:10.1089/thy.2015.0020
14. Giovanella L, Trimboli P, Verburg FA et al (2013) Thyroglobulin levels and thyroglobulin doubling time predict independently a positive 18F-FDG PET/CT scan in patients with biochemical recurrence of differentiated thyroid carcinoma. Eur J Nucl Med Mol Imaging 40:874–880
15. Treglia G, Castaldi P, Villani MF et al (2013) Comparison of different positron emission tomography tracers in patients with recurrent medullary thyroid carcinoma: our experience and a review of the literature. Recent Results Cancer Res 194:385–393
16. Archier A, Heimburger C, Guerin C et al (2015) 18F-DOPA PET/CT in the diagnosis and localization of persistent medullary thyroid carcinoma. Eur J Nucl Med Mol Imaging [Epub ahead of print]
17. Slavikova K, Montravers F, Treglia G et al (2013) What is currently the best radiopharmaceutical for the hybrid PET/CT detection of recurrent medullary thyroid carcinoma? Curr Radiopharm 6:96–105

Part III

Pediatric Radiology Satellite Course “Kangaroo”

Children with Epilepsy: Neuroimaging Findings

W.K. 'Kling' Chong

Introduction

Epilepsy most often begins in childhood and is therefore an important paediatric disorder. Seizures, which are abnormal movements or behaviour which result from abnormal electrical activity in the brain, are a symptom of epilepsy. Not all patients who appear to have seizures have epilepsy. Epilepsy is the group of disorders which are characterised by a tendency for recurrent seizures and are alternatively known as 'seizure disorders'.

Abnormal movements or behaviour without abnormal electrical activity in the brain are considered pseudoseizures or nonepileptic seizures. Seizures may be provoked by trauma, electrolyte imbalance and hypoglycaemia, pyrexia and certain medications.

A good resource for the definition and classification of the different types of epilepsy is the International League Against Epilepsy website (http://www.ilae.org/). It is a particularly important resource because it also includes recommendations for *not* imaging in certain epilepsy syndromes, e.g. in juvenile myoclonic epilepsy. Therefore, it is certainly *not* the case that every child with a seizure or with epilepsy should undergo neuroimaging.

Nevertheless, when neuroimaging is performed, MRI is the modality of choice. Imaging protocols should include sequences in all three planes, ideally volume imaging with both T1 and T2 weighting. Neuroimaging at 3 T may have an advantage over 1.5 T. CT can occasionally be helpful in characterising an abnormality already identified on MR, but should not be used as the primary imaging modality for the investigation of epilepsy.

Many cases with epilepsy have normal brain MRI, even after repeated examination with advanced neuroimaging techniques. This should not be surprising as epilepsy is a functional disorder. The aim for neuroimaging remains the identification of a structural lesion as a potential candidate for the cause of that functional disorder. As well as providing a better understanding of the disease, in some patients this may lead to the offering of surgery for epilepsy as a treatment option to support the more conventional medical therapy.

Some Basic Definitions

Epilepsy is a disease of the brain defined by any of the following conditions:

1. At least two unprovoked (or reflex) seizures occurring >24 h apart
2. One unprovoked (or reflex) seizure and a probability of further seizures similar to the general recurrence risk (at least 60 %) after two unprovoked seizures, occurring over the next 10 years
3. Diagnosis of an epilepsy syndrome

A review of the organisation of the epilepsies is underway, but under the current 2010 revision [2], the terms 'generalised' and 'focal' have been redefined and simplified and the concepts of 'idiopathic', 'symptomatic' and 'cryptogenic' disorders were replaced.

For the practising radiologist, a basic understanding of this classification is helpful particularly when combined with some knowledge of functional neuroanatomy [3].

Generalised seizures are conceptualised as originating from a point and rapidly engaging in bilaterally distributed networks. They can be asymmetric. Focal seizures are conceptualised as originating within networks limited to one hemisphere. It is the author's experience that focal seizures more often have a structural abnormality which is identifiable on neuroimaging.

Epilepsy syndromes organised according to age groups. This is logical because the pattern in which these seizures

W.K. 'Kling' Chong
Radiology, Great Ormond Street Hospital for Children,
Great Ormond Street, London WC1N 3JH, UK
e-mail: kling.chong@gosh.nhs.uk

J. Hodler et al. (eds.), *Diseases of the Brain, Head and Neck, Spine 2016–2019: Diagnostic Imaging*, DOI 10.1007/978-3-319-30081-8_31

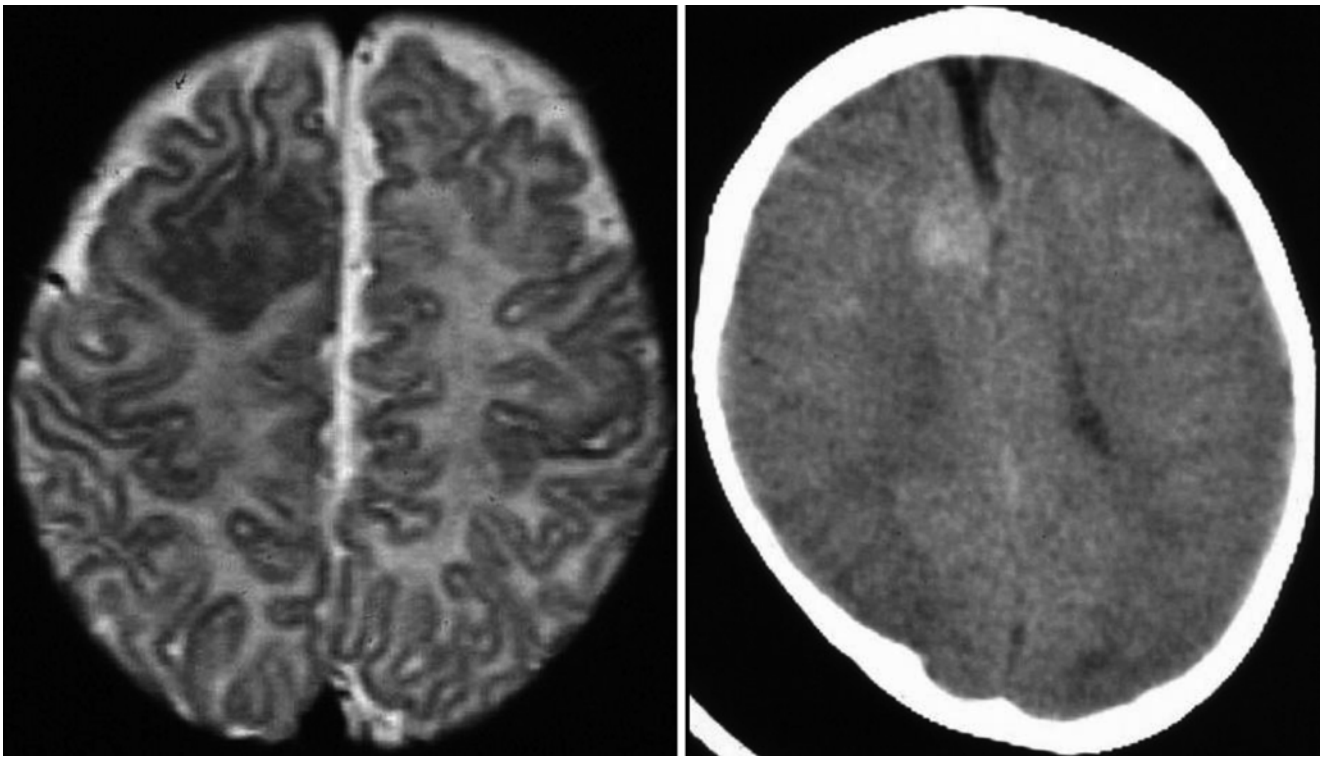

Fig. 1 A focal malformation of cortical development in an infant with focal epilepsy. Early imaging before the brain is myelinated and can sometimes identify lesions more easily. Occasionally, malformations can have dystrophic calcification and be seen on CT

manifest are dependent in part on the degree of development and maturation of the structures of the underlying brain.

Epilepsies may also be organised by their aetiology [3] which provides a convenient format for the descriptions in rest of this syllabus contribution.

Malformations of Cortical Development

Many but not all malformations of cortical development result in a clinical presentation of seizures or epilepsy. The specific entity of focal cortical dysplasia is most often identified as best candidates for epilepsy surgery. Other commonly encountered malformations include polymicrogyria, hemimegalencephaly and neuronal migration disorders [4, 5].

The malformations are usually not small, but they can be difficult to identify because they blend imperceptably with surrounding normal brain tissue. Some malformations are easier to identify when the brain is not fully myelinated (Figs.1 and 2). Others cause focal regions of accelerated myelination as a result of excessive focal seizure activity. The seizures themselves can cause secondary brain changes, so in some cases repeat scanning is required before a lesion can be confidently identified.

Hypothalamic hamartomas can present with a distinct epilepsy syndrome of gelastic seizures, particularly when they involve the mammillary bodies.

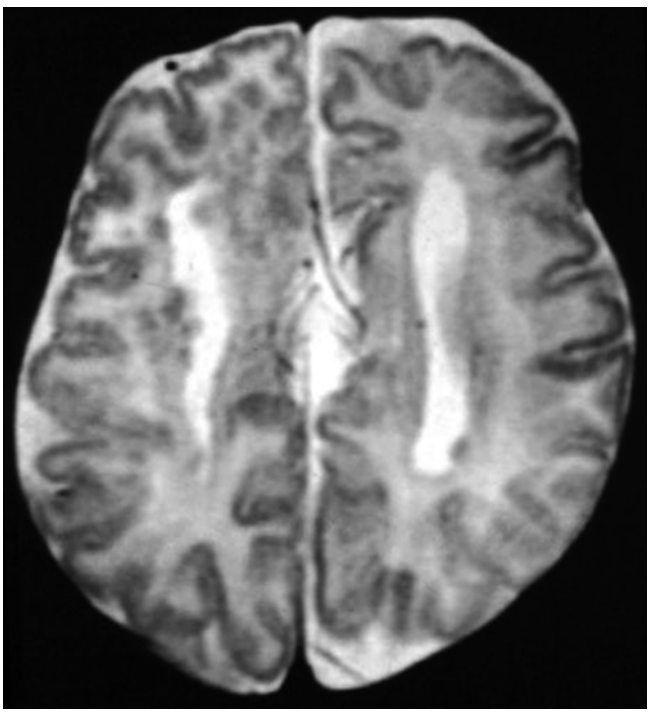

Fig. 2 A girl with agenesis of the corpus callosum and subcortical and subependymal heterotopia in a case of Aicardi syndrome

Neurocutaneous Syndromes

Tuberous sclerosis is a multisystem genetic neurocutaneous syndrome characterised by subependymal hamartomatous nodules, cortical tubers and benign neoplastic lesions (giant cell astrocytomas). The cortical tubers are histopathologically indistinguishable for focal cortical dysplasia type IIb. In the context of imaging for epilepsy surgery, the tubers which are most heavily calcified are the ones considered to be the best candidates for surgery. Neuroimaging is also used for monitoring the progress of any large subependymal nodules at the foramina of Munro, which may progress over time to become giant cell astrocytomas. The latter are benign locally invasive and rarely aggressive tumours which are only found in this syndrome and in this anatomical location.

Patients with unilateral Sturge-Weber syndrome may also be candidates for consideration of epilepsy surgery. The imaging is used for identifying the extent of brain involvement with the pial angioma. It may occasionally be difficult to identify the pial angiomas in neonates and infants [6].

Tumours Causing Epilepsy

There are a few types of tumour which present with epilepsy as the dominant clinical feature and for whom seizure control may be aided by surgery. Some are sufficiently low grade that they may be managed conservatively if their seizures come under control. These include dysembryoplastic neuroepithelial tumours (DNT) and other low-grade glioneuronal tumours characteristically located in the temporal lobes and occasionally parietal lobes.

Immune Epilepsies

Probably the most distinctive immune-mediated epilepsy syndrome is the Rasmussen syndrome, characterised by the onset of intractable often focal motor seizures or epilepsia partialis continua (EPC). The pattern of progressive hemiatrophy on imaging continues after functional hemispherectomy and seizure control.

Infections

These are the commonest causes of epilepsy worldwide, especially in developing countries. For those presenting in the developed world, neurocysticercosis and cerebral toxoplasmosis are important diagnoses to be made. Cerebral tuberculosis, other types of bacterial or viral encephalitis, HIV infection, malaria and other parasites are less often encountered.

Metabolic Epilepsies

In these conditions, the epilepsy is an important part in the manifestation of metabolic imbalance, and early treatment of this improves outcomes. Whilst most have normal imaging, some have characteristic features which may be identifiable on neuroimaging. These include mitochondrial disorders, such as Alpers' syndrome (presenting with status epilepticus or EPC), MELAS or MERRF (presenting as progressive myoclonic epilepsy), and disorders of creatine metabolism which may require the assistance of MR spectroscopy for diagnosis.

Miscellaneous Conditions

Hippocampal sclerosis – this is the most common structural brain abnormality treated with epilepsy surgery in adults. It is also seen in children and such cases also become candidates for surgery, but the incidence is lower. Seizures typically start following a latent period after a febrile convulsion, especially if prolonged (Fig. 3).

Early stroke or vascular injury – a proportion of these patients will present with epilepsy; this is difficult to control. Imaging is used to confirm the underlying diagnosis and in the workup for epilepsy surgery.

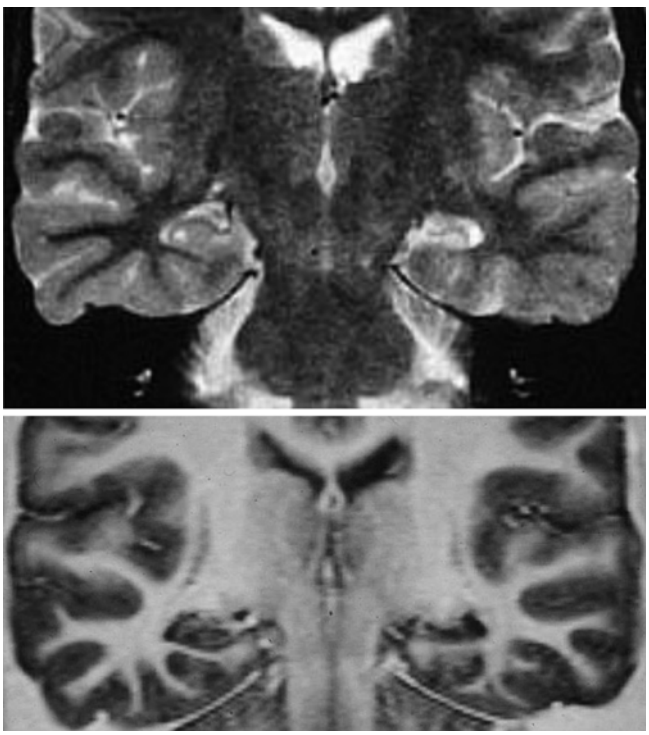

Fig. 3 A typical example of left hippocampal sclerosis

Findings Cause by Seizures or the Consequence of the Treatment of Seizures

Seizures themselves, especially if frequent and intractable, can cause brain changes. Focal signal abnormalities in the splenium are thought to be the result of seizures or the anti-epileptic drugs used to treat them (Fig. 4). Localised brain swelling, oedema and even enhancement have been attributed to seizures.

Detailed neuroimaging is often required in the post-operative assessment following epilepsy surgery, to help determine if an electrical disconnection or resection has been completed [7].

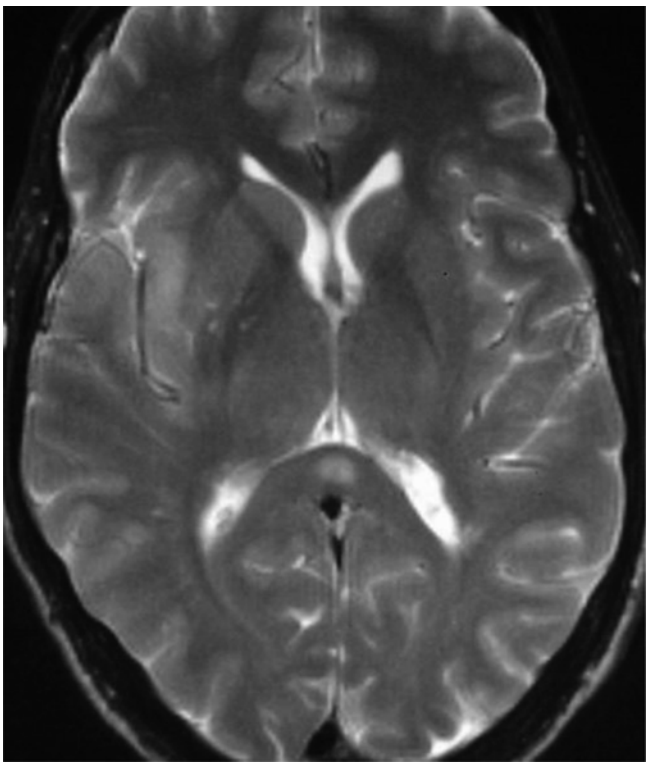

Fig. 4 Focal signal abnormality in the splenium caused by seizures, in a patient with gliomatosis cerebri of the right insular cortex

Summary and Conclusions

Epilepsy is a disorder of brain function. Neuroimaging, particularly MRI, is an invaluable tool in identifying structural abnormalities which may underlie that functional brain disorder and assist with its management, particularly if surgery is being contemplated to assist with medical therapy.

Lesions may be difficult to identify. Detailed and repeat imaging may be required in complex cases of intractable epilepsy.

References

Good General Reading and Reference Text

1. Barkovich AJ, Raybaud C (2011) Pediatric neuroimaging. 5th edn. ISBN/ISSN: 9781605477145

Some Related Peer Reviewed Papers

2. Berg AT, Berkovic SF, Brodie MJ, Buchhalter J, Cross JH, van Emde BW, Engel J, French J, Glauser TA, Mathern GW, Moshé SL, Nordli D, Plouin P, Scheffer IE (2010) Revised terminology and concepts for organization of seizures and epilepsies: report of the ILAE commission on classification and terminology, 2005–2009. Epilepsia 51(4):676–685
3. https://www.epilepsydiagnosis.org/index.html
4. Barkovich AJ, Kuzniecki RI, Jackson GD et al (2005) Developmental and genetic classification for malformations of cortical development. Neurology 65:1873–1887
5. Blumcke I, Thom M, Aronica E et al (2010) The clinicopathological spectrum of focal cortical dysplasias: a consensus classification proposed by an ad hoc task force of the ILAE diagnostic Methods Commission. Epilepsia 1–17
6. Adams ME, Aylett SE, Squier W, Chong W (2009) A spectrum of unusual neuroimaging findings in patients with suspected Sturge-Weber syndrome. AJNR Am J Neuroradiol 30(2):276–281
7. Yoong M, Madari R, Martinos M, Clark C, Chong K, Neville B, Chin R, Scott R (2012) The role of magnetic resonance imaging in the follow-up of children with convulsive status epilepticus. Dev Med Child Neurol 54(4):328–333

Advanced MR Techniques in Pediatric Neuroradiology: What Is Ready for Clinical Prime Time?

P. Ellen Grant

Introduction

For an advanced MR technique to be ready for *clinical* prime time, (1) it must reliably detect abnormalities in individuals, not just provide statistical group differences; (2) processed images must be available rapidly; (3) acquisition times must be reasonable; and (4) time required by professional or supporting staff to create relevant images must be financially sustainable. Also ideally individual differences are visible on an image for the most rapid adaption in clinical practice. In this chapter diffusion imaging, MR spectroscopy, arterial spin labeling, fetal triplane reconstruction, and quantitative T1 and T2 imaging will be discussed, and examples where these sequences have clinical utility in individual pediatric patients will be provided.

Diffusion Imaging

All major vendors provide sequences that perform diffusion-weighted imaging in at least six noncollinear and noncoplanar orientations and provide automatic online reconstruction of the following maps for interpretation:

1. Apparent diffusion coefficient (ADC) maps that provide voxel-based measures of the mean water diffusivity.
2. Fractional anisotropy (FA) maps with intensity representing the degree of coherence of water diffusion with increasing intensity representing greater coherence.
3. Color-coded FA maps representing the primary direction of water diffusion with the convention that blue represents water diffusion in the superior to inferior or inferior to superior direction, red represents left to right or right to left diffusion, and green represents anterior to posterior or posterior to anterior diffusion.
4. Tractography images that provide information on the coherence of water diffusion over many voxels through reconstruction of "tracts." If the same color coding as in the FA maps is used, blue fibers represent primarily projection fibers, red fibers represent primarily interhemispheric connections and fibers, and green fibers represent interhemispheric connections.

There are many different diffusion acquisition schemes and analysis approaches. The most common acquisition scheme used in clinical practice is the acquisition of 6–30 noncollinear and noncoplanar orientations at b values of 1000 s/mm^2 with up to one volume at $b = 0$ s/mm^2 for every six gradient directions. Newer acquisition methods such as simultaneous multislice (SMS) combined with parallel acquisition schemes and high-density phased-array coils at 3 T have significantly decreased acquisition times, allowing 35 gradient directions to be acquired in under 3 min [1]. Additional background on DTI principles can be found in many reviews articles [2–4].

The ability of ADC maps to detect acute ischemic events, metabolic compromise, collections of pus, and tumors with high cellular density in individual patients has been recognized for many years [5, 6]. In general, ADC maps are read visually informed by the individual reader's knowledge of normal ADC values. In infants and young children, the regional variability and normal evolution of ADC values with brain maturation make interpretation of pediatric ADC maps challenging, particularly to those who do not read a high number of pediatric studies. There are references that provide general guidelines for regional ADC values with age, but typically only a few regions are reported or the focus is preterms and the entire reference data sets are not available [7–9]. There are emerging interactive atlases that will provide mean and standard deviations for ADC maps in normal infants and young children

P.E. Grant
Departments of Radiology and Medicine, Boston Children's Hospital and Harvard Medical School,
300 Longwood Ave, Boston, MA 02115, USA
e-mail: Ellen.grant@childrens.harvard.edu

J. Hodler et al. (eds.), *Diseases of the Brain, Head and Neck, Spine 2016–2019: Diagnostic Imaging*, DOI 10.1007/978-3-319-30081-8_32

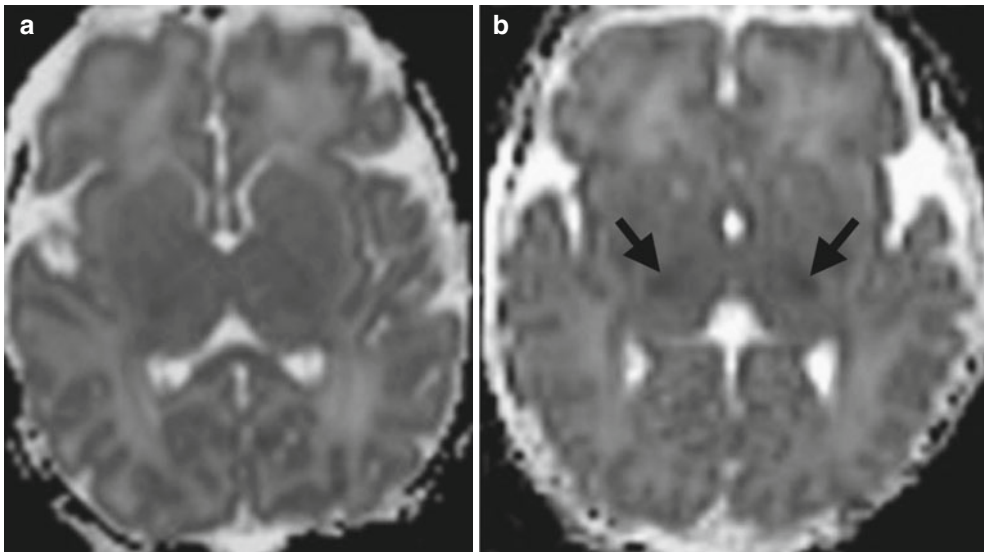

Fig. 1 (**a**) Normal ADC map in a neonate. Note the regional variation in ADC values due to incomplete myelination. (**b**) ADC map in a neonate suffering from hypoxic ischemic encephalopathy (HIE). *Arrows* point to the abnormally low ADC values in the ventrolateral thalamus, a common area of injury when there is a short but significant loss of blood flow and oxygen to the neonatal brain. Note that in the normal neonate, this region is also slightly lower in ADC values than adjacent thalamus making it difficult in subtle cases to determine how low is abnormal

(e.g., http://mi2b2beta.babymri.org/). These interactive, high spatial and temporal density atlases are intended to guide clinical interpretation and help decrease the variance in clinical interpretations by providing a uniform reference standard. Such reference standards become helpful when interpreting neonatal ADC maps for evidence of hypoxic ischemic encephalopathy (Fig. 1).

The clinical interpretation of FA maps is less common but can provide highly relevant clinical information in certain clinical situations. In particular the presence of preserved FA in the context of decreased diffusion indicates preservation of tissue microstructure at the time of the image acquisition [10]. This information can be a helpful hint that a region of decreased diffusion may not be due to an evolving ischemic event but another mechanism such as metabolic compromise (Fig. 2) or tumor infiltration (Fig. 3).

Color FA maps are even less commonly viewed for clinical purposed but are often available for interpretation. These color maps may be helpful when trying to further assess preservation of tissue microstructure or characterize abnormal organization of major white matter tracts and different types of cerebral malformations such as brainstem and corpus callosum abnormalities (Fig. 4).

There are many tools and methods to create tractography images with many vendors now providing tools for tractography reconstruction on the MR console. As a result many radiologists can now easily perform tractography on clinical studies. Controversy over the utility of clinical tractography persists [11], but if the radiologist understands the limitations of the technique and does not over-interpret, useful information may be provided. For example, information regarding the displacement or involvement of specific white matter tracts may be helpful [12] (Figs. 2 and 3).

MR Spectroscopy

Proton (^{1}H) MRS acquisition provides unique information about cerebral metabolites and has been proven useful in many pediatric applications such as hypoxic ischemic encephalopathy, metabolic disorders, tumors, demyelinating disorders, and trauma [13–16] (Fig. 5). The major brain metabolites feasible to assess clinically include myoinositol (mI), choline (Ch), creatine (Cr), glutamine and glutamate (glx), and N-acetylaspartate (NAA) with ratios to Cr as the most common approach. Many abnormal peaks are feasible to detect clinically and include lipids, lactate, glycine, alanine, pyruvate, succinate, valine, acetate, isoleucine, and leucine [16]. Absolute quantification of peaks requires additional technical expertise and additional software (most often LC Model) not available on clinical scanners. Separation of glutamine and glutamate requires longer scan times but is feasible; however, GABA requires much longer scan times at lower resolution as well as special editing techniques and is therefore not currently feasible for routine clinical studies.

Although now FDA approved, clinical application of MR spectroscopy has been limited by the ability to sample the same region in different imaging sessions, the lack of easy quantification, the lack of normal regional data at different TEs and different ages, as well as the time required for image acquisition. Newer 3D ^{1}H MRS acquisition schemes provide multivoxel data making it possible to obtain regional measurements of major metabolites within 5 min (Fig. 6) [17]. The fact that these new methods can be co-registered to volumetric T1 images allows tracking of MRS changes over time. Although there is some information on the normal spectroscopy changes over time [18], the ability of 3D ^{1}H-MRS to be registered to volumetric T1 images opens the door for future development of ^{1}H-MRS atlases with regional information across development.

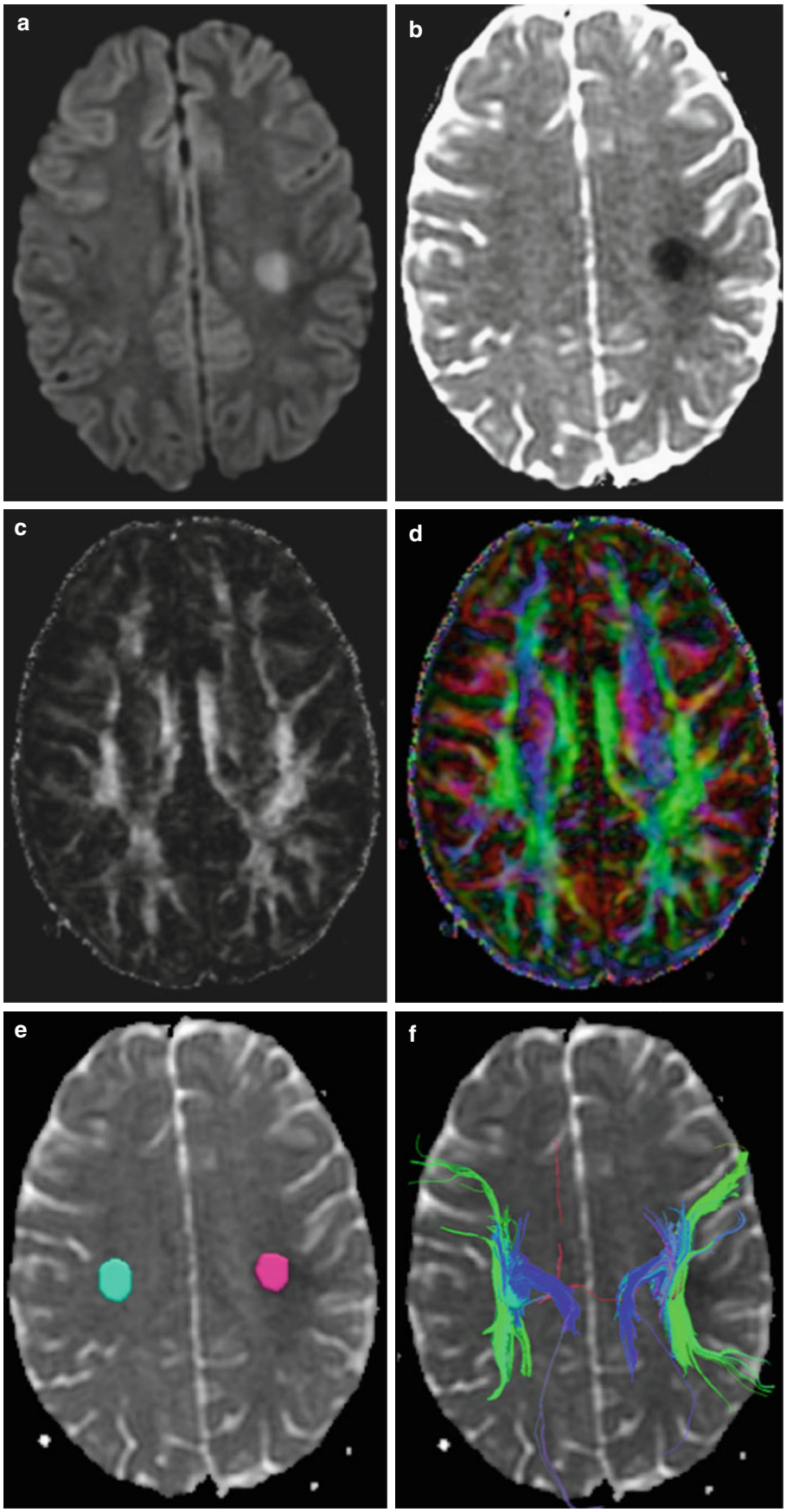

Fig. 2 Young girl with acute lymphoblastic leukemia undergoing intrathecal methotrexate (MTX) therapy presenting with acute onset of right-sided weakness. (**a**) DWI and (**b**) ADC map shows a focal lesion with decreased diffusion. (**c**) FA map shows similar FA values in the lesion compared to the contralateral normal side. (**d**) Color FA map shows similar directions to the diffusion coherence as in the contralateral side. (**e**) ROIs were placed in the lesion and in the contralateral brain to generate tracts. (**f**) Tractography shows preservation of the long-range coherence and confirms that descending tracts, likely corticospinal tract, pass through the lesion. On the T2 images (not shown), the lesion was difficult to detect. The differential includes MTX toxicity, arterial ischemic stroke, or a demyelinating process. Given the clinical history of MTX therapy, this lesion likely corresponds to an area of metabolic compromise or white matter vacuolation with preservation of tissue microstructure at the time of the MRI. The child completely recovered

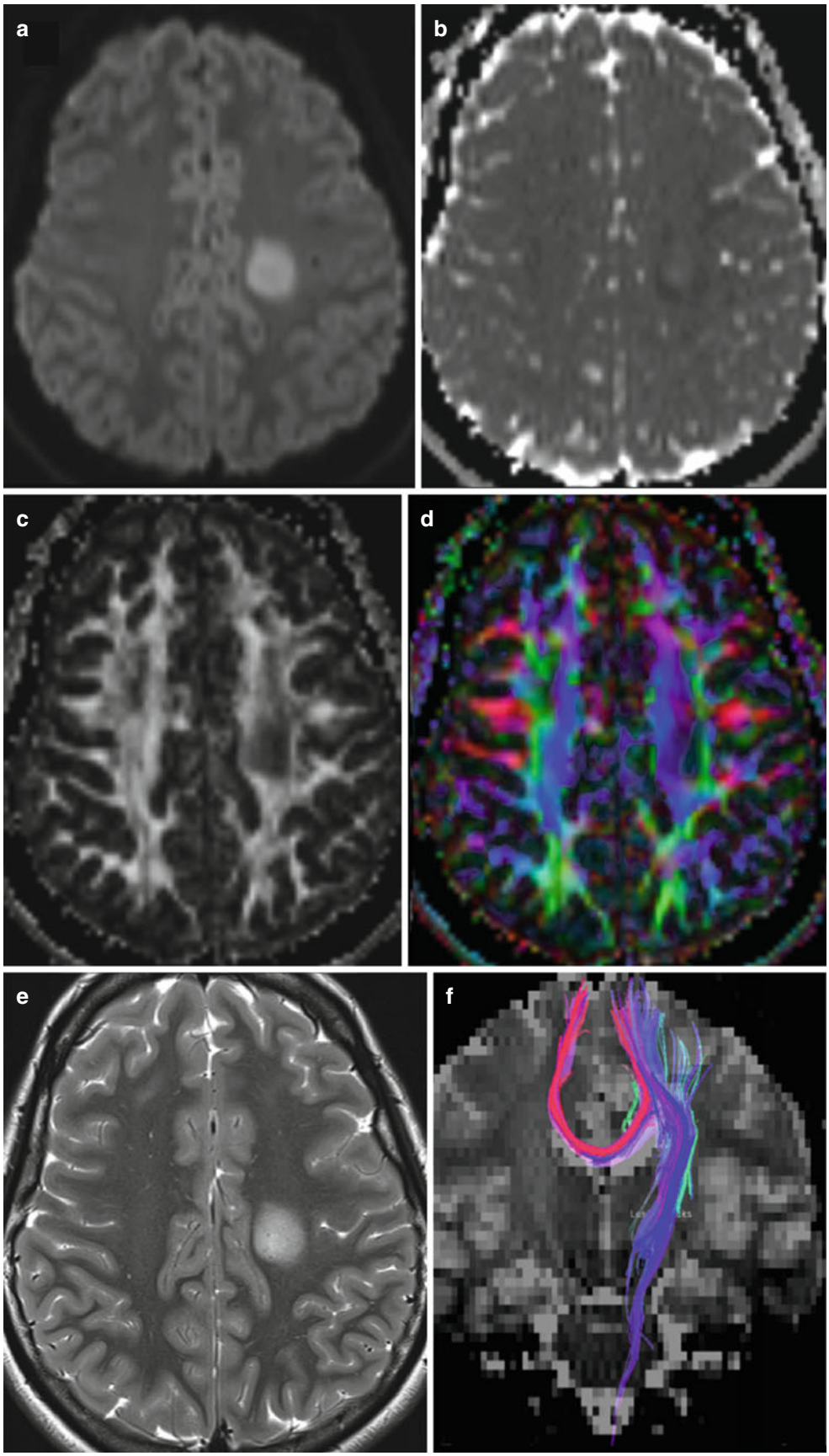

Fig. 3 A 17-year-old girl presenting with new-onset right-sided weakness. (**a**) DWI and (**b**) ADC map show lesions with mixed ADC values. (**c**) FA map showed decreased FA and (**d**) color FA map shows similar diffusion directions as in the contralateral hemisphere. On the T2 image (**e**), the lesion has slightly ill-defined margins. (**f**) Tracks reconstructed using an ROI in the lesion show preservation of long-range coherence. The differential includes a demyelinating lesion or an infiltrative neoplasm. Over the next few months, the lesion continued to grow and was biopsied, revealing an infiltrating glioma grade III. As in this case, infiltrating neoplasms can decrease ADC due to increased cellularity and preserve overall tissue coherence

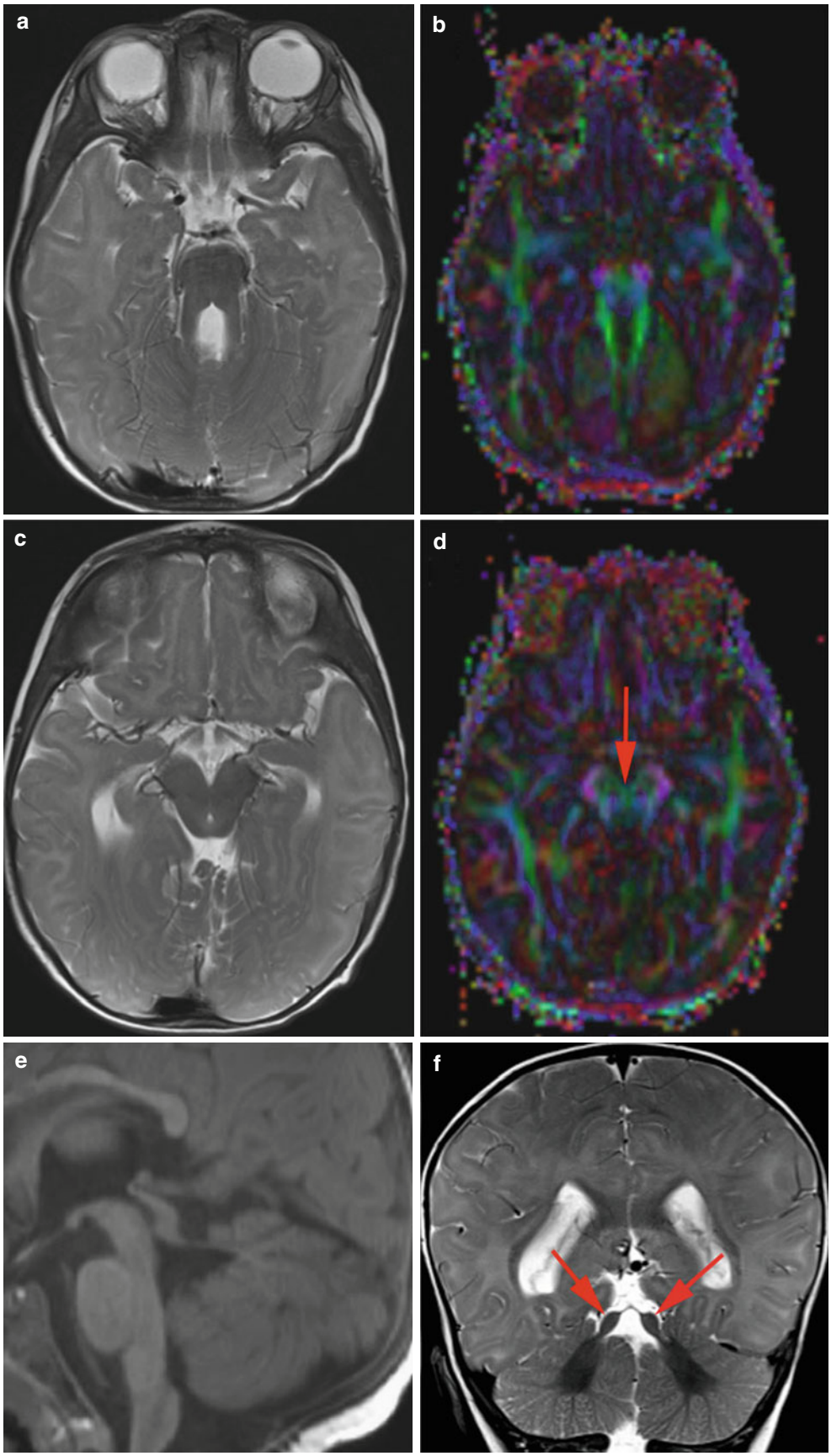

Fig. 4 A 5-month-old female with intermittent apnea and hypoxia. (**a**) Axial T2 at the level of the superior cerebellar peduncles shows large superior cerebellar peduncles giving a molar tooth appearance. (**b**) Color FA map shows the green anterior-posterior direction of the axonal bundles. (**c**) Axial T2 at the level of the midbrain appears normal but on (**d**) color FA map, the normal red spot indicating the decussation of the superior cerebellar peduncles is absent (*arrow*). (**e**) Hypoplastic and dysmorphic vermis and (**f**) coronal T2 showing enlarged superior cerebellar peduncles (*arrows*). The molar tooth appearance with lack of decussation of the superior cerebellar peduncles and small dysplastic vermis is diagnostic of Joubert syndrome

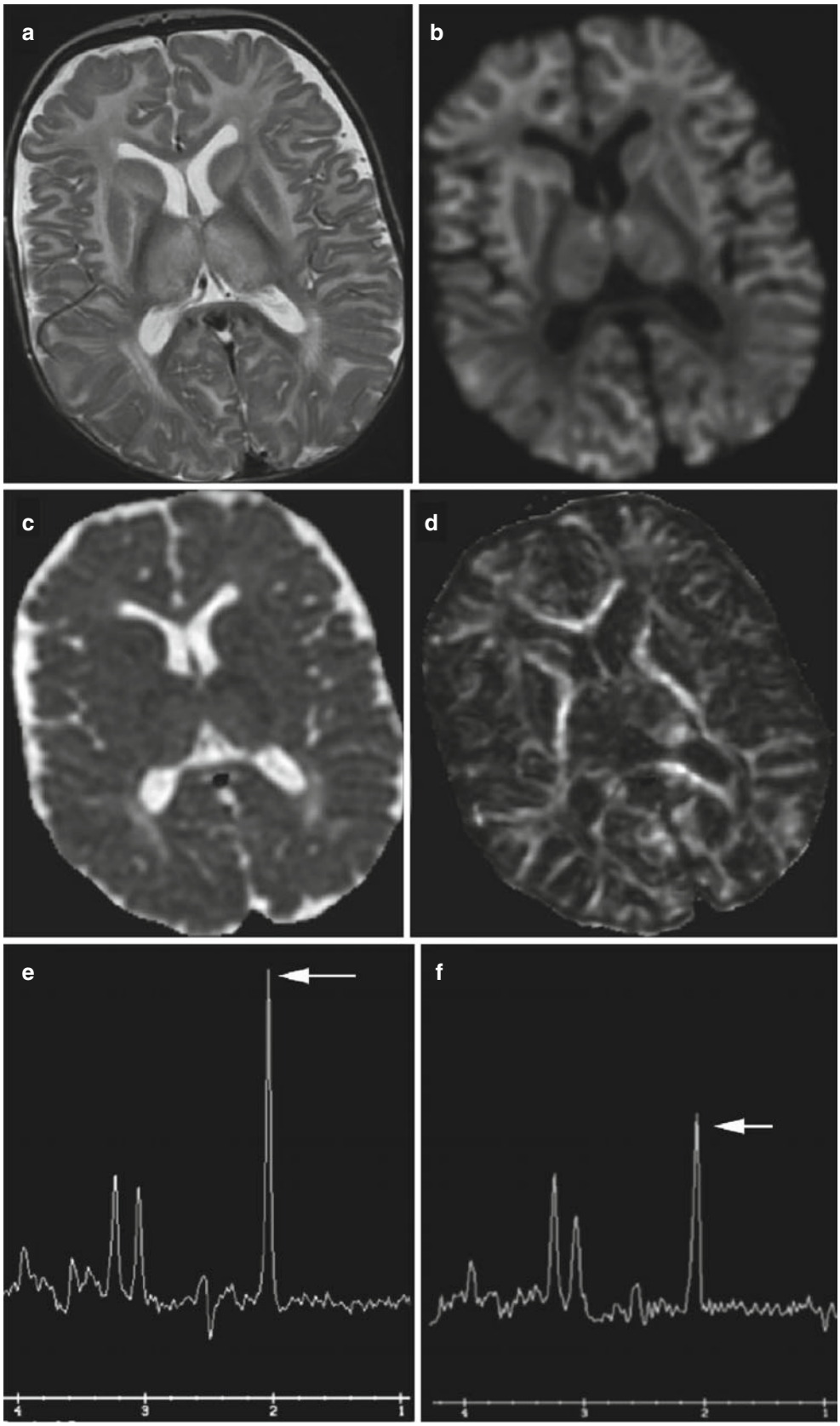

Fig. 5 A 6-month-old presenting with a large head and hypotonia. (**a**) There is diffuse increased signal throughout the white matter on T2 with relative sparing of the corpus callosum and posterior limb internal capsule but involvement of the deep gray nuclei. (**b**) On DWI the white matter appears diffusely bright. (**c**) The ADC map is isointense despite the diffuse increased T2 seen throughout the white matter indicating that the edema is not extracellular. (**d**) FA values are normal to increased. (**e**) The patient's MRS has an elevated NAA peak (*arrow*) compared to (**f**) an age matched typically to a developing toddler. These findings are consistent with the diagnosis of Canavan disease with the white matter changes representing spongiform degeneration. The toddler had high urine N-Acetylaspartate, confirming the diagnosis

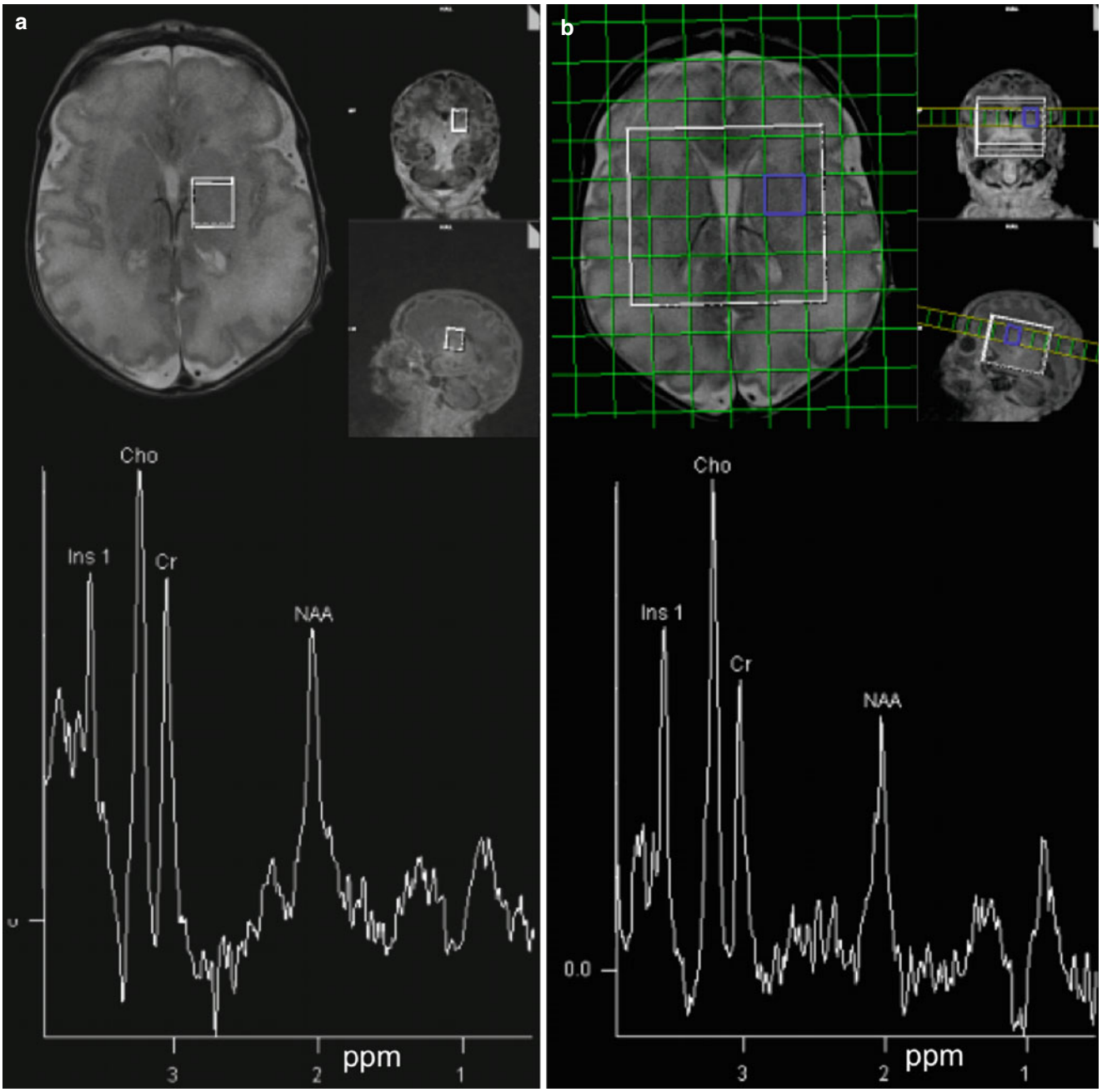

Fig. 6 (**a**) Spectra from a 3 min single-voxel PRESS ^{1}H-MRS acquisition in one 3.4 cc voxel . (**b**) Spectra from a 3 min accelerated 3D spiral CSI ^{1}H-MRS acquisition providing 30 voxels of 2 cc volume to cover a total of 16×16×10 cm regions with LASER-box excitation as shown by the box in the figure inset

Arterial Spin Labeling

Arterial spin labeling (ASL) is a method for noninvasively labeling water molecules in flowing blood to assess cerebral parenchymal perfusion at the capillary level. In ASL inflowing arterial blood is labeled by one of many different methods. The most common labeling scheme on commercial scanners is pulsed ASL (PASL) where a short rf pulse is applied over a volume in the neck. After a delay, designed to allow transit of labeled protons from the carotid and vertebral arteries into the capillaries and extra-axial space of the brain, images of the brain are acquired. The control images are obtained with no label and the two subtracted to provide a perfusion image. ASL is also a low signal-to-noise technique due to the small cerebral capillary vascular volume (5–6 %) and therefore requires multiple repetitions making it susceptible to motion

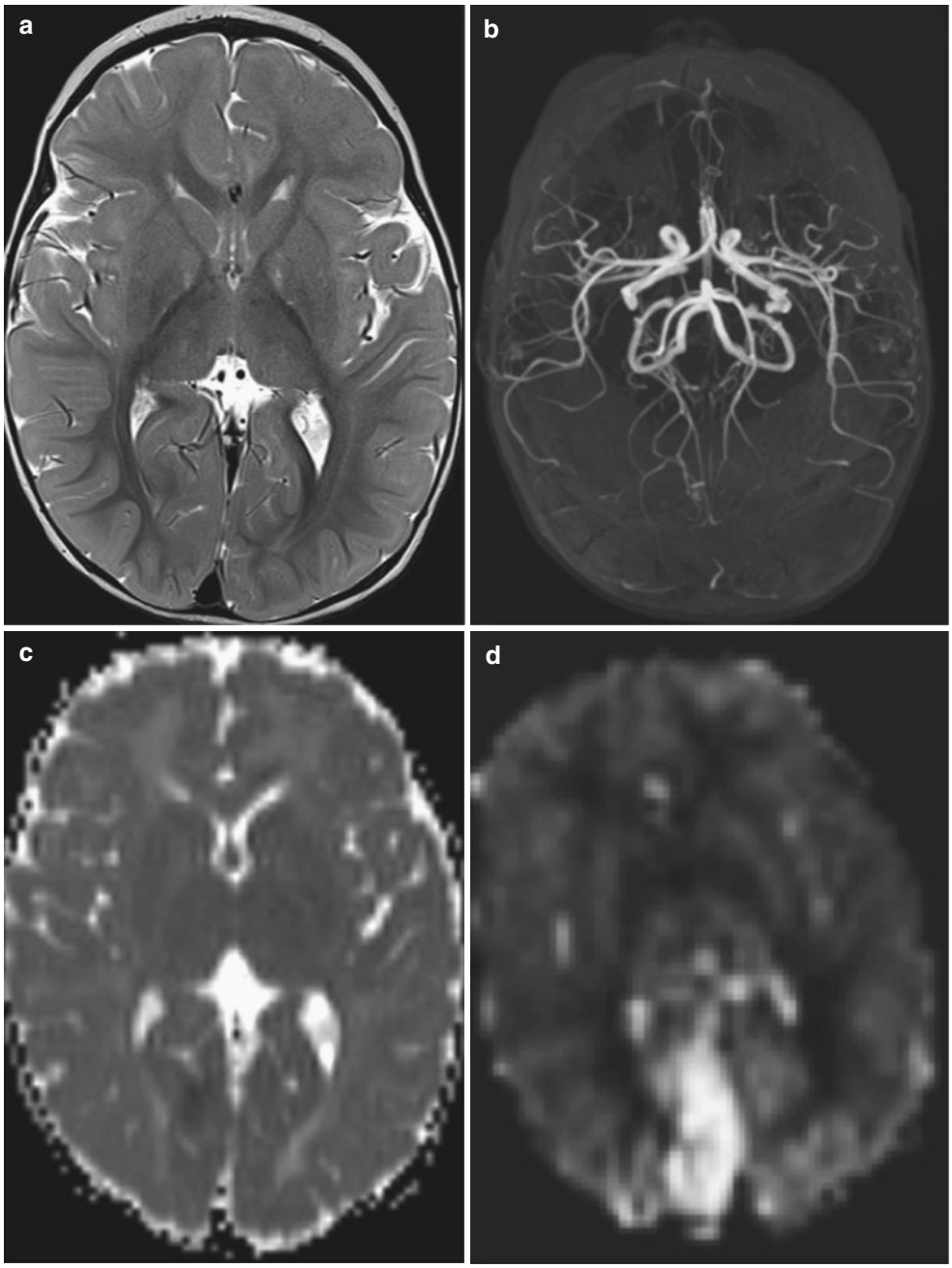

Fig. 7 An 11-month-old girl presenting with epilepsia partialis continua. (**a**) Axial T2-weighted imaging was normal apart from subtle loss of gray white distinction in the right parasagittal occipital lobe. (**b**) Axial MIP from the 3D TOF MRA shows relative prominence of the right PCA compared to the right. (**c**) Subtle decreased ADC is evident in the right parasagittal occipital lobe. (**d**) Right parasagittal occipital lobe hyperperfusion is clearly visible on axial PASL. EEG revealed rhythmic high-amplitude delta with superimposed spikes (RHADS), a hallmark of Alpers' syndrome. The imaging findings are consistent with hyperfusion and mild metabolic compromise from ongoing seizure activity. The child was confirmed to have a POLG1 mutation

artifacts. ASL is a T1-based technique and therefore must be performed prior to contrast administration. Further details on ASL methods can be found in review articles [19, 20].

Controversy exists over ability of ASL methods to provide accurate quantitation of cerebral perfusion due to the need to know the T1 of blood, the labeling efficiency, and label delay, as well as the need to control for magnetization transfer effects [19]. In pediatric imaging many of these factors vary making quantitation even more challenging than in adults. However, despite these issues, numerous articles describing the potential clinical utility exist [20–25], and in addition a consensus article providing guidance to optimizing ASL across vendors is available [26].

Due to the above noted issues with absolute quantitation, clinical applications of ASL are most robust when assessing regional changes in cerebral perfusion. Such changes in cerebral perfusion are extremely useful in identifying alterations in cerebral perfusion in symptomatic patients when no structural abnormalities are identified or in further characterizing an abnormality visible on other sequences. Abnormal increases or decreases in regional cerebral perfusion can be driven by (1) alterations in regional demand, typically due to

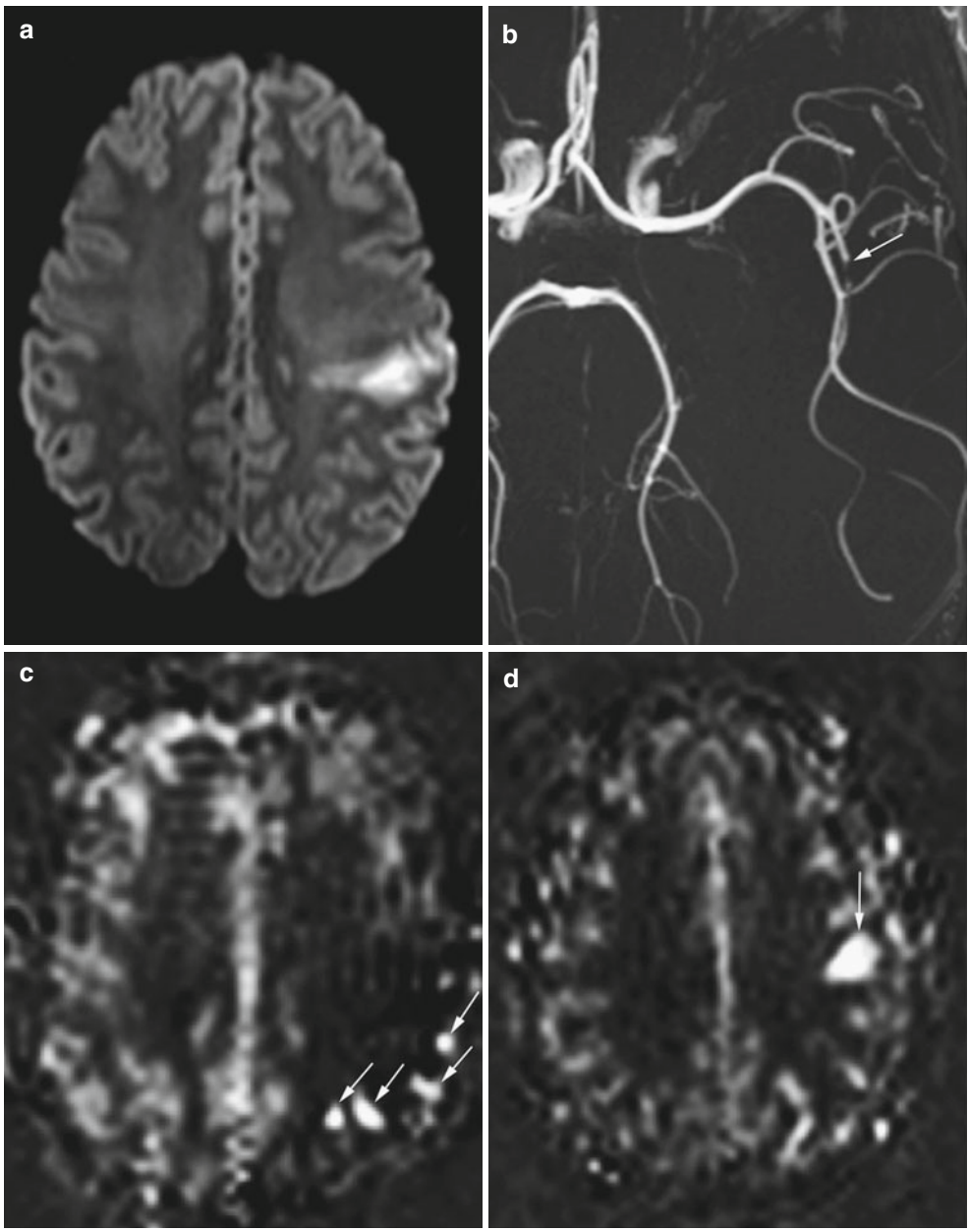

Fig. 8 (**a**) DWI showing decreased diffusivity from an acute arterial ischemic stroke in the left MCA territory. (**b**) On the 3D TOF MRA, loss of flow-related enhancement is detected in the superior division of the left MCA (*arrow*). (**c**) Initial PASL at presentation shows a region of hypoperfusion is larger region than the DWI lesion indicating a penumbra. High signal in the vessels occurs due to delayed arrival of label (*arrows*). (**d**) After TPA, the PASL now shows near-complete resolution of the region of hypoperfusion with now a focal region of parenchymal hyperperfusion (*arrow*)

alterations in regional neural activity (Fig. 7), or (2) regional abnormalities of the vascular system related to vascular anomalies, ischemic events, neovascularization in tumors, arteriovenous fistulas, etc. (Fig. 8).

Fetal Triplane Imaging

Single-shot T2-weighted images such as HASTE or SSFSE are used in sagittal, coronal, and axial planes for clinical evaluation of the fetal brain. Due to motion degradation of slices, these acquisitions are often not exactly in the desired plane and often not exactly orthogonal. Many groups have developed post-processing approaches to combine the three planes together to create a coherent higher resolution 3D brain volume (Fig. 9) [27–30], but these methods currently require manual intervention and many hours of computational time. In addition most tools fail approximately 50 % of the time due to poor image quality as a result of motion or image artifacts. As a result such much needed tools for clinical fetal imaging are not yet available.

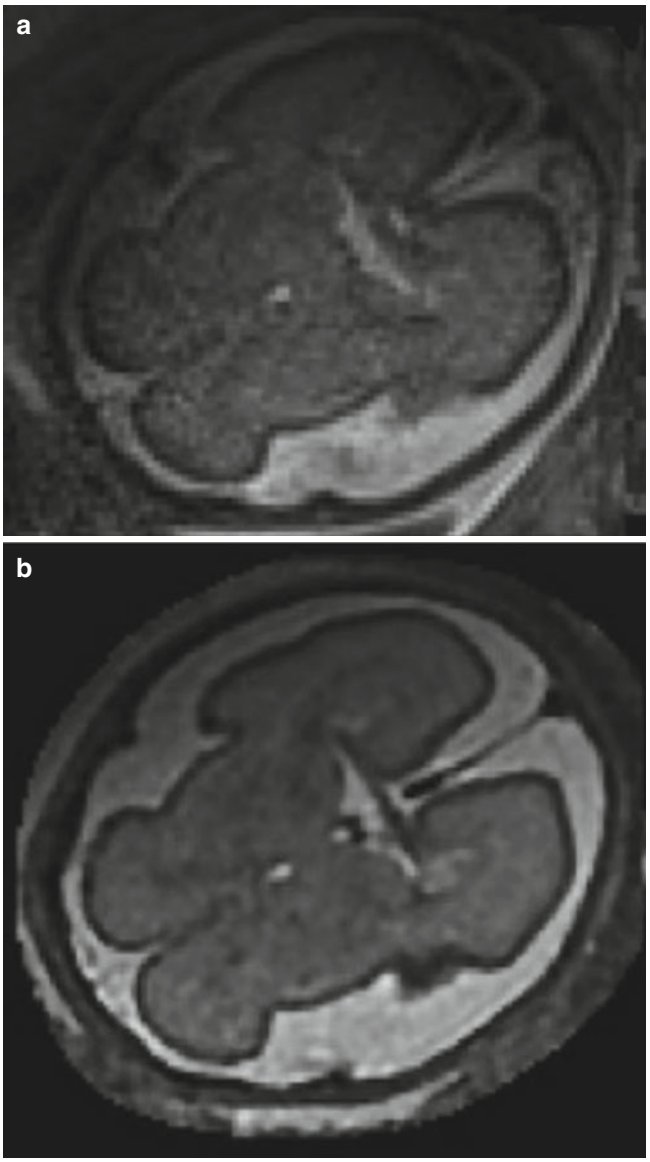

Fig. 9 (**a**) One axial HASTE image of a fetal brain. (**b**) Axial image through a synthesized volume of a fetal brain that is higher in resolution and has less motion degradation after an offline super-resolution reconstruction using as input multiple orthogonal HASTE acquisitions

Quantitative T1 and T2

In the quest for more accurate lesion detection, particularly in children with focal epilepsy, there is a continual push to improve image resolution and contrast as detection of focal cortical lesions significantly improves surgical outcomes and confirmation of multiple lesions in the same clinical context will prompt a more thorough evaluation before surgical resection is attempted. With 32-channel phased-array coils now commonly available at 3 T, image quality has significantly improved with 1 mm isotropic T1-weighted and FLAIR T2 volumetric acquisitions commonly performed in combination with 2 mm-thick T2 TSE images with high in-plane resolution. However, as the search for lesions intensifies, subtle differences in cortical signal due to variations in proximity to the phased-array coils can prove challenging. This has led the desire for quantitative T1- and T2-weighted imaging.

Sequences that provide estimates of T1 with automatically reconstructed T1 maps for visual inspection such as MPXRAGE are becoming commercially available. Such sequences remove signal intensity biases due to the reception profiles of the coils and assist in the visual detection of focal lesions. Sequences that provide estimates of T2 are also available on some systems; however, the application of such sequences is limited by the long acquisition times required (~10 min) but may be clinically justified in complex epilepsy cases as a second-line evaluation (Fig. 10).

Summary

Although there is still progress to be made, many advanced techniques are becoming integrated into the workflow of clinical pediatric neuroradiology. Over-interpretation and definitive statements regarding processed data can be misleading and dangerous. Therefore, these advanced techniques require the neuroradiologist to understand the breadth of physiologies and pathophysiologies that can alter signal intensity or a processed result as well as the potential artifacts that can lead to misleading results.

In the past, quantitation has been viewed with skepticism, but as our tools improve, neuroradiologists need to be open-minded about the potential of quantitative neuroimaging. However, as the field is being pushed toward standardization and quantitation, there will be an increasing need to provide normative measures across development that will require collaboration and incorporation of data from multiple sites with access to patient populations of different ethnic and environmental backgrounds.

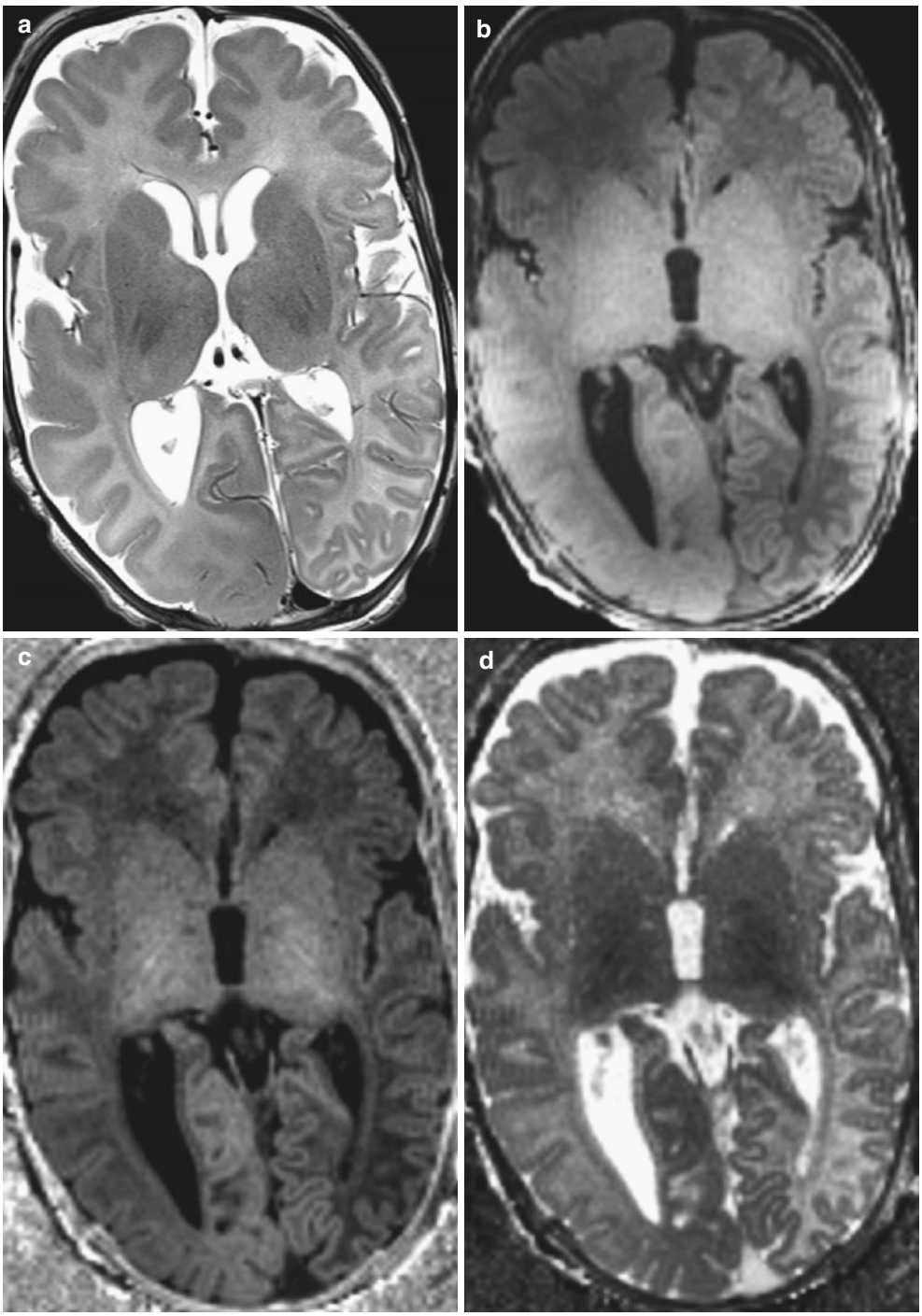

Fig. 10 A 7-week-old infant presenting with fever and concern for sepsis followed by persistent seizure activity. (**a**) Axial T2 shows an asymmetrically large right hemisphere with an enlarged genu of the corpus callosum. T2 signal throughout the right hemisphere white matter is abnormally low and there is apparent thickening of the cortex diffusely. The left temporal and occipital lobe looks normal but the right frontal lobe is concerning for involvement. (**b**) Axial reformation of a sagittal MPRAGE has nonuniform signal due to the phased-array coils making further evaluation of the left frontal lobe difficult. (**c**) Axial reformation of the uniform intensity image created from the MP2RAGE acquisition shows subtle differences in white matter signal in the left frontal and occipital lobe. (**d**) Axial reformation of the T1 map created from the MP2RAGE acquisition confirms the abnormal T1 values in the left frontal white matter compared to the occipital lobe and more similar to the right frontal lobe. These findings are consistent with right hemimegalencephaly with additional involvement of the left frontal lobe

References

1. Setsompop K, Cohen-Adad J, Gagoski BA, Raij T, Yendiki A, Keil B et al (2012) Improving diffusion MRI using simultaneous multi-slice echo planar imaging. Neuroimage 63(1):569–580
2. Mori S, Zhang J (2006) Principles of diffusion tensor imaging and its applications to basic neuroscience research. Neuron 51(5):527–539
3. Basser PJ, Jones DK (2002) Diffusion-tensor MRI: theory, experimental design and data analysis – a technical review. NMR Biomed 15(7–8):456–467
4. Hagmann P, Jonasson L, Maeder P, Thiran JP, Wedeen VJ, Meuli R (2006) Understanding diffusion MR imaging techniques: from scalar diffusion-weighted imaging to diffusion tensor imaging and beyond. Radiographics 26(Suppl 1):S205–S223
5. Schaefer PW, Grant PE, Gonzalez RG (2000) Diffusion-weighted MR imaging of the brain. Radiology 217(2):331–345
6. Grant PE, Matsuda KM (2003) Application of new MR techniques in pediatric patients. Magn Reson Imaging Clin N Am 11(3):493–522
7. Nossin-Manor R, Card D, Morris D, Noormohamed S, Shroff MM, Whyte HE et al (2013) Quantitative MRI in the very preterm brain: assessing tissue organization and myelination using magnetization transfer, diffusion tensor and T(1) imaging. Neuroimage 64:505–516
8. Sadeghi N, Prastawa M, Fletcher PT, Wolff J, Gilmore JH, Gerig G (2013) Regional characterization of longitudinal DT-MRI to study white matter maturation of the early developing brain. Neuroimage 68:236–247
9. Miller JH, McKinstry RC, Philip JV, Mukherjee P, Neil JJ (2003) Diffusion-tensor MR imaging of normal brain maturation: a guide to structural development and myelination. AJR Am J Roentgenol 180(3):851–859
10. Grant PE, He J, Halpern EF, Wu O, Schaefer PW, Schwamm LH et al (2001) Frequency and clinical context of decreased apparent diffusion coefficient reversal in the human brain. Radiology 221(1):43–50
11. Pujol S, Wells W, Pierpaoli C, Brun C, Gee J, Cheng G et al (2015) The DTI challenge: toward standardized evaluation of diffusion tensor imaging tractography for neurosurgery. J Neuroimaging 25(6):875–882
12. Campanella M, Ius T, Skrap M, Fadiga L (2014) Alterations in fiber pathways reveal brain tumor typology: a diffusion tractography study. PeerJ 2, e497
13. Panigrahy A, Nelson MD Jr, Bluml S (2010) Magnetic resonance spectroscopy in pediatric neuroradiology: clinical and research applications. Pediatr Radiol 40(1):3–30
14. Cecil KM (2006) MR spectroscopy of metabolic disorders. Neuroimaging Clin N Am 16(1):87–116, viii
15. Cecil KM (2013) Proton magnetic resonance spectroscopy: technique for the neuroradiologist. Neuroimaging Clin N Am 23(3):381–392
16. Oz G, Alger JR, Barker PB, Bartha R, Bizzi A, Boesch C et al (2014) Clinical proton MR spectroscopy in central nervous system disorders. Radiology 270(3):658–679
17. Yazbek S, Prabhu SP, Connaughton P, Grant PE, Gagoski B (2015) Comparison of accelerated 3-D spiral chemical shift imaging and single-voxel spectroscopy at 3T in the pediatric age group. Pediatr Radiol 45(9):1417–1422
18. Bluml S, Wisnowski JL, Nelson MD Jr, Paquette L, Gilles FH, Kinney HC et al (2013) Metabolic maturation of the human brain from birth through adolescence: insights from in vivo magnetic resonance spectroscopy. Cereb Cortex 23(12):2944–2955
19. Petersen ET, Zimine I, Ho YC, Golay X (2006) Non-invasive measurement of perfusion: a critical review of arterial spin labelling techniques. Br J Radiol 79(944):688–701
20. Deibler AR, Pollock JM, Kraft RA, Tan H, Burdette JH, Maldjian JA (2008) Arterial spin-labeling in routine clinical practice, part 1: technique and artifacts. AJNR Am J Neuroradiol 29(7):1228–1234
21. Amukotuwa SA, Yu C, Zaharchuk G (2016) 3D Pseudocontinuous arterial spin labeling in routine clinical practice: A review of clinically significant artifacts. J Magn Reson Imaging 43(1):11–27
22. Deibler AR, Pollock JM, Kraft RA, Tan H, Burdette JH, Maldjian JA (2008) Arterial spin-labeling in routine clinical practice, part 2: hypoperfusion patterns. AJNR Am J Neuroradiol 29(7):1235–1241
23. Deibler AR, Pollock JM, Kraft RA, Tan H, Burdette JH, Maldjian JA (2008) Arterial spin-labeling in routine clinical practice, part 3: hyperperfusion patterns. AJNR Am J Neuroradiol 29(8):1428–1435
24. Petcharunpaisan S, Ramalho J, Castillo M (2010) Arterial spin labeling in neuroimaging. World J Radiol 2(10):384–398
25. Telischak NA, Detre JA, Zaharchuk G (2015) Arterial spin labeling MRI: clinical applications in the brain. J Magn Reson Imaging 41(5):1165–1180
26. Alsop DC, Detre JA, Golay X, Gunther M, Hendrikse J, Hernandez-Garcia L et al (2015) Recommended implementation of arterial spin-labeled perfusion MRI for clinical applications: a consensus of the ISMRM perfusion study group and the European consortium for ASL in dementia. Magn Reson Med 73(1):spcone
27. Tourbier S, Bresson X, Hagmann P, Thiran JP, Meuli R, Cuadra MB (2015) An efficient total variation algorithm for super-resolution in fetal brain MRI with adaptive regularization. Neuroimage 118:584–597
28. Rousseau F, Kim K, Studholme C, Koob M, Dietemann JL (2010) On super-resolution for fetal brain MRI. Med Image Comput Comput Assist Interv 13(Pt 2):355–362
29. Gholipour A, Estroff JA, Barnewolt CE, Connolly SA, Warfield SK (2011) Fetal brain volumetry through MRI volumetric reconstruction and segmentation. Int J Comput Assist Radiol Surg 6(3):329–339
30. Kuklisova-Murgasova M, Quaghebeur G, Rutherford MA, Hajnal JV, Schnabel JA (2012) Reconstruction of fetal brain MRI with intensity matching and complete outlier removal. Med Image Anal 16(8):1550–1564

Non-accidental Injury of the Pediatric Central Nervous System

Marjolein H.G. Dremmen and Thierry A.G.M. Huisman

Introduction

Inflicted or non-accidental central nervous system (CNS) injury compromises a constellation of injuries to the pediatric brain and spine resulting from direct or indirect forces acting on the cranium and spine and the intracranial and intrathecal components. The recognition of inflicted injury has significantly improved over the past years. Imaging plays a major role in the early and specific detection and documentation of inflicted physical injury. Inflicted injuries can involve any body part and cover every type of injury (e.g., fractures, organ injuries, thermal injuries).

The pediatric skull, brain, and spine go through continuous anatomical and functional developmental phases. As a consequence, the type, pattern, extent, and distribution of traumatic CNS injuries differ depending on the age group of the affected child. Furthermore, the primary and secondary complications and the neurological and functional outcome are different for each age group.

The goals of this manuscript are to enlarge awareness of the epidemiology, mechanisms, and imaging features of inflicted injury of the pediatric CNS, to discuss the "accuracy" of dating of inflicted injury based on imaging findings, and to propose a diagnostic workup for suspected inflected neurotrauma.

M.H.G. Dremmen
Division of Pediatric Radiology and Pediatric Neuroradiology, Department of Radiology and Radiological Science, Johns Hopkins Hospital, Baltimore, MD, USA

Division of Pediatric Radiology, Department of Radiology, Erasmus MC – University Medical Center, Rotterdam, The Netherlands
e-mail: marjolein.dremmen@gmail.com

T.A.G.M. Huisman (✉)
Division of Pediatric Radiology and Pediatric Neuroradiology, Department of Radiology and Radiological Science, Johns Hopkins Hospital, Baltimore, MD, USA

Historical Background

The French forensic physician Tardieu described a diverse range of physical and sexual injuries to children, including meningeal hemorrhage and brain injuries, as early as in the nineteenth century [1]. More than 80 years later, in 1946 the American pediatrician and radiologist Caffey first described the unusual association of chronic subdural hemorrhages and long-bone fractures [2]. In 1972, he published a description of the radiologic and clinical features attributed to shaking injuries [3]. Two pediatricians, Ludwig and Warman, introduced the term shaken baby syndrome in 1983 in the published review of infants and young toddlers injured by shaking. In 1987, Duhaime (neurosurgeon) reported that many victims of shaken baby syndrome showed evidence of blunt impact to the head at the time of diagnosis [4]. In the past decades, extensive efforts to progressively understand causations and mechanisms of inflicted injury have led to abundant objective research data regarding this specific type of injury.

Confusion of Definition

Diverse nomenclature has been used to describe the entity of inflicted CNS injury.

In 2009, the American Academy of Pediatrics (AAP) appealed for the introduction of more encompassing and less specific medical terminology covering the range of injuries to the skull and brain ("abusive head trauma") rather than implying a single injury mechanism ("shaken baby syndrome") by publishing a policy statement [5]. Inflicted or abusive injury is the more recent terminology applied to the outdated terms as battered child syndrome and shaken impact syndrome [5].

J. Hodler et al. (eds.), *Diseases of the Brain, Head and Neck, Spine 2016–2019: Diagnostic Imaging*, DOI 10.1007/978-3-319-30081-8_33

Definition

The definition of child abuse according to the World Health Organization "includes all forms of physical and emotional ill-treatment, sexual abuse, neglect, and exploitation that results in actual or potential harm to the child's health, development or dignity." Inflicted neurotrauma focuses on the physical type of abuse to the CNS of infants and children by adults. Physical injury comprises approximately 20 % of all type of maltreatment injuries. Inflicted physical injury should be suspected in the context of an inappropriate or inconsistent history.

In terms of clinical, laboratory, and imaging findings, there is lack of consistent and reliable criteria for standardizing the diagnosis of inflicted injury. The pattern of abnormalities associated with inflicted injury does not follow circular logic to serve as diagnostic criteria to establish the diagnosis. Inflicted CNS injury remains a diagnostic and medicolegal challenge.

Epidemiology

The estimated incidence of inflicted injury to the brain and spine in the pediatric age group under the age of 1 is 14–40 per 100,000. Inflicted injury is the most common cause of neurotrauma in the age group younger than 2 years [6, 7]. Exact incidence numbers of inflicted CNS injury cannot be determined since there is no standardized definition; a portion of the involved infants and children is not in need of acute medical care and will not enter the medical system, and a subdivision of the medical presented cases are (initially) not recognized as inflicted injury cases. In general, the affected pediatric population consists of a higher proportion of boys (62–77 %), and the majority of cases manifests before 6 months of age (median age 2.2–5.9 months) [8].

Inflicted injury of the brain and spine is the most common cause of traumatic death in infancy [9, 10]. A substantial part of the survivors of inflicted CNS injury demonstrates impaired neurodevelopmental function, is moderately (14 %) to severely (50 %) disabled, and will have a lower life expectancy [10]. The poor outcome is predominantly due to the damage to an intensely developing CNS at this young age.

Perpetrators of inflicted injury are found across various socioeconomic demographics. Risk factors for mistreatment are being established and categorized into risk factors intrinsic to the child (e.g., male, young age), risk factors intrinsic to the perpetrator (e.g., young parent/caregiver, psychiatric problems), and risk factors intrinsic to family structure and socioeconomic situation (e.g., unmarried, minority group) [11].

Mechanisms and Pathophysiologic Processes of Inflicted Injury

Primary CNS injury occurs at the time of injury, whereas secondary injury to the brain and spine evolves over a certain time period (hours, days, months) after the initial trauma. Neurotrauma injury, accidental or inflicted, is initiated by either impulsive loading (movement of head by angular acceleration/deceleration forces to other part of body) or impact loading (direct linear forces to the head). Unique age-dependent anatomical and biomechanical features of the developing skull, brain, and spine cause these traumatic events to have different mechanisms and pathophysiologic injury patterns compared to adults.

Brain Characteristics

Unmyelinated cerebral white matter in a neonate/infant consists of more water (and less myelin) and smaller axonal size if compared to completely myelinated white matter in an older child. As a consequence, the brain tissue is softer and more susceptible to diffuse acceleration-deceleration axonal injury in case of impulsive loading. Predilection sites for diffuse axonal injury are the dorsal brainstem, parasagittal white matter, corpus callosum, and gray-white matter junctions of the cerebral hemispheres (Fig. 1). Moreover, the programmed brain myelination pattern causes myelinated brain regions to absorb external forces distinct from unmyelinated brain regions resulting in cortical tear or cleft injuries rather than cortical contusions [12].

Skull Characteristics

The pediatric skull is thin and demonstrates a high degree of plasticity and deformity with transmission of impact forces to deeper brain structures compared to adults. Open sutures tolerate a small degree of motion of the bones of the cranial vault in relation to each other. Impulsive loading to an unsupported neck (shaking) causes the head to rotate/move along the fulcrum of the cervical spine. The younger the child, the more superior/cranial cervical spine or even the craniocervical junction will be injured. The relative large size and heavy weight of the pediatric head compared to the adult head causes altered dynamics of head acceleration due to external forces. The additional plasticity of the skull results in significant shear forces on the skull and dura versus the subdural vessels and brain with subsequent stretching and tearing injuries of the bridging vessels and the relative soft unmyelinated brain (e.g., subdural/subarachnoid hemorrhages, diffuse axonal injury) [12, 13]. The prominent

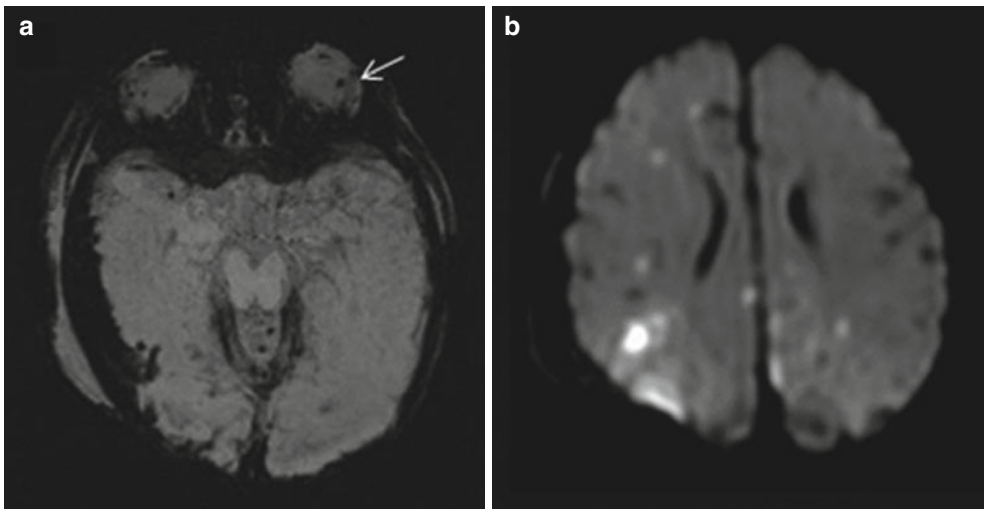

Fig. 1 Axial SWI MR image (**a**) reveals subdural hemorrhage over the right temporal region. Additional subarachnoid hemorrhage in this region is seen. Focal retinal hemorrhages are identified bilateral, left more than right (*white arrow*). Axial DWI MR image (**b**) demonstrates parenchymal shear injuries representing diffuse axonal injury in the subcortical and parasagittal white matter in the frontal and parietal regions

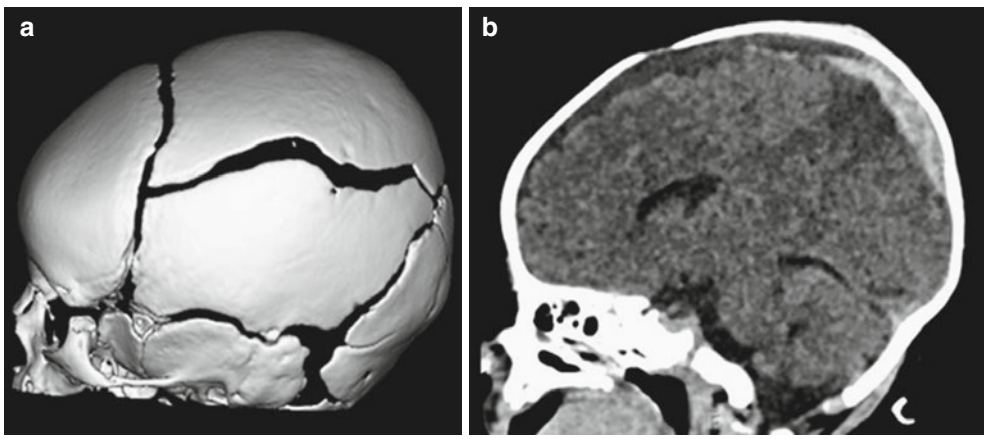

Fig. 2 3D CT image (**a**) shows a linear mild diastatic non-displaced fracture through the left parietal bone extending from the coronal suture to the lambdoid suture. Sagittal 2D CT image (**b**) reveals a hyperdense subdural hematoma in the left parietal region. Moreover, cortical contusion with subcortical edema is noted in the underlying left parietal lobe

extra-axial cerebrospinal fluid (CSF) spaces in the young age group even further increase the traction forces to the bridging veins with subsequent high risk of subdural hemorrhage (Fig. 2).

The inner table of the skull of an infant is not as irregular and uneven as in older children, resulting in less cortical contusions in the young age group. Furthermore, the groove of the middle meningeal artery is shallow (more mobility of the artery), and the pediatric dura is more firmly adherent to the inner table of the skull, decreasing the risk of epidural hemorrhages in infants and young children and causing epidural hemorrhages to be more often from venous rather than arterial quality.

Facial Characteristics

The relative small surface of the pediatric facial bones and the undeveloped and unaerated paranasal sinuses result in considerable more direct transmission of external forces to the skull and brain (potentially resulting in brain injury) and substantial less absorption of applied external forces by the paranasal sinuses [12].

Spinal Characteristics

The mechanisms of injury to the spine consist of hyperflexion, hyperextension, axial loading, axial rotation, and distraction. The younger the child, the weaker the neck muscles and relatively the bigger and heavier is the head in relation to the torso. The immature osseous structures of the cervical spine in infants and younger children are reflected by an anterior wedge-shaped morphology of the vertebral bodies, horizontal-oriented facet joints, and flat morphology of uncinate processes [14, 15]. The stability of the craniocervical junction and cervical spine in the pediatric population is more dependent on the ligaments compared to the osseous elements of the spine [12, 15]. This causes relative ease of vertebral subluxation with complete recovery of the bony elements to normal anatomical alignment. As a consequence, acceleration/deceleration and rotational

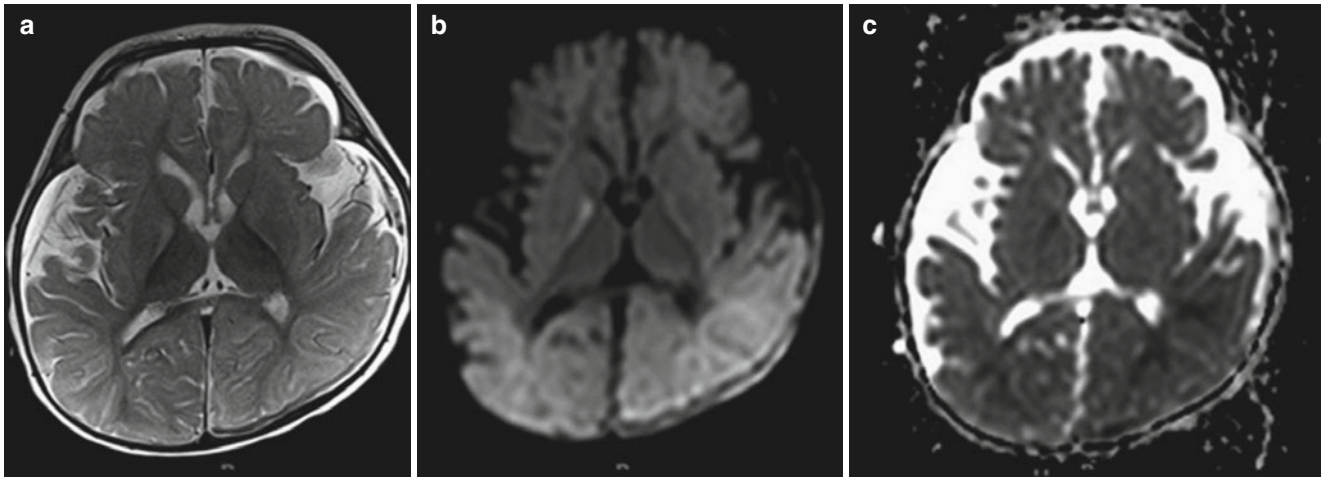

Fig. 3 Axial magnetic resonance images of a young infant exposed to inflicted injury with resultant concomitant hypoxic-ischemic injury. Axial T2-weighted MR image (**a**) shows bilateral hemorrhages along the convexities and focal shear injury of the splenium. Additional T2 hyperintense signal in the bilateral medial segment of the globus pallidus and diffuse T2 hyperintensity in the bilateral parieto-occipital brain parenchyma and adjacent cortex in conjunction with reduced gray-white matter differentiation are noted. Trace of diffusion MR image (**b**) and corresponding apparent diffusion coefficient (ADC) map (**c**) reveal acute hypoxic-ischemic injury with restricted diffusion in the bilateral medial segment of the globus pallidus, bilateral parieto-occipital white matter regions, and less pronounced in the bilateral frontal white matter regions

trauma (impulsive loading) of the spine in neonates and young infants have a potential to cause stretch injury particular to the cervical spine/spinal cord. Cervicomedullary cord damage (e.g., axonal injury) or vascular injury (e.g., epidural hemorrhage) potentially results in apnea or respiratory arrest ultimately leading to hypoxic-ischemic brain and spinal cord injury.

Secondary CNS injury is the consequence of various complex biochemical and physiological events in response to or as a complication of the primary CNS injury. The initiating traumatic event leads more frequent to hyperemic cerebral edema in the pediatric age group compared to adults, likely resulting from immature or impaired autoregulation of the pediatric brain perfusion, increased (immature) permeability of the blood-brain barrier, and an enhanced inflammatory response of the injured developing brain. Decreased cerebral arterial blood flow occurs more rapidly in children, because of a relative low baseline mean arterial blood pressure. Hypoxic-ischemic brain injury (Fig. 3) can result from global cerebral edema, focal compression of vascular structures due to herniation or mass effect of intracranial hemorrhages or from primary vascular injury. In addition, spinal injury with consequent asphyxia and compression of major cervical arterial vessels as well as chest compression (while the child is forcefully shaken) leading to hypoventilation or cardiac arrest can potentially result in hypoxic-ischemic brain injury (Fig. 4) [12]. Diastasis of remaining open sutures can prevent sudden and rapid rise of intracranial pressure to a certain degree.

The chronic sequelae of inflicted traumatic brain injury include, e.g., hydrocephalus, encephalomalacia, and CSF leak.

Age-Specific Patterns of Inflicted Injury

The traditional classical triad of inflicted brain injury due to impulsive loading includes subdural hematomas, associated brain abnormalities (encephalopathy), and retinal hemorrhages (Fig. 1). Additional related spinal, skeletal, and skin abnormalities are potentially present. The presence of the characteristic triad is no definite evidence of inflicted CNS injury in the absence of other corroborative findings. At present, apnea is considered the single critical distinctive feature for inflicted CNS injury compared to accidental neurotrauma. Retinal hemorrhages (severe grade) and rib fractures are considered as significant risk factors for inflicted brain injury [16]. The presence of a subdural hematoma in neonates and infants is more suggestive for inflicted brain injury compared to accidental injury [17].

Inflicted brain injury patterns depend on the type of loading mechanism and the impact of the specific mechanism related to the age of the affected child. Impulsive loading (e.g., "shaken baby phenomenon") with consequent diffuse axonal injury, white matter tear, or cleft and subdural hemorrhages are more frequent in neonates and infants. Occult damage to the brain due to inflicted injury is more frequently observed in children under the age of 1 year [18]. Impact loading (e.g., "beating up") causes more focal injury, e.g., skull fracture, cortical contusions, and epidural hematoma, in older children [12]. In addition, midface fractures are less prevalent in the young group.

Inflicted spinal injury demonstrates two distinct patterns of injury depending on the age of the affected child. Infants less than 1 year of age show a higher incidence of cervical

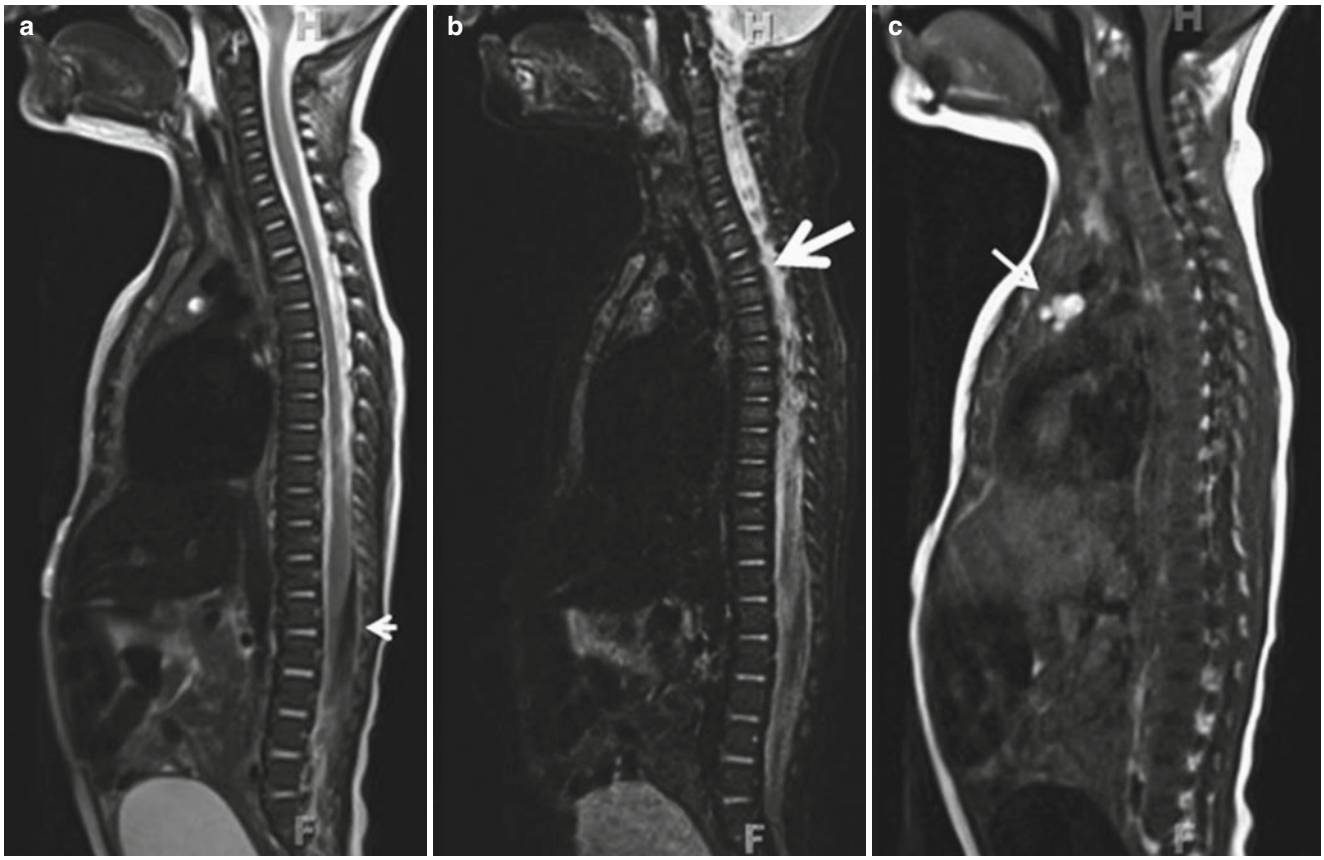

Fig 4 Sagittal midline T2-weighted MR image (**a**) shows an epidural hematoma in the posterior lumbar spinal canal (*white arrow head*). The sagittal STIR image (**b**) reveals a compression fracture at the level T2 (*white arrow*). In the sagittal T1-weighted image (**c**), a hyperintense mediastinal hematoma is demonstrated (*small white arrow*)

spinal cord injuries without osseous abnormalities (SCIWORA), potentially leading to instantaneous damage to the respiratory centers at the cervicomedullary junction, respiratory distress, and subsequent hypoxic-ischemic brain and spinal cord injury. The infants over 1 year of age present more common with thoracolumbar injury with visible spinal deformity and/or focal neurological signs (Fig. 4) [15, 19].

Imaging Findings of Inflicted Injury in the Brain

There is not one single radiologic finding pathognomonic or specific for inflicted brain injury.

The morphology of a skull fracture is not a discriminative factor to differentiate inflicted brain injury from accidental brain injury. Multiple or complex skull fractures are more frequently diagnosed in case of inflicted neurotrauma. Non-visualization of scalp or skull abnormalities on imaging studies should not be interpreted as absence of impact injury.

Subdural hemorrhage is the most frequent neuroradiological finding in the setting of inflicted brain injury as subdural hemorrhage is identified in about 80 % of the cases (Fig. 2) [8, 20]. The typical distribution in the pediatric age group is bilateral over the cerebral convexities, extending into the posterior interhemispheric fissure and into the posterior fossa. The interhemispheric subdural hematoma is not considered characteristic of inflicted injury. The typical characteristics of the different types of extracerebral hemorrhages (subarachnoid, subdural, epidural) can be obscured because of membrane layer disruption with subsequent merging of the features of various types of hemorrhage [13, 21].

Various other types of intracranial injuries are associated with inflicted neurotrauma, in descending order: diffuse axonal injuries, tear or cleft injuries, subarachnoid hemorrhages, intracerebral hemorrhages, and epidural hemorrhages [8].

Diffuse axonal injury demonstrates focal MR susceptibility artifacts and/or focal restricted diffusion (Fig. 1). If the lesions encountered on diffusion-weighted imaging are

arranged within a vascular distribution rather than at the predilection sites of DAI, a vascular injury should be suspected. The severity grade of diffuse axonal injury, quantified by the number and volume of microhemorrhages on susceptibility-weighted imaging (SWI), correlates with the long-term neurologic outcome of the affected child [22, 23].

Diffuse cerebral edema, focal compression of vascular structures due to herniation or mass effect of intracranial hemorrhages, or primary vascular injury can result in hypoxic-ischemic brain injury.

The subacute to chronic sequelae of inflicted injury of the brain comprise hydrocephalus, atrophy, encephalomalacia, gliosis, mineralization, and chronic extracerebral fluid collections. Radiological imaging studies are an important tool in assessing a short-term and long-term prognosis for the affected child based on the severity of brain abnormalities.

Imaging Findings of Inflicted Injury in the Spine

The spectrum of injuries differs with degree of spinal development and therefore differs with age. Overall, the spine is not considered to be a common site of trauma due to inflicted injury. However, in the age group under the age of 2 years, inflicted injury is a relative frequent cause of spinal trauma [14]. The cervical spine, in particular the craniocervical junction and upper cervical spine, are predilection sites of inflicted injury to the spine in neonates, infants, and young children. The majority of inflicted spinal injury is associated with simultaneous injury to the brain [14, 15, 19].

Due to the immaturity of the spine and the consequent morphology and position of the vertebrae and laxity of the surrounding ligamentous structures, the pediatric cervical spine is at risk for spinal cord injuries without demonstrating osseous abnormalities, known as spinal cord injury without radiographic abnormality (SCIWORA). In addition, ligamentous injury of the cervical spine with lack of osseous involvement is a relative common inflicted injury. Furthermore, craniocervical subdural and epidural hemorrhage is reported in inflicted spinal injury in infants [15, 19]. Spinal fracture types associated with inflicted injury include vertebral body compression fractures (Fig. 4).

Imaging Findings of Inflicted Injury in the Rest of the Body

The most common findings concerning inflected injury are skin lesions (bruises, contusions). The second most frequent type of injury is fractures. The fractures potentially involve multiple sites and typically appear in diverse healing stages [24]. In particular, posterior and lateral rib fractures, spiral long-bone fractures, and metaphyseal fracture lesions are strongly associated with inflicted injury. Fractures inconsistent with the nature of the reported trauma or inappropriate for the age of the child are suggestive for inflicted injury. In neonate and infants, the fractures often coexist without any external physical findings or skin lesions. Therefore, the absence of external findings can at no time exclude inflicted injury.

Nonskeletal injuries to the chest, abdomen, and pelvis can occur in the setting of inflicted injury. Potential thoracic imaging findings are pleural effusion, lung contusion, chylothorax, hemopericardium, and cardiac contusion/laceration. Abdominal injuries detected on imaging include contusion/laceration of solid organs, injury to or rupture of bowel/bladder, mesenteric root injury, and (sequela of) pancreatitis [25].

Dating of the Imaging Findings of Inflicted Injury

There is a general impression that radiological imaging is able to date the demonstrated abnormalities to a certain accuracy. In medical decision-making, criminal investigations, and legal proceedings, dating of the imaging findings is a recurring issue.

The temporal evolution of intraparenchymal hemorrhages in general is reasonable consistent; however, the evolution of subdural hemorrhages is reported to be variable or not consistent [13, 17]. Recent literature reveals a wide range and broad overlap of the time intervals reported for the different appearances of subdural hemorrhages on CT and MR imaging studies. Hemorrhage with both CT hyperdense and hypodense features can indicate hyperacute hemorrhage or chronic hemorrhage with sign of rebleed. Intracranial hemorrhagic material may intermix with cerebrospinal fluid. In addition, the hemoglobin concentration of the blood affects the density of the acute hemorrhage. Particularly in the pediatric age group, no significant differences are established between the time intervals for the different CT densities of subdural hemorrhages [17]. A hypothesis for the distinct temporal evolution of parenchymal and subdural hemorrhages in children is the high oxygen tension in the subdural space caused by the vascularized dura [26]. As a consequence, CT or MR imaging appearances of subdural hemorrhages are inappropriate to accurately date the subdural hemorrhages.

The exact dating of fractures based on the presence of periosteal reaction, hard callus formation, or signs of remodeling is not sufficiently consistent to rely on. Therefore, dating of fractures is limited to differentiate recent from old fractures [24]. In addition, due to the membranous origin of the calvarial bones, skull fractures demonstrate lack of periosteal reaction in the healing process. The healing time of a

simple linear skull fracture mandates up to 6 months in an infant and as long as 1 year in an older child [21]. Consequently, dating of a skull fracture is even less consistent and lacks the possibility of distinguishing recent from old fractures.

Differential Diagnosis of Inflicted Injury of the Central Nervous System

In regard of the fact that inflicted injury of the brain and spine is the most common cause of neurotrauma in the pediatric age group under the age of 2, the diagnosis of inflicted injury has to be considered in all children presenting to the medical care system with features of neurotrauma. Furthermore, in various non-neurologic and vague clinical settings, inflicted neurotrauma should always be in the differential diagnosis. Alternative hypotheses for the pattern of injury or clinical presentation have to be considered at all times. Follow-up or additional diagnostic workup may be necessary for differential diagnosis. Radiological imaging studies are important to demonstrate abnormalities associated with inflicted neurotrauma; on the other hand, these studies can reveal features of underlying disease clarifying the clinical presentation and imaging findings.

The differential diagnosis for intracranial hemorrhage and/or related brain abnormalities is extensive and comprises of congenital as well as acquired medical conditions. Birth trauma is a plausible differential diagnosis in the neonatal age group. Birth trauma is frequently causative for the development of subdural hemorrhages. These types of neonatal hemorrhages tend to involute completely within 4 weeks of age [24]. Another relative common condition to consider in the young age group is benign enlargement of the subarachnoid spaces. Furthermore, conditions causing hypoxic-ischemic injury (e.g., apnea, cardiac arrest, seizure), vascular abnormalities (e.g., arterial or venous thrombosis, AVM), infectious diseases, coagulation disorders (e.g., vitamin K deficiency), and metabolic disorders (e.g., glutaric acidosis type 1, Menkes disease) are appropriate differential diagnoses in all pediatric age groups. Connective tissue disorders (e.g., osteogenesis imperfecta) must be considered in case of multiple fracture sites. Alternative diagnoses have to be ruled out by knowledge of the medical history, complete clinical examination, or laboratory tests before trauma is considered as the possible diagnosis. To distinguish accidental trauma from inflicted trauma, detailed evaluation of the constellation of clinical and imaging findings in the context of the provided history is essential (Fig. 5).

Workup of Inflicted Injury of the Central Nervous System

The diagnosis of inflected CNS injury has to be approached with careful consideration of every available detail of current clinical symptoms and mode of presentation, complete medical and family history (including siblings), growth curve, physical examination, laboratory testing, radiologic

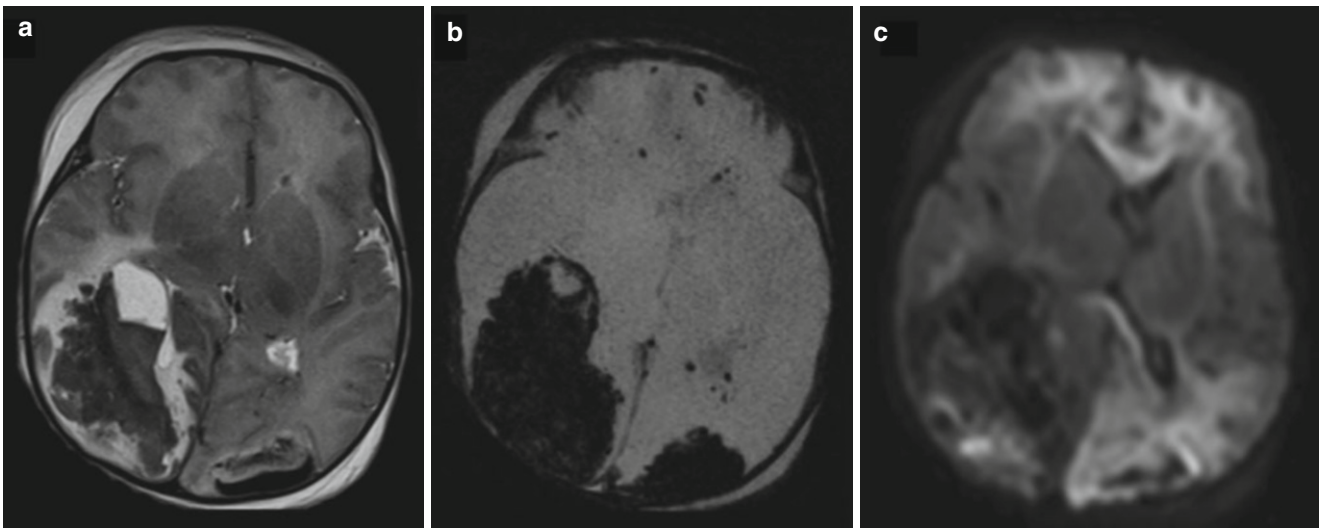

Fig. 5 Axial T2-weighted MR image (**a**), axial SWI MR image (**b**), and axial trace of diffusion MR image (**c**) in a child with liver failure and consequent coagulopathy. In addition, the patient was resuscitated from cardiac arrest. The axial T2-weighted image and SWI image (**a**) show extensive intraparenchymal hemorrhages in the right parieto-occipital region and to a lesser extent in the left parieto-occipital region. Subdural and subarachnoid hemorrhages are noted. The axial SWI image (**b**) reveals additional microhemorrhages scattered in the bilateral frontoparietal regions. On the axial trace of diffusion MR image (**c**), the extensive concomitant diffuse hypoxic-ischemic injury is best appreciated

evaluation, and assessment of possible risk factors. The workup is focused on identifying related injuries, evaluation of the pattern of injuries, detecting injuries of differing age, and exclusion of entities mimicking inflicted injury. One important issue is to determine if the described trauma or situation is considered adequate to cause and/or explain the presenting injury pattern.

Conventional radiography, CT, and MRI are complimentary imaging techniques in the context of suggested inflicted injury. The only available guideline for standardized overall use of different imaging modalities in inflicted neurotrauma is published by the Royal College of Radiologists (RCR) and the Royal College of Paediatrics and Child Health (RCPCH) in 2008 [6]. The time interval between the inflicted injury and the moment of presentation (acute or delayed) and the timing of the specific imaging modality are taken into account. The combined use of CT and MR imaging techniques enables more accurate detection, localization, and characterization of intracranial injury. The role of repeated CT or MR imaging studies is controversial and is completely dependent on the clinical situation of the affected child. The decision to image thoracoabdominal structures is based on the clinical presentation or concerning features on conventional radiographs. Depending on the anatomical region of concern and the age of the affected child, potential useful imaging studies include abdominal ultrasound and CT scan of chest and/or abdomen with intravenous contrast administration.

Computed Tomography

In the setting of (accidental or inflicted) traumatic injury to the CNS, CT is the first-line imaging modality of choice. Cranial CT offers reliable identification of skull fractures as well as intracranial pathology. The standard use of 3D reconstructions improves the detection of fractures even further (Fig. 2). Evaluation of the images in multiple window-level settings is essential to depict subtle hyperdense hemorrhages adjacent to the skull. Multiplanar reconstructions are recommended to include the craniocervical junction for evaluation of fractures, (sub)luxations, and hemorrhages. In any event of a child presenting with signs of abuse combined with signs of possible neurotrauma or retinal hemorrhages, a cranial CT imaging study has to be performed [6, 7, 20]. Due to the possibility of occult brain injury in young children, the ACR appropriateness criteria advise CT evaluation in "any child younger than 24 months of age and suspected physical abuse with or without focal neurologic signs or symptoms" [7]. The RCPCH/RCR guidelines recommend a CT study in "any child under the age of one where there is evidence of physical abuse" [6].

Spinal CT of the cervical or thoracolumbar spine is recommended if there is clinical or radiographical suspicion for vertebral fracture or dislocation.

Magnetic Resonance Imaging

MR imaging of the brain is less sensitive for detection of acute hemorrhage in comparison with CT [20]. Additional long scan times, limited availability, and the potential need for general anesthesia or sedation in the pediatric population result in the use of MR imaging as second-line imaging tool in the setting of inflicted injury of the brain and spine. The importance of complementary MR imaging of the brain is highlighted by detection of additional imaging findings in 25–30 % of inflicted injury cases [20, 23] due to the superior contrast resolution of MRI versus CT. MRI gives a detailed picture of potential parenchymal injury (e.g., diffuse axonal injury) and offers valuable information about the character and time evolution of intracranial hemorrhages. Furthermore, MRI demonstrates more detailed visualization of the posterior fossa structures. The published standard of the RCPCH/RCR for MR imaging of the brain and spine in case of suspected inflicted CNS injury offers different imaging protocols depending on the acute or non-acute presentation of the affected child [6]. The American College of Radiology and Society of Pediatric Radiology (ACR/SPR) and the RCPH/RCR recommend T1- and T2-weighted sequences, gradient echo or susceptibility-weighted sequences, and diffusion-weighted sequences as minimal imaging protocol. MRI has superior ability in monitoring the pattern of cascade of secondary brain injury compared to CT. If the abnormalities demonstrated with conventional imaging techniques do not adequately explain the neurological deficits, the added value of advanced functional imaging techniques, like DTI and fMRI, is emphasized.

In neonates and infants, MR imaging of the cervical spine is advisable to add to the standard MR imaging of the brain, because of the relative high risk of inflicted spinal cord injury of the cervical spine without radiographic abnormality (SCIWORA). The low threshold for MR imaging of the cervical spine is all the more important because upper cervical injuries typically demonstrate lack of external signs in this young age group.

MR imaging of the thoracolumbar spine is recommended if there are clinical features or findings on conventional radiographs suggesting thoracolumbar spinal injury.

Conventional Radiography

The role of conventional radiography in inflicted CNS injury is focused on the skeletal survey to confirm clinical evident

conditions, detect potential occult trauma, and reveal and identification of underlying disease processes. Because of the importance of the detected skeletal abnormalities in supporting or rejecting the diagnosis of inflicted injury or potential alternative diagnoses, it is of major concern to perform the skeletal survey according to international guidelines. The most recent guidelines (2014) of the ACR/SPR and the 2008 guidelines of the RCPCH/RCR have reached consensus about the skeletal survey protocol [6, 7]. The skull radiograph is a consistent and obligatory part of the skeletal survey in both guidelines (regardless of performing a CT scan of the skull and brain). In case of equivocal imaging findings or persistent clinical suspicion, a repeat skeletal survey after 14 days is recommended. The follow-up skeletal survey excludes the skull radiograph due to the absence of periosteal reaction in the healing process of skull fractures. The use of whole-body MR imaging instead of standard skeletal survey is discouraged as a consequence of to the low sensitivity in detecting inflicted injury-related skeletal abnormalities. In particular situations, site-specific MR imaging proves to be useful for further evaluation and characterization of abnormalities [24].

Ultrasound

Ultrasound of the pediatric skull and brain is not routinely used in the diagnostic workup of inflicted brain injury. The structures located in the periphery of the brain and in the extra-axial spaces, under the convexity of the skull, being exact the areas of major concern in the workup of inflicted CNS injury, are difficult or impossible to visualize by means of cranial ultrasonography. In specific cases, ultrasound of the brain is useful for establishing a suspected alternative diagnosis (e.g., benign enlargement of the subarachnoid spaces) or for follow-up of already identified intracranial pathology.

Making the diagnosis of inflicted injury has major social, psychosocial, and legal consequences. Therefore, the used medical terminology must accurately reflect the medical diagnosis. The radiology report should include a detailed factual and objective description of the imaging abnormalities, as well as the pattern, distribution, and severity of the abnormalities. The relevant differential diagnoses have to be included in the report. A remark regarding the quality of the study and the adherence of the study to international guidelines has to be incorporated. In case of suspected inflicted injury based on radiological imaging findings, immediate communication with the responsible clinician is essential for the safety of the affected child and the siblings [20].

The consequential ethical and legal mandates to report suspected inflicted injury to authoritative institutions for further investigation and intervention in the form of child protection procedures are of particular importance. Non-diagnosis or delayed diagnosis in the case of child abuse potentially has severe consequences for the involved child as well as the siblings.

A multidisciplinary approach to child abuse is essential in order to deal with and resolve this specific medical entity in the best possible way.

Conclusion

Timely recognition and early identification of features suggestive for inflicted injury are essential to minimize the consequences of primary injury to the brain and spine and limit or prevent the occurrence of secondary CNS injury. A multidisciplinary approach to child abuse is essential. Radiological imaging plays a crucial role in the detection of physical child abuse. The imaging studies can provide confirmatory evidence of inflicted injury or, on the other hand, contribute by narrowing down a differential diagnosis. If the diagnosis of inflicted injury is not considered or delayed, involved children and siblings are at high risk of repeated abuse. In case inflicted injury is suspected, an appropriate referral to child protection programs should be made as soon as possible.

References

1. Roche JA, Fortin G, Labbe J, Brown J, Chadwick D (2005) The work of Ambroise Tardieu: the first definitive description of child abuse. Child Abuse Negl 29(4):325–334
2. Caffey J (1946) Multiple fractures in long bones of infants suffering from chronic subdural hematoma. Am J Roentgenol 56:163–173
3. Caffey J (1972) On the theory and practice of shaking infants. Am J Dis Child 124(2):161–169
4. Ludwig S, Warman M (1984) Shaken baby syndrome: a review of 20 cases. Ann Emerg Med 13(2):104–107
5. Christian CW, Block R (2013) Committee of Child Abuse and Neglect (2009, reaffirmed in 2013) Abusive head trauma in infants and children. Pediatrics 123(5):1409–1411
6. The Royal College of Radiology, Royal College of Paediatrics and Child Health (2008) Standards for radiological investigations of suspected non-accidental injury
7. American College of Radiology (2014) ACR practice guideline for skeletal surveys in children
8. Sieswerda-Hoogendoorn T, Boos S, Spivack B, Bilo RAC, van Rijn RR (2012) Abusive head trauma part I. Clinical aspects. Eur J Pediatr 171:415–423
9. Duhaime AC, Gennarelli TA, Thibault LE, Bruce DA, Margulies SS, Wiser R (1987) The shaken baby syndrome: a clinical, pathological, and biomechanical study. J Neurosurg 66(3):409–415
10. Duhaime AC, Christian CW, Rorke LB, Zimmerman RA (1998) Nonaccidental head injury in infants – the "shaken-baby-syndrome". N Engl J Med 338:1822–1829
11. Mulpuri K, Slobogean BL, Tredwell SJ (2011) The epidemiology of nonaccidental trauma in children. Clin Orthop Relat Res 469(3):759–767
12. Pinto PS, Poretti A, Medoded A, Tekes A, Huisman TAGM (2012) The unique features of traumatic brain injury in children. Review of

the characteristics of the pediatric skull and brain, mechanisms of trauma, patterns of injury, complications and their imaging findings – part 1. J Neuroimaging 22:e1–e17
13. Huisman TA, Phelps T, Bosemani T, Tekes A, Poretti A (2015) Parturitional injury of the head and neck. J Neuroimaging 25(2): 151–166
14. Knox J, Schneider J, Wimberly RL, Riccio AI (2014) Characteristics of spinal injuries secondary to nonaccidental trauma. J Pediatr Orthop 34:376–381
15. Huisman TA, Wagner MW, Bosemani T, Tekes A, Poretti A (2015) Pediatric spinal trauma. J Neuroimaging 25(3):337–353
16. Maguire S, Pickerd N, Farewell D et al (2009) Which clinical features distinguish inflicted from non-inflicted brain injury? A systematic review. Arch Dis Child 94(11):860–867
17. Sieswerda T, Postema FA, Verbaan D et al (2014) Age determination of subdural hematomas with CT and MRI: a systematic review. Eur J Radiol 83:1257–1268
18. Rubin DM, Christian CW, Bilaniuk LT et al (2003) Occult head injury in high-risk abused children. Pediatrics 111: 1382–1386
19. Kemp AM, Joshi AH, Mann M, Tempest V, Liu A, Holden S, Maguire S (2010) What are the clinical and radiological characteristics of spinal injuries from physical abuse: a systematic review. Arch Dis Child 95:355–360
20. Sieswerda-Hoogendoorn T, Boos S, Spivack B, Bilo RAC, van Rijn RR (2012) Abusive head trauma part II. Radiological aspects. Eur J Pediatr 171:617–623
21. Barnes PD, Krasnokutsky M (2007) Imaging of the central nervous system in suspected or alleged nonaccidental injury, including the mimics. Top Magn Reson Imaging 18:53–74
22. Colbert CA, Holshouser BA, Aaen GS et al (2010) Value of cerebral microhemorrhages detected with susceptibility-weighted MR imaging for prediction of long-term outcome in children with nonaccidental trauma. Radiology 256(3):898–905
23. Hsieh KLC, Zimmerman RA, Kao HW, Chen CY (2015) Revisiting neuroimaging of abusive head trauma in infants and young children. Am J Roentgenol 204:944–952
24. van Rijn RR, Spevak MR (2011) Imaging of neonatal child abuse with an emphasis on abusive head trauma. Magn Reson Imaging Clin N Am 19:791–812
25. American College of Radiology (2012) American College of Radiology ACR appropriateness criteria: suspected physical abuse – child
26. Bradley WG Jr (1994) Hemorrhage and hemorrhagic infections in the brain. Neuroimaging Clin N Am 4:707–732

The Acute Pediatric Spine and Spinal Cord

Andrea Rossi

Introduction

Acute lesions involving the spine and spinal cord in the pediatric age group are rare, but comprise several different pathomechanisms and entities. Patients presenting in the emergency room with acute back pain and/or signs of acute neurological involvement including sensorimotor deficit of the upper and/or lower limbs and sphincter dysfunction warrant emergent clinical evaluation and neuroimaging studies. The risk of a spinal cord compression must always be borne in mind by referring clinicians, since neurological recovery often depends primarily on surgical decompression and stabilization, and the impact of permanent paralysis in an otherwise normal child may result in severe psychological trauma to the child as well as the parents. Often, however, neurological deterioration occurs subacutely in the context of preexisting conditions. It is not uncommon for patients with acute spinal injury to complain with back pain or, in younger children, pain equivalents such as refusal to crawl, sit, or walk. The presence of back pain in prepubertal children almost always heralds a serious underlying disorder; however, families and even physicians overlooking the problem may cause a significant delay in the diagnosis. Red flags for children with back pain include age less than 4 years, presence of a functional disability, duration of greater than 4 weeks, presence of a fever, postural shift of the trunk caused by the pain, limitation of motion due to the pain, and presence of a neurologic abnormality. Head tilt, or torticollis, may be indicative of injury to the craniocervical injury which, if unstable, can further lead to severe neurological deterioration and even death.

A. Rossi
Neuroradiology Unit, Istituto Giannina Gaslini,
Via Gerolamo Gaslini 5, Genoa 16135, Italy
e-mail: andrearossi@gaslini.org

Neuroimaging: General Principles

Diagnostic imaging in patients presenting with an acute spinal injury is aimed at identifying the location, degree, and quality of primary injury in order to institute an immediate treatment and to limit or prevent secondary injury. Imaging should be fast, be readily available, and not interfere with the emergent treatment, and be highly sensitive and specific [1]. Among available imaging modalities, consisting of conventional X-rays, computerized tomography (CT), and magnetic resonance imaging (MRI), the choice should be made based on the patient's clinical status and the available equipment.

In the setting of spinal trauma, X-rays are still often used as the first imaging modality, although helical CT with multiplanar reformat and including bone and soft tissue algorithms should be preferred, especially in patients with serious trauma. MRI is typically performed rapidly as a second line of imaging if focal neurological signs are present, suspecting a spinal cord lesion. Conversely, non-trauma patients presenting in the emergency room with acute neurological signs compatible with a spinal cord lesion should directly be referred for emergent MRI with the goal of identifying potentially curable causes of spinal cord compression. The MR field of view should always cover the entire spine on the sagittal plane and include both T1- and T2-weighted images; axial imaging is typically focused on any focal pathological finding. Coronal imaging with STIR sequences is also useful to obtain a panoramic coverage of the spine while exploiting the exquisite sensitivity of STIR to vertebral bone edema. Post-contrast imaging is also strongly advised in the context of acute neurological presentations, in order to characterize lesions and to evidence areas of blood-cord or blood-root barrier breakdown. In the pediatric age group, sedation is often required to carry out

J. Hodler et al. (eds.), *Diseases of the Brain, Head and Neck, Spine 2016–2019: Diagnostic Imaging*, DOI 10.1007/978-3-319-30081-8_34

MRI studies if the patient is too young or too ill to cooperate.

Spine Trauma

The type, severity, and consequences of trauma significantly depend on the peculiar properties of the immature pediatric spine [2]. These include the predominantly cartilaginous composition of the spine and the relatively lax ligaments, which render the pediatric spine mobile and deformable compared to adults. As a consequence, vertebral fractures are less frequent than dislocations, ligamentous injuries, epiphyseal detachments, and lesions of the ossification centers. The craniocervical junction of infants and small children is also especially vulnerable because of their comparatively larger head with respect to the torso and the weaker neck musculature, especially in the context of sudden acceleration and deceleration. Only from about 10 years of age does the more typical adult distribution start to prevail, with predominantly cervicothoracic or lumbar injuries. Knowledge of the peculiar biomechanics and structure of the pediatric spine, as well as of normal variants or pitfalls (such as the physiological C2–C3 subluxation), is essential for a correct interpretation of imaging studies in the pediatric age group.

The leading cause of spinal trauma in children is motor vehicle accidents (52 %), followed by sports-related injuries (27 %) [3]. Patients with craniocervical junction or cervical trauma have a typically acute presentation with neurological deficit and have a poor prognosis. Intracranial lesions such as hematomas or diffuse axonal injury may coexist and also have a profound impact on the clinical picture and prognosis.

SCIWORA The term indicates a form of spinal cord injury without radiographic abnormality, i.e., lacking evidence on either X-ray or CT scan [4], but evident on MRI studies. This form of spinal cord injury is typical of infants and children and is caused by the high mobility and flexibility of the pediatric spine, which allows for an

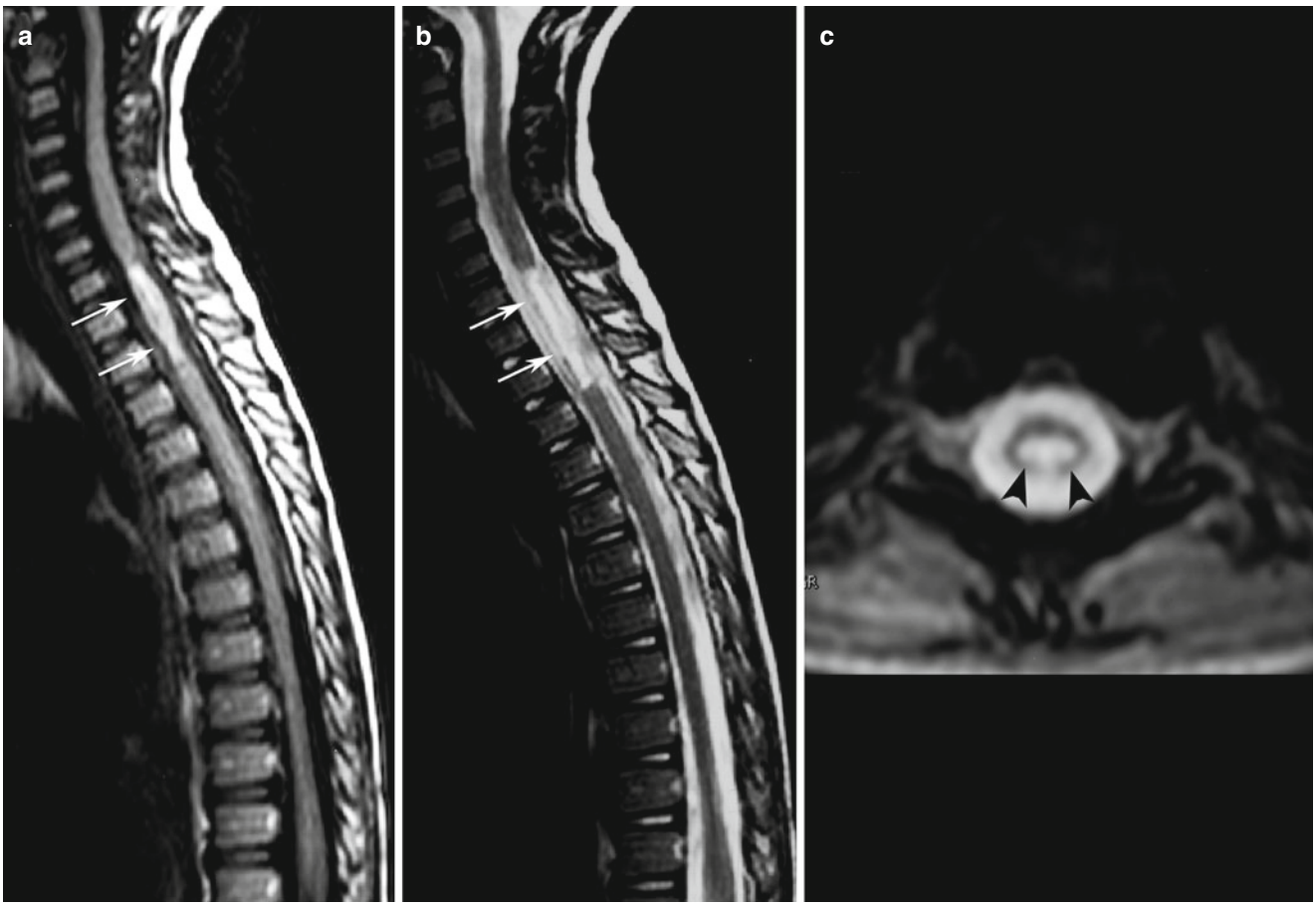

Fig. 1 SCIWORA in a 2-year-old girl involved in a motor vehicle accident. Sagittal FLAIR (**a**) and T2-weighted images (**b**) show intramedullary hyperintense lesion at the C7–T2 level (*arrows*). The osteocartilaginous spine is unremarkable. Axial T2-weighted image (**c**) shows cross-sectional spinal cord involvement (*arrowheads*)

intermittent luxation with consequent impact and contusion of the spinal cord. MRI usually shows a swollen, T2 hyperintense spinal cord in the affected segment (Fig. 1); petechial hemorrhages or frank hematomyelia may complicate the picture.

Atlanto-occipital and Atlanto-axial Dislocation In these severe cases of dislocation, there is typically an anteriorization of the atlas with acute narrowing of the spinal canal, which in turn causes injury to the bulbomedullary junction and spinal cord (Fig. 2). This form of injury is almost invariably severe and leads to a very guarded, if not constantly dismal, prognosis, especially when a complete ligamentous rupture causes a true axial/vertical atlanto-occipital dissociation. Less severe forms of progressive atlanto-axial dislocation may occur also outside the context of trauma, and especially in patients with inflammatory disorders of the craniocervical junction (especially juvenile idiopathic arthritis) or with common otolaryngeal conditions including pharyngitis, adenotonsillitis, tonsillar abscess, cervical abscess, and otitis media that results in hyperemia and pathological relaxation of the transverse ligament of the atlanto-axial joint (Grisel syndrome) [5].

Vertebral Fractures Most vertebral fractures seen in the pediatric clinical practice are compression fractures are characterized by wedge-shaped deformity of the involved vertebral body with interruption/fracture of the anterior vertebral contour [1]. These fractures typically result from falls and are stable if they only involve the anterior column. More severe fractures include burst fractures, in which both the anterior and posterior contour of the vertebral body are involved, resulting in an intrinsically unstable condition which can further be complicated by intraspinal dislocation of bony fragments causing direct spinal cord damage. Peculiar regional fractures can also be encountered, such as the Jefferson fracture of the atlas and the Anderson and Hangman fractures of the axis. In the lumbar region, the Chance fracture occurs due to flexion distraction, typically as a result of a seat or lap belt

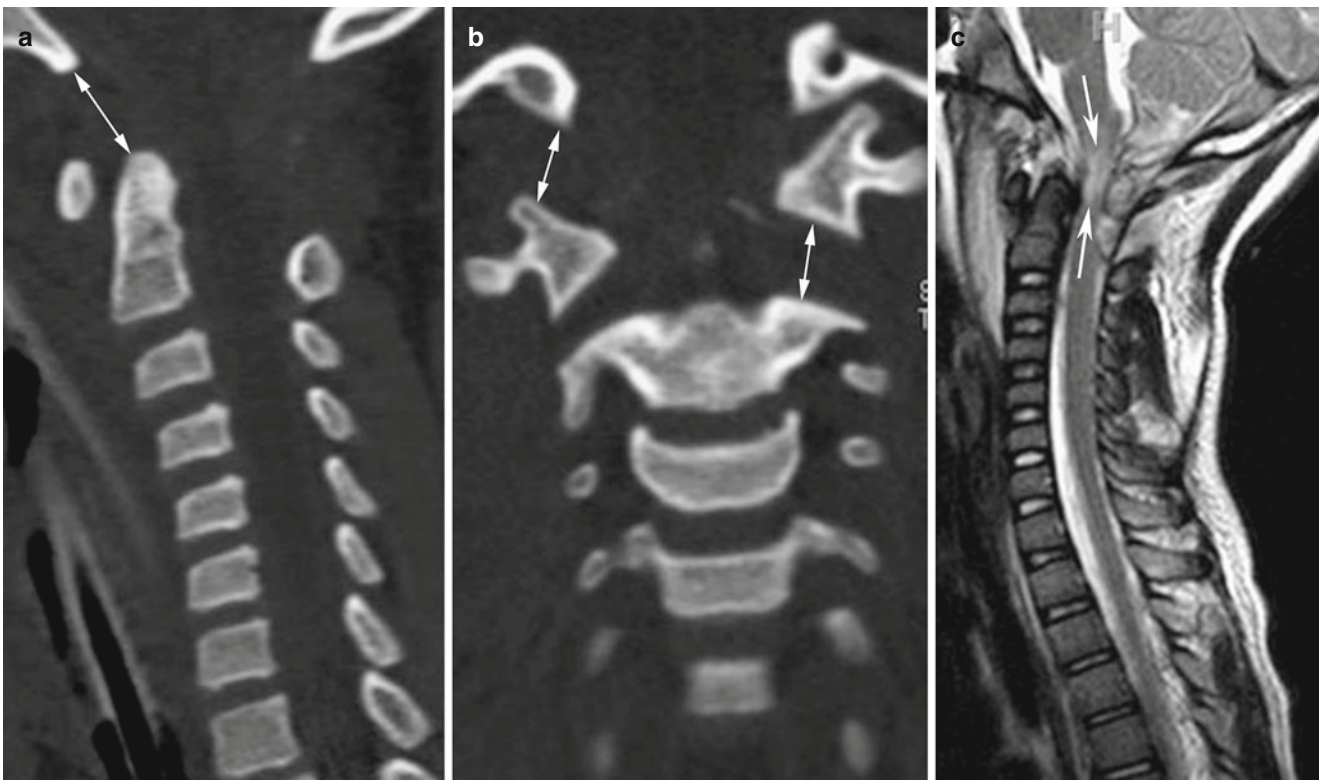

Fig. 2 Atlanto-occipital dislocation. Sagittal (**a**) and coronal (**b**) CT images show asymmetrical dislocation of C1 in relation to C0/skull base with an increased distance between the basion and the tip of the dens (*double arrow*, **a**) and widened right atlanto-occipital and left atlanto-axial joints (*double arrows*, **b**). Sagittal T2-weighted MR image (**c**) shows focal contusion of the lower brain stem and upper cervical spinal cord (*arrows*) as well as a significant ligamentous injury of the craniocervical junction (Case courtesy of T.A. Huisman, Johns Hopkins, Baltimore, USA)

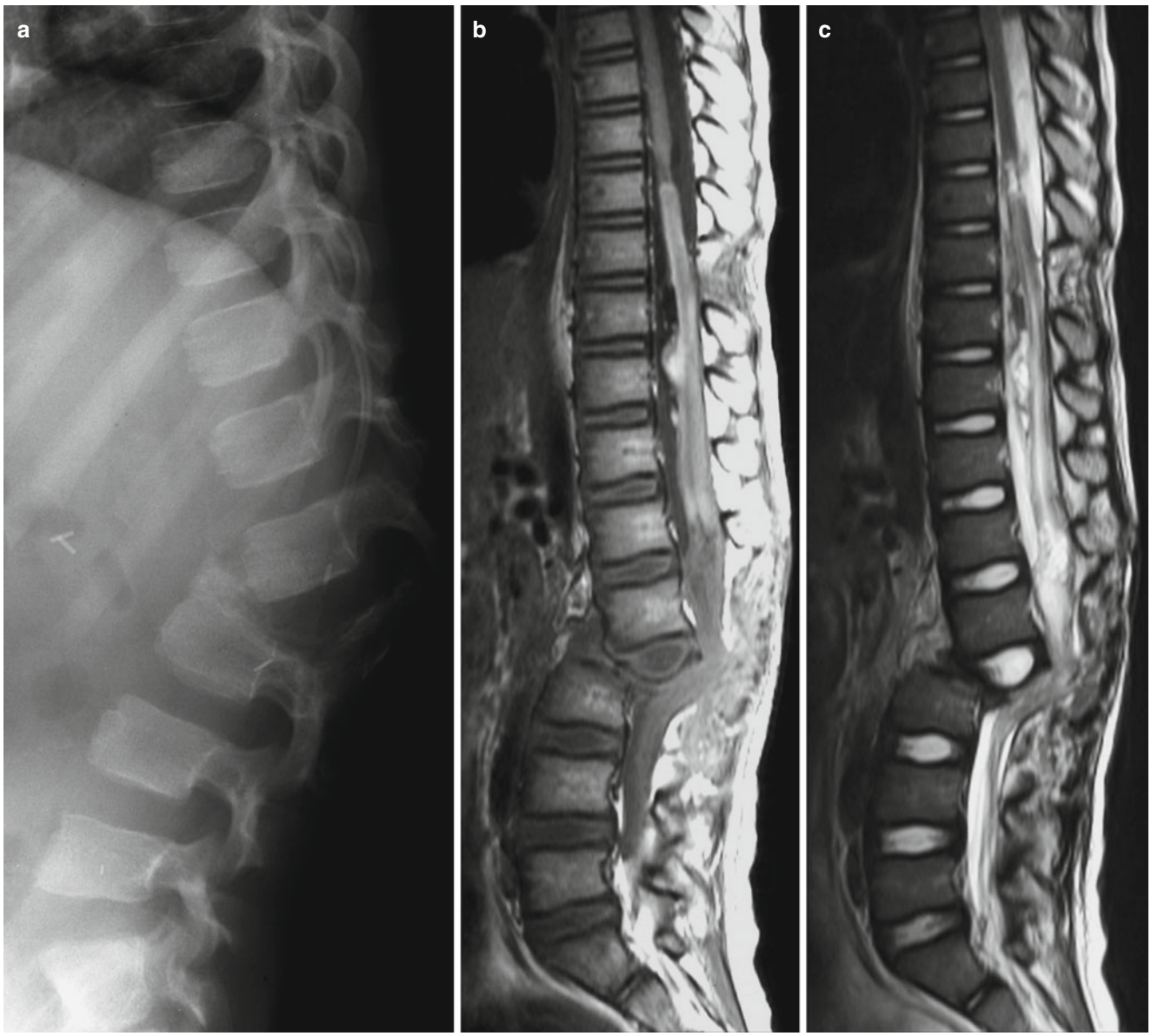

Fig. 3 Lumbar Chance fracture with spinal cord damage in a 7-year-old boy involved in high-speed car accident. Lateral radiogram (**a**) shows disruption of the superior L3 end plate with marked dislocation and kyphosis. Sagittal T1-weighted (**b**) and T2-weighted (**c**) MR images obtained 2 days after emergency decompression show extensive spinal cord and caudal nerve root damage

injury, and is intrinsically unstable as it involves all three longitudinal vertebral columns (Fig. 3).

CT scan is obviously dictated to detect the characteristics of vertebral fracture and to plan surgical management wherever needed; however, MRI including STIR sequences is especially sensitive to even minimal degrees of bone marrow edema (Fig. 4) and is helpful to confirm minimal compression fractures, which may sometimes escape detection on conventional X-ray. MRI is mandatory to assess spinal cord damage or intraspinal hematomas in patients who experience neurological deficit as a result of their trauma.

Infectious/Inflammatory Diseases

Inflammatory and infectious disorders of the spine and spinal cord are less common in children than in adults. The most common infectious spinal disorder in children is bacterial meningitis, which generally does not require imaging studies and is diagnosed and treated on a clinical and physical

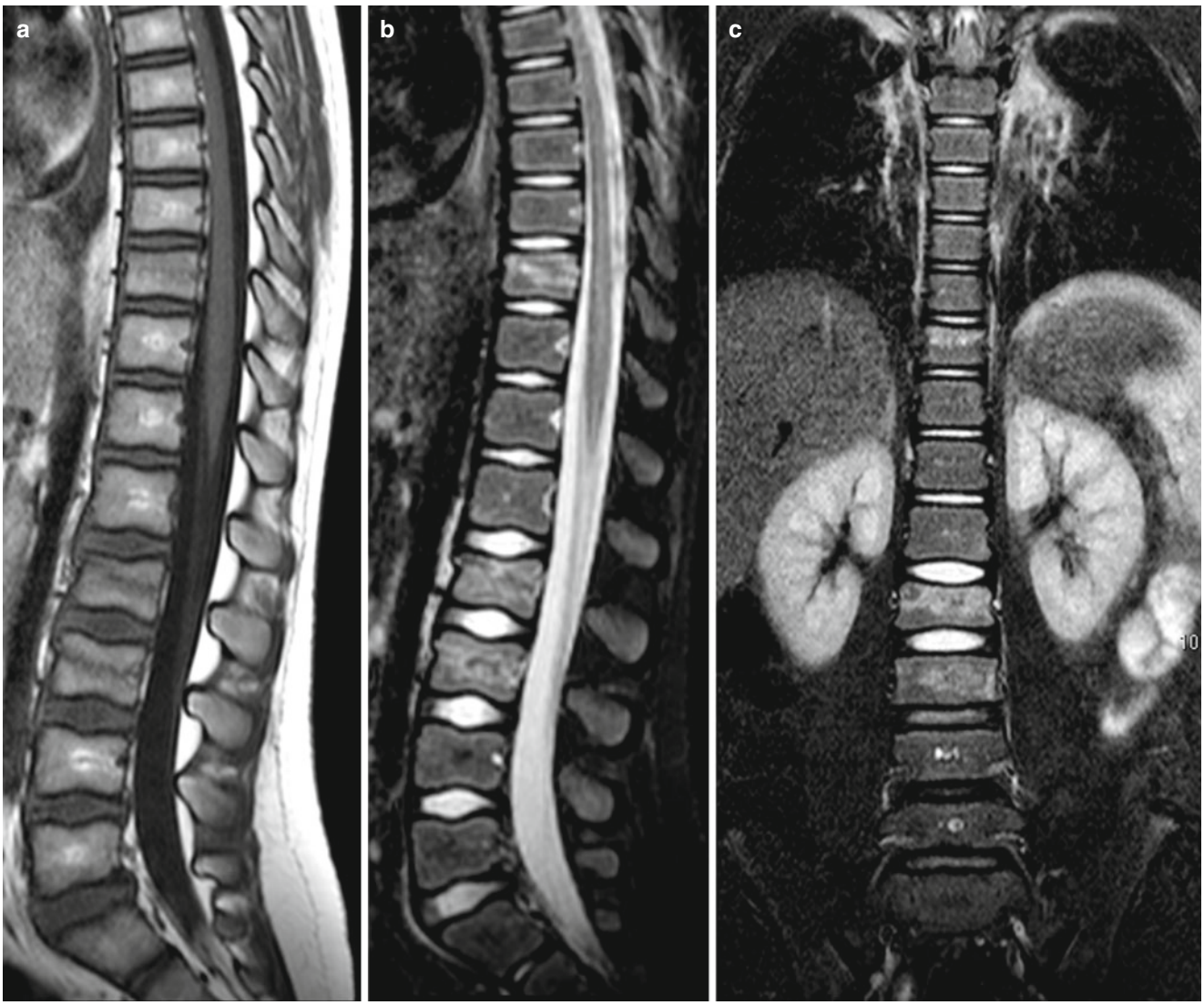

Fig. 4 Compression fractures in a 9-year-old boy. Sagittal T1-weighted image (**a**) shows ill-defined hypointensity of the T10, L2, and L3 vertebral bodies, with a mild reduction in height. Sagittal (**b**) and coronal (**c**) STIR images exquisitely depict hyperintensity of the involved vertebral bodies consistent with bone marrow edema

examination basis. MRI is essential for diagnosing spinal infectious/inflammatory conditions of the spine and spinal cord, while CT does not play a role outside certain specific conditions. Although many of these disorders also show brain abnormalities, I will focus on the abnormalities found in the spine and spinal cord.

Acute Transverse Myelitis Acute transverse myelitis (ATM) is a focal inflammatory disorder of the spinal cord characterized by an acute onset of motor, sensory, and autonomic dysfunction. Clinical presentation is with pain, paresthesias, leg weakness, and sphincter dysfunction, all of which more or less rapidly progress in the hours to days following the onset. Cerebrospinal fluid (CSF) analysis shows pleocytosis or elevated IgG index. The diagnosis of idiopathic ATM involves exclusion of other causes of acute neurological involvement such as extrinsic spinal compression, ischemia, tumor, arteriovenous malformation, and toxicities [6]. Identified causes of ATM such as connective tissue disease, ADEM, multiple sclerosis, and neuromyelitis optica (NMO) must also be ruled out.

MRI plays a fundamental role in patients suspected of harboring ATM and should be done in emergency, because the presentation of compressive lesions such as extramedullary tumor or hemorrhage can be identical [7]. It is wise to also include the brain in order to assess possible additional lesions (such as those typical of ADEM or multiple sclerosis) without delay while minimizing the need for additional seda-

tion [7]. Spinal MRI (Fig. 5) should include high-resolution sagittal T1- and T2-weighted images; sagittal short-tau inversion recovery (STIR) is also extremely useful to detect subtle signal intensity abnormalities of the spinal cord. Optimal slice thickness for sagittal studies should be 3 mm or less. Axial T2-weighted images across lesional areas help to determine the cross-sectional extent of the spinal cord involvement, an important element in the differential diagnosis [8]. Post-contrast images should be acquired in the three planes of space. In ATM, MRI shows normal or slightly expanded, T2-hyperintense spinal cord segment involving more than 3–4 vertebral levels in length and more than 2/3 of the cross-sectional area. Gadolinium enhancement depends on the degree of inflammation and timing of imaging with respect to clinical onset, and can be thoroughly absent [3]. Brain imaging is normal in patients with idiopathic ATM.

Acute Disseminated Encephalomyelitis Acute disseminated encephalomyelitis (ADEM) involves a first episode of inflammatory demyelination with polyfocal neurological signs implicating involvement of multiple sites of the CNS. Patients present with a rapid onset of encephalopathy and motor and/or sensory deficits with brainstem signs and symptoms and ataxia, and mandatory presence of encephalopathy [9, 10]. Most patients with ADEM present in the aftermath of infection or vaccination. The disorder commonly begins 1–2 weeks after a viral, and seemingly minor, illness. CSF analysis may show increased proteins and leukocytosis.

On MRI, multiple, more or less well-defined or demarcated areas of increased T2 signal intensity within the cord are found [11]. Usually, the lesions do not enhance with gadolinium administration. The single most common differential feature from ATM is the presence of brain involvement, as evidenced by clinical signs of encephalopathy and MRI evidence of signal abnormalities, in ADEM but not in ATM (Fig. 6).

Neuromyelitis Optica Neuromyelitis optica (NMO) is a rare, severe, mono- or multiphasic demyelinating disease of the CNS that preferentially affects the optic nerves and spinal cord. The diagnosis of NMO is made in the presence of optic neuritis and acute myelitis, associated with either a spinal MRI lesion extending over three or more segments or positive NMO serology [10]. The presence of at least two of three findings, (1) contiguous spinal cord MRI lesion extending over 3 vertebral segments, (2) brain MRI not meeting criteria for MS, and (3) NMO-IgG seropositive status, is 99 % sensitive and 90 % specific for NMO [12]. The neuromyelitis optica immunoglobulin G (NMO-IgG) is an autoantibody found in the serum of patients affected by NMO that binds to aquaporin 4 (AQP4), the main channel that regulates water

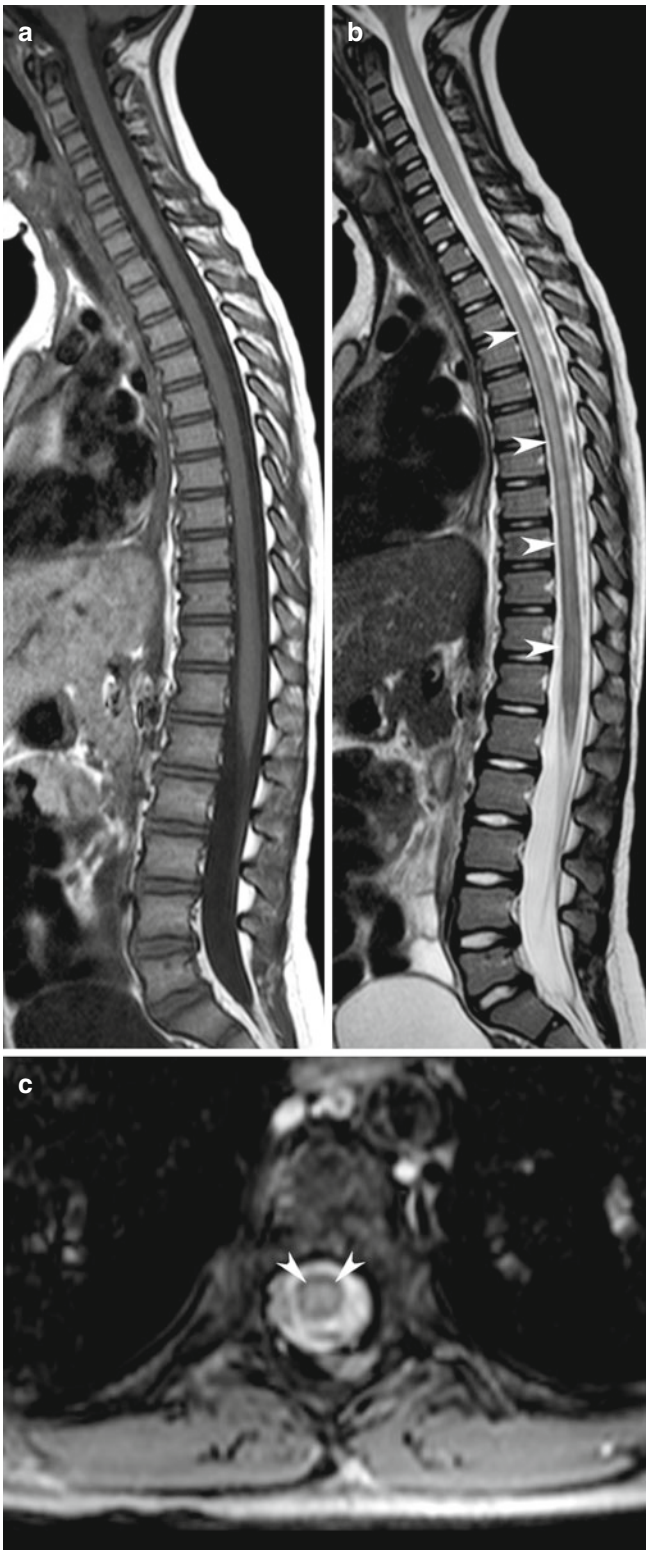

Fig. 5 Acute transverse myelitis in a 5-year-old girl. Sagittal T1-weighted image (**a**) is unrevealing. Sagittal T2-weighted image (**b**) shows ill-defined central hyperintensity of the spinal cord involving most of the thoracic cord and conus medullaris (*arrowheads*). There is not significant swelling of the cord in this case. Axial T2*-weighted image (**c**) confirms hyperintensity of the central portion spinal cord (*arrowheads*), exceeding 2/3 of the cross-sectional area of the cord

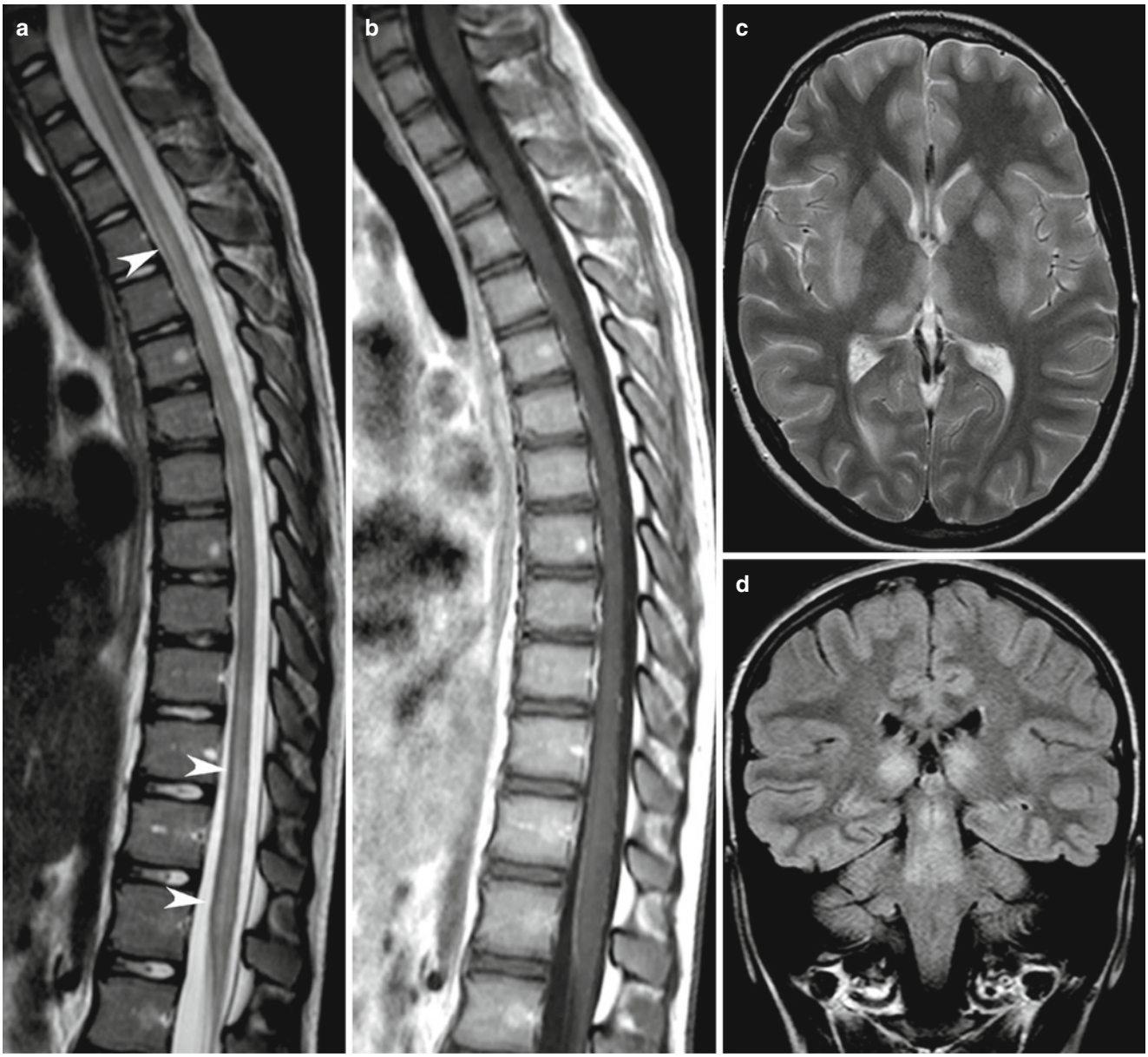

Fig. 6 Acute disseminated encephalomyelitis (ADEM) in a 12-year-old girl. Sagittal T2-weighted image (**a**) shows ill-defined areas of hyperintensity involving the spinal cord at multiple levels (*arrowheads*), while Gd-enhanced sagittal T1-weighted image (**b**) is unrevealing. The imaging findings at level of the spinal cord are not unlike those of isolated ATM. However, axial T2-weighted (**c**) and coronal FLAIR (**b**) images of the brain show multiple hyperintense areas at level of the nucleobasal regions and brainstem, consistent with a diffuse neuraxial process

homeostasis in the CNS, causing disruption of water homeostasis, demyelination, and necrosis with little or no inflammation. In NMO, attacks of acute myelitis precede optic neuritis in only 20 % of cases; in these cases, patients present with severe symmetric paraplegia, sensory loss below the lesion, and bladder dysfunction. The majority of children with an eventual diagnosis of NMO present with isolated LETM, optic neuritis, or brainstem encephalitis, thus failing to meet the diagnostic criteria at the time of their first presentation.

Spinal MRI shows large areas of high T2 signal intensity involving the spinal cord extensively and enhancing inhomogeneously, with a necrotic-cystic pattern that may simulate an intramedullary tumor (Fig. 7) [13, 14]. Imaging of the entire craniospinal axis should always be performed in patients suspected of harboring NMO, and the optic nerves and chiasm should be specifically evaluated. Hypothalamic, periaqueductal gray, and area postrema lesions can also be found in the brain of NMO patients.

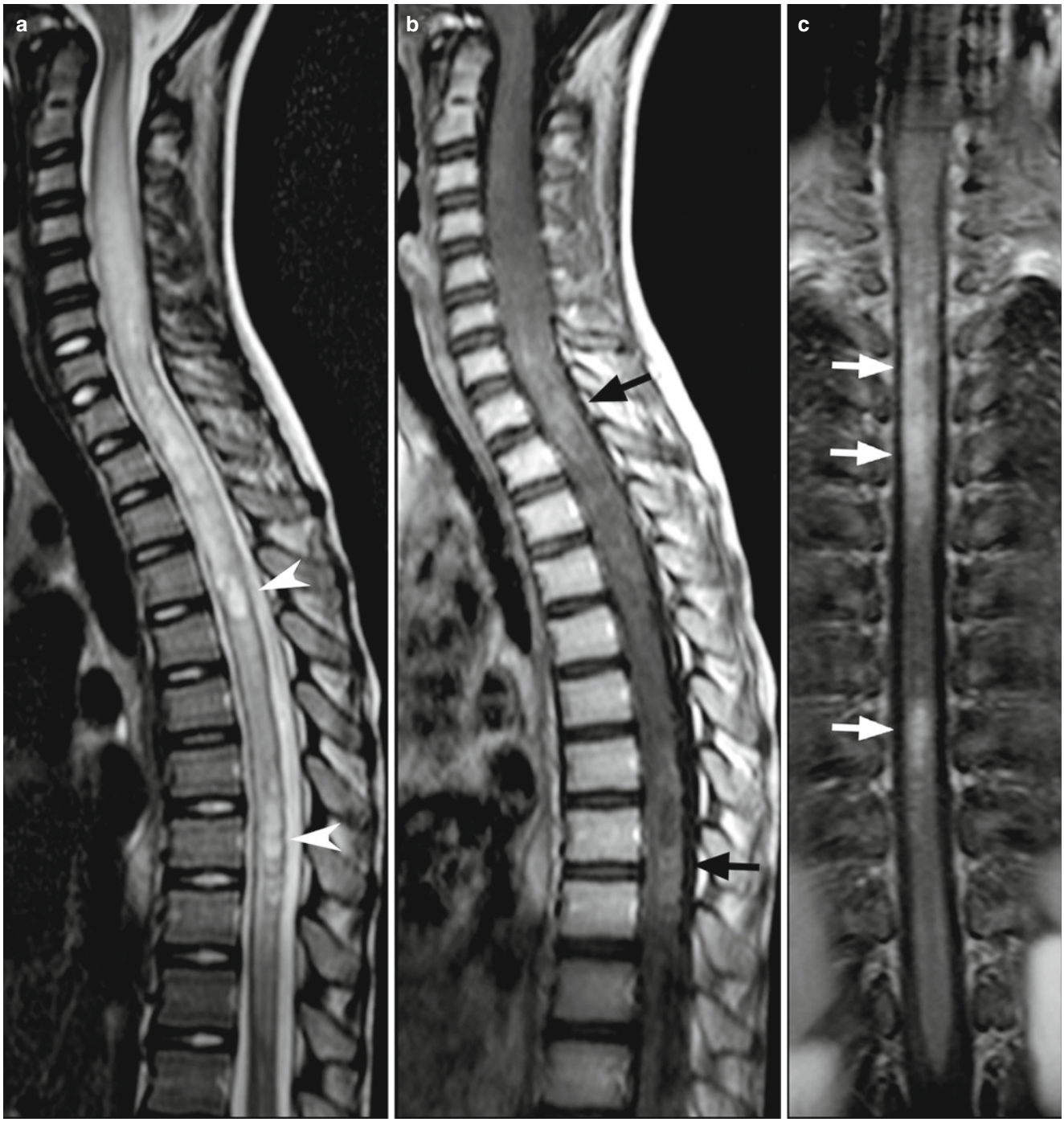

Fig. 7 NMO-IgG-positive longitudinally extensive transverse myelitis (neuromyelitis optica spectrum) in a 9-year-old girl. Sagittal T2-weighted image (**a**) shows marked swelling and hyperintensity of the spinal cord with a holocord extension. Areas of necrotic-cystic changes are shown (*arrowheads*). Gd-enhanced sagittal (**b**) and coronal (**c**) T1-weighted images show irregular areas of enhancement. This patient did not have optic neuritis, and only positive serology revealed the diagnosis, effectively ruling out neoplasm

Spinal Cord Abscess Spinal cord abscesses are extremely rare; predisposing conditions are usually required for germs to colonize the spinal cord, including congenital heart disease, disorders of the immune system, underlying spinal cord tumors, and especially dermal sinuses [15], which allow for a direct communication between the skin and the CNS.

MRI shows increased T2 signal intensity and expansion of the cord; more or less well-defined marginal enhancement occurs after gadolinium administration. A large part or even the whole length of the spinal cord may be involved in the most serious cases (Fig. 8).

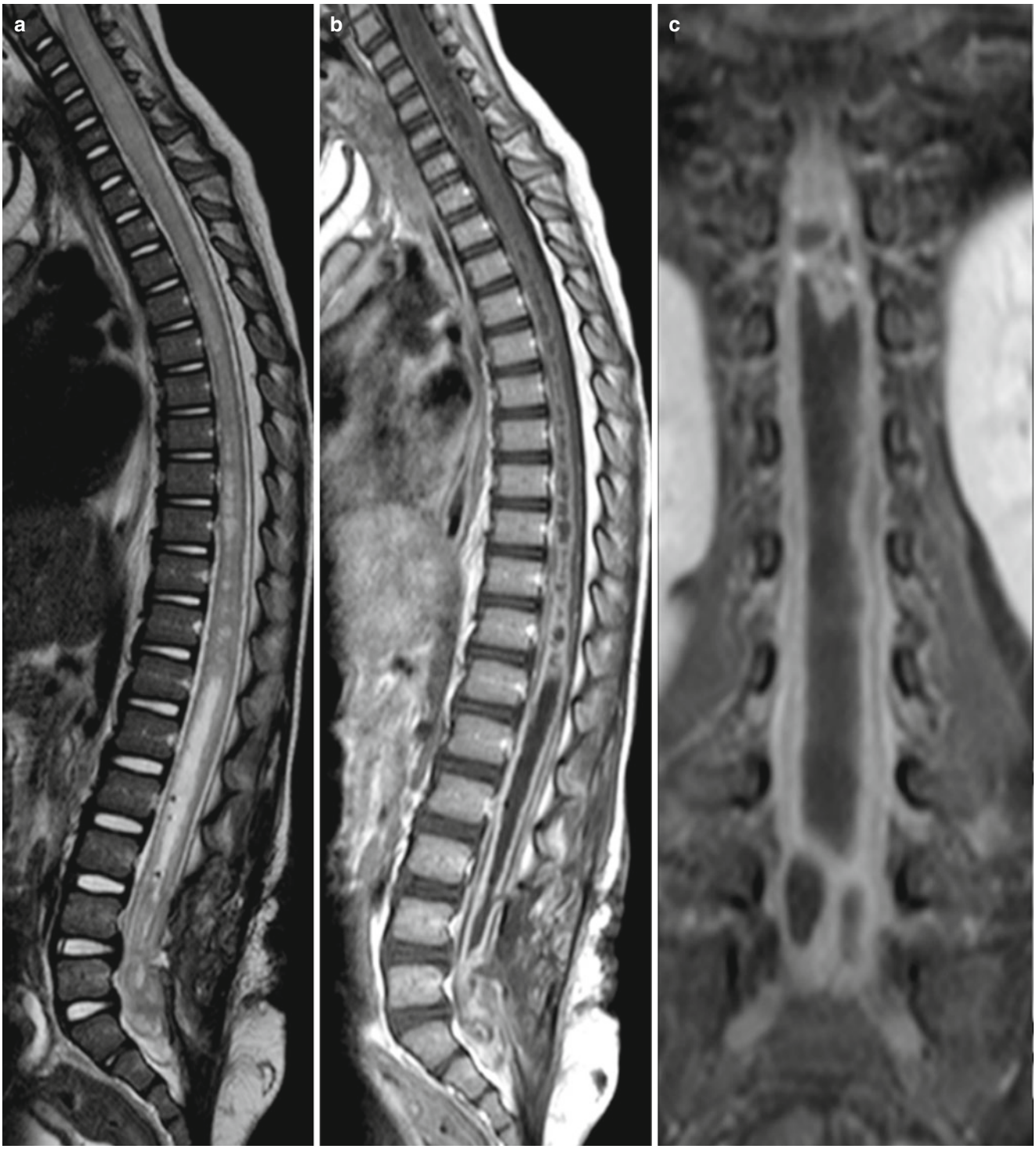

Fig. 8 Diffuse spinal cord abscess in a 2-year-old with prior surgery for lipomyelomeningocele. Sagittal T2-weighted image (**a**) shows diffuse swelling of the whole spinal cord, with signs of cavitation at the lumbar level. The termination of the spinal cord is low due to the pre-existing malformation. Gd-enhanced sagittal (**b**) and coronal (**c**) T1-weighted images show diffuse enhancement of the spinal cord, forming a syrinx-like abscess at the T12–L4 level

Guillain-Barré Syndrome Guillain-Barré syndrome (GBS) is an acute inflammatory disorder involving the spinal and peripheral nerves [16, 17], typically presenting after a recent viral disease (usually a respiratory illness or gastroenteritis). Patients present acutely with lower extremity weakness progressing to flaccid paralysis, often accompanied by sensory disturbances such as pain and paresthesia but rarely associated with sphincter dysfunction.

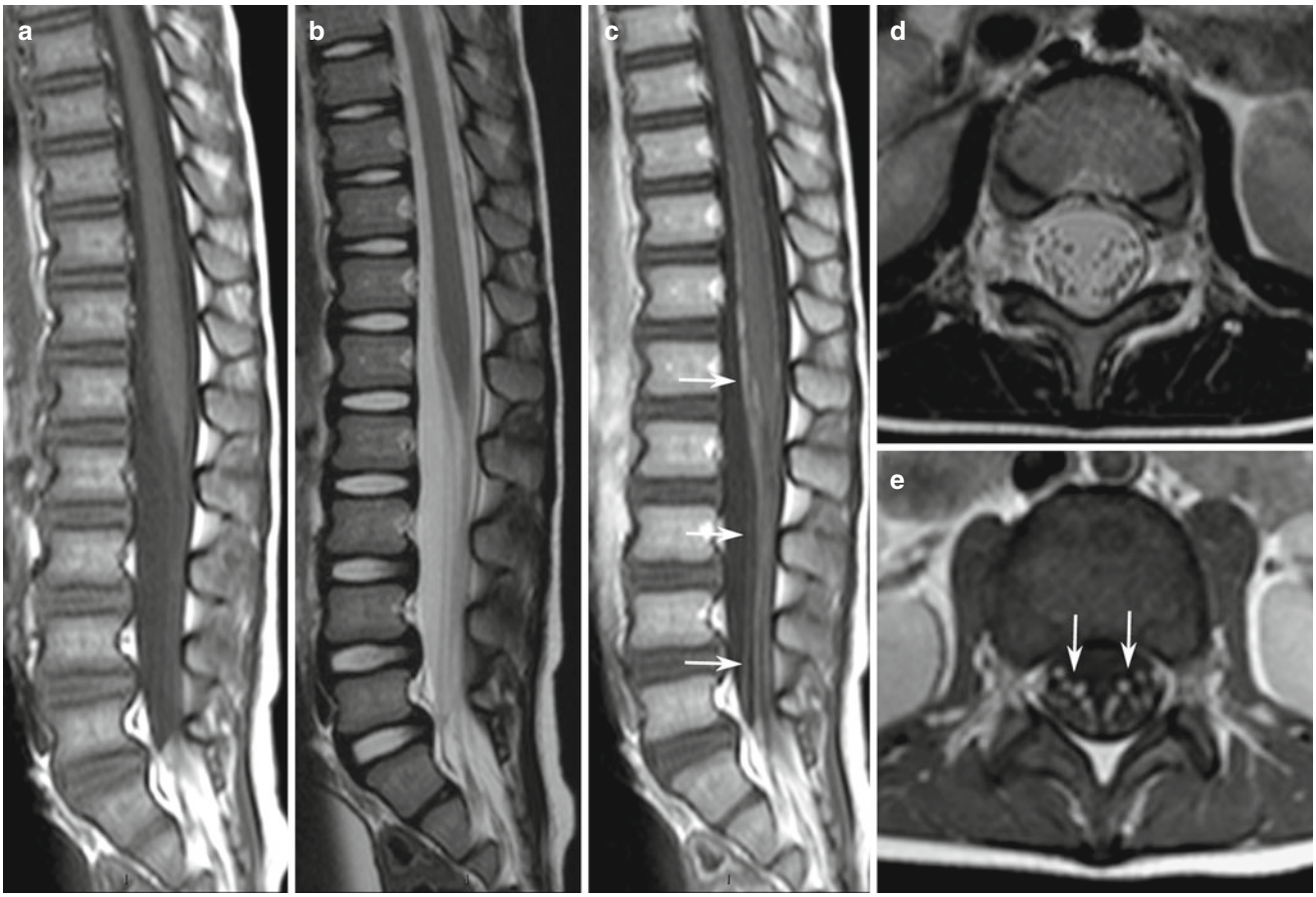

Fig. 9 Guillain-Barré syndrome in a 2-year-old girl presenting with rapidly progressive paraparesis. Sagittal T1-weighted (**a**) and T2-weighted (**b**) images are unremarkable, while Gd-enhanced sagittal T1-weighted image (**c**) shows enhancement of nerve roots of the cauda equina (*arrows*). Axial T2-weighted image (**d**) shows the caudal nerve roots are not thickened, while Gd-enhanced axial T1-weighted image (**e**) shows enhancement of anterior nerve roots in the cauda equine (*arrows*). The diagnosis would be missed without contrast material administration

CSF analysis shows elevation of proteins reflecting nerve root demyelination and a lack of inflammatory cells. GBS progresses rapidly, reaching a maximal deficit within 4 weeks of the onset, during which time approximately 40 % of children become non-ambulant and up to 20 % require ventilatory support [17].

The peculiarity of MRI in patients with GBS is that unenhanced scans are typically unrevealing, as spinal root thickening may be difficult to appraise or even totally absent. On the other hand, gadolinium administration reveals enhancement predominantly of the anterior nerve roots of the cauda equina (Fig. 9) and sometimes global thickening and enhancement of the whole cauda equina. Involvement of cranial nerves in the same inflammatory process is called Miller Fisher syndrome [18]. Affected patients complain with ophthalmoplegia, ptosis, facial weakness, and ataxia, and MRI shows enhancement of multiple cranial nerves.

Spondylodiscitis In children, spondylodiscitis can be pyogenic or tubercular (TB); infection typically originates in the vertebral body adjacent to the end plate and spreads to the disc secondarily. Patients present with nonspecific findings such as failure or refusal to walk, abdominal pain, fever, and chronic back pain; back pain is often the predominant complaint. When the cervical spine is affected, manifestations may include dysphagia and stiff neck. Progression to weakness and paralysis suggests the formation of an epidural abscess with compression of the spinal cord and nerve roots. Abscesses can be particularly large in TB spondylodiscitis and involve the paravertebral region extensively.

Conventional X-rays have very low sensitivity and specificity [19]; loss of definition and irregularity of the vertebral end plate, narrowing, and erosion of the disc space are seen. On MRI, reduction in the height of the intervertebral disc, swelling of the annulus, and T2 hyperintensity of the disc

Fig. 10 Tubercular spondylodiscitis in an 8-year-old boy. Sagittal T1-weighted (**a**), T2-weighted (**b**), and Gd-enhanced T1-weighted (**c**) images show involvement of the central portion of the L4 vertebral body with disruption of the posterior vertebral wall and propagation into the spinal canal below the posterior longitudinal ligament, forming an epidural abscess (*arrows*). The L3–L4 disc space is irregular and probably already involved, albeit without frank, diffuse enhancement (*arrow*). Gd-enhanced axial T1-weighted image (**d**) shows the thecal sac is markedly compressed by the ventrally located collection, while axial CT scan (**e**) shows centroposterior vertebral body necrosis (*arrowheads*) with disruption of the posterior body wall

with enhancement after gadolinium administration are seen in the early stage of the disease. Signal changes of the vertebral end plates and subchondral regions are initially very subtle and are more easily picked up by STIR sequences. As the disease progresses, loss of integrity and definition of the vertebral end plates are detected.

Vertebral collapse can occur, especially in TB cases. Epidural abscesses are frequently seen and appear as a rim-enhancing abnormality in the epidural space whose nonenhancing center generally corresponds to pus (Fig. 10) [20].

Vascular Lesions

Spinal Cord Ischemia Spinal cord ischemia is rare in children and requires a predisposing condition such as cardiovascular surgery, arterial dissection, or fibrocartilaginous embolism. Patients experience a stroke-like presentation, with signs of acute spinal cord dysfunction which progress to nadir more rapidly than in inflammatory ATM, typically within 4 h of the onset. The neurologic presentation of spinal cord infarction is largely defined by the vascular territory involved [21]. The severity of the impairments can vary widely, from paraplegia to minor weakness On MRI (Fig. 11), typical anterior spinal artery distributions will result into involvement of the anterior horns of the gray matter, giving the so-called "snake's eye" appearance on axial T2-weighted images. Diffusion-weighted imaging (DWI) will show areas of restricted diffusion as in cerebral ischemia; however, implementation of DWI sequences is usually more cumbersome and less reliable in the spinal compartment than in the brain [22].

Spinal Cord Hemorrhage Hemorrhagic lesions of the spinal cord are exceedingly rare in the pediatric age group. Apart from exceptional idiopathic cases (Fig. 12), hematomyelia can be caused by bleeding diathesis due to

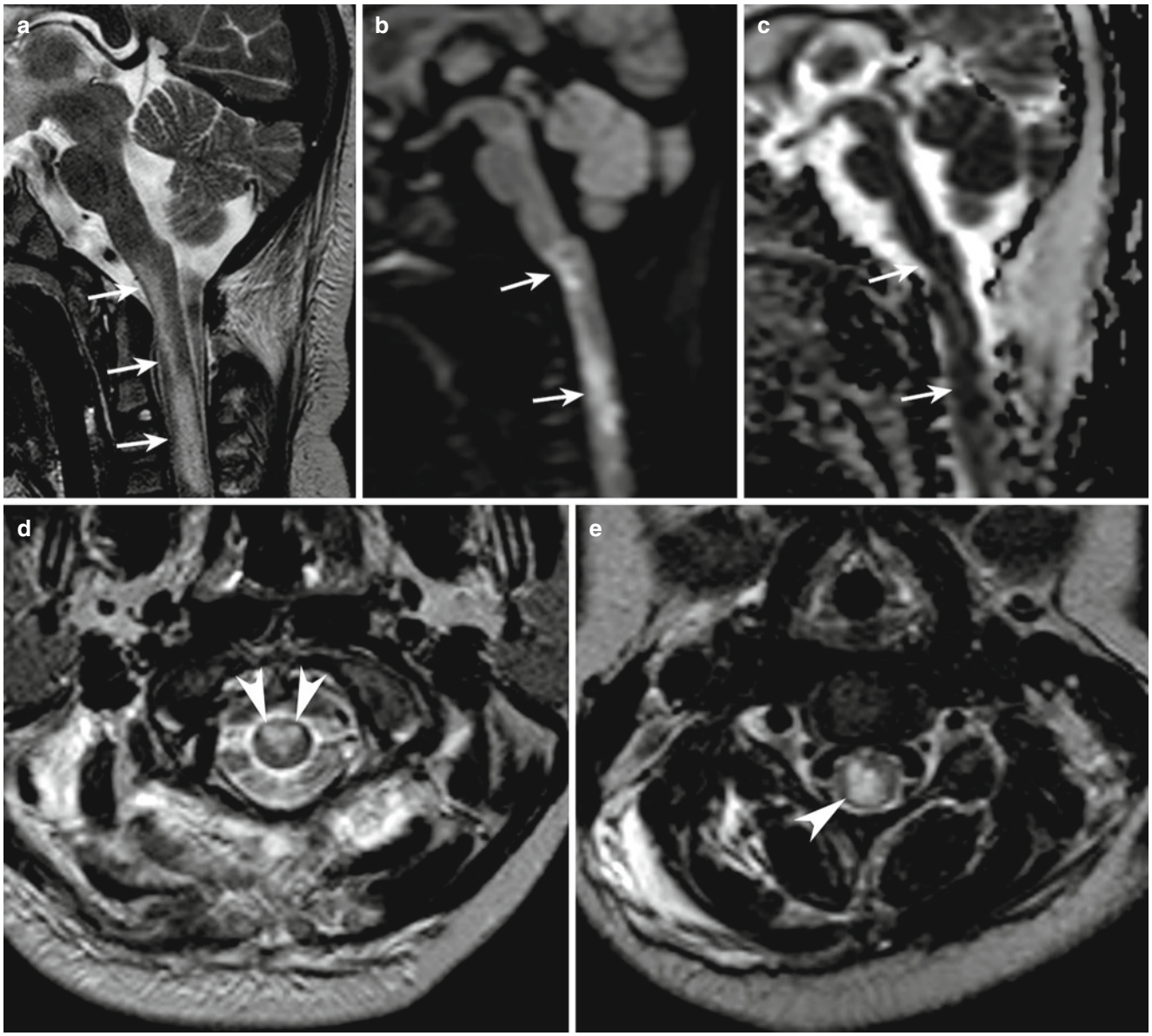

Fig. 11 Spinal cord ischemia in an 8-year-old girl with Down syndrome, craniocervical instability, and a stroke-like presentation with tetraparesis. Sagittal T2-weighted image (**a**) shows hyperintense signal (*arrows*) that involves the anterior aspect of the cervical cord cranially and has a more diffuse distribution caudally. Sagittal diffusion-weighted image (**b** 1000 m/s^2) (**b**) and corresponding ADC map (**c**) show areas of restricted diffusion. Axial T2-weighted images (**d**, **e**) show a typical "snake's eye" sign (*arrowheads*, **d**) due to the involvement of the anterior gray matter horns corresponding to the anterior spinal artery territory; at a more caudal level, the cross-sectional area of the cord is more diffusely involved (*arrowheads*, **e**). MR angiography (not shown) revealed left vertebral artery dissection

coagulation imbalance, trauma, or vascular malformations, such as arteriovenous malformations (AVM) or cavernous malformations. AVMs are usually identifiable because of the presence of tangles of dilated vessels forming an intramedullary or pial nidus [23]. Cavernomas are exceptionally found in the spinal compartment; spinal cord cavernomas produce blooming T2* hypointensities due to hemosiderin staining, similar to their cerebral counterparts.

Tumors

Tumors of the spine and spinal cord may present with chronic back pain; however, frequently these patients present in the emergency room despite the long-standing duration of their complaints, mainly when additional neurological deficits related to either compression or infiltration of the spinal cord and nerve roots occur. Spinal

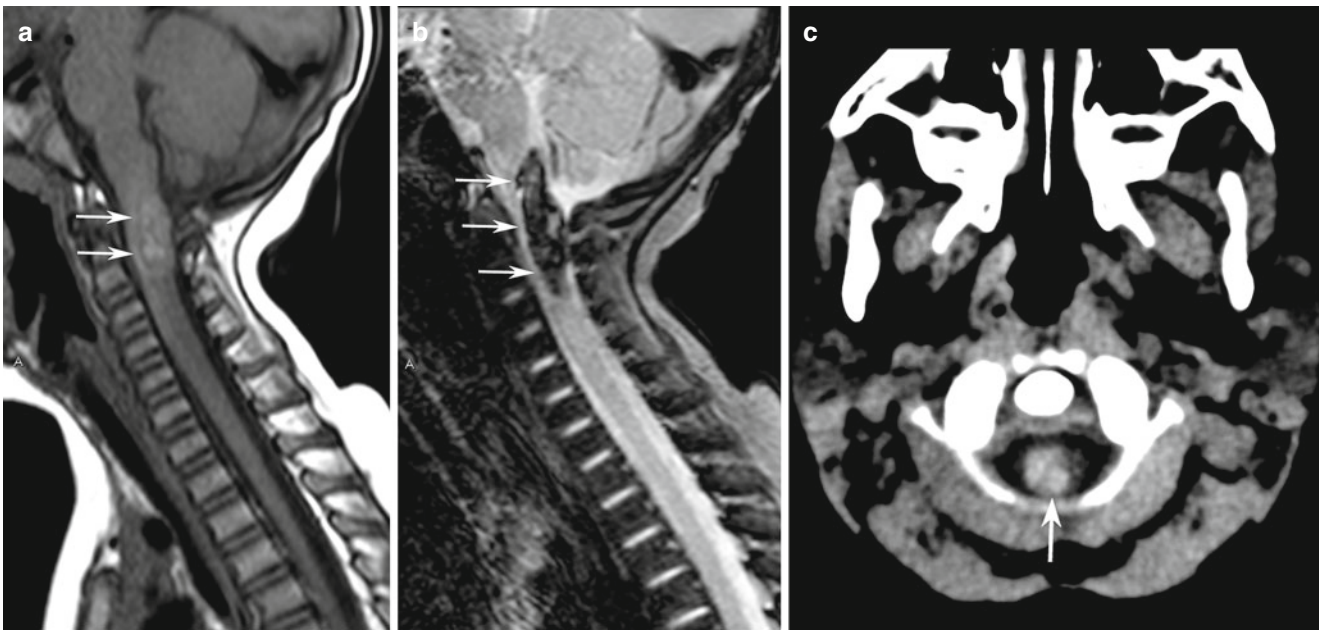

Fig. 12 Bulbo-medullary hemorrhage in a 1-year-old girl. Sagittal T1-weighted image (**a**) shows ill-defined hyperintensity at the bulbo-medullary junction (*arrows*). Sagittal gradient-echo T2*-weighted image (**b**) shows extensive hypointensity (*arrows*) consistent with fresh blood. Hemorrhage is confirmed by unenhanced CT scan (*arrow*, **c**). No cause could be identified in this case

tumors are classified according to the involved compartment into intramedullary, intradural extramedullary, and extradural [24].

Intramedullary Tumors They account for 25 % of pediatric spinal tumors and prevail in children between 1 and 5 years of age [24]. Astrocytomas (especially pilocytic) are the most common intramedullary tumor in the pediatric age group (82 % of cases) followed by gangliogliomas, whereas ependymomas are distinctly uncommon in children outside the setting of neurofibromatosis type 2. The presentation, duration, and course of the disease may be variable. Affected patients may have a prolonged duration of symptoms before a diagnosis is established. Back pain is often the earliest and most persistent complaint, and should prompt to MRI in order to rule out intraspinal pathology. Rigidity and contracture of the paravertebral muscles may result from thecal sac enlargement, involvement of adjacent bone, and impairment of cerebrospinal fluid (CSF) dynamics. Progressive scoliosis may cause delays in the diagnosis if underestimated. Head tilt and torticollis, as well as lower cranial nerve palsies with dysphagia, dyspnea, and dysphonia, may represent early signs of cervicomedullary neoplasms due to involvement of the spinal roots of the accessory nerve. Hydrocephalus with raised intracranial pressure may rarely represent the clinical presentation of intramedullary tumors and is caused by obstruction of the spinal subarachnoid spaces, CSF seeding, or increased CSF protein content.

On MRI, intramedullary neoplasms (Fig. 13) produce enlargement of the spinal cord giving heterogeneous signal intensity. They may be solid or associated with cysts, either neoplastic or nonneoplastic, which are better defined after gadolinium administration. They frequently involve a large portion of the cord, spanning multiple vertebral levels in length. Among intramedullary tumors, ependymomas are especially prone to spontaneous hemorrhage, which may cause abrupt clinical presentations.

Intradural Extramedullary Tumors In the pediatric age group, primitive tumors in this location are the least common among spinal tumors and are mostly represented by schwannomas and neurofibromas in neurofibromatosis patients. A host of other neoplasms, including filar ependymomas, meningiomas, and atypical teratoid rhabdoid tumors, can also be found. Clinical features basically are represented by pain and signs of cord or nerve root compression, depending on the location of the mass.

Extradural Tumors Extradural tumors account for about 2/3 of all spinal tumors in the pediatric age group and may be grouped into bone tumors, tumors of the epidural space, and extraspinal tumors invading the spine. Affected children usually complain with back pain and myeloradiculopathy. Neuroimaging of extradural tumors requires both MRI and CT. MRI depicts extradural soft tissue components,

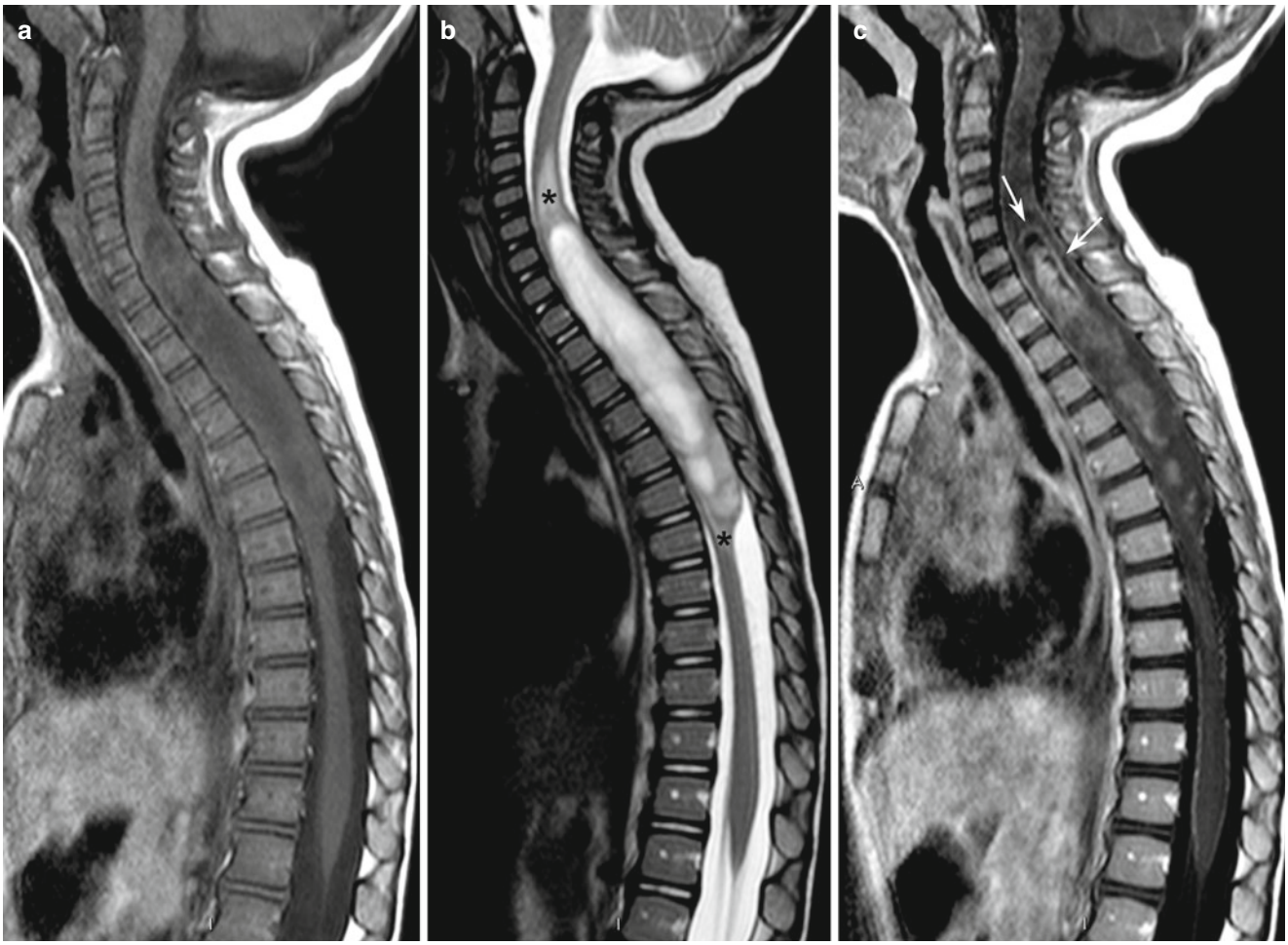

Fig. 13 Intramedullary pilocytic astrocytoma in a 2-year-old girl. Sagittal T1-weighted (**a**) and T2-weighted (**b**) images show intrinsic spinal cord lesion at the C6–T7 level, causing significant expansion of the cord and eliciting perifocal edema (*asterisks*, **b**). Gd-enhanced sagittal T1-weighted image (**c**) shows patchy enhancement, consistent with a mostly solid lesion, although a small peripheral cystic component with enhancing neoplastic walls (*arrows*) is seen at the cranial margin of the lesion. Aspecific venous engorgement is also seen along the pial surface of the thoracolumbar cord

bone marrow infiltration, and compressive myelopathy compression from the tumor, whereas CT detects the osteolytic or osteosclerotic nature of the lesion and the degree of involvement of bone [24].

Among primary bone tumors, *osteoid osteomas* are characterized by an acute presentation with nocturnal pain that recedes with nonsteroid anti-inflammatory medications and/or with painful scoliosis. CT shows the nidus of the osteoma as a rounded hypodense lesion surrounded by a hyperdense sclerotic ring and containing a calcified spot resulting in a "target" appearance. Because of the small size of the lesion, accuracy of MRI in identification of osteoid osteomas is not high; however, MRI clearly detects the extensive reactive soft-tissue masses that are frequently associated with the osteoma (Fig. 14) [25].

Extrinsic compression of the spinal cord and/or nerve roots is the presenting sign of paravertebral *neuroblastoma.* These tumors are the most common non-CNS solid tumors in the pediatric age group and typically affect children younger than 5 years. The tumor mass is typically huge and may show extensive necrotic-hemorrhagic areas and calcification. The clinical presentation is variable depending on the variable location and size of the mass; however, neurologic signs typically ensue with intraspinal extension and thecal sac compression. Neuroblastomas originating from the paravertebral sympathetic chains typically display a "dumbbell" growth through one or more neural foramina, extending a variably sized component into the spinal canal that compresses and displaces the thecal sac and spinal cord (Fig. 15). Other extradural tumors causing spinal cord compression

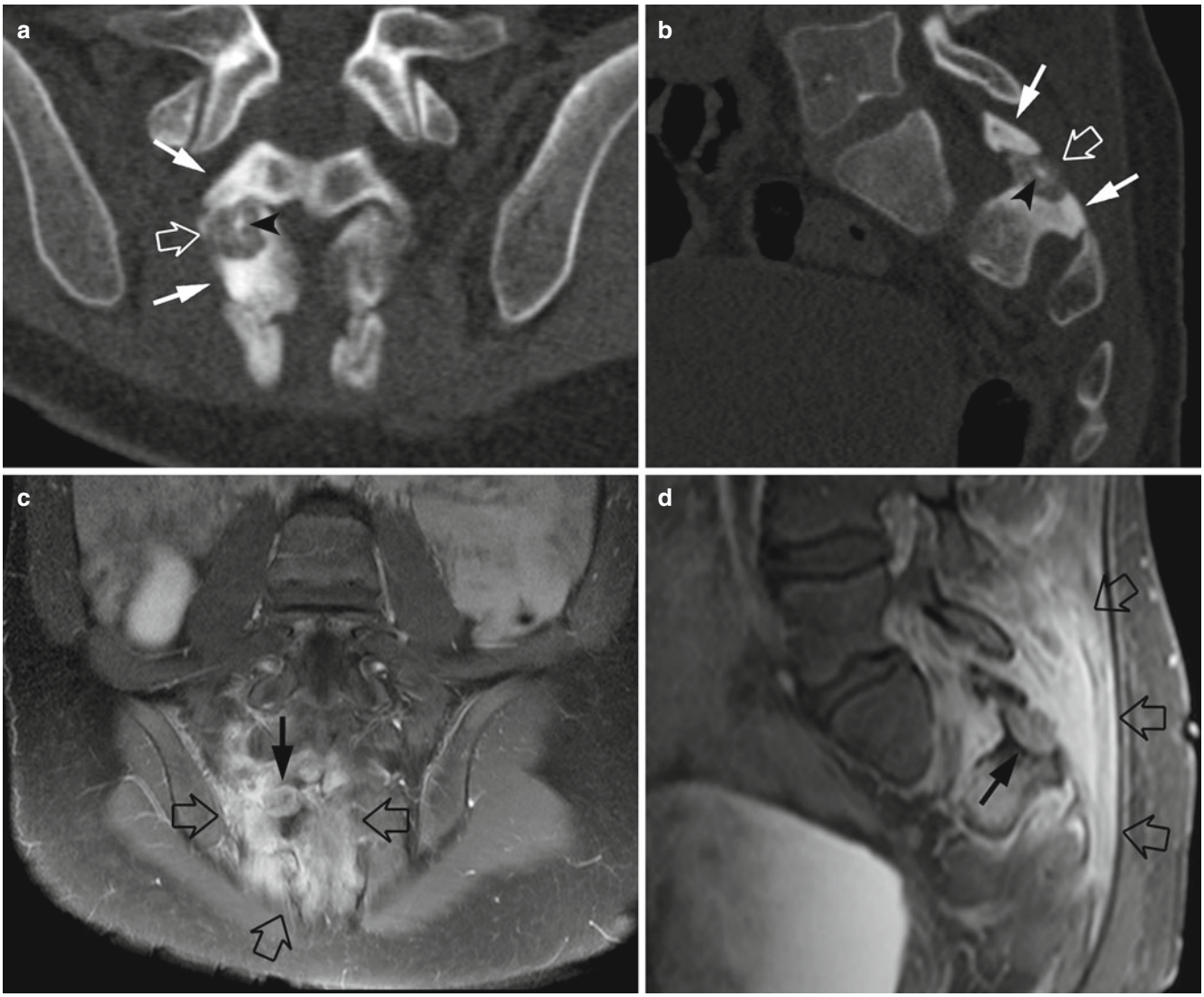

Fig. 14 Osteoid osteoma in a 12-year-old boy with intense low back pain. Coronal (**a**) and sagittal (**b**) reformatted CT images show radiolucent lesion (*empty arrow*) with central sclerotic spot (*arrowhead*, **a**) involving the right S2 lamina and inducing a perifocal sclerotic reaction (*thin arrows*). Contrast-enhanced coronal (**c**) and sagittal (**d**) MR images acquired with a fat suppression technique barely show the lesion (*arrow*), engulfed by a marked inflammatory reaction of the surrounding soft tissues (*empty arrows*)

include Ewing's sarcoma, hematological malignancies, and nerve sheath tumors [24].

Musculoskeletal Disorders

A large host of musculoskeletal conditions may present with acute or chronic pain, often resulting in an emergency room presentation. Only the most common entities will be briefly discussed here.

Juvenile Idiopathic Arthritis Arthritis is a heterogeneous group of musculoskeletal disorders, comprising a large host of different diseases or conditions that affect the joints, bones, muscles, cartilage, and other connective tissues, hampering or halting physical movement. The most common form in children is juvenile idiopathic arthritis (JIA). In the spine, JIA most commonly involves the cervical region; symptomatic patients present with pain, stiffness, torticollis, and limited range motion of the head.

MRI reveals synovitis and joint effusion, bone marrow edema, and bone erosions generally involving the C2–C3 level (Fig. 16). There can be malalignment of the articular surfaces of atlanto-occipital, atlanto-axial or cervical facet joints, or of two adjacent vertebrae. Interruption of the osseous joint

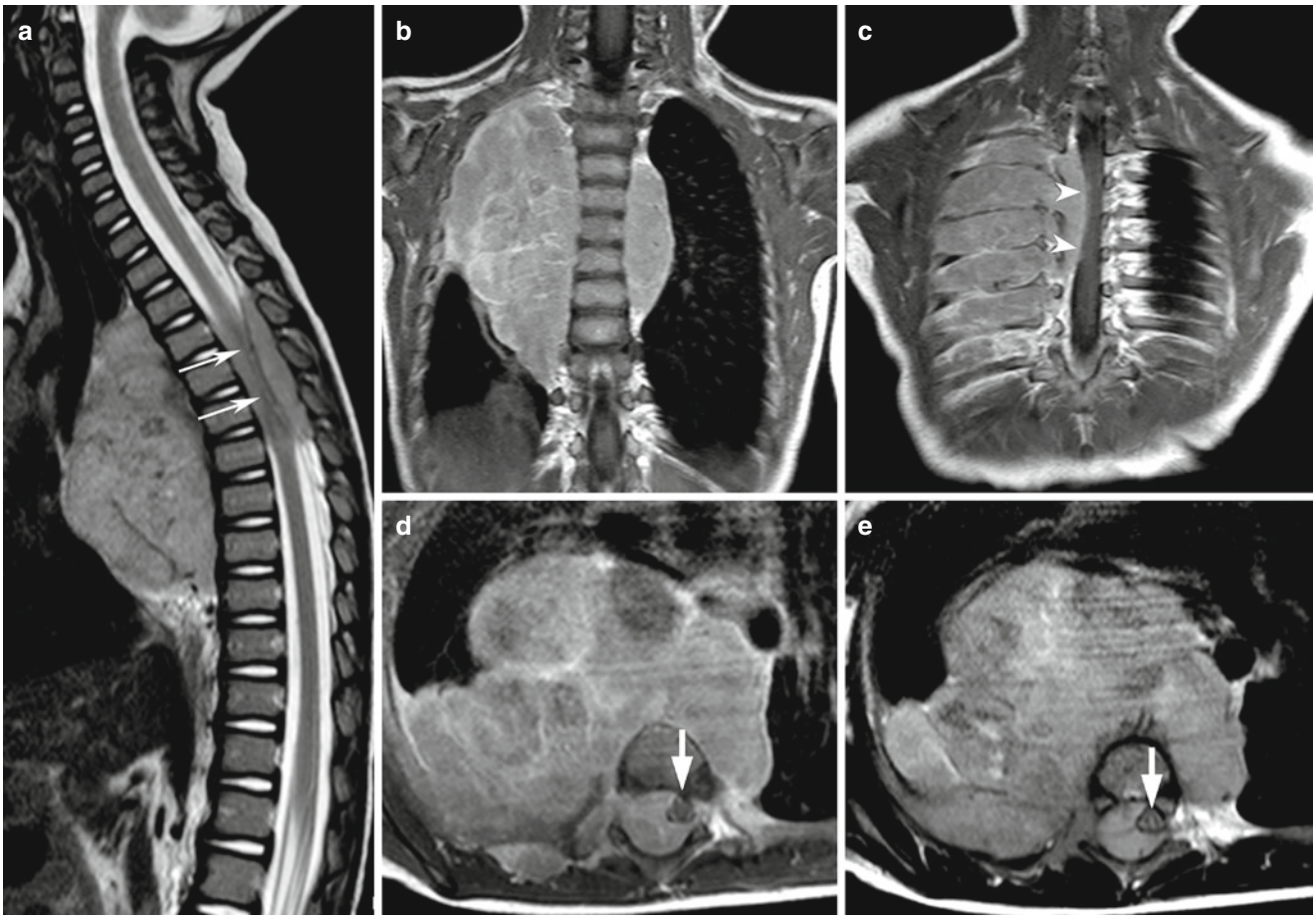

Fig. 15 Thoracic neuroblastoma causing spinal cord compression in a 1-year-old boy. Sagittal T2-weighted image shows huge prevertebral mass that has extended intraspinally, causing spinal cord compression (*arrows*). Contrast-enhanced coronal T1-weighted images (**b**, **c**) show intraspinal extension (*arrows*) has occurred through multiple neural foramina. Notice the absence of scoliosis despite the huge size of the mass, a typical feature of neuroblastoma. On contrast-enhanced axial T1-weighted image (**d**) and axial T2-weighted image (**e**) the thecal sac containing the cord is seen to be markedly displaced (*arrow*, **d**); central spinal cord T2 hyperintensity (*arrow*, **e**) is consistent with edema due to mechanical compression

surface with signs of inflammation, including hyperintense signal of the interarticular space, synovia, and subjacent bone in STIR images with corresponding enhancement on post-contrast T1-weighted images, is classically found [26]. The dens becomes eroded, first anteriorly and then posteriorly, and may become hypertrophic causing narrowing of the spinal canal at the craniocervical junction with possible neurological impairment due to spinal cord compression.

Disc Space Calcification Disc space calcification (DSC), or intervertebral disc calcification, is a poorly understood, uncommon condition characterized by calcification of the intervertebral disc, usually in the cervical spine. Most patients are boys aged 6–10 years who complain with local pain or torticollis; intraspinal herniation of a calcified disc fragment may cause acute neurologic signs such as radiculopathy or sensorimotor signs, similar to other forms of disc herniation. The etiology of DSC is unknown, and the entity is considered idiopathic in the pediatric age group; it is typically self-limiting, and conservative treatment is advocated [27].

Conventional X-rays may show an ovoid calcification in the intervertebral disc space. CT scan confirms the presence of the calcification in the disc space as well as any extruded disc fragment that may impinge on the thecal sac and spinal cord [28]. The vertebral end plates may appear irregular, with areas of subchondral sclerosis or Schmorl nodes. MRI is especially useful to depict associated herniations and the effects on the spinal cord (Fig. 17).

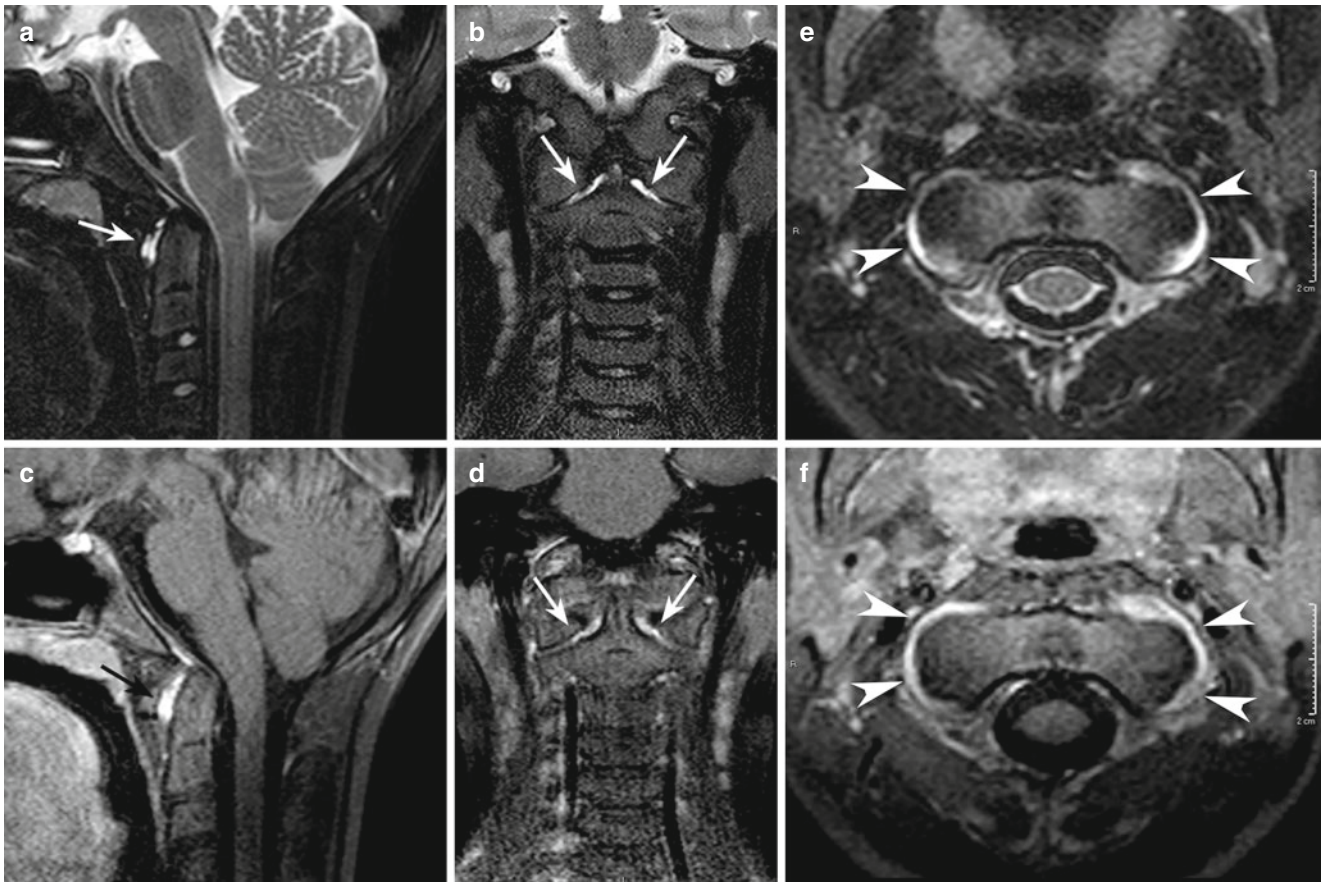

Fig. 16 Juvenile idiopathic arthritis in a 9-year-old girl presenting with acute cervical pain. (**a**) Sagittal and (**b**) coronal STIR images show fluid collection in the atlanto-axial interarticular space bilaterally (*arrows*). (**c**) Sagittal and (**d**) coronal Gd-enhanced T1-weighted images with fat suppression show the collections enhance (*arrows*), consistent with synovitis. (**e**) Axial STIR image and (**f**) Gd-enhanced, fat-suppressed T1-weighted image show enhancing collection surrounding the lateral masses of the atlas bilaterally (*arrows*)

Chronic Recurrent Multifocal Osteomyelitis Chronic recurrent multifocal osteomyelitis (CRMO) is a sterile skeletal inflammation occurring primarily in childhood and adolescence, predominantly in girls. The cause is unknown; autoimmune mechanisms and genetic susceptibility have been implicated. The disease has a long, fluctuating course with exacerbations and remissions. Pain, rigidity, and malaise are the most common complaints. The diagnosis is often one of exclusion in a patient with multiple localized skeletal lesions. Vertebral involvement is often multifocal, with the thoracic spine being involved most commonly. When present, vertebral collapse may progress to kyphosis and vertebra plana.

On CT, the involved vertebrae show a mottled lytic-sclerotic appearance and wedge-like deformation. MRI shows osseous edema of the involved vertebrae, which is exquisitely depicted by STIR images, while the intervertebral discs are typically spared. On post-contrast T1-weighted images, enhancement of the involved vertebrae is best appreciated when fat-suppressed techniques are used [29] (Fig. 18).

Spondylolysis and Spondylolisthesis Spondylolysis is a bone defect of the neural arch, usually at level of the pars interarticularis. Its cause may be traumatic (stress fracture) or dysplastic. Spondylolysis accounts for the majority of cases of low back pain in children older than 7–8 years and is commonly seen in individuals who practice sports [30]. It is more often bilateral than unilateral and involves L5 in the vast majority of cases. This condition allows for excessive motility, and therefore potential instability, of the lumbar spine with respect to the sacrum, often leading to spondylolisthesis, i.e., anterior dislocation, of L5 with respect to S1.

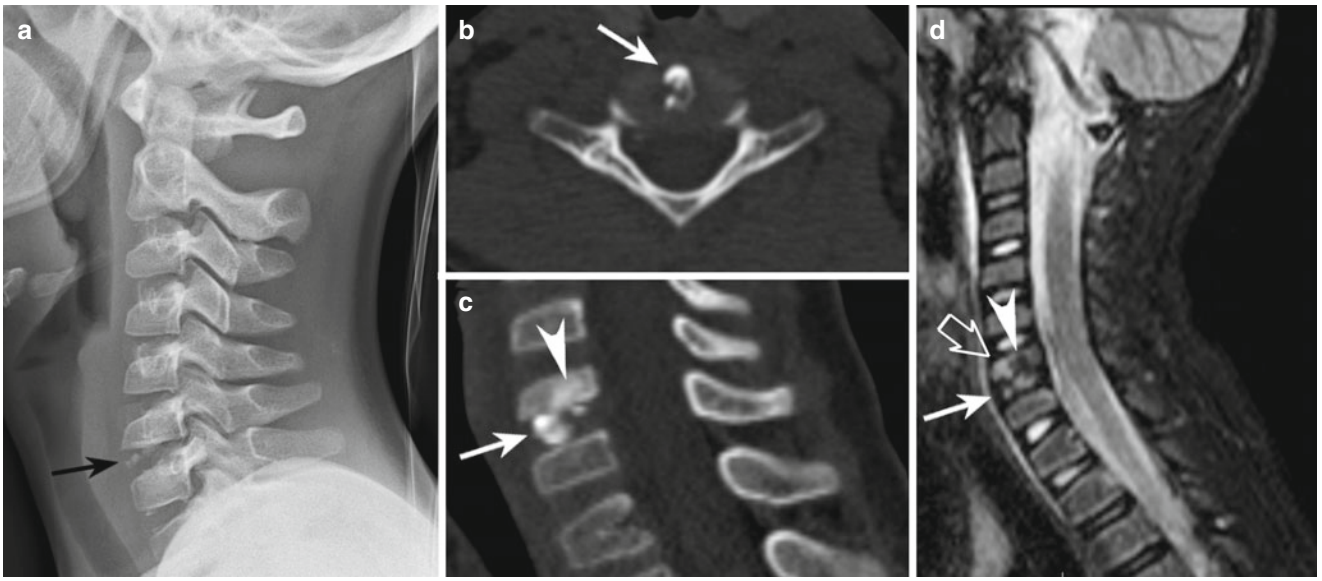

Fig. 17 Disc space calcification in a 7-year-old girl. (**a**) Conventional X-ray of the cervical spine in lateral projection shows densities in the C6–C7 intervertebral space (*arrow*). (**b**) Axial CT scan and (**c**) sagittal reformatted CT image shows calcified clusters involving the C6–C7 intervertebral disc. The C6 vertebral body is slightly reduced in height and shows a subchondral hyperdensity (*arrowhead*). (**d**) Sagittal STIR image shows the C6–C7 disc (*arrow*) is slightly hypointense compared to unaffected discs; the subchondral calcification also appears hypointense (*arrowhead*) and stands out on a diffuse background of mild hyperintensity (*empty arrow*) indicative of bone marrow edema

Fig. 18 Chronic recurrent multifocal osteomyelitis in a 12-year-old girl. (**a**) Coronal and (**d**) sagittal STIR images show multiple ill-defined areas of abnormal signal intensity involving several vertebral bodies in the whole spine (*arrowheads*). (**b**) Coronal fat-suppressed T1-weighted image is inconspicuous; (**c**) coronal and (**e**) sagittal Gd-enhanced fat-suppressed T1-weighted images show enhancement of the vertebral abnormalities (*arrowheads*). Notice there is no vertebral collapse in this case, and the intervertebral discs are spared. There is incidental hydrosyringomyelia

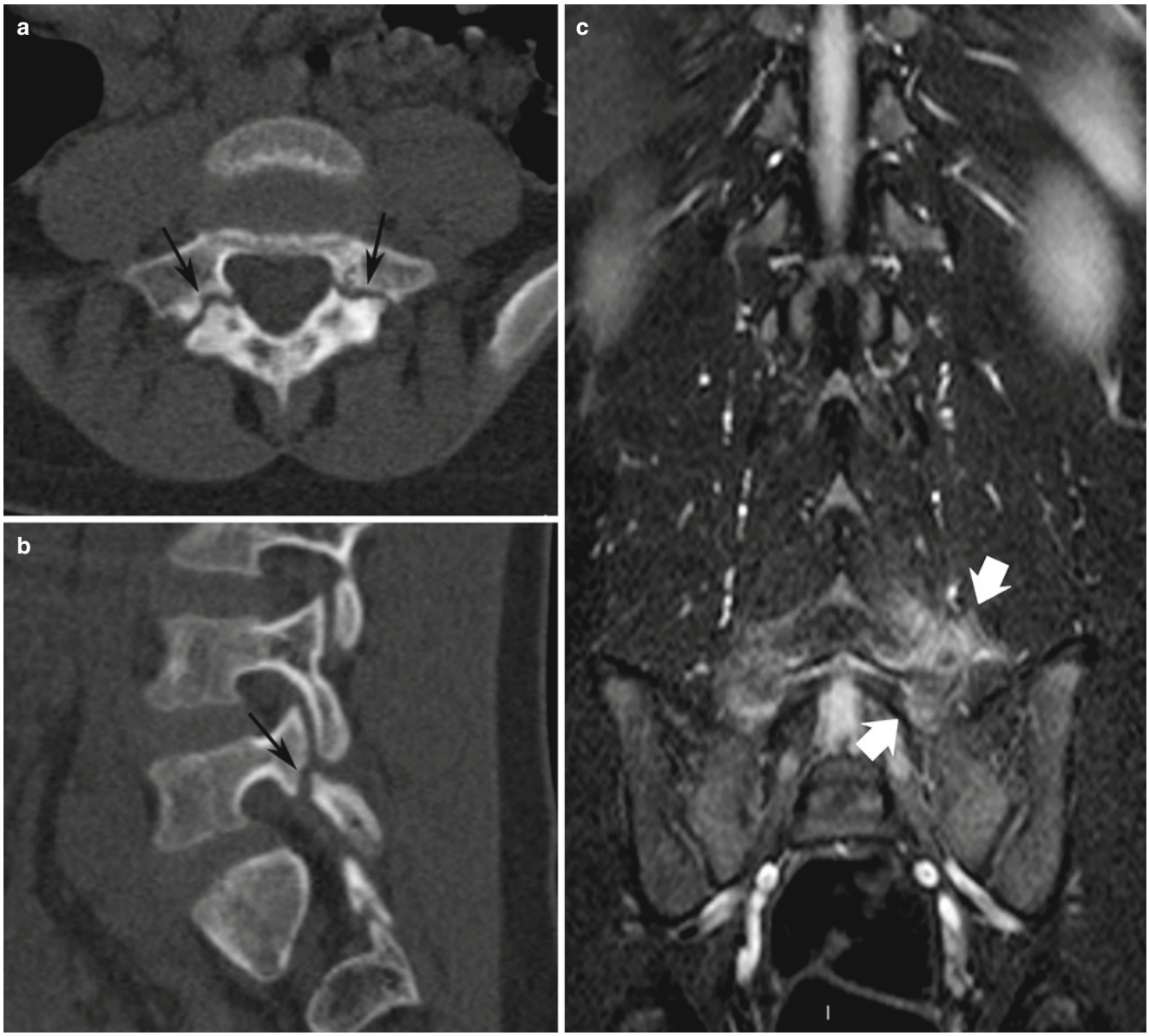

Fig. 19 Isthmic spondylolysis of L5 in a 9-year-old boy presenting with low back pain. CT scan on axial (**a**) and parasagittal (**b**) projections shows radiolucent line crossing the isthmus (or pars interarticularis) bilaterally (*arrows*), surrounded by reactive sclerosis. There is not associated spondylolisthesis in this case; however, note that images were acquired in the supine position, i.e., without the normal axial load which could exacerbate listhesis. Coronal STIR MR image (**c**) does not directly show the lysis, but reveals inflammatory reaction involving the surrounding soft tissues (*arrows*)

CT shows a thin, irregular interruption of the neural arch at level of the isthmus; sagittal reformats perfectly display the possible associated listhesis. On MRI, the defect may not be seen equally well; however, MRI is more useful to evaluate associated features, such as disc bulging and foraminal stenosis. MRI also shows redundant masses of inflammatory tissue surrounding the pars defect as well as edema of the spongious bone, well seen on STIR images (Fig. 19).

References

1. Huisman TA, Wagner MW, Bosemani T, Tekes A, Poretti A (2015) Pediatric spinal trauma. J Neuroimaging 25:337–353
2. Hollingshead MC, Castillo M (2011) Trauma to the spinal column. In: Naidich TP, Castillo M, Cha S, Raybaud C, Smirniotopoulos J, Kollias S, Kleinman GM (eds) Imaging of the spine. Saunders/Elsevier, Philadelphia, pp 219–36
3. Jones TM, Anderson PA, Noonan KJ (2011) Pediatric cervical trauma. J Am Acad Orthop Surg 219:600–611

4. Pang D, Wilberger JE Jr (1982) Spinal cord injury without radiographic abnormalities in children. J Neurosurg 57:114–129
5. Bocciolini C, Dall'Olio D, Cunsolo E, Cavazzuti PP, Laudadio P (2005) Grisel's syndrome: a rare complication following adenoidectomy. Acta Otorhinolaryngol Ital 25:245–249
6. Scott TF, Frohman EM, De Seze J, Gronseth GS, Weinshenker BG, Therapeutics and Technology Assessment Subcommittee of American Academy of Neurology (2011) Evidence-based guideline: clinical evaluation and treatment of transverse myelitis: report of the Therapeutics and Technology Assessment Subcommittee of the American Academy of Neurology. Neurology 77:2128–2134
7. Rossi A (2015) Pediatric spinal infection and inflammation. Neuroimaging Clin N 25:173–191
8. Thurnher MM, Cartes-Zumelzu F, Mueller-Mang C (2007) Demyelinating and infectious diseases of the spinal cord. Neuroimaging Clin N Am 17:37–55
9. Yiu EM, Kornberg AJ, Ryan MM, Coleman LT, Mackay MT (2009) Acute transverse myelitis and acute disseminated encephalomyelitis in childhood: spectrum or separate entities? J Child Neurol 24:287–296
10. Krupp LB, Banwell B, Tenembaum S, International Pediatric MS Study Group (2007) Consensus definitions proposed for pediatric multiple sclerosis and related disorders. Neurology 68:S7–s12
11. Rossi A (2008) Imaging of acute disseminated encephalomyelitis. Neuroimaging Clin N Am 18:149–161
12. Wingerchuk DM, Lennon VA, Lucchinetti CF, Pittock SJ, Weinshenker BG (2007) The spectrum of neuromyelitis optica. Lancet Neurol 6:805–815
13. Tackley G, Kuker W, Palace J (2014) Magnetic resonance imaging in neuromyelitis optica. Mult Scler 2014 May 14 [Epub ahead of print]
14. Tortori-Donati P, Fondelli MP, Rossi A, Rolando S, Andreussi L, Brisigotti M (1993) La neuromielite ottica. Una ulteriore sfida nella diagnosi differenziale con le neoplasie intramidollari. Rivista di Neuroradiologia 6:53–59
15. Dev R, Husain M, Gupta A, Gupta RK (1997) MR of multiple intraspinal abscesses associated with congenital dermal sinus. AJNR Am J Neuroradiol 18:742–743
16. van den Berg B, Walgaard C, Drenthen J, Fokke C, Jacobs BC, van Doorn PA (2014) Guillain-Barré syndrome: pathogenesis, diagnosis, treatment and prognosis. Nat Rev Neurol 10:469–482
17. Ryan MM (2013) Pediatric Guillain-Barré syndrome. Curr Opin Pediatr 25:689–693
18. Urushutani M, Ueda F, Kameyama M (1995) Miller-Fisher-Guillain-Barré overlap syndrome with enhancing lesions in the spinocerebellar tracts. J Neurol Neurosurg Psychiatry 58:241–243
19. Fucs PM, Meves R, Yamada HH (2012) Spinal infections in children: a review. Int Orthop 36:387–395
20. Sandhu FS, Dillon WP (1991) Spinal epidural abscess: evaluation with contrast-enhanced MR imaging. AJNR Am J Neuroradiol 12:1087–1093
21. Vargas MI, Gariani J, Sztajzel R, Barnaure-Nachbar I, Delattre BM, Lovblad KO, Dietemann JL (2015) Spinal cord ischemia: practical imaging tips, pearls, and pitfalls. AJNR Am J Neuroradiol 36:825–830
22. Thurnher MM, Bammer R (2006) Diffusion-weighted MR imaging (DWI) in spinal cord ischemia. Neuroradiology 48:795–801
23. Davagnanam I, Toma AK, Brew S (2013) Spinal arteriovenous shunts in children. Neuroimaging Clin N Am 23:749–756
24. Rossi A, Gandolfo C, Morana G, Tortori-Donati P (2007) Tumors of the spine in children. Neuroimaging Clin N Am 17:17–35
25. Woods ER, Martel W, Mandell SH, Crabbe JP (1993) Reactive soft-tissue mass associated with osteoid osteoma: correlation of MR imaging features with pathologic findings. Radiology 186:221–225
26. Hospach T, Maier J, Müller-Abt P, Patel A, Horneff G, von Kalle T (2014) Cervical spine involvement in patients with juvenile idiopathic arthritis – MRI follow-up study. Pediatr Rheumatol Online J 12:9
27. Garg M, Kumar S, Satija B, Gupta R (2012) Pediatric intervertebral disc calcification: a no touch lesion. J Craniovertebr Junction Spine 3:23–25
28. Calderone M, Severino M, Pluchinotta FR, Zangardi T, Martini G (2009) Idiopathic intervertebral disc calcification in childhood. Arch Dis Child 94:233–234
29. Falip C, Alison M, Boutry N, Job-Deslandre C, Cotten A, Azoulay R, Adamsbaum C (2013) Chronic recurrent multifocal osteomyelitis (CRMO): a longitudinal case series review. Pediatr Radiol 43:355–375
30. Lim MR, Yoon SC, Green DW (2004) Symptomatic spondylolysis: diagnosis and treatment. Curr Opin Pediatr 16:37–46

Part IV

Breast Imaging Satellite Course “Pearl”

Contrast-Enhanced Digital Mammography

Elizabeth A. Morris

Full field digital mammography has more or less replaced conventional film screen mammography. Nevertheless, breast density still remains a concern with possible summation and obscuration of underlying cancers. Digital mammography offers advanced application such as tomosynthesis and contrast-enhanced mammography. Both of these are promising for improved cancer detection that would otherwise be obscured by dense breast tissue. Contrast-enhanced digital mammography is a promising new technology that can combine anatomic and physiologic information at the same time. Similar to magnetic resonance imaging, it uses contrast to delineate neovascularity that is associated with malignancy. The contrast used is iodinated contrast, a familiar contrast agent in most radiology departments.

Contrast-enhanced mammography was first described in 2003. There are two subtraction methods that have been tried: temporal subtraction in which a postcontrast image is subtracted from a precontrast image and dual-energy subtraction image where a low-energy image and a high-energy image are obtained after iodine injection is mathematically combined in such a way that unenhanced breast tissue is eliminated but iodine is well seen. The first paper from Charité Hospital in Berlin [1] described initial experience using the first subtraction technique on seven women who underwent digital mammography after iodine-based contrast injection at 60 and 120 in the 180 s following injection. Preliminary images demonstrated improved visualization of breast tumors. This was followed several months later by a group in Canada [2] who used the same dynamic technique similar to MRI subtraction where a full-field digital mammogram without contrast was subtracted from a full-field digital mammogram with contrast at various time points. Emphasis was placed on the kinetic curve with this technique, and the conclusion of the preliminary study was that contrast-enhanced digital mammography potentially may be useful in identifying lesions in the mammographically dense breast.

Later that same year, a third paper appeared in the literature using the second different dual-energy contrast-enhanced digital subtraction technique which is the current technique that is employed today [3]. This technique relies on the fact that iodine attenuation has a K-edge 33 keV. Two exposures are taken – one exposure is taken below and another is taken above 33 keV, thereby suppressing the background breast parenchyma and highlighting contrast uptake within the tumor. No dynamic information is obtained. Mammography systems with specialized detectors distinguish photons with high energy and photons with high energy; photons with low energy within the single imaging are required and are called slot-scan systems with slit-shaped detectors that scan the breast with a narrow X-ray beam. This limits motion artifacts. Both of the above-described techniques in the early studies performed well-demonstrating cancers with fewer false positives. The advantage of the dual-energy technique is that the breast does not have to remain immobilized during and after the contrast agent injection, so this allows multiple projections to be obtained versus a single projection possible with temporal subtraction. Acquisition of multiple views of the same fast breast or bilateral examination is feasible with the dual-energy technique, and therefore this is replaced with the temporal technique.

E.A. Morris, MD
Radiology, Memorial Sloan Kettering Cancer Center,
New York, NY, USA
e-mail: morrise@mskcc.org

J. Hodler et al. (eds.), *Diseases of the Brain, Head and Neck, Spine 2016–2019: Diagnostic Imaging*, DOI 10.1007/978-3-319-30081-8_35

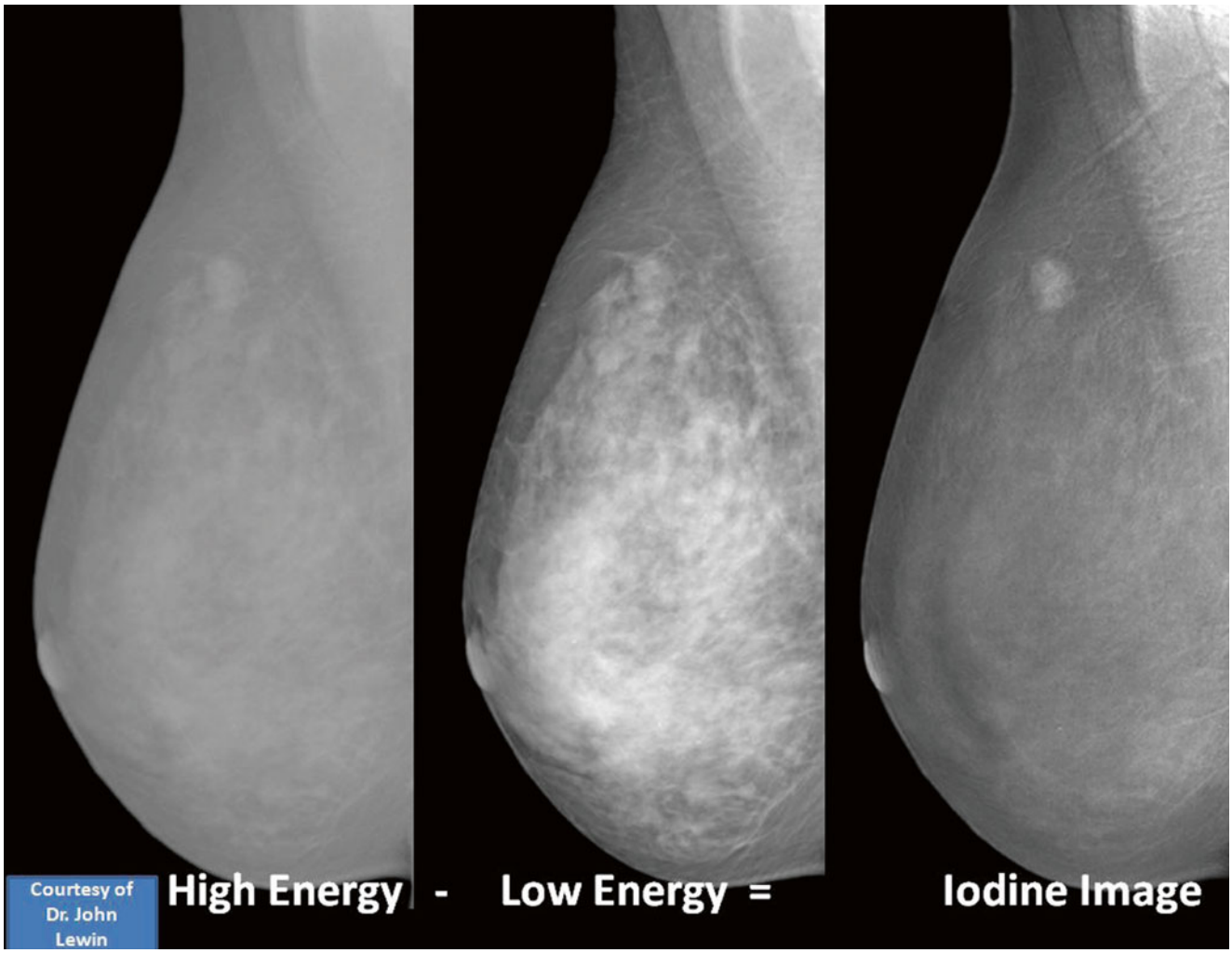

A few years later in 2006, a group in Paris demonstrated that contrast-enhanced digital mammography was able to depict angiogenesis in breast cancer using the temporal subtraction technique [4]. A year later in 2007, the group at University of Pennsylvania published experience on contrast-enhanced digital breast tomosynthesis [5] which is still not in routine use. Conclusion of this study was that early experience demonstrated better morphologic and vascular characteristics of breast lesions equally as well as the combination of digital mammography and MRI.

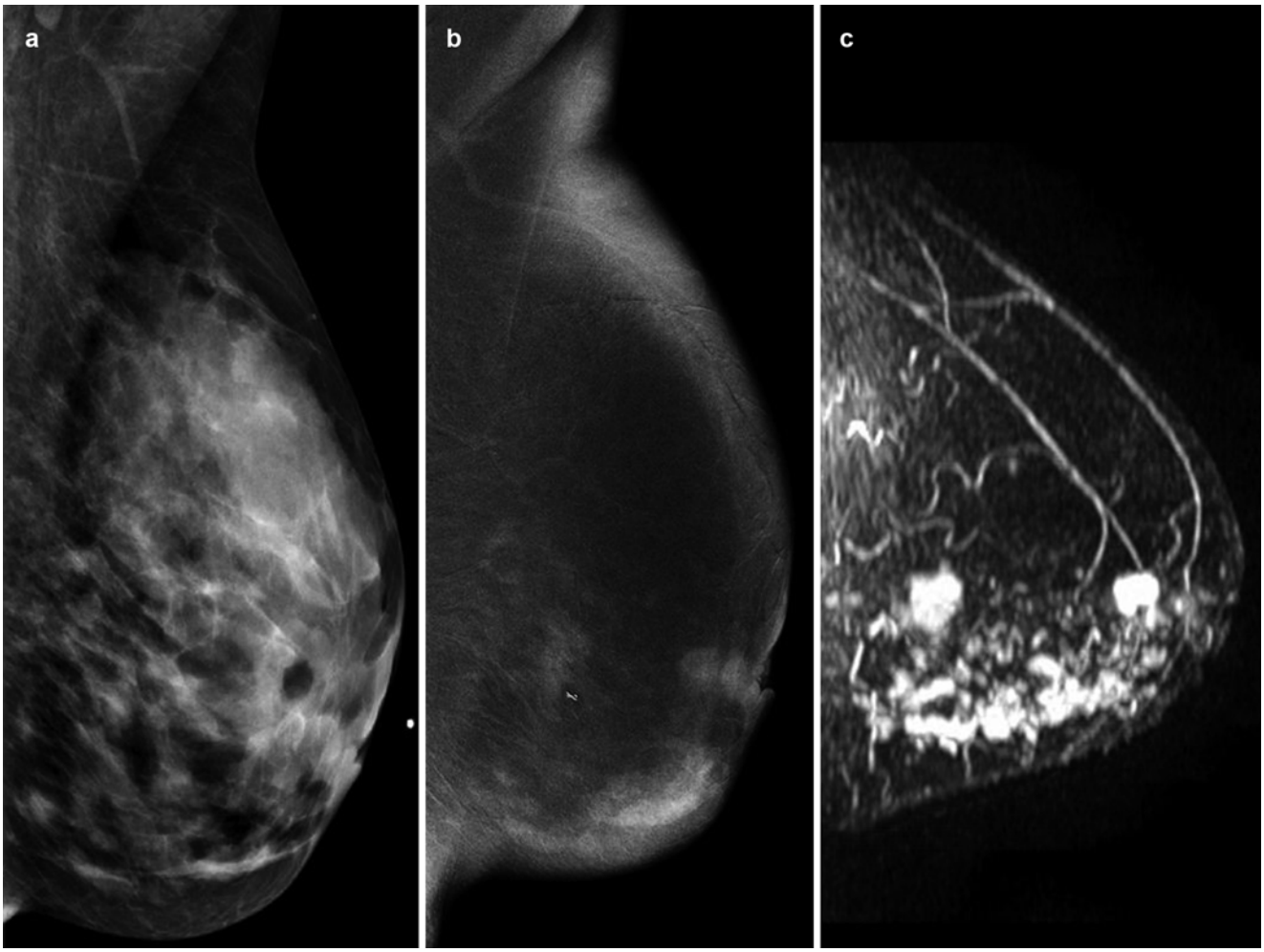

(**a**) FFDM demonstrates dense breast with no mammographic finding. (**b**) CEDM demonstrates a clip following US biopsy at a site of invasive cancer. Additional suspicious mass and nonmass enhancement is present in a segmental distribution compatible with multicentric cancer. (**c**) Contrast enhanced MRI confirms the findings on CEDM

It was not until about 2011 however that clinical studies were attempted with the dual-energy technique. The first study [6] compared CEDM to mammography and mammography plus ultrasound finding that CEDM had better diagnostic accuracy than mammography or mammography plus ultrasound. The lesion size was closer to the histologic size for CEDM and all multifocal lesions were identified. This is then followed by publications [7] demonstrating that dual-energy CEDM is an adjunct to mammography, and ultrasound improves diagnostic accuracy compared to mammography and ultrasound alone. In a prospective trial comparing MRI to CEDM in newly diagnosed breast cancer, both CEDM and MRI identified all primary tumors; however, CEDM had a slightly lower sensitivity for detecting additional ipsilateral disease, although the specificity was higher [8].

The benefits of contrast-enhanced digital mammography are numerous which has led to people calling it a possible replacement to contrast-enhanced MRI. It is easy to install, is inexpensive, requires little training for technologist to perform, has good patient tolerance, requires less maintenance than MRI, and does not have a steep learning curve for diagnostic interpretation. There is relatively good news about radiation exposure in that the low-energy mammogram obtained during the CEDM acquisition is comparable to a routine full-field digital mammogram, and therefore the patient need not undergo additional radiation [9]. Radiation dose is 20 % greater than a routine normal mammogram

which translates to the equivalent of one extra image. With this examination there is an obvious risk of administering iodinated contrast medium.

It appears that the enhancement of lesions on CEDM is slightly different than that observed on MRI. With contrast-enhanced mammography, many cancers demonstrate gradual enhancement as opposed to rapid enhancement and washout seen with MRI. It is also curious that the specificity with CEDM appears to be improved over MRI where many of the false-positive findings seen on MRI are not seen on CEDM. Why this occurs is not certain and may be possibly related to the differences in the contrast agents. Clearly, iodinated contrast interacts differently with the tumors within the breast than gadolinium, and these differences need to be better understood. It is interesting that bilateral exams can be performed in any acquisition order without loss of contrast and therefore sensitivity.

Despite the improved specificity over MRI, benign lesions within the breast include fibroadenoma, radial scar, and pseudo-angiomatous stromal hyperplasia (PASH). Additionally, background parenchymal enhancement can be observed on CEDM, as with MRI.

Clinical uses of contrast-enhanced digital mammography remain currently unclear. Early experience suggests that contrast-enhanced digital mammography may be more sensitive than digital mammography in the detection of cancer and may be more specific than MRI producing fewer false-positive findings in the preoperative setting. Potential clinical uses may be similar to MRI which would include staging of known breast cancers, evaluation for recurrent tumor in the post-treated breast, and screening for breast cancer. Prospective trials are needed to further elucidate the clinical value.

References

1. Diekmann F, Diekmann S, Taupitz M, Bick U, Winzer KJ, Hüttner C, Muller S, Jeunehomme F, Hamm B (2003) Use of iodine-based contrast media in digital full-field mammography–initial experience. Rofo 175(3):342–345
2. Jong RA, Yaffe MJ, Skarpathiotakis M, Shumak RS, Danjoux NM, Gunesekara A, Plewes DB (2003) Contrast-enhanced digital mammography: initial clinical experience. Radiology 228(3):842–850. Epub 2003 Jul 24
3. Lewin JM, Isaacs PK, Vance V, Larke FJ (2003) Dual-energy contrast-enhanced digital subtraction mammography: feasibility. Radiology 229(1):261–268. Epub 2003 Jul 29
4. Dromain C, Balleyguier C, Muller S, Mathieu MC, Rochard F, Opolon P, Sigal R (2006) Evaluation of tumor angiogenesis of breast carcinoma using contrast-enhanced digital mammography. AJR Am J Roentgenol 187(5):W528–537
5. Chen SC, Carton AK, Albert M, Conant EF, Schnall MD, Maidment AD (2007) Initial clinical experience with contrast-enhanced digital breast tomosynthesis. Acad Radiol 14(2):229–238
6. Dromain C, Thibault F, Muller S, Rimareix F, Delaloge S, Tardivon A, Balleyguier C (2011) Dual-energy contrast-enhanced digital mammography: initial clinical results. Eur Radiol 21(3):565–574. doi:10.1007/s00330-010-1944-y. Epub 2010 Sep 14
7. Dromain C, Thibault F, Diekmann F, Fallenberg EM, Jong RA, Koomen M, Hendrick RE, Tardivon A, Toledano A (2012) Dual-energy contrast-enhanced digital mammography: initial clinical results of a multireader, multicase study. Breast Cancer Res 14(3):R94
8. Jochelson MS, Dershaw DD, Sung JS, Heerdt AS, Thornton C, Moskowitz CS, Ferrara J, Morris EA (2013) Bilateral contrast-enhanced dual-energy digital mammography: feasibility and comparison with conventional digital mammography and MR imaging in women with known breast carcinoma. Radiology 266(3): 743–751. doi:10.1148/radiol.12121084. Epub 2012 Dec 6
9. Francescone MA, Jochelson MS, Dershaw DD, Sung JS, Hughes MC, Zheng J, Moskowitz C, Morris EA (2014) Low energy mammogram obtained in contrast-enhanced digital mammography (CEDM) is comparable to routine full-field digital mammography (FFDM). Eur J Radiol 83(8):1350–1355. doi:10.1016/j.ejrad.2014.05.015. Epub 2014 May 16

Current Challenges in Mammography Screening and Diagnostic Assessment

Michael James Michell

Screening

Screening Mammography

The aim of breast cancer screening is to decrease the number of deaths from breast cancer by detecting and treating cancers when they are small, when there is a low risk of metastatic spread and when treatment is most likely to be effective. The detection of small breast cancers continues to present challenges to mammography film readers and is dependent on specialist film reader training, ongoing audit and reader performance monitoring and high-quality digital images obtained with modern mammography equipment [1–3]. In the UK screening programme, all screening mammograms are independently double read by trained film readers, and systematic audit of screening detected cancers demonstrates that 9 % of screen-detected cancers are detected by one reader only. Analysis of the mammographic features of such discordant read cancers is important in enabling film readers to be aware of the mammographic features which may be missed [4]. Over 70 % of such cancers are small (less than 15 mm diameter), and the mammographic features include irregular and spiculate masses and clusters of microcalcification. Readers may fail to detect such lesions either on the craniocaudal or medial lateral oblique view, and histological analysis of the cancers shows no significant difference in distribution of tumour type compared to non-discordant read tumours.

The findings support the continued use of double reading to maximise the small invasive cancer detection rate in routine breast screening practice. Cases will be demonstrated to illustrate subtle mammographic signs which readers may find difficult to perceive.

M.J. Michell
Breast Radiology Department, King's College Hospital NHS Foundation Trust, London, UK
e-mail: Michael.michell@nhs.net; fleur.huxster@nhs.net

Interval Cancer Review and Radiology Classification

Data on interval cancers is an important indicator of the effectiveness of breast cancer screening programmes. All UK screening programmes routinely identify interval cancers, and this data is used to inform the epidemiological assessment of the effectiveness of breast cancer screening services. In addition the interval cancer cases are reviewed by the screen film readers together with the previous screening mammograms. Cases are then classified according to the presence or absence of abnormal features on the prior screening mammograms and following national breast screening quality assurance guidelines. The previous screening mammograms may be classified as (1) normal; (2) uncertain, there are features which can be identified in retrospect on the screening mammograms but where there is uncertainty over whether the case should be recalled; or (3) suspicious, there are features on the previous screening mammograms which are suspicious for malignancy [1]. Routine review of such cases is carried out in all screening programmes and ensures that film readers see and discuss subtle mammographic features of malignancy and maintain their skills in detection of small breast cancers. Cases will be demonstrated to illustrate subtle mammographic features.

Use of New Technology: Tomosynthesis in Breast Cancer Screening

Three European studies and a North American study have demonstrated significantly increased invasive cancer detection rates using tomosynthesis in addition to 2D mammography for screening. These studies have demonstrated no significant change in the DCIS detection rates, and three of the four studies have demonstrated a significant decrease in the false-positive recall rates. Tomosynthesis is very effective at demonstrating areas of spiculation or parenchymal distortion and improving the visibility of such subtle

J. Hodler et al. (eds.), *Diseases of the Brain, Head and Neck, Spine 2016–2019: Diagnostic Imaging*, DOI 10.1007/978-3-319-30081-8_36

mammographic findings. These studies of tomosynthesis in screening have not shown a significant increase in the DCIS detection rate because tomosynthesis does not improve the visualisation of microcalcification compared to 2D digital mammography. There remains, however, uncertainty regarding the implementation of tomosynthesis for routine screening in national programmes because of uncertainty over whether the increased cancer detection rate with tomosynthesis results in improved effectiveness of mammography screening in preventing breast cancer deaths. There is in addition some uncertainty regarding the cost of implementation of tomosynthesis for routine screening and in particular the implications for film reading time and number of film readers required. A trial proposal for addressing these questions will be discussed.

Diagnostic Assessment

Diagnostic Work-up

Approximately 5 % of women undergoing routine screening are recalled for further diagnostic assessment. The aim of the assessment is to obtain a definitive diagnosis of screen-detected lesions so that women with no significant breast problems can be reassured as quickly as possible and discharged from the clinic, and women with cancer can be diagnosed without delay. For women with breast cancer, appropriate imaging and biopsy workup is required to enable the multidisciplinary treating team to decide on appropriate surgical and oncological management [6]. Demonstration of the extent of both invasive and non-invasive tumour and the presence of tumour foci in other quadrants of the breast are crucial in determining whether breast-conserving therapy or mastectomy is the most appropriate treatment. Diagnostic assessment may be complex because the image features are subtle or difficult to characterise, the disease is more extensive than on initial baseline imaging, or biopsy pathology shows borderline or low-grade lesions. Systematic review of interval cancers shows that a small proportion (less than 5 %) have previously undergone diagnostic assessment.

Best quality diagnostic assessment is provided in a specialist radiology led clinic offering the triple diagnostic method. The risk of errors is reduced by close teamwork between radiology, radiographic, nursing and administrative staff. Cases with difficult or equivocal imaging features should be discussed and reviewed with colleagues, and all patients undergoing needle biopsy should be reviewed at a multidisciplinary meeting, together with pathology and surgery colleagues [2].

Cases will be demonstrated to illustrate complex and difficult diagnostic assessment cases.

Management of Borderline Lesions [5, 7, 8, 13, 20]

Approximately 7 % of lesions undergoing core biopsy at assessment are categorised as B3 (uncertain malignant potential), such lesions include:

- Atypical intra-ductal epithelial proliferation [18]
- Non-pleomorphic classical lobular in situ neoplasia (ALH or LCIS) [9–11]
- Flat epithelial atypia [12]
- Radial scar with or without epithelial atypia [14]
- Papillary lesion with or without epithelial atypia [15, 16]
- Cellular fibro-epithelial lesion
- Mucocele-like lesion [17]

Such lesions have been identified more frequently probably because of increased sensitivity of digital mammography and superior detection of low suspicion microcalcification, increased use of core biopsy and vacuum-assisted biopsy techniques and increased recognition of such lesions by pathologists. Surgical excision has been the diagnostic procedure of choice for such lesions in order to remove the lesion for full histological assessment. However, the increase in concern regarding overtreatment of such lesions and the increased availability of effective image-guided tissue sampling techniques such as vacuum-assisted core biopsy (VACB), a non-surgical approach to the management of such lesions, is proposed [12, 19]. Following an initial diagnostic 14G core biopsy or VACB, it is proposed that for some borderline lesions, it is safe to carry out image-guided vacuum-assisted excision (VAE), instead of surgery. VAE sampling should provide more than 3.5 g of tissue for examination. VAE is currently proposed for the management of cases of atypical intra-ductal epithelial proliferation, classical lobular in situ neoplasia, flat epithelial atypia, radial scar/complex sclerosing lesion without atypia and papillary lesion without atypia. The aim is to decrease the number of cases with borderline lesions requiring diagnostic surgical procedures.

Cases of borderline screening detected mammographic lesions will be demonstrated with imaging and histopathological correlation to show where non-surgical management is same and appropriate.

Low-Grade Ductal Carcinoma In Situ

There is considerable uncertainty regarding the natural history and clinical significance of low-risk ductal carcinoma in situ. There has been recent concern regarding possible overtreatment of patients with such lesions, and they are now being offered entry into a trial (the LORIS trial). In this trial, following image-guided diagnostic tissue sampling, patients

who consent to participate are randomised to either standard surgical management or active surveillance. Examples of such cases and the trial protocol will be discussed.

References

1. Quality assurance guidelines for breast cancer screening radiology second edition NHSBSP Publication No 59 March 2011 Editors Robin Wilson and Joyce Liston. NHS Cancer Screening Programmes
2. Quality assurance guidelines for breast cancer screening assessment third edition NHSBSP Publication No 49 June 2010 Editors Joyce Liston and Robin Wilson NHS Cancer Screening Programmes
3. Hackshaw AK, Wald NJ, Michell MJ, Field S, Wilson AR (2000) An investigation into why two-view mammography is better than one-view in breast cancer screening. Clin Radiol 15:454–458. doi:10.1053/crad.2000.0448
4. Cornford EJ et al (2005) The pathological and radiological features of screen-detected breast cancers diagnosed following arbitration of discordant double reading opinions. Clin Radiol 15:1182–1187. doi:10.1016/j.crad.2005.06.003
5. El-Sayed ME, Rakha EA, Reed J, Lee AH, Evans AJ, Ellis IO (2008) Predictive value of needle core biopsy diagnoses of lesions of uncertain malignant potential (B3) in abnormalities detected by mammographic screening. Histopathology 53(6): 650–657
6. Quality assurance guidelines for surgeons in breast cancer screening. 2009. (Surgical guidelines for the management of breast cancer. Association of Breast Surgery at BASO. EJSO 2009; S1-S22). Edited by Mark Sibbering, Roger Watkins, John Winstanley and Julietta Patnick
7. Huber S, Wagner M, Medl M, Czembirek H (2003) Benign breast lesions: minimally invasive vacuum-assisted biopsy with 11-gauge needles—patient acceptance and effect on follow-up imaging findings. Radiology 226:783–790
8. Rakha EA, Lee AH, Jenkins JA, Murphy AE, Hamilton LJ, Ellis IO (2011) Characterization and outcome of breast needle core biopsy diagnoses of lesions of uncertain malignant potential (B3) in abnormalities detected by mammographic screening. Int J Cancer 129(6):1417–1424
9. Buckley ES, Webster F, Hiller JE, Roder DM, Farshid G (2014) A systematic review of surgical biopsy for LCIS found at core needle biopsy – do we have the answer yet?. Eur J Surg Oncol 40(2):168–175
10. Hussain M, Cunnick GH (2011) Management of lobular carcinoma in-situ and atypical lobular hyperplasia of the breast – a review. Eur J Surg Oncol 37(4):279–289
11. Hwang H, Barke LD, Mendelson EB, Susnik B (2008) Atypical lobular hyperplasia and classic lobular carcinoma in situ in core biopsy specimens: routine excision is not necessary. Mod Pathol 21(10):1208–1216
12. Verschuur-Maes AH, van Deurzen CH, Monninkhof EM, van Diest PJ (2012) Columnar cell lesions on breast needle biopsies: is surgical excision necessary? A systematic review. Ann Surg 255(2):259–265
13. Jackman RJ, Nowels KW, Rodriguez-Soto J, Marzoni FA Jr, Finkelstein SI, Shepard MJ (1999) Stereotactic, automated, large-core needle biopsy of nonpalpable breast lesions: false-negative and histologic underestimation rates after long-term follow-up. Radiology 210(3):799–805
14. Brenner RJ, Jackman RJ, Parker SH, Evans WP 3rd, Philpotts L, Deutch BM, Lechner MC, Lehrer D, Sylvan P, Hunt R, Adler SJ, Forcier N (2002) Percutaneous core needle biopsy of radial scars of the breast: when is excision necessary? AJR Am J Roentgenol 179(5):1179–1184
15. Eiada R, Chong J, Kulkarni S, Goldberg F, Muradali D (2012) Papillary lesions of the breast: MRI, ultrasound, and mammographic appearances. AJR Am J Roentgenol 198(2):264–271
16. Page DL, Salhany KE, Jensen RA, Dupont WD (1996) Subsequent breast carcinoma risk after biopsy with atypia in a breast papilloma. Cancer 78:258–266
17. Rakha EA, Shaaban AM, Haider SA, Jenkins J, Menon S, Johnson C, Yamaguchi R, Murphy A, Liston J, Cornford E, Hamilton L, James J, Ellis IO, Lee AHS (2013) Outcome of pure mucocele-like lesions diagnosed on breast core biopsy. Histopathology 62:894–898
18. Rakha EA, Ho BC, Naik V, Sen S, Hamilton LJ, Hodi Z, Ellis IO, Lee AH (2011) Outcome of breast lesions diagnosed as lesion of uncertain malignant potential (B3) or suspicious of malignancy (B4) on needle core biopsy, including detailed review of epithelial atypia. Histopathology 58(4):626–632
19. Green S, Khalkhali I, Azizollahi E, Venegas R, Jalil Y, Dauphine C (2011) Excisional biopsy of borderline lesions after large bore vacuum-assisted core needle biopsy – is it necessary? Am Surg 77(10):1358–1360
20. Bianchi S, Caini S, Renne G, Cassano E, Ambrogetti D, Cattani MG, Saguatti G, Chiaramondia M, Bellotti E, Bottiglieri R, Ancona A, Piubello Q, Montemezzi S, Ficarra G, Mauri C, Zito FA, Ventrella V, Baccini P, Calabrese M, Palli D (2011) Positive predictive value for malignancy on surgical excision of breast lesions of uncertain malignant potential (B3) diagnosed by stereotactic vacuum-assisted needle core biopsy (VANCB): a large multi-institutional study in Italy. VANCB Study Group. Breast 20(3):264–270

Mammography: BI-RADS® Update and Tomosynthesis

Elizabeth A. Morris

BI-RADS® Update

The illustrative BI-RADS® fifth edition is a product of years of collaboration between subsection heads, committees, the American College of Radiology, and most importantly input from users of the lexicons. It is a living document, and therefore every edition tries to incorporate current state-of-the-art imaging interpretation. It is designed for everyday practice and should make possible unambiguous breast imaging reports and meaningful evaluation of individual and practice performance. The fifth edition includes mammography, ultrasound, and MRI. It includes a new section on follow-up in outcome monitoring. It does not include tomosynthesis, contrast-enhanced mammography, or molecular imaging. Each section has undergone major changes since the prior edition which shall be outlined as follows.

General

There has been a marked increase in the number of pages and number of images. An electronic version is available. Descriptors for all three modalities were harmonized and consistent across all modalities so that the same terms could be used. Breast tissue descriptors are no longer given numeric BI-RADS values to prevent confusion with numeric BI-RADS assessment categories. Management recommendations have been separated from assessment categories to allow for occasions where discordance between assessment and management is necessary. Each modality section as well as follow-up in outcome monitoring section includes frequently asked questions with responses.

E.A. Morris, MD
Radiology, Memorial Sloan Kettering Cancer Center, New York, NY, USA
e-mail: morrise@mskcc.org

Mammography

Breast density descriptions have changed to the following and percentage quartiles have been eliminated:

A. The breasts are almost entirely fatty.
B. There are scattered areas of fibroglandular density.
C. The breasts are heterogeneously dense, which may obscure small masses.
D. The breasts are extremely dense, which lowers the sensitivity of mammography.

Asymmetries have been expanded:

Asymmetry: An area of fibroglandular density tissue that is visible on only one mammographic projection. Most of these findings represent summation artifacts and superimposition of normal breast structures.

Global asymmetry: Global asymmetry is judged relative to the corresponding area and the contralateral breast and represents a large amount of fibroglandular density tissue over a substantial portion of the breast (at least one quadrant). There is no mass, architectural distortion, or associated suspicious calcifications. Global asymmetry usually represents a normal variant.

Focal asymmetry: Focal asymmetry is judged relative to the corresponding location in the contralateral breast and represents a relatively small amount of fibroglandular density tissue over a confined portion of the breast (less than one quadrant). It is visible on and has similar shape on different mammographic projections and hence is a real finding rather than superimposition of normal breast structures but it lacks a convex outward border and conspicuity of a mass. Usually the borders are concave outward and may be seen interspersed with fat.

Developing asymmetry: This is a focal asymmetry that is new, larger, and more conspicuous than on previous examination. Approximately 15 % of developing

J. Hodler et al. (eds.), *Diseases of the Brain, Head and Neck, Spine 2016–2019: Diagnostic Imaging*, DOI 10.1007/978-3-319-30081-8_37

asymmetries are found to be malignant, so these cases warrant further imaging evaluation and biopsy unless found to be characteristically benign with further workup.

Category 3, 4, or 5 should not be used for mammographic screening. These assessments should only be given after full diagnostic workup.

Ultrasound

New section that includes anatomy, tissue composition, image quality, and labeling/measurement.

Definition of standard images for screening ultrasound was described. For screening ultrasound performed with hand-held transducer, the operator (physician or sonographer) records a small set of images that are representative of the breast. This is defined at least five images per breast (one each quadrant and one in the retroareolar region). If any findings are identified on a screening ultrasound examination in which more additional diagnostic images are recorded, this represents a positive screening examination as further additional diagnostic images will be obtained.

MRI

A new section on implant assessment, fat-containing lesions, and nonenhancing findings was added. The amount of fibroglandular tissue added to the lexicon:

A. Almost entirely fat
B. Scattered fibroglandular tissue
C. Heterogeneous fibroglandular tissue
D. Extreme fibroglandular tissue

Amount of background parenchymal enhancement (BPE) added to the lexicon to describe the volume and intensity of normal parenchymal enhancement:

Minimal/mild/moderate/marked

Stippled has been removed from the lexicon as this reflects a type of background parenchymal enhancement that has a specific pattern. Multiple foci similarly have been removed from the lexicon as this also generally reflects a pattern of background parenchymal enhancement. The single focus has been retained as a descriptor.

Auditing

Objective and reproducible auditing practices for all three major breast imaging modalities are described so that more internally consistent and more meaningful cross-modality comparison of outcomes can be obtained. Cross modality comparison will become increasingly more important since as newer modality of screening breast ultrasound of breast MRI become more widely used. Additionally, as BI-RADS incorporates newer modality such as tomosynthesis and contrast-enhanced mammography, it will be important to have firm outcome measures.

Tomosynthesis

The role of tomosynthesis in breast cancer screening programs is maximizing the benefits for women.

Mammography as we currently know it is the best screening test for the early detection of breast cancer. There is no doubt it saves lives. As an imaging modality, mammography had not changed for many years until the advent of digital imaging technology. Most breast imaging in the Western world is now currently performed with digital technology rather than film screen. The benefits of digital imaging are numerous: improved contrast, increased speed of acquisition and display, improved storage and retrieval, and the possibility of advanced applications. Disappointingly, digital mammography (DM) did not improve the cancer detection rate in women to the extent that was hoped, although it did show a modest improvement in women with dense breasts. Digital technology allowed the development of digital breast tomosynthesis (DBT), an advanced application, informally called 3D mammography (in contrast to conventional 2D DM).

DBT has arrived on the world stage in time to address many of the limitations of mammography. Dense tissue has always been the challenge of mammography due to the masking effect. Trials have shown that cancer detection rate with DBT is improved as the cancers are "unmasked" as the issue of overlapping tissue or summation artifacts is eliminated. Additionally, recent criticism of mammography has centered false-positive examinations and overdiagnosis. In numerous trials, the callback rates are lower when DBT is used compared to standard DM. Fewer women are asked to return for summation shadows as DBT easily resolves these at interpretation. A recent multicenter study published in the *Journal of the American Medical Association (JAMA)* found that when tomosynthesis is used in addition to digital screening mammography, there is a 41 % increase in invasive cancer detected, a 15 % decrease in unnecessary callbacks for false alarms, and a 29 % increase in the detection of all breast cancers. The conclusion is that DBT finds more of the invasive, harmful cancers and saves women the anxiety and cost of having additional screenings for what turns out to be a false alarm.

Conventional full-field digital mammography produces one image of overlapping tissue making it often difficult to detect obscured underlying breast cancers. It has been well documented that the detection of cancer and women with radiographically dense breasts can be limited. While nearly

all cancers will be apparent of fatty breasts, only half will be visible in extremely dense breasts. Digital breast tomosynthesis (DBT) was pioneered in 1992 at Massachusetts General Hospital and takes multiple images of the entire breast and provides a clear more accurate view of the breast resulting in improved breast cancer detection, especially invasive cancers and decreasing callbacks which may lessen anxiety for patients. In 2011 DBT was approved by the FDA in the USA. DBT is rapidly becoming a part of routine clinical practice despite increase interpretation times. It is thought that the reduction of false positives however could counterbalance this with fewer diagnostic workups involving additional views. Approximately 40 % of practices have adopted tomosynthesis in the northeast of the USA.

Tomosynthesis is here to stay and likely will replace FFDM in most practices. It however will not solve all issues with false negatives as cancers can still be missed on tomosynthesis. Advanced screening will still likely be used. It is uncertain if tomosynthesis will obviate screening with US or perhaps contrast-based techniques such as CEDM or MRI. These studies need to be undertaken.

Reference

1. Friedewald SM, Rafferty EA, Rose SL et al (2014) Breast cancer screening using tomosynthesis in combination with digital mammography. JAMA 311(24):2499–2507

Breast Ultrasound: BI-RADS Update and Imaging Pathologic

Alexander Mundinger

Introduction

Radiology and pathology share some characteristics such as intensive multidisciplinary cooperation, standardised communication and discussion of any discrepancy. Both disciplines have to survey many details to detect and characterise index lesions within the breast based on a perception concept that resembles the recognition of a signal within noise. Appropriate correlation of all imaging and pathological findings with clinical symptoms, underlying risk and anamnestic information is prerequisite for quality assurance. Both disciplines also depend on continuous education and international exchange to achieve and maintain highest standards. To date interdisciplinary conferences have become standard in breast centres. The consensus on radiologic-pathologic correlation is one of several critical parameters to fulfil state-of-the-art management of patients with breast disease. Management options focus on a second expert opinion, the gaining of additional information by minimally invasive tissue sampling or surgical re-biopsy or imaging follow-up to exclude the new development of breast cancer.

BI-RADS Ultrasound Update

History and Intention The breast imaging and reporting data system (BI-RADS) was introduced by the American College of Radiology (ACR) at the beginning of the 1990s for mammograms. The last update in 2003 expanded the content to a breast imaging lexicon and included ultrasound and MRI. This multimodality book has been translated and commented in many languages including German [1–3]. Meanwhile, ACR published a new renamed fifth version, the Breast Imaging Atlas 2013. Under the editorship of Ellen B. Mendelson, the ultrasound section includes four main chapters (general considerations, breast imaging – ultrasound lexicon, reporting system, guidance) that are framed by preface, introduction and an appendix with tables. Again this update standardises the international terminology, the uniform approach and the subsequent verification of actions following breast imaging. Special features of the US audit for ultrasound are designed for the US health system only and can only be transferred to European quality assurance with severe modifications.

Features and Descriptors Table 1 lists the refined sonographic diagnostic major and minor criteria, i.e. imaging features and descriptors. Table 2 sums up the categories. In the main chapters of the new BI-RADS Atlas Imaging – Ultrasound, numerous details have been completely or partially revised. In addition to many newly inserted details, the description depth in some places has been reduced deliberately. Thus, only the distinction between "circumscribed" and "not circumscribed" is relevant for the assessment of the margin. The focus of the image analysis holds still on the B-image morphology. The former boundary zone (hyperechoic halo) was abandoned as a separate feature and is now subsumed under the "indistinct edge" of a lesion. The simple cyst was incorporated as a special case for the first time. To avoid confusion, the nomenclature has been adapted. It now differs between a simple cyst, clustered microcysts, the complicated cyst (all category special cases) and the "complex cystic and solid lesion" (category mass, feature echo pattern) (Table 3). The latter used to be called "complex mass" previously. In addition now a new localisation exists in the category calcifications: intraductal. The former wording of microcalcifications has been switched to calcifications. The previous two descriptors, architectural distortion and duct changes, are now listed as associated features (Table 4). Both can be found as accompanying findings of a lesion or standing alone. Respecting the new technical developments of the

A. Mundinger
Radiological Department and Breast Centre,
Niels-Stensen-Clinics, Bischofsstraße 1,
Osnabrück 49074, Germany
e-mail: alexander.mundinger@gmail.com

J. Hodler et al. (eds.), *Diseases of the Brain, Head and Neck, Spine 2016–2019: Diagnostic Imaging,* DOI 10.1007/978-3-319-30081-8_38

last year's elasticity has been introduced as an associated feature. Other new special cases include simple cyst, vascular abnormalities (arteriovenous malformations and pseudoaneurysms), postoperative fluid collections and fat necrosis [14]. All special cases are considered as pathognomonic and need no further differentiation by shape, orientation or margin descriptors (Tables 5 and 6).

Categories, Recommendations and Management The formerly very strict coupling between BI-RADS category and the resulting management recommendations was reduced in favour of a greater freedom to manoeuvre (Table 2). If a lesion is consistent with BI-RADS category 3, the patient

Table 1 Classification of diagnostic ultrasound criteria in the ACR BI-RADS® Atlas

Tissue composition (screening only)	(a) Homogeneous background echotexture – fat	
	(b) Homogeneous background echotexture – fibroglandular	
	(c) Heterogeneous background echotexture	
Masses	Shape	Oval
		Round
		Irregular
	Orientation	Parallel
		Not parallel
	Margin	Circumscribed
		Not circumscribed
		Indistinct[a]
		Angular
		Microlobulated
		Spiculated
	Echo pattern	Anechoic
		Hyperechoic
		Complex cystic and solid
		Hypoechoic
		Isoechoic
		Heterogeneous
	Posterior features	No posterior features
		Enhancement
		Shadowing
		Combined pattern
Calcifications	Calcifications in a mass	
	Calcifications outside of a mass	
	Intraductal calcifications	
Associated features	Architectural distortion	
	Duct changes	
	Skin changes	Skin thickening
		Skin retraction
	Oedema	
	Vascularity	Absent
		Internal vascularity
		Vessels in rim
	Elasticity assessment	Soft
		Intermediate
		Hard
Special cases	Simple cysts	
	Clustered microcysts	
	Complicated cyst	
	Mass in or on skin	
	Foreign body including implants	
	Lymph nodes – intramammary	
	Lymph nodes – axillary	
	Vascular abnormalities	AVMs (arteriovenous malformations/ pseudoaneurysms)
	Postsurgical fluid collection	
	Fat necrosis	

New wordings or topics are assigned red

[a]The former lesion boundary has been deleted. The margin descriptor "indistinct" now comprises the previous echogenic halo. An echogenic rim may also be interpreted as sign of architectural distortion owing to effects of a mass on its surrounding (amongst associated features)

Table 2 Assessment categories, management recommendations and likelihood of cancer

Assessment categories	Management	Likelihood of cancer
0 Diagnosis incomplete	Recall for additional imaging	–
1 Negative	Normal follow-up	Almost 0 %
2 Benign	Normal follow-up	Almost 0 %
3 Probably benign	Short-interval follow-up (6 month) or continued surveillance	>0 % but ≤2 %
4 Suspicious	Tissues diagnosis	>2 % but <95 %
4a Slightly suspicious		>2 % but ≤10 %
4b Moderately suspicious		>10 % but ≤50 %
4c Highly suspicious		>50 % but <95 %
5 Highly suggestive of malignancy	Tissue diagnosis	≥95 %
6 Biopsy-proven malignancy	Surgery, if adequate	–

ACR BI-RADS® Atlas. Breast Imaging Reporting and Data System 2013. Ultrasound [1]

Table 3 Imaging-pathology correlation and differential diagnosis of complex cystic and solid lesions

Complex cystic and solid lesions
Imaging features
Anechoic and hyperechoic components
Wall thickening
Broad septations
Intracystic or mural solid mass
Mainly solid mass in cystic compartments
Pathologic correlation
Papillary carcinoma
Papillomas
Fibrocystic breast disease
Inflammation

Table 4 Tissue characteristics associated with architectural distortion

Associated features: *architectural distortion*
Compression of the tissue around space occupying lesion
Obliteration of tissue layers by infiltration
Straight or thickened Cooper ligaments
Aberrations of duct patterns
Hyperechoic halo

ACR BI-RADS Atlas. Breast Imaging Reporting and Data System 2013. Ultrasound [1]

Table 5 C (cytology) and B-(bore) classification of FNA and core biopsy specimens

Fine needle aspiration: *cytology*
C1 Inadequate for diagnosis
C2 Benign epithelial cells
C3 Atypia probably benign
C4 Suspicious of malignancy
C5 Malignant
Core biopsy: *histology*
B1 Unsatisfactory/normal breast tissue
B2 Benign
B3 Benign but of uncertain malignant potential
B4 Suspicious of malignancy
B5 Malignant

and physician may nevertheless, contrary to the statement of the BI-RADS, agree on a biopsy. Like every lexicon the BI-RADS Atlas gradually develops further and is guided by the findings of the research. The use of modern technologies including elastography and automated 3-D volume breast ultrasound (ABUS or AVUS) is explicitly encouraged. The final importance for patient care or screening is still to be defined in further studies [4]. If new methods will not prove themselves, they can be eliminated in future versions and give way to others. The translation of a lexicon into foreign languages will be controlled by the ACR in order to ensure the linguistic transfer correctly and accurately to the last detail. Further, legal and copyright issues have to be considered.

Table 6 Characteristics of phyllodes tumour

Histology	Benign PT	Borderline PT	Malignant PT
Margin	Well-defined	Well-defined, may be focally permeating	Permeating
Cellularity	Usually mild	Usually moderate	Usually marked
Atypia	Mild or none	Mild or moderate	Marked
Mitoses	Usually few	Usually frequent	Usually abundant
Stromal overgrowth	Absent	Absent or very focal	Often present
Proportion	60–75 %	15–20 %	10–20 %

Modified according to Ref. [15]

Imaging and Pathology Correlation

Basics Most proliferative benign and malignant breast diseases arise from TDLUs. The DCIS extends to or may start also from the larger ducts of the breast. Dilated TDLUs can be caused by cystic remodelling, proliferation of benign cells (adenosis, sclerosing adenosis) or monoclonal proliferation of malignant cells within the basal membrane (DCIS, CLIS). If the malignant cells break through the basal membrane, a carcinoma is given by definition. Carcinomas develop their "typical" malignant macroscopic appearance with increasing size. Then carcinomas exhibit a wide range of growth forms, regressive changes, desmoplastic reactions of the tumour environment and locoregional propagation. Numerous suspicious diagnostic characters reflect this diversity of carcinoma presentations at ultrasound and other imaging modalities [4].

Molecular Pathology of Breast Cancer Progression Genomic, transcriptomic (gene expression) profiling and epigenetic analyses of the various stages of breast cancer have increased the insights in the complex process of breast cancer progression. Breast cancer appears to progress along two distinct molecular genetic pathways that strongly associate with tumour grade. In the epithelial and non-epithelial components of the tumour microenvironment, the greatest molecular alterations occur prior to local invasion representing gene instability at the gene expression level. In the epithelial compartment, no major additional gene expression changes occur between the preinvasive and invasive stages of breast cancer, while only modest genome copy number abnormalities and a continuing loss of telomerase length characterise this phase of proliferative advantages for tumour cells. The non-epithelial compartment of the tumour micromilieu undergoes dramatic epigenetic and gene expression alterations during the

transition from preinvasive to invasive disease. Thus, cancer progression results from an orchestrated series of bidirectional signalling between non-epithelial cells and malignant epithelial cells in the tumour microenvironment [5]. Today, genomic assays such as Oncotype, MammaPrint, Mammostrat and Prosigna are used to analyse the activity of a group of genes within breast cancer tissue in order to predict the risk of the breast cancer returning later.

The Sick Lobe Theory

The sick lobe theory presented by Tibor Tot complements the insights in molecular tumour progression and may explain the various distribution patterns of cancer [6]. In a first step, breast stem cell or committed progenitor cells such as the common progenitor cell, myoepithelial progenitor cell and luminal progenitor cell of a lobe acquire genetic aberrations during embryogenesis. The committed myoepithelial and luminal progenitors transfer their instability when finally differentiating to the myoepithelial, luminal and ductal epithelial cells to a defined area within the lobe. Secondly, these mutations progress and accumulate depending on exogenic and endogenic hits. Finally, a malignant transformation to in situ precursors and at the last stage to breast cancer develops that is restricted to the barriers of a single lobe initially in most cases. The malignant transformation of stem cells may explain the simultaneous and diffuse malignant transformation of TDLUs and ductal structures [6]. Intense interactions between the parenchymal and stromal elements and the epithelial-mesenchymal transition of some parenchymal cells lead to invasive malignant growth. As the committed progenitor cells may be either evenly or unevenly distributed within the sick lobe, malignant transformation of the cells could appear at a single discrete locus, simultaneously at several loci or at many different points within the entire lobe. Consequently, the development of in situ precursors within the sick lobe may be unifocal, multifocal or diffuse. Similarly, invasive growth may appear at a single locus, at several distant loci or over a large area within the breast tissue [7]. Approximately one-third of invasive cases are unifocal, with a single invasive focus and an in situ component within and/or in the vicinity of this focus. Another third of the cases are characterised by the presence of a single invasive focus but associated with a diffuse or multifocal in situ component. The final third of the cases exhibit a multifocal invasive component. Almost half of these cases are extensive in which the individual foci occupy a tissue volume of greater than four cm in the largest dimension [8]. The lobar nature of breast carcinoma is easiest to observe at in situ or early millimetres' scale invasive phase. The consequences of the lobar tumour growth extend to both the lobar approach to preoperative imaging and segmental surgery.

How Do Radiology and Pathology Diagnose and Correlate Findings? Both disciplines make use of a multifaceted approach to breast lesions. First, they have to detect and then characterise the index lesions in a representative location within the breast at imaging or within the biopsy or excision specimen at pathological analysis. The previous BI-RADS chapter emphasised both the variety of malignant features and also the overlap between malignant and benign features at ultrasound. This is true for all other imaging approaches correspondingly. Imaging modalities and pathology refer to different scales of the spatial spectrum and focus on macroscopic structure and architectural features at imaging and microscopic cellular characteristics at pathology. The golden standard for establishing the malignant diagnosis has been traditionally pathology at the cellular level. The increased rate of mitosis, increased nuclear size, altered nuclear/cytoplasm relation and the loss of the basal membrane and myoepithelial are the main pillars to establish the diagnosis of malignancy correspondingly. In contrast, imaging methods including ultrasound detect and characterise the macroscopic extension of the tumour front (margin) and the characteristic imaging phenotype of the tumour matrix (texture) within and surrounding tissue with special focus on the interface (architectural distortion, halo). Any microscopic extension of tumour foci will not be detected by imaging and thus any multifocal spread will be underweighted by the intrinsic characteristic of macroscopic imaging. Knowing about the limitations of each discipline allows recognising discordances between the BI-RADS category and the pathologic B (bore) category following biopsy and impacts patient management in up to 5 % of cases. Improving patient care by incorporation of multidisciplinary breast radiology-pathology correlation conference decreases follow-up imaging and avoids unnecessary surgical intervention [8, 9]. The B3 lesions of uncertain malignant potential comprise two subcategories. (1) Lesions with risk of associated DCIS or invasive cancer. These comprise atypical ductal hyperplasia (ADH), lobular neoplasia (ALH, LCIS) and flat epithelial atypia (FEA). (2) Inhomogeneous lesions with sampling risk. These include phyllodes tumour, cellular fibroadenoma, incompletely removed papilloma and radial scar or complex sclerosing lesion ([10], Table 5).

What Is the Blind Side of Imaging and Pathology? Macroscopic imaging modalities with the exception of receptor-based molecular imaging cannot make use of cellular information. This is the intrinsic blind side of macroscopic imaging. Some radiologic characteristics of a tumour do not catch the attention of the pathologist when establishing the malignant diagnosis. Pathology nearly ignores tissue changes within and around the tumour that may be relevant for the radiologist. Desmoplastic reactions of the tumour surrounding tissue, altered vessel architecture and regressive tissue

reactions illustrate such background changes that usually are not worth to be high lightened in a pathology report. They are part of the background tissue changes that contrast the signal information of malignancy. Further, it takes a lot of interdisciplinary standardised cooperation and feedback to ensure that all malignant foci are visualised within the volume of the excision specimen. Only the complete analysis of thin-sliced gross section specimen using large-format histology would represent a perfect golden standard of pathology to prove the extension of all malignant foci as recommended by Tot and co-workers [11]. To date, MRI may show more invasive foci than described by pathological analysis after resection of a mastectomy or segmental specimen if only the representative approach of current margin analysis and no gross section specimens are used [12]. For ultrasound and mammography, this is true to a less extent. Large-format gross section histopathology demonstrates both the macroscopic extent and also the cell characteristics of a tumour [6–8]. This preparation technique, however, is associated with higher costs and limited to few centres to date. The supporters of large-format histology argue with the consequences of undetected invasive foci on the treatment plan. The opponents doubt that better pathologic staging can be transferred to better survival in the times of state-of-the-art-oncologic therapy. Clinical experience has shown that histologically undetected foci are controlled with radiotherapy, and their incidence significantly exceeds local recurrence rates in modern studies of BCT. Although it is clear that the clinical importance of microscopic multifocal disease is related to its volume, the threshold volume that influences clinical outcome is unknown [13].

Histologic Types and Imaging Characteristics

Invasive Cancers They are highly heterogeneous with regard to growth pattern, contour, cytological features, intercellular cohesion, mitosis, associated DCIS, necrosis, desmoplastic activity, admixed lymphoplasmacytic infiltrates and neovascularisation. Besides the histopathological type, the major classification approaches are grade of the tumour, the stage of the tumour and the expression of proteins and genes [14]. As knowledge of cancer cell biology develops, these classifications are updated regularly. The latest WHO tumour classification of the breast covers not only invasive breast cancers but also precursor lesions, lesions of low malignant potential, benign epithelial proliferations, fibroepithelial and myoepithelial and mesenchymal neoplasms, amongst others. Histologic grade often varies from one part of the tumour to the next. Assigning the highest grade within the malignancy to the whole tumour is advisable [15]. To prevent misunderstanding, it must be emphasised that the following US features are only more or less characteristic for the addressed tumour types [16, 17]. This means that for an individual case, even the opposite observations may be true.

The term *NOS* (*not otherwise specified*) *cancer* stands for the previous term ductal carcinoma. The histological growth pattern in ductal cancers arranges tumour cells as glandular structures, nests, cords, trabeculae or solid sheets. The margin features may be infiltrating, pushing, circumscribed or mixed.

US features: High-grade tumours are likely to be more cellular and fast growing than hypocellular and slowly growing. They tend to lie rather at the round and circumscribed end of the malignant nodule spectrum, and they rather induce more inflammatory and less desmoplastic response compared with low-grade lesions. Further they more frequently present with necrosis and extensive DCIS compared to low-grade lesions. A subgroup of high-grade cancers may even resemble a cyst at first fundamental US examination. Only the tumour hypervascularisation in Doppler techniques and elastographic stiffness may point to the solid nature of the lesion.

All features of the ACR-BI-RADS Atlas can be found in NOS cancers [1, 2, 16].

Triple-negative cancer is a subset of invasive cancers with poor diagnosis that is often (68 %) clinically detected and show grade 3 in 71 % compared to non-triple-negative cancers. Ultrasound findings of a recent study (AJR 2012) showed hypoechoic or complex masses with an irregular shape (78/120 (65 %)) and ill-defined (57/120 (48 %)) or microlobulated (38/120 (32 %)) margins.

The hallmark of *lobular cancer* is the loss of intercellular cohesion that results in the invasion of the stroma in a singly and in a single file pattern that results in the formation of linear strands. Typically associated desmoplastic reaction is present, and advanced disease is associated with a volume loss of the breast. US is considered more sensitive than mammography in detecting ILC. Literature reports sensitivities ranging from 68 to 98 % [18]. Jones and co-workers specified that of 509 invasive lobular carcinomas, 27 (5 %) were hyperechoic, of which 13 (48 %) were associated with posterior acoustic shadowing. Heterogeneously echogenic cancer was seen in 57 (11 %) cases. The most common sonographic finding was a hypoechoic, irregular mass with or without posterior shadowing ($n=323$; 63 %). In 66 (13 %) lesions, focal shadowing was seen without a discrete mass. Fourteen (3 %) lesions were isoechoic with respect to surrounding normal adipose tissue without acoustic shadowing [19] (Fig. 1).

The hallmark of *tubular cancer* is the proliferation of well-formed glands or tubules without myoepithelial lining. The associated stroma shows desmoplastic reaction and elastosis. Low-grade DCIS and FEA are often found in association with tubular carcinoma.

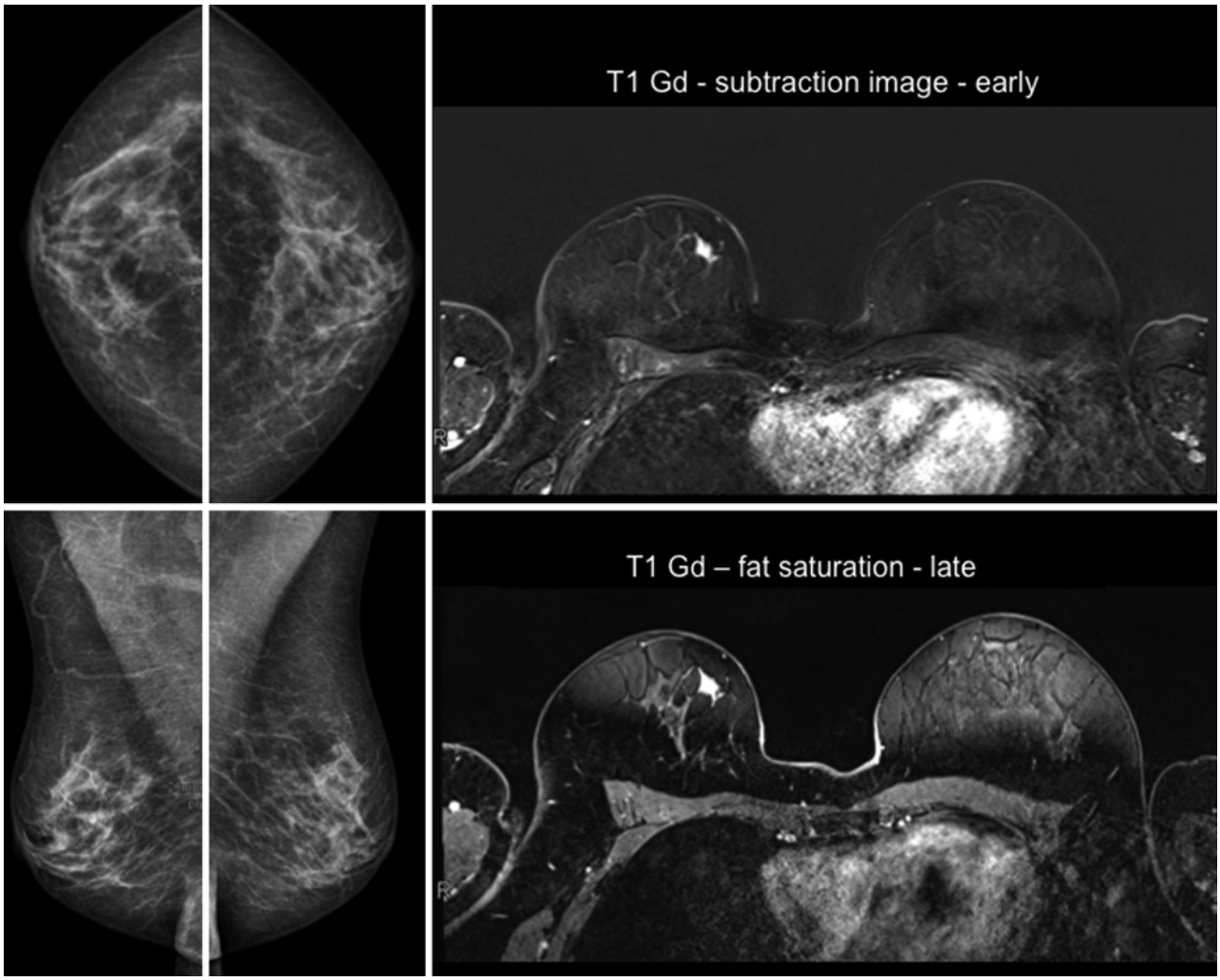

Fig. 1 A 68-year-old patient noticed a subtle palpable finding at 12.00–1:00 o'clock of the right breast. Ultrasound and mammography examination elsewhere are negative which is a discrepancy. Advanced high-resolution ultrasound detects and characterises a corresponding lesion. The lesion is slightly hypervascularised and stiff

US features: The most frequent finding is an irregular hypoechoic mass with spiculations or an indistinct margin, with or without shadowing and associated architectural distortion [20].

The hallmark of *mucinous carcinoma* (*colloid*) is extracellular mucin production and small uniform cells within. Two subtypes of mucinous carcinoma may be differentiated histologically: pure and mixed. Of these two subtypes, pure mucinous carcinoma is characterised by less aggressive growth and less frequent metastasis to axillary lymph nodes.

US features: Pure mucinous breast carcinomas commonly have indistinct or lobulated sonographic margins. On ultrasound, these neoplasms are commonly observed as a mass with an oval shape (60 %), isoechoic (51 %) with normal posterior acoustic appearances (80 %). However, most (77 %) of these lesions have suspicious or definite imaging features of malignancy [16, 21] (Fig. 2).

The hallmarks of *medullary carcinoma* are a syncytial growth pattern (>75 %) without ducts or lobules, circumscription, lympho-plasmacellular infiltrates and grade 2 or 3 nuclear pleomorphism.

US features: The most frequent finding is a round, oval or lobulated hypoechoic mass. The mass can present either homogeneously, hypoechoic or hypoechoic with mild heterogeneity. Enhanced transmission may be present and simulate a cystic appearance. Necrosis may result in mild heterogeneity or even pseudocystic substructures [20, 22].

The hallmark of *DCIS* is a neoplastic proliferation of epithelial cells confined to the mammary ductal-lobular system and characterised by subtle to marked cytological atypia and an inherent but necessarily obligate tendency for progression to invasive breast cancer. By definition the myoepithelial cells are able to produce and preserve a basal membrane that is intact.

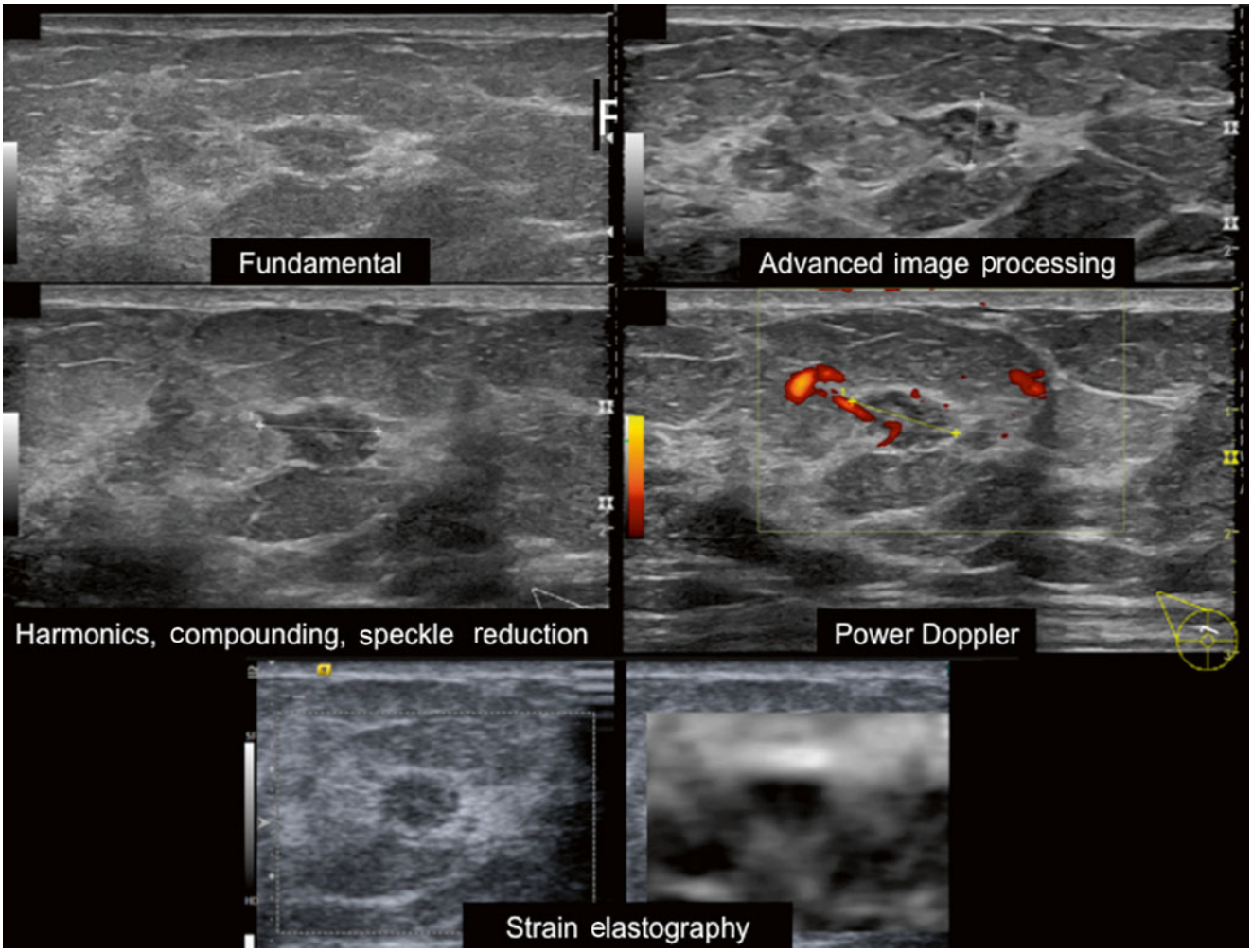

Fig. 2 Same patient. Digital mammography is negative. 3T MRI shows a corresponding suspicious lesion

DCIS of low nuclear grade typically develops within dilated TDLU. The DCIS has a solid and luminal component. Calcifications develop following secretion to the very tiny luminal spaces. In contrast DCIS of intermediate and nuclear grade represent calcifications within necrotic spaces within TDLUs or ducts. Typical characteristics of high-grade DCIS comprise unicentric local growth and for large DCIS segmental distribution towards periphery and nipple. In contrast low-grade DCIS shows a multicentric distribution that may present metachronously or synchronously. It is unclear whether or not DCIS spreads beyond anastomoses of adjacent duct segments or develops in multiple dysplastic lobes synchronously. Risk of microinvasion, multifocality and multicentricity increases with extension of spread. The prognostic relevance is highest for high-grade DCIS, less striking for intermediate and not proven for low-grade DCIS.

US features: Cystic or solid lesions accounted for approximately 80 % of US findings of DCISs detected by US alone. In general more benign-looking ultrasound features are associated with the absence of microinvasion and lower nuclear grade [23].

Dilatation and unfolding of TDLU due to DCIS predominantly grades 1 and 2 correlates with a round or lobulated small "solid" US mass in fundamental US. DCIS growing within multiple dilated TDLUs represents the extension within the whole ductal-lobular tree (grade 3 > 2) or multifocal development (grade 1). DCIS grade 3 with casting calcifications may develop in the major ducts only and correlates with a "non-mass" appearance in fundamental US.

Thin slices can depict echogenic intraductal masses and non-floating linear and/or echogenic foci (<1 mm) that are consistent with calcifications. A lump, shadowing of the mass in fundamental US and hypervascularisation, can be explained by inflammatory and desmoplastic reactions of the surrounding tissue (predominantly grade 3) [3, 4]. Special types of DCIS may be clinically detectable and comprise intracystic papillary carcinoma, tumour-forming DCIS, apocrine papillary DCIS (nipple discharge) and Paget disease (eczema).

Lobular carcinoma in situ, atypical ductal hyperplasia, atypical lobular hyperplasia and peripheral duct papillomas usually are too small to present with an ultrasound correlate.

Clinical follow-up studies have indicated that intraductal proliferative lesions are associated with different levels of risk for subsequent development of invasive breast cancer that ranges from approximately 1.5 times that of the reference population for usual ductal hyperplasia, four- to five-fold (range, 2.4- to 13.0-fold) for ADH and eight- to tenfold for DCIS. The main clinical significance of the diagnosis of ADH lies in the increased risk of invasive breast carcinoma that is about 4–5 times that of the general population and may be even greater for premenopausal women. The risk of CLIS and DCIS is similar [24].

These proliferative changes are diagnosed by a pathologist as an associated finding or represent the origin of calcifications at tissue sampling. At medical audits according to the ACR-BI-RADS®, follow-up and outcome monitoring of the lobular carcinoma in situ, atypical ductal hyperplasia, atypical lobular hyperplasia, peripheral duct papillomas and phyllodes tumour are considered negative pathology results [24]. Pleomorphic lobular carcinoma in situ (LCIS) is categorised as an invasive cancer and may be treated as breast cancer. However, to maintain consistency in BI-RADS auditing, a uniform definition of cancer is required (no exceptions permitted), so this definition does not include the diagnosis of pleomorphic LCIS. Nor does the definition of cancer in the BI-RADS audit include malignant phyllodes tumour (Table 6), breast sarcoma, metastasis, lymphoma and leukaemia (Table 6). These are malignancies that occur within the breast but are not breast cancer [25].

Management of Discrepancies Between Imaging and Pathological Findings

Discrepancies can be defined as controversial meanings of information that induce cognitive dissonance. The discrepancy can occur at the level of morphologic information, the assumed meaning or interpretation of the detected abnormality or the management recommendation to the patient. Both the radiologist and the pathologist have to detect any relevant abnormality, exclude an artefact, make a threshold decision in borderline cases and correlate the finding to an imaging or pathologic classification that determines the management decisions such as BI-RADS or B-classification. A radiologic intermodality correlation needs to assign the index lesion to corresponding findings in other modalities, palpation or clinical signs and symptoms. In health systems without strict litigation, a specificity approach allows to downgrade the BI-RADS classification from tissue diagnosis to follow-up, if benign indicators of one modality override the suspicious judge of another modality. The new overall assessment category may end up in BI-RADS 3 or 2 overall assessment categories. In health systems with strict litigation, a given biopsy recommendation cannot be taken back upon on the results of other modalities. This would decrease sensitivity and increase the frequency of litigation. The final imaging-pathology consensus has to agree whether or not the localisation of the biopsy is representative and whether or not the quality of the specimens is representative for the imaging index lesion. The most suspicious judgement of experts defines the further management. Experts may use same diagnostic criteria and note the same morphological features in a case but sometimes have different opinions about whether or not the features meet a diagnostic threshold [26]. As a consequence management options focus on a second expert opinion, the gaining of additional information by minimally invasive or surgical re-biopsy or imaging follow-up along with guideline recommendations (Fig. 3).

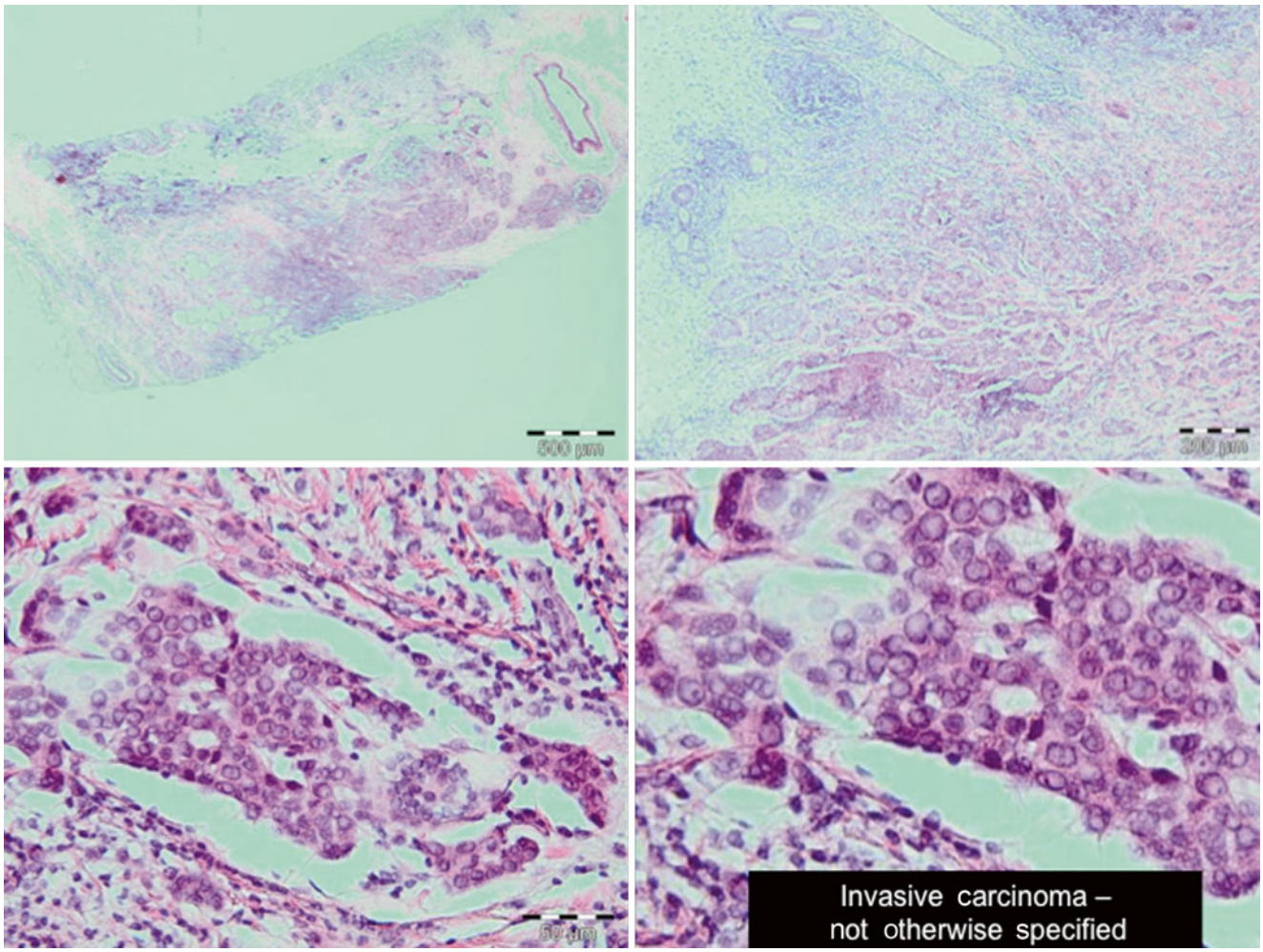

Fig. 3 Ultrasound-guided large core needle biopsy and surgical specimen agree in the diagnosis of invasive cancer – not otherwise specified (NOS)

References

1. Mendelson EB, Böhm-Vélez M, Berg WA et al (2013) ACR BI-RADS® Ultrasound. In: ACR BI-RADS® atlas, breast imaging reporting and data system. American College of Radiology, Reston
2. Madjar H, Ohlinger R, Mundinger A et al (2006) BI-RADS-analogue DEGUM criteria for findings in breast ultrasound – consensus of the DEGUM Committee on Breast Ultrasound. Ultraschall Med 27(4):374–379
3. Mundinger A, Madjar H (2015) Mammasonografie Update. Radiologie up2date 15(02):107–134
4. Mundinger A (2014) BI-RADS: ultrasound update including elastography. Where do we stand now? In: Hodler J, von Schulthess GK, Zollikofer CHL (eds) Diseases of the abdomen and pelvis. 2014–2017. Springer, Milan, pp 259–266
5. Bombonati A, Sgroi DC (2011) The molecular pathology of breast cancer progression. J Pathol 223(2):307–317
6. Tot T (2005) DCIS, cytokeratins, and the theory of the sick lobe. Virchows Arch 447(1):1–8
7. Amy D, Durante E, Tot T (2015) The lobar approach to breast ultrasound imaging and surgery. J Med Ultrason 42(3):331–339
8. Tot T (2012) The role of large-format histopathology in assessing subgross morphological prognostic parameters: a single institution report of 1000 consecutive breast cancer cases. Int J Breast Cancer 2012:395415
9. Prakash S, Venkataraman S, Slanetz PJ, Dialani V, Fein-Zachary V, Littlehale N, Mehta TS (2015) Improving patient care by incorporation of multidisciplinary breast radiology-pathology correlation conference. Can Assoc Radiol J. pii: S0846-5371(15)00086-8
10. http://www.ago-online.de/fileadmin/downloads/leitlinien/mamma/maerz2014/en/2014ER_06_Lesions_of_Uncertain_Malignant_Potential_(B3).pdf
11. Tabár L, Dean PB, Lindhe N, Ingvarsson M (2012) The ongoing revolution in breast imaging calls for a similar revolution in breast pathology. Int J Breast Cancer 2012:489345
12. Gonzalez V, Sandelin K, Karlsson A, Åberg W, Löfgren L, Iliescu G, Eriksson S, Arver B (2014) Preoperative MRI of the breast (POMB) influences primary treatment in breast cancer: a prospective, randomized, multicenter study. World J Surg 38(7):1685–1693
13. Morrow M (2008) How much can improved molecular and pathologic discriminants change local therapy? Breast Cancer Res 10(Suppl 4):S5
14. Sinn HP, Kreipe H (2013) A Brief Overview of the WHO Classification of Breast Tumors, 4th Edition, Focusing on Issues and Updates from the 3rd Edition. Breast Care 8:149–154
15. Lakhani S, Ellis I, Schnitt S et al (2012) WHO Classification of tumours of the breast, 4th edn. IARC Press, Lyon

16. Stavros AT (2015) Breast ultrasound. Lippincott Williams & Wilkins. ISBN 1609138112, 9781609138110
17. Krizmanich-Conniff KM, Paramagul C, Patterson SK, Helvie MA, Roubidoux MA, Myles JD, Jiang K, Sabel M (2012) Triple receptor-negative breast cancer: imaging and clinical characteristics. AJR Am J Roentgenol 199(2):458–464
18. Menezes GL, van den Bosch MA, Postma EL, El Sharouni MA, Verkooijen HM, van Diest PJ, Pijnappel RM (2013) Invasive ductolobular carcinoma of the breast: spectrum of mammographic, ultrasound and magnetic resonance imaging findings correlated with proportion of the lobular component. SpringerPlus 2:621
19. Jones KN, Magut M, Henrichsen TL, Boughey JC, Reynolds C, Glazebrook KN (2013) Pure lobular carcinoma of the breast presenting as a hyperechoic mass: incidence and imaging characteristics. AJR Am J Roentgenol 201(5):W765–W769
20. Berg WA et al (2007) Diagnostic imaging: breast. Amirsys
21. Tan JZ, Waugh J, Kumar B, Evans J (2013) Mucinous carcinomas of the breast: imaging features and potential for misdiagnosis. J Med Imaging Radiat Oncol 57(1):25–31
22. Martinez SR, Beal SH, Canter RJ, Chen SL, Khatri VP, Bold RJ (2011) Medullary carcinoma of the breast: a population-based perspective. Med Oncol 28(3):738–744
23. Izumori A, Takebe K, Sato A (2010) Ultrasound findings and histological features of ductal carcinoma in situ detected by ultrasound examination alone. Breast Cancer 17(2):136–141
24. Ellis IO (2010) Intraductal proliferative lesions of the breast: morphology, associated risk and molecular biology. Modern Pathology 23:1–7
25. Sickles EA, D' Orsi O (2013) ACR BI-RADS® -follow-up and outcome-monitoring. In: ACR BI-RADS® atlas, breast imaging reporting and data system. American College of Radiology, Reston
26. Allison KH, Reisch LM, Carney PA, Weaver DL, Schnitt SJ, O'Malley FP, Geller BM, Elmore JG (2014) Understanding diagnostic variability in breast pathology: lessons learned from an expert consensus review panel. Histopathology 65(2): 240–251

Breast MRI: An Update on Guidelines and BI-RADS®

Lale Umutlu

Introduction

Within the past 15 years, breast MR imaging has been well established as a noninvasive diagnostic tool for diagnosis and staging of breast cancer, therapy monitoring, and post-therapeutic surveillance as well as screening for high-risk females [1–4]. While breast MRI is currently considered one of the most sensitive imaging methods to diagnose breast cancer, having proven its potential to outperform both mammography and ultrasound [2], it is important to retain the overview and complementary diagnostic capacity of all breast cancer diagnosis tools, including mammography, ultrasound, and image-guided needle biopsy.

While there is a broad agreement for the standardization of wording and reporting of breast MRI in accordance with the BI-RADS® MRI lexicon (Breast Imaging Reporting and Data System) first introduced by the American College of Radiology (ACR) in 2003, technical considerations on how to perform breast MR examinations have yet to be standardized and are currently addressed by different guidelines [2, 5–7].

An Update on Guidelines

Over the years numerous organizations have conceptualized guidelines to help standardize indications as well as clinical practice of breast MR examinations [5–7]. While the European guidelines were mainly based on the recommendations of the EUSOMA (European Society of Breast Cancer Specialists) and EUSOBI (European Society of Breast Imaging) groups, the American College of Radiology (ACR) is the principal organization of radiologists, radiation oncologists, and clinical medical physicists in the United States. The main goal of these guidelines is to address the lack of standardization and uniformity in the indication and application of breast MRI to improve its diagnostic capacity and minimize potential errors.

The most current recommendations on indications for breast MRI were published by the EUSOBI group, naming seven key indications: (1) screening of women at high risk of breast cancer; (2) preoperative staging of newly diagnosed breast cancer (ipsilateral and contralateral); (3) therapy monitoring under neoadjuvant chemotherapy; (4) breast implant imaging; (5) detection of occult primary cancer, when mammography and ultrasound are negative; (6) suspected local recurrence; and (7) as a tool for problem solving in case of equivocal findings in mammography and ultrasound [6].

Another important issue addressed within the same guidelines is the need for correct scheduling of the examinations. It is important to discriminate between pre- and postmenopausal women for correct scheduling, as postmenopausal scans are free of considerations regarding limitations due to the menstrual cycle and postmenopausal hormone replacement therapy has been shown to have negligible effect on parenchymal background enhancement [8]. In premenopausal women, contrast-enhanced breast MRI should preferably be scheduled between days 7 and 14 of the menstrual cycle, to minimize potential masking of lesions due to fortified background parenchymal enhancement of normal fibroglandular breast tissue [9]. However, in any case, breast MRI scheduling should not substantially delay therapy planning; hence, suboptimal scheduling causing a potential reduction of the diagnostic value of the examination should be accepted when needed.

Technical considerations regarding the applied pulse sequences may vary distinctively depending on the used magnetic field strength and scanner system and should be optimized in accordance with the system and the guidelines. In general, a dedicated breast MRI protocol should comprise

L. Umutlu
Department of Diagnostic and Interventional Radiology and Neuroradiology, University Hospital Essen, Essen 45122, Germany
e-mail: Lale.Umutlu@uk-essen.de

J. Hodler et al. (eds.), *Diseases of the Brain, Head and Neck, Spine 2016–2019: Diagnostic Imaging,* DOI 10.1007/978-3-319-30081-8_39

T2-weighted imaging to distinguish potential cysts, edema, or necrosis. Furthermore, a two-dimensional (2D) or 3D T1-weighted gradient echo (GRE) pulse sequence should be obtained prior as well as several times after the application of contrast agent, preferably with submillimeter in-plane spatial resolution in both the frequency-encoding and the phase-encoding direction, incorporating thin slices (≤3 mm, but preferably with nearly isotropic voxels). A total acquisition time of less than 2 min for each phase of the dynamic series (60–90s, if possible) is required. Fat suppression is mandatory to prevent potential masking of contrast-enhancing lesions and can be performed either in a primary fat saturation manner or during post-processing, by subtraction of the enhanced sequences from the non-enhanced dataset [10, 11]. Diffusion-weighted imaging has been strongly established within breast MRI over the last few years and is known to provide valuable additional information to distinguish between malignant and benign lesions [12]. However, apart from its known diagnostic value, it has not made the step into current recommendations yet.

An Update on Reporting

Breast imaging was the first subspecialty to establish standardized wording and standardized reporting to ensure correct and unambiguous understanding of the given diagnoses [13].

The Breast Imaging Reporting and Data System® (BI-RADS®) initiative, instituted by the ACR, was started in the late 1980s to address a lack of standardization and uniformity in mammography practice reporting and resulted in the preparation of a so-called BI-RADS® lexicon, comprising a dictionary of descriptors of specific imaging features. After successful introduction for the standardized reporting of mammography, the current updated and revised fifth edition provides standardized breast imaging finding terminology, report organization, assessment structure, and a classification system for mammography, ultrasound, as well as breast MRI. Furthermore, current changes include a web-based format, the recognition of T2-weighted sequences, as well as the background parenchymal enhancement in MRI [5].

The ACR BI-RADS® lexicon is subdivided into five sections (with an additional appendix) comprising (1) clinical information and acquisition parameters, (2) breast imaging lexicon MRI, (3) reporting system, (4) implant assessment, and (5) guidance [5]. In a first step, a succinct description of the overall breast composition including the amount of fibroglandular tissue (Fig. 1) as well as the background parenchymal enhancement is performed.

The evaluation of the background parenchymal enhancement is a new feature to assess the diagnostic potential of the MR examination, considering potential masking of foci or

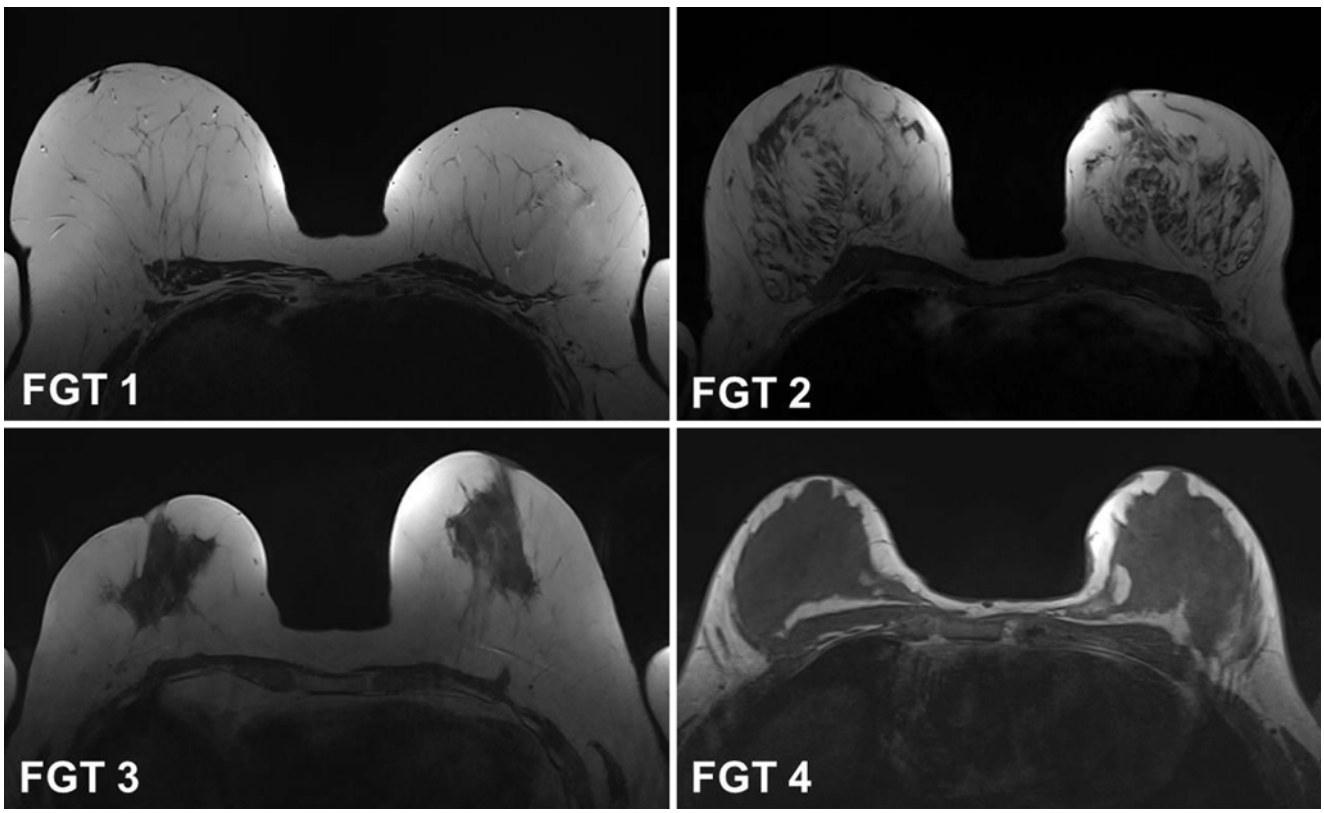

Fig. 1 Demonstration of the different categorizations of the amount of fibroglandular tissue

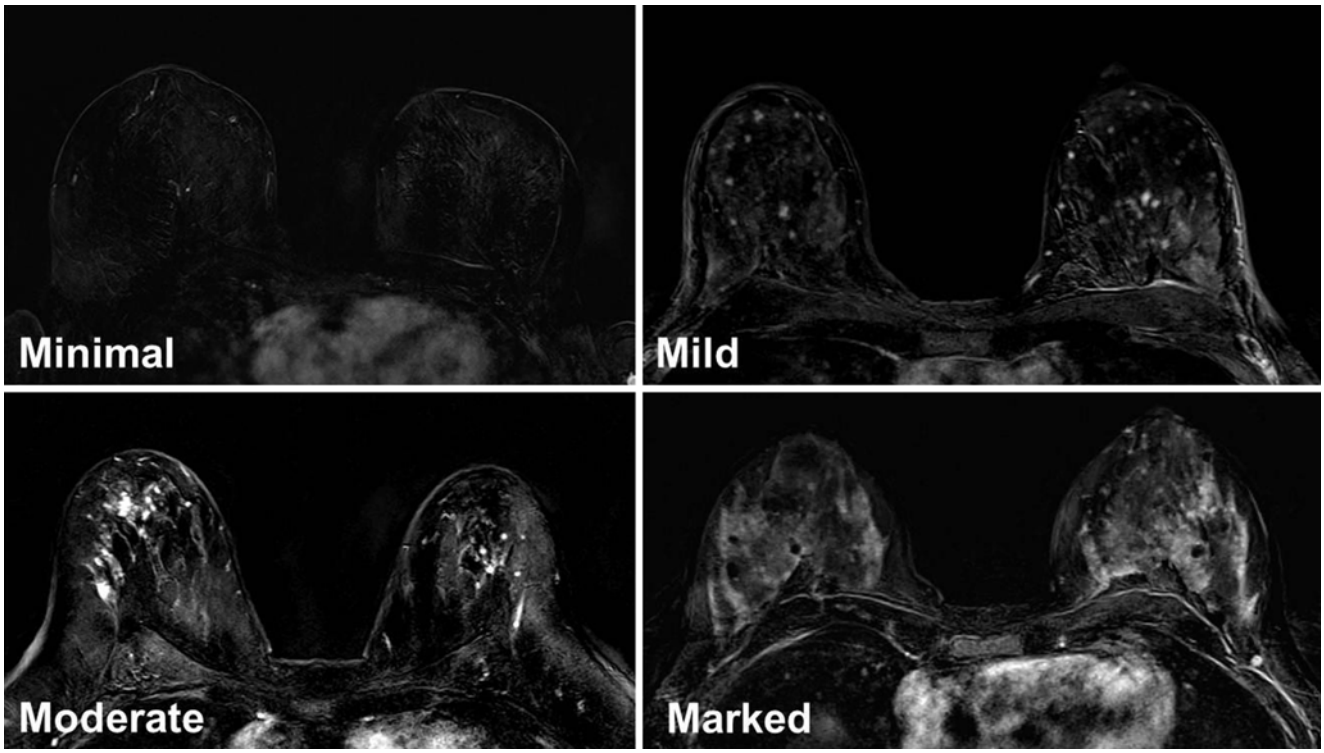

Fig. 2 Demonstration of the different categorizations of background parenchymal enhancement

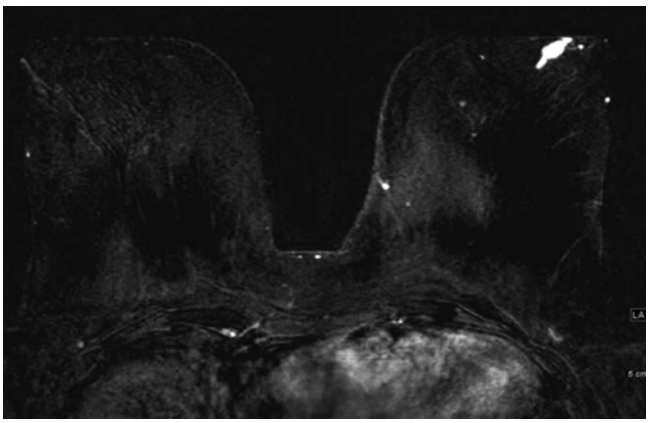

Fig. 3 The subtraction image shows an oval, well-circumscribed mass lesion in the left retromamillar region with homogeneous enhancement

small mass lesions, and is graded into (1) minimal, (2) mild, (3) moderate, and (4) marked (Fig. 2).

In a second step, any important finding should be reported while stating the size and location (breast side, quadrant and clock-face position, and distance from the nipple/chest wall). Descriptors for abnormal enhancement include (1) focus, (2) mass, or (3) non-mass enhancement and should be furtherly characterized by modifiers, such as the description of the shape, margin, and internal enhancement characteristics of mass lesions (Fig. 3)

Further considerable findings comprise intramammary lymph nodes, skin lesion, non-enhancing findings, associated features, and fat-containing lesions such as fat necrosis (Fig. 4).

As there is general agreement that the combined analysis of morphology and enhancement kinetics provides best diagnostics and characterization of breast lesions, the BI-RADS® lexicon also gives assistance in kinetic curve assessment, categorizing the enhancement into initial (strong/moderate/slight enhancement) and postinitial phases (continuous increase/plateau kinetics/washout).

In case of previous implant surgery, the BI-RADS® lexicon also offers distinguished descriptors for implant (rupture) assessment.

As a final step toward standardized reporting, a BI-RADS® category should be given, ranging from BI-RADS 0 (assessment incomplete) to BI-RADS 6 (known biopsy-proven malignancy) [5].

Summary

High-quality breast MR imaging requires high standards in technical considerations as well as strong expertise for reading and reporting the datasets. To improve and unify the imaging quality as well as the reading and reporting of breast MRI, it is generally recommended to adhere to the guidelines and the BI-RADS® lexicon [2, 5–7].

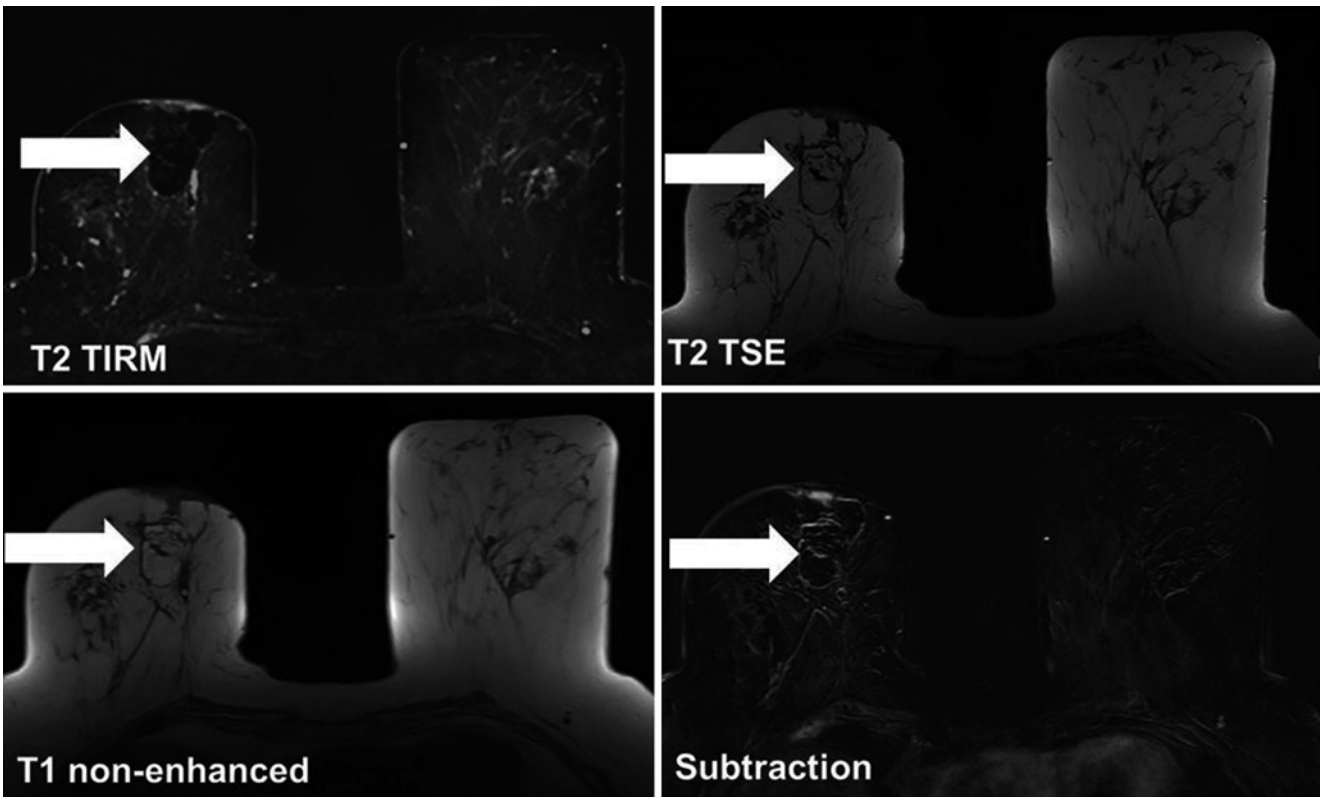

Fig. 4 The images show an example of a fat necrosis (marked by *arrow*)

References

1. Kuhl CK (2007) Current status of breast MR imaging. Part 2. Clinical applications. Radiology 244(3):672–691
2. Mann RM, Balleyguier C, Baltzer PA et al (2015) Breast MRI: EUSOBI recommendations for women's information. Eur Radiol 25(12):3669–3678
3. Pinker K, Grabner G, Bogner W et al (2009) A combined high temporal and high spatial resolution 3 Tesla MR imaging protocol for the assessment of breast lesions: initial results. Invest Radiol 44(9):553–558
4. Pinker-Domenig K, Bogner W, Gruber S et al (2012) High resolution MRI of the breast at 3 T: which BI-RADS® descriptors are most strongly associated with the diagnosis of breast cancer? Eur Radiol 22(2):322–330
5. American College of Radiology (ACR) (2015) ACR BI-RADS—mammography; ultrasound; magnetic resonance imaging. In: ACR breast imaging reporting and data system, breast imaging atlas, 2nd edn. American College of Radiology, Reston
6. Mann RM, Kuhl CK, Kinkel K, Boetes C (2008) Breast MRI: guidelines from the European Society of Breast Imaging. Eur Radiol 18(7):1307–1318
7. Sardanelli F, Boetes C, Borisch B et al (2010) Magnetic resonance imaging of the breast: recommendations from the EUSOMA working group. Eur J Cancer 46(8):1296–1316
8. Hegenscheid K, Schmidt CO, Seipel R et al (2012) Contrast enhancement kinetics of normal breast parenchyma in dynamic MR mammography: effects of menopausal status, oral contraceptives, and postmenopausal hormone therapy. Eur Radiol 22(12): 2633–2640
9. Baltzer PA, Dietzel M, Vag T et al (2011) Clinical MR mammography: impact of hormonal status on background enhancement and diagnostic accuracy. Rofo 183(5):441–447
10. Kuhl C (2007) The current status of breast MR imaging. Part I. Choice of technique, image interpretation, diagnostic accuracy, and transfer to clinical practice. Radiology 244(2):356–378
11. Hendrick RE (2008) Breast MRI: fundamentals and technical aspects. Springer, New York
12. Spick C, Pinker-Domenig K, Rudas M, Helbich TH, Baltzer PA (2014) MRI-only lesions: application of diffusion-weighted imaging obviates unnecessary MR-guided breast biopsies. Eur Radiol 24(6):1204–1210
13. Kuhl CK (2015) The changing world of breast cancer: a radiologist's perspective. Invest Radiol 50(9):615–628